Mechanisms of Resistance to Targeted Therapy in Urothelial Carcinoma

Geoffrey Alasdair Pettitt

Submitted in accordance with the requirements for the degree of
Doctor of Philosophy

The University of Leeds
School of Medicine

October, 2018

The candidate confirms that the work submitted is his own and that appropriate credit has been given where reference has been made to the work of others.

Acknowledgements

I would like to express my gratitude to Professor Margaret Knowles, Dr Carolyn Hurst and Dr Julie Burns for their encouragement and guidance throughout this project. I am very grateful to Helen McPherson who produced the resistant lines studied in this project. I would like to thank Dr Olivia Alder for her assistance with the analysis of next generation sequencing and microarray data. I am greatly appreciative of the PD173074 and linsitinib cell viability assays conducted by Matt Dunning and the work that Emma Black and Fiona Platt conducted towards the copy number analysis of resistant lines. I would like to thank the Leeds Genetics Laboratory for conducting the examination of samples for EGFR mutations.

I am very grateful to Yorkshire Cancer Research who provided the funding which made this project possible and the Leeds Institute of Cancer and Pathology who provided me with additional funding to conduct my research.

Finally, I would like to thank my parents, Geoff and May Pettitt, for their encouragement and support which they have provided continuously, throughout, and long before I began this project.

Abstract

Fibroblast growth factor receptor 3 (FGFR3) signalling is altered in ~80% of non-muscle-invasive and ~40% of muscle-invasive bladder cancers via activating mutations (point mutations or gene fusions), overexpression or both. FGFR inhibitors have entered clinical trials in advanced bladder cancer. As with other targeted therapies, resistance is expected to limit treatment efficacy. We have used *in vitro* models to explore resistance to FGFR inhibition. The urothelial cancer cell lines RT112 and RT4 express FGFR3-TACC3 fusion proteins and are sensitive to FGFR inhibition. Isogenic resistant cell lines, termed RT112 R1, R2, R3 and RT4 R1 were derived by long-term culture of parental cells in the FGFR inhibitor PD173074.

RT112 R1, R2 and RT4 R1 had an altered morphology and reduced proliferation rate compared to the parental lines. These changes were reversed when the resistant cells were cultured without PD173074 for four passages. Following this 'drug holiday' RT112 R1 and R2 retained PD173074 resistance, whereas RT4 R1 did not. The resistance mechanism in RT112 R1, R2 and RT4 R1 appears to be epigenetic. RT112 R3 retained an epithelial morphology and a proliferation rate similar to parental RT112. Exome sequencing uncovered a *HRAS* G12S mutation in RT112 R3. The retroviral transduction of a *HRAS* G12 mutation in RT112 parental induced PD173074 resistance. Microarray analysis was conducted to examine expression changes between parental and resistant lines. Metacore™ analysis identified the differential expression of pathways relating to cell cycle, epithelial-mesenchymal transition and Oncostatin M signalling. Microarray and immunoblot analysis identified a number of tyrosine kinases as potential resistance mediators. Viability assays showed that RT4 parental and R1 were sensitive to the EGFR inhibitor erlotinib and that RT112 parental and resistant lines were sensitive to the IGF1R inhibitor linsitinib.

Investigation of PD173074-resistant derivatives suggests that genetic and epigenetic mechanisms of resistance occur following prolonged FGFR inhibition.

Table of Contents

List of Tables

List of Figures

Chapter 4

Chapter 5

Chapter 6

List of Abbreviations

°C	Degrees Celsius
^{14}C	Carbon-14
µg	Microgram
µl	Microlitre
µM	Micromolar
ABC	ATP-binding cassette
ACER3	Alkaline ceramidase 3
ALL	Acute lymphoblastic leukaemia
ANOVA	Analysis of variance
AP1	Activating protein 1
ATP	Adenosine triphosphate
BAIAP2L1	BAI1-associated protein 2-like 1
BCG	Bacillus Calmette-Guérin
BET	Bromodomain and extraterminal
cDNA	Complementary DNA
cfDNA	Cell-free DNA
cm	Centimetres
CO_2	Carbon dioxide
CML	Chronic myeloid leukaemia
Ct	Threshold cycle
dH_2O	Distilled water
DMSO	Dimethyl sulphoxide
DNA	Deoxyribonucleic acid
dNTPs	Deoxyribonucleoside triphosphates
DTT	Dithiothreitol
EC50	Half maximal effective concentration
EDTA	Ethylenediaminetetraacetic acid
EGFR	Epidermal growth factor receptor
ELOVL5	Elongation of very long chain fatty acids protein 5
EMA	European Medicines Agency
EMT	Epithelial mesenchymal transition
ERBB	Erb-B2 Receptor Tyrosine Kinase (HER)
ETS	E-twenty-six
FABP4	Fatty acid binding protein 4

FCS	Foetal calf serum
FDA	United States Food and Drug Administration
FGF	Fibroblast growth factor
FGFR	Fibroblast growth factor receptor
FGFRL1	Fibroblast growth factor receptor like-1
FISH	Fluorescence *in situ* hybridization
g	Gram
g	Gravity of Earth
GemCis	Gemcitabine plus cisplatin
GIST	Gastrointestinal stromal tumour
gp130	Glycoprotein 130
GDP	Guanine diphosphate
GTP	Guanine triphosphate
h	Hour
H3K27	Histone H3 lysine-27
HBSS	Hanks' balanced salt solution
HGF	Hepatocyte growth factor
HCl	Hydrochloric acid
HMGCR	3-hydroxy-3-methylglutaryl-CoA reductase
HMM	Hidden Markov Model
HRAS	Harvey Rat Sarcoma Viral Oncogene Homolog
HRP	Horseradish peroxidase
HSD17B2	Hydroxysteroid 17-beta dehydrogenase 2
IC50	Half maximal inhibitory concentration
Ig	Immunoglobulin
IGF1R	Insulin-like growth factor 1 receptor
IGV	Integrative genomics viewer
Indels	Insertions and deletions
InsR	Insulin receptor
JAK	Janus kinase
KCl	Potassium chloride
kDa	Kilo Daltons
LIFR	Leukaemia inhibitory factor receptor
LRP8	Low-density lipoprotein receptor-related protein 8
mAbs	Monoclonal antibodies
MAF	Mutation annotation format
MAP	Mitogen-activated protein
Mb	Megabase
ME1	Malic enzyme 1
mg	Milligram

$MgCl_2$	Magnesium chloride
MIBC	Muscle-invasive bladder cancer
min	Minute
ml	Millilitre
mM	Millimolar
mRNA	Messenger RNA
MTT	3-(4,5-dimethylthiazol)-2,5-diphenyl tetrazolium
MVAC	Methotrexate, vinblastine, doxorubicin plus cisplatin
ng	Nanogram
NGS	Next-generation sequencing
NLS	Nucear localisation signal
NMIBC	Non-muscle-invasive bladder cancer
NRG	Neuregulin
OSM	Oncostatin M
OSMR	Oncostatin M receptor
PARP	Poly (ADP) ribose polymerase
PBS	Phosphate buffered saline
PBS-T	PBS containing 0.1% (v/v) Tween 20
PCA	Principal component analysis
PCR	Polymerase chain reaction
PCSK9	Proprotein convertase subtilisin/kexin Type 9
PD	PD173074
PD-1	Programmed cell death protein 1
PD-L1	Programmed death ligand 1
PDGFR	Platelet derived growth factor receptor
PDSS1	Decaprenyl diphosphate synthase subunit 1
PI3	Phosphatidylinositol-3
PIP_2	Phosphatidylinositol-4,5-bisphosphate
PIP_3	Phosphatidylinositol-3,4,5-triphosphate
PKC	Protein kinase C
PLCγ	Phospholipase C gamma
PolyPhen	Polymorphism Phenotyping v2
PPAR	Peroxisome proliferator activator receptor γ
OD	Optical density
qRT-PCR	Quantitative reverse transcription polymerase chain reaction
RIN	RNA integrity number
RIPA	Radioimmunoprecipitation assay
RNA	Ribonucleic acid
RNAi	RNA interference
RQ	Relative quantification

RT	Room temperature
s	Seconds
SAP	Shrimp alkaline phosphatase
SCD1	Stearoyl-CoA desaturase-1
SDHA	Succinate dehydrogenase complex flavoprotein subunit A
SDR16C5	Short chain dehydrogenase/reductase family 16C member 5
SDS-PAGE	Sodium dodecyl sulphate polyacrylamide gel
shRNA	Short hairpin RNA
SIFT	Sorting intolerant from tolerant
SNV	Single nucleotide variation
SST-RMA	Signal Space Transformation-Robust Multichip Average
STAG2	Stromal antigen 2
STAT	Signal transducer and activator of transcription
TACC3	Transforming acid coiled coil 3
TBE	Tris/Borate/EDTA
TGF-α	Transforming growth factor alpha
TGS	Tris/Glycine/SDS
TKI	Tyrosine kinase inhibitor
Tris	Tris (hydroxymethyl) aminoethane
TURBT	Transurethral resection of the bladder tumour
TV	Trypsin-versene
Tween	Polyxyethylene sorbitan monolaurate
v/v	Volume/volume
VEGFR	Vascular endothelial growth factor
VEP	Variant Effect Predictor
w/v	Weight/volume
WHO	World Health Organisation

Chapter 1
Introduction

1.1 Bladder cancer

1.1.1 Epidemiology and treatment of bladder cancer

It is estimated that there were 429,000 new cases and 165,000 deaths from bladder cancer worldwide in 2012 (Ferlay *et al.*, 2015). The median age at diagnosis with bladder cancer is approximately 67 and in the western world approximately 95% of bladder cancers are urothelial carcinoma (Eble *et al.*, 2004; Malats and Real, 2015). Bladder cancer occurs more frequently in males than females with a worldwide sex ratio of 3.5:1 (Ferlay *et al.*, 2015). Smoking cigarettes, exposure to chemicals such as aromatic amines and consumption of phenacetin are major risk factors for developing bladder cancer (Miyazaki and Nishiyama, 2017). Bladder cancer patients commonly present with painless haematuria. Cystoscopy, transurethral resection of the bladder tumour (TURBT), computed tomography and magnetic resonance imaging are used in the diagnosis, staging and grading of bladder cancer (Witjes *et al.*, 2014).

Bladder cancers are classified with the TNM staging system as follows: Tis: known as carcinoma *in situ*, the tumour is non-invasive; Ta: the tumour is non-invasive with a papillary structure protruding into the bladder lumen; T1: the tumour has invaded the subepithelial connective tissue; T2: the tumour has invaded the bladder's muscle wall; T3: the tumour has invaded the perivesical fatty tissue surrounding the bladder, and T4: the tumour has invaded adjacent organs such as the uterus, vagina, prostate, pelvic wall or abdominal wall (Cheng *et al.*, 2009). Non-invasive urothelial carcinomas are graded with the 2004 World Health Organisation (WHO) classification system according to cellular appearance as papillary urothelial malignancy of low malignant potential, non-invasive, low grade papillary urothelial carcinoma or non-invasive, high grade papillary urothelial carcinoma (Eble *et al.*, 2004). Previously bladder cancers were graded with the 1973 WHO classification with the most differentiated tumours assigned grade 1,

tumours with an intermediate level of differentiation assigned grade 2 and the least differentiated tumours assigned grade 3 (World Health Organization, 1973).

Worldwide, 70-80% of bladder cancers present as non-muscle-invasive. These non-muscle-invasive bladder cancers (NMIBCs) recur in 50-70% of patients following treatment and progress to muscle-invasive disease in 10-15% of cases (Prout *et al.*, 1992). The high rate of recurrence means that patients require lifetime surveillance and often multiple treatments during their lifetime. Therefore, bladder cancer is expensive to treat (Svatek *et al.*, 2014). Sylvester *et al.* analysed the records of 2596 patients with superficial bladder cancer treated with TURBT and identified that the presence of multiple tumours, larger tumours and a higher prior recurrence rate were all prognostic of a greater risk of disease recurrence. Classification of the tumour as T1 rather than Ta, concomitant carcinoma *in situ* and a higher tumour grading were all prognostic of a greater risk of progression to muscle-invasive bladder cancer (MIBC) (Sylvester *et al.*, 2006). Following the diagnosis of NMIBC, which is dependent upon the histological analysis of a tissue sample obtained with TURBT, patients with low risk of recurrence and progression receive treatment with a single immediate postoperative instillation of chemotherapy such as the DNA crosslinking agent mitomycin C. Patients with a high risk of recurrence and progression receive intravesical Bacillus Calmette-Guérin (BCG) vaccine instillations (Babjuk *et al.*, 2016). BCG reduces recurrence and progression of NMIBC (Kamat *et al.*, 2017). NMIBC patients with the highest risk of progression may receive radical cystectomy (Babjuk *et al.,* 2016). MIBC is treated with the neoadjuvant chemotherapy combination of methotrexate, vinblastine, doxorubicin plus cisplatin (MVAC) or gemcitabine plus cisplatin (GemCis) and radical cystectomy. Neoadjuvant chemotherapy has been demonstrated to increase overall patient survival in randomized controlled trials (Hermans *et al.*, 2017). Adjuvant chemotherapy, most commonly GemCis, is offered to patients who did not receive neoadjuvant chemotherapy or have stage T3 or T4 disease (Pradere *et al.*, 2017; Witjes *et al.*, 2016). Meta-analysis has shown that adjuvant therapy increases overall patient survival and disease-free survival in MIBC patients (Leow *et al.*, 2014). There is a need to improve survival in MIBC patients: patients with locally advanced or metastatic MIBC have a 5-year survival rate of approximately 15% (von der Maase *et al.*, 2005). Although more tumours are diagnosed in males, females have a higher mortality rate from their disease and are more likely to present with MIBC. This may be due to females experiencing a greater time from the onset of symptoms to GP referral and to treatment with TURBT (Bryan *et al.*, 2015).

The immunotherapeutic monoclonal antibodies atezolizumab, pembrolizumab, nivolumab are approved by the United States Food and Drug Administration (FDA) and the European Medicines Agency (EMA) for use as postplatinum single agents for the treatment of advanced urothelial carcinoma. Avelumab and durvalumab are also approved by the FDA but not the EMA for treatment of this condition. Atezolizumab and pembrolizumab are also approved by the FDA and EMA as single agent, first-line treatments of advanced urothelial carcinoma patients ineligible for treatment with cisplatin (Godwin *et al.*, 2018). Pembrolizumab and nivolumab bind programmed cell death 1 (PD-1) and atezomomab, avelumab and durvalumab bind programmed death ligand 1 (PD-L1). Monoclonal antibodies targeting PD-1 and PD-L1 prevent the PD-1 and PD-L1 interaction and therefore prevent the inhibition of T-cell activation and enable T-cells to induce cancer cell death (Topalian *et al.*, 2015). Atezolizumab was approved for use in urothelial carcinoma following a phase II clinical trial which assessed its efficacy in advanced urothelial carcinoma patients whose disease had progressed since, or who were ineligible for treatment with, platinum-based chemotherapy. The objective response rate of 15% was statistically significant compared to the historical objective response rate of 10% (Rosenberg *et al.*, 2016). Since then a phase III clinical trial has been published assessing the efficacy of atezolizumab in advanced urothelial carcinoma patients whose disease had progressed following platinum-based chemotherapy. Overall survival was not significantly different between the atezolizumab and chemotherapy treatment groups (Powles *et al.*, 2018). The efficacy of pembrolizumab was assessed in a phase III clinical trial with patients whose urothelial carcinoma had recurred or progressed following chemotherapy. Median overall survival was 10.3 months for the pembrolizumab group and 7.4 months for the chemotherapy group. This increase in overall survival was significant (Bellmunt *et al.*, 2017). The efficacy of nivolumab was assessed in a phase II clinical trial in patients whose urothelial carcinoma had recurred or progressed following chemotherapy. An overall objective response was observed in 19.6% of patients. This was significantly greater than the historical control objective response rate of 10% (Sharma *et al.*, 2017).

1.1.2 Molecular features of bladder cancer

NMIBC and MIBC have distinct molecular profiles. FGFR3 overexpression and mutations in *FGFR3*, *KDM6A, STAG2* and RAS occur more frequently in NMIBC whilst alterations in genes which regulate TP53 and the cell cycle pathways occur

more frequently in MIBC. TERT mutations occur frequently in both NMIBC and MIBC. Mutation rates are higher in MIBC (Hurst *et al.*, 2017; Robertson *et al.*, 2017).

Genetic alterations in the TP53/cell cycle pathway occur frequently in bladder cancer (Lianes *et al.*, 1994). The frequency of *TP53* mutations increases with stage and grade and alterations in *TP53* are weakly predictive of mortality, tumour progression and recurrence (Esrig *et al*., 1993; Malats *et al*., 2005). *TP53* encodes the transcription factor TP53, which is a tumour suppressor. TP53 regulates expression of genes which control cell cycle, metabolism, DNA repair and apoptosis (Fischer, 2017). Robertson *et al.* conducted analysis including RNA-seq, whole exome sequencing and copy number analysis on a cohort of 412 MIBC tumours (Robertson *et al.*, 2017). They reported that the TP53/cell cycle pathway was inactivated in 89% of MIBC tumours. 48% of the MIBC tumours had mutant *TP53* (Robertson *et al.*, 2017). Pietzak *et al,* who examined genomic changes in NMIBC from 105 patients and primary MIBC from 40 patients using targeted exon sequencing analysis, observed that *TP53* was mutated in 21% of NMIBCs (Pietzak *et al.*, 2017). MDM2 ubiquitinates the C-terminus of TP53 causing it to be degraded by the proteasome (Merkel *et al.*, 2017). *CDKN2A* encodes $p16^{INK4A}$ which binds and inhibits CDK4 and CDK6 preventing the phosphorylation of RB1 and so inhibits cell cycle progression. *CDKN2A* also encodes p14ARF which inhibits MDM2 (Pomerantz *et al.*, 1998; Zhao *et al.*, 2016). Amplification and overexpression of MDM2 occurs in bladder cancer (López-Knowles *et al*., 2006; Maluf *et al*., 2006; Tuna *et al*., 2003). *TP53* mutations occur mutually exclusively with amplification of *MDM2* and deletion of *CDKN2A* (López-Knowles *et al*., 2006; Veerakumarasivam *et al*., 2008; Robertson *et al.*, 2017). *MDM2* amplification and overexpression were found in 6% and 19% of tumours, respectively in a cohort of 412 MIBC (Robertson *et al.*, 2017). Additionally, it was observed that focal deletion of 9p21.3, which contains the tumour suppressor *CDKN2A,* occurred in 22% of MIBCs and *CDKN2A* mutations occurred in 7% of MIBCs. Alterations between *CDKN2A* were mutually exclusive with mutations observed in *TP53* and *RB1* (Robertson *et al.*, 2017). Pietzak *et al.* observed genomic alteration, predominantly amplification, of *MDM2* in 8% of NMIBCs and genomic alteration, predominantly deletion, of *CDKN2A* in 19% of NMIBCs (Pietzak *et al.*, 2017). They observed that alterations in *TP53* and *MDM2* were associated with a higher stage and grade of bladder cancer (Pietzak *et al.*, 2017). Homozygous deletion of CDKN2A occurs more frequently in bladder cancers with mutant *FGFR3* than those with wildtype *FGFR3* and homozygous deletion of CDKN2A associated with a higher stage in tumours with mutant *FGFR3*

but not those with wildtype *FGFR3* (Rebouissou *et al*., 2012). *RB1* encodes the tumour suppressor RB1 which regulates cell cycle progression by modulating the activity of E2F transcription factors. Inactivating mutations in RB1 are a frequent event in bladder cancer and are associated with a higher stage and grade (Hong-Ji *et al*., 1993; Horowitz *et al*., 1990; Ishikawa *et al*., 1991). *RB1* mutations, which were predominantly inactivating, were observed in 17% of MIBCs and deletion of *RB1* was observed in 4% of MIBCs (Robertson *et al.*, 2017). Pietzak *et al.* observed deletion and mutation of *RB1* in 6% of NMIBCs. Alterations in cell cycle control genes were significantly associated with a higher stage and grade (Pietzak *et al.*, 2017).

Fibroblast growth factor receptor 3 (FGFR3) is frequently overexpressed and *FGFR3* is frequently mutated in bladder cancer. Alterations in *FGFR3* occur more frequently in bladder cancers of a lower stage and grade (Kimura *et al.*, 2001). Tomlinson *et al.* screened 158 urothelial carcinoma samples for mutations in *FGFR3* exons 7, 10 and 15 with direct sequencing and examined FGFR3 protein expression in 149 samples with immunohistochemistry. Bladder cancer tumours were of a range of stages and grades. It was observed that 81% of non-invasive and 54% of invasive urothelial carcinomas had an activating *FGFR3* mutation or overexpressed FGFR3 (Tomlinson *et al.*, 2007). Robertson *et al.* observed *FGFR3* mutations in 14% of MIBCs, *FGFR3* fusion events in 2% of MIBC and focal copy number gain of the *FGFR3* locus (4p16.3) in 2% of MIBCs (Robertson *et al.*, 2017). Genomic alterations were observed in *FGFR3* in 49% of 105 NMIBC patients, *FGFR3* amplification was observed in 2 tumours (2% of the cohort), FGFR3 fusion events were observed in 4 tumours (4%) and missense mutations were observed in 47 tumours (45%) (Pietzak *et al.*, 2017). *FGFR3* mutations occurred in 79% of a cohort of 82 Ta urothelial tumours examined with either exome sequencing or selective target capture followed by next-generation sequencing (NGS) (Hurst *et al.*, 2017). FGFR expression in urothelial carcinoma is further discussed in section 1.3.2.

Expression, mutation and copy number gain of members of the EGFR family of receptor tyrosine kinases (RTKs) are common in bladder cancer. Approximately 6% of MIBC exhibit gain of copy number of region 7p11.2 which contains *EGFR* (Robertson *et al.*, 2017). Examination of membranous EGFR expression with immunohistochemistry showed that 61% of 74 bladder tumours of a variety of stages and grades expressed EGFR. This expression did not correlate with the stage or grade of the tumours (Ibrahim *et al.*, 2009). 12% and 10% of MIBC tumours have mutations in *ERBB2* and *ERBB3* respectively. Gain of chromosome

7q12, which contains *ERBB2,* occurs in 5% of MIBC (Robertson *et al.*, 2017). Examination of ERBB2 expression with immunohistochemistry in 1005 MIBC tumours showed that ERBB2 overexpression occurred in 9% of tumours (Laé *et al.*, 2010). Fluorescence *in situ* hybridization (FISH) in the tumours in which immunohistochemistry had identified ERBB2 overexpression, revealed that 5% of the cohort of 1005 tumours exhibited *ERBB2* amplification (Laé *et al.*, 2010). A single *ERBB2* missense mutation and no *ERBB2* amplifications were found in a panel of 23 low-grade NMIBCs and *ERBB2* amplifications or missense mutations were observed in 15 out of 82 (18%) high grade NMIBCs. *ERBB2* alterations were associated with a higher stage and grade and *FGFR3* and *ERBB2* alterations were observed to be mutually exclusive (Pietzak *et al.*, 2017).

Alterations in the PI3 kinase pathway are frequently found in bladder cancers (Askham *et al*., 2010; Aveyard *et al*., 1999; Cairns *et al*., 1998; Knowles *et al*., 2003; Platt *et al*., 2009; Ross *et al*., 2013; Wang *et al*., 2000). *PIK3CA* encodes the phosphatidylinositol-3 (PI3) kinase p110α subunit. PI3 kinase phosphorylates phosphatidylinositol-4,5-bisphosphate (PIP_2) to produce phosphatidylinositol-3,4,5-triphosphate (PIP_3). This leads to AKT activation which promotes cell growth and survival (Fruman *et al*., 2017). TSC1 forms part of the TSC complex which inhibits the activity of the mTORC1 complex which in turn regulates cell growth via the promotion of translation. TSC1 is inhibited by AKT (Mieulet and Lamb, 2010). Of the 412 MIBCs examined with whole exome sequencing, 22% harboured *PIK3CA* mutations, which were predominantly activating, and 8% had *TSC1* mutations, which were often truncating (Robertson *et al*., 2017). *PIK3CA* and *TSC1* mutations were observed in 28% and 11% of a cohort of 105 NMIBC respectively. *PIK3CA* and *TSC1* mutations were found not to be significantly associated with bladder cancer stage and grade (Pietzak *et al*., 2017).

Mutations in members of the RAS family of GTPases, which activate the mitogen activated protein (MAP) kinase and PI3 kinase pathways, are observed in bladder cancer. Robertson *et al.* observed *HRAS*, *KRAS* and *NRAS* mutations in 5, 4 and 2% of MIBCs respectively (Robertson *et al.*, 2017). RAS mutations are usually found mutually exclusively with FGFR3 mutations in bladder cancer suggesting the mutations have an overlapping function (Jebar *et al.*, 2005). RAS mutations occur more frequently in NIBCs than MIBCs (Hurst *et al.*, 2017).

Genes encoding chromatin modifiers, such as *KDM6A*, *CREBBP*, *EP300* and *ARID1A* are frequently mutated in bladder cancer (Gui *et al.*, 2011; van Haaften *et al.*, 2009). *KDM6A* encodes a histone H3 lysine-27 (H3K27)

demethylase. One consequence of the histone demethylation activity of KDM6A in fibroblasts is an increase in expression of retinoblastoma binding proteins required for the function of RB1 as a tumour suppressor (Wang *et al.*, 2010). Its role in epithelial cells, including the urothelium, is unknown. *CREBBP* and *EP300* encode CREB-binding protein and p300 respectively which can act as both tumour suppressors or oncogenes. These proteins have a similar structure, with 63% amino acid sequence identity, and are largely functionally redundant. CREB-binding protein and p300 function as histone acetyltransferases, interact with transcription factors and recruit transcription machinery and transcriptional coactivators to the promoter. The tumour suppressive role of these proteins may be due to their interaction with TP53, BRCA1, and FOXO3a (Wang *et al.*, 2013a). ARID1A is a subunit of the BAF chromatin remodelling complex. BAF has been found to bind RB1, aiding RB1 repression of E2F1 activity: this could be a key tumour suppressive function of the BAF complexes (Hodges *et al.*, 2016; Trouche *et al.*, 1997).

Gui *et al.* identified mutations in 9 MIBC with whole exome sequencing. Genes identified as mutated in this initial cohort were then examined with targeted exon sequencing in a further 51 MIBC and 37 NMIBC (Gui *et al.*, 2011). They observed that mutations in chromatin remodelling genes occurred in 59% of samples, the most common of which were in *KDM6A,* which was mutated in 21% of tumours, and *CREBBP*, *EP300* and *ARID1A* which were each mutated in 13% of tumours (Gui *et al.*, 2011)*. KDM6A* mutations were frequent in tumours of a low stage and grade with 32% of Ta and T1 tumours and 13% of tumours stage T2 or greater exhibiting mutated *KDM6A. ARID1A*, *CREBBP* and *EP300* mutations were not significantly associated with tumour stage and grade (Gui *et al.*, 2011). In the Robertson *et al.* cohort of 412 MIBCs, mutations, predominantly inactivating, were observed in greater than 5% of tumours in each of the following chromatin remodelling genes: *KDM6A* (26%), *KMT2A* (11%), *KMT2C* (18%), *KMT2D* (28%), *CREBBP* (12%), *EP300* (15%), *KANSL1* (6%), *ARID1A* (25%), *ASXL1* (6%) and *ASXL2* (9%) (Robertson *et al.*, 2017). In a panel of 105 NMIBC, *KDM6A, ARID1A, CREBBP* and *EP300* were mutated in 38%, 21%, 21% and 15% of NMIBCs respectively (Pietzak *et al.*, 2017). Hurst *et al.* observed predominantly inactivating mutations in *KDM6A* (52%), *KDMT2D* (30%), *EP300* (18%), *ARID1A* (18%), *KDMT2C* (15%) and *CREBBP* (15%) in a cohort of 82 Ta urothelial tumours (Hurst *et al.*, 2017).

Reduced expression of stromal antigen 2 (STAG2) occurs in bladder cancer due to truncating and missense mutations (Gui *et al.*, 2011; Taylor *et al.*,

2014). STAG2 functions as a subunit of the cohesin complex to adhere to the centromeric regions of sister chromatids following DNA replication in the cell cycle. This maintains the cohesion of sister chromatids until they are required to separate during metaphase (Aquila *et al.*, 2018; Peters *et al.*, 2008). *STAG2* mutations were observed in 22% of a cohort of 307 bladder tumours and *STAG2* mutations were associated with a low stage and grade of bladder cancer (Taylor *et al.*, 2014). Examination of STAG2 with immunohistochemistry showed that 18% of 295 urothelial carcinomas, of a range of stages and grades, did not express STAG2. Additionally, Sanger sequencing on a cohort of 47 NMIBC and 64 MIBC found that 32% of the NMIBC and 13% of the MIBC exhibited *STAG2* mutations. (Solomon *et al.*, 2013). It has been suggested that the loss of *STAG2* expression may promote aneuploidy and tumour evolution due to its role in regulating chromosomal segregation. However, examination of STAG2 expression, with immunohistochemistry, and chromosomal alterations, with high resolution SNP or BAC arrays, in a panel of 23 TaG1/TaG2 urothelial carcinomas showed that 9 tumours lacked STAG2 expression and loss of STAG2 expression often occurred in chromosomally stable tumours (Balbás-Martínez *et al.*, 2013). Additionally knockdown of STAG2 in the bladder cancer cell lines RT112, UM-UC-11 and 639V did not increase the development of aneuploidy (Balbás-Martínez *et al.*, 2013). Furthermore, Taylor *et al.* observed that *STAG2* mutation was not associated with an increase in copy number alterations in bladder cancer (Taylor *et al.*, 2014). Therefore, loss of *STAG2* may exert its function as a tumour suppressor in urothelial carcinoma through a mechanism other than preventing the development of aneuploidy.

TERT promoter mutations are found in approximately 80% of bladder cancer patients, most commonly G>A base changes -124 bp and -146 bp upstream of the ATG start site. *TERT* promoter mutations are not associated with stage and grade in bladder cancer and therefore *TERT* mutations may occur early in tumour development (Allory *et al.*, 2014; Hurst *et al.*, 2014; Killela *et al.*, 2013; Kinde *et al.*, 2013; Liu *et al.*, 2013). *TERT* encodes the enzymatic subunit of telomerase (TERT) which prevents shortening of telomeres during DNA replication. Cells which do not express TERT are able to undergo only 50-90 rounds of replication prior to the induction of cell senescence (Heidenreich and Kumar, 2017). *TERT* promoter mutations create binding sites for the E-twenty-six (ETS) transcription factors (Bell *et al.*, 2015; Horn *et al.*, 2013). Borah *et al.* showed that TERT promoter mutations were associated with increased expression of *TERT* mRNA and protein and an increase in telomere length in urothelial carcinoma cell lines (Borah *et al.*, 2015).

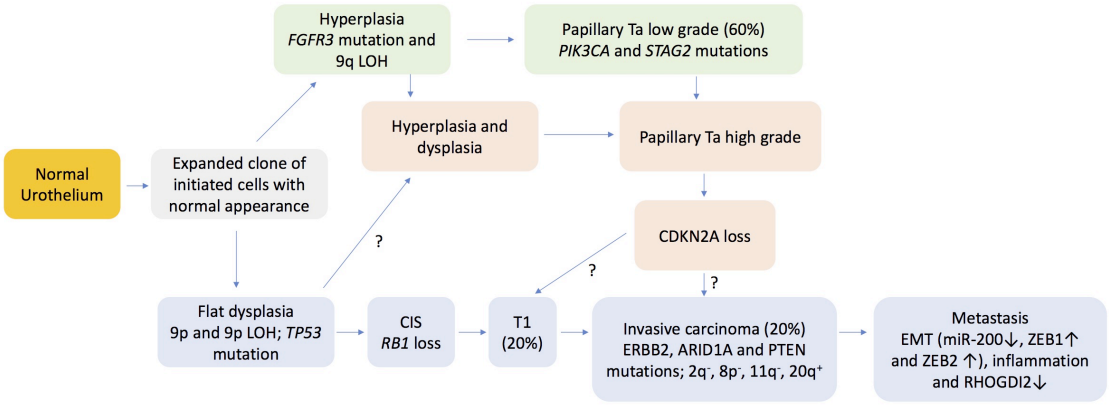

Figure 1.1 Molecular pathogenesis of urothelial carcinoma. The two major pathways of urothelial carcinoma pathogenesis are shown in green and blue. Key molecular alterations and percentages at diagnosis are shown. Image adapted from Knowles and Hurst (2015).

Gene expression profiling of bladder tumours has been used to identify molecular subtypes with differing clinical outcomes. Sjödahl *et al.* performed mRNA microarray expression analysis and unsupervised hierarchical cluster analysis on a cohort of 308 NMIBCs and MIBCs. Additionally, tumours were examined for the presence of *FGFR3*, *PIK3CA* and *TP53* mutations and the expression of key genes was determined with immunohistochemistry. This identified 5 subtypes of bladder cancer: urobasal A, urobasal B, genomically unstable, infiltrated and squamous cell carcinoma (SCC)-like. The tumour subtype with the best prognosis was urobasal A whilst urobasal B and SCC-like had the worst prognosis. Urobasal A and B subtypes both exhibited high expression of *FGFR3, CCND1* and *TP63* and frequently harboured *FGFR3* mutations. However, whilst urobasal A had a similar pattern of cytokeratin expression to normal urothelium, urobasal B exhibited high expression of *KRT6A*, *KRT6C* and *KRT14*. Urobasal B also had a high frequency of *TP53* mutations. The SCC-like subtype also exhibited high expression of basal markers but did not exhibit the FGFR3 gene expression signature observed in urobasal A and B. The genomically unstable subtype had a high frequency of *TP53* mutations and grossly rearranged genomes. The infiltrated subtype exhibited high expression of immunologic and extracellular matrix genes. Immunohistochemistry revealed a high expression of CD3 and ACTA2 in the infiltrating subtype tumours, confirming the presence of T cells and myofibroblasts (Sjodahl *et al.*, 2012).

Damrauer *et al.* performed consensus clustering on gene expression data, curated from publically available datasets, from 262 high grade NMIBCs. This

analysis identified two subtypes. In one subtype tumours exhibited higher expression of urothelial basal markers (*KRT14*, *KRT5*, *KRT6B* and *CD44*) and had a higher frequency of alterations in the RB1 pathway. In the other subtype tumours exhibited higher expression of markers associated with urothelial umbrella cells (*UPK1B*, *UPK2*, *UPK3A* and *KRT20*) and this subtype had a higher frequency of *FGFR3* and *TSC1* mutations. It was observed that the basal-like subtype of tumours had a significantly shorter disease specific and overall survival (Damrauer *et al.*, 2014).

Choi *et al.* performed mRNA microarray expression profiling and unsupervised hierarchical cluster analysis with 73 MIBCs. The MIBCs clustered into 3 molecular subtypes: basal, luminal and p53-like (Choi *et al.,* 2014). Basal tumours exhibited high expression of basal markers (*CD44*, *CDH3*, *KRT14*, *KRT16*, *KRT5*, *KRT6A*, *KRT6B* and *KRT6C*), mesenchymal markers (*TWIST1/2*, *SNAI2*, *ZEB2* and *VIM*) and p63 pathway genes. This subtype had a significantly shorter disease specific survival. Luminal tumours expressed luminal markers (*FGFR3, FOXA1, GPX2, ERBB2, ERBB3, CYP2J2, GATA3, PPARG, KRT19, KRT7, KRT6, FABP4, KRT20, CD24, KRT18* and *XBP1*), exhibited PPARγ pathway activation and this subtype was enriched with activating *FGFR3* mutations. The p53-like subtype also expressed luminal markers but possessed the determining feature of an activated wild-type p53 gene expression signature. p53-like subtype tumours were typically resistant to chemotherapy. Expression profiling was conducted with a cohort of 43 MIBC prior to and following neoadjuvant chemotherapy. It was observed that post-treatment, resistant tumours were enriched with the p53-like subtype (Choi *et al.*, 2014).

Robertson *et al.* conducted consensus clustering with the RNA-seq data generated from 408 MIBCs. This split the MIBCs into 5 subtypes: luminal, luminal papilliary, luminal infiltrated, basal-squamous and neuronal (Robertson *et al.*, 2017). The luminal, luminal papilliary and luminal infiltrated subtypes had high expression of *UPK2*, *UPK1A*, *PPARG*, *FOXA1* and *GATA3*. The luminal papilliary subtype was enriched with tumours with a papillary structure whilst the luminal infiltrated subtype exhibited a myofibroblast and smooth muscle expression signature and had increased expression of immune markers. The basal-squamous subtype exhibited high expression of the basal and stem-like markers *CD44*, *KRT5*, *KRT6A* and *KRT14* and high expression of *TGM1*, *DCS3* and *PI3* which are markers of squamous differentiation. This subtype was enriched with *TP53* mutations. The neuronal subtype exhibited high expression of markers of neuronal differentiation and neuroendocrine markers. Three of the tumours in this subtype

had a neuroendocrine histology whilst the other 17 tumours in this subtype did not display histological features suggestive of a neuroendocrine origin. Overall survival after 5 years was highest for the luminal papilliary subtype, intermediate for the luminal and basal squamous subtypes and lowest for the luminal infiltrated and neuronal subtype (Robertson *et al.*, 2017).

Sjodahl *et al.* conducted hierarchical cluster analysis with microarray expression data and examined the expression of 28 proteins with immunohistochemistry in 307 MIBCs. This categorised tumours into the following subtypes: urothelial-like, genomically unstable, basal/SCC-like, mesenchymal-like, and small-cell/neuroendocrine-like. The urothelial-like and genomically unstable subtypes both exhibited expression of luminal markers. However, the urothelial-like subtype was distinct from the genomically unstable subtype as it exhibited higher expression of FGFR3, CCND1 and RB1 and lower expression of E2F3. The basal/SCC-like, mesenchymal-like, and small-cell/neuroendocrine-like subtypes exhibited lower expression of luminal markers. The basal/SCC-like subtype exhibited high expression of KRT5 and KRT14 and low expression of GATA3 and FOXA1 whereas the mesenchymal-like subtype exhibited high expression of the mesenchymal markers vimentin and ZEB2 and the small-cell/neuroendocrine-like subtype exhibited high expression of the neuroendocrine marker TUBB2B and the epithelial marker EpCAM (Sjödahl *et al.*, 2017).

Seiler *et al.* conducted expression profiling with 343 MIBC prior to these tumours being treated with neoadjuvant chemotherapy and developed a single-sample genomic subtyping classifier to categorize tumours as claudin-low, basal, luminal-infiltrated or luminal. 476 MIBC, which were not treated with neoadjuvant chemotherapy, from previously published datasets were assigned subtypes. This study found that patients with basal tumours had a poor prognosis when not given neoadjuvant chemotherapy but that the overall survival of patients in this subtype was improved when treated with neoadjuvant chemotherapy. Patients with luminal subtype tumours had a good prognosis whilst the luminal-infiltrated and claudin-low subtypes had a poor overall survival. Treatment with neoadjuvant chemotherapy had little effect on the prognosis of the luminal, luminal-infiltrated or claudin-low subtypes (Seiler *et al*., 2017).

Hedegaard *et al.* conducted RNA-seq analysis on a cohort of 460 NMIBCs and conducted consensus clustering with this expression data. This identified three subtypes which were named class 1-3 and a 117 gene classifier was developed to assign independent samples to a subtype/class. Hedegaard *et al.* suggested that

the luminal-like class 2 may represent a Tis pathway of progression whilst the basal-like class 3 tumours may represent a Ta pathway of progression. Class 1 and 2 tumours both exhibited high expression of uroplakins compared to class 3 tumours. However, class 1 tumours had high expression of genes associated with early cell cycle in contrast to class 2 tumours which exhibited high expression of genes associated with late cell cycle. Additionally, class 2 tumours exhibited higher expression of *KRT20* which is a luminal marker and associated with carcinoma *in situ*. The class 3 subtype did not exhibit high expression of early or late cell cycle genes. Low expression of uroplakins and high expression of the basal markers *KRT5* and *KRT15* was observed in class 3 tumours and some class 3 tumours exhibited high expression of *CD44*. High expression of *KRT14*, was observed in both class 2 and 3 tumours. Class 1 and 2 tumours exhibited a higher frequency of *FGFR3* mutations whilst class 3 tumours exhibited a higher frequency of *TP53* mutations. Tumours of a high stage and grade or with concomitant carcinoma in situ were more frequent in classes 2 and 3. Class 1 tumours had the highest rate progression-free survival followed by class 3 whilst class 2 tumours had the lowest. (Hedegaard *et al.*, 2016).

The different attempts to use gene expression profiling to classify bladder cancer have differed in the subtypes identified. However, there is a consensus that there are basal and luminal subtypes of bladder cancer and that tumours expressing basal markers have a worse prognosis than those expressing luminal markers.

1.2 Targeted therapy for cancer

1.2.1 Targeted therapies

Targeted therapies act against molecules specific to, or aberrantly expressed in, cancerous cells to induce cell death and reduce cell division. In contrast, traditional chemotherapy acts less specifically by targeting rapidly dividing cells whether or not they are cancerous. Targeted therapies can take the form of either monoclonal antibodies, small molecule inhibitors or gene therapy. Gene therapy, including oncolytic viral therapy, involves the delivery of DNA or RNA to target cells. The aim is to induce gene expression of an absent or defective gene in target cells, to increase expression of a gene which will induce cell death, by for example

stimulating an immune response, or to cause cell death due to viral infection. Delivery of the DNA is usually achieved with a viral vector (Fukuhara *et al.*, 2016; Naldini, 2015). This Introduction will focus on monoclonal antibody and small molecule inhibitor treatments as these therapies are most relevant to this project.

Many targeted therapies have been developed against RTKs, a class of proteins which are frequently activated in cancer. Upon ligand binding RTKs undergo a conformational change which results in oligomerisation. The oligomers then use ATP to autophosphorylate tyrosine residues in the RTK tyrosine kinase domain and to phosphorylate intracellular signalling molecules (Ullrich and Schlessinger, 1990). RTKs activate intracellular signalling pathways such as the MAP kinase and the PI3 kinase pathways. Small molecule inhibitors commonly have specificity for the ATP binding site of tyrosine kinases which enables them to competitively or non-competitively inhibit RTK activity and downstream signalling (Klein *et al.*, 2005). Monoclonal antibodies have been developed with specificity for RTKs. These monoclonal antibodies can induce cell death by a number of mechanisms including cell surface receptor agonist or antagonist activity, induction of phagocytosis and antibody-dependent cell-mediated cytotoxicity. Monoclonal antibodies and small molecule inhibitors specific for tyrosine kinases are now established treatments for cancer (Fabbro, 2015; Scott *et al.*, 2012). Examples of targeted agents which have been found to increase patient survival are detailed below.

The monoclonal antibody trastuzumab is specific for the human epidermal receptor 2 (ERBB2/HER2). Binding of trastuzumab to ERBB2 reduces downstream signalling through the PI3 and MAP kinase pathways and induces antibody-dependent cellular cytotoxicity (Vu and Claret, 2012). Trastuzumab increased the ten-year overall survival rate from 75.2 to 84% in women with primary, operable node positive or high-risk node negative, ERBB2-positive breast cancer without metastasis when used in conjunction with adjuvant chemotherapy (Perez *et al.*, 2014).

Hussain *et al.* examined the efficacy of treatment with trastuzumab, paclitaxel, carboplatin, and gemcitabine in patients with ERBB2-positive advanced urothelial carcinoma. Out of the cohort of 44 patients, there were 5 complete responses and 26 partial responses to treatment (Hussain *et al.*, 2007). Powles *et al.* conducted a phase III clinical trial in patients with EGFR- or ERBB2-positive metastatic urothelial carcinoma. The efficacy of maintenance treatment with lapatinib, an EGFR and ERBB2 small molecule inhibitor, following first-line

chemotherapy, was compared to treatment with a placebo. Lapatinib did not significantly increase progression-free survival or overall survival (Powles *et al.*, 2017).

The small molecule inhibitor erlotinib is a first-generation EGFR tyrosine kinase inhibitor (TKI). Erlotinib reversibly binds the adenosine triphosphate (ATP) binding site on the epidermal growth factor receptor (EGFR) intracellular domain. Erlotinib was the first EGFR TKI to be approved by the FDA, following a phase III clinical trial in patients with non-small cell lung cancer (NSCLC) which accounts for 80-85% of lung cancers. This trial found that erlotinib could prolong survival in these patients following the failure of one or two chemotherapy regimens (Gridelli *et al.*, 2010; Zhang, 2016).

Seront *et al.* assessed the efficacy of the mTOR inhibitor everolimus in patients whose urothelial carcinoma had progressed following treatment with platinum-based chemotherapy. A disease control rate of 27% was observed at 8 weeks (Seront *et al.*, 2012). Milowsky *et al.* assessed the efficacy of everolimus in patients with progressive metastatic urothelial carcinoma previously treated with chemotherapy in a phase II clinical trial. The primary endpoint of 2-month progression-free survival was not met (Milowsky *et al.*, 2013). However, a patient from this clinical trial, who achieved a durable and complete response to everolimus was examine by Iyer *et al.* with whole exome sequencing. This identified a E636fs mutation in *TSC1* (Iyer *et al.*, 2012). TSC1 acts in complex with TSC2 to regulate the GTPase activity of Rheb and therefore inhibit activation of the mTORC1 complex which contains mTOR (Huang and Manning, 2008). Iyer *et al.* examined the tumours of a further 13 patients who were enrolled in the same clinical trial with a targeted deep sequencing assay and identified that three other tumours had *TSC1* nonsense mutations. Two of the three patients whose tumours had a *TSC1* mutation had a minor response to everolimus, as did a patient who had a somatic TSC1 missense mutation of unknown consequence. Of the 9 patients whose tumours were identified to have wildtype TSC1, only one patient's disease did not progress (Iyer *et al.*, 2012).

FGFR TKIs have been assessed in clinical trials with bladder cancer patients. These are discussed in section 1.4.1.

1.2.2 Mechanisms of resistance to targeted therapies

Resistance to therapy can be classified as intrinsic, if the cancer does not show any response to treatment, or acquired where the cancer initially responds to treatment before resistance develops. Targeted agents typically have specificity for RTKs or intracellular signalling molecules which induce cell proliferation and survival by activating intracellular signalling pathways such as the PI3 kinase and MAP kinase pathways. Resistance to targeted agents frequently occurs via maintaining activation or re-activation of the intracellular signalling pathways vital for cell proliferation and survival. This can occur via the activation of an RTK not inhibited by the targeted agent or maintenance of signalling via the targeted RTK due to upregulation or mutation of the receptor. Alternatively, resistance to targeted agents can occur due to alterations in intracellular signalling molecules which induce intracellular pathway activation independent of upstream signalling. Examples of how resistance has arisen against a wide variety of targeted agents are detailed below.

The first generation EGFR small molecule TKIs erlotinib, gefitinib and icotinib, which are reversible ATP-competitive inhibitors, were developed to treat NSCLC (Zhang, 2016). The most common NSCLC EGFR mutations are exon 19 in-frame deletions and L858R point mutations. In Europe, mutant EGFR is found in approximately 15% of NSCLC. This subtype of NSCLC responds to first generation EGFR TKIs in more than 60% of cases (Midha *et al.*, 2015; Russo *et al.*, 2015). The T790M EGFR mutation was first detected in a patient with NSCLC. The mutation was absent in the patient's original biopsy specimen but present after the patient relapsed after treatment with gefitinib. This mutation introduces a methionine side chain, which impedes EGFR TKI binding to the ATP binding site of EGFR (Kobayashi *et al.*, 2005). Activation of the T790M mutation accounts for approximately 60% of cases of acquired resistance to first generation EGFR TKIs (Zhang, 2016). Second generation EGFR TKIs were developed to overcome resistance arising from the T790M mutation. These TKIs irreversibly inhibit EGFR by covalent bonding to the ATP binding site in the EGFR tyrosine kinase domain. However, patients treated with second generation EGFR TKIs suffer epithelium-based toxicities due to inhibition of wildtype EGFR, limiting the tolerated dose and clinical usage of these molecules (Huang and Fu, 2015; Zhang, 2016). Third generation TKIs, like second generation inhibitors, covalently bind EGFR. However, these have greater affinity for mutant EGFR receptors and therefore can be given to patients at an effective dose without inducing intolerable side effects (Hossam *et al.*, 2016). Clinical trials with a number of third generation EGFR TKIs have been

conducted or are in progress (Wang *et al.*, 2016). The third generation EGFR TKI osimertinib has been approved by the FDA and conditionally approved by the EMA for the treatment of advanced or metastatic NSCLC with the T790M EGFR mutation (Santarpia *et al.*, 2017). Other EGFR mutations that induce resistance to EGFR TKIs include D761Y, L747S and T854A, which are located in the tyrosine kinase domain. The mechanisms by which these mutations induce resistance are unknown (Balak *et al.*, 2006; Bean *et al.*, 2008; Costa *et al.*, 2007).

Overexpression or mutation of an alternative RTK, or overexpression of a receptor ligand, are mechanisms by which resistance to EGFR-targeted agents can arise. These mechanisms enable the activation of growth and survival pathways such as MAP kinase and PI3 kinase. Signalling via other EGFR family members, MET, insulin-like growth factor 1 receptor (IGF1R), vascular endothelial growth factor receptors (VEGFRs), FGFRs and platelet derived growth factor receptor (PDGFR) have all been implicated in resistance to inhibition of EGFR (Akhavan *et al.*, 2013; Azuma *et al.*, 2014; Bianco *et al.*, 2008; Engelman *et al.*, 2007; Nakata *et al.*, 2014; Peled *et al.*, 2013). For example, amplification of *ERBB2* and downstream re-activation of the MAP kinase pathway has been identified as a mechanism of resistance to cetuximab in derivatives of colorectal cancer and NSCLC cell lines which had undergone long-term culture in cetuximab (Yonesaka *et al.*, 2011). *ERBB2* amplification has been identified as a mechanism of both intrinsic and acquired resistance to treatment with anti-EGFR monoclonal antibodies in colorectal cancer patients (Martin *et al.*, 2013; Yonesaka *et al.*, 2011). Sartore-Bianchi *et al.* conducted a phase II clinical trial testing the combination of trastuzumab and lapatinib in ERBB2-positive metastatic colorectal cancer previously treated with cetuximab or panitumumab. An objective response was observed in 8 out of 27 patients (Sartore-Bianchi *et al.*, 2016).

Mutant *KRAS* is found in lung adenocarcinomas with wildtype EGFR, most commonly mutated at G12, G13 or Q61, which reduce GTPase activity and permanently activate RAS. Constitutively active KRAS induces MAP kinase pathway signalling irrespective of RTK activation. Patients with mutant *KRAS* have a worse response rate to EGFR TKIs (Pan *et al.*, 2016; Pao *et al.*, 2005). Colorectal cancer is treated with the anti-EGFR monoclonal antibodies cetuximab and panitumumab. Approximately 50% of metastatic colorectal tumours have mutations in *KRAS* or *NRAS,* most commonly at residues G12, G13, Q61 or A146 (Boleij *et al.*, 2016). These patients do not benefit from treatment with anti-EGFR monoclonal antibodies (Amado *et al.*, 2008; Karapetis *et al.*, 2008). This result suggests that the anti-tumour effect of anti-EGFR monoclonal antibodies is mediated by inhibition of

the MAP kinase pathway downstream of EGFR and that the efficacy of EGFR-targeted agents can be limited by MAP kinase reactivation.

Another member of the MAP kinase pathway which is frequently mutated in cancer is BRAF, a kinase activated by RAS. Activating *BRAF* mutations are found in cancers including melanoma, papillary thyroid carcinoma, serous micropapillary ovarian carcinoma, colorectal and NSCLC (Niault and Baccarini, 2010). The most common activating *BRAF* mutation is V600E which accounts for 90% of *BRAF* mutations in cancer (Obaid *et al.*, 2017). Approximately 6% of colorectal tumours have mutant *BRAF*, most commonly V600E which is located in the kinase domain (Mao *et al.*, 2015). V600E mutant BRAF is not dependent on RAS-mediated RAF dimerization for activation (Haling *et al.*). Metastatic colorectal cancers treated with cetuximab and chemotherapy that have mutant *BRAF* have a significantly worse prognosis than those with wildtype *BRAF* (De Roock *et al.*, 2010). Additionally, colorectal cancers exhibit intrinsic resistance to BRAF inhibition due to activation of EGFR (Corcoran *et al.*, 2012; Prahallad *et al.*, 2012). Examination of the efficacy of the combination of BRAF and EGFR inhibition or BRAF, MEK and EGFR inhibition in patients with BRAF-mutant advanced colorectal cancer has been examined in phase I/II clinical trials and found to have acceptable tolerability and clinical activity (Atreya *et al.*, 2015; Schellens *et al.*, 2015; Yaeger *et al.*, 2015). *BRAF* activating mutations are also reported in NSCLC patients with acquired resistance to EGFR TKIs (Ohashi *et al.*, 2012).

Clinical trials have found the BRAF TKIs vemurafenib and dabrafenib to be effective in the treatment of metastatic melanoma (Chapman *et al.*, 2011; Hauschild *et al.*). Melanomas have been found to activate the MAP kinase pathway to overcome treatment with BRAF TKIs. Mutations in *NRAS*, *KRAS* and *MEK1* as well as amplification and alternative splicing of *BRAF* are found in melanoma patients who developed resistance to BRAF TKI monotherapy (Shi *et al.*, 2014). The RTKs EGFR, IGF1R and PDGFRβ have been reported to be activated as mechanisms of acquired resistance to BRAF inhibition (Girotti *et al.*, 2013; Nazarian *et al.*, 2010; Villanueva *et al.*, 2010). Treatment of melanomas with the MEK inhibitors cobimetinib and trametinib used in combination with BRAF TKIs has been found to be more effective than BRAF TKI monotherapy. The combinatorial treatment hinders the emergence of resistance via re-activation of the MAP kinase pathway and is less toxic (Grimaldi *et al.*, 2017). The combination of BRAF and MEK inhibition is also effective in some *BRAF*-mutant metastatic colorectal cancer patients (Corcoran *et al.*, 2015).

Activation of the PI3 kinase pathway can also lead to resistance to BRAF inhibition. Mutations in the PI3 kinase pathway genes *AKT1*, *AKT3*, *PIK3CA*, *PIK3CG, PIK3R2*, *PTEN*, *PHLPP1* have been reported in BRAF TKI-resistant melanoma (Shi *et al.*, 2014). Activation of ERBB3 and AKT has been reported as a mechanism of resistance to BRAF or MEK inhibition in melanoma cell lines (Fattore *et al.*, 2013).

Monoclonal antibodies and TKIs have been developed that are specific to ERBB2. Aberrant activation of ERBB2 signalling, via overexpression, amplification or, less frequently, mutation is found in cancers including breast, gastric, lung, bladder, colon, ovary, endometrium and head and neck. The monoclonal antibody trastuzumab is used in the treatment of ERBB2-overexpressing breast, gastric and gastroesophageal cancer (Iqbal and Iqbal, 2014). In order to determine the suitability of patients for treatment with trastuzumab, ERBB2 overexpression or amplification is determined by immunohistochemistry or *in situ* hybridisation (Bartley *et al.*, 2016; Wolff *et al.*, 2013).

One mechanism of resistance to trastuzumab is the synthesis of truncated ERBB2, termed p95HER2, which lacks the extracellular portion of the protein due to cleavage of the extracellular domain of full length ERBB2 by matrix metalloproteases (Codony-Servat *et al.*, 1999). Alternatively, initiation of translation can occur from methionine residues located close to the ERBB2 transmembrane domain at codons 611 and 678 of full-length ERBB2, generating a C-terminal ERBB2 fragment (Anido *et al.*, 2006). p95HER2 proteins can be classified by their size: either 100 to 115kDa or 95 to 100kDa. 100-115kDa fragments are constitutively active homodimers due to intermolecular disulphide bonds formed between cysteine residues in the short extracellular portion of this protein. 95-100kDa sized proteins lack these cysteine residues and most likely form dimers due to homotypic affinity between the ERBB2 transmembrane and intracellular domains (Arribas *et al.*, 2011). The trastuzumab binding site is in the extracellular domain of ERBB2 and therefore this antibody does not bind p95HER2. It has been demonstrated that inducing expression of p95HER2 in breast cancer cell lines and xenograft models results in resistance to trastuzumab. However, p95HER2 expression did not induce resistance to lapatinib as lapatinib binds the ATP-binding site in the kinase domain of EGFR and ERBB2. (Scaltriti *et al.*, 2007). Lapatinib has since been shown to inhibit tumour growth and ERBB2 signalling in patients whose tumours express p95HER2 (Han *et al.*, 2012; Scaltriti *et al.*, 2010).

Heterodimerisation of IGF1R with ERBB2 has been described as a mechanism of resistance in the breast cancer cell line SK-BR-3 which became trastuzumab resistant following long-term culture in trastuzumab. Inhibition of IGF1R increased sensitivity to trastuzumab by reducing IGF1R and ERBB2 heterodimerization (Nahta *et al.*, 2005). Patients whose breast tumours express IGF1R at the cell membrane, as opposed to those with tumours with mainly cytoplasmic IGF1R expression, have been shown to be significantly less likely to respond to trastuzumab and vinorelbine (Harris *et al.*, 2007).

Whilst *ERBB2* mutations are rare in cancer, they have been reported in the ERBB2 tyrosine kinase domain in lung, breast, colorectal, head and neck, bladder and gastric cancer (Bekaii-Saab *et al.*, 2006; Bellmunt *et al.*, 2015; Cohen *et al.*, 2005; Kubo *et al.*, 2009; Lee *et al.*, 2006; Stephens *et al.*, 2004; Zito *et al.*, 2008). *ERBB2* mutations are most commonly located in the extracellular domain or kinase domain. *ERBB2* mutations have been reported in breast cancers including T798M which was observed to induce resistance to lapatinib, an EGFR- and ERBB2-targeted TKI, when expressed in breast cancer cell lines. The T798M ERBB2 mutation is analogous to the EGFR T790M mutation in the EGFR kinase domain ATP binding site (Bose *et al.*, 2013; Rexer *et al.*, 2013). Lapatinib resistance could be overcome by treatment with the irreversible EGFR and ERBB2 TKI neratinib. In July 2017, neratinib was approved by the FDA for early stage breast cancer with amplification or overexpression of *ERBB2* previously treated with trastuzumab (Deeks, 2017).

Studies of breast cancer cell lines have found low expression of *PTEN* and presence of *PIK3CA* mutations to correlate with resistance to trastuzumab (Kataoka *et al.*, 2010; O'Brien *et al.*, 2010). Rexer *et al.* observed that the breast cancer cell line BT474 acquired a *PI3KCA* helical domain mutation, E542K, following long-term culture in lapatinib. This mutation enabled the resistant derivative to maintain activation of the PI3 kinase pathway in the presence of lapatinib, as PIK3CA is downstream of ERBB2. In contrast, lapatinib inhibited the PI3 kinase pathway in parental BT474 (Rexer *et al.*, 2014). Rexer *et al.* also observed that treatment with the PI3K inhibitor BKM120 in addition to trastuzumab and lapatinib induced tumour regression in an *ERBB2* amplified, mutant *PIK3CA* mouse xenograft model of breast cancer whereas, treatment with trastuzumab and lapatinib without BKM120 did not (Rexer *et al.*, 2014). The link between PI3 kinase pathway alterations and trastuzumab resistance has been examined in breast cancer patients. Further research is required to elucidate the effect of *PIK3CA* mutations and PTEN loss and the response to trastuzumab (Razis *et al.*, 2011; Wang *et al.*, 2013b). *In vitro*

work established that the combination of an mTOR or AKT small molecule inhibitor and trastuzumab could overcome resistance to trastuzumab in breast cancer cell line and xenograft models (Lu *et al.*, 2007). The efficacy and safety of adding everolimus, an mTOR inhibitor, to the combination of trastuzumab and the chemotherapeutic agent vinorelbine was tested in a phase III clinical trial in patients with ERBB2-positive, trastuzumab-resistant breast cancer. It was found that everolimus increased the progression-free survival of patients although this additional treatment also increased adverse effects (André *et al.*, 2014).

The Philadelphia chromosome is found in greater than 90% of cases of chronic myeloid leukaemia (CML) and 10-15% of cases of adult acute lymphoblastic leukaemia (ALL). This genetic alteration is formed by the Philadelphia chromosomal translocation: t(9;22)(q34;q11), and results in the production of BCR-ABL fusion protein which has constitutive activity, unlike ABL kinase (Salesse and Verfaillie, 2002; Wong and Witte, 2004). Treatment of Philadelphia chromosome-positive CML with imatinib, an inhibitor of BCR-ABL, improves patient survival (Hochhaus *et al.*, 2017; O'Brien *et al.*, 2003). However, resistance to imatinib is common, with 60-95% of chronic stage CML patients becoming unresponsive to the TKI within 12 to 24 months. Mutations in *BCR-ABL* are a mechanism of intrinsic and acquired resistance; the kinase domain of the protein is a mutation hotspot. The most common BCR-ABL mutations to arise following treatment with imatinib are T315I, G250E, M244V, M351T, and E255K/V (Soverini *et al.*, 2014). The second generation ABL TKIs nilotinib, dasatinib and bosutinib have greater potency than imatinib and were designed to overcome imatinib resistance mediated by point mutation in *BCR-ABL* (Chen and Chen, 2015; Weisberg *et al.*, 2006). Following clinical trials which demonstrated the superiority of nilotinib and dasatinib over imatinib, these TKIs were approved by the FDA and EMA as first line treatments for use in Philadelphia chromosome-positive CML and for treatment of Philadelphia chromosome-positive CML resistant to or intolerant to prior therapy (Jabbour *et al.*, 2015). However, treatment with second generation ABL TKIs does not overcome the T315I *BCR-ABL* mutation (Hochhaus *et al.*, 2007; Kantarjian *et al.*, 2007). This mutation prevents the formation of a hydrogen bond between the oxygen atom in threonine 315 and an imatinib amino group, hindering the binding of imatinib to BCR-ABL (Gorre *et al.*, 2001; Schindler *et al.*, 2000). The TKI ponatinib, which inhibits a number of kinases including ABL, VEGFRs and FGFRs, was developed to avoid the steric clash with the bulky isoleucine residue and therefore inhibits T315I BCR-ABL in addition to wildtype ABL. Ponatinib has been approved by the EMA and FDA for Philadelphia chromosome positive CML

harbouring the T315I mutation and for the treatment of Philadelphia positive CML resistant to or intolerant to other TKIs (Jabbour *et al.*, 2015). However, resistance to ponatinib has been found to arise via further mutation of residue 315: I351M, or via compound *BCR-ABL* mutations including E255V/T315I (Zabriskie *et al.*, 2014). A less common mechanism of resistance to imatinib is an increase in *BCR-ABL* copy number via amplification of *BCR-ABL* or gain of an additional Philadelphia chromosome. The additional copies of *BCR-ABL* induce increased protein expression and activation of BCR-ABL (Hochhaus *et al.*, 2002; le Coutre *et al.*, 2000).

Studies using cancer cell lines have shown that cells can enter a drug-tolerant or resistant state mediated by gene expression changes and epigenetic resistance mechanisms with an apparent lack of genetic alteration. Sharma *et al.* generated derivatives of the NSCLC line PC9 tolerant to EGFR TKIs by culturing parental PC9 in gefitinib for 9 days. These cells mediated their resistance by activation of IGF1R and this drug tolerant state was dependent upon the activation of the histone demethylase KDM5A (Sharma *et al.*, 2010). Hou *et al.* reported that KDM5A protein and RNA expression was increased in the breast cancer lines SUM149 and SUM102 following 6 and 9 days culture in erlotinib. They conducted stable knockdown of KDM5A in the breast cancer cell lines SUM149 and HCC1937. It was observed that stable *KDM5A* knockdown reduced the number of drug tolerant SUM149 and HCC1937 cells following 30-day culture in erlotinib (Hou *et al.*, 2012). Gale *et al.* developed the KDM5A inhibitor YUKA1. It was observed that treatment with YUKA1 reduced the formation of gefitinib-resistant colonies during the long-term culture of PC-9 with gefitinib. YUKA1 also reduced the formation of trastuzumab-resistant colonies during the long-term culture of the breast cancer cell line BT474 with trastuzumab (Gale *et al.*, 2016).

Hata *et al.* cultured greater than 1200 pools of approximately 5000 parental PC9 cells in gefitinib for 2 weeks. Some pools of PC9 cells produced resistant derivatives with the EGFR T790M mutation and some PC9 pools produced drug tolerant derivatives which did not have this gatekeeper mutation, similar to the PC9 derivatives described by Sharma *et al.* (Hata *et al.*, 2016; Sharma *et al.*, 2010). Repetition of this procedure with the third generation EGFR TKI WZ4002, which effectively inhibits EGFR T790M, yielded only the drug tolerant derivatives which lacked the T790M mutation. Further culture of the drug tolerant derivatives in gefitinib led to acquisition of the EGFR T790M mutation. However, these cells retained resistance to WZ4002 induced apoptosis. This study indicates that further

resistance mechanisms can arise from cancer cells persisting in a drug tolerant state, highlighting the importance of targeting drug tolerant cells (Hata *et al.*, 2016).

Ramires *et al.* expanded a single clone of PC9 for approximately 20 doublings. This population of cells was then treated with erlotinib for approximately 2 months at which point the emergent colonies of drug tolerant cells were isolated and cultured in erlotinib for a further 6-8 months. In total, this process yielded 17 different resistant colonies. These colonies all retained greater resistance to erlotinib than PC9 following culture without erlotinib for 40 weeks. They then conducted a drug screen, testing the sensitivity of the resistant cells to 560 compounds in combination with erlotinib. Exome sequencing data was then used to attempt to identify a genetic basis for the drug sensitivities identified in the drug screen. Despite the fact that the resistant cells were derived from a single clone, the cells exhibited differential sensitivity to drugs in the screen. Some colonies exhibited broad resistance to the drugs tested. One resistant clone exhibited sensitivity to MET inhibitors and was found to contain a MET amplification. Some exhibited sensitivity to EGFR inhibitors capable of inhibiting EGFR T790M, and were observed to have acquired this mutation. Other colonies were sensitive to MEK inhibitors and were observed to have acquired *NRAS* or *RAF1* mutations (Ramirez *et al.*, 2016). This study demonstrates that several mechanisms of resistance can emerge from a single clone in a drug tolerant state.

Gastrointestinal stromal tumours (GISTs) often have activating mutations in the RTK encoding genes *KIT* and *PDGFRA* (Heinrich *et al.*, 2003; Hirota *et al.*, 1998). Mühlenberg *et al.* observed that the combination of the non-selective histone deacetylase inhibitor vorinostat and imatinib was additive in KIT-positive GIST cell lines. Vorinostat was shown to reduce KIT mRNA expression and increase acetylation of HSP90, a KIT chaperone, inducing KIT degradation (Muhlenberg *et al.*, 2009). Bauer *et al.* conducted a phase I clinical trial assessing the efficacy of the combination of imatinib and the non-selective histone deacetylase inhibitor panobinostat in overcoming resistance in patients with GISTs refractory to the combination of imatinib and the multitargeted TKI sunitinib. One out of the 11 patients showed a partial response, 7 had stable disease and 3 patients had progressive disease (Bauer *et al.*, 2014).

15-20% of colorectal cancer patients have global high CpG island methylation phenotype which induces inactivation of tumour suppressors such as the mismatch repair gene *MLH1* (Mojarad *et al.*, 2013). Garrido-Laguna *et al.* conducted a phase I/II clinical in treated metastatic colorectal cancer patients with

wildtype *KRAS* and a minimum of 2 prior therapies. All but one patient had previously been treated with cetuximab. 20 patients were treated with combination of decitabine, a hypomethylating agent, and panitumumab. A partial response was observed in 2 patients, stable disease was observed in 11 patients and progressive disease was observed in 7 patients (Garrido-Laguna *et al.*, 2013).

Non-cancerous cells in the tumour microenvironment have been reported to affect tumour drug resistance. Paulsson *et al*. used immunohistochemistry to examine the stromal expression of PDGFRβ, a regulator of fibroblasts, in 360 tumours from premenopausal, and 528 tumours from postmenopausal, breast cancer patients treated with and without tamoxifen, a selective oestrogen receptor modulator. Kaplan-Meier analysis showed that pre- and postmenopausal patients with low expression of PDGFRβ had a significant increase in recurrence-free survival when treated with tamoxifen. In contrast, a significant treatment benefit was not observed in patients with high stromal PDGFRβ expression. This study did not identify a causal link between high stromal PDGFRβ expression and tamoxifen resistance (Paulsson *et al*., 2017). Park *et al*. reported that depletion of CD8+ cytotoxic lymphocytes with an anti-CD8α- antibody induced rapid tumour relapse in BALB/c mice bearing tumours established from the neu-positive mammary carcinoma cell line TUBO treated with an anti-neu antibody. This suggests a T-cell dependent resistance mechanism (Park *et al*., 2010).

1.3 Altered FGFR signalling in cancer

1.3.1 Structure of FGFRs

The FGFR family of transmembrane glycoproteins (FGFRs1-4) bind to and are activated by 18 FGFs and 4 FGF homologous factors that have differing affinities for each of the FGFRs and their splice variants. The different FGFs signal through FGFR in a paracrine or endocrine manner by forming a complex of 2 FGFs, 2 FGFRs and 2 heparan sulphate molecules (Ornitz *et al.*, 1996; Zhang *et al.*, 2006). Fibroblast growth factor receptor like-1 (FGFRL1), also known as FGFR5, is the most recently identified member of the FGFR family (Sleeman *et al.*, 2001). It has been suggested that FGFRL1 is a decoy receptor (Steinberg *et al.*, 2010; Trueb *et al.*, 2003) although more recent evidence indicates that it may activate the MAP kinase pathway independently of ligand (Silva *et al.*, 2013). Upon ligand binding,

FGFRs1-4 form homodimers, and intracellular autophosphorylation can lead to signalling through the MAP kinase, PI3 kinase, PLCγ and JAK/STAT pathways (Böttcher and Niehrs, 2005; Klint and Claesson-Welsh, 1999). From the extracellular N-terminus through to the C-terminus FGFR1-4 contain the following: a signal peptide, immunoglobulin (Ig)-like domain I, an acid box consisting of a sequence of glutamic and aspartic acids, the heparan sulphate binding domain, Ig-like domain II, Ig-like domain III, a transmembrane domain, a juxtamembrane linker, a split tyrosine kinase domain and an inhibitory carboxy-terminal tail (Fig. 1.1)(Belov and Mohammadi, 2013). The Ig-like domains I-III are named D1-3 with D1 at the N-terminus and D3 proximal to the membrane. D1 and the acid box are autoinhibitory whilst D2 and D3 bind FGFs and therefore are responsible for specificity of each receptor. FGFR1 can be alternatively spliced to produce FGFR1α, which contains Ig-like domains I-III or FGFR1β which contains only Ig-like domains II and III (Johnson *et al.*, 1991). FGFR1α exhibits greater affinity for FGF1 and heparan than FGFR1β (Shi *et al.*, 1993; Wang *et al.*, 1995). FGFR1-3 can undergo alternative splicing expressing either exon 8 or 9, producing IIIb or IIIc isoforms respectively. Exons 8 and 9 encode the C-terminus of D3 and therefore this alternative splicing event affects ligand specificity. For example, FGF1 activates all FGFRs whereas FGF2 preferentially activates the FGFR IIIc isoforms. Expression of FGFR IIIb isoforms is found in epithelial tissue, in contrast to IIIc isoforms which are expressed in mesenchymal tissue (di Martino *et al.*, 2012; Olsen *et al.*, 2004; Ornitz *et al.*, 1996; Zhang *et al.*, 2006). FGFR3 IIIb contains the following tyrosine phosphorylation sites: Y579, Y649/650, Y726, Y762 and Y772 (Fig. 1.1). Phosphorylation of residue Y726 is important in the activation of the MAP kinase, PI3 kinase, STAT1 and STAT3 pathways. Phosphorylation of Y649/650, which are situated in the protein's activation loop, is required for kinase activity. Phosphorylation of Y762 allows binding of PLCγ and the PI3 kinase p85 subunit and may induce greater phosphorylation of STAT1 and STAT3. Y772 inhibits activation of the PI3 kinase pathway (Hart *et al.*, 2001). Pathway activation downstream of FGFR3 is summarised in Fig. 1.2.

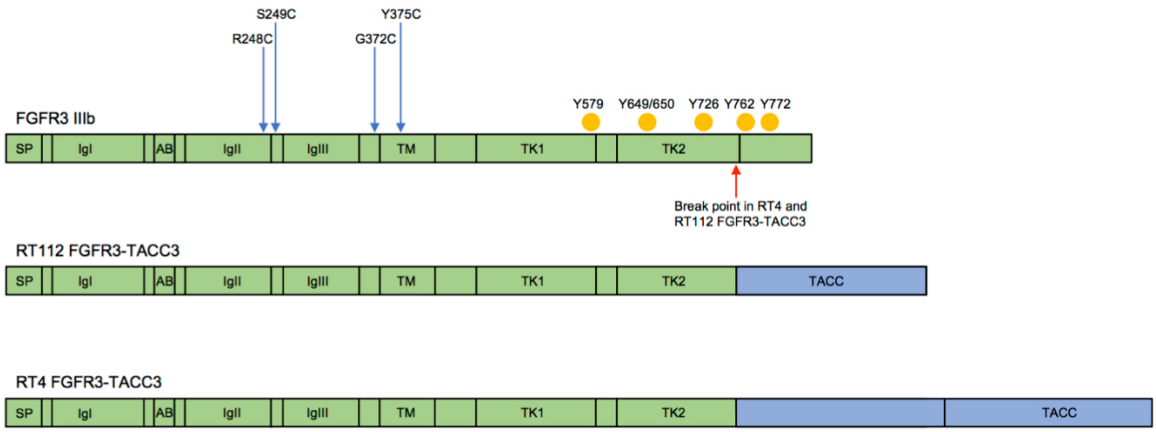

Figure 1.2 Protein structure of FGFR3 IIIb (green) and the FGFR3-TACC3 (blue) fusion proteins found in RT112 and RT4. Yellow spots highlight the location of FGFR3 phosphorylation sites. The red arrow indicates the breakpoint in RT112 and RT4 FGFR3-TACC3. Blue arrows indicate the most common sites of FGFR3 mutation in bladder cancer. SP: signal peptide, IgI-III immunoglobulin like domains, AB: acid box, TM: transmembrane domain, TK1 and TK2: tyrosine kinase domain, TACC: Transforming acid coiled-coil. Image adapted from di Martino *et al.*, 2016.

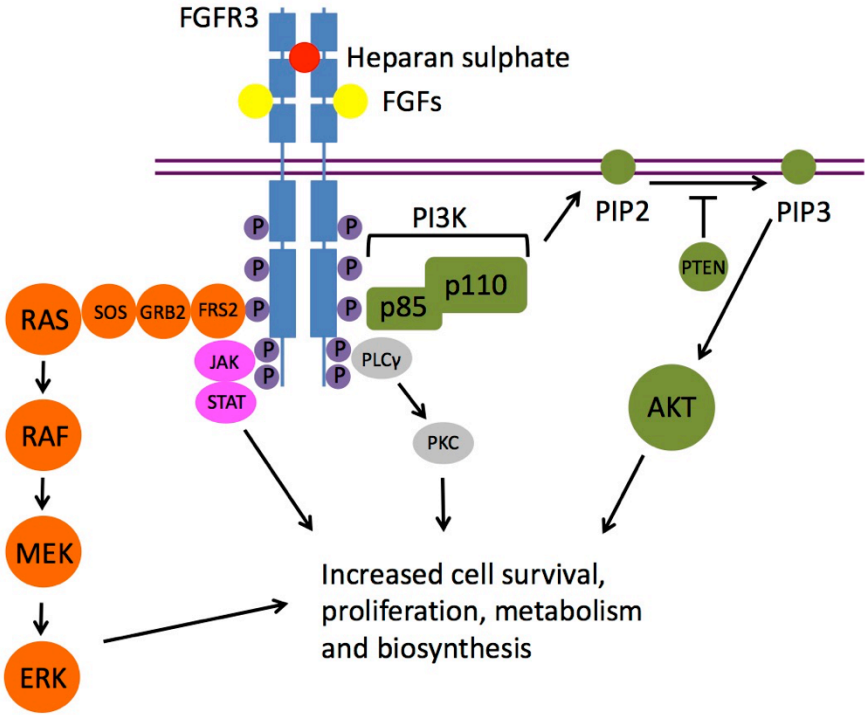

Figure 1.3 Signalling pathways activated by FGFR3. Orange denotes the MAP kinase pathway, magenta: the JAK/STAT pathway, grey: the PLCγ pathway and green: the PI3 kinase pathway. Blue denotes the FGFR3 homodimer, red: heparan sulphate and yellow: FGFs. P indicates the FGFR3 phosphorylation sites. Image adapted from di Martino *et al.*, 2016.

1.3.2 FGFR mutation and overexpression

FGFR signalling is activated in many different cancers: some examples are summarised below.

Moelans *et al.* observed amplification of *FGFR1* in 17% of 104 invasive breast cancers examined with multiplex ligation-dependent probe amplification (Moelans *et al.*, 2010). Turner *et al.* interrogated whole genome gene expression data from 295 invasive breast cancers, examining overexpression of genes located in the 8p11-12 amplicon, which contains *FGFR1*. It was observed that amplification of *FGFR1* was associated with the luminal B breast cancer subtype which has a poor prognosis. 16-27% of luminal B subtype breast cancers had *FGFR1* amplification (Turner *et al.*, 2010). Hiest *et al.* determined that 16% of a cohort of squamous NSCLCs had amplification of *FGFR1* using FISH (Heist *et al.*). Theelen *et al.* conducted immunohistochemistry on 653 NSCLC tumours and observed high protein expression of FGFR1 in 10.6% of samples (Theelen *et al.*, 2016).

Amplification and mutation of *FGFR1* are uncommon events in bladder cancer. Fischbach *et al.* identified *FGFR1* amplification in 2 out of 122 bladder cancers of a range of stages and grades with FISH (Fischbach *et al.*, 2015). Ross *et al.* conducted NGS targeting the exons of 182 cancer related genes and the introns of 14 genes often rearranged in cancer on a panel of 35 stage IV, predominantly high grade urothelial carcinomas. Three tumours had FGFR1 gene amplification, one patient had a T141R *FGFR1* mutation and one tumour had a FGFR1-NTM fusion (Ross *et al.*, 2014). Tomlinson *et al.* examined expression of *FGFR1* in 27 bladder cell lines and 73 bladder tumours with quantitative real time PCR (qRT-PCR) and observed that *FGFR1* mRNA expression was increased in the majority of bladder cancer cell lines and tumours compared to normal human urothelial cells. Knockdown of FGFR1 and treatment with the FGFR TKI PD173074 (PD) identified the bladder cancer cell line JMSU1 as dependent upon FGFR1 expression for survival (Tomlinson *et al.*, 2009). Tomlinson *et al.* examined expression of *FGFR1α* and *FGFR1β* with isoform specific qRT-PCR in 37 bladder cancer cell lines and 50 bladder tumours and observed that the majority of bladder cancer cell lines and tumours had undergone a *FGFR1α* to *FGFR1β* isoform switch. A higher ratio of *FGFR1β* to *FGFR1α* expression was associated with a higher stage and grade in tumours. Low concentrations of FGF1 were found to activate the MAP kinase pathway and cell proliferation to a greater extent in immortalized normal human urothelial cells transduced to express FGFR1α compared to cells transduced to express FGFR1β (Tomlinson and Knowles, 2010). FGFR1

expression has been associated with a mesenchymal phenotype in bladder cancer cell lines in contrast to expression of FGFR3 which has been associated with an epithelial phenotype (Cheng *et al.*, 2013).

Activating FGFR2 mutations are found in approximately 10% of endometrial cancers. The most common is S252W, which increases FGFR2 binding affinity for several FGFs (Helsten *et al.*, 2016; Pollock *et al.*, 2007). Theelen *et al.* observed high protein expression of FGFR2 in 12.9% of samples of the 653 NSCLC tumours examined with immunohistochemistry. Diez de Medina *et al.* examined *FGFR2* mRNA expression in 54 urothelial carcinomas of a variety of stages and grades and observed FGFR2 expression to be increased in 2 tumours and 18 tumours expressed FGFR2 below 30% of the level observed in normal urothelium. In MIBCs loss of FGFR2 expression correlated with a poor prognosis. Therefore, FGFR2 may be tumour suppressive in urothelial carcinoma (Diez de Medina *et al.,* 1997).

In multiple myeloma, about 40% of patients have a t(4:14) translocation and approximately 70% of tumours with this translocation overexpress wildtype FGFR3 due to the juxtaposition of *FGFR3* with *IGH* gene regulatory sequences (Kalff and Spencer, 2012). FGFR3 mutations are found at a low frequency in multiple myeloma, colorectal cancer, and cervical carcinoma (Cappellen *et al.*, 1999; Chesi *et al.*, 1997; Jang *et al.*, 2001). FGFR3 mutations are found at a high frequency in seborrheic keratoses (Hafner *et al.*, 2010; Hafner *et al.*, 2006)

The prevalence of *FGFR3* mutation and overexpression in NMIBC and MIBC is discussed in section 1.1.2. The most common *FGFR3* mutations in bladder cancer are S249C, Y375C, R248C and G372C (Fig. 1.1). All these mutations introduce a cysteine in or close to D2 or the transmembrane domain of the receptor, inducing the formation of intermolecular disulphide bonds and constitutive phosphorylation and activation of FGFR3 (Bernard-Pierrot *et al.*, 2006). K650E/M/Q/T FGFR3 kinase domain mutations are found in less than 1% of urothelial carcinomas and stabilise the kinase in its active state (Huang *et al.*, 2013). *FGFR3* mutations are normally mutually exclusive with *RAS* mutations in bladder cancer, suggesting that mutations in these genes perform an overlapping function (Jebar *et al.*, 2005).

Altered expression of FGFR4 has not been described in urothelial carcinoma (di Martino *et al.*, 2016). *FGFR4* kinase domain mutations are found in approximately 8% of rhabdomyosarcomas (Taylor *et al.*, 2009).

1.3.3 FGFR Fusion Proteins

The first FGFR fusion protein to be identified was FGFR3-TACC3 in glioblastoma multiforme (Singh *et al.*, 2012). FGFR1-TACC1 or FGFR3-TACC3 fusions are found in approximately 3% of glioblastoma multiforme (Singh *et al.*, 2012). FGFR fusion protein transcripts have been detected in bladder, prostate, oral and breast cancer as well as others (Wu *et al.*, 2013).

FGFR3 fusion proteins were first observed in bladder cancer by Williams *et al.* It was observed that the bladder cancer cell lines RT112, RT4 and SW780 express FGFR3 fusion proteins of a higher molecular weight than wildtype FGFR3 in addition to wildtype FGFR3 (Williams *et al.*, 2013). RT112 expresses an FGFR3-transforming acid coiled coil 3 (TACC3) fusion containing residues 1-760 (exons 1-18 of IIIb isoform) of FGFR3 and TACC3 residues 649-838. RT4 also expresses an FGFR3-TACC3 fusion containing residues 1-760 (IIIb isoform) of FGFR3, but this fusion contains TACC3 residues 433-638 (Fig 1.1) (Williams *et al.*, 2013). TACC3 forms a complex with ch-TOG and clathrin which aids the formation of inter-microtubule bridges, stabilising kinetochore fibres during mitosis (Booth *et al.*, 2011; Peset and Vernos, 2008). These FGFR3-TACC3 fusions are due to a rearrangement of the 4p16.3 region containing both FGFR3 and TACC3. SW780 expresses an FGFR3-BAI1-associated protein 2-like 1 (BAIAP2L1) fusion with residues 1-760 (IIIb isoform) of FGFR3 and BAIAP2L1 residues 18-522 as a result of a reciprocal translocation between chromosome 4 and 7 (Williams *et al.*, 2013). BAIAP2L1, also called IRTKS (insulin receptor tyrosine kinase substrate), regulates the actin cytoskeleton (Millard *et al.*, 2007).

FGFR3 exon 19 is not encoded in the *FGFR3-TACC3* fusion. FGFR3 exon 19 contains a PLCγ binding site, Y762, and a site involved in the negative regulation of the PI3 kinase pathway, Y772 (Hart *et al.*, 2001). As anticipated, when expressed in immortalized normal human urothelial cells, the FGFR3 fusion proteins did not induce phosphorylation of PLCγ but did induce ERK phosphorylation (Williams *et al.*, 2013). Williams *et al.* considered the possibility that the FGFR3-TACC3 fusion proteins may possess aberrant activation compared to wildtype FGFR3 due to the loss of FGFR3 exon 19. The fusion proteins induced anchorage-independent growth and a more spindle-like morphology when ectopically expressed in the mouse embryonic fibroblast cell line NIH3T3. This is in contrast to the result of ectopic expression of a truncated FGFR3 with a stop codon at the end of exon 18 to prevent expression of C-terminal exon 19. This did not induce a morphological change and induced anchorage-independent growth to a lesser extent. This suggests that the fusion partner rather than simply loss of the

FGFR3 terminal exon is important for the oncogenic potential of the fusion proteins (Williams *et al.*, 2013). TACC3 is thought to regulate microtubule stability via the formation of a complex with ch-TOG and clathrin (Ding *et al.*, 2017). The FGFR3-TACC3 fusion contains the TACC3 TACC domain which mediates dimerization (Guo *et al.*, 2015; Simpson *et al.*, 2004). The inclusion of the TACC domain in FGFR3-TACC3 may mediate homodimerization of the fusion protein, inducing activation of the tyrosine kinase domain. Compared to wildtype FGFR3, FGFR3-TACC3 is reported to have increased total kinase activity, additional phosphorylation sites and an increase in FGF independent activation of the MAPK pathway (Nelson *et al.*, 2016).

Sequencing of 126 urothelial tumours identified the following gene fusions: one *FGFR1-NTM*, four *FGFR3-TACC3*, one *FGFR3-JAKMIP1* and one *FGFR3-TNIP2*. Information on the stage and grade of tumours was not provided in this study (Helsten *et al.*, 2016). Guo *et al.* identified two *FGFR3-TACC3* fusion events in a panel of 42 urothelial carcinomas of a variety of stages and grades with RNA-Seq (Guo *et al.*, 2013). One FGFR3-TACC3 fusion event was present in a superficial tumour and one was present in an invasive tumour (Guo *et al.*, 2013). Robertson *et al.* examined 412 MIBCs with RNA-Seq and identified that FGFR3-TACC3 fusions were present in 10 (2%). Pietzak *et al.* identified that of the 105 NMIBCs examined with targeted exon sequencing, FGFR3 fusion events occurred in 4 (4%) (Pietzak *et al.*, 2017). These studies show that FGFR3 fusion events are present at a low frequency in both NMIBC and MIBC.

1.4 Previous Research into FGFR-targeted therapy

1.4.1 Current FGFR-targeted therapies in development

Many FGFR TKIs have been assessed in clinical trials. Dovitinib is a multitargeted TKI. Trudel *et al.* observed that dovitinib inhibited FGFR1, FGFR3, KIT, vascular endothelial growth factor receptor 1 (VEGFR1), VEGFR2, VEGFR3, FLK3, platelet-derived growth factor receptor α (PDGFRα) and PDGFRβ with IC50s less than 28nM in an *in vitro* kinase assay (Trudel *et al.*, 2005). It has been trialled in patients with NSCLC, bladder cancer, endometrial cancer and multiple myeloma, (Das *et al.*, 2015; Keam *et al.*, 2015; Konecny *et al.*, 2015; Milowsky *et al.*, 2014; Scheid *et al.*, 2015). It was assessed in a phase II clinical trial in advanced urothelial cancer

patients. Although it was well tolerated it had limited single agent activity in urothelial cancer patients with either mutant or wildtype FGFR3 (Milowsky *et al.*, 2014).

The FGFR1-2, VEGFR1-3, PDGFR α and PDGFRβ TKI lucitanib was evaluated in a phase I/IIa clinical trial in 76 patients with advanced metastatic solid tumours including breast, colon, rectal, lung and thyroid cancer. Lucitanib was assessed in patients with FGFR1 or FGF3/4/19 amplification or whose disease was of a histological type potentially sensitive to anti-angiogenic therapy patients and whose disease was progressing following previously stable disease in response to anti-angiogenic-based treatment. The objective response rate was 30.4% in the FGF aberrant tumours and 25.9% in the angiogenesis-sensitive tumours (Soria *et al.*, 2014).

The FGFR1-3 TKI AZD4547 has been tested in phase I and II clinical trials in *FGFR1*-amplified NSCLC, *FGFR1*-amplified breast cancer and *FGFR2*-amplified gastroesophageal cancer. In these trials AZD4547 was well tolerated but the efficacy of AZD4547 was often disappointing; however, Smyth *et al.* did report a confirmed response in 3 out of 9 patients with *FGFR2*-amplified gastroesophageal cancer (Arkenau *et al.*, 2014; Paik *et al.*, 2017; Smyth *et al.*, 2015). Other trials with AZD4547 are in progress or yet to commence, including a phase I trial, ID NCT02546661, in metastatic MIBC patients who have progressed on prior treatment (Powles *et al.*, 2016).

The FGFR1-3 TKI BGJ398 has been assessed in a phase I clinical trial in patients with advanced solid tumours with *FGFR* alterations. BGJ398 was found to have a tolerable safety profile and a partial response was observed in some patients with *FGFR1*-amplified squamous NSCLC and *FGFR3*-mutant urothelial cancer (Nogova *et al.*, 2017). Pal *et al.* evaluated the efficacy of single agent treatment with BGJ398 in 67 patients with metastatic urothelial carcinoma who had progressed on or were intolerant to platinum-based chemotherapy and whose tumours had alterations in FGFR3. There was an overall response rate of 25% and disease stabilisation was observed in an additional 39% of patients. FGFR3 gatekeeper mutations (V443L, V443M, and L496V) were detected in the cell-free DNA (cfDNA) of 4 patients during treatment (Pal *et al*., 2018).

The FGFR1-4 TKI erdafitinib has been assessed in a phase I trial in a number of advanced solid tumours. Of the 8 urothelial carcinoma patients in this trial, a partial response was reported in 2 patients with *FGFR3-TACC3* translocations and a patient with a *FGFR2-BICC1/FGFR2-CASP7* translocation

(Tabernero *et al.*, 2015a). Erdafitinib was assessed in another phase I clinical trial in patients with advanced solid tumours and found to have a manageable safety profile. No patients had a partial or complete response. This trial had only one bladder cancer patient (Tabernero *et al.*, 2015b). Completed, ongoing or planned clinical trials examining treatment with FGFR targeted agents in bladder cancer patients are detailed in table 1.1.

FGFR targeted agent	Manufacturer	Molecular targets	Clinical trials (NCT number, phase)
Dovitinib	Novartis Pharmaceuticals	FLT3, KIT, FGFR1-3, VEGFR1-4	NCT01496534, phase I NCT01732107, phase II NCT00790426, phase II NCT01831726, phase II
AZD4547	AstraZeneca	FGFR1-3	NCT02546661, phase I NCT02465060, phase II
BGJ398	Novartis Pharmaceuticals	FGFR1-4	NCT02657486, pilot study NCT01004224, phase I NCT02160041, phase I
Erdafitinib	Janssen Pharmaceuticals	FGFR1-4	NCT03473743, phase I and II NCT02699606, phase II NCT03390504, phase III
Vofatamab	BioClin Therapeutics	FGFR3	NCT02925533, phase I NCT03123055, phase I/II NCT02401542, phase I/II
BIBF1120	Boehringer Ingelheim	VEGFR1-3, FGFR1-4, FLT3, LCK	NCT02278978, phase II
BAY1163877	Bayer	FGFR1-3	NCT01976741, phase I NCT03473756, phase I/II
PRN1371	Principia Biopharma	FGFR1-4, CSF1R	NCT02608125, phase I
LY3076226	Lilly Oncology	FGFR3	NCT02529553, phase I

Table 1.1 Completed, ongoing or planned clinical trials examining treatment with FGFR targeted agents in bladder cancer patients. Clinical trials identified using clinicaltrials.gov.

1.4.2 Previous work on resistance to FGFR inhibitors

The V561 residue is the FGFR1 ‘gatekeeper’ residue, responsible for FGFR1 ATP binding site nucleotide and small molecule inhibitor specificity. The FGFR1 V561M mutation introduces a large methionine side chain mutation that causes steric hindrance with the FGFR inhibitors PD and E3810 but not others such as AZD4547. AZD4547 retains binding affinity due to flexibility caused by an ethyl linker in its structure. This mutation also increases the stability of the hydrophobic

spine of residues indicative of the active form of the catalytic domain (Sohl *et al.*, 2015; Yoza *et al.*, 2016).

Long-term culture of the myeloma cell line KMS-11 with the FGFR inhibitor AZ12908010, which was discovered during the development of, and is closely related to, AZD4547, produced a resistant derivative with an FGFR3 V555M mutation, analogous to the FGFR1 V561M gatekeeper mutation. The KMS-11 AZ12908010-resistant derivative had also acquired resistance to AZD4547 and PD. The methionine side chain introduced by this mutation, similarly to the FGFR1 V561M mutation, appears to disrupt binding of TKIs to the ATP-binding site (Chell *et al.*, 2013).

The murine Il-3-dependent, pro-B cell line, Ba/F3, was stably transduced to overexpress FGFR2. The stable FGFR2-expressing Ba/F3 cells were seeded into 96 well plates and cultured in the presence of dovitinib and colonies which grew out were expanded. This screening procedure was repeated with Ba/F3 cells stably expressing the FGFR2-activating mutations, S252W or N550K. In total 14 *FGFR2* mutations which induced resistance to dovitinib were identified, 13 of which occurred in the FGFR2 tyrosine kinase domain (M536I, M538I, I548V, N550H/K/S/T, V565I, E566A/G, L618M, K642N and E719G). One mutation, Y770fsX14, was in the FGFR2 c-terminal tail. One of these mutations was N550K, which accounts for 25% of FGFR2-mutant endometrial cancers. This mutation induced the greatest cross-resistance to PD. N550 is part of an autoinhibitory network of residues, and mutations affecting this site allow the kinase to adopt an active state. The only mutation identified that caused resistance to ponatinib, a TKI that inhibits BCR-ABL and FGFR1-4, was V565I. The gatekeeper residue V565I stabilizes the hydrophobic spine, in a similar way to some of the other reported mutations, but also sterically hinders FGFR TKI binding. This steric hindrance is a possible cause of the ponatinib resistance (Byron *et al.*, 2013).

A siRNA screen identified EGFR as limiting the sensitivity of three bladder cancer cell lines with mutant FGFR3, RT4, RT112 and MGH-U3, to PD. RT112 and 639V, a bladder cancer cell line with an *FGFR3* point mutation, showed increased phosphorylation of EGFR upon acute treatment with PD. A RT112 xenograft mouse model showed that treatment with PD and gefitinib reduced tumour volume to a greater extent than either of the drugs given separately (Herrera-Abreu *et al.*, 2013).

Long term treatment of RT112 with the pan-FGFR TKI BGJ398 yielded resistant derivatives with phosphorylated ERBB2 and ERBB3 and sensitivity to a combination of inhibitors of the EGFR family (Wang *et al.*, 2014).

A screen of a shRNA library that targeted kinases and kinase-related genes in RT112 identified that inhibition of the PI3 kinase pathway and EGFR enhanced the effect of AZD4547. Phosphorylation of EGFR and ERBB3 was observed in RT112 following AZD4547 treatment. The pan-PI3 kinase inhibitor BKM120 plus AZD4547 synergistically reduced proliferation in RT112 and JMSU-1, a urothelial carcinoma cell line with *FGFR1* amplification (Wang *et al.*, 2017b).

A secreted protein cDNA library was screened in RT112 cultured in BGJ398. The EGF family ligands neuregulin 1 (NRG1), NRG2 and transforming growth factor alpha (TGF-α) and the MET ligand HGF were identified as able to rescue RT112 from this FGFR TKI (Harbinski *et al.*, 2012).

1.4.3 RT112 and RT4

In order to examine how urothelial carcinomas may acquire resistance to FGFR TKIs this study has made use of the cell lines RT112 and RT4. RT112 was derived in 1973 from a female of unknown age with untreated urothelial carcinoma, histological grade 2. Clinical stage of the disease was not recorded (Marshall *et al.*, 1977; Masters *et al.*, 1986). RT4 was derived in 1968 from a 63 year old male with urothelial carcinoma treated with gold beads, clinical stage T2, histological grade 1 (Rigby and Franks, 1970). RT112 is mainly diploid (Williams *et al.*, 2005). This cell line has a *BRCA2* Q2731R missense mutation, a *CDH6* S2380X nonsense mutation, a *TERT* promoter mutation and homozygous deletion of *CDKN2A* (Aveyard and Knowles, 2004; Earl *et al.*, 2015; Nickerson *et al.*, 2017). BRCA2 is crucial in the repair of DNA double strand breaks by homologous recombination maintaining genomic stability (Fradet-Turcotte *et al.*, 2016). *CDH6* encodes cadherin 6 which is a type II classical cadherin (Shimoyama *et al.*, 1999).

RT4 is mainly tetraploid, has a *DNMT3A* S129L missense mutation, an *ELF3* 217_219del frameshift deletion, *ESPL1 P1937A* missense mutation, *FAT4* R3716H missense mutation, a *PALB2* L337S missense mutation and a *TSC1* D505fs frameshift deletion. RT4 also has *TP53* loss of heterozygosity and homozygous deletion of *CDKN2A* (Aveyard and Knowles, 2004; Earl *et al.*, 2015; Nickerson *et al.*, 2017; Williams *et al.*, 2005). *DNMT3A* encodes DNA (cytosine-5)-methyltransferase 3A. ELF3 is a transcriptional regulator in the urothelium (Bock *et*

al., 2014). *ELF3* frameshift deletions and insertions, splice site and missense mutations are found in bladder cancer (Dadhania *et al.*, 2016). Guo *et al.* found *ESPL1* mutations in 6% of urothelial carcinomas (Guo *et al.*, 2013). *ESPL1* encodes separase which enables the segregation of sister chromatids at the metaphase to anaphase transition (Solomon *et al.*, 2014). FAT4, a member of the cadherin superfamily, inactivates the oncogenic transcription co-activators YAP and TAZ which promote cell proliferation (Katoh, 2012). PALB2 is a tumour suppressor which binds BRCA2 and recruits it to the site of DNA damage (Park *et al.*, 2014). RT112 and RT4 express wildtype FGFR3 and FGFR3-TACC3 fusion proteins (Fig. 1.1) (Williams *et al.*, 2013).

RT112 and RT4 were chosen for this study as they are reported to be sensitive to PD (Lamont *et al.*, 2011). PD acts by binding the ATP-binding pocket in the tyrosine kinase domain of FGFR1 and FGFR3 (Mohammadi *et al.*, 1998). Lamont *et al.* reported RT112 and RT4 as having IC50s of 15nM and 5nM respectively for PD (Lamont *et al.*, 2011). Herrera-Abreu *et al.* found that treatment of RT112 with 1mM PD for 3 days reduced cell viability by over 50% (Herrera-Abreu *et al.*, 2013). In order to produce a model of acquired resistance to FGFR inhibition, RT112 and RT4 were cultured in PD for 20 passages. Resistant derivatives that arose from this treatment were examined in this project and are denoted RT112 R1, RT112 R2, RT112 R3 and RT4 R1.

1.5 Aims

There is a need to improve the survival of patients with MIBC. FGFR inhibitors are now entering clinical trials to assess their suitability for the treatment of urothelial carcinoma. Whilst intrinsic and acquired resistance has reduced the efficacy of targeted agents specific for tyrosine kinases in other types of cancer, research into these resistance mechanisms has enabled further improvements in the treatment of cancer patients. This project has been conducted in anticipation that resistance to FGFR inhibitors will develop in patients with urothelial carcinoma. The aims of this research are the following:

1. Examine the differences in morphology, cell proliferation and sensitivity to PD between RT112 parental and RT112 R1, R2 and R3 and between RT4 parental and RT4 R1.

2. Determine the mechanisms by which the RT112 and RT4 resistant derivatives continue to grow in the presence of PD.

3. Suggest drug combinations which may overcome resistance based upon the identified resistance mechanisms and test the efficacy of these drug combinations.

Chapter 2
Materials and Methods

Manufacturer names are detailed after the first mention of each product. See Appendix A for full name and address of all suppliers. See Appendix B for buffers and solutions.

2.1 Tissue culture

2.1.1 Tyrosine kinase inhibitors (TKIs) used in this study

The TKIs used in this study were the FGFR inhibitor PD173074 (Sigma-Aldrich), the EGFR inhibitor Erlotinib (Cayman Chemical), the EGFR, ERBB2 and ERBB3 inhibitor Sapitinib (ApexBio Technology), the IGF1R inhibitor Linsitinib (Biovision) and the MET inhibitor Capmatinib (Adooq Bioscience). All TKIs were dissolved in DMSO and stored at -20°C: PD173074 and Sapitinib were stored as 10mM solutions, Erlotinib was stored as a 40mM solution, Linsitinib was stored as a 20mM solution and Capmatinib was stored as a 4.85mM solution.

2.1.2 Cell lines used in this study

The epithelial cell lines RT112 and RT4 were used (Marshall *et al.*, 1977; Masters *et al.*, 1986). The cell line identity of parental RT112 and parental RT4 was confirmed with short tandem repeat profiling in 2012. The RT112 and RT4 profiles were compared with reference profiles from the ATCC and DSMZ databases. All resistant derivatives were previously generated in the Knowles lab (described in Chapter 3). RT112 R1, RT112 R3 and RT4 R1 were cultured in 1μM PD173074 (Sigma-Aldrich) whilst RT112 R2 was cultured in 2μM PD173074. During production of the resistant derivatives RT112 R1, R2 and RT4 R1 were split 1 in 3 and R3 was split 1 in 5.

2.1.3 Cell culture

All cell culture was performed under aseptic conditions in a Biomat class II laminar flow hood (MAT). Cells were removed from liquid nitrogen storage, rapidly thawed at 37°C, recovered into 10ml of growth medium, pelleted by centrifugation at 1000 x *g* for 4 min then resuspended in an appropriate volume of growth medium and transferred to sterile 25cm^2 or 75cm^2 vented canted-neck cell culture flasks (Corning). Cells were maintained at 37°C in a humidified incubator (Sanyo) in an atmosphere of 5% CO_2 in air. RT112 cells were cultured in RPMI-1640 growth medium (Sigma-Aldrich) supplemented with 10% foetal calf serum (FCS; Biosera) and 2mM GlutaMAX (Life Technologies). RT4 was cultured in McCoy's 5A growth medium (Sigma-Aldrich) supplemented with 10% FCS and 2mM GlutaMAX. Resistant derivatives were cultured in the same media as their parental cell line supplemented with PD173074. The resistant derivatives RT112 R1, RT112 R3 and RT4 R1 were routinely cultured in 1μM PD173074 whilst RT112 R2 was cultured in 2μM PD173074. Cells were cultured for no more than 10 passages from frozen stocks.

2.1.4 Cell passage

Cells were routinely passaged at, or just prior to, confluence. Medium was aspirated, cells were rinsed in calcium- and magnesium-free phosphate buffered saline (PBS) solution then incubated in PBS containing 0.1% (w/v) EDTA for 2 min at 37°C. The PBS-EDTA was aspirated and cells were incubated with 1ml 0.05% trypsin-0.02% EDTA (TV; Sigma-Aldrich) for a 75cm^2 flask, for approximately 5 min until the cells detached. TV was inhibited by re-suspension of cells in fresh medium containing 10% FCS. A fraction of this single cell suspension was transferred to a new flask containing fresh growth medium.

2.1.5 Cell counting

Cells were counted to seed plates with the correct number of cells per well for growth curves and cell viability assays, and to calculate cell numbers during growth curves. A single cell suspension was produced as described above. Cells were counted with a Beckman Coulter Z2 cell and particle counter (Beckman Coulter). Counts were performed twice per sample and a mean value was calculated.

2.1.6 Growth curves

A single cell suspension was produced from cells at 70-80% confluence as described above. Cells were seeded in 6 well plates (Corning) at a density of 1 x 10^4 cells/well in 2ml of medium. Medium was changed every 3 to 4 days. Triplicate wells were counted for each time point and a mean value calculated.

2.1.7 Cell Viability Assay - CellTiter-Blue™

For each cell line a 70-80% confluent 75cm^2 flask was selected and a single cell suspension produced as described above. A flat-bottomed 96 well plate (Corning) was seeded with 100µl of cells per well in medium without any TKI or vehicle present. Cells were seeded at a density that would give 80% confluence at the end of the assay in the untreated control. After 24 h incubation medium was replaced with 100µl of medium containing the appropriate concentration of TKI(s) or vehicle. Cells were then incubated for 72 h after which medium was replaced and cells were incubated for a further 48 h. Throughout this assay cells were incubated at 37°C in 5% CO_2. After 120 h of incubation with TKI(s), 20µl of CellTiter-Blue pre-warmed to 37°C was added to each well. The plates were kept dark and incubated for 2 h at 37°C in 5% CO_2. Fluorescence was measured on a Berthold Mithras LB 940 Multimode microplate reader. Excitation was at 540nM and emission was at 590nM respectively. Results were blanked with a medium no cell control and normalized to the vehicle (DMSO) control. Dose response curves and IC50 values were calculated using GraphPad Prism® 7. Cell viability assays in Figure 3.8, Figure 7.7 and Figure 7.8 were conducted by Matt Dunning.

2.1.8 Retroviral transduction of RT112 parental

Retroviral transduction was performed by Dr Julie Burns:

Amphotropic retrovirus was produced as follows: 50% confluent Phoenix Ampho cells were transfected overnight with virus backbone plasmids: pBABEpuro, pBABEpuro-RAS V12, pLXSNneo or pLXSNneo-RAS V12 using transfection reagent *Trans*IT-293 (Mirus) according to the manufacturer's protocol. Medium was changed daily and virus-containing medium was harvested after 72 and 96 h. The 72 and 96 h virus supernatants were pooled, passed through a 0.45µm filter and stored at -80^{o}C in 1.5ml aliquots. RT112 parental cells were transduced as follows: 50% confluent cells in a 25cm^2 flask were transduced overnight with retroviral

supernatant (1.5 ml virus supernatant + 1.5 ml normal medium + 8μg/ml polybrene (Sigma-Aldrich 107689)). The following morning the transduction mix was replaced with normal growth medium and selection with 1μg/ml puromycin or 600μg/ml G418 was started after 48 h. Selection was maintained until stocks were frozen after 14 days (LXSN) or 19 days (BABE). When thawed the cells were maintained in half of the selection drug concentration.

2.2 Examination of protein expression

2.2.1 Protein extraction

70-80% confluent cells in 75cm^2 cell culture flasks were selected and washed twice with phosphate buffered saline (PBS). Cells were lysed on ice in 250μl of RIPA buffer (Appendix A) containing 6.25μl protease inhibitor cocktail (P8340) and 2.5μl phosphatase inhibitor cocktail 2 (P5726) (Sigma-Aldrich). The flasks were incubated on ice for 5 min then cells were detached using a cell scraper (Sarstedt). Cell lysates were transferred to 1.5ml micro-centrifuge tubes and cell debris pelleted by centrifugation at 12850 x *g* for 10 min at 4°C. The supernatants were transferred to new 1.5ml micro-centrifuge tubes and stored at -80°C.

2.2.2 Bradford assay (protein quantification)

Proteins used for immunoblotting and immunoprecipitation were quantified by Bradford assay. Protein concentrations were measured using the Bio-Rad protein assay, which is based on the Bradford dye-binding method, according to the manufacturer's protocol. The absorbance of a series of bovine serum albumin standards was measured on a Bio-Rad SmartSpec Plus spectrophotometer and used to generate a standard curve. The absorbance of the samples was then measured and the standard curve used to calculate protein concentrations.

2.2.3 Immunoblotting

Protein samples were diluted with RIPA buffer to contain 30μg of protein in 20μl. 5μl of 5x SDS loading buffer (Appendix A) was added and samples were denatured for 3 min at 100°C then placed on ice for 3 min. 10μl of Precision Plus Protein

Prestained Standard (Bio-Rad) and 20µl of samples were loaded onto 7.5% polyacrylamide Bio-Rad Mini-PROTEAN TGX precast gels. Gels were electrophoresed in 1x TGS buffer (Bio-Rad) (Appendix A) at 3W per gel, until the blue dye front reached the bottom of the gel. Proteins were transferred to nitrocellulose membranes using the high molecular weight program on a Trans-Blot Turbo Transfer System (Bio-Rad) with a Trans-Blot Turbo transfer pack (Bio-Rad) of either mini or midi format. Membranes were blocked in 4% (w/v) non-fat milk (Panreac AppliChem) in PBS containing 0.1% (v/v) Tween 20 (Fisher Scientific) (PBS-T) for 30 min. Membranes were then incubated with primary antibody in 2% (w/v) non-fat milk in PBS-T for 1 h at room temperature (RT) or overnight at 4°C on a shaking platform. Hybridised membranes were washed 4 x 10 min in PBS-T and incubated with HRP-conjugated secondary antibody in 2% (w/v) non-fat milk in PBS-T for 1 h at RT or overnight at 4°C on a shaking platform. Membranes were then washed for 4 x 10 min in PBS-T. HRP-labelled antibody was detected by chemiluminescence using Luminata Forte Western HRP Substrate (Merk Millipore) and imaged with a ChemiDoc MP System and Image Lab software (Bio-Rad). Membranes were stripped at 55°C for 40 min in stripping buffer (Appendix A), washed 3 x 10 min in PBS-T and re-hybridised to examine β-actin expression as a loading control. See Table 2.1 for a list of antibodies and their concentrations.

Table 2.1 Antibodies used in immunoblotting.

Antibodies	Manufacturer and Catalogue number	Species	Dilution
1° antibodies			
β-actin (ACTBD11B7)	Santa Cruz sc-81178	Mouse monoclonal	1/3000
AKT (C67E7)	Cell Signalling #4691	Rabbit monoclonal	1/1000
CD44H (2C5)	R & D Systems BBA10	Mouse monoclonal	1/1000
CK5/6 (D5/16B4)	Dako M7237	Mouse monoclonal	1/1000
E-cadherin [HECD-1]	Abcam ab1416	Mouse monoclonal	1/500
EGFR (1005)	Santa Cruz sc-03	Rabbit polyclonal	1/1000
Erbb2	Abcam ab2428	Rabbit polyclonal	1/1000
Erbb3 (C-17)	Santa Cruz sc-285	Rabbit polyclonal	1/1000
Erk (K23)	Santa Cruz sc-94	Rabbit polyclonal	1/1000
FGFR3 (B-9)	Santa Cruz sc-13121	Mouse monoclonal	1/1000
FLG (C-15) (FGFR1)	Santa Cruz sc-121	Rabbit polyclonal	1/500
N-cadherin (13a9)	Santa Cruz sc-59987	Mouse monoclonal	1/500
Met	Cell Signalling #4560	Rabbit polyclonal	1/1000

phospho-Akt (Ser473) (D9E)	Cell Signalling #4060	Rabbit monoclonal	1/1000
phospho-EGFR (Tyr1068) (D7A5)	Cell Signalling #3777	Rabbit monoclonal	1/1000
phospho-Erbb2 (Tyr1221/1222) (6B12)	Cell Signalling #2243	Rabbit monoclonal	1/1000
phospho-Erbb3 (Tyr1289) (21D3)	Cell Signalling #4791	Rabbit monoclonal	1/1000
phospho-Erk (Tyr204) (E-4)	Santa Cruz sc-7383	Mouse monoclonal	1/1000
phospho-Met (Tyr1234/1235) (D26)	Cell Signalling #3077	Rabbit monoclonal	1/1000
phospho-Stat1 (Tyr701) (58D6)	Cell Signalling #9167	Rabbit monoclonal	1/1000
phospho-Stat3 (Tyr705)	Cell Signalling #9131	Rabbit polyclonal	1/1000
SCD1 (M38)	Cell Signalling #2438	Rabbit polyclonal	1/1000
SREBP1 (A4)	Santa Cruz sc-13551	Mouse monoclonal	1/1000
Stat1	Cell Signalling #9172	Rabbit polyclonal	1/1000
Stat3 (79D7)	Cell Signalling #4904	Rabbit monoclonal	1/1000
Vimentin (H-84)	Santa Cruz sc-5565	Rabbit polyclonal	1/500
2° Antibodies			
Anti mouse-HRP	Bio-Rad 170-6516	Goat	1/3000
Anti rabbit-HRP	Southern Biotech 4010-05	Goat	1/3000

2.3 Examination of RNA expression

2.3.1 RNA extraction and quantification

RNA was extracted using an RNeasy Mini Kit (Qiagen) according to the manufacturer's protocol and the concentration determined by measuring the absorbance at 260nm using a NanoDrop 8000 UV-Vis Spectrophotometer (LabTech). RNA was stored at -80°C.

2.3.2 DNase treatment and examination of RNA concentration, purity and integrity prior to DNA microarray analysis

RNA samples were DNase-treated prior to examination with the Affymetrix GeneChip® Human Transcriptome Array 2.0. 10µg of RNA was treated with 3U of DNase I in DNase reaction buffer containing 40U RNase OUT™ in a total volume of

34µl for 15 minutes at RT. The reaction was inhibited by the addition of 4µl of 25mM EDTA (all reagents from Life Technologies). The sample volume was adjusted to 100µl with RNase-free water and RNA was purified with an RNeasy Mini Kit (Qiagen) using the RNA Clean-up protocol according to the manufacturer's protocol. A NanoDrop 8000 UV-Vis Spectrophotometer was used to establish the concentration and purity of RNA samples by measuring the absorbance at 260nm and the 260/280nm absorbance ratio respectively. The integrity of the RNA was examined on a 2200 TapeStation (Agilent) using the RNA ScreenTape System (Agilent) according to the manufacturer's instructions, and RIN values recorded. An example RNA profile of one sample is shown in Fig. 2.1 RNA was stored at -80°C.

2.3.3 Wet lab microarray procedure - conducted by Hologic/Tepnel

Total RNA was amplified using the Affymetrix GeneChip® WT PLUS Reagent Kit according to manufacturer's instructions. The resulting cDNA was quantified using optical density (OD) (NanoDrop). The cDNA was normalised and hybridised onto Affymetrix Human Transcriptome 2.0 microarrays for 16 hours at 45°C. Microarrays were washed and stained using the Affymetrix GeneChip® Hybridization, Wash, and Stain Kit according to manufacturer's instructions using the Affymetrix GeneChip® Fluidics Station 450. Microarrays were scanned using an Affymetrix GeneChip® 7G microarray scanner. Data quality was analysed using Affymetrix® Expression Console™ Software.

2.3.4 Microarray data analysis

Quality control of individual sample hybridisations and normalisation of data was conducted with Affymetrix Expression Console. To adjust for the variability in probe cell intensity data between microarray samples, Signal Space Transformation - Robust Multichip Average (SST-RMA) normalisation was conducted with CEL files generating CHP files. SST removes significant fold change compression and RMA minimises probe variance (Irizarry *et al.*, 2003). Affymetrix Transcriptome Analysis Console was used to determine which genes had undergone a significant change in gene expression between experimental conditions. The criteria for a significant change in intensity were a) a linear fold change greater than or equal to 2 and b) an unpaired one-way Analysis of Variance (ANOVA) p-value less than 0.05. MetaCore™ was used to examine which pathways were significantly altered

between experimental conditions. Partek Genomic Suite® was used to conduct hierarchical clustering with Euclidean distance and complete linkage.

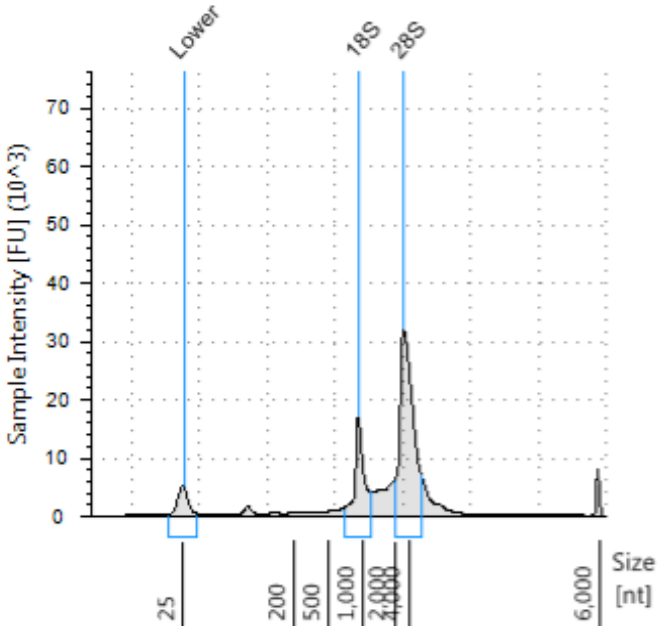

Figure 2.1 Profile of a RNA sample from RT4 R1 No PD generated on the 2200 TapeStation. The 18S and 28S ribosomal subunits are quantified from the electropherogram and the software uses the ratio of these subunits to produce a RNA Integrity Number (RIN). RINs range from 1 to 10 with a value of 1 indicating total RNA degradation and a value of 10 indicating no degradation (Schroeder *et al.*, 2006). All RNA samples used in the microarray analysis had RINs greater than or equal to 8.7.

2.3.5 cDNA synthesis

RNA was reverse transcribed into first strand cDNA using SuperScript II Reverse Transcriptase (Life Technologies) according to the manufacturer's protocol. 1µg of RNA, 250ng random primers and 1µl dNTP mix (10mM each) were added to a 0.5ml micro-centrifuge tube and the volume was made up to 12µl with molecular biology grade water (Sigma Aldrich). Samples were heated at 65°C for 5 min and quick chilled on ice. 4µl 5X First Strand Buffer [250 mM Tris-HCl pH 8.3, 375 mM KCl, 15 mM $MgCl_2$], 2µl 0.1M Dithiothreitol (DTT) and 1µl RNaseOUT™ was added to each tube. Samples were incubated at room temperature for 2 min then 200 units of SuperScript II reverse transcriptase were added to each tube. Samples were incubated at 42°C for 50 min and the reactions were stopped by heating at 70°C for 15 min. Finally, 80µl of molecular biology grade water was added. cDNA was stored as 25µl aliquots at -80°C.

2.3.6 PCR of cDNA

PCR was performed using first strand cDNAs to examine the expression of total FGFR2, FGFR2 IIIb, FGFR2 IIIc and HPRT1. Each reaction contained 1x AmpliTaq Gold® 360 buffer, 1.5mM $MgCl_2$, 0.2μM of forward and reverse primers (see Table 2.2 for primer sequences), 200μM dNTPs, 1U AmpliTaq Gold® 360 DNA Polymerase and 5μl cDNA in a total reaction volume of 25μl. Reactions were performed in non-skirted 96 well PCR plates (Thermo Scientific) in a Veriti thermal cycler (Applied Biosystems). Cycling conditions were 95°C for 5 min, 35 cycles of 95°C for 30 s, 56°C for 30 s and 72°C for 60 s followed by a final extension step of 72°C for 5 min.

2.3.7 Agarose gel electrophoresis of PCR products

5μl of DNA loading dye (Appendix A) was added to PCR products. 500ng of 100bp DNA ladder (New England Biolabs, N3231S) and 10μl of PCR products were loaded onto 2% agarose (w/v) gels cast using 1x TBE (Severn Biotech)(Appendix A) and containing 0.6μg/ml ethidium bromide (Severn Biotech). Gels were electrophoresed in 1x TBE buffer at 90 V for 1 h and imaged using a Bio-Rad ChemiDoc MP.

Table 2.2 Primers used in *FGFR2* standard PCR.

Primer	**Sequence (5'-3')**
***FGFR2* exons 7-11 (all isoforms)**	
Forward	GTGGTCGGAGGAGACGTAGA
Reverse	AACTCCCATTTTGGGTCCTC
***FGFR2* exons 7-8 (IIIb isoforms)**	
Forward	GTGGTCGGAGGAGACGTAGA
Reverse	TGTTTTGGCAGGACAGTGAG
***FGFR2* exons 7-9 (IIIc isoforms)**	
Forward	GTGGTCGGAGGAGACGTAGA
Reverse	CAACCATGCAGAGTGAAAGG
***HPRT1* control primers**	
Forward	CCTGCTGGATTACATTAAAGCACTG
Reverse	CTGAAGTACTCATTATAGTCAAGGG

2.3.8 Quantitative real time PCR (qRT-PCR)

Quantitative real-time PCR was performed using first strand cDNAs and TaqMan or SYBR Green assays. For TaqMan assays, pre-made and optimised gene expression assays (Applied Biosystems) were used (Table 2.3). Each reaction contained 10µl 2x TaqMan Gene Expression Master Mix (Applied Biosystems), 1µl TaqMan gene expression assay, 7µl dH_20 and 2µl cDNA. Previously optimised SYBR Green assays were used for analysis of *KDM6A* mRNA levels. Each reaction contained 12.5µl 2x SYBR Green mix, 1.5µl of each forward and reverse primer (10µM stock) (see Table 2.4 for primer sequences), 9µl dH_20 and 2µl cDNA. Reactions were performed in triplicate in 96-well optical plates (Applied Biosystems) in a 7500 Real-Time PCR System (Applied Biosystems). Cycling conditions consisted of an initial hold at 50°C for 2 min, followed by 95°C for 10 min, then 40 cycles of 95°C for 15 s and 60°C for 1 min. Melt curve analysis was performed for SYBR Green assays after the PCR amplification step. Expression levels were normalised to the expression of the housekeeping gene succinate dehydrogenase complex flavoprotein subunit A (SDHA) (Ohl *et al*., 2006) and measured relative to the parental cell lines value.

Table 2.3 TaqMan assays used in qRT-PCR.

Gene	Assay ID
CDH1	Hs01013963_m1
ERBB3	Hs00176538_m1
ESRP1	Hs00214472_m1
FGF1	Hs00265254_m1
FGF2	Hs00266645_m1
FGFR1	Hs00241111_m1
FGFR3	Hs00179829_m1
FOXA1	Hs04187555_m1
GATA3	Hs00231122_m1
IL6ST	Hs00174360_m1
JUN	Hs01103582_s1
KRT5	Hs00361185_m1
KRT6C	Hs00752476_s1
KRT14	Hs00265033_m1
KRT20	Hs00300643_m1
LIFR	Hs01123581_m1

MMP1	Hs00899658_m1
OSMR	Hs00384276_m1
PPARG	Hs00234592_m1
PTGS2	Hs01573476_g1
SDHA	Hs00417200_m1
SREBF1	Hs01088691_m1
STAT3	Hs01047580_m1
UPK2	Hs00171854_m1

Table 2.4 Primers used in *KDM6A* SYBR Green qRT-PCR

Primer	**Sequence (5'-3')**
Forward	TTCACCATACCCTCCCTTGC
Reverse	AGAAAAGTCCCAGGTCTAACTTAA

2.4 DNA sequencing

2.4.1 DNA extraction

DNA used for exome sequencing and copy number analysis was purified from cells using a Gentra Puregene Kit (Qiagen) following the cultured cells protocol according to the manufacturer's instructions. DNA used for Sanger sequencing and SNaPshot assay was purified using a QIAamp DNA Mini kit (Qiagen) following the blood or body fluids spin protocol. For each protocol, DNA was purified from one 80-100% confluent 75cm^2 culture flask

2.4.2 DNA quantification

DNA used for exome sequencing and copy number analysis was quantified using the PicoGreen dsDNA quantitation assay (Thermo Scientific) as follows: Lambda DNA standards were prepared to final concentrations of 1000, 100, 10, 1 and 0 ng/ml and samples were diluted 1 in 500 in 1 x TE buffer. 100µl of these standards and diluted samples were pipetted into a black 96 well optical plate (BMG Labtech Ltd). Then 100µl of PicoGreen reagent (diluted 200 fold in 1x TE) was added to each well. Standards and samples were mixed by pipetting and incubated at RT for 2 minutes before being quantified by measurement of fluorescence (excitation

480nm, emission 520nm) with a BMG Fluostar Galaxy plate reader. DNA used for Sanger sequencing and SNaPshot assay was quantified and tested for purity with a NanoDrop 8000 UV-Vis spectrophotometer by measuring the absorbance at 260nm and the calculation of a 260/280nm absorbance ratio respectively.

2.4.3 Exome sequencing

Exome sequencing was conducted with RT112 R1, RT112 R3 and parental RT112 samples. 3µg of DNA was made up to a final volume of 250µl with TE buffer (pH 8 0.1mM EDTA). DNA was sonicated with a Covaris S2 sonicator with the following settings:

38 cycles of:

1. 500 cycles per burst, intensity 8, duty cycle 15%.
2. 1000 cycles per burst, intensity 9.9, duty cycle 19.9%.

Libraries were generated and enriched for exomic regions using the SureSelect^{XT} Human All Exon V6 capture library (Agilent) according to the manufacturer's protocols. An overview of the production of libraries for NGS is shown in Fig. 2.2. The concentration and size of DNA fragments was assessed using a 2200 TapeStation (Agilent) with High Sensitivity D1000 ScreenTapes (Agilent) according to the manufacturer's instructions. The points at which the 2200 TapeStation (Agilent) was used to determine the concentration and size of DNA fragments are detailed in Fig 2.2. RT112 parental, RT112 R1, RT112 R3 and 2 samples not relevant to this project were indexed, pooled and run in a single lane on an Illumina HiSeq 3000 in paired-end mode. DNA sequencing was performed by the Leeds Institute of Molecular Medicine Next Generation Sequencing Facility.

2.4.4 Exome sequencing data analysis

Procedure conducted by Dr Olivia Alder: Base calling and quality control was performed using Illumina's Real Time Analysis software with standard settings. Sequence files were QC checked using FastQC (v0.10.0) before preprocessing. Adapter contamination and low-quality read ends (< 20) were trimmed using cutadapt 1.3 and fastq-tools 0.8. Any read in which either pair had a length less than 19 was removed from subsequent analysis. Read Mapping and Genotype Calling Alignment was performed using BWA 0.7.10 mem GRch38 reference. Duplicate reads were removed using the Picard v1.56 MarkDuplicates program. Local realignment around indels was performed using the GATK v1.3

RealignerTargetCreator and IndelRealigner in Smith-Waterman mode with reference to dbSNP v132. The Picard v1.56 FixMateInformation program was used to ensure that all mate-pair information was in sync between each read and its mate following local realignment. Base quality scores were recalibrated using GATK v1.3 CountCovariates and TableRecalibration with reference to dbSNP v132. BAM files were sorted and then indexed using SAMtools index. Somatic Variant Analysis Pileup files (created using SAMtools mpileup, with parameters – d 5000 and q- 20) were used as input to VarScan2 v2.3.5. This was used in somatic mode, with a strand filter, to identify somatic single nucleotide variations (SNVs) and small insertions and deletions (indels). Results were then processed using processSomatic to extract the somatic mutations with the specification that zero reads were to support the variant in the normal sample. SNVs and indels were identified in RT112 R1 and RT112 R3 with parental RT112 as the normal sample. To be called, a mutation needed to satisfy the following two criteria:

1) a variant allele frequency of greater than 20%

2) an absence of the mutation in RT112 parental.

High confidence somatic variant and indel calls were converted to mutation annotation format (MAF) using Variant Effect Predictor (VEP) version 81 via the Ensembl Virtual Machine.

2.4.5 Copy number analysis

Copy number alterations were examined by low pass genomic sequencing. Emma Black constructed NGS libraries with NEBNext® reagents according to the manufacturer's instructions. Data was processed by Fiona Platt. BAM files were generated as described in the exome sequencing section (2.5.4). Following the generation of BAM files, ngCGH was used to compare number of read counts between the cell line and blood or parental samples using a window size of 1000. The Nexus Copy Number software package was used to conduct GC correction and copy number calling using the FASST2 Segmentation Algorithm which is a Hidden Markov Model (HMM) based approach. Segmentation was conducted with a significance threshold of 1.0E-5, with a requirement of at least 3 probes per segment and a maximum probe spacing of 1000 between adjacent probes before breaking a segment.

The $\log_2$ ratio thresholds were set as follows: single copy gain; 0.25, single copy loss; -0.25, two or more copy gain; 1.25 and homozygous loss; -1.25.

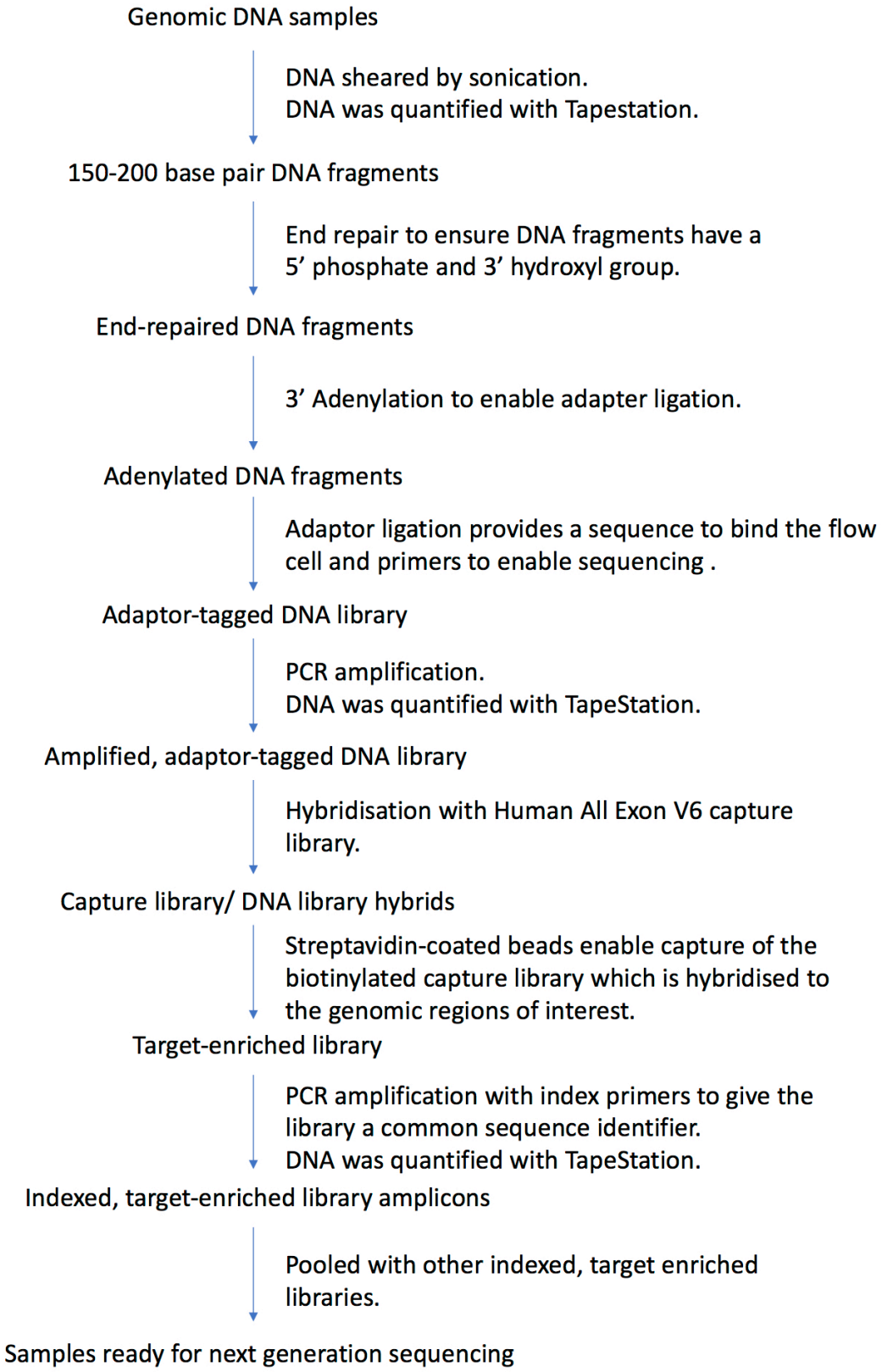

Figure 2.2 Overview of production of next-generation sequencing libraries. Adapted from SureSelectXT Target Enrichment System for Ilumina Paired-End Multiplexed Sequencing Library protocol.

2.4.6 PCR and Sanger sequencing of *HRAS* exon 1

Standard PCR was performed with each reaction containing 1x AmpliTaq Gold® 360 buffer, 2.5mM $MgCl_2$, 0.2µM of forward and reverse primers (see Table 2.5 for primer sequences), 1mM dNTPs, 1U AmpliTaq Gold® 360 DNA Polymerase and 20ng of DNA in a total reaction volume of 25µl. Reactions were performed in non-skirted 96 well PCR plates (Thermo Scientific) in a Veriti thermal cycler (Applied Biosystems). Cycling conditions were 95°C for 5 min, 35 cycles of 95°C for 30 s, 60°C for 30 s and 72°C for 30s followed by a final extension step of 72°C for 10 min. Agarose gel electrophoresis was used to check that PCR was successful.

1µl ExoProStar (Illumina) was added to 2.5µl PCR products. This was mixed by pipetting, incubated at 37°C for 15 min then incubated at 80°C for 15 min. Sequencing was conducted with the BigDye™ Terminator v1.1 Cycle Sequencing Kit (Applied Biosystems) according to the manufacturer's instructions (see Table 2.5 for primer sequences). Products were purified by adding 1µl of 3M sodium acetate (pH5.3) and 25µl 95% (v/v) ethanol to each sample, incubating at RT for 30 min and centrifugation at 2000 x *g* for 30 min at 4°C. The PCR plate was inverted on absorbent paper to remove the supernatant. 75µl 95% (v/v) ethanol was added to each sample and samples were spun at 2000 x *g* for 15 min at 4°C. The PCR plate was spun inverted on tissue paper at 730 x *g* for 1 min. Pellets were dried for 5 min at 95°C and resuspended in 15µl Hi-Di formamide (Applied Biosystems). Samples were heated at 95°C for 2 min and then kept on ice. Samples were then run on a ABI 3130xl Genetic Analyzer (Applied Biosystems).

Table 2.5 Primers used for PCR amplification, Sanger sequencing and SNaPshot of *HRAS* exon 1

Primer	**Sequence (5'-3')**
Forward	CAGGAGACCCTGTAGGAGGA
Reverse	TCGTCCACAAAATGGTTCTG

2.4.7 SNaPshot analysis of *HRAS* c.DNA 34

Standard PCR was performed following the same methodology as for Sanger sequencing. 3µl of PCR product was run on a 2% agarose gel to check the PCR was successful. 3µl of shrimp alkaline phosphatase (Sigma-Aldrich) and 2µl Exonuclease I (Affymetrix) were added to the remaining 12 µl PCR product. This was then spun down for 10 s at 190 x *g*, incubated for 60 min at 37°C and 15 min at

72°C. Each SNaPshot reaction contained 1µl shrimp alkaline phosphatase(SAP)/exonuclease-treated PCR product, 2.5µl SNaPshot Multiplex Ready Reaction Mix, 1 x BigDye Terminator sequencing buffer, 5µM *HRAS* c.DNA 34 probe, and molecular biology grade water to a final volume of 9µl (all reagents Applied Biosystems). The sequence (5'->3') of the *HRAS* c.DNA 34 probe was $T_{(17)}$CTGGTGGTGGTGGGCGCC. SNaPshot analysis was conducted with the following cycling conditions: 35 cycles of 95°C for 10 s, 58.5°C for 40 s, hold at 4°C. 1µl shrimp alkaline phosphatase was added to the labelled SNaPshot extension products which were then incubated for 60 min at 37°C followed by 15 min at 72°C and spun down for 10 s at 190 x *g*. SNaPshot products and GeneScan™ 120 LIZ™ dye size standard (Applied Biosystems) were diluted 1 in 10. 1µl diluted SNaPshot product, 0.2 µl 120 LIZ™ dye size standard and 9.8µl Hi-Di formamide were mixed, spun down for 10 s at 190 x *g*, denatured for 5 min at 100°C, cooled on ice and run on a ABI 3130xl Genetic Analyzer.

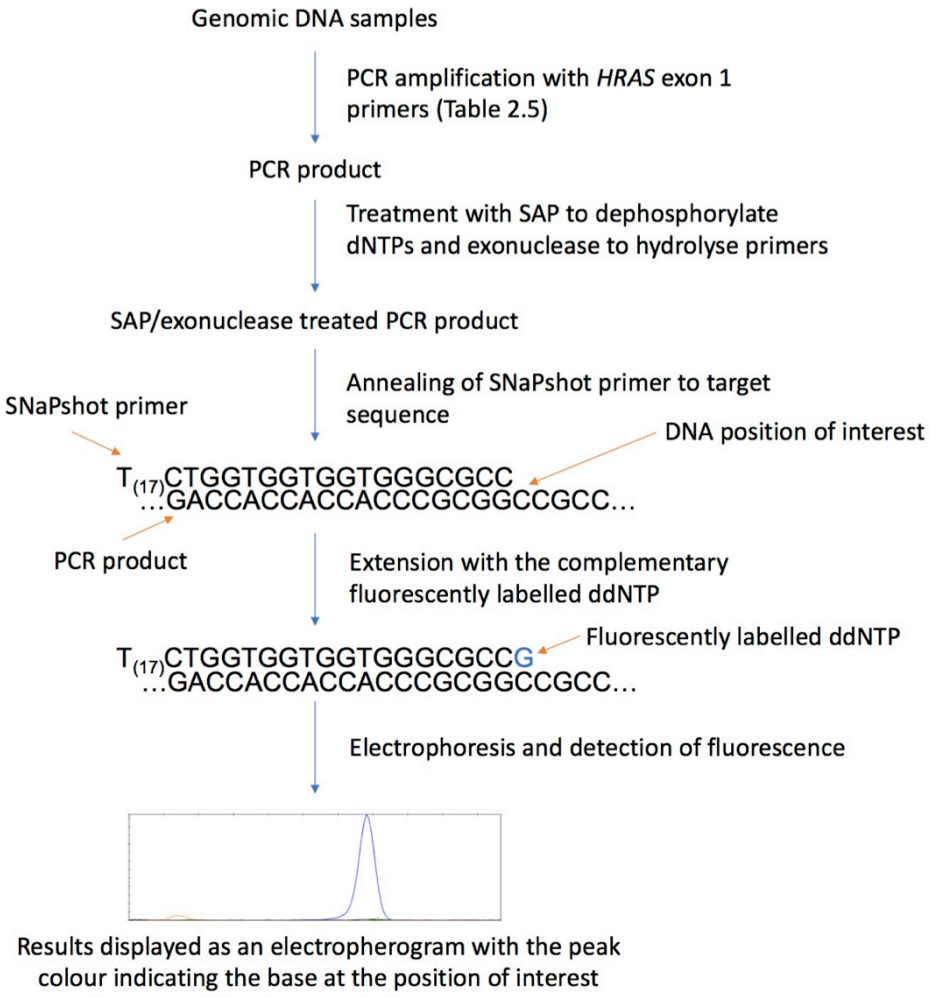

Figure 2.3 Overview of the SNaPshot analysis of *HRAS* c.DNA 34. Abbreviations: SAP; shrimp alkaline phosphatase, ddNTP; dideoxynucleoside triphosphate. Adapted from the SNaPshot® Multiplex System for SNP genotyping product bulletin.

Chapter 3
Characterisation of Parental and PD173074 Resistant cells

3.1 Introduction

The FGFR TKI PD173074 (PD) is a potent selective inhibitor of the FGFR family of receptor tyrosine kinases. Mohammadi *et al.* reported that in an *in vitro* kinase inhibition assay FGFR1 was inhibited with an IC50 of 21.5nM. FGFR1 autophosphorylation was inhibited with a half maximal inhibitory concentration (IC50) of 1-5nM in the fibroblast cell line NIH3T3 which endogenously expresses FGFR1 (Mohammadi *et al.*, 1998). Pardo *et al.* demonstrated that 100nM of PD inhibited autophosphorylation of FGFR2 in NCI-H510A, a small cell lung cancer cell line (Pardo *et al.*, 2009). In another study PD inhibited FGFR3 autophosphorylation in NIH3T3 transfected with FGFR3 with an IC50 of approximately 5nM (Trudel *et al.*, 2004). Mohammadi *et al.* demonstrated that, in an *in vitro* kinase inhibition assay, PD inhibited the cytoplasmic domain of PDGFR with an IC50 of 17.6μM and Src with an IC50 of 19.8μM. EGFR, insulin receptor (InsR), MEK and protein kinase C (PKC) were inhibited with IC50s greater than 50μM. VEGFR2 was inhibited with an IC50 of 100-200nm in the fibroblast cell line NIH3T3. PD binds the ATP-binding site of FGFRs via the formation of hydrogen bonds and van der Waal forces, competitively inhibiting ATP-binding (Mohammadi *et al.*, 1998).

PD has been found to reduce cell viability in bladder cancer cell lines which express point mutated FGFR3 or FGFR3-TACC3 fusion proteins (Herrera-Abreu *et al.*, 2013; Lamont *et al.*, 2011; Miyake *et al.*, 2010). Lamont *et al.* reported RT112 and RT4 to have IC50s of 15nM and 5nM in PD respectively. Herrera-Abreu *et al.* reported a half maximal effective concentration (EC50) of 27nM in RT112. FGFR TKIs including PD have been used previously to study resistance in FGFR-expressing cell lines including RT112 and RT4. The findings of these previous studies are summarised in section 1.4.2 of the Introduction. This chapter will describe how isogenic resistant lines were derived from parental RT112 and RT4 and compare the morphology, cell proliferation and sensitivity to PD of parental and resistant lines. Expression of FGFR3 and, due to a morphological change in some resistant lines, markers of epithelial-mesenchymal transition (EMT) were examined.

3.2 Results

3.2.1 Derivation of resistant lines

RT112 and RT4 resistant derivatives were derived by long-term culture in PD by Helen McPherson. Characterisation of resistant derivatives was not conducted prior to this project. 1μM was selected as the initial concentration of PD to culture parental RT112 and RT4 in to generate resistant derivatives. This was because PD exerted maximal effect on the growth of RT112 and RT4 at these concentrations but some RT112 and RT4 cells could survive in these PD concentrations. RT112 was cultured in PD for a total of 21 passages in order to generate isogenic resistant derivatives (Fig. 3.1). Cells were passaged when 90% confluent throughout the generation of resistant derivatives. Parental RT112 was cultured in 1μM PD and split 1 in 2 between passages 40 and 43. This took 74 days. At passage 43 two sublines were created, one which was split 1 in 3 and one split 1 in 5 for the rest of the resistant line derivation. The subline split 1 in 3 was cultured until passage 45, 15 days later, when this subline was further split to produce two sublines. One continued to be cultured in 1μM PD and the other was cultured in 2μM PD. The subline cultured 1 in 3 in 1μM PD was cultured for a further 117 days when it was frozen down at passage 61 and termed R1. The subline cultured 1 in 3 in 2μM PD was cultured for a further 120 days from passage 45 when it was frozen down at passage 61 and called R2. The subline split 1 in 5 was cultured in 1μM PD for a further 135 days from passage 43. Stocks of this resistant derivative were frozen at passage 61. This resistant derivative was termed R3.

Initially during the derivation of RT112 R1, R2 and R3 the media contained many floating dead cells. The number of floating cells in all sublines had reduced by passage 52. RT112 parental cells grow as a tightly packed layer of small epithelial cells when cultured without PD. Treatment with PD induced RT112 to have a spindle-shaped mesenchymal morphology with a loss of intercellular adhesion. (Fig. 3.2). The cells gradually began to proliferate at a faster rate, based upon the time taken to reach confluence between passages.

RT4 R1 was produced by long-term culture of RT4 in 1μM PD for 211 days from passage 12 to passage 28, splitting at 90% confluence (Fig. 3.1). At passage 28 the resistant derivative was frozen down and termed RT4 R1. With the initial PD treatment, as with RT112, there were many dead floating cells. The number of floating cells had reduced by passage 23. During the treatment with PD the RT4 cells became flatter and had many peripheral cytoplasmic extensions in contrast to

the morphology of RT4 when not cultured in PD (Fig. 3.3). Parental RT4 cells, cultured without PD, grow in tightly packed clusters. During the derivation of the RT4 resistant line, the RT4 cells continued to grow in clusters but did not grow on top of each other (Fig. 3.3). When initially treated with PD the RT4 cells stopped proliferating or proliferated very slowly. With continued PD treatment, the RT4 cells began proliferating at a faster rate. However, the proliferation rate continued to be slower than the rate observed in parental RT4. With both RT112 and RT4 there were no obvious pre-existing resistant cells or a specific time when resistance appeared to develop. The development of resistance was gradual. The morphology and proliferation rate of the final resistant derivatives is examined in sections 3.2.2 and 3.2.3. RT112 and RT4 resistant lines were maintained in their respective concentrations of PD at all times unless otherwise stated.

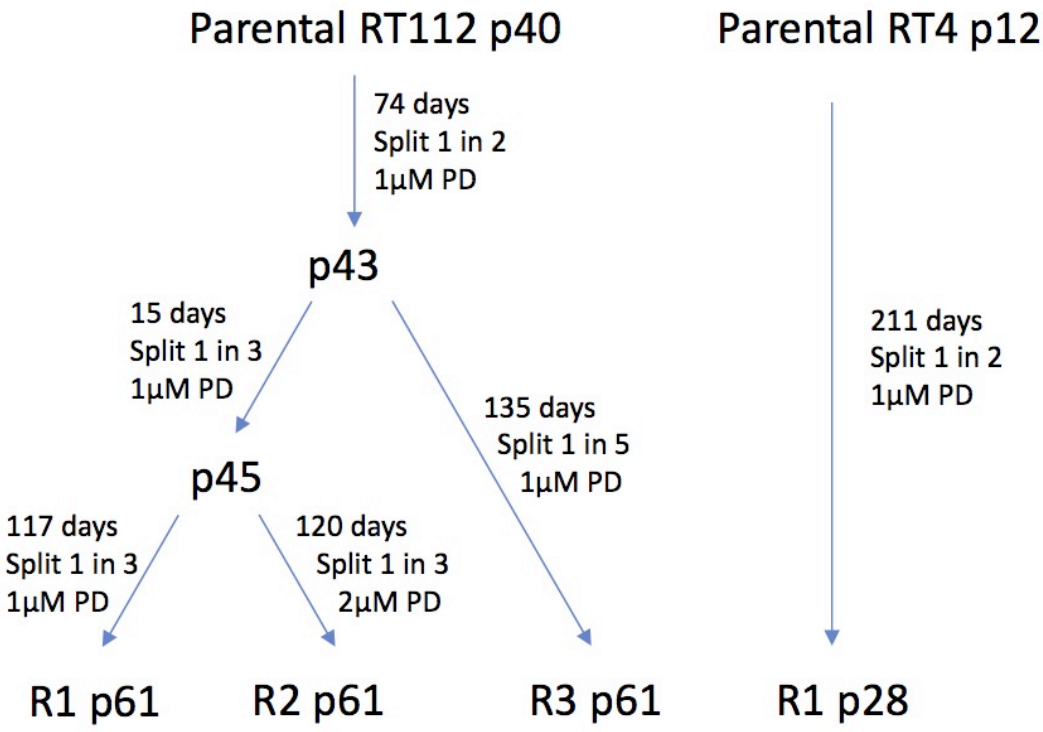

Figure 3.1 Derivation of resistant derivatives from parental RT112 and RT4. Passage number is denoted with a 'p' prior to the passage number.

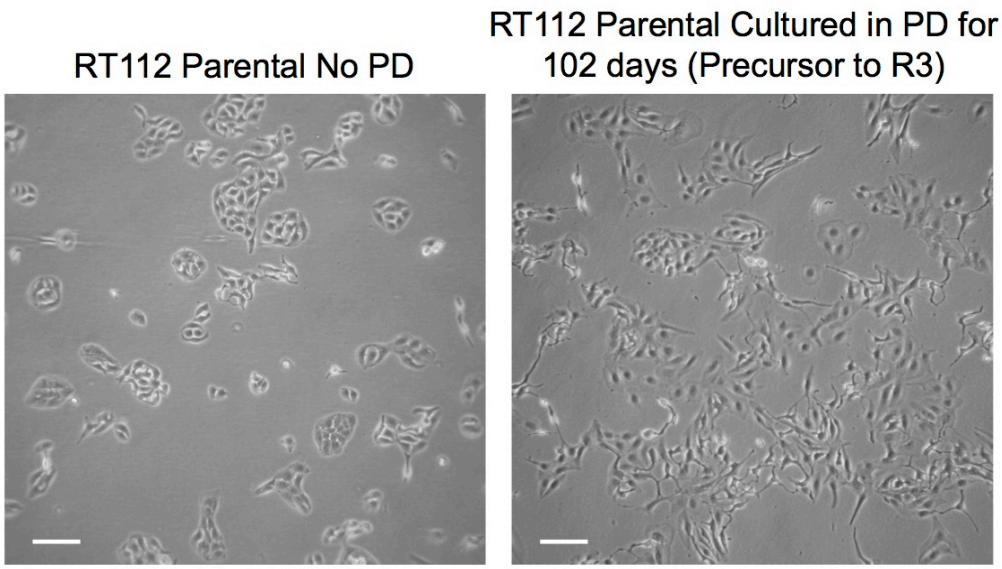

Figure 3.2 Morphology of parental RT112 in the presence and absence of PD173074. Images were taken with phase contrast microscopy. The white bar indicates 100μm.

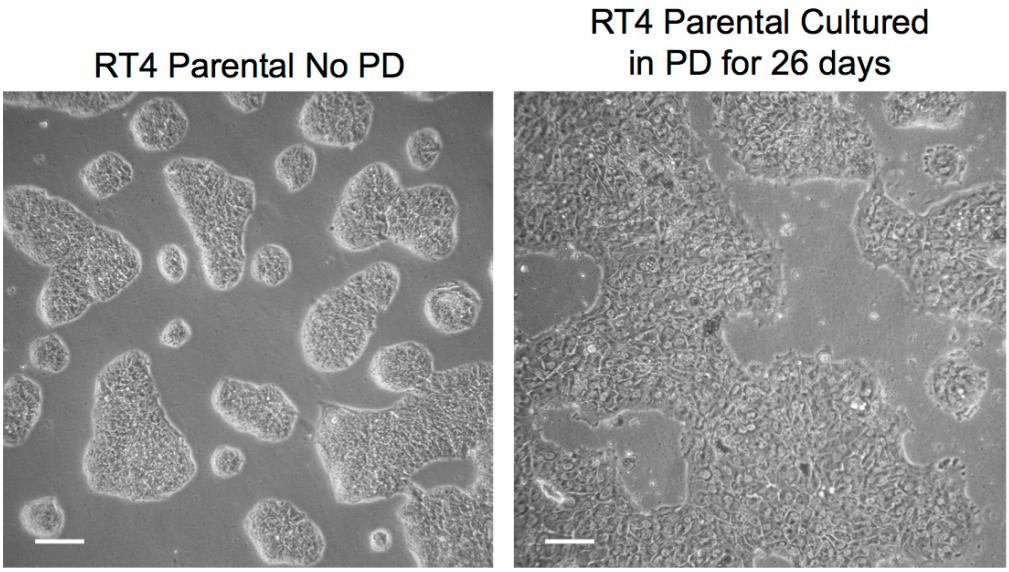

Figure 3.3 Morphology of parental RT4 in the presence and absence of PD173074. Images were taken with phase contrast microscopy. The white bar indicates 100μm.

3.2.2 Morphology of resistant lines cultured with and without PD173074

RT112 parental cells have an epithelial morphology when cultured with no PD. This is in contrast to the mesenchymal morphology observed during the derivation of resistant lines by long-term culture of RT112 parental in PD (Fig. 3.2). RT112 R1 and R2 cultured in PD exhibited a mesenchymal morphology whilst R3 had a more epithelial morphology (Fig. 3.4). Wang *et al.* reported that RT112 cells cultured long-term in the FGFR TKIs BJG398 and ponatinib to produce RT112 resistant derivatives exhibited a mesenchymal morphology. It was found that removal of the

FGFR TKIs resulted in the derivatives regaining an epithelial morphology within 2-4 weeks (Wang *et al.*, 2014). In order to determine if resistance to PD and the morphological change observed in R1 and R2 were dependent on continual culture in PD, RT112 resistant derivatives were cultured without PD. Following culture for 2 passages without PD, approximately 2 weeks, the cells reverted to an epithelial morphology (Fig. 3.5).

RT4 parental cells, RT4 R1 cells cultured in PD and R1 cells cultured without PD for 4 passages are pictured in Fig. 3.6. RT4 has an epithelial morphology and RT4 grow as a tall palisade of tightly clustered cells rather than spreading out across the culture surface. RT4 R1 also grows in clusters but the cells have many cytoplasmic extensions. These cytoplasmic extensions are not observed in RT4 parental. RT4 R1 regained a morphology similar to RT4 parental after being cultured without PD for 2 passages.

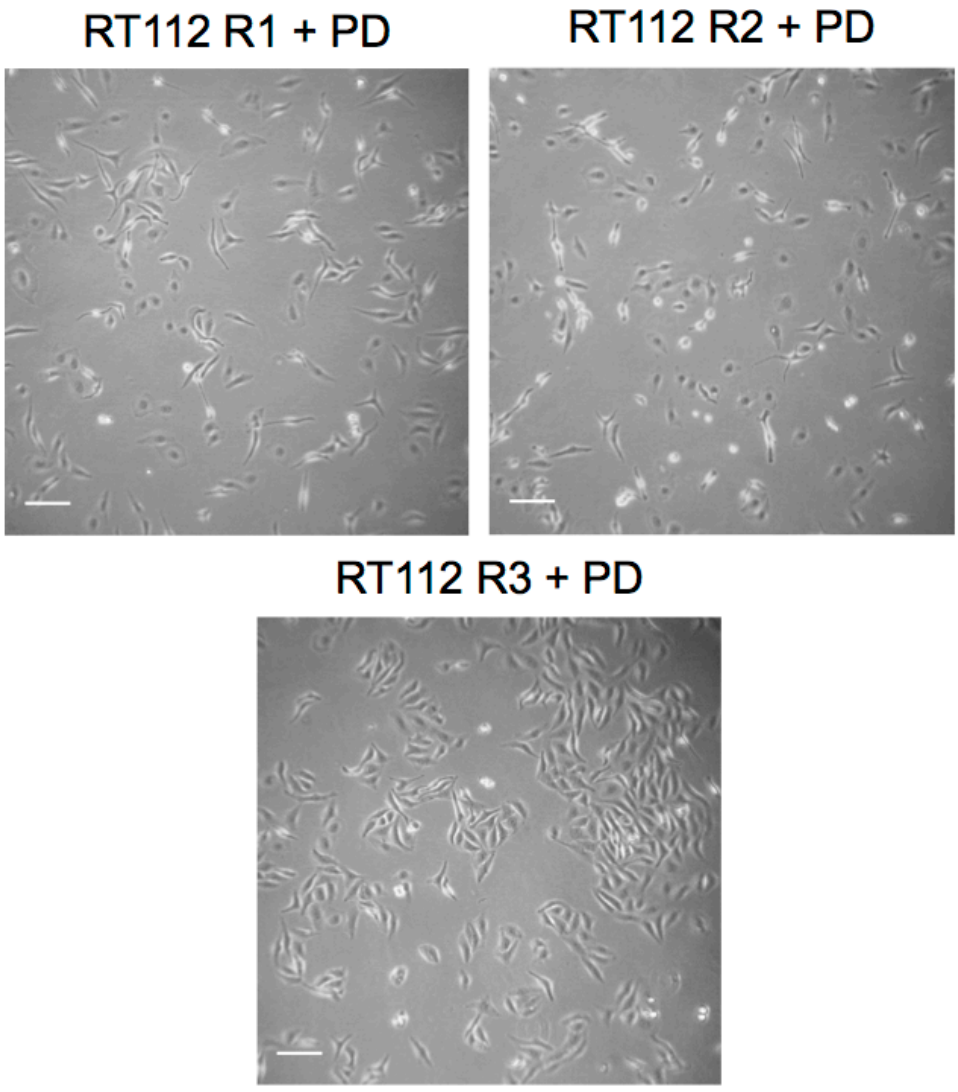

Figure 3.4 Morphology of RT112 resistant derivatives. Images were taken with phase contrast microscopy. The white bar indicates 100μm.

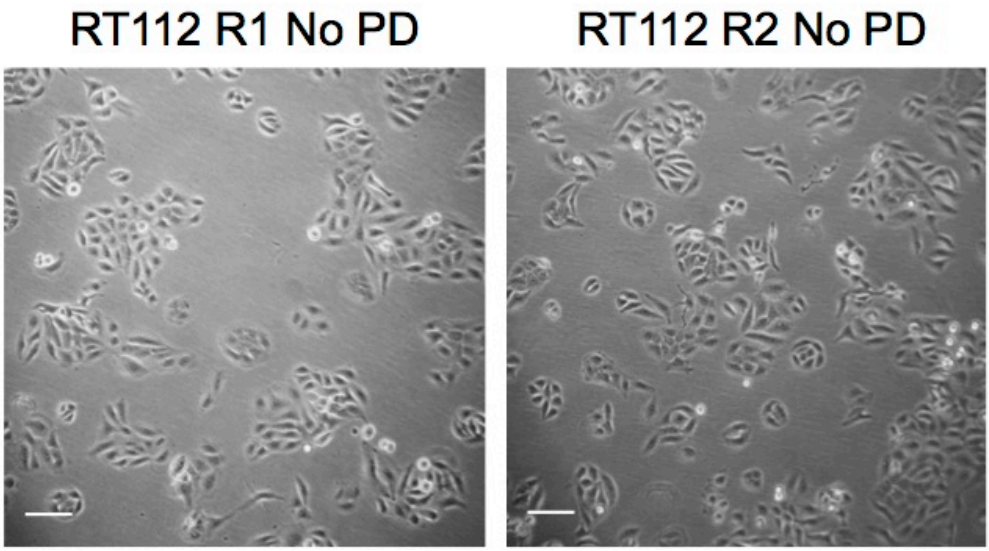

Figure 3.5 Morphology of RT112 R1 and R2 cultured without PD for 4 passages. Images were taken with phase contrast microscopy. The white bar indicates 100μm.

3.2.3 Proliferation of parental and resistant lines

To determine if the cell density at confluence and growth rate of the RT112 resistant lines differed from parental RT112, proliferation assays were conducted with RT112 parental, R1, R2 and R3 and growth curves constructed (Fig. 3.7). RT112 parental was cultured in medium not supplemented with PD. R1 and R3 were cultured in 1μM PD and R2 was cultured in 2μM PD. Parental RT112 reached a final density of 6.65 x 10^6 cells/well whereas R1 and R2 reached a final density of 8.38 x 10^5 cells/well and 1.06 x 10^6 cells/well respectively. R3 reached a final density of 1.64 x 10^6 cells/well. It seemed likely that PD was limiting the proliferation of RT112 resistant derivatives, rather than the resistant cells having an intrinsically slower growth rate than RT112 parental. To test this, RT112 resistant derivatives were cultured out of PD for 4 passages, 3-5 weeks, and proliferation assays were conducted with these cells without PD. Population doubling times were calculated for RT112 parental and resistant derivatives and are summarised in Table 3.1. The doubling time was shortest for RT112 parental not cultured with PD at 25.6 h. R2 and R3 cultured in PD both had doubling times of 38.2 h and R1 + PD had the longest doubling time of 51.1 h. The doubling times of R1 and R2 were reduced, 31.3 h and 34.5 h respectively, when cultured without PD (Table 3.1). The doubling time of parental + PD and R3 no PD was not examined. These results indicate that PD treatment hampered proliferation and cell density at confluence of the RT112 resistant lines despite these lines exhibiting PD resistance. The reduced rate of cell

proliferation in RT112 R1 and R2 was partially reversed when the cells were cultured in the absence of PD for 4 passages.

Proliferation assays were not conducted in RT4 parental and RT4 R1. However, from cell culture it was apparent that RT4 R1 cultured in PD proliferated at a slower rate than RT4 parental cultured without PD. It was also clear that, despite the long-term culture in PD during the production of RT4 R1, the proliferation rate of RT4 R1 increased upon culture without PD.

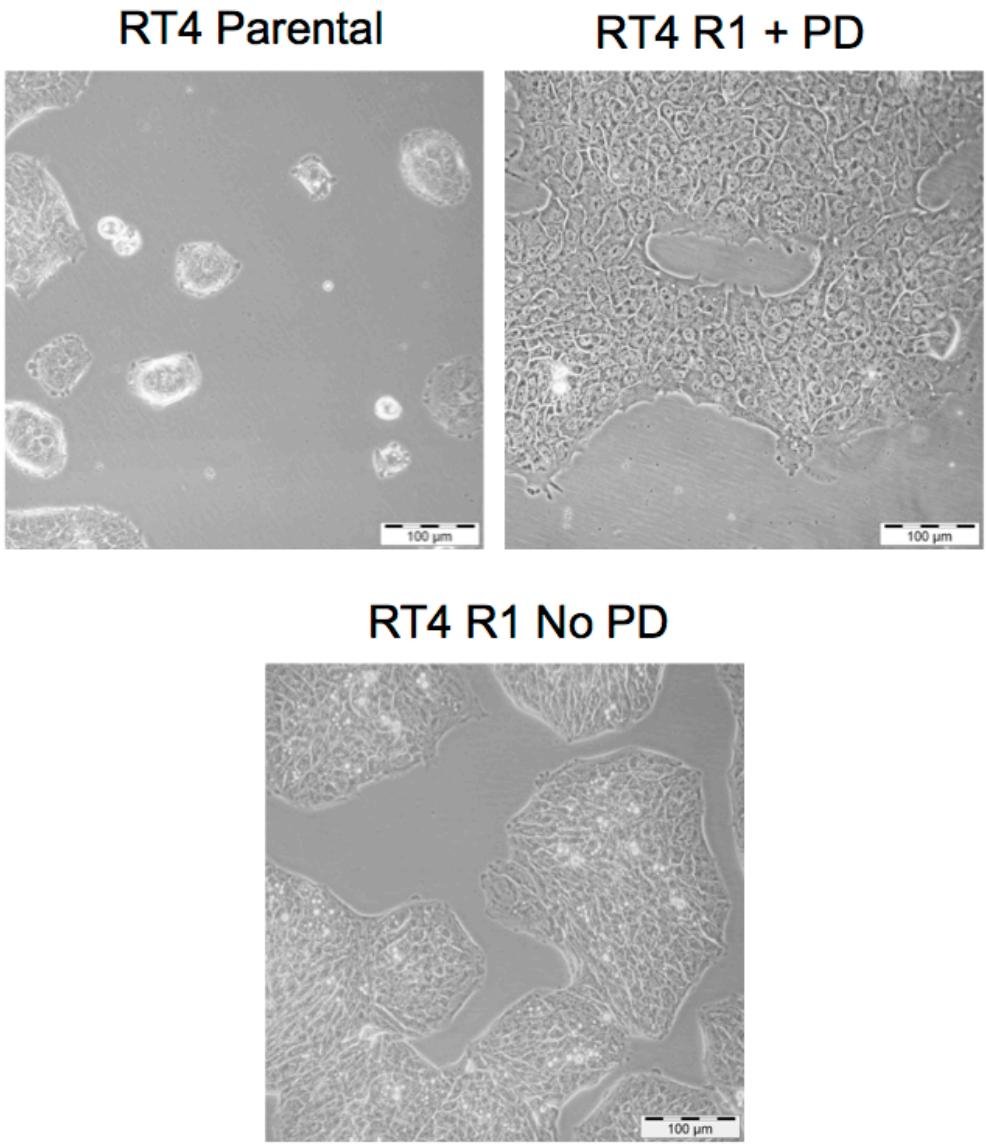

Figure 3.6 Morphology of RT4 parental cultured without PD, RT4 R1 cultured with PD and R1 cultured without PD for 4 passages. Images were taken with phase contrast microscopy.

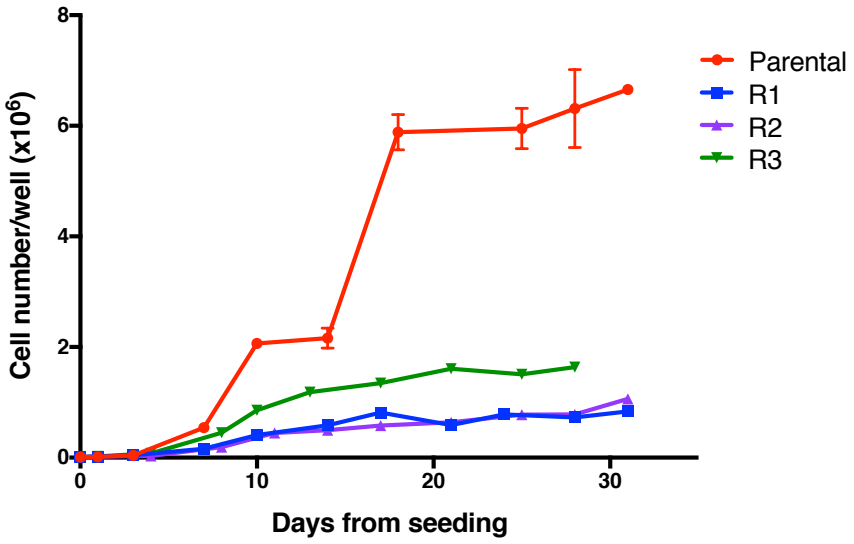

Figure 3.7 Growth curves for RT112 parental and resistant derivatives. Cells were seeded in 6 well plates, with a growth area of approximately 9.5 cm² per well, at a density of 1 x 10^4 cells/well in 2ml of medium. RT112 parental was cultured in media not supplemented with PD. R1 and R3 were cultured in 1μM PD and R2 was cultured in 2μM PD. Error bars show standard error of the mean. GraphPad Prism software was unable to plot some error bars due to small standard error of the mean.

Table 3.1 RT112 parental and resistant derivative doubling times. Cells were seeded in 6 well plates, with a cell growth area of approximately 9.5 cm² per well, at a density of 1 x 10^4 cells/well in 2ml of medium. RT112 R1 and R2 were cultured without PD for 4 passages prior to seeding for doubling time experiments. Doubling times were calculated from cell counts at days 3 and 7 or 4 and 8 post seeding. ND stands for no data.

RT112 line	Doubling time (h) Cells cultured without PD173074	Doubling time (h) Cells cultured with PD173074
Parental	25.6	ND
R1	31.3	51.1
R2	34.5	38.2
R3	ND	38.2

3.2.4 Sensitivity to PD173074

To examine the sensitivity of RT112 parental and RT112 resistant lines to PD, cell viability assays were conducted (Fig. 3.8). RT112 parental had 33% viability, R1 had 53% viability, R2 had 67% viability and R3 had 90% viability in 1μM PD relative to the vehicle control. Therefore, sensitivity to PD increased in the order R3 < R2 < R1 < parental. This confirmed that the derivatives had gained resistance to PD, with

R3 being most resistant and showing no sensitivity up to 1μM PD. Viability was approximately 30% in parental cells treated with between 0.1 and 1μM PD indicating that some parental cells survived this PD treatment. Parental RT112 had an IC50 of 36nM PD estimated from sigmoidal dose response curve plotted in GraphPad Prism®.

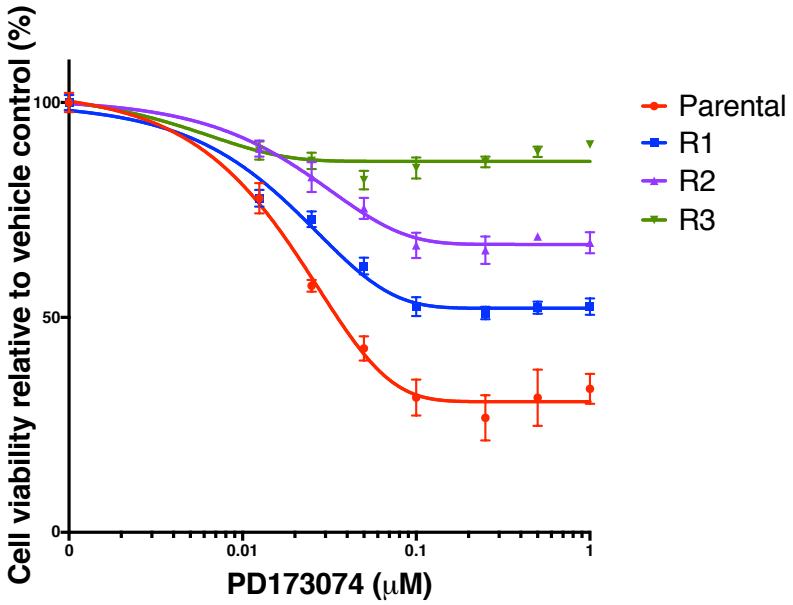

Figure 3.8 Cell viability of parental RT112 and resistant derivatives in PD173074. Viability of cells was assayed following 120 h treatment with PD173074 and normalised to the vehicle control. Error bars show standard error of the mean. This assay was repeated 3 times and a representative example is shown. Sigmoidal dose response curve was plotted in GraphPad Prism®. GraphPad Prism® software was unable to plot some error bars due to small standard error of the mean.

We had observed that RT112 R1 and R2 cells regained an epithelial morphology similar to parental RT112 following culture without PD for 2 passages (approximately 2 weeks). To determine if sensitivity to PD was retained following culture without PD and a return to an epithelial morphology, resistant derivatives were cultured without PD for 4 passages, 3-5 weeks, and viability in 1μM PD was examined (Fig. 3.9). Despite R1 and R2 reverting to an epithelial morphology the cells remained resistant to PD compared to RT112 parental. However, the difference in sensitivity to PD between RT112 R1 cultured without PD and the parental line was not striking. R3 also retained PD resistance compared to RT112 parental. In this aspect RT112 R1, R2 and R3 differed from the mesenchymal-like BGJ398 and ponatinib resistant RT112 derivatives described by Wang *et. al.* Upon culture without PD for 2-4 weeks and morphological reversion, these RT112

resistant cells were almost as sensitive to FGFR inhibition as parental RT112 (Wang *et al.*, 2014).

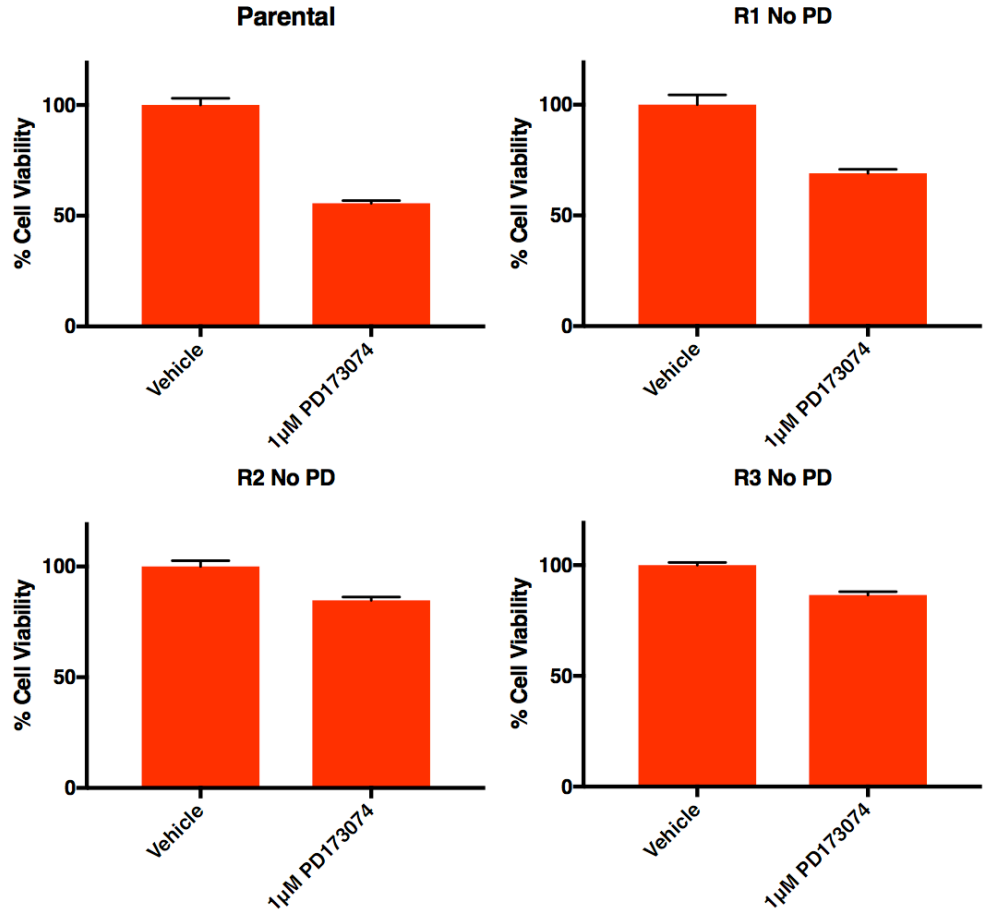

Figure 3.9 Cell viability of parental RT112 and resistant derivatives in PD173074 following a drug holiday. Resistant derivatives were cultured without PD173074 for 4 passages (3-5 weeks). Viability of cells was assayed following 120 h treatment with PD173074 and normalised to the vehicle control. Error bars show standard error of the mean. This assay was repeated twice and a representative example is shown.

To determine if RT4 R1 was less sensitive to PD than RT4 parental and if RT4 R1 retained its resistance following culture without PD, viability assays were conducted. Sensitivity to PD was assessed in RT4 parental, R1 which had been cultured with PD and R1 cultured without PD for 4 passages (3-5 weeks) (Fig. 3.10). RT4 parental was sensitive to PD with an IC50 of 19nM. RT4 R1 + PD had some resistance to PD and did not reach IC50. R1 no PD was sensitive to PD with an IC50 of 17nM. IC50s were estimated from sigmoidal dose response curve plotted in GraphPad Prism®. RT4 parental had 11% viability, R1 cultured in PD had 55% viability and R1 cultured out of PD for 4 passages had 22% viability in 1μM PD relative to the vehicle control. These results indicate that RT4 R1 had gained resistance to PD but that this resistance was not maintained following culture

without PD. The sensitivity of RT4 R1 cultured without PD was in contrast to the RT112 PD resistant derivatives cultured without PD for the same number of passages, as these retained PD resistance.

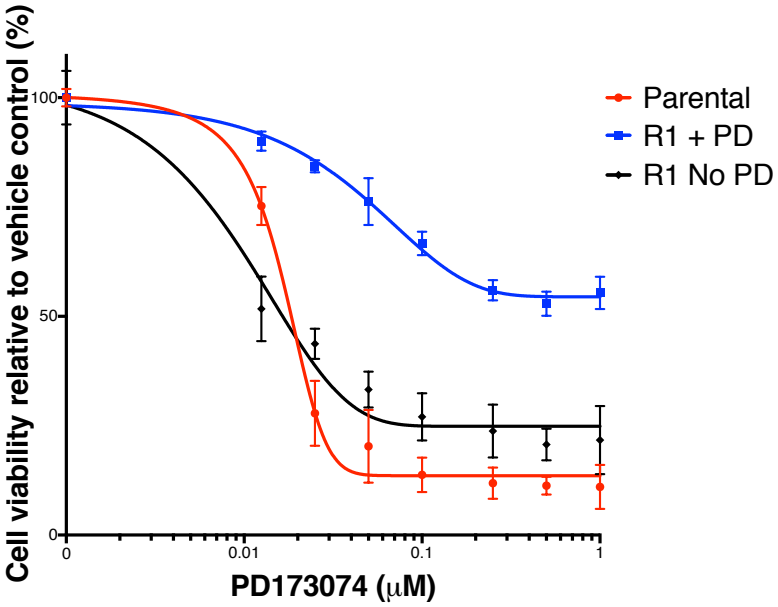

Figure 3.10 Cell viability of RT4 parental and R1 in PD173074. Viability of cells was assayed following 120 h treatment with PD173074 and normalised to the vehicle control. Error bars show standard error of the mean. This assay was repeated twice and a representative example is shown. Sigmoidal dose response curve was plotted in GraphPad Prism®.

3.2.5 Expression of FGFR3 and EMT markers

Due to the mesenchymal-like morphology observed in RT112 R1 and R2, expression of mesenchymal and epithelial markers was examined to determine if these cells had undergone an EMT. Cadherins are a class of membrane proteins which form part of the adherens junctions. Adherens junctions facilitate the attachment of neighbouring cells to one another (Singh *et al.*, 2017). FGFR3 expression is of clear importance due to the dependency of RT112 and RT4 on FGFR3 signalling and the specificity of PD for the FGFR family. In addition to this, FGFR3 expression has been associated with an epithelial phenotype in bladder cancer cell lines (Cheng *et al.*, 2009). Expression of FGFR3 and the mesenchymal marker N-cadherin were examined in RT112 parental and resistant derivatives (Fig. 3.11). Expression of FGFR3 was highest in parental cells cultured without PD and treated with PD for 24 h, lower in the resistant derivatives cultured without PD and lowest in the resistant derivatives cultured in PD. Herrera-Abreu *et al.* and Wang *et*

al. both reported that total FGFR3 expression is maintained in RT112 during 24 h treatment with an FGFR TKI (Herrera-Abreu *et al.*, 2013; Wang *et al.*, 2014). This is concordant with our results. N-cadherin was increased in RT112 R1 + PD and R2 + PD compared to the parental line cultured without PD. Like RT112 R1 and R2, the FGFR TKI resistant cells produced by Wang *et al.* had increased protein expression of N-cadherin.

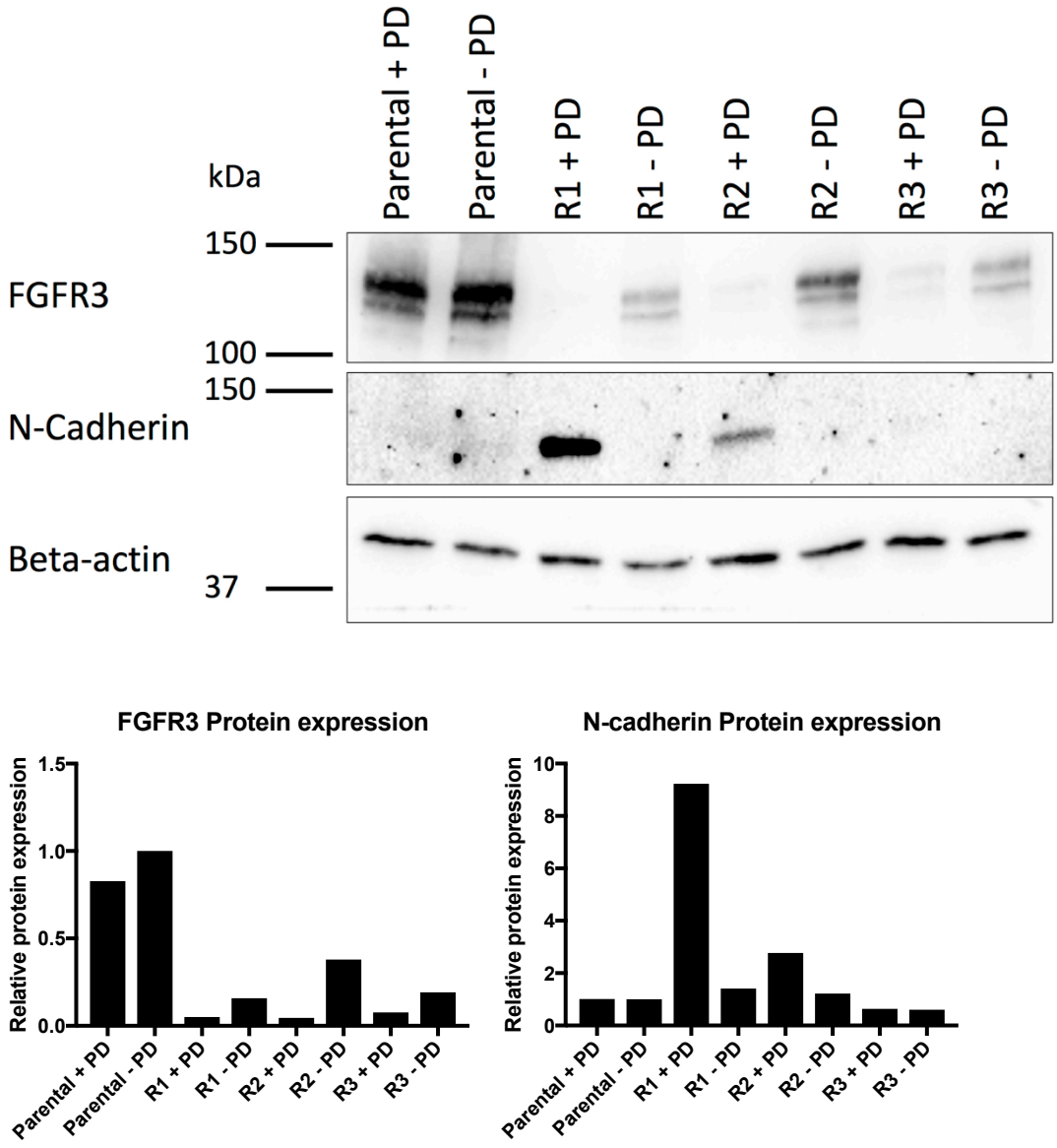

Figure 3.11 Immunoblot of FGFR3 and N-Cadherin protein expression in parental RT112 and resistant derivatives. A) Immunoblot analysis. B) Protein expression relative to parental – PD. Expression was examined in parental, parental treated with PD173074 for 24 h, R1, R2 and R3 cultured with PD173074 and R1, R2 and R3 cultured without PD173074 for 4 passages. β-actin was used as a loading control. Immunoblots were conducted three times and a representative example is shown. The immunoblot shown was used to normalise FGFR3 and N-cadherin relative to β-actin using Image Lab software.

Vimentin, a mesenchymal marker, provides mechanical strength to intermediate filaments. Intermediate filaments are a cytoskeleton component and vimentin makes intermediate filaments less likely be damaged during cell migration (Singh *et al.,* 2017). As expression of N-cadherin was increased in RT112 R1 and R2 cultured in PD, expression of the epithelial marker E-cadherin and vimentin was also examined in these resistant derivatives (Fig. 3.12). E-cadherin expression was not reduced in RT112 R1 and R2. Vimentin expression was increased in RT112 R1 and R2, though only by a small magnitude. RT112 R1 and R2 are therefore distinct from the Wang *et al.* resistant derivatives which had reduced expression of E-cadherin protein (Wang *et al.,* 2014). The results so far suggest that RT112 R1 and R2 have undergone a partial EMT. RT112 R3 appears to have not undergone an EMT.

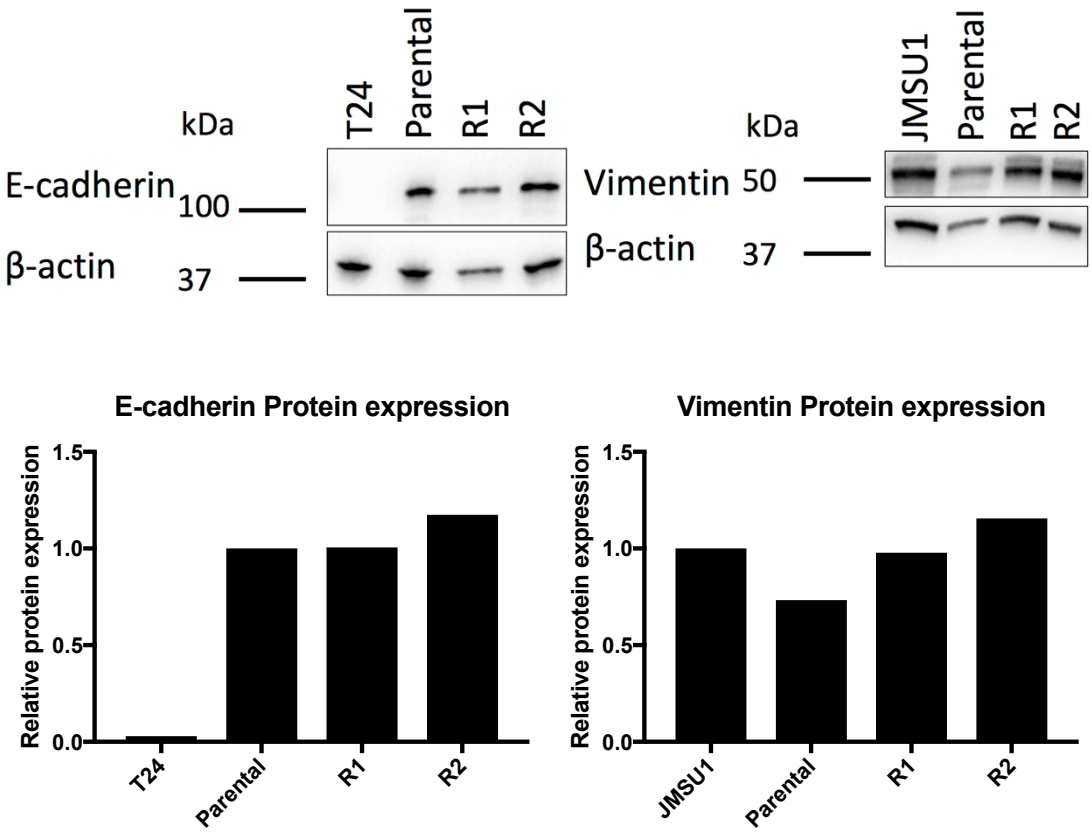

Figure 3.12 Immunoblot of E-Cadherin and vimentin protein expression in RT112 parental, R1 and R2. A) Immunoblot analysis. B) Relative protein expression. T24 was included as a negative control for E-cadherin and JMSU1 was included as a positive control for vimentin. β-actin was used as a loading control. Immunoblots were conducted three times and a representative example is shown. The expression of E-cadherin and vimentin relative to β-actin was calculated using Image Lab software. E-cadherin expression was quantified relative to RT112 parental and Vimentin was quantified relative to JMSU1.

To determine if EMT-like changes were present in RT4 R1 as observed in RT112 R1 and R2, expression of N-cadherin, vimentin, E-cadherin and FGFR3 were examined in RT4 parental and R1 (Fig. 3.13). The increase in expression of N-cadherin and decrease in expression of FGFR3 observed in RT112 R1 and R2 was not observed in RT4 R1. Vimentin expression was low in RT4 parental and RT4 R1. E-cadherin expression was not reduced in RT4 R1 relative to RT4 parental. These results indicate that RT4 R1 did not undergo an EMT during its derivation.

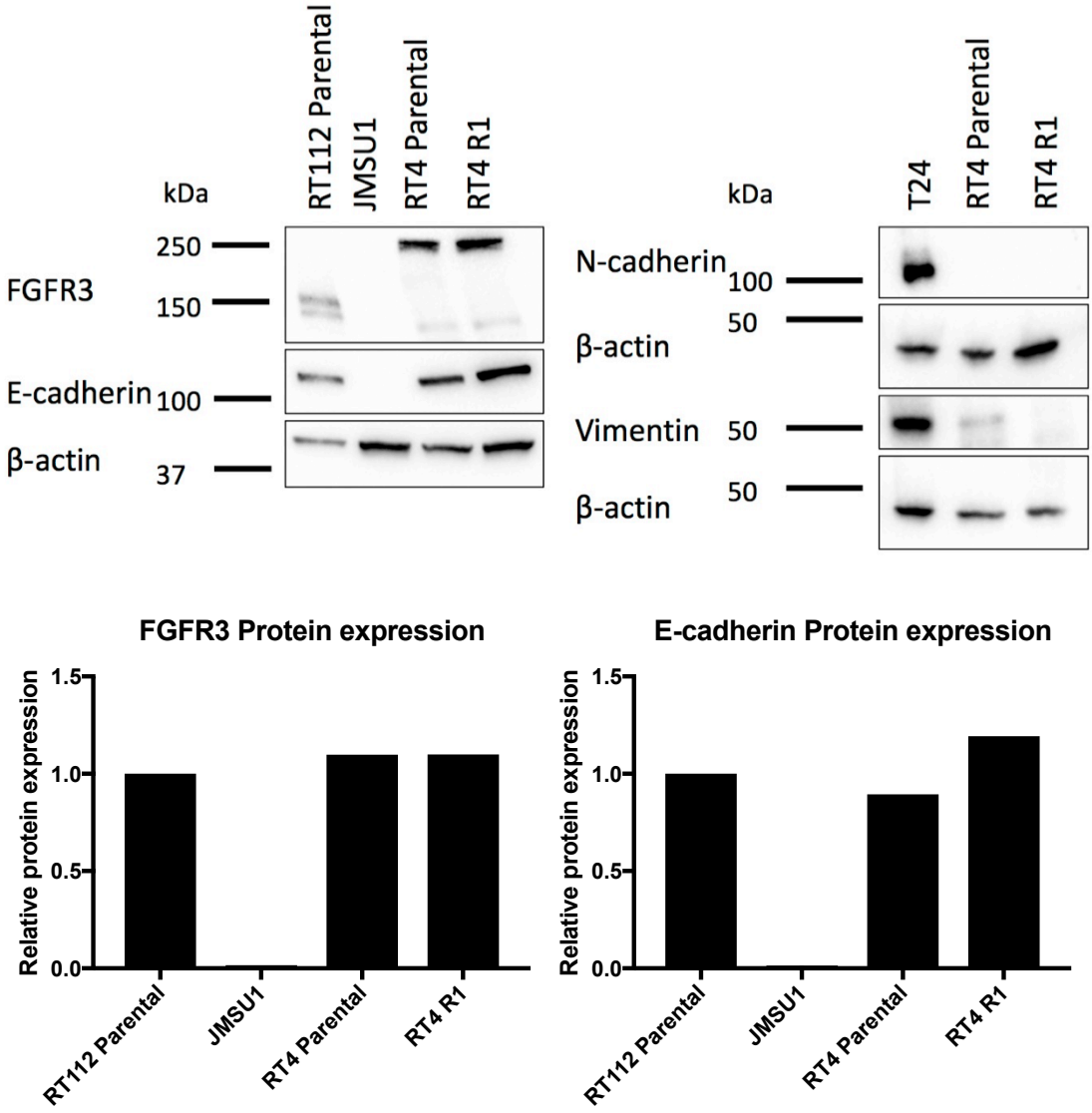

Figure 3.13 Immunoblot of N-cadherin, vimentin FGFR3 and E-Cadherin protein expression in RT4 parental and R1. A) Immunoblot analysis. B) Protein expression relative to parental RT112. T24 was included as a positive control for N-cadherin and vimentin. RT112 parental and JMSU1 were included as positive and negative controls for FGFR3 and E-cadherin respectively. β-actin was used as a loading control. Immunoblots were conducted three times and a representative example is shown. The expression of FGFR3 and E-cadherin relative to β-actin was calculated using Image Lab software. FGFR3 and E-cadherin expression were quantified relative to RT112 parental.

3.3 Discussion

The sensitivity of RT112 to PD has previously been examined. Lamont *et al.* found RT112 to have an IC50 of 15nM and 10-20% viability in 1μM PD in a 120 h assay (Lamont *et al.*, 2011). Herrera-Abreu *et al.* found RT112 to have an EC50 of 27nM and a cell viability of 36% in 1μM PD in a 72 h assay (Herrera-Abreu *et al.*, 2013). In this study, it was found that the viability of RT112 in PD was not entirely abolished with viability approximately 1/3 of the vehicle control in parental cells treated with between 0.1 and 1μM PD. The viability of RT4 parental was not abolished with PD with approximately 12% viability relative to the vehicle control being maintained with treatment with between 0.1 and 1μM PD. This indicates that some RT112 and RT4 parental cells were able to survive PD treatment. Lamont *et al.* reported RT4 to have an IC50 of 5nM in a 120 h assay, whereas we found RT4 to have an IC50 of 19nM in an assay of the same time length (Lamont *et al.*, 2011). The differences in the viability results between Herrera-Abreu *et al.* and Lamont *et al.* and our viability assays could be due to differences in methodology. Herrera-Abreu *et al.* treated with PD for 72 h and assayed viability with CellTiter-Glo whereas for our assay, PD treatment was for 120 h and viability was assessed with Cell-Titer Blue. Herrera-Abreu *et al.* calculated an EC50 whereas we calculated an IC50. Lamont *et al.* treated with PD for 120 h, similar to our assay but changed media 48 h post PD treatment whereas in our assay medium was replaced after 72 h. Lamont *et al.* assessed viability with a 3-(4,5-dimethylthiazol)-2,5-diphenyl tetrazolium (MTT) assay. The RT112 used by Herrera-Abreu *et al.* was obtained from the same laboratory in which this project was conducted. The Lamont *et al.* paper was produced in the same laboratory as this project. It is therefore unlikely that the observed differences in viability are due to differences in the RT112 and RT4 cells used. There was large variability between individual cell viability assays, for example, in figure 3.8 the cell viability of parental RT112 treated with 1μM PD was reduced to 33% whereas in figure 3.9 the viability of RT112 parental treated with 1μM PD was reduced to approximately 50%. Therefore, it is not possible to draw conclusions by comparing the results of different viability assays. It would have been beneficial to have included the resistant lines cultured in PD as a control when the resistant lines cultured out of PD were assayed for their PD resistance. This would have determined whether the RT112 resistant lines maintained the same level of PD resistance when cultured with and without PD rather than simply demonstrating that the resistant derivatives cultured out of PD were more resistant than parental RT112. Additionally, for each cell viability experiment it would have

been more reliable to have presented the average of the cell viability assay repeats, rather than presenting one representative example. This would have enabled a statistical test to have been conducted to determine whether observed differences in viability were significant.

RT112 R1, RT112 R2 and RT4 R1 cells had a different morphology from their parental lines. These resistant lines returned to the parental morphology upon culture without PD. RT112 R1 and R2 retained their resistance to PD following culture without PD whereas RT4 R1 did not. RT112 R3 was distinct from RT112 R1, RT112 R2 and RT4 R1 in that it retained the epithelial morphology of its parental line. Despite the mesenchymal-like morphology of RT112 R1 and R2 cultured in PD these cells did not appear to have undergone a complete EMT. Expression of E-cadherin was not decreased in these resistant derivatives. Expression of N-cadherin and vimentin was increased suggesting that RT112 R1 and R2 had undergone a partial EMT. No evidence was found to suggest that RT4 R1 had undergone an EMT. However, the analysis of epithelial and mesenchymal markers was limited to only a few proteins and therefore it is possible that RT4 R1 or RT112 R3 may have also undergone some expression changes associated with an EMT. In bladder cancer cell lines, expression of FGFR3 has been associated with an epithelial phenotype, in contrast to FGFR1 expression which has been associated with a mesenchymal phenotype (Cheng *et al.*, 2013). Hanze *et al.* found that phenotypically mesenchymal bladder cancer cell lines were more resistant to the FGFR TKI dovitinib than epithelial bladder cancer cell lines (Hanze *et al.*, 2013). This could be related to the activation of FGFR3 versus FGFR1 signalling in these lines, as there was some overlap between the panel of bladder cancer cell lines examined by Cheng *et al.* and Hanze *et al.* Therefore, a shift from an epithelial phenotype to a more mesenchymal phenotype as a result of FGFR inhibition is logical in the FGFR3-dependent lines used in this project. This switch to a more mesenchymal phenotype is of interest as a mesenchymal phenotype is associated with greater cell migration and invasion. Therefore, if FGFR inhibitors induce an EMT in patients this could lead to tumour metastasis (Singh *et al.*, 2017).

Some studies examining the response of RT112 to FGFR inhibition, which have focused on the short-term mechanisms of survival, have not detailed EMT-like changes occurring in RT112 (Harbinski *et al.*, 2012; Herrera-Abreu *et al.*, 2013; Wang *et al.*, 2017b). This would be expected as this study found that the EMT-like morphological changes in RT112 became apparent only after long-term culture in PD rather than acute exposure. Wang *et al.* reported a mesenchymal morphology, increased cell migration, increased protein expression of the mesenchymal markers

fibronectin and N-cadherin and reduced expression of E-cadherin with long-term culture of RT112 in the FGFR TKIs BGJ398 and ponatinib. They derived resistant cells via gradual increase in exposure to the TKI and treatment with an initial high dose of TKI. These changes were reversed upon culturing the cells out of drug for 2-4 weeks. In contrast to our RT112 resistant derivatives which maintained their resistance following culture out of PD for 4 passages, the Wang *et al.* resistant cells did not maintain their FGFR TKI resistance following culture without drug for 2-4 weeks. Wang *et al.* do not detail the time taken to derive their resistant cells (Wang *et al.*, 2014). Our RT4 resistant derivative, RT4 R1, did re-acquire PD sensitivity when cultured out of PD for 4 passages. If resistance to FGFR inhibition could be reversed in patients simply by pausing treatment with the FGFR TKI, then this would be an ideal way to overcome the resistance as it avoids the use of potentially toxic drug combinations. Our results suggest that pausing treatment would not induce the cancer cells to revert to sensitivity to an FGFR TKI in all cases. However, our RT112 resistant derivatives may have re-acquired sensitivity to PD if cultured out of PD for a greater length of time.

The rapid reversibility of the phenotypes of RT112 R1, RT112 R2 and RT4 R1 indicates that the phenotypic changes are induced by alterations in transcription rather than via stable genomic changes. The altered transcription is likely to be mediated by epigenetic modifications. Sharma *et al.*, reported that a treatment of the NSCLC cell line PC-9 with the EGFR TKIs gefitinib or erlotinib for 9 days yielded a population of drug tolerant cells with increased protein expression of the histone demethylase KDM5A. KDM5A demethylates lysine 4 of histone 3 (H3K4me2 and H3K4me3) thereby repressing transcription (Santos-Rosa *et al.*, 2002). KDM5A promotes cell proliferation and inhibits cell differentiation, this activity is modulated by the tumour suppressor *RB1* (Benevolenskaya *et al.*, 2005; Lin *et al.*, 2011). Knockdown of *KDM5A* with RNA interference significantly reduced the number of drug tolerant PC-9 cells generated by culture in an EGFR TKI (Sharma *et al.*, 2010). Hypermethylation of *PDLIM4* which encodes PDZ and LIM domain protein 4 has been associated with shortened survival in CML patients treated with imatinib. Gene hypermethylation normally reduces gene transcription, therefore this epigenetic alteration may induce imatinib resistance by reducing PDLIM4 inactivation of the tyrosine kinase Src (Jelinek *et al.*, 2011). Roh *et al.* reported that, in the urothelial carcinoma cell lines KU-7 and 5637, overexpression and knockdown of *FOXM1* significantly increased and decreased cell viability in the presence of the chemotherapeutic agent doxorubicin respectively. FOXM1 is a global regulator of DNA methylation. FOXM1 was shown to regulate expression of

ABCG2 and drug efflux. ABCG2 is a member of the ATP-binding cassette (ABC) transporter family which induce drug resistance via drug efflux (Roh *et al.*, 2018; Teh *et al.*, 2012). As epigenetic alterations are heritable, it is possible that an epigenetic alteration maintains expression changes in RT112 R1 and R2 following the culture of these cells without PD for 4 passages. An epigenetic alteration could therefore enable the persistence of the PD resistant in RT112 R1 and R2.

The reduction in FGFR3 expression in the RT112 PD resistant derivatives suggests that signalling via FGFR3 in these cells is reduced and indicates that FGFR3 overexpression or mutation or drug efflux is not the cause of resistance in these cells. Resistance could be mediated by activation of an alternative RTK, as has been described previously in response to FGFR TKIs in RT112. Harbinski *et al.* showed that inducing expression of HGF, NRG1, NRG2 or TGF-α in RT112 could mediate short-term survival to exposure to PD in RT112 (Harbinski *et al.*, 2012). Herrera-Abreu *et al.* identified EGFR signalling as mediating short-term survival to PD in RT112 (Herrera-Abreu *et al.*, 2013). Wang *et al.* produced RT112 resistant derivatives via long-term culture in FGFR inhibitors which owed their resistant phenotype to the activation of ERBB2 and ERBB3 (Wang *et al.*, 2014). As RT112 R3 is able to maintain a phenotype more similar to its parental line than RT112 R1, RT112 R2 or RT4 R1, this resistant derivative may have developed resistance via a mutation. A V555M mutation in the FGFR3 kinase domain was reported in KMS-11, a myeloma cell line, following long-term treatment with a FGFR TKI, AZ12908010. This mutation prevents the binding of TKIs to the ATP-binding site (Chell *et al.*, 2013). However, as FGFR3 expression was downregulated in R3, it is unlikely that resistance has arisen in this line via a mutation in *FGFR3*. Alternative genetic mechanisms by which resistance may have arisen include other mutations in *FGFR3* which induce activity by a different mechanism, an activating mutation in a different RTK, or mutation in a signalling molecule downstream of FGFR3. Chapter 5 will examine if there is a genetic mechanism of resistance in the RT112 and RT4 resistant derivatives.

Chapter 4
Receptor Tyrosine Kinase Signalling

4.1 Introduction

FGFR3 expression is associated with an epithelial morphology and FGFR1 expression is associated with a mesenchymal morphology in bladder cancer cell lines (Cheng *et al.*, 2013; Tomlinson *et al.*, 2012). It was therefore thought that RT112 R1 and R2, which have a more mesenchymal morphology, could have increased activation of FGFR1, possibly by altered FGF expression. FGFR1, FGF1 and FGF2 expression was examined in this Chapter for this reason. However, any mechanism which induced FGFR1 activation in the resistant lines would have to overcome the inhibition of FGFR1 by PD, which inhibits FGFR1-3 (Mohammadi *et al.*, 1998; Pardo *et al.*, 2009; Trudel *et al.*, 2004). Activation of an alternative RTK is a commonly reported mechanism of resistance to targeted agents. Such activation of a replacement RTK would re-activate intracellular signalling pathways inhibited by FGFR3 inhibition. Wang *et al.* found RT112 activated ERBB2 and ERBB3 signalling as a mechanism of resistance to the FGFR TKIs BGJ398 and ponatinib upon long-term culture in these inhibitors (Wang *et al.*, 2014). Herrera-Abreu *et al.* identified EGFR activation as a mechanism of short-term survival in RT112 treated with PD (Herrera-Abreu *et al.*, 2013). Harbinski *et al.* identified MET activation by HGF as a mechanism of short-term survival in response to BGJ398 (Harbinski *et al.*, 2012). This previously conducted research is examined in section 1.4.2 of the Introduction. As these RTKs had been previously implicated in FGFR TKI resistance it was imperative to examine total expression and phosphorylation of EGFR family members and MET. Examination of RTK expression was conducted predominantly in RT112 R1, RT112 R2 and RT4 R1. This was because it was thought that RT112 R3 was the most likely resistant derivative to have a genetic mechanism of resistance because, compared to RT112 R1 and R2, it maintained a maximal cell density and morphology were more similar to RT112 parental. Exome sequencing will be conducted in Chapter 5 with the aim of determining whether RT112 R3 has a genetic mechanism of resistance. Expression and phosphorylation of AKT, a serine/threonine kinase which is part of the PI3 kinase pathway, and ERK, a serine/threonine kinase in the MAP kinase signalling cascade, will be examined in RT112 parental and resistant lines in this Chapter. The PI3 kinase and

MAP kinase pathways, amongst others, are activated by FGFR3 and are key determinants of cell proliferation and survival (di Martino *et al.*, 2016). Intracellular pathways activated in resistant cells could potentially be targeted as a mechanism to overcome resistance. For example, the PI3 kinase inhibitor BKM120 and FGFR TKI AZD4547 have been found to be synergistic in reducing cell proliferation in RT112 and urothelial carcinoma cell line JMSU1, which has amplification of *FGFR1* (Wang *et al.*, 2017b).

4.2 Results

4.2.1 FGFR and FGF expression

FGFR1 mutations are not found in bladder cancer but *FGFR1* DNA amplifications are reported albeit infrequently (Fischbach *et al.*, 2015). Cheng *et al.* examined a panel of bladder cancer cell lines and found FGFR3 dependence to be associated with an epithelial phenotype and FGFR1 dependence to be associated with a mesenchymal phenotype (Cheng *et al.*, 2013). Increased activation of FGFR1 could be a cause of resistance. However, PD is a pan-FGFR TKI, which inhibits FGFR1 with an IC50 in the nanomolar range (Mohammadi *et al.*, 1998). Therefore, a significant increase in protein expression or an FGFR1 gatekeeper mutation would be required to activate FGFR1 signalling. Exome sequencing, which is described in Chapter 5, will uncover any genetic alterations involving FGFR1 or other FGFRs. *FGFR1* and *FGFR3* expression was examined by qRT-PCR in the epithelial RT112 parental line as well as R1 and R2, which had undergone phenotypic changes associated with a mesenchymal phenotype (Fig. 4.1). *FGFR1* expression was significantly increased and *FGFR3* expression was significantly reduced in R1 and R2. The reduction in *FGFR3* mRNA expression is concordant with immunoblot analysis conducted in Chapter 3 which found reduced expression of FGFR3 protein in RT112 R1 and R2 (Fig. 3.11). Protein expression of FGFR1 was examined in RT112 parental, RT112 R1, RT112 R2, RT4 parental and RT4 R1 by immunoblot (Fig. 4.2). There was no increase in FGFR1 expression in the resistant derivatives compared to their parental lines. Expression of FGFR1 was low in all RT112 samples compared to the JMSU1 positive control. Therefore, the increased *FGFR1* mRNA expression in RT112 R1 and R2 did not result in a detectable increase in FGFR1 protein expression. Phosphorylation of FGFR1 was not examined.

However, the low expression of this receptor suggests that it is not inducing resistance in the resistant lines or inducing the EMT-associated changes observed in RT112 R1 and R2.

The FGFR family undergoes alternative splicing, mutually exclusively including exons 8 and 9 to produce isoforms with different specificities for FGFs. If exon 8 is included the IIIb isoform is produced whereas if exon 9 is included the IIIc isoform is produced. FGF1 activates FGFR1-3 IIIb and IIIc isoforms. FGF2 has a greater specificity for the IIIc isoforms of FGFR1-3 which are associated with a mesenchymal phenotype, rather than the IIIb isoforms associated with an epithelial morphology (Chellaiah *et al.*, 1994; Ornitz *et al.*, 1996; Zhang *et al.*, 2006). It was thought that differential expression of these FGFs could be inducing greater activation of IIIc rather than IIIb isoforms in RT112 R1 and R2. FGF1 and FGF2 expression was examined in RT112 parental, R1 and R2 by qRT-PCR (Fig. 4.3). Expression of FGF1 was not consistently higher or lower in R1 and R2 compared to parental in the 4 repeats of the qRT-PCR analysis. FGF2 levels were increased in R1 and R2 compared to parental by over 200-fold. However parental RT112 had a high cycle threshold and therefore the parental FGF2 mRNA level was low.

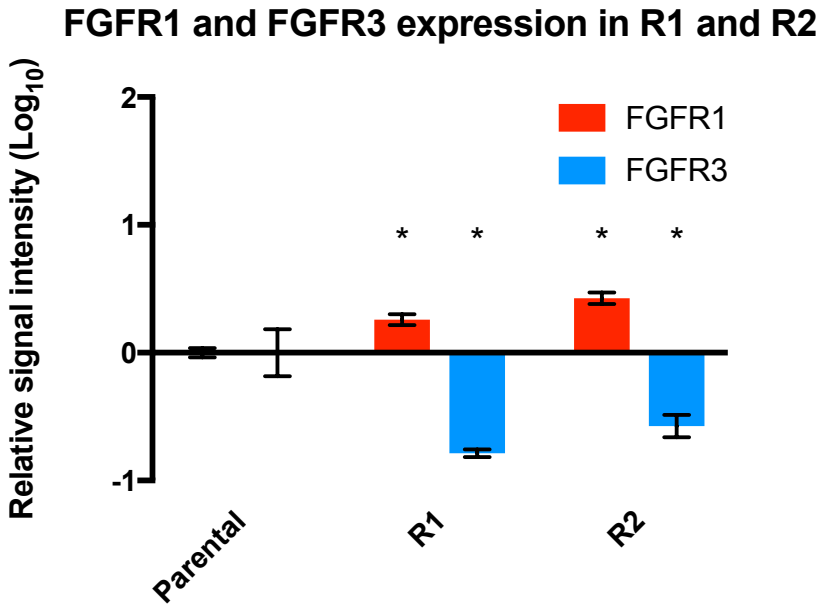

Figure 4.1 qRT-PCR of FGFR1 and FGFR3 in RT112 parental R1 and R2. Expression was normalised to parental to produce relative quantification values (RQ). Error bars indicate RQmin and RQmax which indicate the 95% confidence interval calculated by the 7500 Real-Time PCR System software. qRT-PCR was repeated 3 times and one representative result is shown. Resistant derivatives were tested against parental for significantly different gene expression with the Mann Whitney U test, two-tailed, $p<0.05$. Asterisks indicate which genes were significantly differentially expressed between resistant derivatives and parental cells.

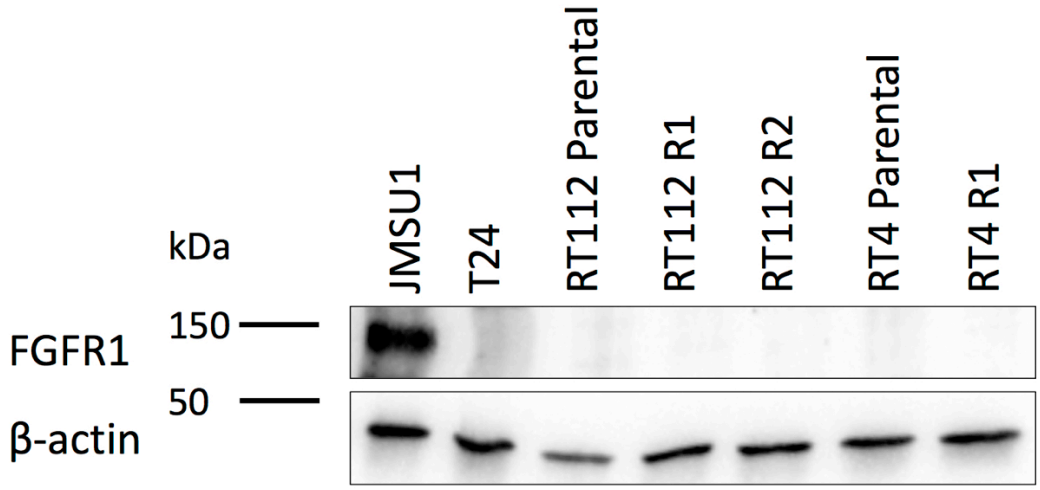

Figure 4.2 Immunoblot analysis of FGFR1 protein expression in RT112 and RT4. Expression was examined in RT112 parental, RT112 R1, RT112 R2, RT4 parental and RT4 R1. JMSU1 and T24 were included as positive and negative controls for FGFR1 respectively. β-actin was used as a loading control. Immunoblots were conducted three times and a representative example is shown.

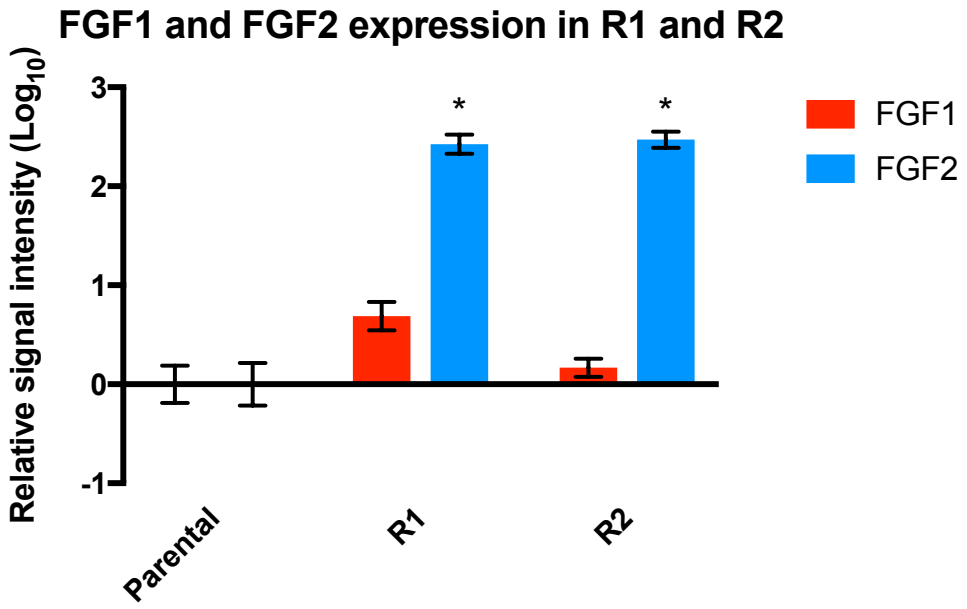

Figure 4.3 qRT-PCR of FGF1 and FGF2 in RT112 parental, R1 and R2. Expression was normalised to parental to produce relative quantification values (RQ). Error bars indicate RQmin and RQmax which indicate the 95% confidence interval calculated by the 7500 Real-Time PCR System software. qRT-PCR was repeated 4 times and one representative result is shown. Resistant derivatives were tested against parental for significantly different gene expression with the Mann Whitney U test, two-tailed, $p<0.05$. Asterisks indicate which genes were significantly differentially expressed between resistant derivatives and parental.

As with other FGFRs, expression of FGFR2IIIb is associated with an epithelial phenotype whereas FGFR2IIIc expression is associated with a mesenchymal morphology (Ranieri *et al.*, 2016). Expression of FGFR2 isoforms was examined in RT112 R1 and R2 to determine if isoform switching had occurred (Fig. 4.4). PCR of

exons FGFR2 7-11 produces a 623-626 bp product and detects both FGFR2 IIIb and IIIc. PCR of exons 7-8 produces a 278 bp product and detects FGFR2 IIIb expression. PCR of exons 7-9 produces 267 bp product and detects FGFR2 IIIc. The FGFR2 IIIb isoform but not the FGFR2 IIIc isoform was detected in all of the RT112 samples. Therefore, R1 and R2 had not switched expression of FGFR2 isoforms and this had not induced the mesenchymal change in RT112 R1 and R2. It is possible that isoform switching has occurred in other FGFRs, although expression of FGFR3 is decreased and FGFR1 expression is low in the RT112 resistant derivatives (Fig. 3.11 and Fig. 4.2).

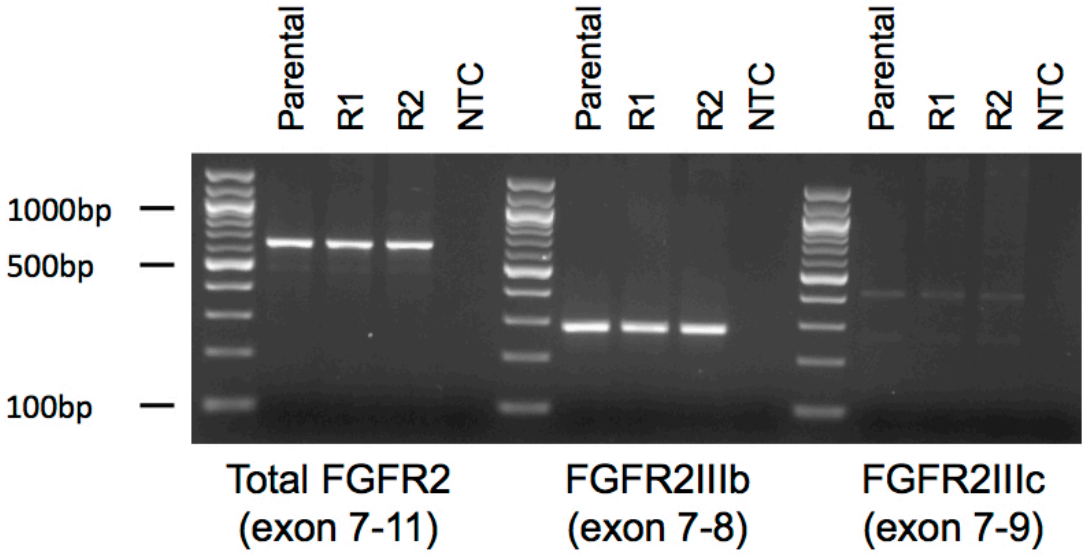

Figure 4.4 FGFR2 isoform RT-PCR products from RT112 parental, R1 and R2. Non-template control is abbreviated to NTC. This analysis was conducted only once.

4.2.2 EGFR and ERBB2 activation

The EGFR family of RTKs homodimerize or heterodimerize resulting in phosphorylation of the intracellular kinase domain and activation of the MAP kinase, PI3 kinase and PLCγ pathways. (Roskoski, 2014). *EGFR* amplification, *ERBB2* amplification and mutations and *ERBB3* mutations are found in MIBC (Robertson *et al.*, 2017). Increased signalling via EGFR has been reported as a method of survival in RT112 following short term treatment with PD (Herrera-Abreu *et al.*, 2013). For this reason, immunoblot analysis of total and phospho-EGFR was examined in RT112 parental, R1 and R2 (Fig. 4.5). Expression of phospho-EGFR and total EGFR was low in RT112 parental, R1 and R2. Phospho-EGFR expression

was not increased in R1 and R2 compared with parental cells indicating that activation of EGFR is not mediating resistance in these resistant lines.

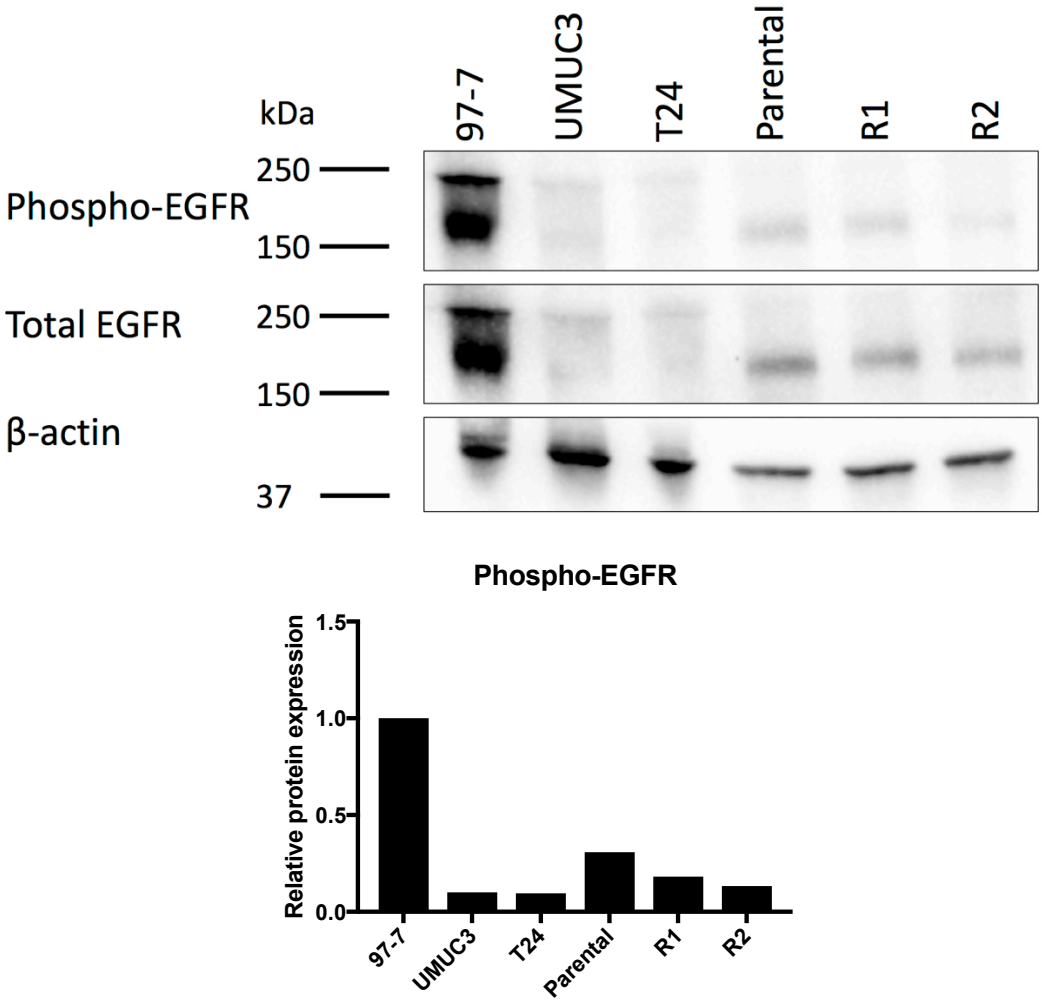

Figure 4.5 Immunoblot analysis of phospho-EGFR and total EGFR protein expression in RT112. A) Immunoblot analysis. B) Protein expression relative to 97-7. Expression was examined in parental, R1 and R2. 97-7 was included as a positive control for phospho-EGFR and total EGFR. UMUC3 and T24 were included as negative controls for phospho-EGFR and total EGFR. β-actin was used as a loading control. Immunoblots were conducted three times and a representative example is shown. The immunoblot shown was used to normalise phospho-EGFR relative to β-actin using Image Lab software.

Expression of phospho-EGFR (Y1068) and total EGFR was also examined in RT4 parental and RT4 R1 (Fig. 4.6). Growth factor receptor-bound protein 2 (Grb2) binds to the phosphorylated Y1068 of EGFR. Therefore, autophosphorylation of this residue is required for EGFR-mediated activation of the MAP kinase pathway (Rojas *et al.*, 1996). Expression of both phospho-EGFR and total EGFR was increased in RT4 R1 compared to parental R1. Therefore, signalling via EGFR is a possible mechanism of resistance in RT4 R1.

No ligand with specificity for ERBB2 has been identified, so it is suspected that ERBB2 only signals via heterodimerization with other EGFR family members.

The other EGFR family members preferentially dimerize with ERBB2 (Roskoski, 2014). The ERBB3 kinase domain is impaired in its ability to undergo autophosphorylation and so ERBB3 homodimers are unable to elicit activation of intracellular signalling pathways (Shi *et al.*, 2010). Activation of ERBB2 and ERBB3 signalling has been reported as a mechanism of resistance in RT112 to BGJ398 and ponatinib (Wang *et al.*, 2014). For this reason, protein expression of phospho-ERBB2, total ERBB2 and phospho-ERBB3 was examined in RT112 parental, R1 and R2. Examination of total ERBB3 was attempted but was unsuccessful. No increase in phospho-ERBB2 or total ERBB2 was observed in RT112 R1 or R2 (Fig. 4.7). Therefore, activation of ERBB2 does not appear to contribute to resistance in these cells.

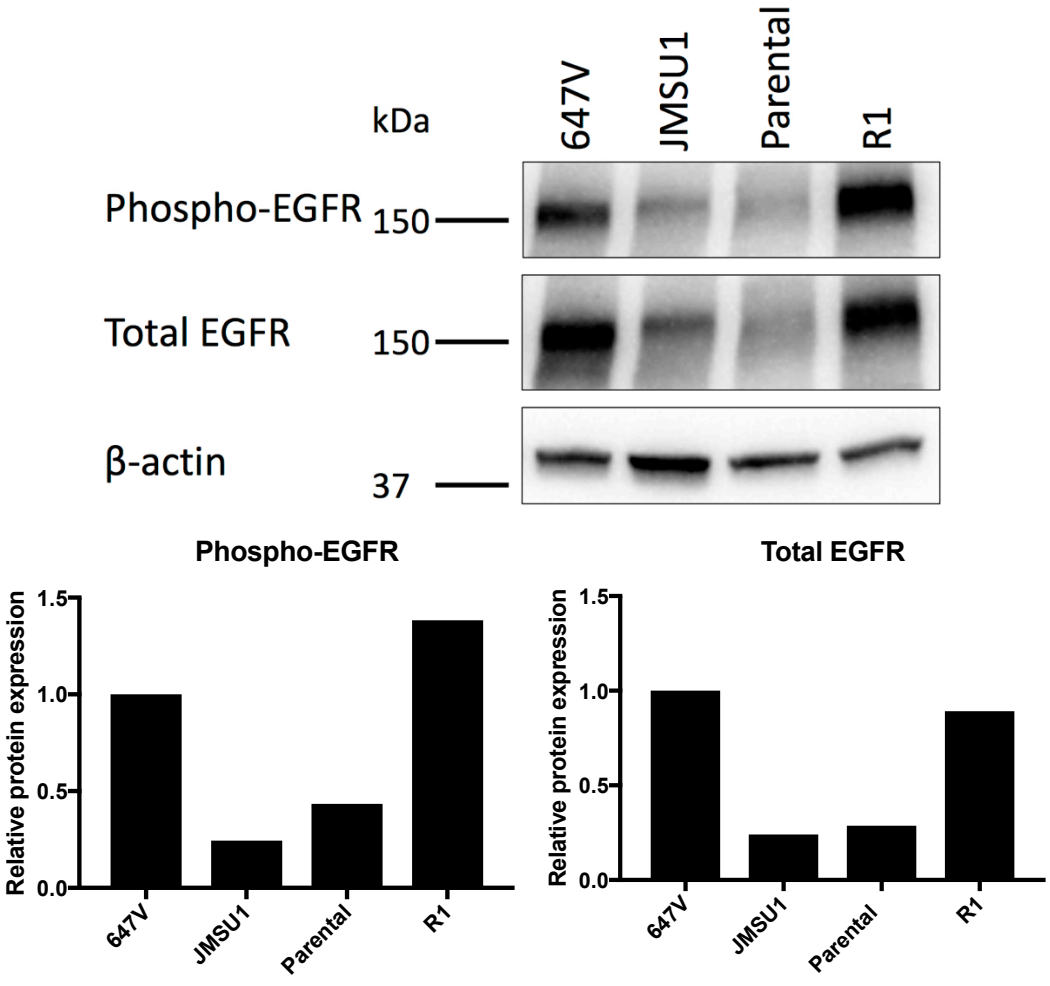

Figure 4.6 Immunoblot analysis of phospho-EGFR and total EGFR protein expression in RT4. A) Immunoblot analysis. B) Protein expression relative to 647V. Expression was examined in parental and R1. 647V was included as a positive control for phospho-EGFR (Tyrosine 1068) and total EGFR. JMSU1 was included as a negative control for phospho-EGFR and total EGFR. β-actin was used as a loading control. Immunoblots were conducted three times and a representative example is shown. Protein expression from the immunoblots shown was normalised compared to the total protein per well using Image Lab software and quantified relative to the positive control.

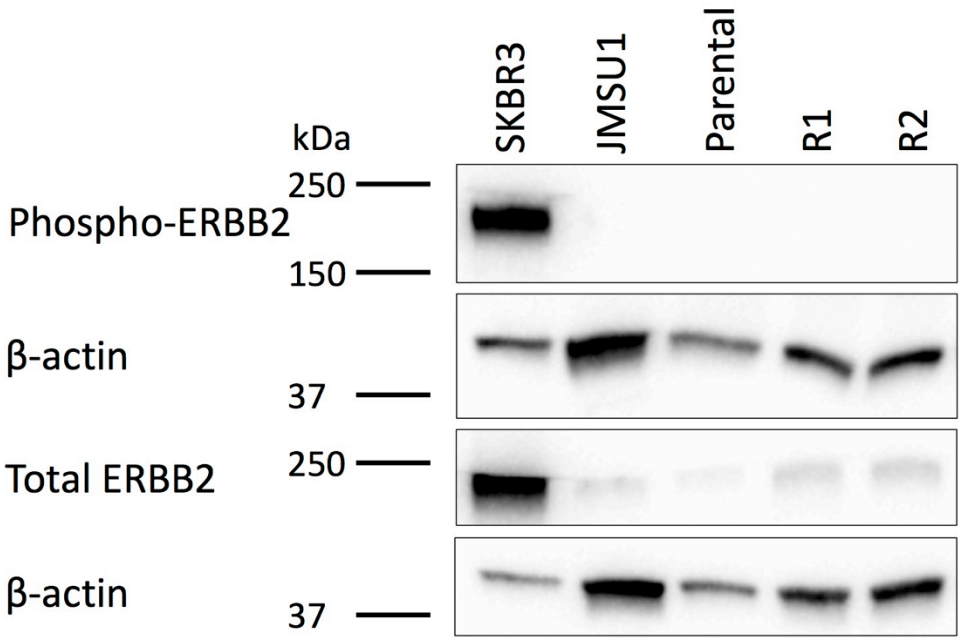

Figure 4.7 Immunoblot analysis of phospho-ERBB2 and total ERBB2 protein expression in RT112. Expression was examined in parental, R1 and R2. SKBR3 and JMSU1 were included as positive and negative controls for phospho-ERBB2 and total ERBB2 respectively. β-actin was used as a loading control. Immunoblots were conducted three times and a representative example is shown.

4.2.3 ERBB3 activation

Phosphorylation of ERBB3 in RT112 parental, R1 and R2 was examined with immunoblotting (Fig. 4.8). An increase in ERBB3 phosphorylation was observed in RT112 R1 and R2 compared to parental. It is possible that this activation of ERBB3 signalling contributes to resistance in these derivatives. As immunoblotting for total ERBB3 was unsuccessful, it is not possible to tell if the increase in ERBB3 phosphorylation is accompanied by an increase in ERBB3.

Expression of phospho-ERBB2, total ERBB2 and phospho-ERBB3 was examined in RT4 parental and R1 (Fig. 4.9). Expression of phospho-ERBB2 and total ERBB2 was low in RT4 parental and R1 compared to the positive control SKBR3. Expression of phospho-ERBB3 was increased in R1, although it remained much lower than in the positive control, the breast cancer cell line SKBR3. The increase in phospho-ERBB3 could also contribute to PD resistance in this line.

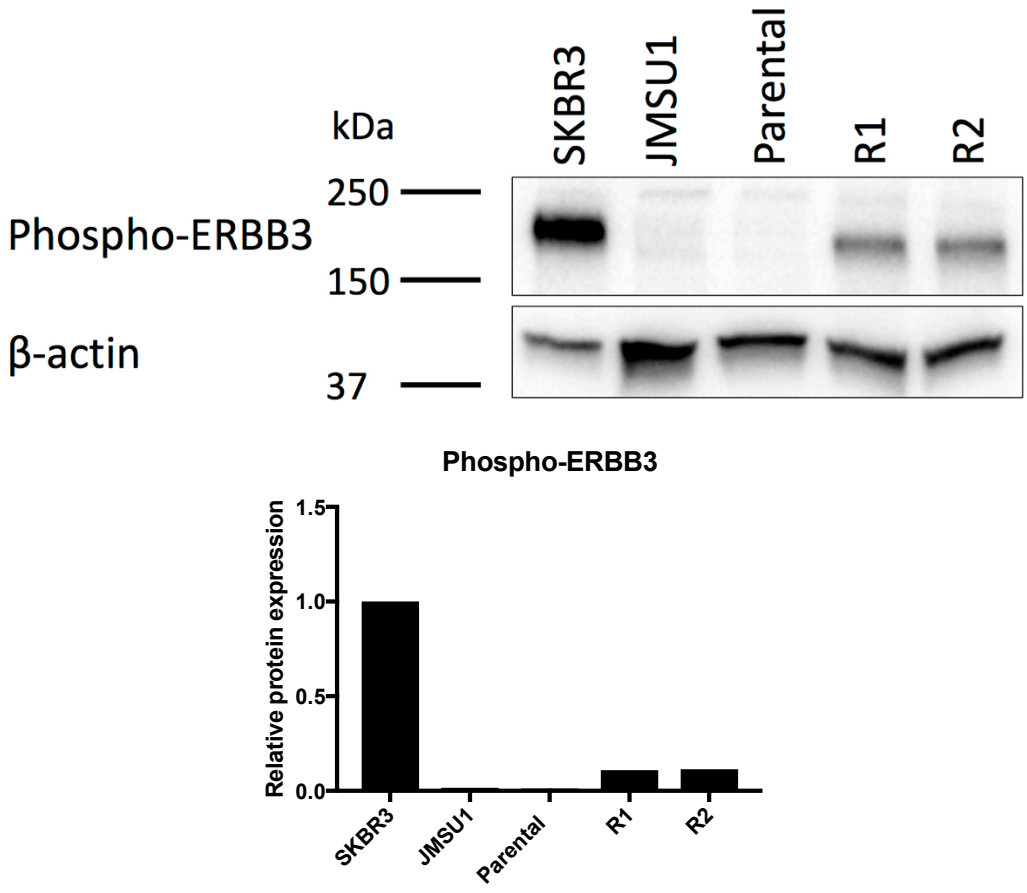

Figure 4.8 Immunoblot analysis of phospho-ERBB3 protein expression in RT112. A) Immunoblot analysis. B) Protein expression relative to SKBR3. Expression was examined in parental, R1 and R2. SKBR3 and JMSU1 were included as positive and negative controls for phospho-ERBB3 respectively. β-actin was used as a loading control. Immunoblots were conducted three times and a representative example is shown. The immunoblot shown was used to normalise phospho-ERBB3 relative to β-actin using Image Lab software.

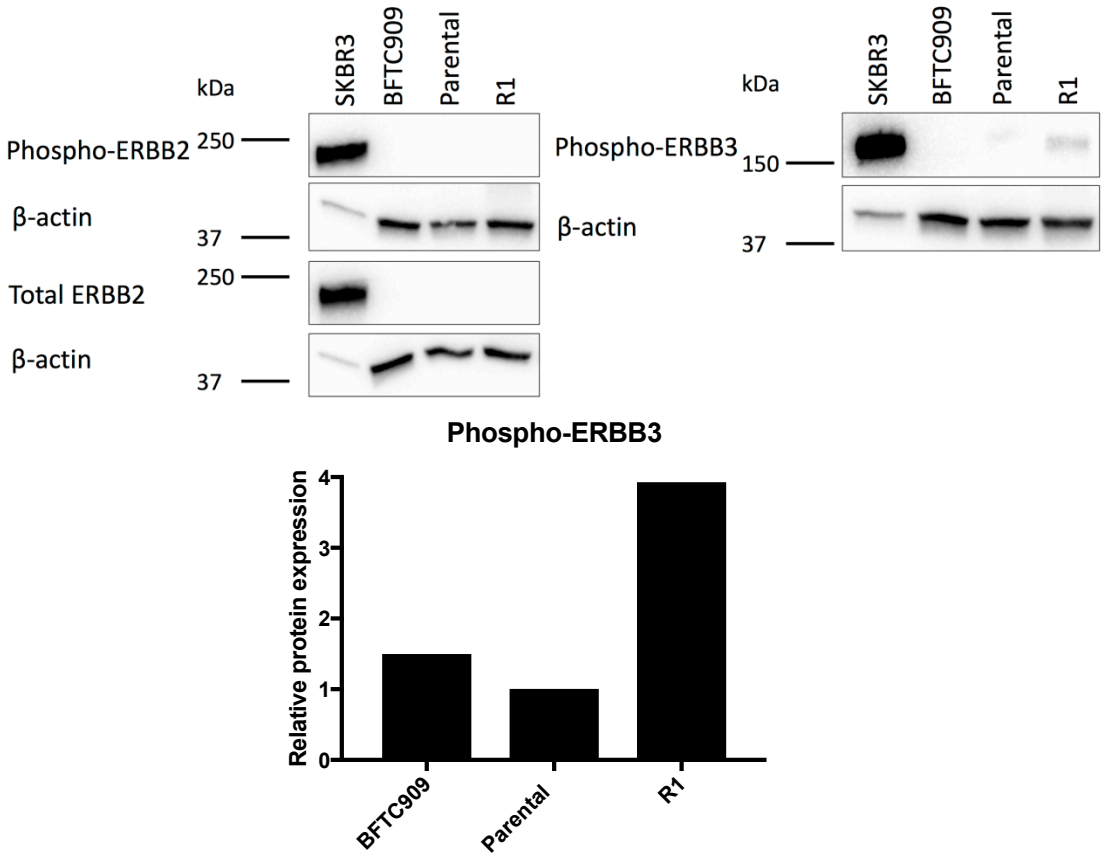

Figure 4.9 Immunoblot analysis of phospho-ERBB2, total ERBB2, phospho-ERBB3 and total ERBB3 protein expression in RT4. A) Immunoblot analysis. B) Protein expression relative to parental RT4. Expression was examined in parental and R1. SKBR3 and BFTC909 were included as positive and negative controls for phospho-ERBB2, total ERBB2, phospho-ERBB3 and total ERBB3. β-actin was used as a loading control. Immunoblots were conducted three times and a representative example is shown. The immunoblot shown was used to normalise phospho-ERBB3 relative to β-actin using Image Lab software.

Expression of the ERBB3 and ERBB4 ligand neuregulin 1 was reported to be upregulated in BGJ398 resistant derivatives. Treatment with neuregulin 1 was also found to rescue RT112 and RT4 from BGJ398-induced reduction in cell viability (Wang *et al.*, 2014). It was thought that neuregulin 1 could be inducing phosphorylation of ERBB3 in RT112 R1, RT112 R2 and RT4 R1. Expression of *NRG1*, which encodes neuregulin 1, was examined in RT112 parental, R1 and R2 by qRT-PCR. Expression of *NRG1* was increased by approximately 3 and 2-fold in RT112 R1 and R2 compared to parental respectively (Fig. 4.10). This increase in *NRG1* expression, although of a low magnitude, could be the cause of the increased phosphorylation of ERBB3 in RT112 R1 and R2.

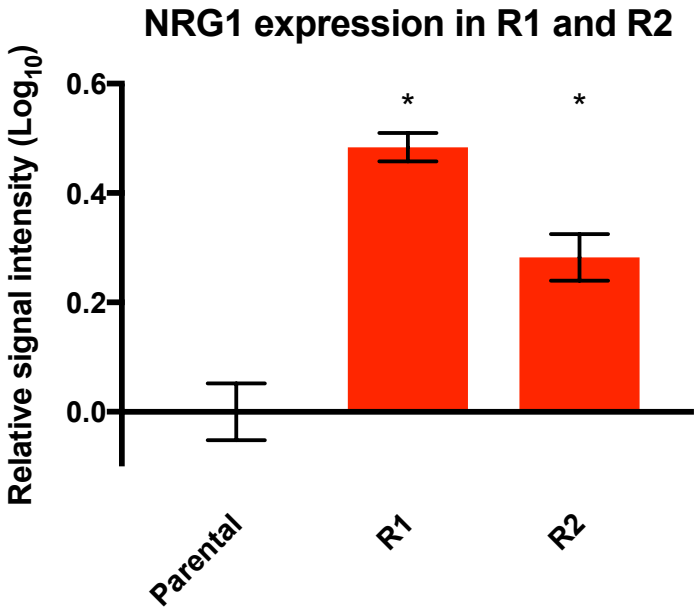

Figure 4.10 qRT-PCR of NRG1 in RT112 parental, R1 and R2. Expression was normalised to parental to produce relative quantification values (RQ). Error bars indicate RQmin and RQmax which indicate the 95% confidence interval calculated by the 7500 Real-Time PCR System Software. qRT-PCR was repeated 3 times and one representative result is shown. Resistant derivatives were tested against parental for significantly different gene expression with the Mann Whitney U test, two-tailed, $p<0.05$. Asterisks indicate the resistant derivatives with significantly different gene expression to parental.

4.2.4 MET activation

Activation of MET with hepatocyte growth factor (HGF) has been reported to rescue RT112 treated with BGJ398 (Harbinski *et al.*, 2012). Cheng *et al.*, using immunohistochemistry, identified high MET expression in 7 out of 142 urothelial carcinoma patients (Cheng *et al.*, 2002). MET, in addition to other EGFR family members, is able to heterodimerize with ERBB3 to induce intracellular signalling (Pérez-Ramírez *et al.*, 2015; Tanizaki *et al.*, 2011). Engelman *et al.* reported that *MET* amplification induced resistance to EGFR inhibition in the NSCLC cell line HCC827 cultured in gefitinib. MET activation mediated phosphorylation of ERBB3 which induced activation of the PI3 kinase pathway. This resistance could be overcome by combined EGFR and MET inhibition. Engelman *et al.* also reported *MET* amplification in NSCLC patient samples with acquired resistance to gefitinib (Engelman *et al.*, 2007).

It was thought that activation of MET could be mediating the increase in ERBB3 phosphorylation observed in RT112 R1 and R2. Expression of phospho-MET and total MET was measured in RT112 parental cultured in PD for 24 h, parental cultured without PD and R1, R2 and R3 each cultured with PD or without PD for 4 passages. Expression of phospho-MET and total MET was not examined

in RT4 parental and R1 due to time limitations and because it was thought that the increased phosphorylation of EGFR was the likely mediator of PD resistance in RT4 R1. An increase in phospho-MET was observed in R3 cultured with and without PD and a smaller increase was observed in R1 and R2 cultured with PD. However, phospho-MET expression remained low in R1 and R2 compared to the positive control 5637. (Fig. 4.11). It is possible that MET activation could be inducing survival in the RT112 resistant derivatives.

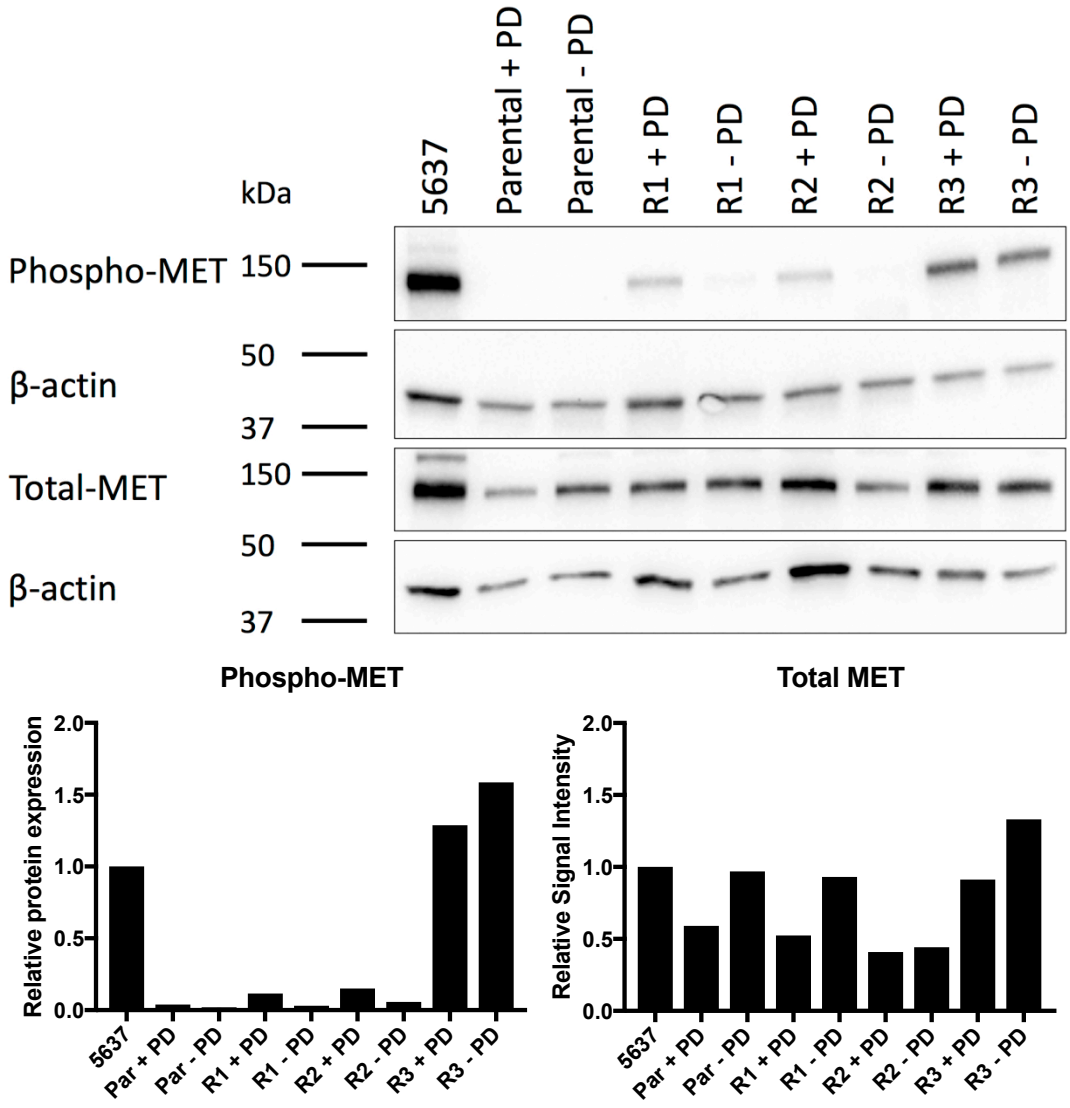

Figure 4.11 Immunoblot analysis of phospho-MET and total MET protein expression in RT112. A) Immunoblot analysis. B) Protein expression relative to 5637. Expression was examined in parental, parental treated with PD173074 for 24 h, R1, R2 and R3 cultured with PD173074 and R1, R2 and R3 cultured without PD173074 for 4 passages. 5637 was included as a positive control for phospho-MET and total MET and β-actin was used as a loading control. Immunoblots were conducted twice and a representative example is shown. The immunoblots shown were used to normalise phospho-MET and total MET relative to β-actin using Image Lab software.

4.2.5 AKT and ERK activation

The MAP kinase and PI3 kinase pathways regulate cell proliferation and survival and are activated downstream of FGFR3 (Hart *et al.*, 2001). Therefore, the activation of these pathways could be the determinant of the differences in cell proliferation between parental and resistant derivatives observed in Chapter 3. To determine whether the PI3 kinase and MAP kinase pathways were activated, expression of phospho-AKT, total AKT, phospho-ERK and total ERK was examined in RT112 parental acutely treated with PD, parental cultured without PD, and resistant derivatives cultured with and without PD (Fig. 4.12). Expression of phospho-AKT was increased in R1 and R2 + PD and reduced in parental + PD. Expression of phospho-ERK was also decreased in parental + PD. Expression of total ERK remained fairly constant between parental and resistant derivatives. The reduction of phospho-ERK and phospho-AKT in RT112 parental acutely treated with PD is likely to contribute to the reduced proliferation in these cells. All resistant derivatives cultured in PD maintained ERK phosphorylation. These results suggest that finding an alternative mechanism of activating the MAP kinase and PI3 kinase pathways may be key to overcoming FGFR inhibition with PD. The increase in phosphorylation of AKT observed in R1 and R2 cultured with PD but not R3 cultured with PD highlights a difference in the resistance mechanism between these lines. The mechanism of resistance employed in R1 and R2 appears to strongly activate the AKT pathway; whereas the resistance mechanism in R3 activates the PI3 kinase pathway only to a similar level to parental RT112 not treated with PD.

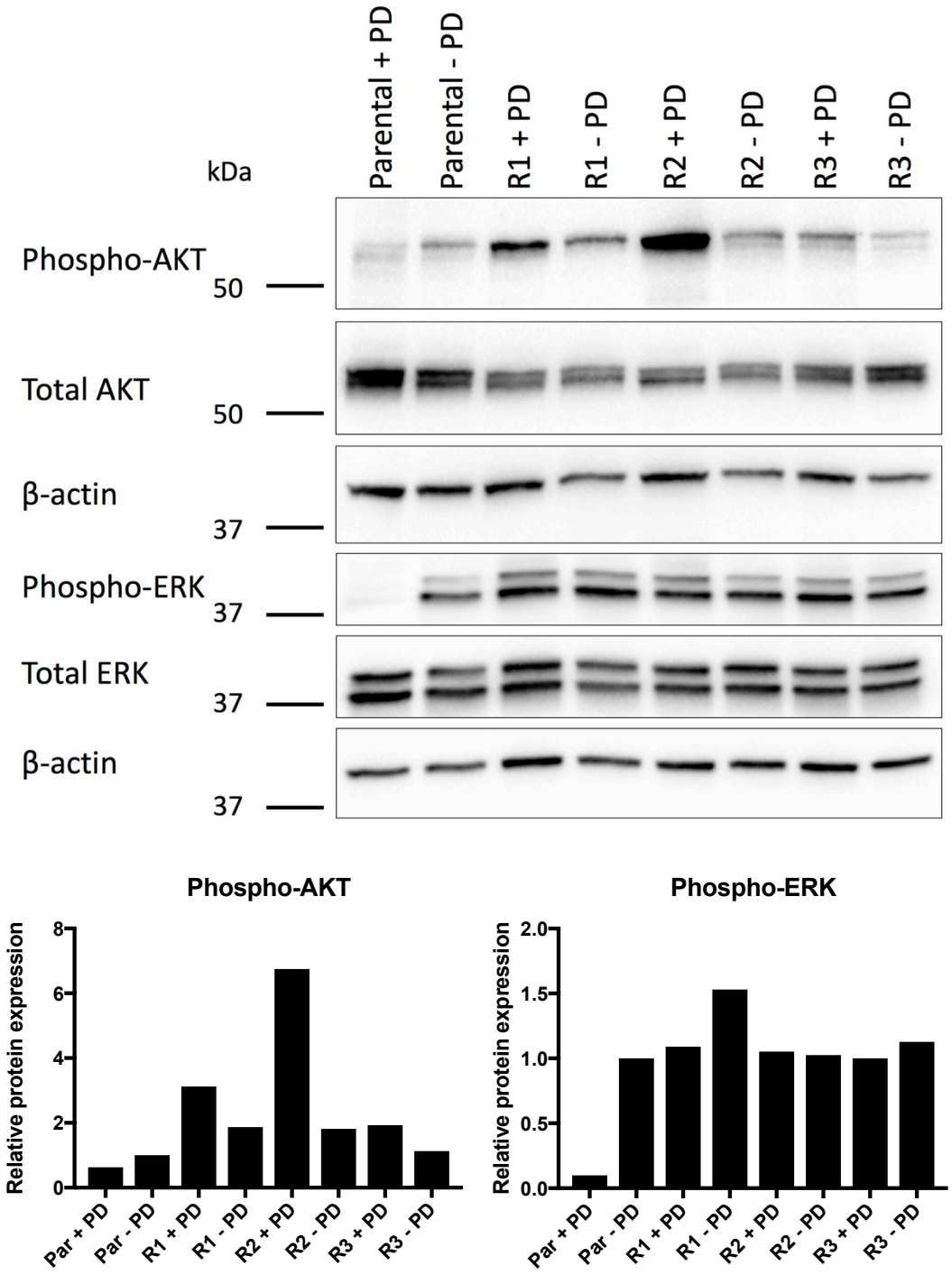

Figure 4.12 Immunoblot analysis of phospho-AKT, AKT, phospho-ERK and ERK protein expression in RT112. A) Immunoblot analysis. B) Protein expression relative to parental - PD. Expression was examined in parental, parental treated with PD73074 for 24 h, R1, R2 and R3 cultured with PD173074 and R1, R2 and R3 cultured without PD173074 for 4 passages. β-actin was used as a loading control. Immunoblots were conducted twice and a representative example is shown. Phospho-AKT expression from the immunoblot shown was normalised compared to the total protein per well using Image Lab software and quantified relative to parental no PD. The immunoblot shown was used to normalise phospho-ERK relative to β-actin using Image Lab software. Phospho-ERK expression was quantified relative to parental no PD.

4.3 Discussion

FGFR1 expression has been associated with a mesenchymal phenotype and FGFR3 has been associated with an epithelial phenotype (Cheng *et al.*, 2013). FGFR1 activation is known to induce EMT in urothelial carcinoma cell lines (Tomlinson *et al.*, 2012). It was thought that the mesenchymal phenotypic changes observed in RT112 R1 and R2 could be caused by a switch in dependency from FGFR3 to FGFR1. FGFR1 protein expression remained low in the resistant derivatives and therefore the partial EMT observed in RT112 R1 and R2 and PD resistance is not induced by increased expression of this RTK. It was also considered that activation of the FGFR IIIc rather than IIIb isoform could be inducing the mesenchymal phenotypic changes observed in RT112 R1 and R2. An increase in FGF2 expression was observed in RT112 R1 and R2. This FGF preferentially activates FGFR IIIc isoforms. However, no switching to the IIIc isoform was observed in FGFR2 in RT112 R1 and R2. Other FGFRs were not examined for isoform switching. However, as FGFR1 and FGFR3 expression is low in RT112 R1 and R2 cultured in PD isoform switching of these receptors is unlikely to be a cause of the partial EMT in these lines. It is crucial to note that, as PD is a pan-FGFR inhibitor, signalling via FGFRs including IIIc isoforms should not be possible in the presence of PD unless a gatekeeper mutation has occurred. The V555M FGFR3 mutation has been identified as a mechanism of acquired resistance to FGFR inhibition (Chell *et al.*, 2013). Unless an activating FGFR mutation or FGFR amplification is identified in the resistant derivatives the hypothesis that FGFR isoform switching is inducing phenotypic changes in the PD resistant derivatives can be discounted. Genetic analysis of resistant derivatives will be described in Chapter 5.

Increased phosphorylation of ERBB3 and MET was observed in RT112 R1 and R2. An increase in phospho-MET was observed in RT112 R3 but phospho-ERBB3 was not examined in this line. The phosphorylation of these receptors could be contributing to the resistant phenotype in these lines. ERBB3 is not able to signal via homodimerization due to low kinase function. However, MET, in addition to other EGFR family members, is able to heterodimerize with ERBB3 to induce intracellular signalling (Pérez-Ramírez *et al.*, 2015; Tanizaki *et al.*, 2011). It is therefore possible that MET is heterodimerising with ERBB3 in the resistant derivatives and contributing to the resistance to PD. The activation of RTKs in RT112 resistant lines was examined with a phospho-RTK array (PathScan® RTK signaling antibody array Kit #7982). However, as the results of this array were

disappointing with a low signal detected from RTK specific spots, the results of this analysis were not presented in this Chapter. An alternative phospho-RTK array from a different supplier was identified but analysis was not conducted with this array due time limitations.

Phosphorylation of EGFR was markedly increased in RT4 R1 and was considered a strong candidate resistance mechanism. EGFR is able to signal via homodimerization or heterodimerization with other EGFR family members (Roskoski, 2014). A slight increase in phospho-ERBB3 was observed in RT4 R1 but phospho-ERBB2 was not detected in RT4 R1. This analysis of expression and phosphorylation is limited to a few RTKs: other signalling via other RTKs could be inducing resistance. The genetic analysis in Chapter 5 and transcriptomic analysis in Chapter 6 may uncover further signalling pathways implicated in resistance to PD. RTKs can be targeted by TKIs used clinically and the dependence of resistant lines on these RTKs will be tested in Chapter 7 of this thesis.

The increased phosphorylation of AKT in RT112 R1 and R2 compared to RT112 parental and R3 highlights that there is a difference in the resistance mechanism employed in R1 and R2 compared to the mechanism employed in R3. However, the cause of this increased phosphorylation is unknown. The maintenance of ERK and AKT activation in RT112 R3 to a similar level as observed in RT112 parental was expected as R3 has the most similar phenotype to the parental line of all the resistant derivatives. Upon culture without PD, phospho-AKT expression was reduced in RT112 R1 and R2, FGFR3 expression was increased in all RT112 resistant derivatives and cell proliferation was increased in all resistant derivatives. This suggests that the resistant derivatives resume signalling via FGFR3 upon drug removal.

	RT112 R1	RT112 R2	RT112 R3	RT4 R1
N-cadherin	Increased	Increased	Increased	Constant
FGFR3	Reduced	Reduced	Reduced	Constant
Phospho-EGFR	Reduced	Reduced	Not assayed	Increased
EGFR	Constant	Constant	Not assayed	Increased
Phospho-ERBB2	Not detected	Not detected	Not assayed	Not detected
ERBB2	Constant	Constant	Not assayed	Not detected
Phospho-ERBB3	Increased	Increased	Not assayed	Increased
Phospho-MET	Increased	Increased	Increased	Not assayed
MET	Reduced	Reduced	Increased	Not assayed

Figure 4.13 Key protein expression changes identified in RT112 and RT4 resistant derivatives by immunoblot in Chapter 3 and 4. Protein expression of each resistant derivative cultured in PD is given relative to the parental line cultured without PD.

Chapter 5
Genetic Differences Between Parental and Resistant Cells

5.1 Introduction

This Chapter will examine whether there is a genetic mechanism of resistance in any of the RT112 or RT4 derivatives. Genetic mechanisms of resistance to targeted agents discussed in Chapter 1 included the FGFR3 V555M mutation which was previously described as a mechanism of acquired resistance to FGFR inhibition in the myeloma cell line KMS-11 (Chell *et al.*, 2013). One possible mechanism by which resistance could have arisen in the RT112 and RT4 resistant lines is via the acquisition of a mutation in an RTK. It is probable that any genetic change identified as a cause of resistance will induce activation of the MAP kinase and PI3 kinase pathways as these have been identified as inhibited in parental RT112 upon acute treatment but active in RT112 resistant derivatives. In addition to mutations in the receptor itself, mutations may be identified in these pathways, in genes such as the RAS genes, *RAF*, *PIK3CA*, *PTEN* and *AKT* (discussed in Chapter 1, section 1.2.2).

Increased copy number of *ERBB2* has been associated with resistance to EGFR monoclonal antibodies in colorectal cancer patients (Martin *et al.*, 2013). Le Coutre *et al.* cultured the CML cell line LMA84 with imatinib for 6 months. The line became resistant to imatinib due to amplification of the *BCR-ABL* fusion gene which induced an increase in BCR-ABL protein expression (le Coutre *et al.*, 2000). Short-term survival and resistance to FGFR TKIs in RT112 has been reported to arise due to activation of alternative RTKs, but this has not been found to be due to gene amplification (Harbinski *et al.*, 2012; Herrera-Abreu *et al.*, 2013; Wang *et al.*, 2014).

Two studies examined the mechanism by which RT112 cells survive short-term treatment with PD and focused on identifying non-genetic changes in the FGFR TKI-treated cells rather than genetic differences (Harbinski *et al.*, 2012; Herrera-Abreu *et al.*, 2013). They identified MET and EGFR activation respectively as inducing short term survival. During the course of this study, Wang *et al.*, conducted long-term culture of RT112 in FGFR TKIs and conducted mRNA sequencing and reported activation of ERBB2 and ERBB3 as a non-genetic mechanism of resistance in their resistant derivatives (Wang *et al.*, 2014).

In Chapter 4, a small increase in ERBB3 phosphorylation was identified in RT112 R1 and R2 (Fig. 4.8) and an increase in phosphorylation of MET was observed in RT112 R1, R2 and R3 (Fig. 4.11). An increase in total and phosphorylated EGFR was observed in RT4 R1 (Fig. 4.6). It is possible that the phosphorylation of these RTKs could be mediated by an activating mutation in or an increase in the copy number of these RTKs. It was hypothesised that RT112 R3 was the most likely RT112 resistant derivative to have a genetic mechanism of resistance as it maintained a maximal cell density and morphology more similar to RT112 parental than RT112 R1 or R2. It was also thought that RT112 R1 and RT112 R2 may have the same resistance mechanism due to these resistant derivatives having a similar phenotype. Therefore, RT112 R2 was not examined with whole exome sequencing or copy number analysis. If a genetic alteration of interest was identified in RT112 R1, analysis would be conducted to determine if the same mutation was present in RT112 R2. RT4 parental and R1 were not examined by whole exome sequencing as it was considered likely that EGFR was mediating resistance in RT4. Therefore, genetic analysis of the RT4 parental and resistant line focused on determining if *EGFR* was amplified or mutated in RT4 R1.

5.2 Results

5.2.1 Copy number analysis of RT112 Parental, R1 and R3

Copy number analysis was conducted in RT112 parental, R1, R2 and R3 with low pass whole genome sequencing. An unmatched blood sample was used as a reference sample in this study because we do not have a matched reference sample for RT112 or RT4. The sequence of centromeres contains long arrays of near identical tandem repeats. The repetitive nature of these regions prevents accurate sequence alignment (Hayden, 2012). This can result in copy number gains and losses being falsely identified in centromeric regions and therefore apparent copy number alterations identified in these regions were ignored. The genome-wide copy number profiles of chromosomes 1-22 for RT112 parental, R1 and R3 normalised to a blood sample are presented in Fig. 5.1. The copy number profiles of chromosome 8 and 9 for RT112 parental, R1 and R3 are shown in Appendix C, Fig. C.1, to enable the visualization of the smaller copy number alterations present on these chromosomes. Copy number alterations shared

between RT112 parental, R1 and R3 are summarised in Table 5.1. The karyotype of parental RT112 maintained in this laboratory has been analysed previously by M-FISH and copy number changes have been examined with array comparative genomic hybridisation at passage 33 (Hurst *et al.*, 2004; Williams *et al.*, 2005). In this study RT112 parental was passage 37 when DNA was harvested for copy number analysis. The copy number data fits well with the genomic alterations described by Williams *et al.* and Hurst *et al.* (Hurst *et al.*, 2004; Williams *et al.*, 2005). For example, a gain of chromosome 20 was observed by Williams *et al.*, Hurst *et al.* and in this study. Williams *et al.* observed a gain of 4p and Hurst *et al.* reported that RT112 had a gain of 4p11–pter. This was consistent with the copy number gain of 4p16.3-p11 observed in RT112 parental in this study. Williams *et al.* describe RT112 as having a del(1)(p3?4) and Hurst *et al.* observed loss of 1p35.3–pter. In our copy number data, a loss of 1p36.33-p36.21 in RT112 parental, R1 and R3 was observed. No loss of 2q was reported by Williams *et al.* whilst loss of 2q22.1–q23.1 was reported by Hurst *et al.* and a loss of 2q21.3-q23.2 was observed in RT112 parental, R1 and R3. This may be due to the more limited resolution of M-FISH (Hurst *et al.*, 2004).

To examine the differences between the three lines, the copy number data of RT112 R1 and R3 were normalised to parental. Results are presented in Figure 5.2. Copy number differences between RT112 parental and R1 and R3 are summarised in Table 5.2 and Table 5.3, respectively. As RT112 parental is an uncloned line, copy number differences between RT112 parental and the RT112 resistant derivatives may be due to selection of a subclone rather than due to a genomic alteration that has occurred during the derivation of the resistant derivatives. In addition to the 2q21.3-q23.2 copy number loss in RT112 parental, R1 and R3, copy number loss of 2q37.2-q37.3 was observed in RT112 R1. The copy number analysis conducted with RT112 parental as the reference sample indicated that RT112 R1 had gain of 19p13.3-q11. However, RT112 parental and R3 have loss of 19p (Fig. 5.1) and therefore it is likely that RT112 R1 is a subclone with normal chromosome 19.

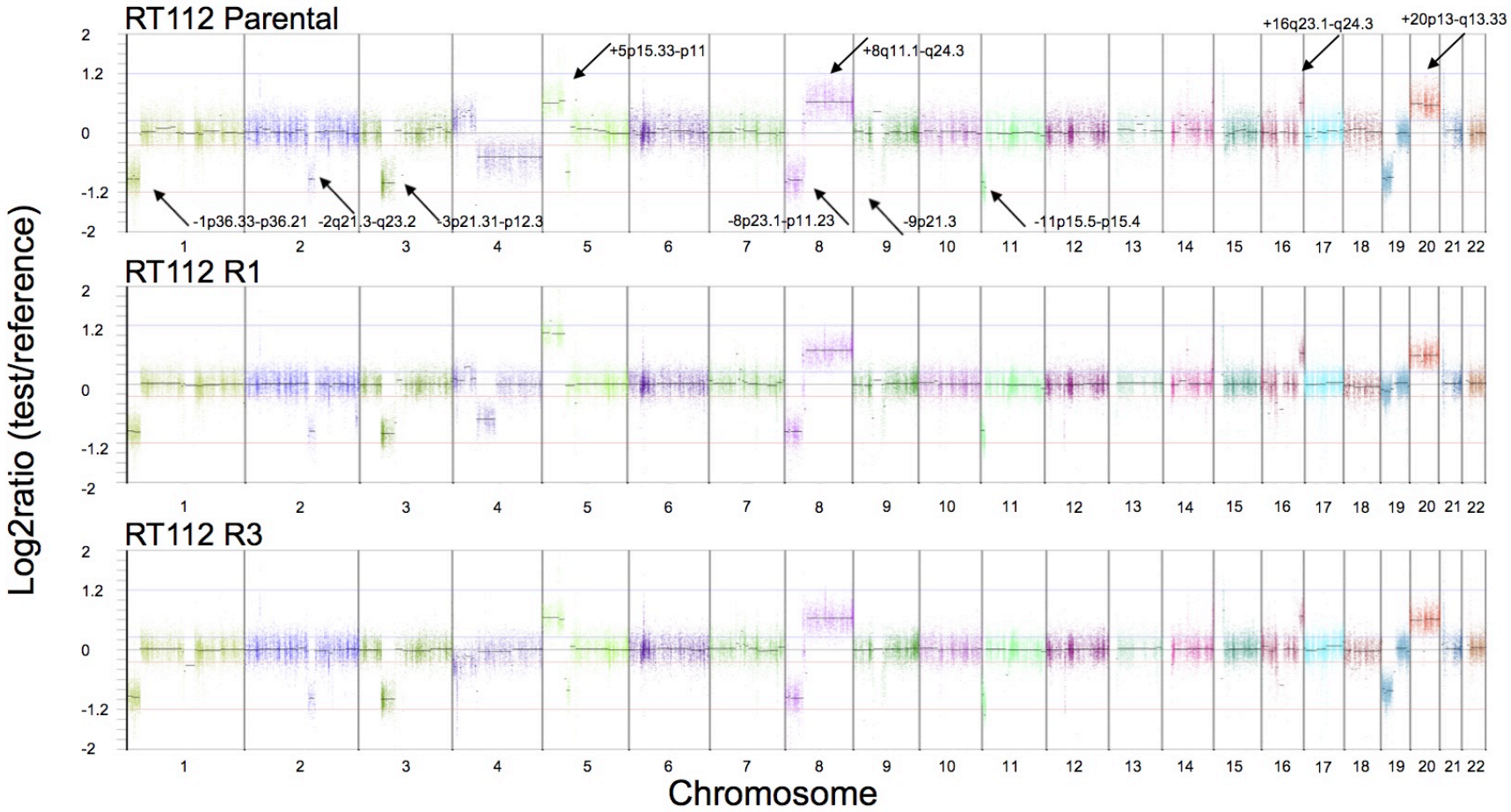

Figure 5.1 Copy number profiles for all autosomes for RT112 parental, R1 and R3 normalised to a patient blood sample. Copy number plots were generated in Nexus Copy Number 8.0 and show $\log_2$ ratio of the read counts of RT112 samples normalised to a patient blood sample for chromosomes 1-22 (GRCh38 reference). Each point represents the $\log_2$ ratio for a section of DNA of window size 1000 bp. Copy number gains (above the zero line) and losses (below the zero line) shared by RT112 parental, R1 and R3 are highlighted with arrows and are also detailed in Table 5.1.

Table 5.1 Copy number alterations shared by RT112 parental, R1 and R3. Copy number data was generated using low-pass whole genome sequencing and normalised to data from an unrelated patient's blood sample.

Chromosome:Position (Mb; hg38)	Cytoband	Copy Number Loss/Gain
1:744,421-29,096,605	p36.33-p36.21	loss
2:135,548,251-149,171,997	q21.3-q23.2	loss
3:47,319,697-77,956,013	p21.31-p12.3	loss
5:0-46,508,621	p15.33-p11	gain
8:7,295,847-38,098,889	p23.1-p11.23	loss
8:39,000,213-41,275,121	p11.22-p11.21	gain
8:43,801,423-45,928,436	p11.1-q11.1	loss
8:45,928,436-145,138,636	q11.1-q24.3	gain
9:21,409,526-23,540,699	p21.3	loss
11:0-8,295,312	p15.5-p15.4	loss
16:78,500,343-90,338,345	q23.1-q24.3	gain
20:0-64,444,167	p13-q13.33	gain

RT112 R1 exhibited copy number loss of 4p16.3-q22.1. There was a possible loss of 4p16.3-p11 in RT112 R3, however this did not reach the required threshold of -0.25 to be classified as a loss. *FGFR3* is located within the chromosome 4 cytoband p16.3. RT112 parental exhibited a gain of 4p16.3-p11 which was not observed in RT112 R1 or R3 (Fig. 5.1). Therefore, the loss of 4p16.3-q22.1 in RT112 R1 appears to be due to this resistant line lacking the 4p gain observed in RT112 parental. Both RT112 R1 and R3 exhibited gain of 8p11.23-p11.1. This region contains *FGFR1*. RT112 R1 exhibited copy number gain of 5p15.33-q11.1 which contains the genes *LIFR* and *OSMR* which encode the oncostatin M (OSM) pathway receptors leukaemia inhibitory factor receptor (LIFR) and oncostatin M receptor (OSMR), respectively. RT112 R1 also exhibited copy number gain of 5q11.1-q11.2 which contains the gene *IL6ST* which encodes the OSM pathway receptor glycoprotein 130 (gp130) (Fig. 5.2, Table 5.2).

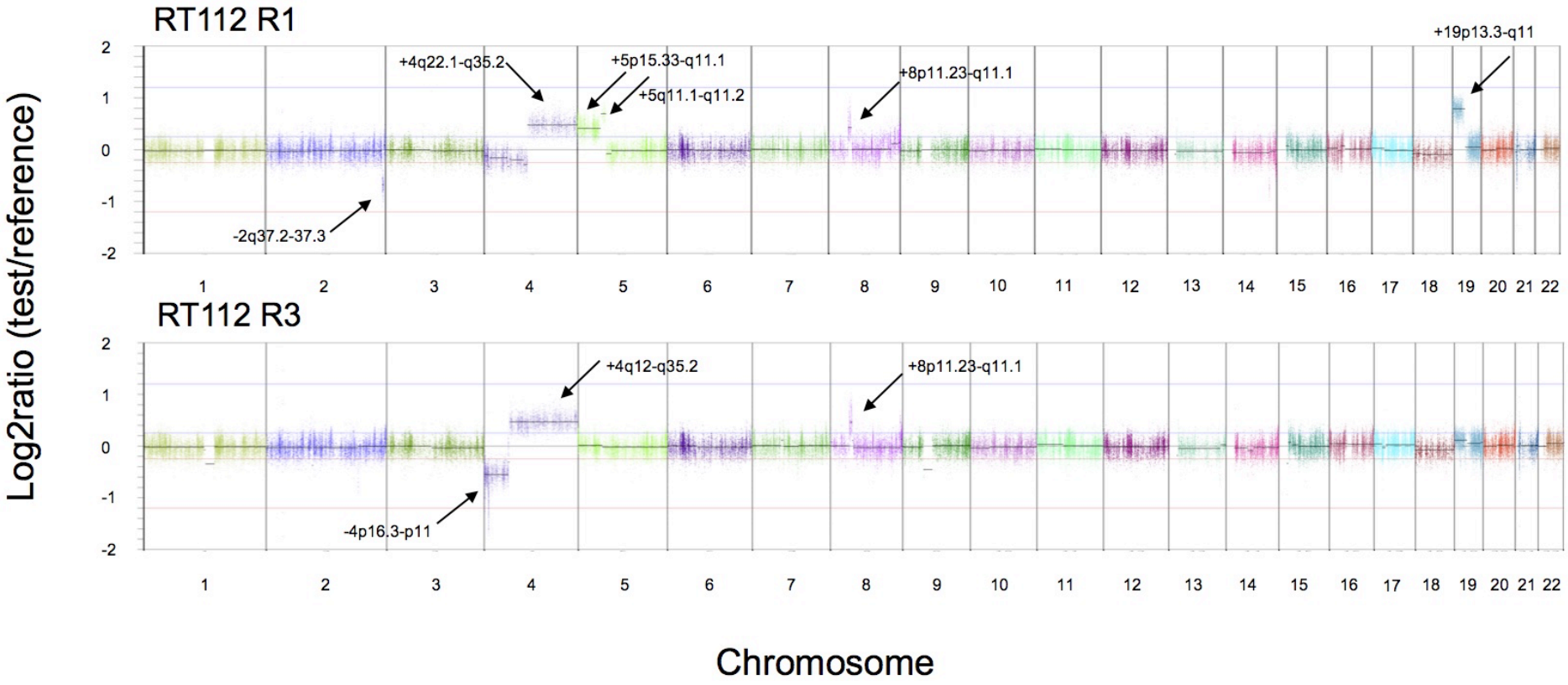

Figure 5.2 Copy number profiles of RT112 R1 and R3 normalised to RT112 parental. Copy number plots were generated in Nexus Copy Number 8.0 and show $\log_2$ ratio of the read counts of RT112 R1 and R3 normalised to parental for chromosomes 1-22 (GRCh38 reference). Each point represents the $\log_2$ ratio for a section of DNA of window size 1000 bp. Copy number gains (above the zero line) and losses (below the zero line) are highlighted with arrows and are also detailed in Table 5.2 and Table 5.3.

Table 5.2 Copy number differences between RT112 parental and R1. Copy number data was generated using low-pass whole genome sequencing and copy number alterations identified using RT112 parental as the reference sample and RT112 R1 as the test sample.

Chromosome:Position (Mb; hg38)	Cytoband	Copy Number Loss/Gain	Potential Candidate Genes	Number of Genes in Region
2:235,053,661-238,107,785	q37.2 – q37.3	loss	*SH3BP4*	17
4:90,569,813-190,026,739	q22.1 – q35.2	gain	*FABP2, SMAD1*	311
5:0-48,800,000	p15.33 – q11.1	gain	*LIFR, OSMR,*	136
5:49,712,701-57,604,516	q11.1 – q11.2	gain	*IL6ST, MAP3K1*	34
8:38,057,101-45,200,000	p11.23 – q11.1	gain	*FGFR1*	47
19:209,898-26,200,000	p13.3 – q11	gain	*FGF22, INSR, JUNB, JUND*	590

Table 5.3 Copy number differences between RT112 parental and R3. Copy number data was generated using with low-pass whole genome sequencing and copy number alterations identified using RT112 parental as the reference sample and RT112 R3 as the test sample.

Chromosome:Position (Mb; hg38)	Cytoband	Copy Number Loss/Gain	Potential Candidate Genes	Number of Genes in Region
4:85,661-49,061,875	p16.3 – p11	loss	*FGFRL1, FGFR3, FGFRBP1, FGFRBP2*	301
4:51,843,881-190,026,739	q12 – q35.2	gain	*KIT, SMAD1*	507
8:38,057,101-43,883,945	p11.23 – p11.1	gain	*FGFR1*	47

5.2.2 Copy number analysis of RT4 parental and RT4 R1

Copy number analysis was conducted with low pass whole genome sequencing in RT4 parental and R1. The copy number profiles of RT4 parental and RT4 R1 normalised to a blood sample are presented in Figure 5.3 and copy number changes shared between RT4 parental and R1 are summarised in Table 5.4. The karyotype of parental RT4 has been analysed previously by M-FISH and copy number changes have been examined by with array comparative genomic hybridisation (Hurst *et al.*, 2004; Williams *et al.*, 2005). The reported genomic alterations in RT4 parental were concordant with the copy number changes observed in our copy number data. For example, Williams *et al.* reported RT4 parental, which is tetraploid, to have three copies of chromosome 9 and five copies of chromosome 12 and Hurst *et al.* reported loss of chromosome 9 and gain of chromosome 12 (Hurst *et al.*, 2004; Williams *et al.*, 2005). This is in agreement with our copy number data in which there was copy number loss of chromosome 9 and gain of chromosome 12 in both RT4 parental and RT4 R1.

The copy number profile of RT4 R1 normalised to RT4 parental is presented in Figure 5.4 and copy number differences between RT4 parental and RT4 R1 are summarised in Table 5.5. As our RT4 parental is a clone, any changes in copy number differences observed in RT4 R1 are likely to be due to alterations acquired during culture in PD, rather than selection of existing subclones, although changes could still be passenger events. The alterations that differed between RT4 parental and RT4 R1 were gain of 5p15.33-q11.1 and the loss of 5q11.1- q35.3. A gain of the region from 5p15.33-q11.1, which contains the *LIFR* and *OSMR* genes was also observed in RT112 R1. These genes encode receptors in the OSM signalling pathway (Fig. 6.15). Transcriptome analysis conducted in Chapter 6 identified differential expression of OSM pathway signalling genes in RT112 resistant derivatives compared to parental RT112 (Fig. 6.9, 6.10, D.6 and D.7). Tables of the genes in 5p15.33-q11.1 which were differentially expressed between RT4 parental and RT4 R1 and between RT112 parental and RT112 R1, determined by transcriptome analysis, are included as supplementary data. It was possible that the increase in EGFR expression in RT4 R1 could be due to *EGFR* amplification. *EGFR* is located on chromosome 7, cytoband p11.2. No change in copy number in this region was observed between RT4 parental and RT4 R1, therefore the increased EGFR expression observed is not due to *EGFR* amplification.

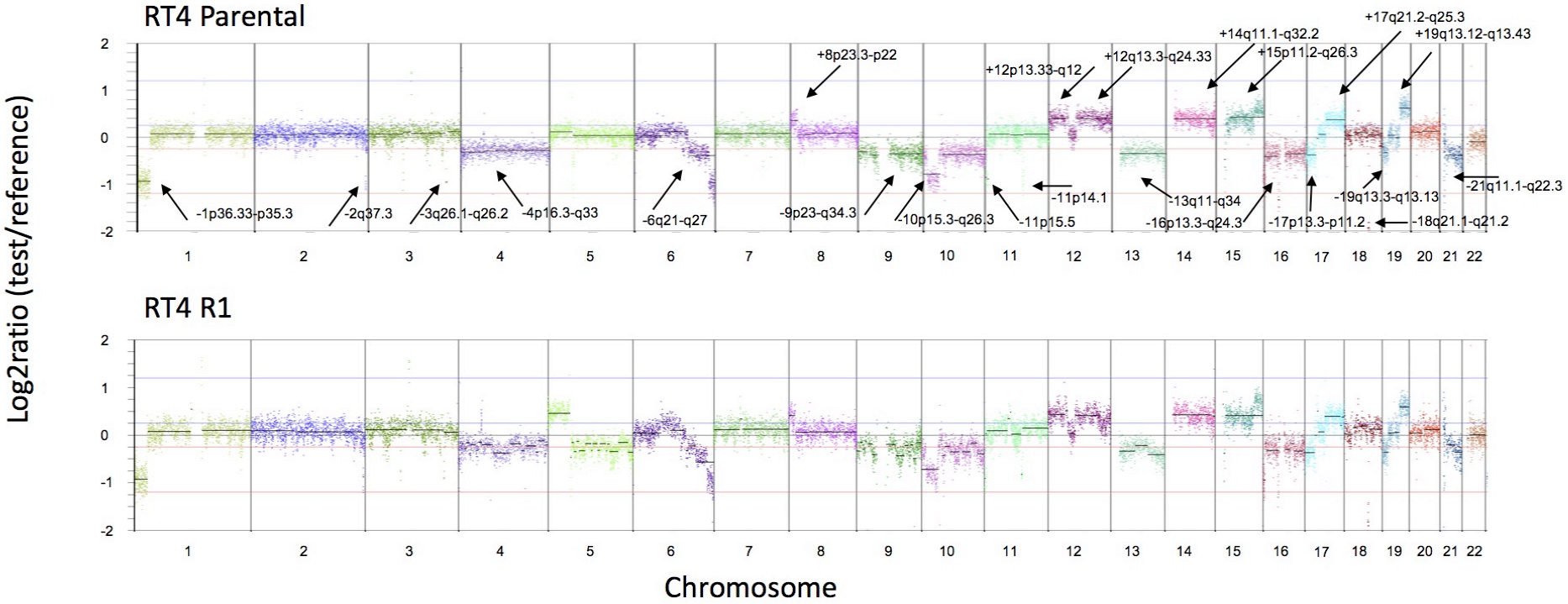

Figure 5.3 Copy number profiles of RT4 parental and R1 normalised to a patient blood sample. Copy number plots were generated in Nexus Copy Number 8.0 and show $\log_2$ ratio of the read counts of RT4 samples normalised to a patient blood sample for chromosomes 1-22 (GRch38 reference). Each point represents the $\log_2$ ratio for a section of DNA of window size 1000 bp. Copy number gains (above the zero line) and losses (below the zero line) shared by RT4 parental and R1 are highlighted with arrows and are also detailed in Table 5.4.

Table 5.4 Copy number alterations shared by RT4 parental and RT4 R1. Copy number data was generated using low-pass whole genome sequencing and normalised to data from an unrelated patient's blood sample.

Chromosome:Position (Mb; hg38)	Cytoband	Copy Number Loss/Gain
1:0-27,636,501	p36.33 – p35.3	loss
2:237,762,632-238,486,412	q37.3	loss
3:167,210,191-168,502,510	q26.1 – q26.2	loss
4:0-169,230,689	p16.3- q33	loss
6:112,662,364-170,805,979	q21 – q27	loss
8:558,052-15,238,333	p23.3 – p22	gain
9:13,808,337-138,394,717	p23 – q34.3	loss
10:0-133,797,422	p15.3 – q26.3	loss
11:0-1,369,711	p15.5	loss
11:3,959,836-5,227,107	p15.4	loss
11:78,639,222-80,827,017	q14.1	loss
12:0-41,345,528	p13.33 – q12	gain
12:57,594,810-132,634,466	q13.3 – q24.33	gain
13:18,798,543-114,364,328	q11 – q34	loss
14:17,200,000-107,043,718	q11.1 – q32.2	gain
15:17,000,502-101,991,189	p11.2 – q26.3	gain
16:0-90,338,345	p13.3- q24.3	loss
17:0-21,227,316	p13.3 – p11.2	loss
17:41,732,953-82,478,901	q21.2 – q25.3	gain
18:49,738,286-51,622,721	q21.1 – q21.2	loss
19:0-12,643,882	p13.3- p13.13	loss
19:36,259,172-58,617,616	q13.12 – q13.43	gain
21: 12,000,000-46,709,983	q11.1 – q22.3	loss

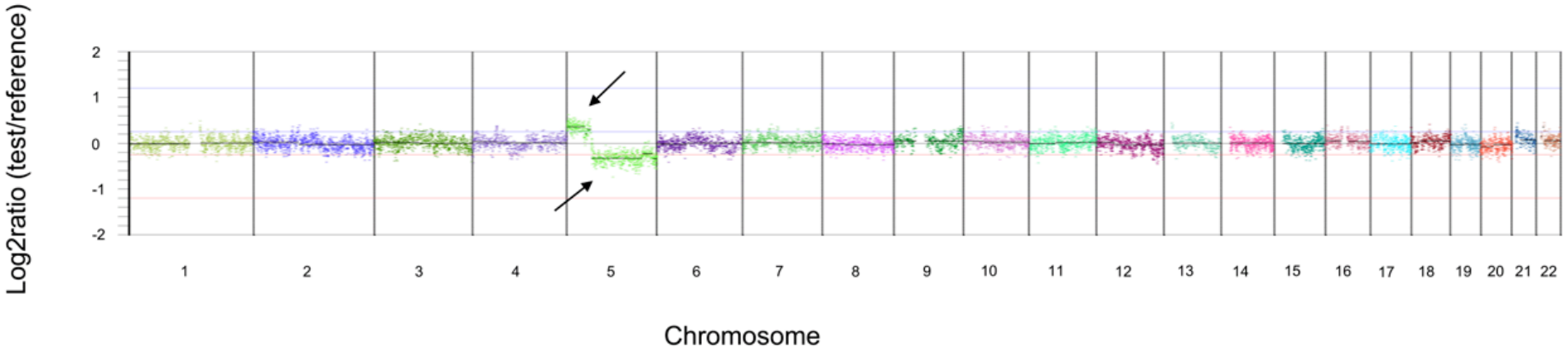

Figure 5.4 Copy number profile of RT4 R1 normalised to RT4 parental. The copy number plot was generated in Nexus Copy Number 8.0 and shows $\log_2$ ratio of the read counts of RT4 R1 normalised to parental RT4 for chromosomes 1-22 (GRch38 reference). Each point represents the $\log_2$ ratio for a section of DNA of window size 1000 bp. Copy number gains (above the zero line) and losses (below the zero line) are highlighted with arrows and are also detailed in Table 5.5.

Table 5.5 Copy number differences between RT4 parental and RT4 R1. Copy number alterations were identified with low-pass whole genome sequencing and a patient blood sample was used as the reference sample which RT4 parental and RT4 R1 were examined against.

Chromosome:Position (Mb; hg38)	Cytoband	Copy Number Loss/Gain	Potential Candidate Genes	Number of Genes in Region
5:0-48,800,000	p15.33 – q11.1	gain	*LIFR, OSMR*	136
5: 50,518,687-181,538,259	q11.1 – q35.3	loss	*IL6ST, IL31RA, MAP3K1, SMAD5, FGF1, RASGEFC, MAPK9*	721

5.2.3 Whole exome sequencing of RT112 R1

In order to identify genetic changes which could be inducing resistance, whole exome sequencing was conducted in RT112 parental, R1 and R3. To be called, a mutation needed to satisfy the following two criteria: 1) a variant allele frequency of greater than 20% and 2) an absence of the mutation in RT112 parental. All variants were visualised in Integrative Genomics Viewer (IGV) and any considered to be artefacts were removed from variant lists. No insertions or deletions in RT112 R1 or RT112 R3 met these criteria. There were forty-three single nucleotide variants (SNVs) which met the criteria in RT112 R1. These are listed in Table C.1, Appendix C. Twenty-one mutations (49%) were non-synonymous. The mutations in RT112 R1 which were thought to be most likely to be inducing resistance, as they were predicted to induce a nonsense mutation, predicted to be deleterious by Polymorphism Phenotyping v2 (PolyPhen) and Sorting Intolerant from Tolerant (SIFT) or as previous research had implicated the mutated gene in cancer, are detailed in Table 5.6.

A missense mutation in *MIB2* resulting in a Q898R amino acid change was observed in RT112 R1 (Table 5.6). *MIB2* encodes Mindbomb E3 Ubiquitin Protein Ligase 2 which ubiquitinates Delta, a Notch ligand, inducing its removal from the cell membrane via endocytosis (Koo *et al.*, 2005). Transfection of wildtype *MIB2* into melanoma cell lines reduced MET protein expression and significantly reduced invasion *in vitro* and *in vivo*. (Takeuchi *et al.*, 2006). Immunoblot analysis conducted in Chapter 4 showed that there was an increase in phospho-MET in R3 cultured without PD and in R1, R2 and R3 cultured with PD compared to RT112 parental acutely treated with PD (Fig. 4.11).

A missense mutation in *ATF2* resulting in an E349K amino acid change was observed in RT112 R1 and was predicted to be deleterious by SIFT and possibly damaging by PolyPhen (Table 5.6). *ATF2* encodes activating transcription factor 2 which elicits its activity by forming homodimers or by heterodimerizing with other activating protein 1 (AP1) family members. ATF2 regulates genes which control the cell cycle, inflammation and cell death (Watson *et al.*, 2017).

A missense mutation in *HACL1* resulting in a S15P amino acid change was observed in RT112 R1 and was predicted to be deleterious by SIFT (Table 5.6). *HACL1* encodes 2-hydroxyacyl-CoA lyase which is involved in the α-oxidation pathway which breaks down branched fatty acid and 2-hydroxylated fatty acids into aliphatic aldehydes in the peroxisome. The resulting aldehyde is then able to be degraded with the β-oxidation pathway (Foulon *et al.*, 2005).

A nonsense mutation (Q144*) in *SLC35G2* was observed in RT112 R1 (Table 5.6). *SLC35G2* encodes solute Carrier Family 35 Member G2. SLC35 family members are involved in the transport of nucleotide sugars or adenosine 3′-phospho 5′-phosphosulfate into the Golgi apparatus. Little is known about the SLCG35 subfamily (Song, 2013).

A nonsense mutation (K143*) in *TRIM51* was observed in RT112 R1 (Table 5.6). *TRIM51* encodes Tripartite Motif-Containing 51. A number of the TRIM family of RING type E3 ubiquitin ligases are involved in the regulation of the p53 pathway and the regulation of nucleotide receptors such as the thyroid receptor and the oestrogen receptors (Hatakeyama, 2011).

A nonsense mutation (E76*) was observed in *SESN3* in RT112 R1 (Table 5.6). *SESN3* encodes sestrin 3. Sestrins 1-3 are reported to act as negative regulators of mTORC1 via their interaction with the GATOR2 complex which occurs most strongly during amino acid deprivation. Sestrins 1-3 appear to be functionally redundant (Chantranupong *et al.*, 2014).

A missense mutation in *GRIP1* resulting in a G188E amino acid change was observed in RT112 R1 and was predicted to be deleterious by SIFT and probably damaging by PolyPhen (Table 5.6). *GRIP1* encodes glutamate receptor interacting protein 1 which mediates the localisation of AMPA-type glutamate receptors at the synapse (Tan *et al.*, 2015).

A missense mutation in *TMPRSS15* resulting in a R583T amino acid change was observed in RT112 R1 and was predicted to be deleterious by SIFT and probably damaging by PolyPhen (Table 5.6). *TMPRSS15* encodes Transmembrane Protease Serine 15, also known as Enteropeptidase, which cleaves the pancreatic precursor protrypsin to trypsin (Holzinger *et al.*, 2002).

All the RT112 R1 SNVs detailed in Table 5.6 had a variant allele frequency of approximately 30%. This may imply the presence of a subclone in RT112 R1.

5.2.4 Whole exome sequencing of RT112 R3

There were twenty-five SNVs which met the criteria in RT112 R3. These are listed in Table C.2, Appendix C. Thirteen mutations (52%) were non-synonymous. The mutations which were thought to be most likely to be inducing resistance in RT112 R3, as they were predicted to induce a nonsense mutation, predicted to be deleterious by PolyPhen and SIFT or as previous research had implicated the mutated gene in cancer, are detailed in Table 5.7.

Table 5.6 Selected mutations identified by whole exome sequencing in RT112 R1. The mutations met the following criteria: the mutation was absent from RT112 parental and had a variant allele frequency of greater than 20%

Gene	Ensembl transcript ID	Chromosome: Position (Mb; hg38)	Variant Effect Predictor (VEP) consequence	Coding DNA sequence change (position from start codon)	Amino acid change	COSMIC ID	Sorting Intolerant From Tolerant (SIFT) Prediction	Polymorphism Phenotyping v2 (PolyPhen) Prediction	Variant allele frequency R1 (%)	Variant allele frequency R3 (%)
MIB2	ENST00000355826	1:1629393	missense variant	c.A2693G	p.Q898R		tolerated	benign	33	0
ATF2	ENST00000264110	2:175093201	missense variant	c.G1045A	p.E349K		deleterious	possibly damaging	24	4
HACL1	ENST00000321169	3:15601421	missense variant	c.T43C	p.S15P		deleterious	benign	33	4
SLC35G2	ENST00000393079	3:136854890	stop gained	c.C430T	p.Q144*		-	-	32	3
TRIM51	ENST00000449290	11:55886138	stop gained	c.A427T	p.K143*		-	-	27	4
SESN3	ENST00000278499	11:95185375	stop gained	c.G226T	p.E76*		-	-	32	7
GRIP1	ENST00000359742	12:66517916	missense variant	c.G563A	p.G188E		deleterious	probably damaging	26	6
TMPRSS15	ENST00000284885	21:18329201	missense variant	c.G1748C	p.R583T		deleterious	probably damaging	29	4

A missense mutation in *CD55* resulting in a Y245F amino acid change was observed in RT112 R3 and was predicted to be deleterious by SIFT and probably damaging by PolyPhen (Table 5.7). CD55, also known as decay accelerating factor, is an inhibitor of the complement system. CD55 inhibits complement dependent cytotoxicity of cancer cells (Reis *et al.*, 2018).

A nonsense mutation (E2243*) was observed in *XIRP2* in RT112 R3 (Table 5.7). XIRP2 encodes Xin Actin Binding Repeat Containing 2 which is expressed in skeletal and cardiac muscle. XIRP2 stabilises the actin cytoskeleton via binding and crosslinking actin filaments (Pacholsky *et al.*, 2004).

A missense mutation in *UGT3A1* resulting in a V244E amino acid change was observed in RT112 R3 and was predicted to be deleterious (low confidence) by SIFT and possibly damaging by PolyPhen (Table 5.7). UGT3A1 transfers N-acetylglucosamine to the bile acid ursodeoxycholic acid from UDP N-acetylglucosamine (Mackenzie *et al.*, 2008).

A missense mutation in PCSK5 resulting in a W681S amino acid change was observed in RT112 R3. PCSK5 is a Calcium-dependent serine protease which cleaves and activates Pro-renin, Integrin α subunit and MMP14 (Klein-Szanto and Bassi, 2017). The COSMIC database v83 catalogues this mutation as having occurred in head and neck cancer cell lines and lung, kidney and colon cancers (Forbes *et al.*, 2017). This missense mutation was predicted to have an unknown effect by PolyPhen and SIFT did not predict the effect of this mutation. According to the Ensembl database v91, the only transcript that this variant has coding effects in (ENST00000376767) is poorly supported by experimental evidence (Zerbino *et al.*, 2018).

A missense mutation in *ZNF114* resulting in a E362K amino acid change was observed in RT112 R3. This mutation was predicted to be possibly damaging by Polyphen. *ZNF114* encodes zinc finger protein 114 which is involved in epigenetic repression of pro-differentiation genes to maintain a pluripotent state (Oleksiewicz *et al.*, 2017).

It was decided that the genetic alteration most likely to be inducing resistance in RT112 R3 was the *HRAS* G12S mutation. The *HRAS* G12S mutation has been previously reported and it is known to act as a gain of function mutation (Hobbs *et al.*, 2016). *RAS* mutations are usually mutually exclusive with *FGFR3* mutations in bladder cancer suggesting the mutations have an overlapping function

(Jebar *et al.*, 2005). The *HRAS* G12S mutation was present in 131 out of 179 (73%) reads in RT112 R3 and was not present in any reads in RT112 parental or R1 (both samples had 151 reads at *HRAS* cDNA position 34) (Table 5.7, Fig. 5.5). This mutation was selected for further investigation. The other variants in RT112 R1 and R3 were not investigated further due to time limitations.

5.2.5 Analysis of *HRAS* G12S mutation

Sanger sequencing was conducted to confirm the presence of the *HRAS* G12S mutation in RT112 R3 and absence in RT112 parental, R1 and R2 (Fig. 5.6). Sanger sequencing identified both a guanine and adenine at position 34 (relative to the first base of the ATG start codon) in exon 1 of the *HRAS* gene in RT112 R3. This confirmed that R3 contained both wildtype and G12S mutant *HRAS*.

As whole exome sequencing and Sanger sequencing found that the RT112 R3 population contained both wildtype and G12S mutant *HRAS*, it was unclear if individual RT112 R3 cells contained both *HRAS* alleles or if this was a mixed population. The *HRAS* genomic coordinates on chromosome 11 are 532,636-534,322 Mb (hg38). Copy number analysis revealed that RT112 parental, R1 and R3 all exhibited loss of chromosome 11 from 0-8,295,312 Mb (Fig. 5.1, Table 5.1). As RT112 is diploid, this suggests that RT112 parental, R1 and R3 have only one copy of *HRAS*. SNaPshot analysis of 36 single cell RT112 R3 clones, conducted by Dr Julie Burns, identified 21 single cell clones with the *HRAS* G12S mutation, 14 with wildtype *HRAS* and 1 heterozygous/mixed clone (data not shown). It is most likely that the heterozygous/mixed clone was not of single cell origin. Therefore, it can be concluded that RT112 R3 is a mixed population of cells with some cells homozygous for wildtype *HRAS* and others homozygous for G12S mutant *HRAS*.

Table 5.7 Selected mutations identified by whole exome sequencing in RT112 R3. The mutations met the following criteria: the mutation was absent from RT112 parental and had a variant allele frequency of greater than 20%

Gene	Ensemble transcript ID	Chromosome: Position (Mb;hg38)	Variant Effect Predictor (VEP) consequence	Coding DNA sequence change (position from start codon)	Amino acid change	COSMIC ID	Sorting Intolerant From Tolerant (SIFT) Prediction	Polymorphism Phenotyping v2 (PolyPhen) Prediction	Variant allele frequency R3 (%)	Variant allele frequency R1 (%)
CD55	ENST00000314754	1:207331177	missense variant	c.A734T	p.Y245F		deleterious	probably damaging	41	0
XIRP2	ENST00000409195	2:167248119	stop gained	c.G6727T	p.E2243*				34	0
UGT3A1	ENST00000333811	5:35962902	missense variant	c.T731A	p.V244E		deleterious low confidence	possibly damaging	23	0
PCSK5	ENST00000376767	9:76175271	missense variant	c.G2042C	p.W681S	COSM4139532		unknown	27	0
HRAS	ENST00000311189	11:534289	missense variant	c.G34A	p.G12S	COSM1644659 COSM1746299 COSM3931342 COSM480 COSM481 COSM482	deleterious	tolerated	73	0
ZNF114	ENST00000315849	19:48286708	missense variant	c.G1084A	p.E362K		tolerated	possibly damaging	35	0

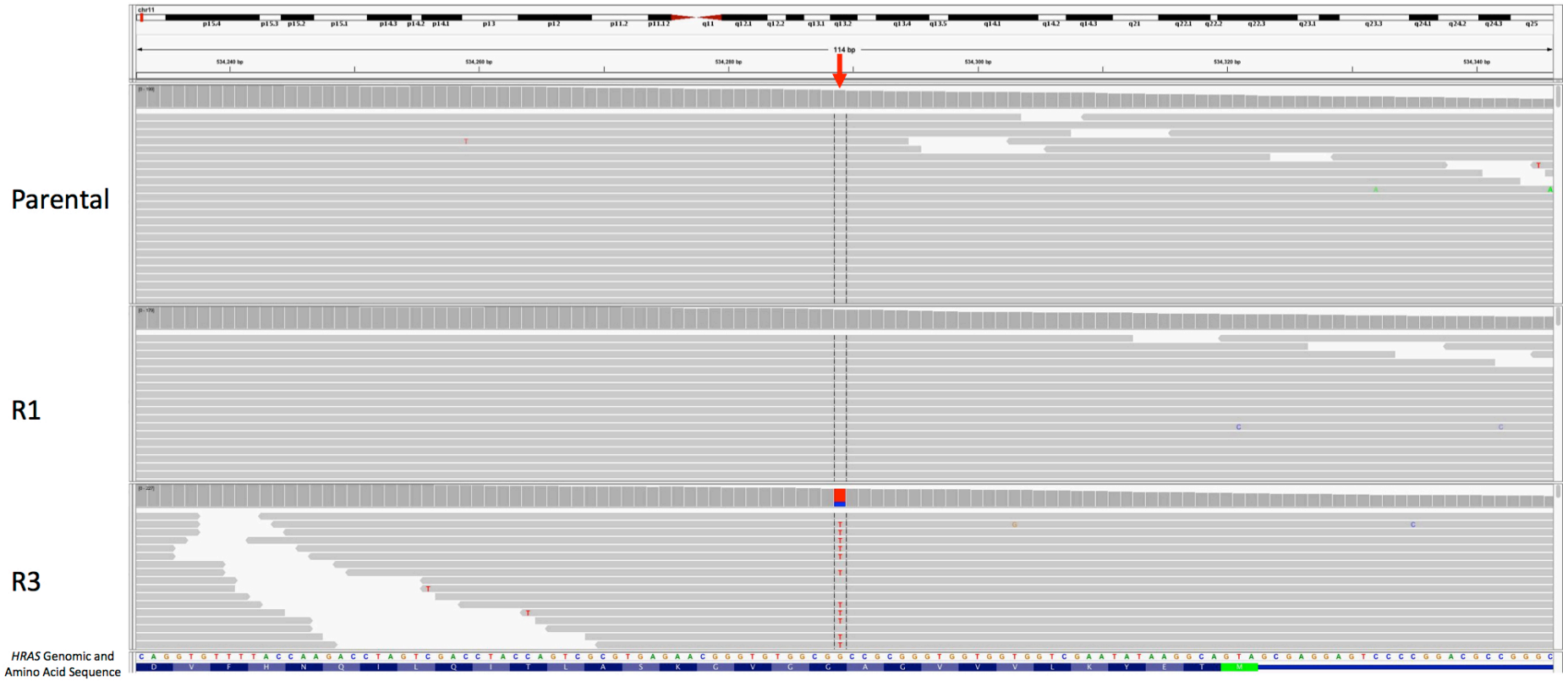

R3: c.34G>A, p.G12S

Figure 5.5 Screenshot of the *HRAS* G12S mutation in RT112 R3 visualised in the Integrative Genomics Viewer (IGV). IGV (version 2.3.59) is a computer application which enables the visualisation of next-generation sequencing data (Thorvaldsdottir *et al.*, 2013). The *HRAS* gene is encoded on the reverse strand therefore the C>T mutation located on chr11 at 534289Mb (hg38) is a G>A mutation in the *HRAS* coding sequence. The wildtype sequences for RT112 parental and R1 are also shown.

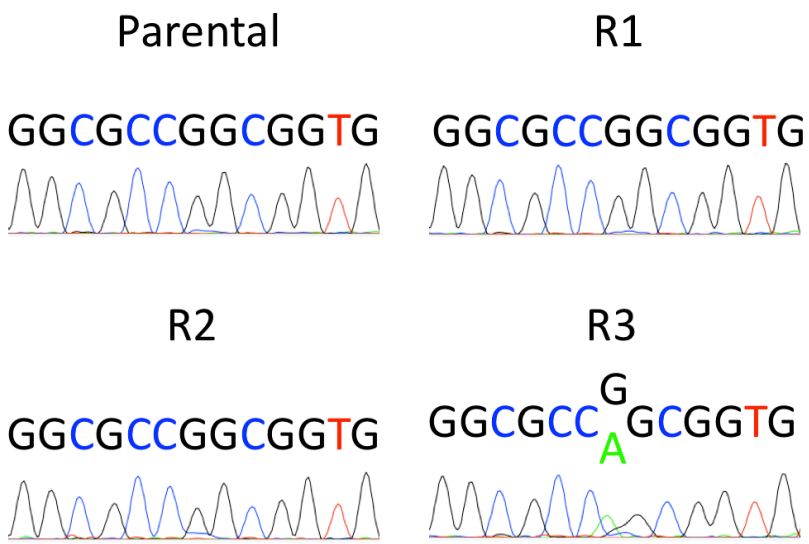

Figure 5.6 Sanger sequencing trace showing nucleotides 28 to 40 of *HRAS* exon 1 in RT112 parental R1, R2 and R3. Numbering is relative to the first base of the ATG start codon.

A SNaPshot assay was conducted with RT112 R3 at passages 63, 73 and 76 maintained in PD. Although SNaPshot analysis is only semi-quantitative, the proportion of mutant *HRAS* could be determined from these results (Fig. 5.7). The proportion of mutant *HRAS* in the R3 population increased with increased passage number and therefore suggests that the HRAS G12S provided a selective advantage.

In order to examine whether mutant *HRAS* could confer resistance to PD, RT112 parental was retrovirally transduced with a construct encoding *HRAS* G12V and selection of transduced cells was conducted. A *HRAS* G12V construct was used because we did not have a *HRAS* G12S available and time was limited. It was observed that these cells had reduced sensitivity to PD (Fig. 5.8). This provides evidence that an activating *HRAS* mutation can induce resistance to FGFR inhibition.

5.2.6 Examination of EGFR mutation status in RT4 parental and R1

Immunoblot analysis conducted in Chapter 4 found that RT4 R1 had increased total and phosphorylated EGFR compared to RT4 parental (Fig. 4.6). RT4 parental and R1 were examined for the presence of activating *EGFR* mutations by The Leeds Genetics Laboratory (St James's Hospital, Leeds) using NGS. This assay covered the following genomic regions (hg38 assembly):

1) 7:55173971-55174022 – This region accounts for the majority of exon 18.
2) 7:55174756-55174820 – This region accounts for the majority of exon 19.
3) 7:55181308-55181337 – This region is in exon 20.
4) 7:55181360-55181410 – This region is in exon 20.
5) 7:55191804-55191846 – This region is in exon 21.

EGFR exons 18-24 encode the tyrosine kinase domain of this RTK (da Cunha Santos *et al.*, 2011). The genomic regions examined by the Leeds Genomics Laboratory include the most common sites of *EGFR* (ENST00000275493) mutation in lung cancer: 7:55174013-7:55174015 which encodes G719 in exon 18 is a common site of missense mutations, 7:55174769-55174795 which encodes I744-P753 in exon 19 is a region in which deletions such as the A746_750del commonly occur, 7:55181312-55181329 encodes S768-V774 in exon 20 which is a region in which insertions commonly occur, 7:55181378 is the site of the T790M exon 20 activating mutation implicated in resistance to EGFR TKIs and 7:55191822-55191831 encodes L858-L861 in exon 21 which is a site in which missense mutations occur, notably the L858R mutation (Tsiambas *et al.*, 2016). Exon 19 deletions and L858 mutations account for greater than 90% of mutations in lung adenocarcinoma (Sholl, 2016). No *EGFR* mutations were detected in RT4 R1 in the regions listed above (data not shown). A mutation in *EGFR* in RT4 R1 could have occurred in the regions not examined by this assay or the increased activation of EGFR in RT4 may not be due to an activating EGFR mutation.

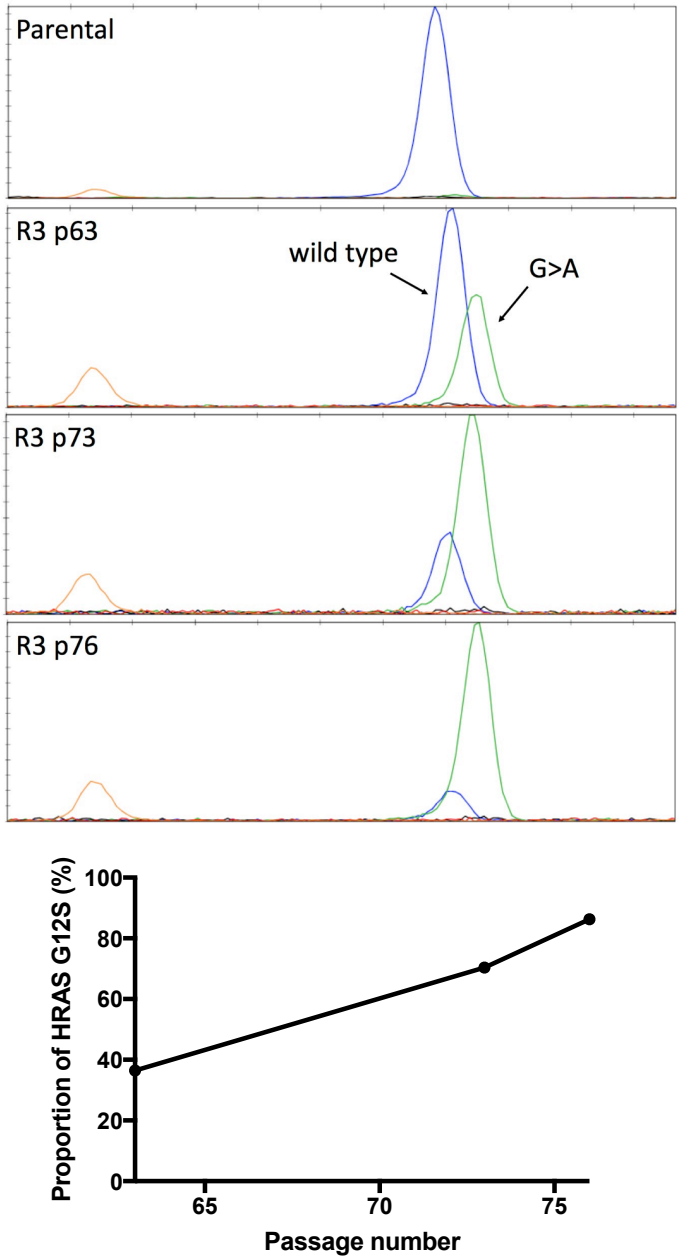

Figure 5.7 Electropherograms from the SNaPshot analysis of HRAS cDNA position 34 in RT112 parental and RT112 R3 at passage 63, 73 and 76. Orange peaks represent Genescan-120LIZ size standards, green peaks represent adenine, blue peaks represent guanine. The proportion of wildtype and mutant *HRAS* in R3 was determined from SNaPshot analysis using the area under the wildtype and mutant curves for each passage.

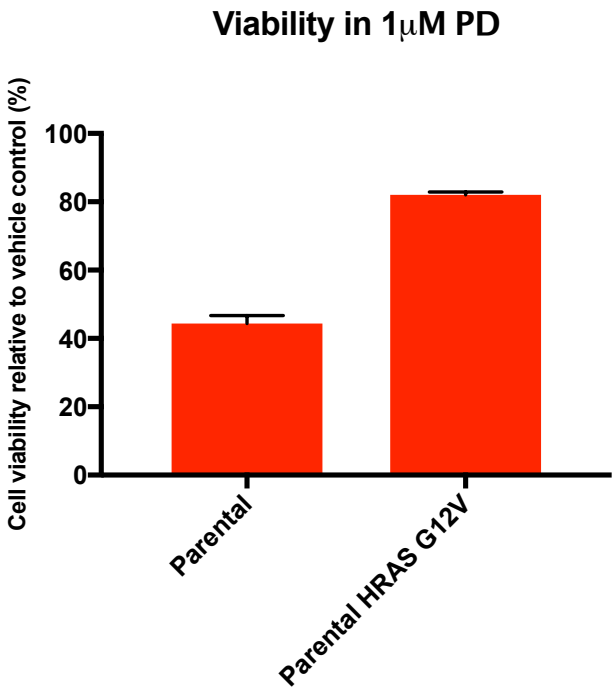

Figure 5.8 Cell viability of RT112 parental and parental HRAS G12V in 1μM PD173074. Viability of cells was assayed following 120 h treatment with PD173074 and normalised to vehicle control. Error bars show standard error of the mean. This assay was repeated twice and a representative example is shown.

5.3 Discussion

Our RT112 resistant derivatives were produced via long-term culture, for a total of 21 passages, in PD. As RT112 parental is not a clone, any genetic differences identified could have been present in a small fraction of cells prior to PD treatment or acquired during culture in PD. RT4 R1 was produced by long-term culture, for 16 passages, of RT4 parental in PD. This RT4 parental cell line was previously cloned and therefore genetic differences identified between RT4 R1 and the parental line are likely to have been acquired during the long-term culture in PD. In both RT112 and RT4, genetic differences between the parental line and the resistant derivatives could have been selected for by the culture in PD or may be passenger mutations.

Copy number alterations in RT112 and RT4 were generally consistent with previous examinations of the copy number changes in these cell lines (Hurst *et al.*, 2004; Williams *et al.*, 2005). Deletion of 2q37.2-q37.3 was observed in RT112 R1 but not RT112 parental or RT112 R3. Distal 2q deletions are associated with a higher histological stage and grade in urothelial carcinoma (Hurst *et al.*, 2012; Lindgren *et al.*, 2012; Nishiyama *et al.*, 2011). It is unclear whether this deletion contributed to the resistant phenotype. The following genes in the 2q37.2-q37.3

region were lost in RT112 R1: *SH3BP4, AGAP1, GBX2, ASB18, IQCA1*, *ACKR3*, *COPS8, COL6A3, MIR6811*, *MLPH*, *PRLH, RAB17, LRRFIP1*, *RBM44, RAMP1*, *UBE2F*, *UBE2F-SCLY*, *SCLY* and *ESPNL*. SH3BP4 modulates the amino acid mediated activation of mTORC1 by binding and inhibiting the activity of the Rag GTPase complex. When amino acids are present, the Rag GTPase complex, in its active guanine triphosphate (GTP) bound form, recruits mTORC1 to the lysosome enabling its activation. SH3BP4 directly binds the Rag GTPase complex stabilising it in its guanine diphosphate (GDP) bound, inactive form preventing the interaction between the Rag GTPase complex and mTORC1. *SH3BP4* deletions have been reported in a number of cancers including NSCLC, renal and breast cancers and SH3BP4 has been mooted as a tumour suppressor (Kim and Kim, 2013). Its loss of function could allow mTORC1 activation in the presence of FGFR3 inhibition. Whether the loss of *SH3BP4* contributed to PD resistance in RT112 R1 could be tested by inducing *SH3BP4* expression in RT112 R1 or knockdown of *SH3BP4* expression in RT112 parental and examining if these alterations increased or reduced sensitivity to PD respectively. Whole exome sequencing identified a nonsense mutation in *SESN3*, which encodes the negative regulator of mTORC1 sestrin 3. This mutation could cooperate with the deletion of *SH3BP4* to enable greater activation of mTORC1. However, as sestrin 1-3 are functionally redundant (Chantranupong *et al.*, 2014), it was thought that this mutation was unlikely to be inducing resistance to PD in RT112 R1.

Both RT112 R1 and RT112 R3 had gain of 8p11.23-q11 which contains *FGFR1*. However, increased copy number of *FGFR1* is unlikely to be the cause of resistance to PD as FGFR1 protein expression was low in RT112 R1 and R2 (Fig. 4.2). Phosphorylation of this receptor was not examined. Copy number analysis showed that there was a loss of 4p16.3-q22.1 in RT112 R1. A possible loss of 4p16.3 - p11 was also observed in RT112 R3, however, the level of this loss did not reach the threshold of -0.25 required for this region to be classified as a loss. *FGFR3* is located in cytoband 4p16.3. Immunoblot analysis conducted in Chapter 3 showed that expression of FGFR3 was reduced in RT112 R1, R2 and R3 cultured in PD compared to RT112 parental cultured out of PD (Fig. 3.11). Culture of the RT112 resistant derivatives without PD for 4 passages induced an increase in expression of both wildtype FGFR3 and the FGFR3-TACC3 fusion. However, expression of both wildtype FGFR3 and the FGFR3-TACC3 fusion remained lower than in RT112 parental cultured without PD (Fig. 3.11). As there is differential expression of wildtype FGFR3 and the FGFR3-TACC3 fusion in the RT112 resistant derivatives depending on exposure to PD, this suggests that the altered

expression is due to transient regulation of gene expression rather than loss of 4p16.3.

RT112 R1 and RT4 R1 exhibited a gain of copy number of 5p15.33-q11.1. As this change in copy number was observed in two separate resistant lines it was thought that this was the most likely copy number alteration to be causing PD resistance. This region contains the genes *OSMR* and *LIFR* which encode the oncostatin M receptor and leukaemia inhibitory family receptor respectively. These receptors are part of the OSM signalling pathway which induces activation of the STAT and MAP kinase pathways (Hermanns, 2015). RT112 R1 also exhibited a gain of copy number of 5q11.1-q11.2 which contains the gene *IL6ST* which encodes glycoprotein 130, another receptor in the OSM signalling pathway (Hermanns, 2015). It is possible that the signalling via the OSM pathway induces resistance via the activation of these pathways in the RT112 and RT4 resistant lines. The OSM pathway is examined in greater detail in Chapter 6 section 6.2.5 following transcriptome analysis of RT112 and RT4 parental and resistant lines.

SNVs in *ATF2*, *SLC35G2, TRIM51, SESN3, HACL1*, *GRIP1* and *TMPRSS15* were identified in RT112 R1. These SNVs were also present in RT112 R3 at a low variant allele frequency. This suggests that these mutations were present in a subclone of parental RT112 or that the mutation arose prior to the point at which the RT112 cells were cultured as separate lines during the derivation of the RT112 resistant derivatives (Chapter 3, Fig. 3.1). Some mutations identified in RT112 R1 and R3 have not yet been catalogued in the COSMIC database. However, this does not mean these mutations are not important as they may be novel mutations which contribute to FGFR TKI resistance. Out of all the mutations identified in RT112 R1 and R3, only the PCSK5 W681S and the HRAS G12S mutations in R3 have been curated in the COSMIC database. The PCSK5 W681S mutation (COSM4139532) has been observed in head and neck cancer (Martin *et al*., 2014), colorectal cancer (van de Wetering *et al*., 2015), gastric cancer (COSMIC study ID COSU371), acute myeloid leukemia (COSU544), lung cancer (COSU583), prostate adenocarcinoma (COSU537) and renal cell cancer (COSU588). Mutations in the RAS family of GTPases occur in many cancers including pancreatic, colorectal and lung adenocarcinomas, multiple myeloma and bladder cancer (Scott *et al*., 2016; Robertson *et al*., 2017).

It was thought that of the SNVs identified in RT112 R1 by whole exome sequencing, E349K *ATF2* and Q898R *MIB2* were the most likely to be inducing resistance. *ATF2* encodes activating transcription factor 2 which elicits its activity by

forming homodimers or by heterodimerizing with other activating protein 1 (AP1) family members. ATF2 regulates genes which control the cell cycle, inflammation and cell death (Watson *et al.*, 2017). The mutation observed in RT112 R1 induces an amino acid substitution, p.E349K, in one of the nuclear localisation signals (NLS) in this protein. The NLS contains two bipartite NLS motifs, both of which are capable of inducing nuclear localisation. One NLS motif is encoded by amino acids 342-358 and the second is encoded by amino acids 356-372 (Liu *et al.*, 2006). A suggested consensus sequence of a bipartite NLS is as follows: BBX10-12BBBBB, where B represents the basic amino acids lysine and arginine and X represents any amino acid. Only 3 residues out of the 5 basic amino acids in the second cluster are required to be lysine or arginine (Robbins *et al.*, 1991). Kosugi *et al.* reported that the introduction of basic amino acids near the centre of the linker region impaired the function of an artificial NLS (Kosugi *et al.*, 2008). Therefore, it is likely that the ATF2 E349K mutation would impair the function of the NLS motif. However, as ATF2 possesses a second functional NLS this mutation is not likely to impair ATF2 function (Liu *et al.*, 2006). Therefore, it is most likely that this mutation is not inducing PD resistance in RT112 R1.

It was thought that the Q898R mutation observed in *MIB2* in RT112 R1, could be inducing resistance to PD (Table 5.6). Takechui *et al.* observed hypermethylation of the *MIB2* promoter in 6 out of 31 invasive melanoma samples whilst hypermethylation was not observed in 25 benign nevi or five non-invasive superficial spreading melanomas. It was also reported that transfection of wildtype *MIB2* into melanoma cell lines reduced MET protein expression and significantly reduced invasion *in vitro* and *in vivo*. (Takeuchi *et al.*, 2006). Total and phospho-MET protein expression was examined in the RT112 resistant derivatives in Chapter 4 (Fig. 4.11). An increase in total MET expression was not observed in RT112 R1 compared to RT112 parental. An increase in phospho-MET was observed in R3 cultured without PD and in R1, R2 and R3 cultured with PD compared to RT112 parental acutely treated with PD. However, as MET phosphorylation was reduced in RT112 R1 and R2 upon culture without PD for 4 passages, the increase in phospho-MET appears to be transient, and suggests that it is not due to a genetic alteration such as *MIB2* mutation.

The resistance mechanism in RT112 R1 may be epigenetic, and could be due to the copy number gain of 5p15.33-q11.1 or loss of 2q37.2-q37.3 or could arise due to one of the SNVs identified in this line. Further investigation of the genetic alterations observed in RT112 R1 was not conducted due to time limitations. As whole exome sequencing and copy number analysis were not

conducted with RT112 R2, whether there is a genetic cause of PD resistance in this resistant line is unknown. However, due to the similar phenotypes of RT112 R1 and R2 it is thought that these lines may have similar mechanisms of resistance to PD. The plasticity of the RT112 R1 and R2 phenotype suggests these lines have an epigenetic mechanism of resistance. Possible resistance mechanisms in RT112 R1 and R2 include the activation of ERBB3 and MET as an increase in phosphorylation of these RTKs was observed in Chapter 4 (Fig. 4.8 and Fig. 4.11).

The RT112 R3 *HRAS* G12S mutation detected by whole exome sequencing was confirmed by Sanger sequencing. Retroviral transduction of RT112 parental with *HRAS* G12V indicated that a *HRAS* mutation can induce resistance to PD. The mutual exclusivity of mutant *RAS* and *FGFR3* in urothelial carcinoma suggests that the mutations perform a similar function (Jebar *et al.*, 2005). Immunoblot analysis conducted in Chapter 4 found that phospho-ERK and phospho-AKT were expressed in RT112 parental cells cultured without PD and the RT112 resistant derivatives in and out of PD. Phospho-ERK and phospho-AKT expression was reduced in RT112 parental cultured in PD for 24 h (Fig. 4.12). The reduced phosphorylation in RT112 parental acutely treated with PD showed that activation of the MAP kinase and PI3 kinase pathways in parental RT112 is dependent on FGFR3 activation. As the RAS family are also able to activate the MAP kinase and PI3 kinase pathways, the *HRAS* G12S mutation in RT112 R3 is likely to be inducing the phosphorylation of ERK and AKT observed in RT112 R3 cultured in PD (Castellano and Downward, 2011). *FGFR3* and RAS mutations occur more frequently in bladder cancers of a lower stage (Hurst *et al.*, 2017; Kimura *et al.*, 2001). In Chapter 3, it was shown that RT112 R3 cultured in PD had a reduced rate of proliferation and cell density at confluence compared to RT112 parental cultured without PD. This suggests that the *HRAS* mutation, whilst providing resistance to PD, does not confer exactly the same intracellular signals to induce cell proliferation as FGFR3.

SNaPShot analysis of RT112 R3 single cell clones indicated that R3 consists of a mixed population of cells, some with wildtype *HRAS* and others with G12S mutant *HRAS*. The increase in prevalence of G12S *HRAS* in this population over time suggests that G12S *HRAS* confers a selective advantage to the cells with the mutation. The survival and proliferation of the RT112 R3 cells with wildtype *HRAS* may be mediated by the activation of ERBB3 and MET observed by immunoblot in Chapter 4.

RAS proteins activate the MAP kinase, PI3 kinase, RAL and PLCε pathways inducing cell survival and proliferation. RAS proteins activate downstream signalling only when bound to GTP (Stephen *et al*., 2014). The RAS family of proteins are GTPases and upon GTP hydrolysis to GDP RAS enters its inactive form. Guanine exchange factors elicit the return of RAS to its GTP bound active form and GTPase activating proteins aid the hydrolysis of GTP (Scott *et al*., 2016). The RAS family of GTPases contain three domains: residues 1-86 of RAS proteins encode the effector lobe, residues 87-166 encode the allosteric lobe and residues 167-188/189 encode the hypervariable region. The effector lobe contains switch 1, encoded by residues 30-40, and switch 2, encoded by residues 60 to 76. Switch 1 and 2 undergo a conformational change depending on the binding of GTP or GDP. When bound to GTP, switch 1 and 2 are able to bind and activate a range of effector molecules due to their flexible structure. These effector molecules include RAF, PI3K, RALGEF and PLCε. Whilst the sequence of the effector lobe is conserved between RAS family members, the sequence of the allosteric and hypervariable regions varies. The allosteric region is involved in RAS dimerization, which is thought be important in activation of the MAP kinase pathway. Post translational modification of the hypervariable region targets RAS to the cell membrane (Spencer-Smith and O'Bryan, 2017). The majority of mutations in *HRAS*, *KRAS* and *NRAS* occur at residues G12, G13 and Q61. These residues are in the RAS G domain which binds to GTP. This domain is also responsible for the hydrolysis of GTP to GDP. Mutations at residues G12, G13 and Q61 disrupt this GTPase activity which results in constitutively active RAS (Hobbs *et al*., 2016). Mutations in the *RAS* family of GTPases occur in many cancers including pancreatic, colorectal and lung adenocarcinomas and multiple myeloma (Scott *et al*., 2016). Robertson *et al*. examined a cohort of 412 MIBCs and found that *HRAS*, *KRAS* and *NRAS* were mutated in 5, 4 and 2% of tumours respectively (Robertson *et al*., 2017). *KRAS* and *NRAS* mutations are known to occur in colorectal cancer patients as a mechanism of intrinsic and acquired resistance to EGFR-targeted therapy (Sforza *et al*., 2016; Van Emburgh *et al*., 2016). Bockorny *et al*. reported that the long-term culture of the *FGFR1*-amplified, NSCLC cell line NCI-H2077 produced a resistant derivative with an *NRAS* Q61R mutation. Treatment of the resistant cells with BGJ398 and the MEK inhibitor trametinib reduced cell proliferation to a greater extent than treatment with either BGJ398 as a single agent. It was observed that the combination of BGJ398 and trametinib was well tolerated, significantly slowed tumour progression and increased progression-free survival in a mouse NCI-H2077 xenograft model (Bockorny *et al*., 2018).

Development of a potent small molecule inhibitor which inhibits RAS for the treatment of *RAS* mutant cancers has so far been unsuccessful. Attempted methods of inhibition have included inhibiting the lipid modification of RAS to prevent the translocation of RAS to the membrane and preventing the exchange of RAS-bound GDP for GTP via inhibition of guanine nucleotide exchange factor interaction with RAS (Scott *et al.*, 2016). Development of inhibitors which target molecules downstream of RAS has been more successful. For example, the MEK inhibitor trametinib has been approved by the FDA and EMA for the treatment of BRAF mutant melanoma and NSCLC (Cheng and Tian, 2017). Inhibitors of MEK, RAF, PI3 kinase, AKT and mTOR, have entered clinical trials in patients with RAS mutant tumours (Scott *et al.*, 2016).

The likely mechanism of resistance in RT4 R1 is the activation of EGFR identified in Chapter 4. Therefore, examination of RT4 focused on identifying an *EGFR* mutation or amplification in this line. No *EGFR* mutation or amplification was found and so EGFR-upregulated expression and activation probably occurs by a non-genetic mechanism. Herrera-Abreu *et al.* reported that RT112 increased activation of EGFR as a mechanism of short-term survival to treatment with PD. They reported that PD treatment induced EGFR accumulation at the plasma membrane and the increased activation of EGFR in RT112 was as a result of reduced MAP kinase pathway repression (Herrera-Abreu *et al.*, 2013).

In conclusion, of the genetic alterations identified in RT112 and RT4 resistant derivatives in this Chapter, the most likely to be inducing PD resistance are the gain of copy number of OSM family receptors in RT112 R1 and RT4 R1, the *HRAS* G12S mutation identified in RT112 R3 and the E349K *ATF2* and Q898R *MIB2* mutations identified in RT112 R1.

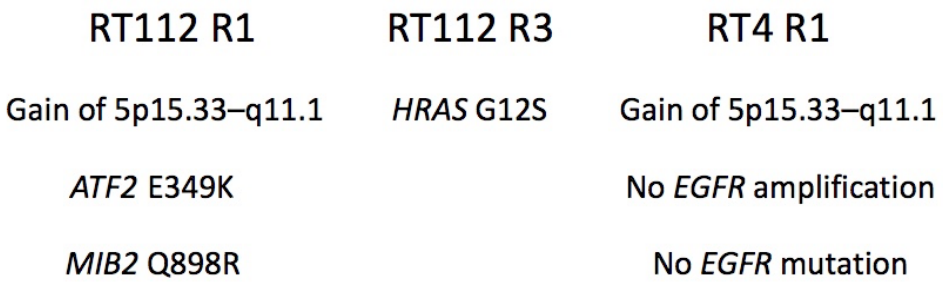

Figure 5.9 Key genetic alterations identified in RT112 and RT4 resistant derivatives. The rational as to why the *ATF2*, *MIB2* and *HRAS* mutations and the gain of 5p15.33-q11.1 were thought to be the most likely genetic alterations to be inducing resistance is outlined in the Chapter 5 discussion.

Chapter 6
Expression analysis of Parental and Resistant lines

6.1 Introduction

In Chapter 5 a *HRAS* G12S mutation was identified as the probable determinant of resistance in RT112 R3. However, RT112 R1, RT112 R2 and RT4 R1 have most likely developed resistance to PD through non-genetic mechanisms. It is probable that RT4 R1 developed resistance due to the overexpression and phosphorylation of EGFR observed in Chapter 4 (Fig. 4.6). Genetic analysis in Chapter 5 uncovered no amplification or mutation of *EGFR*, indicating that this resistance is not caused by a genetic alteration to *EGFR* in RT4 R1. Culture of RT4 R1 without PD for 4 passages re-sensitized this line to PD (Chapter 3, Fig. 3.10). Therefore, RT4 R1 did not maintain an epigenetic state which allowed it to respond to PD treatment. Culture of RT4 R1 for a greater period of time in PD may have led to the resistant line acquiring an epigenetic state which enabled it to maintain its PD-resistant state

A genetic mechanism of resistance in RT112 R1 was not identified in Chapter 5 through exome sequencing or copy number analysis. It was thought that as RT112 R1 and R2 are phenotypically similar, these lines may employ a similar method of resistance to PD. The resistance to PD in RT112 R1 and R2 may be induced by the increased phosphorylation of ERBB3 and MET observed in Chapter 4 (Fig. 4.8 and 4.11). RT112 R1 and R2 retained resistance despite reverting to a phenotype similar to parental RT112 following culture without PD for 4 passages (Fig. 3.9 and 3.5). Therefore, the gene expression profile of RT112 R1 no PD and R2 no PD could provide insight into the mechanism of PD resistance in RT112 R1 and R2. Expression analysis with DNA microarray was conducted to examine the following: 1) other possible determinants of resistance, 2) the potential downstream effect(s) of the *HRAS* G12S mutation on gene expression in RT112 R3 and 3) whether the resistant lines exhibit gene expression features associated with having undergone an EMT.

A well-reported mechanism of resistance to inhibition of a RTK is the activation of an alternative RTK. This was discussed in section 1.2.2 of the Introduction. Increased expression of a RTK in a resistant line cultured in PD may

indicate that the receptor is a possible mediator of resistance. Therefore, expression of RTKs will be examined in this Chapter. The EMT phenotype is of interest as a mesenchymal phenotype is associated with greater cell migration and invasion. Therefore, if FGFR inhibitors induce an EMT in patients this could lead to tumour metastasis (Singh *et al.*, 2017).

Expression analysis was conducted with DNA microarrays. Gene expression changes could be induced due to culture in PD, could be 'passenger' gene expression changes which are present in cells with a selective advantage or could be caused by unintended experimental differences such as cell culture conditions. Once important gene expression changes had been identified, these changes were validated with qRT-PCR and immunoblotting.

6.2 Results

Expression analysis, with Affymetrix® GeneChip® Human Transcriptome Array 2.0, was conducted with the following experimental conditions in triplicate: RT112 Parental + PD 24 h, RT112 Parental no PD, RT112 R1 + PD, RT112 R1 no PD, RT112 R2 + PD, RT112 R2 no PD, RT112 R3 + PD, RT112 R3 no PD, RT4 Parental no PD, RT4 R1 + PD and RT4 R1 no PD. Resistant line 'no PD' samples were cultured out of drug for 4-6 passages. This was long enough for RT112 R1, RT112 R2 and RT4 R1 to regain a faster proliferation rate and morphology similar to their parental line, enabling the identification of non-transient gene expression changes induced by PD. Appendix D summarises the quality control and normalisation of microarray data. Principal component analysis (PCA) was conducted and lists of genes which had undergone a significant gene expression change ($p<0.05$, one-way analysis of variance (ANOVA), 2-fold change) between experimental conditions were generated. These gene lists (included as supplementary data) were analysed with MetaCore™ pathway analysis.

6.2.1 Principal component analysis (PCA)

PCA was conducted on the full RT112 microarray dataset to examine which RT112 samples had similar gene expression (Fig. 6.1). The repeats of each experimental condition clustered close together suggesting that none of the samples were anomalous. The three parental + PD replicates clustered separately from the other

samples. The R1 + PD and R2 + PD replicates formed a second cluster. A third cluster was formed containing the following samples: parental no PD, R1 no PD, R2 no PD, R3 + PD and R3 no PD. PCA1 separated parental + PD, R1 + PD and R2 + PD from the other samples. PCA2 separated parental + PD from R1 + PD and R2 + PD. This indicated that gene expression in RT112 parental + PD was distinct from expression in other experimental conditions. It also indicated that R1 + PD and R2 + PD had similar gene expression profiles to each other, distinct from the other experimental conditions. The remaining experimental conditions have similar gene expression. This analysis fits with RT112 R1 and R2 + PD exhibiting a mesenchymal morphology in contrast to the epithelial morphology of RT112 parental no PD, R1 no PD, R2 no PD R3 + PD and R3 no PD (Chapter 3, Fig. 3.4 and Fig. 3.5). It is logical that RT112 parental + PD formed a separate cluster as this line exhibited greater sensitivity to PD than the RT112 resistant derivatives in Chapter 3 (Fig. 3.8).

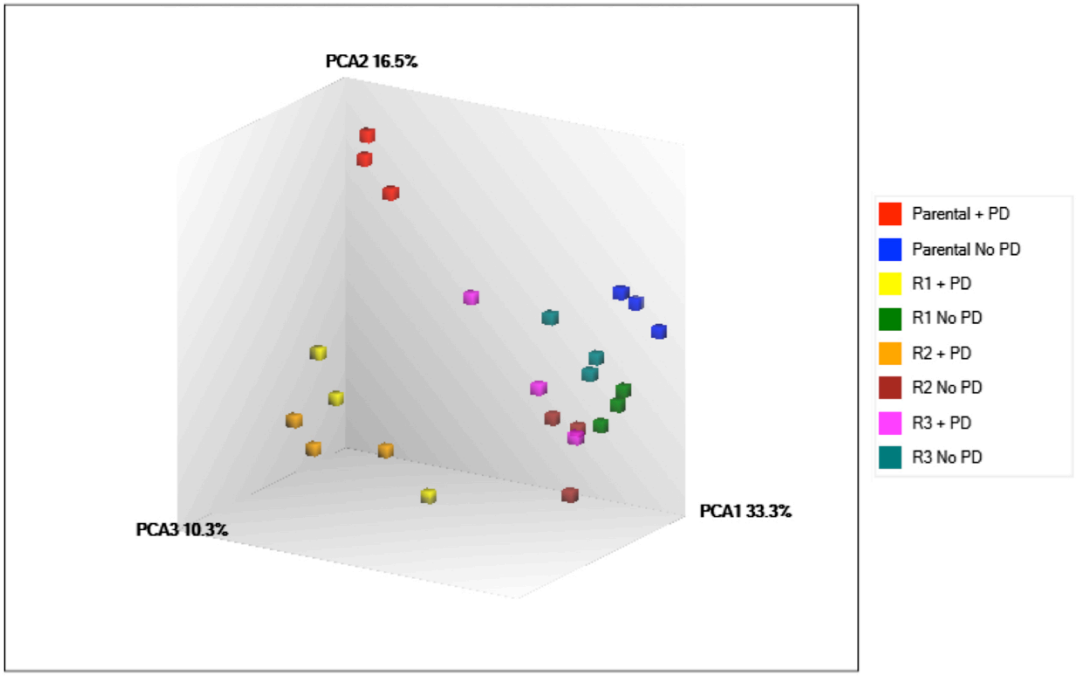

Figure 6.1 Principal component analysis of RT112 expression data. This analysis was conducted in Affymetrix Expression Console™.

PCA was conducted on the full RT4 microarray dataset (Fig. 6.2). The repeats of each experimental condition clustered close together suggesting that none of the samples were anomalous. Parental no PD, R1 + PD and R1 no PD replicates each separated into a different cluster. PCA1 separated parental no PD and R1 no PD from R1 + PD. PCA2 separated R1 no PD replicates from other samples. This indicates that the expression profile of each RT4 experimental condition was

distinct from the others. In PCA analysis the first component accounts for the greatest amount of variability in the data. Therefore, as RT4 parental and RT4 R1 no PD were separated from each other by PCA2 rather than PCA1, the expression in these two conditions was more similar to each other than the gene expression in RT4 R1 + PD. This fits with the observation that RT4 R1 cultured out of PD and RT4 parental had a similar morphology (Chapter 3, Fig. 3.6).

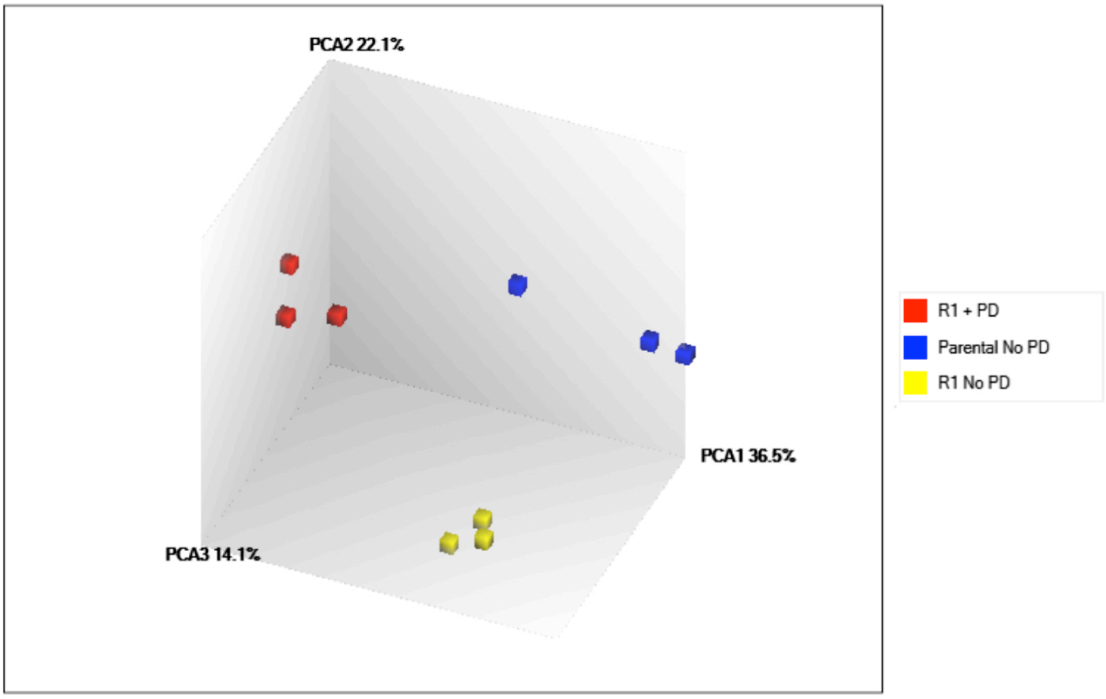

Figure 6.2 Principal component analysis of RT4 expression data. This analysis was conducted in Affymetrix Expression Console™.

6.2.2 Identification of significantly differentially expressed genes

Table 6.1 details the numbers of significantly differentially expressed probes for comparisons of RT112 experimental conditions. The threshold for significant differential expression was a greater than two-fold expression change and a $p<0.05$ in a one-way ANOVA. Additionally, a false-discovery rate p-value was calculated. The lists of the genes which were differentially expressed between experimental conditions are included as supplementary data. The greatest number of significantly differentially expressed probes was found for the comparisons of parental no PD vs parental + PD, R1 + PD, and R2 + PD and parental + PD vs R3 + PD (Table 6.1). This suggests that gene expression is most different between these experimental conditions. The comparisons of parental no PD vs R3 + PD, R1 no PD, R2 no PD and R3 no PD had the least number of significantly differentially expressed probes, each with less than 1500. This suggests that the gene expression of parental no PD

is most similar to R3 + PD and the resistant derivatives cultured out of PD. The results are concordant with the PCA analysis which found similar gene expression between RT112 parental no PD, R1 no PD, R2 no PD, R3 + PD and R3 no PD and found expression in Parental + PD, R1 + PD and R2 + PD to be distinct from expression in other experimental conditions.

Table 6.1 Number of probes which detected significantly different gene expression (ANOVA p<0.05, 2-fold) in comparisons of RT112 experimental conditions.
Identification of differentially expressed probes was conducted with the Affymetrix Transcriptome Analysis Console.

Comparison	Number of probes increased in 1st condition	Number of probes increased in 2nd condition	Total
Parental + PD vs Parental No PD	1728	1928	3716
Parental No PD vs R1 + PD	1910	1861	3771
Parental No PD vs R2 + PD	1706	1962	3668
Parental No PD vs R3 + PD	639	621	1260
Parental + PD vs R1 + PD	1255	1444	2699
Parental + PD vs R2 + PD	1428	1229	2657
Parental + PD vs R3 + PD	1983	1811	3795
R1 No PD vs Parental No PD	289	624	913
R2 No PD vs Parental No PD	726	772	1498
R3 No PD vs Parental No PD	467	349	815

Table 6.2 details the numbers of significantly differentially expressed probes for comparisons of RT4 experimental conditions. As with the analysis of RT112, the threshold for significant differential expression was a greater than two-fold expression change and a p-value <0.05 in one-way ANOVA. The number of significantly differentially expressed probes was greatest in the comparison of R1 + PD vs Parental no PD followed by R1 + PD vs R1 no PD and finally R1 no PD vs Parental no PD. This is concordant with the PCA analysis which found RT4 R1 + PD to be separated from parental no PD and R1 no PD by PCA1. Lists of differentially expressed gene lists are included as supplementary data.

Table 6.2 Number of probes which detected significantly different gene expression (ANOVA p<0.05, 2-fold) in comparisons of RT4 experimental conditions. Identification of differentially expressed probes was conducted with the Affymetrix Transcriptome Analysis Console.

Comparison	Number of probes increased in 1st condition	Number of probes increased in 2nd condition	Total
R1 + PD vs Parental No PD	849	1251	2100
R1 + PD vs R1 No PD	774	1022	1796
R1 No PD vs Parental No PD	366	494	860

6.2.3 Hierarchical cluster analysis of significantly differentially expressed genes

Hierarchical cluster analysis enables the visualisation of expression data from multiple probes and microarray samples and indicates which samples have a similar gene expression profile. Hierarchical cluster analysis was performed for probes significantly differentially expressed between RT112 parental no PD samples and the other RT112 experimental conditions (one-way ANOVA p<0.01, 2-fold) (Fig. 6.3). The samples separated into two clusters, one containing parental + PD, R1 + PD and R2 + PD and a second containing all other experimental conditions. The cluster containing parental + PD, R1 + PD and R2 + PD consisted of 2 smaller clusters: one containing parental + PD samples and another containing R1 + PD and R2 + PD samples, indicating that R1 + PD and R2 + PD have more similar gene expression to each other than to parental + PD. This fits well with the results of the RT112 PCA (Fig. 6.1).

Hierarchical clustering was performed for probes differentially expressed in RT4 experimental conditions (Fig. 6.4). Parental no PD and R1 no PD samples clustered together whilst R1 + PD samples formed a separate cluster. This fits well with the results of the RT4 PCA (Fig. 6.2).

6.2.4 Identification of differentially expressed pathways with MetaCore™

The lists of genes which were significantly differentially expressed between RT112 experimental conditions (ANOVA p<0.05, 2-fold) were analysed with MetaCore™. The comparison of RT112 parental + PD versus parental no PD was conducted to examine the effect of acute treatment on RT112 parental. Eight of the ten most significantly differentially expressed pathway maps for the comparison of RT112

parental + PD versus parental no PD relate to the cell cycle (Fig. 6.5). This reflects the slow growth of parental RT112 when acutely treated with PD, as observed during the derivation of the RT112 resistant lines (described in Chapter 3). The other pathways in the top ten significantly differentially expressed pathways are 'ATM/ATR regulation of G1/S checkpoint' and 'Sirtuin 6 regulation and functions'. ATM and ATR kinases are activated by DNA damage inducing the phosphorylation of targets involved in DNA repair, cell cycle arrest and apoptosis (Maréchal and Zou, 2013). Genes differentially expressed in the 'ATM/ATR regulation of G1/S checkpoint' MetaCore™ pathway included *ATR* and genes involved in the regulation of cell proliferation, such as members of the cyclin family and *MYC*. Expression of these genes was lower in parental + PD. Sirtuin 6 activates PARP1 via mono-ADP ribosylation, stimulating repair of DNA double strand-breaks (Mao *et al.*, 2011). Many of the genes differentially expressed in the 'Sirtuin 6 regulation and functions' MetaCore™ pathway are involved in the regulation of lipid metabolism such as *FASN* and *SCD* which encode fatty acid synthase and stearoyl-CoA desaturase-1, respectively.

MetaCore™ analysis was used to compare the gene expression of RT112 parental acutely treated with PD with the expression of resistant derivatives cultured in PD. These differences in gene expression could be critical to the PD-resistant phenotype of the derivatives. Pathway maps related to cytoskeletal remodelling, EMT and TGF signalling pathways were differentially expressed in RT112 R1 and R2 + PD compared to parental + PD (Fig. 6.6 and Fig. 6.7). This reflects the fact that RT112 R1 and R2 have a mesenchymal morphology in contrast to the epithelial morphology of the parental line (Chapter 3, Fig. 3.4).

Eight of the ten most significantly differentially expressed pathway maps for the comparison of RT112 R3 + PD versus parental + PD relate to the cell cycle (Fig. 6.8). This reflects that RT112 R3 is the most PD-resistant RT112 derivative whilst RT112 parental is sensitive to PD (Chapter 3, Fig. 3.8). The other pathways in the top ten significantly differentially expressed pathways are 'ATM/ATR regulation of G1/S checkpoint' and 'BRCA1 as a transcription factor'. Many of the genes differentially expressed in the 'ATM/ATR regulation of G1/S checkpoint' MetaCore™ pathway are involved in the regulation of cell proliferation, such as members of the cyclin family and *MYC*. Expression of these genes was higher in R3 + PD. Genes differentially expressed in the pathway 'BRCA1 as a transcription factor' included *ATM*, *ATR, BRCA1* and *MYC*. Expression of *BRCA1* and *ATR* was higher in R3 + PD, expression of *ATM* was higher in parental + PD. BRCA1 is a

tumour suppressor which is involved in the homologous recombination of DNA double strand breaks (Scully *et al.*, 1997).

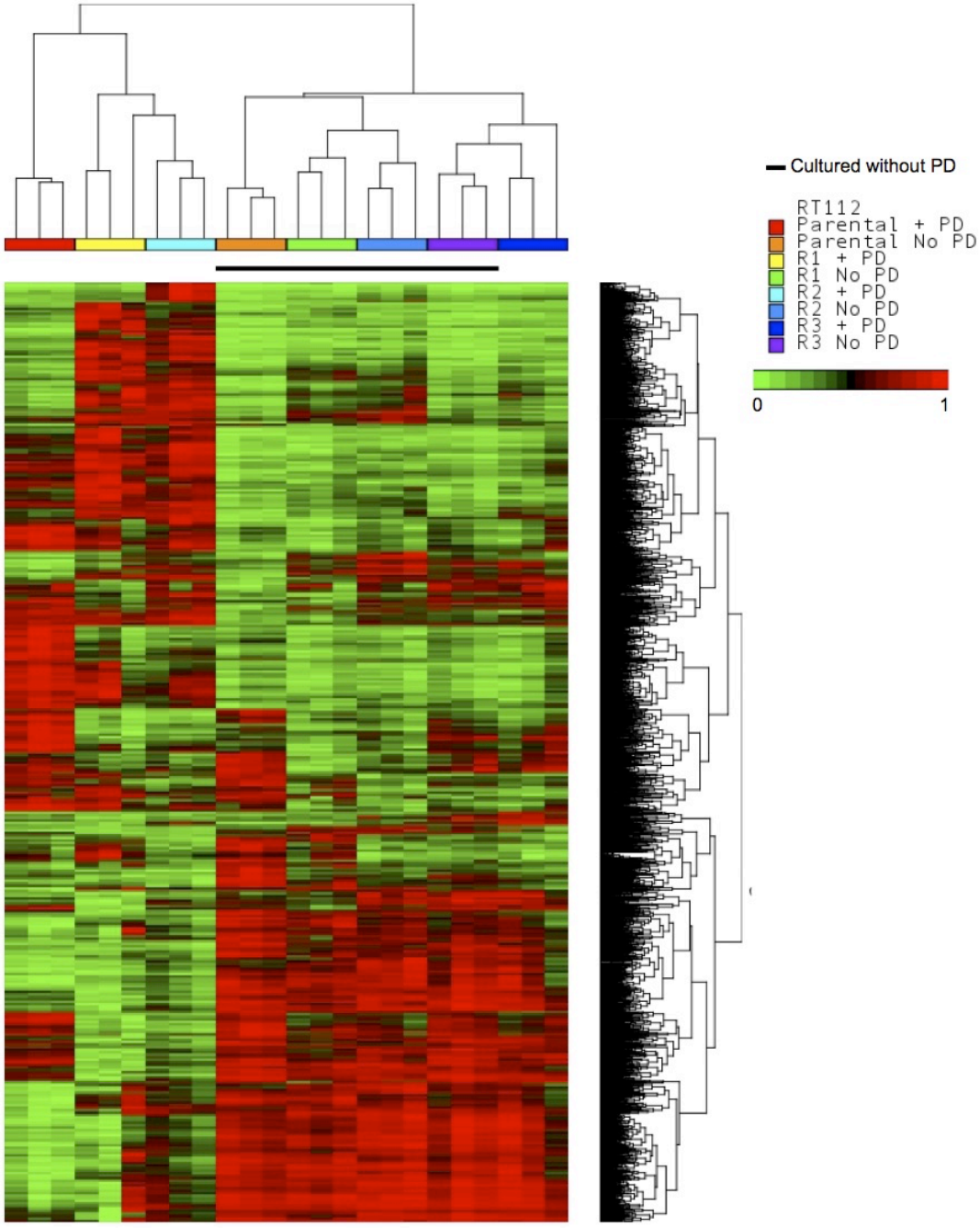

Figure 6.3 Hierarchical clustering of significantly differentially expressed genes between RT112 parental No PD and other RT112 experimental conditions (one-way ANOVA p<0.01, 2-fold change). The $\log_2$ gene expression was standardised between 0 and 1. The expression profiles of samples and genes were clustered using Euclidean distance and complete linkage. Standardisation and hierarchical cluster analysis were conducted in Partek® Genomics Suite® 6.6. Scale bar indicates the normalised $\log_2$ gene expression with colour depicting the level of gene expression as high (red), intermediate (black) and low (green).

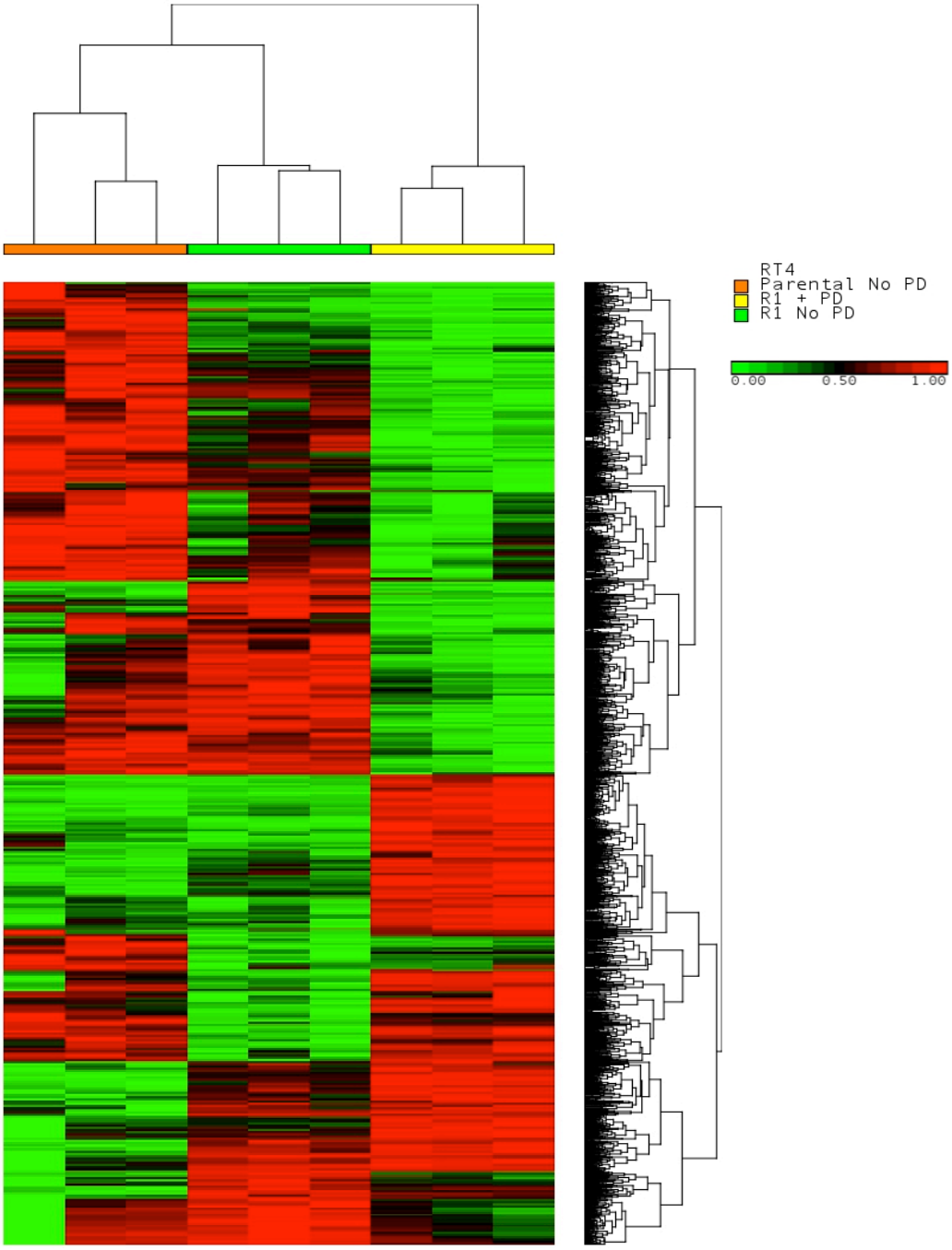

Figure 6.4 Hierarchical cluster analysis of significantly differentially expressed genes between RT4 experimental conditions (one-way ANOVA p<0.05, 2-fold change). The Log_2 gene expression was standardised between 0 and 1. The expression profiles of samples and genes were clustered using Euclidean distance and complete linkage. Standardisation and hierarchical cluster analysis were conducted in Partek® Genomics Suite® 6.6. Scale bar indicates the normalised Log_2 gene expression with colour depicting the level of gene expression as high (red), intermediate (black) and low (green).

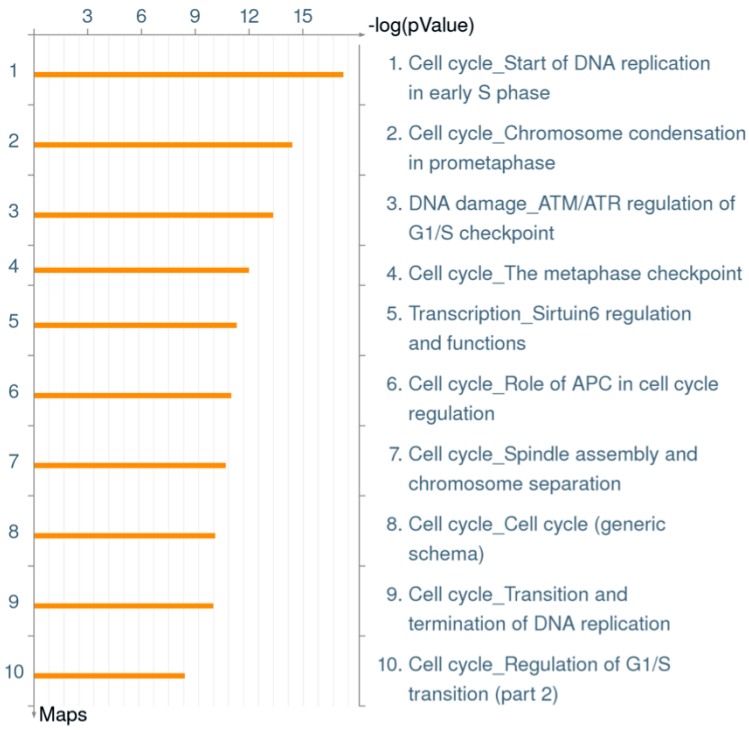

Figure 6.5 The 10 most significantly differentially expressed MetaCore™ pathway maps for RT112 parental + PD vs parental no PD.

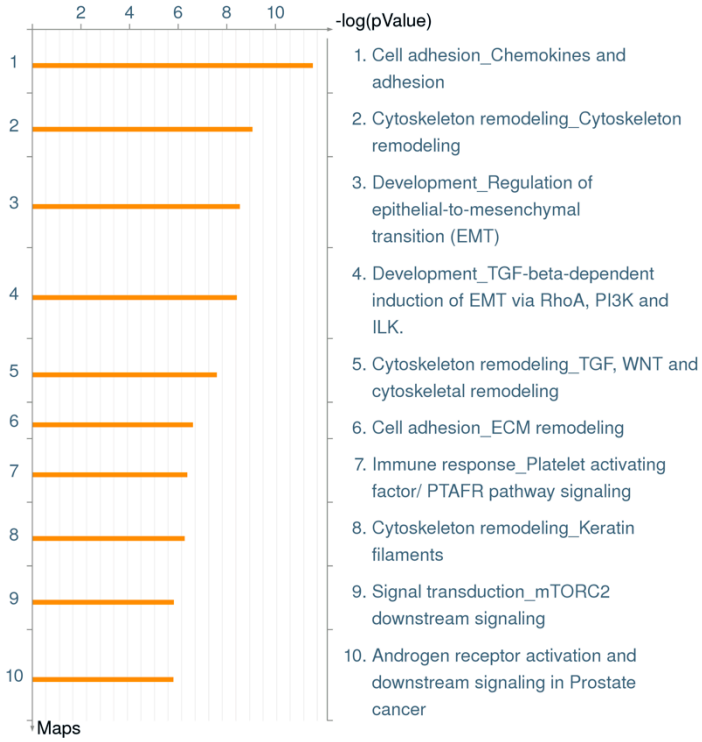

Figure 6.6 The 10 most significantly differentially expressed MetaCore™ pathway maps for RT112 R1 + PD vs parental + PD.

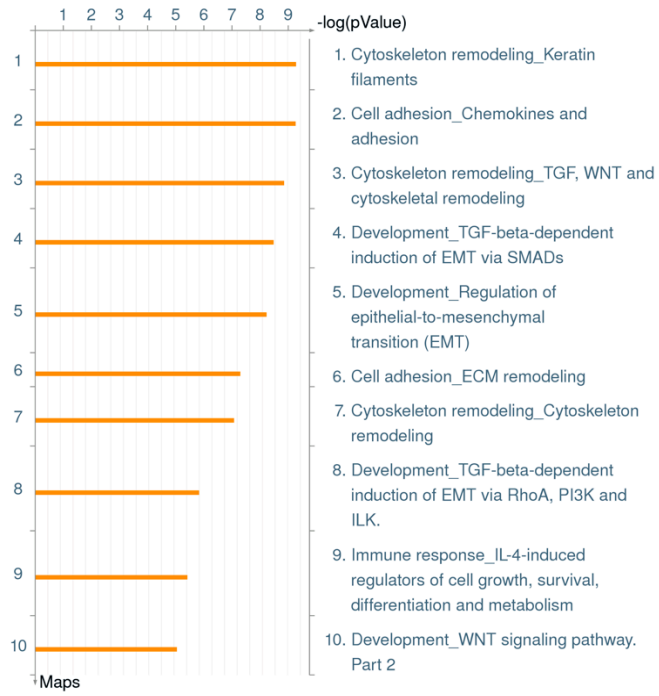

Figure 6.7 The 10 most significantly differentially expressed MetaCore™ pathway maps for RT112 R2 + PD vs parental + PD.

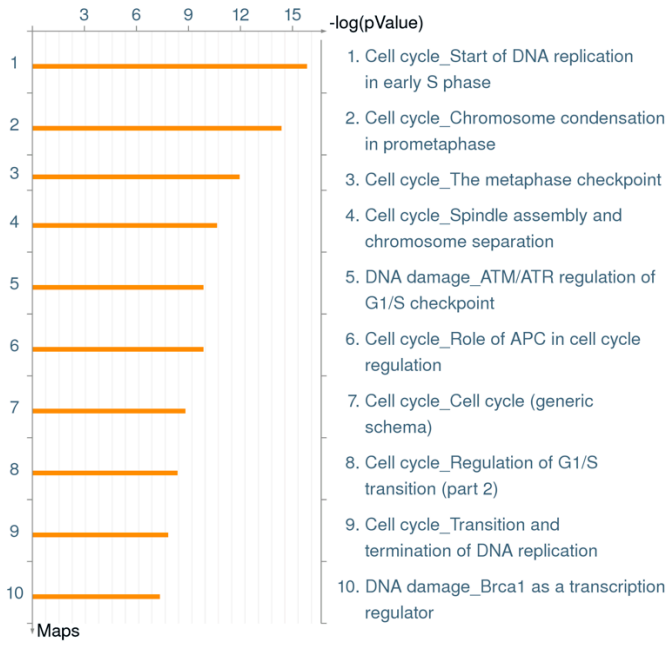

Figure 6.8 The 10 most significantly differentially expressed MetaCore™ pathway maps for RT112 R3 + PD vs parental + PD.

The resistant derivatives retained their resistance following culture without PD for 4 passages whilst exhibiting a morphology similar to the parental line. Therefore, the genes differentially expressed between RT112 parental no PD and R1, R2 and R3 no PD could be causative of this poised resistant state. MetaCore™ analysis was used to compare the gene expression of RT112 parental not cultured in PD with that of the resistant derivatives not cultured in PD. Pathway maps relating to OSM signalling are among the top ten most significantly differentially expressed pathways for R1 and R2 no PD vs parental no PD but not for R3 no PD vs parental no PD (Fig. 6.9, 6.10 and 6.11). The pathway map 'regulation of RAC1 activity' is differentially expressed in R3 no PD vs parental no PD. Rho-like GTPases such as RAC1 regulate EMT, cell migration and cell proliferation (Ungefroren *et al.*, 2017). The most significantly differentially expressed MetaCore™ pathway maps for the comparisons RT112 R1 no PD and parental + PD, R2 no PD and parental + PD and R3 no PD and parental + PD are detailed in Figures D.6, D.7 and D.8, respectively, in Appendix D.

Figure 6.9 The 10 most significantly differentially expressed MetaCore™ pathway maps between RT112 R1 no PD vs parental no PD.

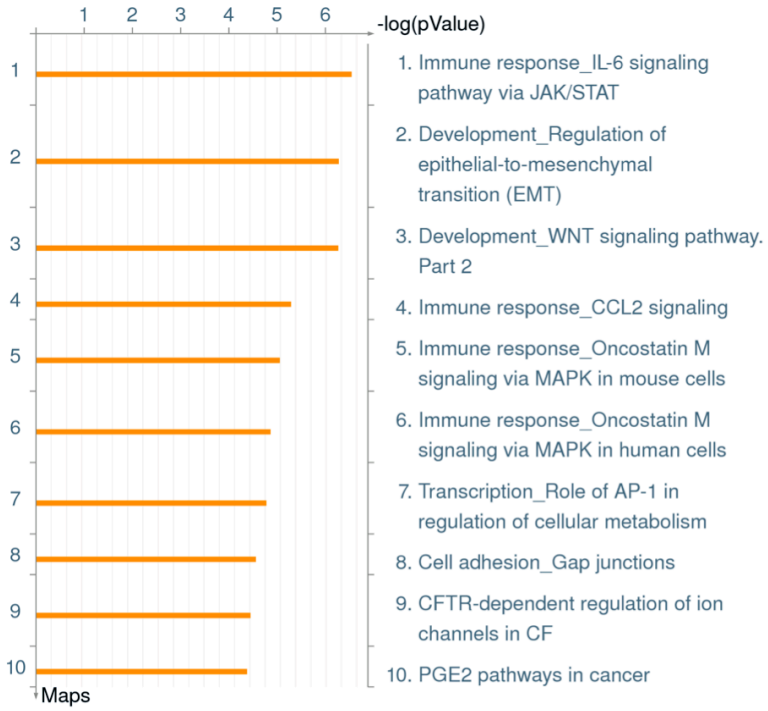

Figure 6.10 The 10 most significantly differentially expressed MetaCore™ pathway maps for RT112 R2 no PD vs parental no PD.

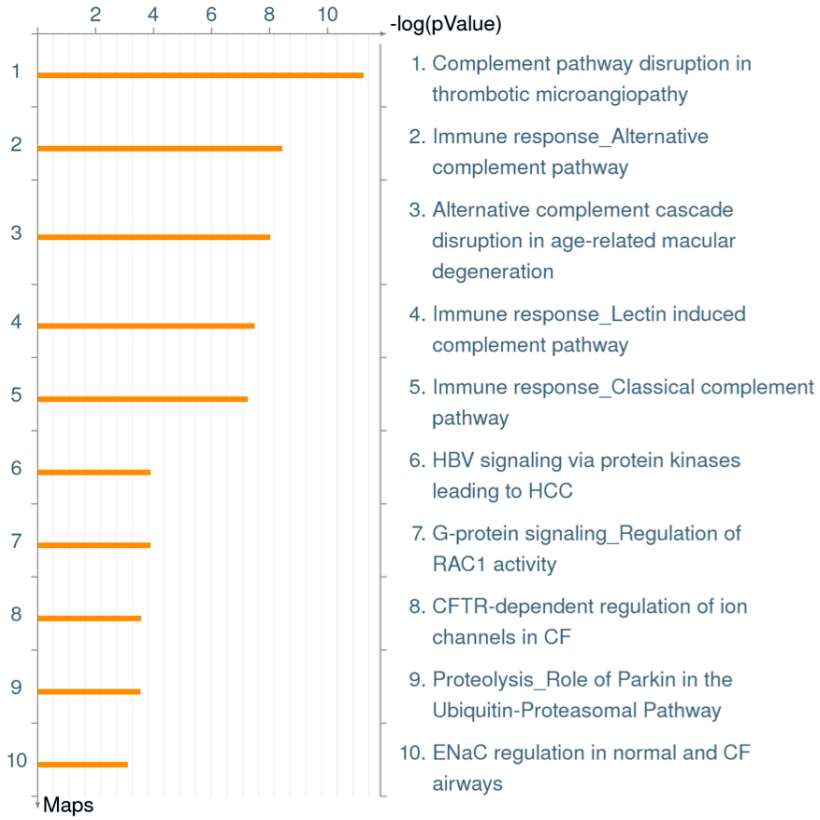

Figure 6.11 The 10 most significantly differentially expressed MetaCore™ pathway maps for RT112 R3 no PD vs parental no PD.

As observed for the MetaCore™ comparisons of RT112 resistant lines with RT112 parental no PD, pathways relating to EMT and cell adhesion were significantly differentially expressed for RT4 R1 + PD vs RT4 parental no PD (Fig. 6.12). The most significantly enriched pathway map for this comparison is 'ENaC regulation in normal and CF airways'. Genes differentially expressed in this pathway include *SCNN1A* and *SCNN1B*, which encode subunits of the epithelial sodium channel ENaC. Expression of these genes was higher in parental no PD. The ENaC sodium channel permits the diffusion of sodium ions across the apical membrane of epithelial cells. ENaC is an important mediator of homeostasis of electrolytes and water. Genes in the 'immune response IFN-alpha/beta signaling via JAK/STAT' pathway map which were differentially expressed included interferon inducible proteins and guanylate binding proteins regulated by STAT signalling. Interferons are antiviral cytokines produced in response to cellular stress which reduce proliferation and induce apoptosis in cancer cells (Snell *et al.*, 2017). Differential expression of other pathways in the list of the top 10 most differentially expressed pathway maps, such as 'effect of *H. pylori* infection on gastric epithelial cell proliferation' and 'B cell antigen pathway' appears to reflect differential regulation of cell proliferation between RT4 R1 + PD and parental no PD.

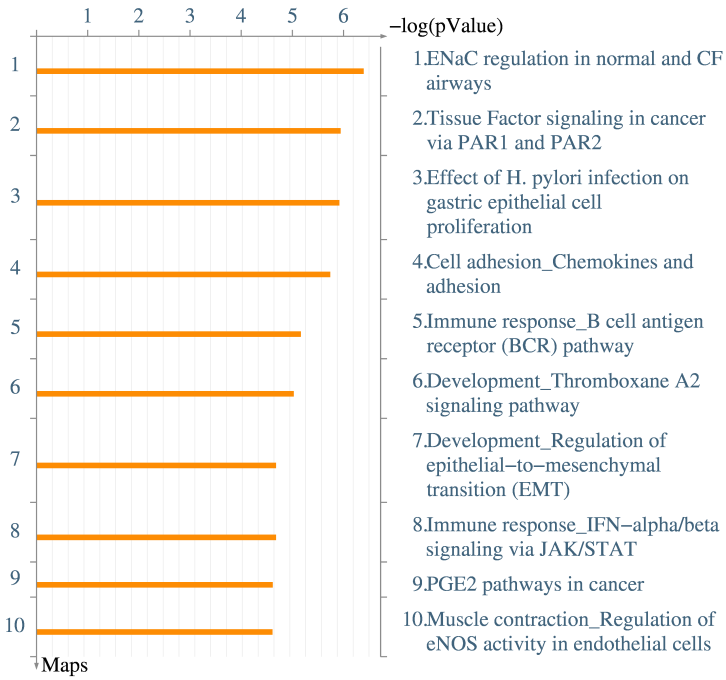

Figure 6.12 The 10 most significantly differentially expressed MetaCore™ pathway maps for RT4 R1 + PD vs parental no PD.

RT4 R1 no PD did not retain resistance to PD following culture without PD for 4 passages. Therefore, the gene expression in this experimental condition did not reflect a resistant state although persistent gene expression changes caused by FGFR inhibition may be present in this line. Increased expression of IL-1 alpha and beta in R1 no PD features in a number of pathways for the comparison of RT4 R1 no PD vs parental no PD (Fig. 6.13). The IL-1 family of cytokines are pleiotropic, can induce migration, apoptosis and proliferation and are pro-inflammatory (Striz, 2017). For the comparison of RT4 R1 no PD vs parental no PD (Fig. 6.13) and RT4 R1 + PD vs RT4 parental no PD (Fig. 6.14) there was differential expression of the 'immune response IFN-alpha/beta signaling via JAK/STAT' pathway map.

For the comparison of RT4 R1 + PD vs R1 no PD the significantly-enriched pathways relate to the cell cycle, which is logical due to the faster growth rate of R1 no PD, interferon signalling and the hippo pathway (Fig. D.9).

6.2.5 Oncostatin M signalling and downstream pathways

MetaCore™ pathway analysis showed the pathway map 'Oncostatin M signalling via MAPK in human cells' to be in the top 10 differentially expressed pathways for the RT112 comparisons: Parental no PD vs R1 no PD (Fig. 6.9), Parental no PD vs R2 no PD (Fig. 6.10), Parental no PD vs RT112 R1 + PD (Fig. D.6) and Parental no PD vs RT112 R2 + PD (Fig. D.7). Additionally, copy number analysis showed that RT112 R1 has gain of 5p15.33 - q11.1 which contains *LIFR* and *OSMR* and gain of 5q11.1 - q11.2 which contains *IL6ST* compared to RT112 parental (Chapter 5, Fig. 5.2, Table 5.2). Therefore, it was considered that signalling via the Oncostatin M (OSM) pathway could be inducing resistance to PD in RT112 R1 and RT112 R2. Signalling downstream of OSM is summarised in Fig. 6.15. OSM binds the receptor glycoprotein 130 (gp130), and then either the Oncostatin M receptor (OSMR) or Leukaemia inhibitory factor receptor (LIFR) are recruited to the complex. The OSM pathway primarily signals via the Janus kinase (JAK) family of non-receptor tyrosine kinases which phosphorylate and activate the signal transducer and activator of transcription (STAT) family of transcription factors. This is known as the JAK/STAT pathway. OSM signalling also activates the MAPK pathway, JNK, the AKT/PI3K pathway and PKCδ. Activation of these pathways could contribute to the resistant phenotype of these cells.

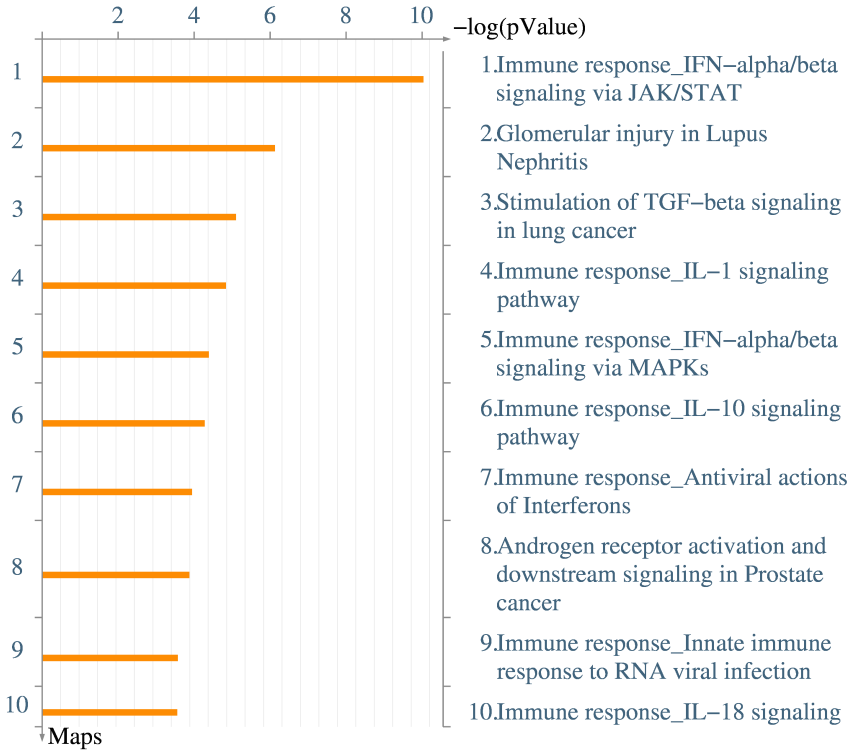

Figure 6.13 The 10 most significantly differentially expressed MetaCore™ pathway maps for RT4 R1 no PD vs parental no PD.

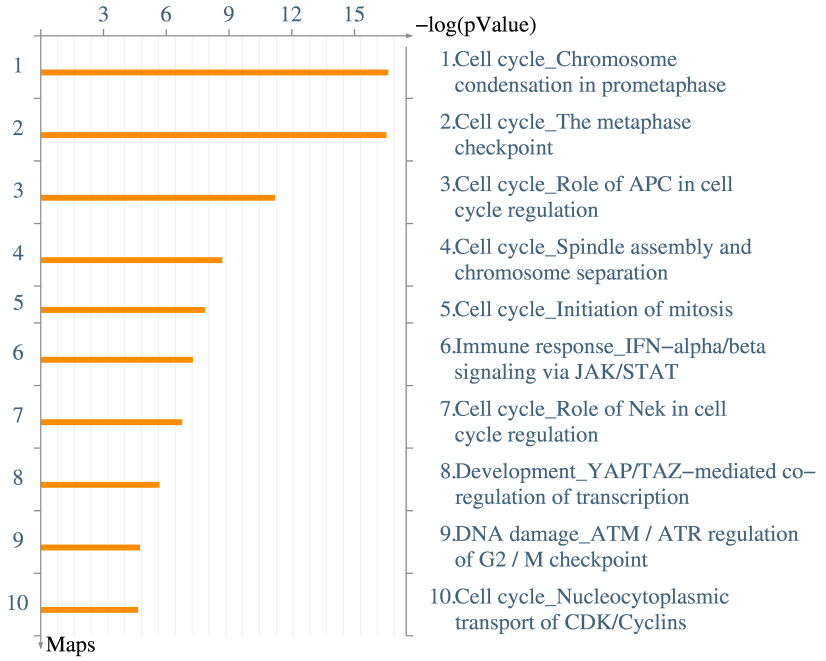

Figure 6.14 The 10 most significantly differentially expressed MetaCore™ pathway maps for RT4 R1 + PD and R1 no PD.

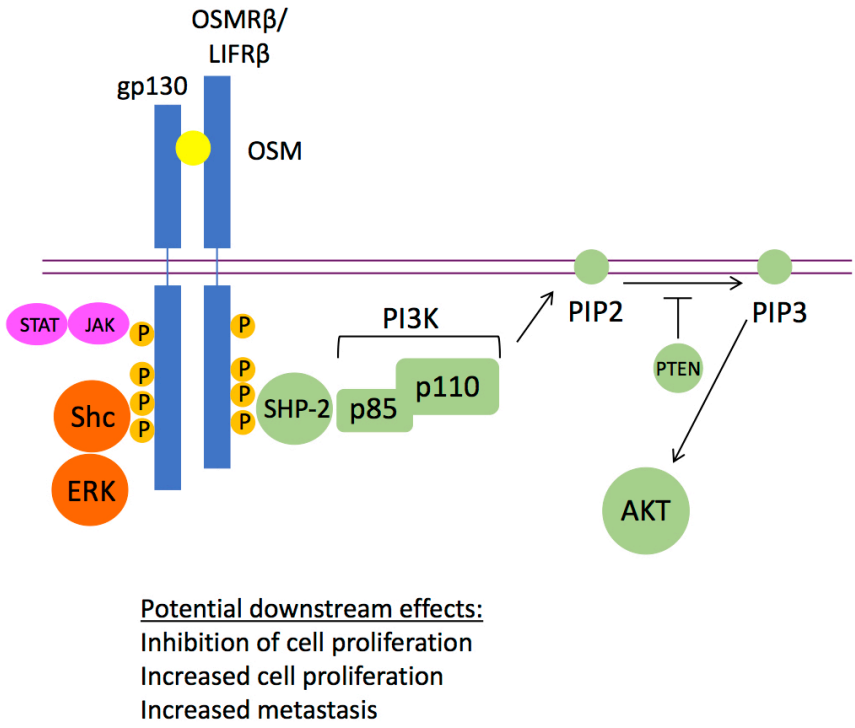

Figure 6.15 Signalling pathways activated by OSM. Orange denotes the MAP kinase pathway, magenta denotes the JAK/STAT pathway, green denotes the PI3 kinase pathway. Blue denotes the gp130 and OSMRβ/LIFRβ heterodimer and yellow denotes OSM. 'P's represent the intracellular phosphorylation of gp130 and OSMRβ/LIFRβ. Image adapted from Hermanns *et al,* 2015.

IL6ST, *OSMR* and *LIFR,* which encode receptors in the OSM signalling pathway, were amongst the genes in the MetaCore™ pathway 'Oncostatin M signalling via MAPK in human cells' which were differentially expressed in RT112 R1 + PD and RT112 R2 + PD compared to RT112 parental no PD. The *IL6ST* gene encodes the receptor glycoprotein 130 (gp130). Microarray analysis found that *IL6ST* expression was highest in R1 + PD and R2 + PD where it was approximately 20-fold and 9-fold higher respectively than in RT112 parental no PD (Fig. 6.16). qRT-PCR analysis of *IL6ST* confirmed that expression was significantly increased in R1 + PD and R1 no PD (Fig. 6.16). Microarray analysis showed that *OSMR* expression was significantly increased in R1 + PD, R1 no PD, R2 + PD and R2 no PD and significantly decreased in parental + PD compared to parental no PD (Fig. 6.17). qRT-PCR analysis confirmed the increase in *OSMR* expression in R1 + PD and R1 no PD (Fig. 6.17). Microarray analysis showed that *LIFR* expression was approximately 3, 5 and 2-fold higher in R1 + PD, R2 + PD and R3 + PD respectively than in parental no PD (Fig. 6.18). qRT-PCR confirmed that *LIFR* was significantly increased in R1 + PD and also showed that expression was significantly increased in R1 no PD (Fig. 6.18). The observed increase in expression of *IL6ST*, *OSMR* and *LIFR* could

be mediating an increase in activation of the OSM signalling pathway in RT112 resistant lines. The RT112 R1 5p15.33 - q11.1 and 5q11.1 - q11.2 gains may be mediating the increase in expression of *IL6ST*, *OSMR* and *LIFR* observed in RT112 R1 no PD compared to parental no PD. However, the 5p gains cannot account for the increased expression of *IL6ST*, *OSMR* and *LIFR* in RT112 R1 + PD compared to R1 no PD.

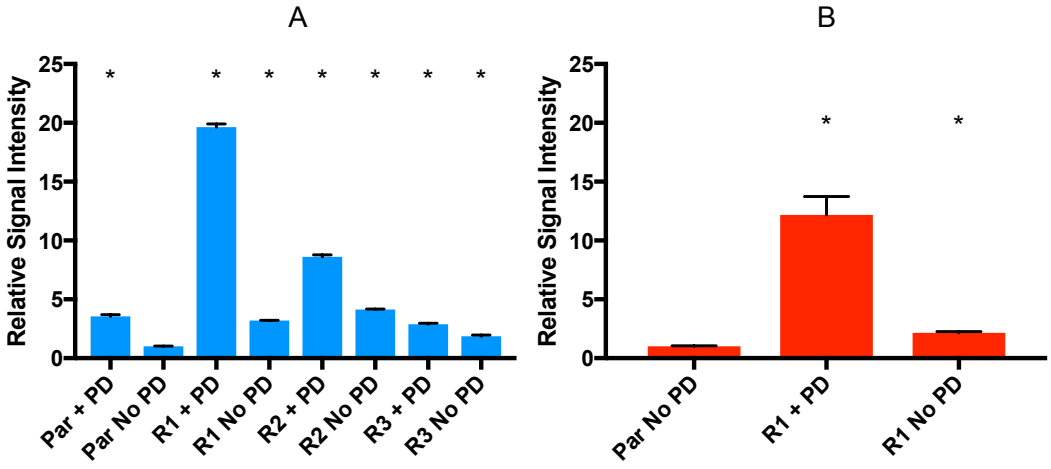

Figure 6.16 Expression of *IL6ST* in RT112 determined by microarray and qRT-PCR analysis. A) microarray analysis. B) qRT-PCR analysis. Error bars indicate standard error of the mean. Signal intensity is given relative to parental no PD. For microarray: asterisks indicate the experimental conditions in which *IL6ST* is differentially expressed compared to parental no PD (ANOVA $p<0.05$, 2-fold expression change). For qRT-PCR: asterisks indicate the experimental conditions in which *IL6ST* is differentially expressed compared to parental no PD (Mann-Whitney U, 2-tailed test, $p<0.05$).

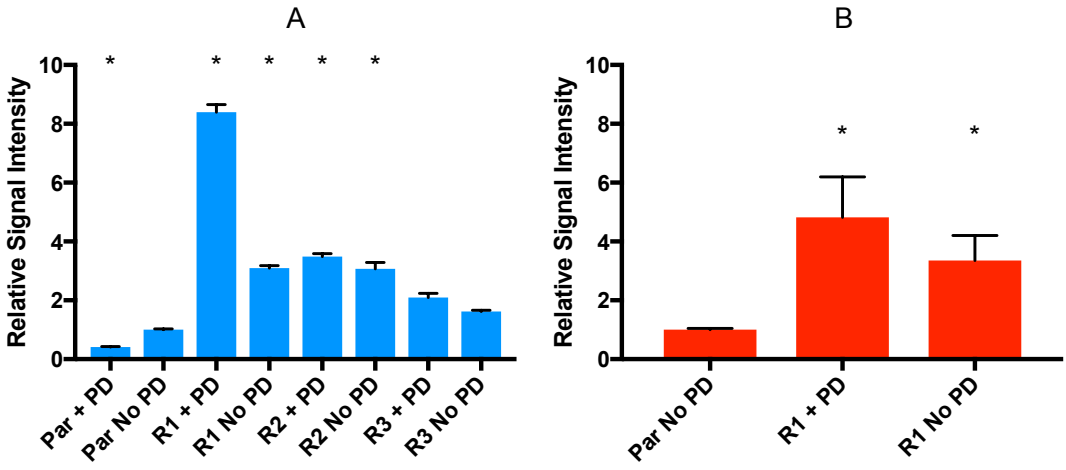

Figure 6.17 Expression of *OSMR* in RT112 determined by microarray and qRT-PCR analysis. A) microarray analysis. B) qRT-PCR analysis. Error bars indicate standard error of the mean. Signal intensity is given relative to parental no PD. Asterisks indicate the experimental conditions in which *OSMR* was differentially expressed compared to parental no PD. Microarray statistical test: ANOVA $p<0.05$, 2-fold expression change. qRT-PCR statistical test: Mann-Whitney U 2-tailed test, $p<0.05$.

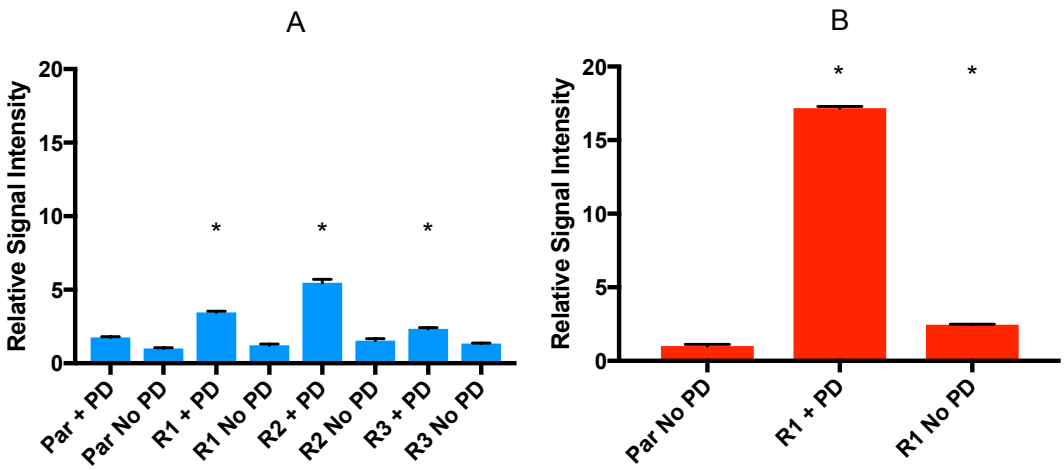

Figure 6.18 Expression of *LIFR* in RT112 determined by microarray and qRT-PCR analysis. A) microarray analysis. B) qRT-PCR analysis. Error bars indicate standard error of the mean. Signal intensity is given relative to parental no PD. Asterisks indicate the experimental conditions in which *LIFR* was differentially expressed compared to parental no PD. Microarray statistical test: ANOVA $p<0.05$, 2-fold expression change. qRT-PCR statistical test: Mann-Whitney U 2-tailed test, $p<0.05$.

Microarray analysis showed that the OSM signalling pathway ligands *OSM* and *IL31* were not significantly differentially expressed between RT112 parental no PD and the other RT112 experimental conditions (Appendix D, Fig. D.10). Therefore, if activation of the OSM signalling pathway is increased in RT112 it is unlikely to be due to increased presence of ligand.

In RT4, MetaCore™ pathway analysis did not suggest that the OSM signalling pathway was differentially expressed in RT4 parental and RT4 R1 (Fig. 6.13, 6.14 and D.9). However, as this pathway had been identified as a possible mediator of resistance to PD in RT112 R1 and R2, it was examined in RT4. Additionally, copy number analysis showed that RT4 R1 had copy number gain of the region 5p15.33 - q11.1 which contains *LIFR* and *OSMR* and loss of the region 5q11.1 - q35.3 which contains *IL6ST*. *IL6ST*, *OSMR* and *LIFR* were not significantly differentially expressed in RT4 R1 + PD compared to RT4 parental no PD (Appendix D, Fig. D.11). *OSM* and *IL31* were not significantly differentially expressed between RT4 experimental conditions (Appendix D, Fig. D.12). Therefore, differential expression of these receptors or ligands is unlikely to be contributing to resistance in RT4 R1 and the copy number alterations on chromosome 5 observed in RT4 R1 are not significantly altering expression of *IL6ST*, *OSMR* and *LIFR*.

As previously stated, OSM signals primarily via the JAK/STAT pathway (Fig. 6.15). For this reason, it was decided to examine the microarray data for expression of the *STATs* in RT112 experimental conditions (Fig. 6.19). Expression of *STAT1*,

STAT3 and, to a lesser extent, *STAT5B* was increased in RT112 R1 + PD and R2 + PD compared to RT112 parental no PD. *STAT5A* expression was similar between the RT112 experimental conditions. The increase in *STAT3* expression in R1 + PD was validated by qRT-PCR (Fig. 6.19).

Phosphorylation of STAT family members induces the translocation of these molecules to the nucleus where they carry out their function as transcription factors (Hermanns, 2015). For this reason, phosphorylation of STAT1 and STAT3 was examined in RT112 parental and resistant lines (Fig. 6.20 and 6.21). A431 treated with EGF was selected as a positive control for STAT1 and STAT3 as previous research has shown that A431 treated with EGF expresses total and phosphorylated STAT1 and STAT3 (Grudinkin *et al.*, 2007). Phosphorylated STAT1 and STAT3 could not be detected by immunoblot in any RT112 samples. Therefore, STAT1 and STAT3 are not mediating resistance in RT112 resistant lines. As the STAT family of transcription factors are commonly activated when OSM and OSMR signalling is active, it is unlikely that the increased expression of *OSMR*, *LIFR* and *IL6ST* is inducing resistance in RT112 R1 and RT112 R2 via STAT activation. However, it is possible that *OSMR*, *LIFR* and *IL6ST* are mediating resistance via activation of the MAP kinase pathway without activating the STAT family of transcription factors. Phosphorylation of STAT1 or STAT3 was not examined in RT4 as the microarray data indicated that there was no significant increase in *OSM, IL31, IL6ST, OSMR, LIFR, STAT1, STAT3, STAT5A* or *STAT5B* expression in RT4 R1 compared to parental.

As previously stated, OSM signalling can activate the MAPK pathway (Fig. 6.15) which regulates the activity of the activator protein 1 (AP-1) transcription factor. Microarray analysis indicated that expression of *JUN*, which encodes AP-1 family member JUN, was significantly increased in RT112 R1 + PD, R2 + PD and R2 no PD compared to RT112 parental (Fig. 6.22). This increase was confirmed for R1 + PD and R1 no PD by qRT-PCR. Jun can homodimerize or heterodimerize with other AP-1 family members to form the AP-1 transcription factor. Jun is a positive regulator of cell proliferation (Shaulian, 2010). A key difference between RT112 parental acutely treated with PD and the RT112 resistant lines is the maintenance of ERK phosphorylation in the resistant lines (Chapter 4, Fig. 4.12). OSM pathway signalling could be activating AP-1 via the MAPK pathway in RT112 R1 and R2. *JUN* expression was also significantly increased in RT4 R1 + PD and non-significantly increased in R1 no PD compared to parental no PD (Fig. 6.22). This may induce cell proliferation in RT4 R1 + PD. JUN protein expression was not examined due to time limitations.

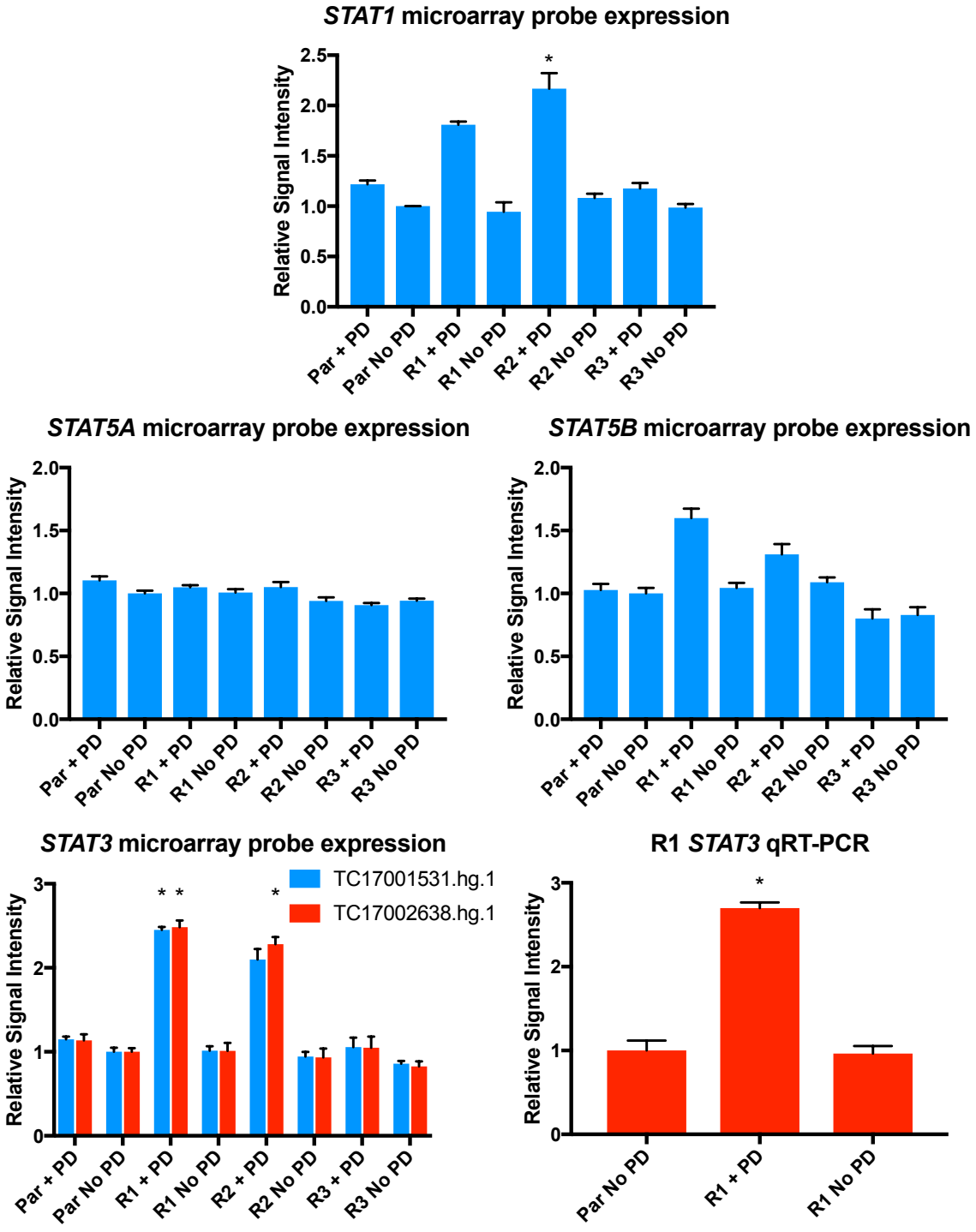

Figure 6.19 Expression of *STATs* in RT112 determined by microarray and qRT-PCR analysis. Error bars indicate standard error of the mean. Signal intensity is given relative to parental no PD. Asterisks indicate the probe and experimental condition for which significantly different expression was detected compared to parental no PD. Microarray statistical test: ANOVA $p<0.05$, 2-fold expression change. qRT-PCR statistical test: Mann-Whitney U 2-tailed test, $p<0.05$. For genes with specificity to more than one probe, all probes are shown with a legend indicating the probe's Affymetrix IDs.

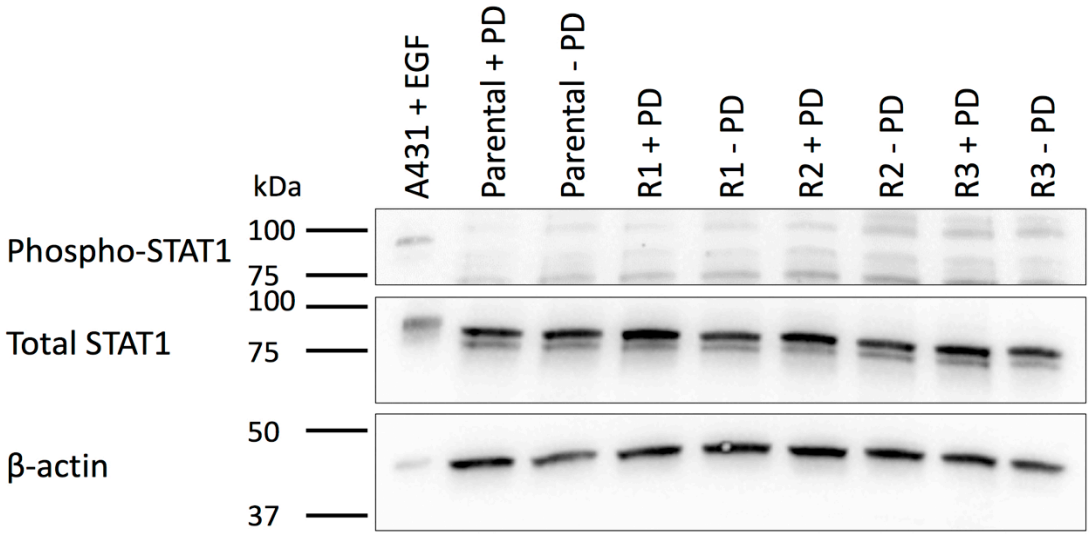

Figure 6.20 Immunoblot analysis of phospho-STAT1 and total STAT1 protein expression in RT112. Expression was examined in parental, parental treated with PD173074 for 24 h, R1, R2 and R3 cultured with PD173074 and R1, R2 and R3 cultured without PD173074 for 4 passages. A431 + EGF was included as a positive control for phospho-STAT1 and total STAT1 and β-actin was used as a loading control.

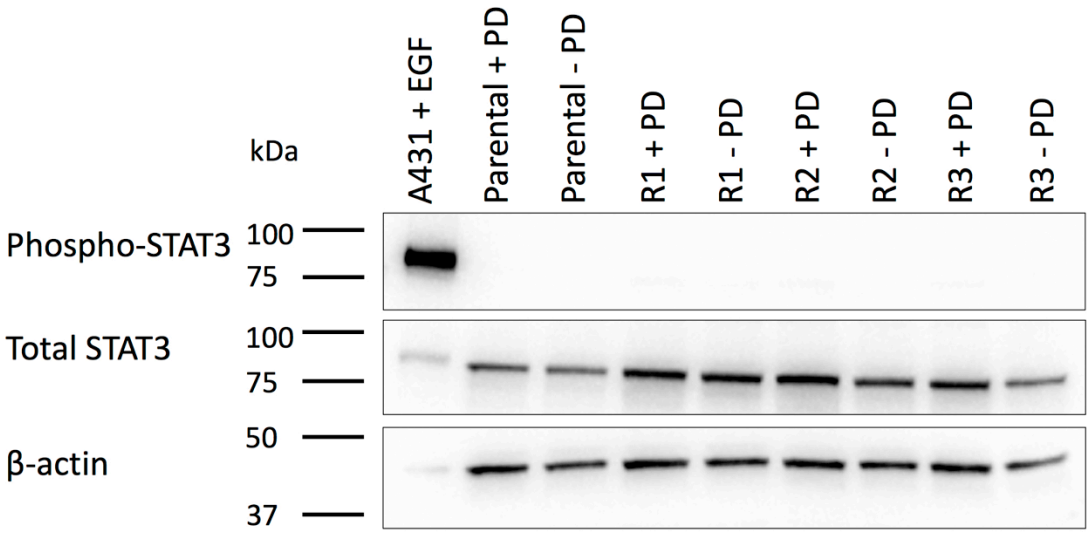

Figure 6.21 Immunoblot analysis of phospho-STAT3 and total STAT3 protein expression in RT112. Expression was examined in parental, parental treated with PD173074 for 24 h, R1, R2 and R3 cultured with PD173074 and R1, R2 and R3 cultured without PD173074 for 4 passages. A431 + EGF was included as a positive control for phospho-STAT3 and total STAT3 and β-actin was used as a loading control.

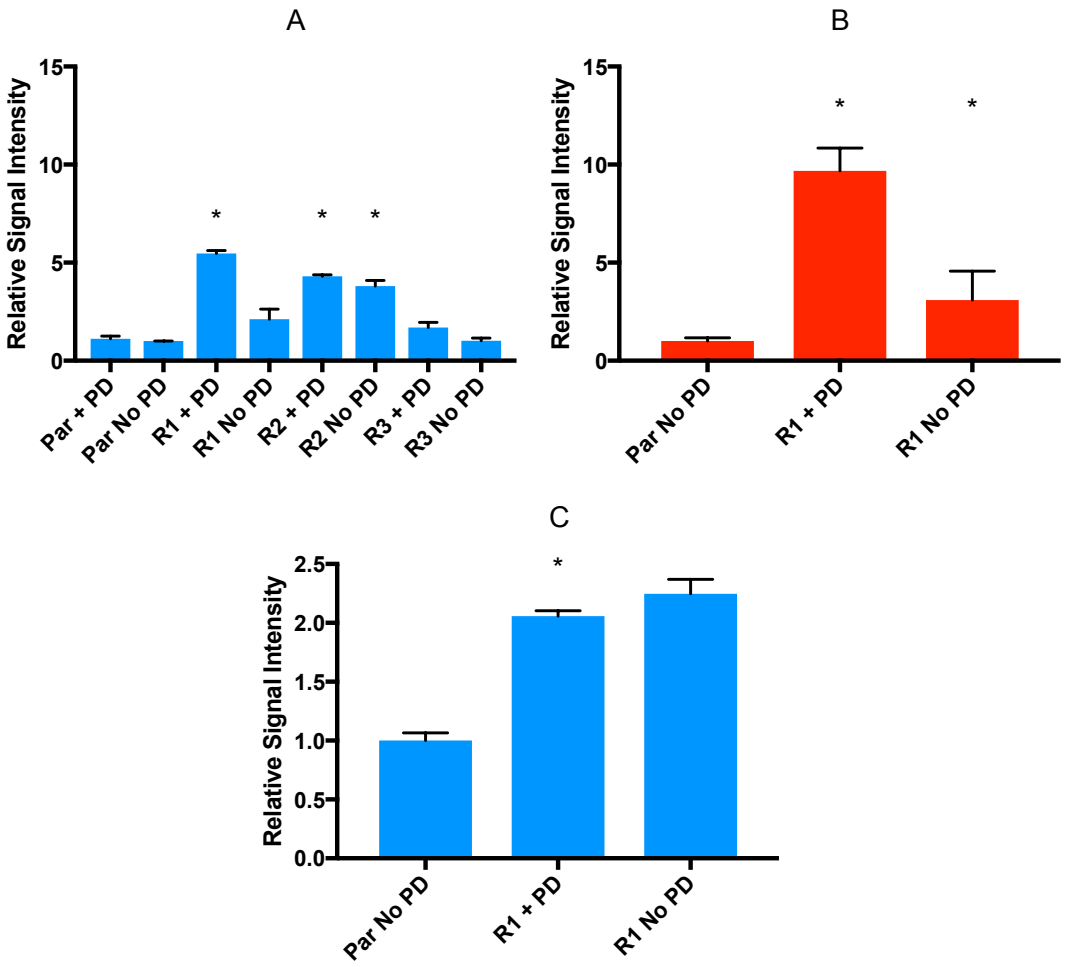

Figure 6.22 Expression of *JUN* in RT112 and RT4 determined by microarray and qRT-PCR analysis. A) microarray analysis of *JUN* in RT112. B) qRT-PCR analysis of *JUN* in RT112. C) microarray analysis of *JUN* in RT4. Error bars indicate standard error of the mean. Signal intensity is given relative to parental no PD. For microarray and qRT-PCR, asterisks indicate the experimental conditions in which *JUN* was differentially expressed compared to parental no PD. Microarray statistical test: ANOVA $p<0.05$, 2-fold expression change. qRT-PCR statistical test: Mann-Whitney U 2-tailed test, $p<0.05$.

6.2.6 Expression of regulators of lipid homeostasis

The regulation of fatty acid synthesis by FGFR3 has been studied in RT112. Du *et al.* reported that *FGFR3* knockdown in RT112 reduced expression of genes involved in fatty acid and sterol biosynthesis and metabolism (Du *et al.*, 2012). The transcription factors SREBP1 and SREBP2, encoded by the genes *SREBF1* and *SREBF2*, preferentially regulate synthesis of unsaturated fatty acids and cholesterol, respectively (Hagen *et al.*, 2010). In RT112, microarray analysis showed that expression of *SREBF1* was significantly differentially downregulated in parental + PD, R1 + PD, R2 + PD and R2 no PD compared to parental no PD. Additionally, *SREBF1* was non-significantly reduced in R1 no PD, R3 + PD and R3 no PD. *SREBF2* was not significantly differentially expressed in the other RT112

experimental conditions compared to parental no PD (Fig. 6.23). qRT-PCR validation found significantly reduced expression of *SREBF1* in parental + PD, R1 + PD, R1 no PD, R2 + PD and R2 no PD compared to parental no PD (Fig. 6.24). In contrast to the microarray analysis, qRT-PCR analysis indicated that *SREBF1* expression in R3 no PD was significantly increased (Fig. 6.24). Therefore, the synthesis of fatty acids could be reduced in RT112 parental + PD and in RT112 resistant lines. Cholesterol synthesis may also be reduced despite the reduction in *SREBF2* expression not being statistically significant.

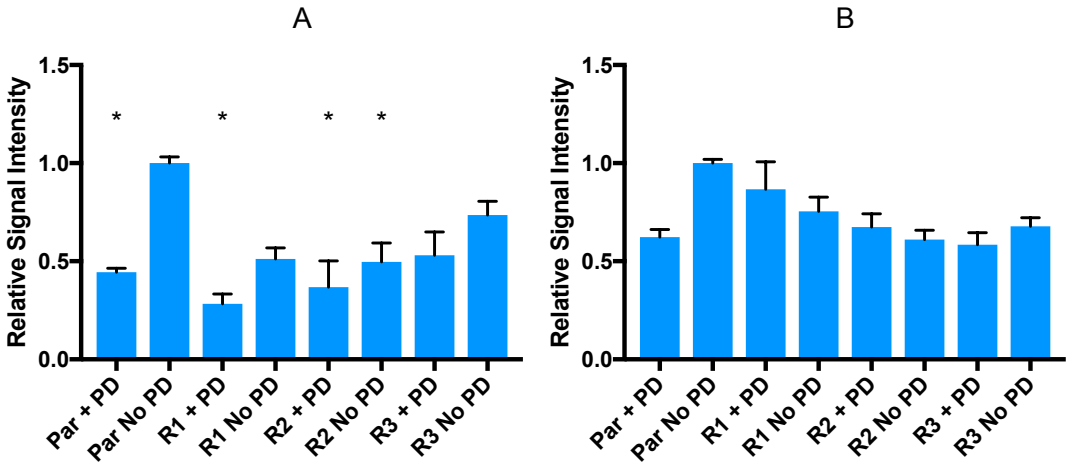

Figure 6.23 Expression of *SREBF1* and *SREBF2* in RT112 determined by microarray analysis. A) *SREBF1.* B) *SREBF2.* Error bars indicate standard error of the mean. Signal intensity is given relative to parental no PD. Asterisks indicate the experimental conditions in which *SREBF1* and *SREBF2* were differentially expressed compared to parental no PD (ANOVA $p<0.05$, 2-fold expression change).

Full-length SREBP1 and SREBP2 are endoplasmic reticulum-bound precursor proteins which are cleaved to produce their mature form (Hagen *et al.*, 2010). Immunoblot analysis showed that expression of mature SREBP1 was reduced in RT112 parental + PD, R1 + PD, R2 + PD, R3 + PD and R3 no PD (Fig. 6.25). Stearoyl-CoA desaturase-1 (SCD1) is the rate-limiting enzyme in the production of mono-unsaturated fatty acids from saturated fatty acids and increases lipogenesis (Igal, 2016). Immunoblot analysis showed that SCD1 protein expression was highest in RT112 parental no PD and R2 no PD, lower in RT112 R1 no PD, R3 + PD and R3 no PD and lowest in RT112 parental + PD, R1 + PD and R2 + PD (Fig. 6.25). These results suggest there is a reduction in mono-unsaturated fatty acid synthesis and lipogenesis in RT112 parental and the RT112 resistant derivatives when cultured in PD. Figure 6.26 illustrates the effects that SREBP1 induces on the synthesis of fatty acids.

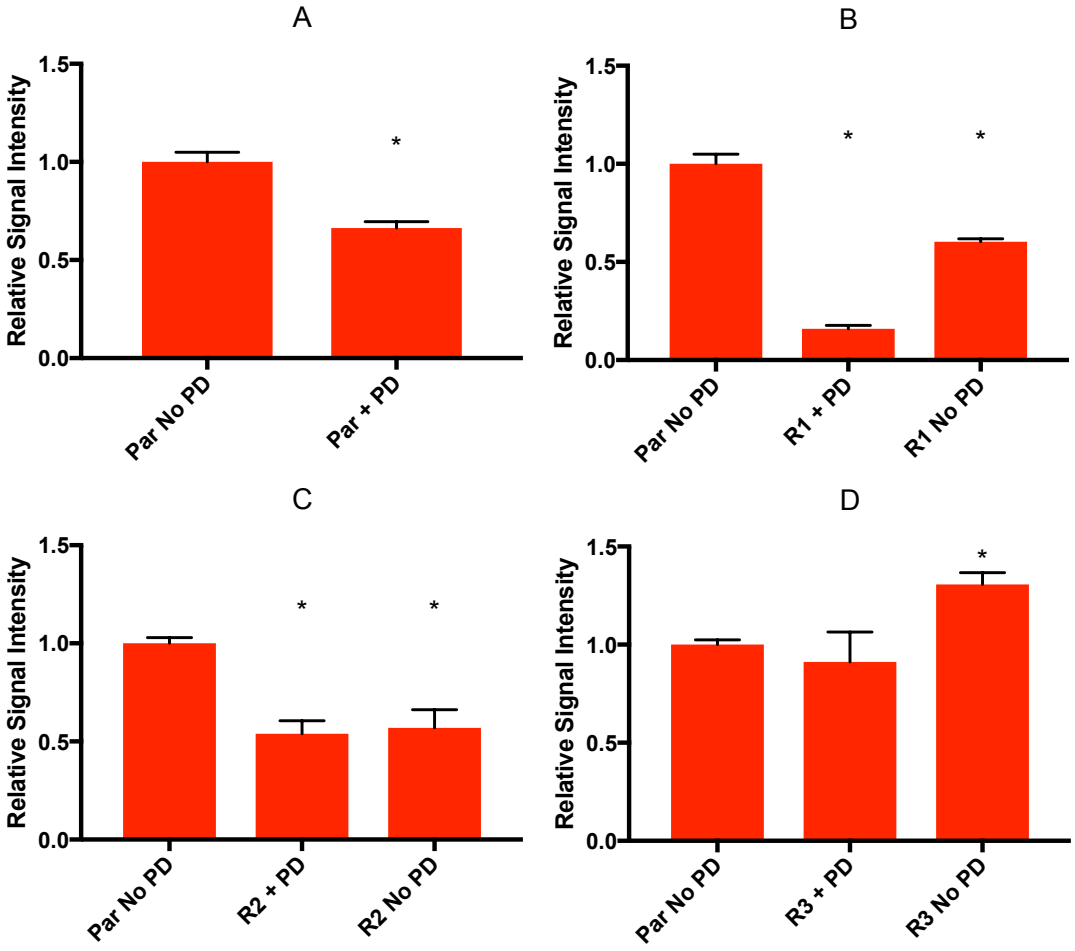

Figure 6.24 qRT-PCR validation of *SREBF1* in RT112. A) parental + PD. B) R1. C) R2. D) R3. Error bars indicate standard error of the mean. Signal intensity is given relative to RT112 no PD. Asterisks indicate the experimental conditions in which *SREBF1* was differentially expressed compared to parental no PD. qRT-PCR statistical test: Mann-Whitney U 2-tailed test, $p<0.05$.

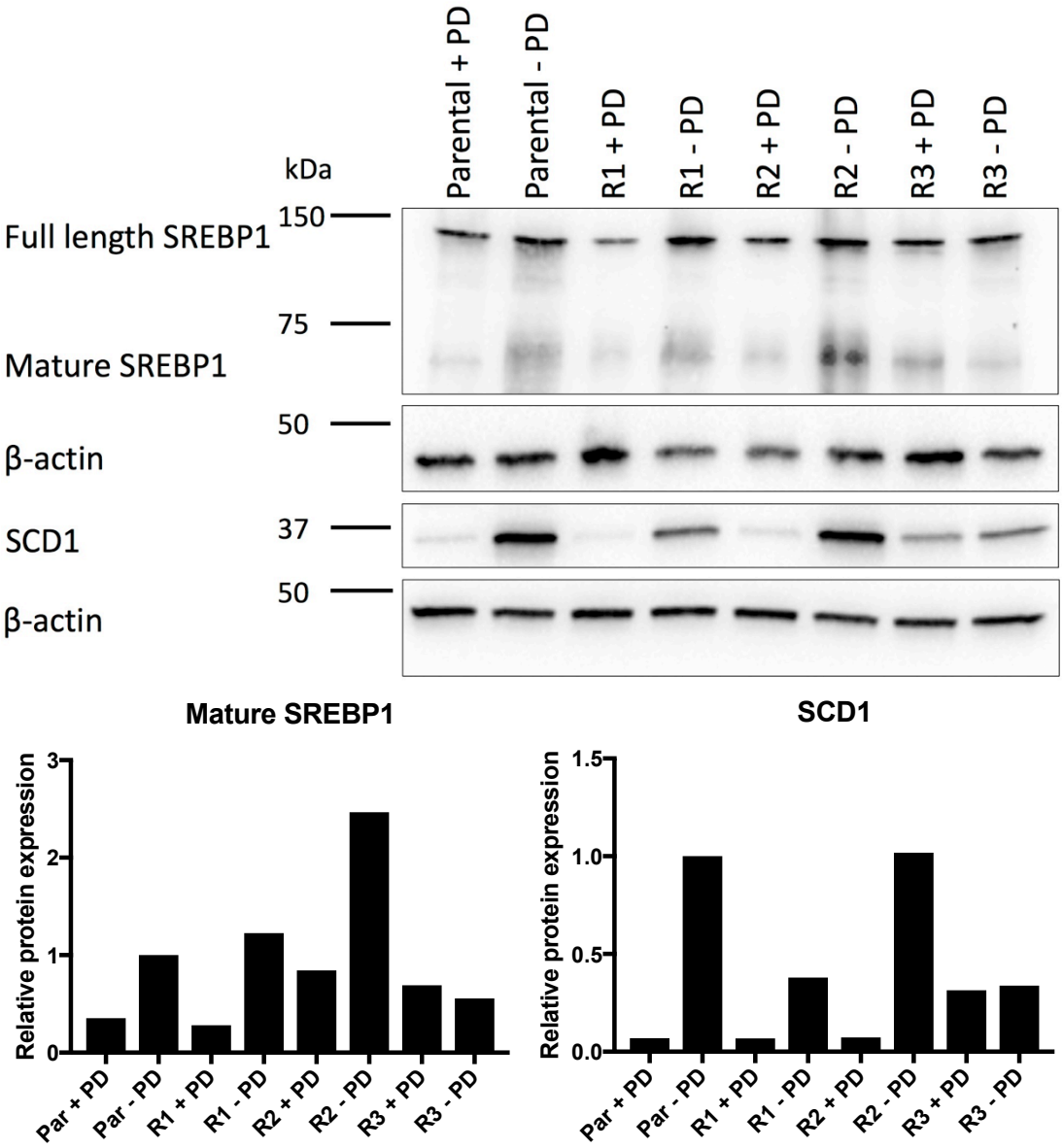

Figure 6.25 Immunoblot analysis of full length SREBP1, mature SREBP1 and SCD1 protein expression in RT112. Expression was examined in parental, parental treated with PD173074 for 24 h, R1, R2 and R3 cultured with PD173074 and R1, R2 and R3 cultured without PD173074 for 4 passages. β-actin was used as a loading control. Image Lab software was used to determine the intensity of the β-actin, mature SREBP1 and SCD1 protein bands and normalise mature SREBP1 and SCD1 expression relative to β-actin. Mature SREBP1 and SCD1 expression were quantified relative to RT112 parental no PD.

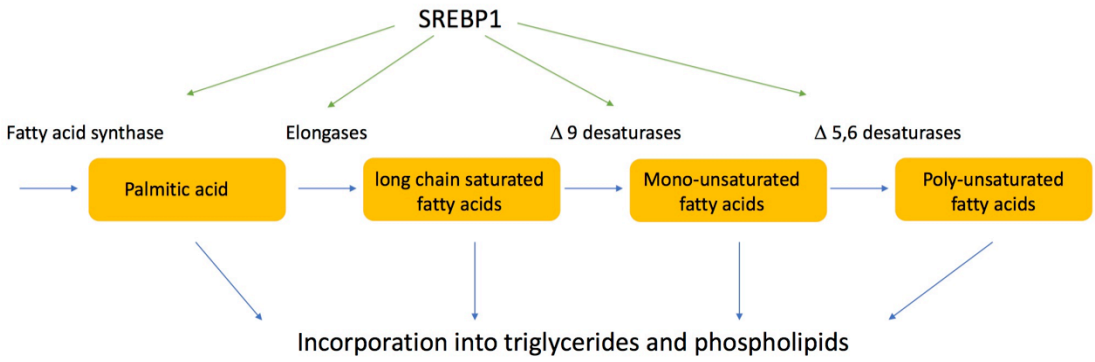

Figure 6.26 Regulation of fatty acid synthesis by SREBP1. Green lines indicate transcriptional upregulation induced by SREBP1. Blue lines indicate a chemical reaction. Modified from Hagen *et al.*, 2010.

Du *et al.* reported a set of 33 genes involved in fatty acid and sterol biosynthesis and metabolism that were downregulated upon knockdown of *FGFR3* in RT112 (Du *et al.*, 2012). Unsupervised hierarchical cluster analysis was performed in RT112 microarray samples for this set of genes (Fig. 6.27). Expression of this cohort of genes was predominantly reduced in RT112 + PD compared to RT112 no PD. A cluster with generally low expression of these genes contained the samples RT112 R1 + PD, R2 + PD and parental + PD. A second cluster was formed containing the samples RT112 parental no PD, R3 + PD, R1 no PD, R2 no PD and R3 no PD with predominantly high expression of this cohort of genes. Overall, the differential expression of this cohort of genes indicated that fatty acid and sterol biosynthesis and metabolism was likely to be reduced in RT112 parental + PD, RT112 R1 + PD and RT112 R2 + PD compared to the other RT112 experimental conditions. Therefore, the mechanism of resistance to PD in RT112 R1 and R2 did not re-establish the expression of fatty acid and sterol biosynthesis genes whereas the mechanism of resistance in RT112 R3, the *HRAS* G12S mutation, did. However, the mutant *HRAS* in RT112 R3 did not activate fatty acid synthesis to the same extent as the signalling via *FGFR3-TACC3* and wildtype *FGFR3* in parental no PD. Du *et al.* observed that treatment with a MEK inhibitor reduced FGF1-induced expression of mature SREBP1 (Du *et al.*, 2012). Therefore, it is logical to suggest that the activation of the MAP kinase pathway via the acquisition of a *HRAS* G12S mutation in RT112 R3 induced the maintenance of fatty acid and sterol biosynthesis genes expression in the presence of PD.

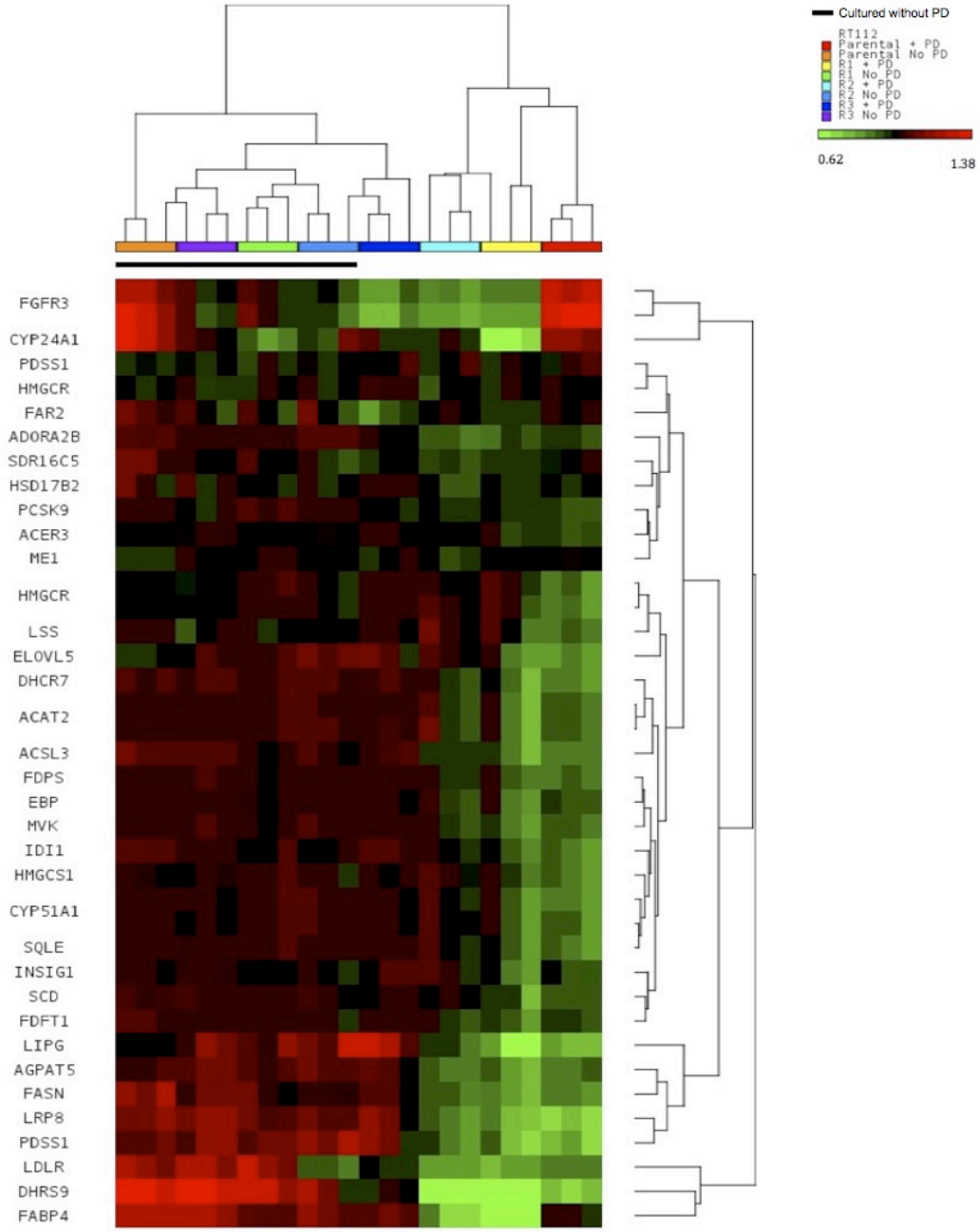

Figure 6.27 Unsupervised hierarchical cluster analysis of Du *et al.* cohort of fatty acid and sterol biosynthesis and metabolism genes in RT112 microarray samples. The log_2 gene expression was normalised by dividing each expression value by the probe's mean log_2 gene expression. Following log_2 gene expression normalisation, the expression profiles of samples and genes were clustered in Partek® Genomics Suite® 6.6 using Euclidean distance and complete linkage. Scale bar indicates the normalised log_2 gene expression with colour depicting the level of gene expression as high (red), intermediate (black) and low (green).

Immunoblot analysis of FGFR3 conducted in RT112 in Chapter 3 (Chapter 3, Fig. 3.11) found reduction in FGFR3 expression in the RT112 resistant lines. Examination of phospho-FGFR3 expression via immunoprecipitation was unsuccessful. A reduction in *FGFR3* expression in RT112 R1 + PD, R1 no PD, R2 + PD, R2 no PD, R3 + PD and R3 no PD compared to parental no PD was observed with microarray analysis and qRT-PCR analysis (Fig. 6.28). In contrast to the immunoblot and microarray analysis, qRT-PCR showed a significant increase in *FGFR3* expression in parental + PD (Fig. 6.28). The low expression of FGFR3 in R3 + PD indicates that R3 maintains expression of the Du *et al.* cohort of genes when cultured in PD by a mechanism other than signalling via FGFR3.

As was observed for RT112 experimental conditions, genes involved in lipid homeostasis were differentially expressed between RT4 experimental conditions (Supplementary data, 2-fold change lists). Microarray analysis showed that expression of *SREBF1* and *SREBF2* was non-significantly reduced in RT4 R1 compared to parental no PD. qRT-PCR analysis found that *SREBF1* mRNA was significantly downregulated in RT4 R1 + PD and R1 no PD (Fig. 6.29).

Hierarchical cluster analysis was performed in RT4 microarray samples for the Du *et al.* cohort of fatty acid and lipid synthesis genes (Fig. 6.30). One RT4 parental no PD sample did not cluster with any of the other RT4 samples. This sample passed the microarray quality control (Appendix D, Fig. D.1, D.2 and D.3), however, in the PCA analysis this sample was separate from the other two parental no PD samples (Fig. 6.2). The remaining two RT4 parental no PD replicates and R1 no PD samples formed a cluster characterised by a predominantly high expression of this gene cohort relative to the other RT4 experimental conditions. R1 + PD samples formed a cluster of samples with predominantly low expression of this gene cohort. Expression of some genes was maintained or upregulated in RT4 R1 + PD relative to parental no PD (*FGFR3*, *PDSS1*, *HMGCR, ELOVL5*, *SDR16C5*, *ACER3* and *PCSK9*). Therefore, RT4 R1 + PD may maintain some fatty acid and sterol biosynthesis and metabolism. However, as expression of this cohort of genes was predominantly reduced in RT4 R1 + PD, including *SCD* which encodes SCD1, this suggests that fatty acid and sterol biosynthesis and metabolism was reduced in RT4 R1 + PD.

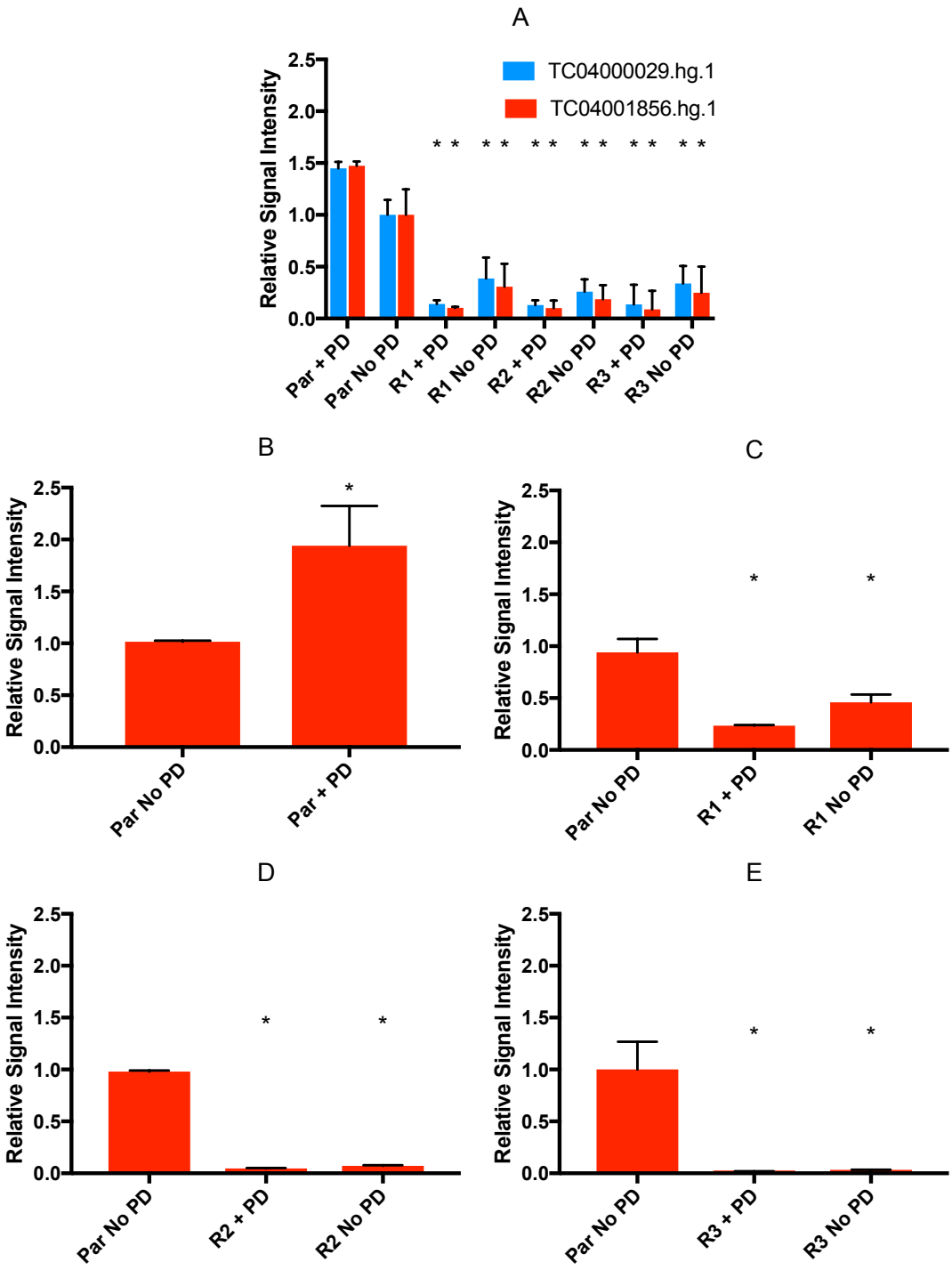

Figure 6.28 Expression of *FGFR3* in RT112 determined by microarray and qRT-PCR analysis. A) microarray analysis in all RT112 experimental conditions. B) qRT-PCR analysis in parental. C) qRT-PCR analysis in R1. D) qRT-PCR analysis in R2. E) qRT-PCR analysis in R3. Error bars indicate standard error of the mean. Signal intensity is given relative to RT112 no PD. For microarray and qRT-PCR, asterisks indicate the probe and experimental condition for which significantly different *FGFR3* expression was detected compared to parental no PD. Microarray statistical test: ANOVA $p<0.05$, 2-fold expression change. qRT-PCR statistical test: Mann-Whitney U 2-tailed test, $p<0.05$. For genes with specificity to more than one probe, all probes are shown with a legend indicating the probe's Affymetrix IDs.

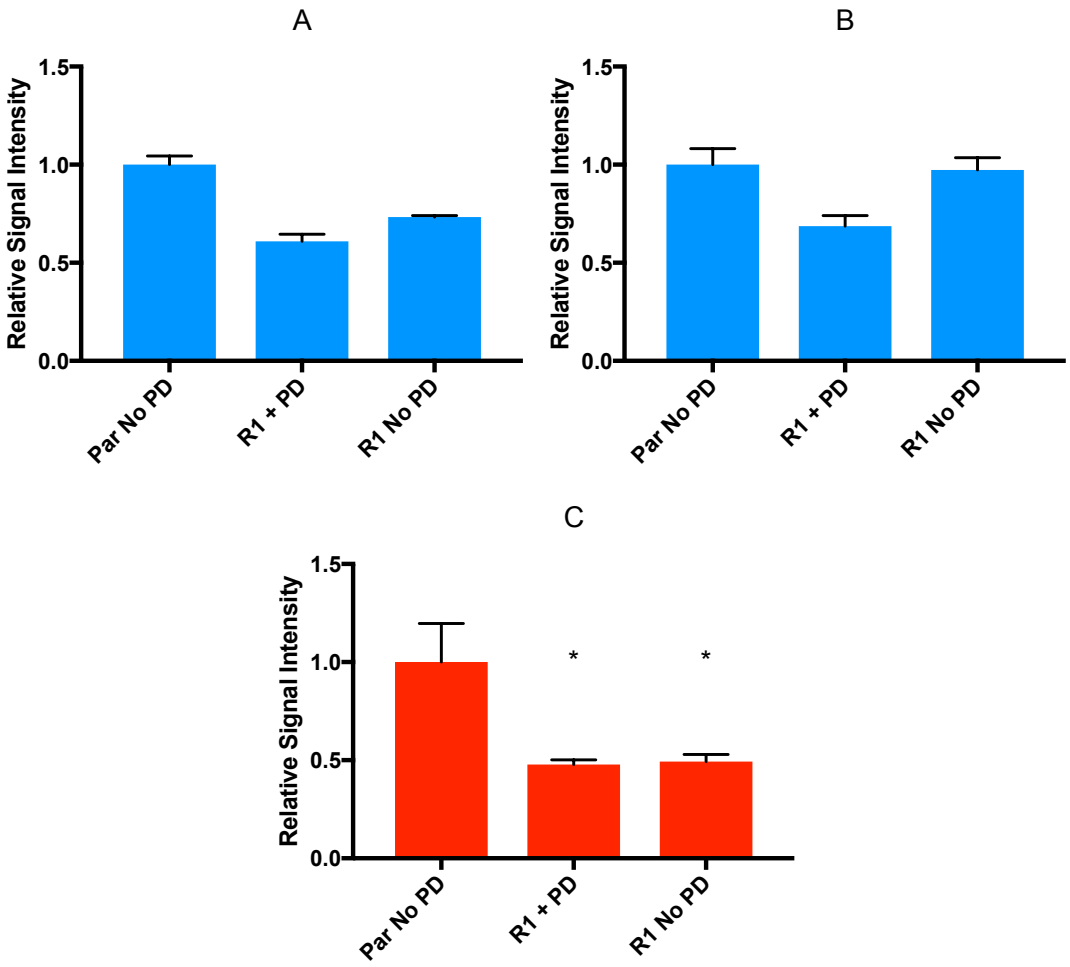

Figure 6.29 Microarray and qRT-PCR analysis of *SREBF1* and *SREBF2* expression in RT4. A) microarray analysis of *SREBF1.* B) microarray analysis of SREBF2. C) qRT-PCR analysis of *SREBF1.* Error bars indicate standard error of the mean. Signal intensity is given relative to parental no PD. For microarray and qRT-PCR, asterisks indicate the experimental conditions in which *SREBF1* or *SREBF2* were differentially expressed compared to parental no PD. Microarray statistical test: ANOVA $p<0.05$, 2-fold expression change. qRT-PCR statistical test: Mann-Whitney U 2-tailed test, $p<0.05$.

Immunoblot analysis in Chapter 3 found FGFR3 to be expressed at the same level in RT4 parental and R1 + PD (Fig. 3.13). Microarray analysis showed there was a non-significant, approximately 1.5-fold increase in *FGFR3* expression in RT4 R1 + PD and a non-significant decrease in *FGFR3* expression in R1 no PD (Fig. 6.31). qRT-PCR analysis showed that *FGFR3* expression was significantly increased approximately 2-fold in R1 + PD and not significantly different in R1 no PD compared to parental no PD (Fig. 6.31). However, it is likely that RT4 R1 does not signal via FGFR3 when cultured in PD as activation of EGFR has been identified as a likely mechanism of resistance to PD in RT4 R1 (Chapter 4, Fig. 4.6).

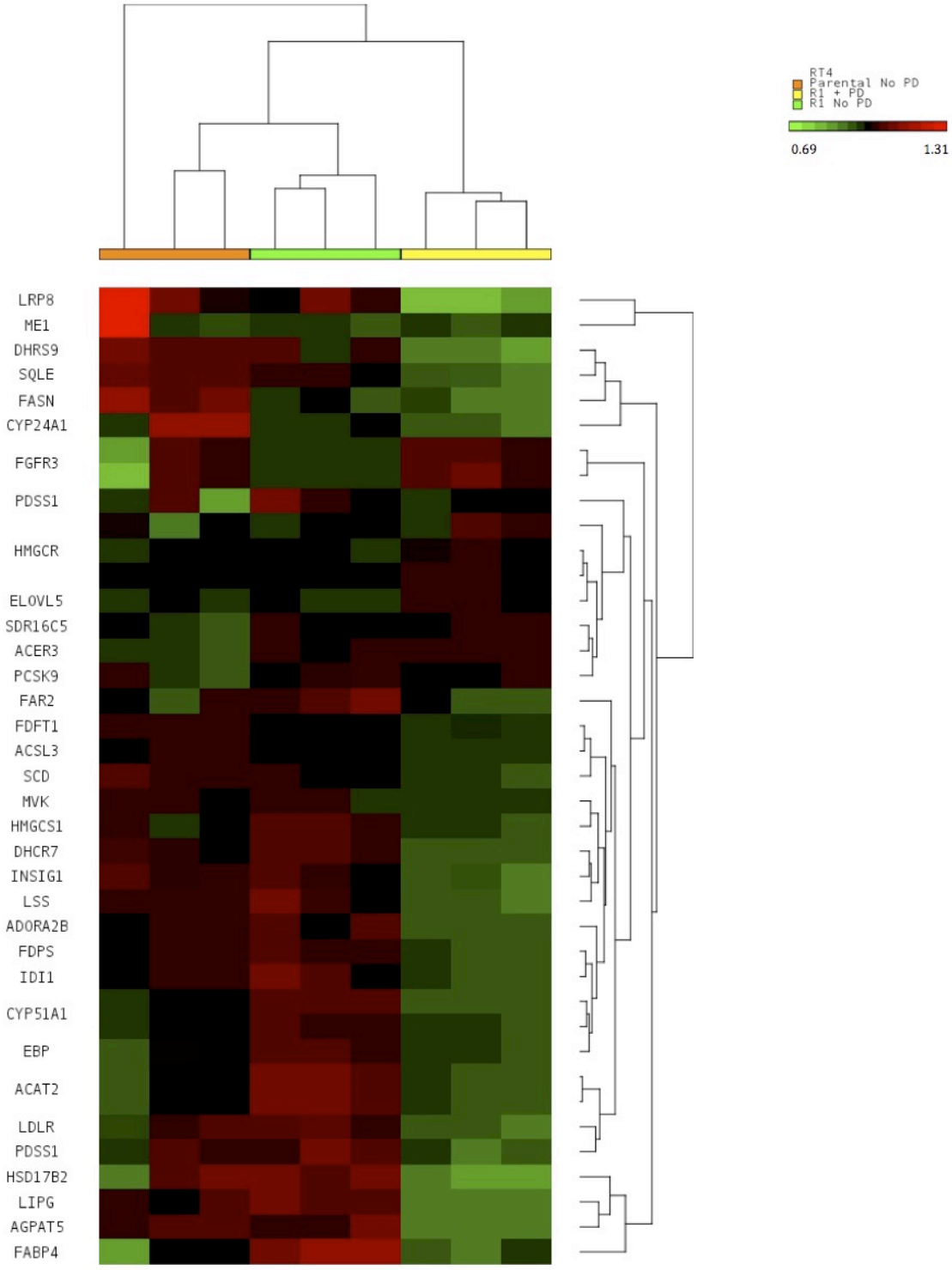

Figure 6.30 Unsupervised hierarchical cluster analysis of Du *et al.* cohort of fatty acid and sterol biosynthesis and metabolism genes in RT4 microarray samples. The log_2 gene expression was normalised by dividing each expression value by the probes mean log_2 gene expression. Following log_2 gene expression normalisation, the expression profiles of samples and genes were clustered in Partek® Genomics Suite® 6.6 using Euclidean distance and complete linkage. Scale bar indicates the normalised log_2 gene expression with colour depicting the level of gene expression as high (red), intermediate (black) and low (green).

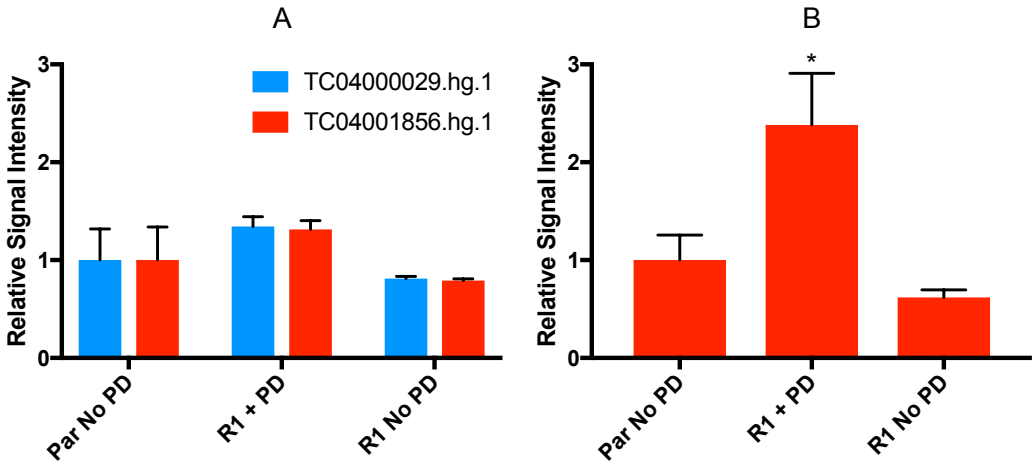

Figure 6.31 Expression of *FGFR3* in RT4 determined by microarray and qRT-PCR analysis. A) microarray analysis B) qRT-PCR analysis. Error bars indicate standard error of the mean. Signal intensity is given relative to parental no PD. Asterisks indicate the experimental conditions in which *FGFR3* is differentially expressed compared to parental no PD. microarray statistical test: ANOVA $p<0.05$, 2-fold expression change. qRT-PCR statistical test: Mann-Whitney U, 2-tailed test, $p<0.05$. For genes with specificity to more than one probe, all probes are shown with a legend indicating the probe's Affymetrix IDs.

6.2.7 Expression of epithelial-mesenchymal transition markers

MetaCore™ pathway analysis found EMT and cytoskeletal remodelling pathways to be differentially expressed between RT112 parental + PD and R1 + PD (Fig. 6.6) and R2 + PD (Fig. 6.7) and between parental no PD and R1 no PD (Fig. 6.9), R2 no PD (Fig. 6.10), R1 + PD (Appendix D, Fig. D.6), R2 + PD (Appendix D, Fig. D.7) and R3 + PD (Appendix D, Fig. D.8). It had previously been observed that RT112 R1 and R2 cultured in PD have a mesenchymal morphology (Chapter 3, Fig. 3.4).

Immunoblot analysis found that expression of the epithelial marker E-cadherin was constant between RT112 parental no PD, R1 + PD and R2 + PD and that N-cadherin expression was increased in RT112 R1 and R2 + PD, and to a lesser extent RT112 R3 + PD compared to RT112 parental no PD (Chapter 3, Fig. 3.12). Microarray analysis of expression of *CDH1*, which encodes E-cadherin, was concordant with this and showed that *CDH1* was not significantly differentially expressed in any experimental condition compared to RT112 parental no PD (Fig. 6.32). Microarray analysis showed that expression of the *CDH2* gene, which encodes N-cadherin, was increased in RT112 R1, R2 and R3 + PD, and by a smaller magnitude in RT112 R1 and R2 no PD compared to parental no PD. This increase was only significant for RT112 R2 + PD (Fig. 6.32). A small increase in protein expression of another mesenchymal marker, vimentin, was observed in RT112 R1 and R2 compared to the parental line (Chapter 3, Fig. 3.12). Concordant with this, a small but non-significant increase in expression of the gene that

encodes vimentin, *VIM*, was seen in RT112 parental, R1, R2 and R3 + PD compared to RT112 parental no PD (Fig. 6.32).

Microarray analysis showed expression of *FN1*, which encodes the mesenchymal marker fibronectin, was significantly increased in RT112 R1+ PD, R1 no PD and R2 + PD approximately 27-fold, 3-fold and 19-fold, respectively, compared to RT112 parental no PD. A smaller, non-significant increase in *FN1* expression was seen in R1 and R2 no PD and R3 + PD (Fig. 6.32). *SNAI2* encodes snail family transcriptional repressor 2 which promotes a mesenchymal phenotype (Alves *et al.*, 2009). Microarray analysis found *SNAI2* expression to be significantly increased in RT112 R1 + PD, R2 + PD, R2 no PD and R3 + PD compared to RT112 parental no PD (Fig. 6.32). *ELF5* encodes E74-like ETS transcription factor 5, which is reported to repress transcription of *SNAI2*, inhibiting EMT (Chakrabarti *et al.*, 2012). Expression of *ELF5* was significantly reduced in RT112 R1 + PD, R2 + PD, R2 no PD, R3 + PD and R3 no PD compared to RT112 parental no PD. (Fig. 6.32). The expression changes observed in *FN1, SNAI2* and *ELF5* were not validated by qRT-PCR or immunoblot due to time limitations. The microarray analysis, in conjunction with the morphological and immunoblot analysis in Chapter 3 indicate that RT112 R1, R2 and possibly R3 have undergone a partial EMT during their derivation which is reversed upon culture out of PD for 4 passages.

MetaCore™ pathway analysis also showed that genes in the pathway map 'regulation of EMT' were differentially expressed between RT4 parental no PD and RT4 R1 + PD (Fig. 6.12). Immunoblot analysis conducted in Chapter 3 found that expression of N-cadherin and vimentin was low in RT4 parental and R1. E-cadherin expression was found to be increased in RT4 R1 compared to the parental line (Chapter 3, Fig. 3.13). Consistent with this, *CDH1*, *CDH2* and *VIM* were not significantly differentially expressed between parental no PD, R1 + PD and R1 no PD (Fig. 6.33). However, *FN1* expression was significantly increased by approximately 6 in R1 + PD and non-significantly increased by approximately 11-fold in R1 no PD (Fig. 6.33). A non-significant increase in *SNAI2* expression of approximately 2 and 1.5-fold was observed in RT4 R1 + PD and RT4 R1 no PD, respectively (Fig. 6.33). Expression of *ELF5* was non-significantly reduced in RT4 R1 no PD to approximately half the expression observed in RT4 parental no PD. (Fig. 6.33). The microarray analysis, in conjunction with the morphological and immunoblot analysis in Chapter 3 suggests that RT4 R1 did not undergo an EMT during its derivation.

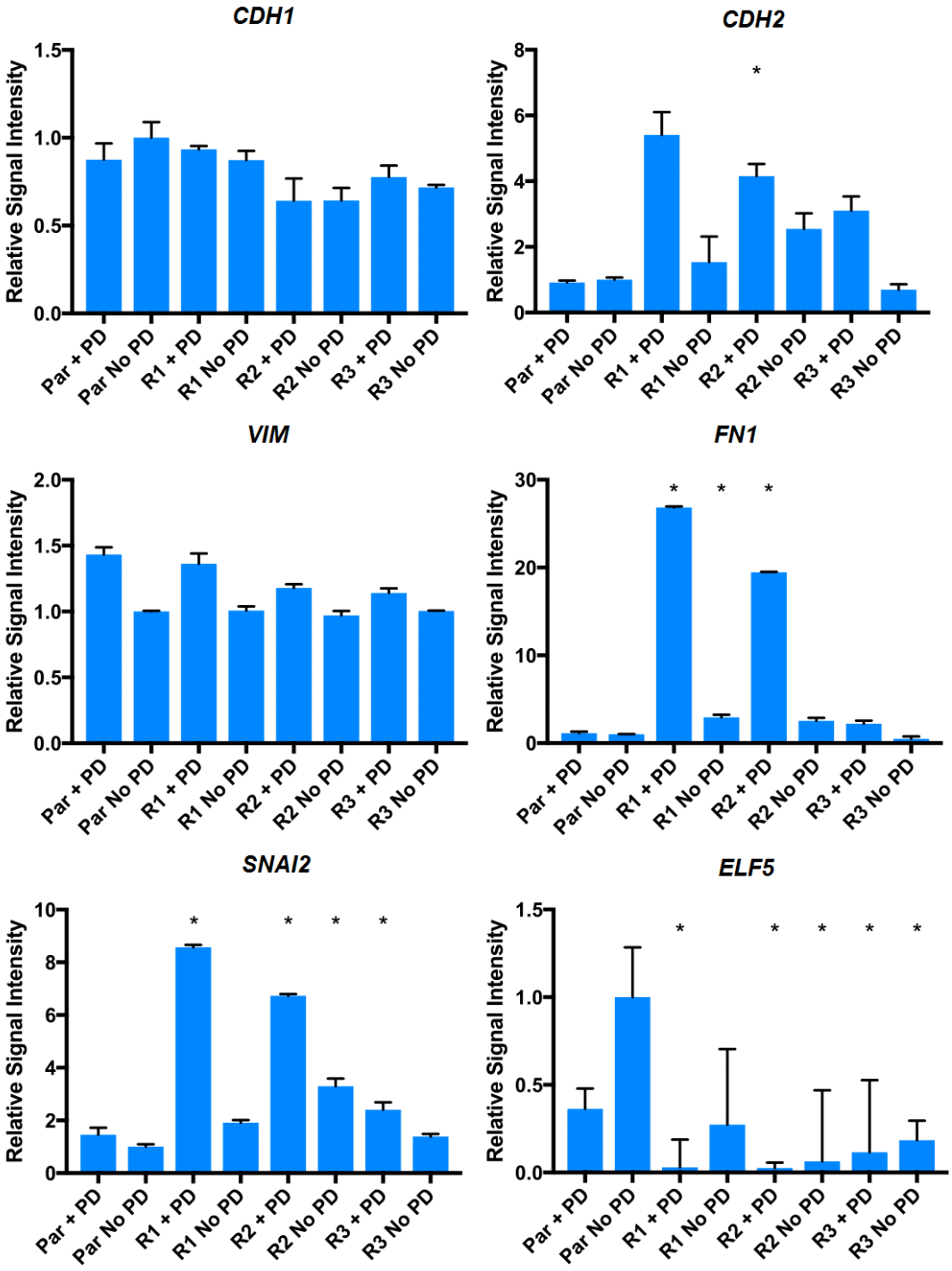

Figure 6.32 Expression of *CDH1*, *CDH2, VIM, FN1, SNAI2 and ELF5* in RT112 determined by microarray analysis. Error bars indicate standard error of the mean. Signal intensity is given relative to parental no PD. Asterisks indicate the experimental conditions in which CDH1, CDH2, VIM, FN1, SNAI2 and ELF5 were differentially expressed compared to parental no PD (ANOVA $p<0.05$, 2-fold expression change).

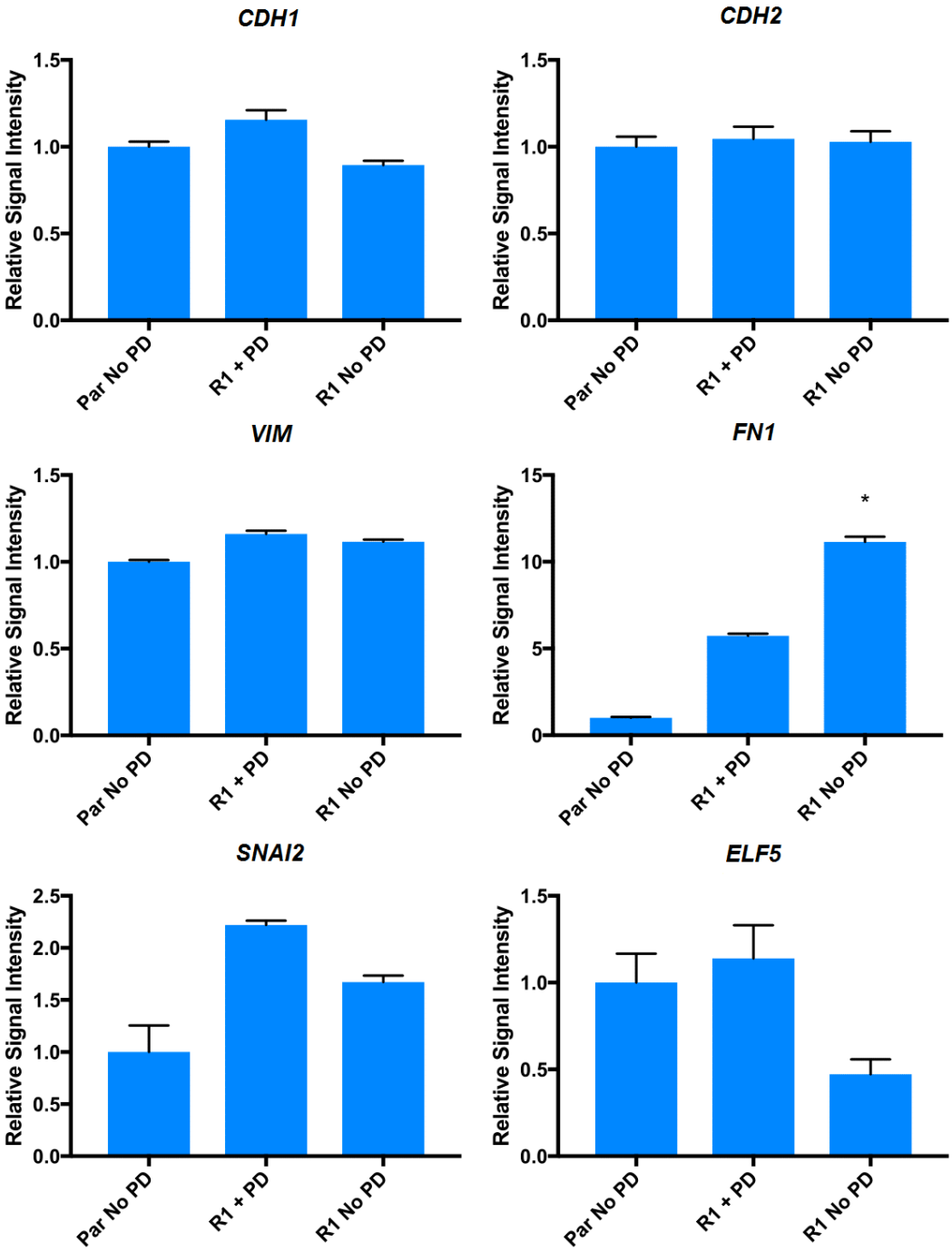

Figure 6.33 Expression of *CDH1*, *CDH2, VIM, FN1, SNAI2 and ELF5* in RT4 determined by microarray analysis. Error bars indicate standard error of the mean. Signal intensity is given relative to parental no PD. Asterisks indicate the experimental conditions in which genes were differentially expressed compared to parental no PD (ANOVA $p<0.05$, 2-fold expression change).

6.2.8 Expression of luminal cell markers in RT112

Bladder cancers can be classified into basal and luminal subtypes (Choi *et al.* 2014, 2014a; Dadhania *et al.*, 2016; Warrick *et al.*, 2016), as discussed in Chapter 1, section 1.1.2. It was observed that basal and luminal markers were differentially

expressed between RT112 parental no PD and RT112 R1 + PD, R2 + PD and R3 + PD (Supplementary data; 2-fold gene lists). Basal tumours are more aggressive than luminal tumours, although they are typically sensitive to chemotherapy (Dadhania *et al.*, 2016). Choi *et al.* reported that p53-like subtype tumours were typically resistant to chemotherapy (Choi *et al.*, 2014a). Both RT112 and RT4 have been previously classified as luminal (Warrick *et al.*, 2016). If the resistant cells have undergone a switch from a luminal to a basal or p53-like subtype during their derivation, the resistant line could be more aggressive or could have reduced sensitivity to treatment. If FGFR inhibitors induce a similar switch subtype in patients, this could result in worse patient survival.

Unsupervised hierarchical cluster analysis was performed with RT112 microarray expression data for the luminal subtype markers reported by Choi *et al.* (Fig. 6.34). Compared to parental no PD, expression of *ERBB2, ERBB3, FGFR3, GPX2 and CYP2J2* was increased in RT112 parental + PD. RT112 R1 + PD and R2 + PD had increased expression of *ERBB2*, *ERBB3* and *KRT7* and reduced expression of *FGFR3*, *FOXA1*, *GPX2 and CYP2J2*. Expression of the luminal markers *ERBB2, ERBB3* and *KRT7* was generally low in RT112 R1 no PD, R2 no PD, R3 no PD, and R3 + PD (Fig. 6.34). This analysis suggests that acute treatment with PD induced a more luminal phenotype in parental RT112. The expression of luminal markers in R1 and R2 culture in PD is more complex with expression of some markers increased whilst other markers exhibit decreased expression. The low expression of luminal markers in R1 and R2 when cultured out of PD suggests that these lines become less luminal upon the removal of PD.

In order to validate the changes in expression of luminal markers observed in the RT112 microarray data, qRT-PCR was performed using assays specific for a selected panel of these markers. Expression of the luminal marker *KRT20* was non-significantly reduced in all RT112 microarray samples compared to parental no PD. qRT-PCR analysis showed that *KRT20* expression was significantly reduced in R1 + PD and R1 no PD (Fig. 6.35).

Expression of the transcription factor *PPARG*, which promotes a luminal phenotype in MIBC, was non-significantly reduced in all RT112 microarray samples compared to parental no PD (Choi *et al.*, 2014a). This reduction was found to be significant in R1 + PD and R1 no PD by qRT-PCR (Fig. 6.36). The transcription factors GATA3 and FOXA1 work with PPARG to promote a luminal phenotype in bladder cancer cell lines (Warrick *et al.*, 2016). Microarray analysis showed *GATA3* expression was significantly increased in R1 + PD compared to parental no PD.

The increase in R1 + PD *GATA3* expression was confirmed by qRT-PCR and *GATA3* expression in R1 no PD was also found to be significantly reduced (Fig. 6.36). Microarray analysis showed that expression of *FOXA1* was reduced in RT112 R1 + PD, R1 no PD, R2 + PD, R2 no PD, R3 + PD and R3 no PD compared to RT112 parental no PD. This reduction was only significant in RT112 R1+ PD and R2 + PD. Reduced expression of this luminal marker was confirmed in RT112 R1 + PD and R1 no PD by qRT-PCR (Fig. 6.36).

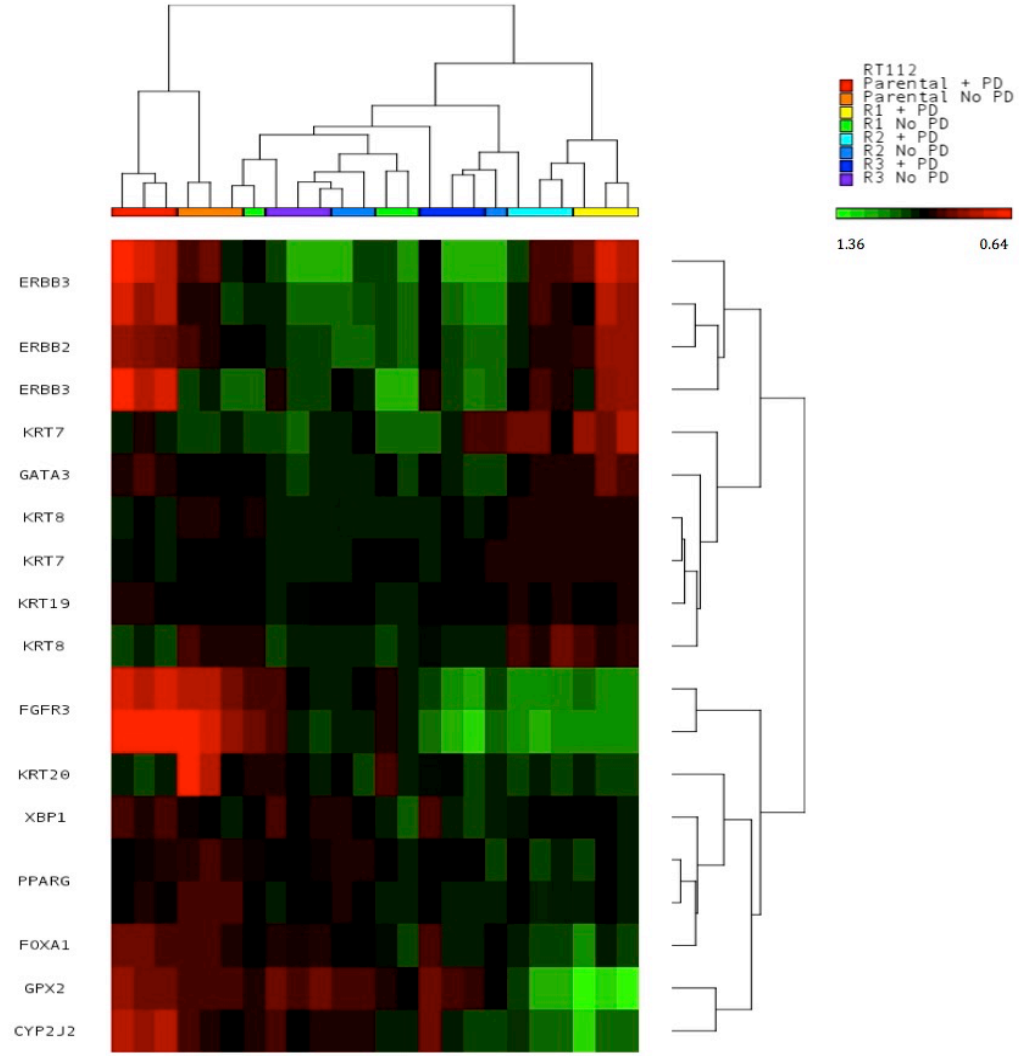

Figure 6.34 Unsupervised hierarchical cluster analysis of Choi *et al.* cohort of luminal markers in RT112 microarray samples. The Log_2 gene expression was normalised by dividing each expression value by the probe's mean Log_2 gene expression. Following Log_2 gene expression normalisation, the expression profiles of samples and genes were clustered in Partek® Genomics Suite® 6.6 using Euclidean distance and complete linkage. Scale bar indicates the normalised Log_2 gene expression with colour depicting the level of gene expression as high (red), intermediate (black) and low (green).

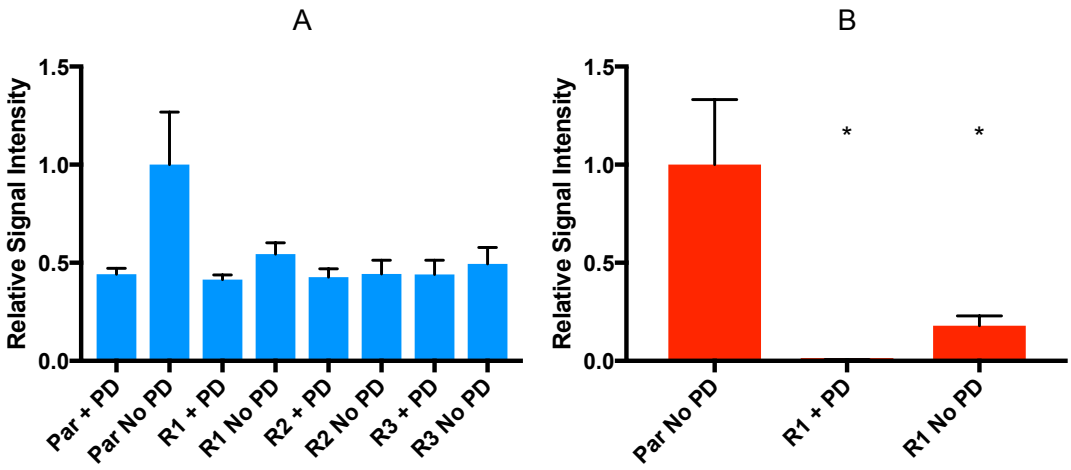

Figure 6.35 Expression of *KRT20* in RT112 determined by microarray and qRT-PCR analysis. A) microarray analysis. B) qRT-PCR analysis. Error bars indicate standard error of the mean. Signal intensity is given relative to parental no PD. For microarray: asterisks indicate the experimental conditions in which *KRT20* is differentially expressed compared to parental no PD (ANOVA $p<0.05$, 2-fold expression change). For qRT-PCR: asterisks indicate the experimental conditions in which *KRT20* is differentially expressed compared to parental no PD (Mann-Whitney U, 2-tailed test, $p<0.05$).

FGFR3 is a luminal marker (Choi *et al.*, 2014). As discussed in section 6.2.6, microarray and qRT-PCR analysis showed that compared to RT112 parental no PD, expression of *FGFR3* was increased in parental + PD and reduced in the resistant derivatives cultured with and without PD (Fig. 6.28). Microarray expression of *ERBB3*, another luminal marker, was significantly increased in RT112 parental + PD and non-significantly increased in RT112 R1 and R2 + PD compared to RT112 parental no PD. qRT-PCR showed *ERBB3* to be significantly increased in RT112 parental + PD, R1 + PD, R1 no PD, R1 + PD and R2 + PD compared to RT112 parental no PD (Fig. 6.37). ERBB3 is a possible mediator of resistance in RT112 R1 and R2 as an increase in phospho-ERBB3 expression was seen in these resistant lines (Chapter 4, Fig. 4.8).

Uroplakins, encoded by *UPK1A*, *UPK2*, *UPK3A* and *UPK3B*, are luminal markers expressed at the apical surface of the urothelium (Hu *et al.*, 2000). Microarray analysis showed that *UPK1A* expression was significantly increased in RT112 parental + PD, R1 + PD and R2 + PD and significantly reduced in R1 no PD, R2 no PD and R3 no PD (Fig. 6.38). *UPK2* expression was significantly increased in RT112 parental + PD and R1 + PD and significantly decreased in R2 no PD. *UPK3A* expression was not differentially expressed and *UPK3B* expression was significantly decreased in R2 + PD and R2 no PD (Fig. 6.38). Microarray analysis found that expression of the transcription factor and luminal marker *ELF3* (Bock *et*

al., 2014) was significantly increased in RT112 parental + PD and non-significantly reduced in R1 no PD and R2 no PD compared to parental no PD (Fig. 6.38).

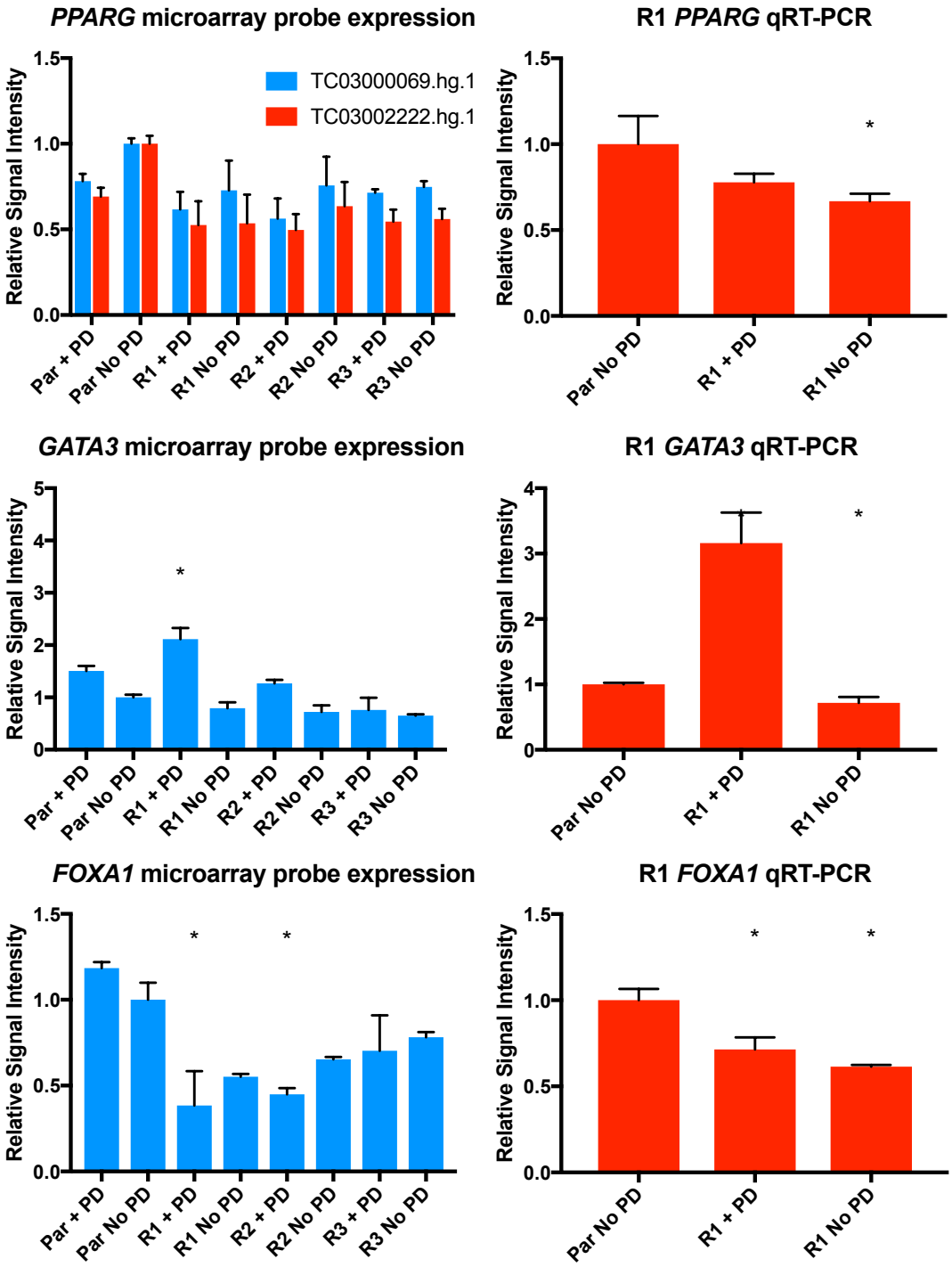

Figure 6.36 Expression of *PPARG, GATA3* and *FOXA1* in RT112 determined by microarray and qRT-PCR analysis. Error bars indicate standard error of the mean. Signal intensity is given relative to parental no PD. Asterisks indicate the experimental conditions in the genes were differentially expressed compared to parental no PD. Microarray analysis: ANOVA $p<0.05$, 2-fold expression change. qRT-PCR analysis: Mann-Whitney U, 2-tailed test, $p<0.05$. For genes with specificity to more than one probe, all probes are shown with a legend indicating the probe's Affymetrix IDs.

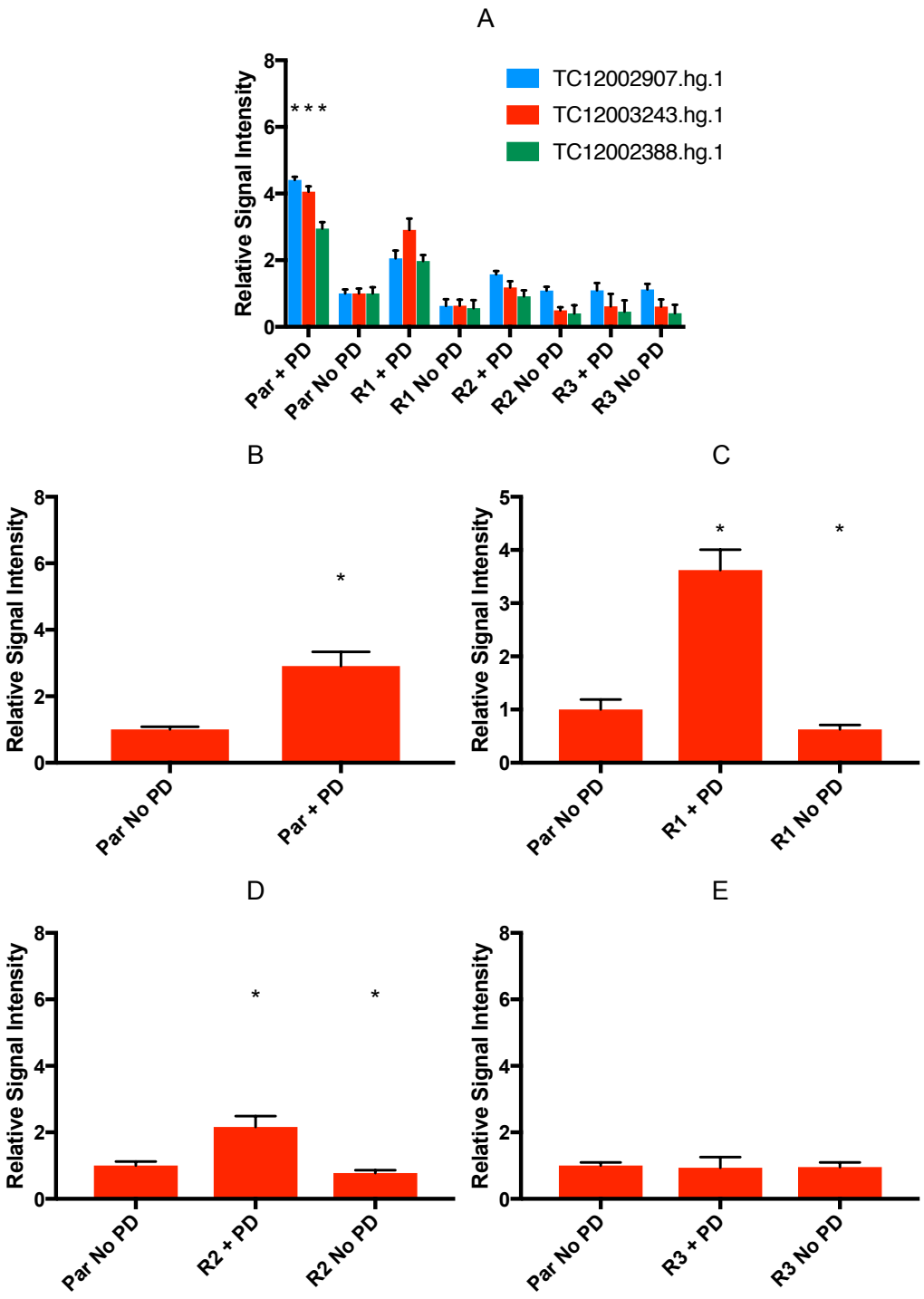

Figure 6.37 Expression of *ERBB3* in RT112 determined by microarray and qRT-PCR analysis. A) microarray analysis in all RT112 experimental conditions. B) qRT-PCR analysis in parental. C) qRT-PCR analysis in R1. D) qRT-PCR analysis in R2. E) qRT-PCR analysis in R3. Error bars indicate standard error of the mean. Signal intensity is given relative to parental no PD. Asterisks indicate the probe and experimental condition for which *ERBB3* was significantly differentially expressed compared to parental no PD. Microarray statistical test: ANOVA $p<0.05$, 2-fold expression change. qRT-PCR statistical test: Mann-Whitney U 2 -tailed test, $p<0.05$. For genes with specificity to more than one probe, all probes are shown with a legend indicating the probe's Affymetrix IDs.

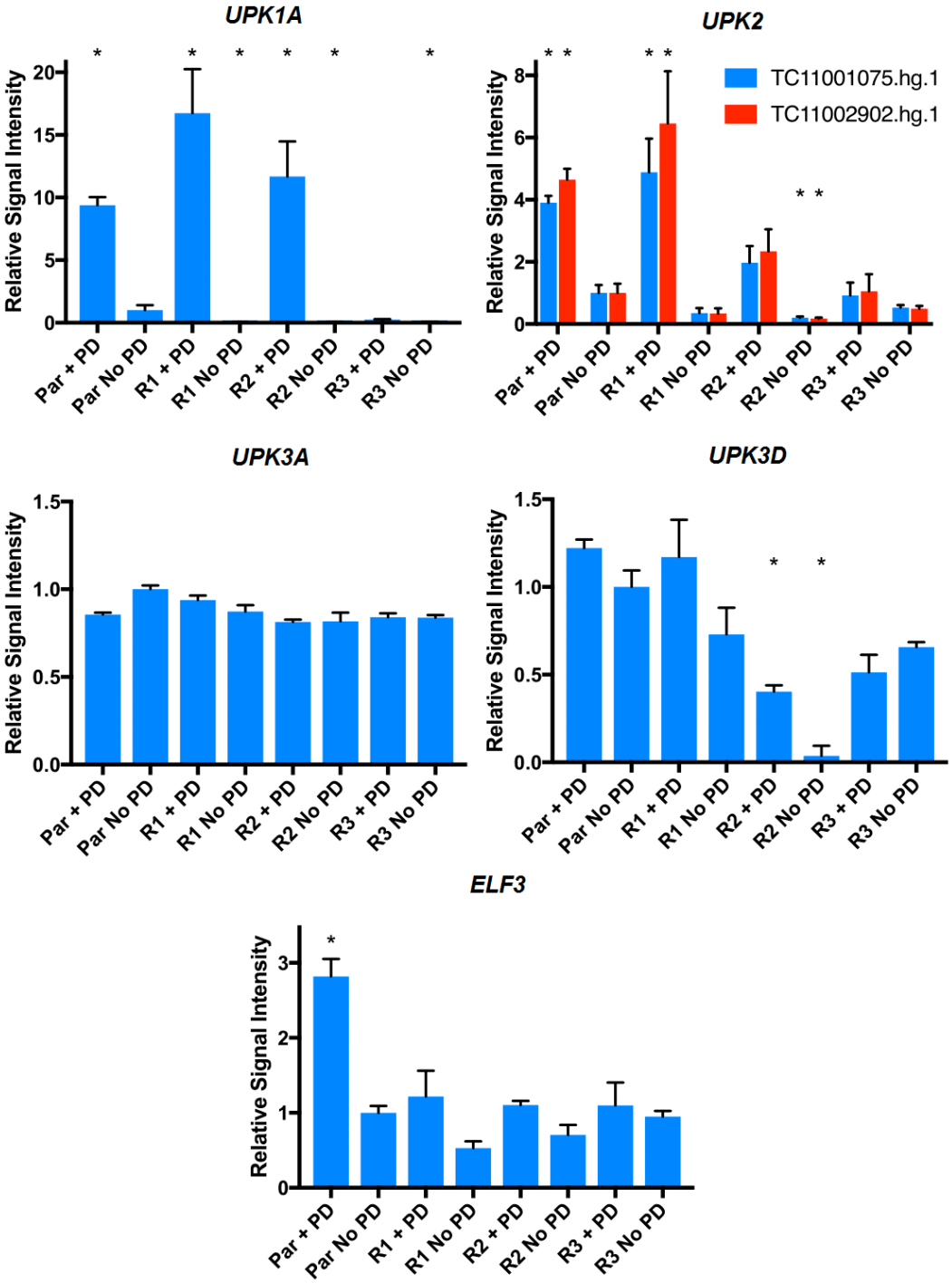

Figure 6.38 Expression of *UPK1A*, *UPK2, UPK3A, UPK3B* and *ELF3* in RT112 determined by microarray analysis. Error bars indicate standard error of the mean. Signal intensity is given relative to RT112 no PD. Asterisks indicate the experimental conditions in which genes were significantly differentially expressed compared to parental no PD (ANOVA $p<0.05$, 2-fold expression change). For genes with specificity to more than one probe, the data generated from each probe is shown separately with a legend indicating the probe's Affymetrix IDs.

The expression of luminal markers in R1 + PD and R2 + PD does not follow a set pattern with some markers exhibiting an increase in expression compared to parental no PD, whilst others exhibit a decrease or no change in expression. The microarray analysis suggests that luminal markers are not differentially expressed between R3 + PD and parental no PD. The expression of a number of luminal markers is significantly reduced in R1 no PD, R2 no PD and R3 no PD, supporting the hypothesis that expression of luminal markers is reduced upon culture of the resistant lines without PD.

The Choi *et al.* p53-like subtype of MIBCs had an activated wildtype *TP53* gene expression signature (Choi *et al.*, 2014). Unsupervised hierarchical cluster analysis was performed with RT112 microarray expression data for the p53-like subtype markers reported by Choi *et al.* These markers were not differentially expressed between RT112 experimental conditions (Appendix D, Fig. D.13). Therefore, it is unlikely that the RT112 resistant lines have adopted a p53-like phenotype.

6.2.9 Expression of basal cell markers in RT112

Unsupervised hierarchical cluster analysis performed with the basal subtype markers reported by Choi *et al.* showed that basal markers were differentially expressed in RT112 microarray samples (Fig. 6.39).

In order to validate the changes in basal marker expression observed in the microarray data, qRT-PCR was performed using assays specific for a selected panel of these markers. Microarray analysis found expression of *KRT6C* to be significantly reduced, by approximately 70%, in RT112 parental + PD and significantly increased approximately 13-fold in R1 no PD compared to parental no PD (Fig. 6.40). qRT-PCR analysis showed significantly higher *KRT6C* expression in R1 + PD and R1 no PD (Fig. 6.40). Microarray analysis showed expression of *KRT5* was increased in RT112 R1 no PD compared to RT112 parental no PD (Fig. 6.40). The expression data generated from one microarray probe indicated that there was an approximate 6-fold significant increase whilst the second microarray probe indicated that there was an approximate 1.4-fold non-significant increase (Fig. 6.40). *KRT5* expression was significantly reduced for at least one probe in RT112 parental + PD, R1 + PD, R3 + PD and R3 no PD compared to RT112 parental no PD. qRT-PCR analysis showed that *KRT5* was significantly reduced in RT112 R1 + PD and significantly increased in R1 no PD (Fig. 6.40). Microarray analysis showed that expression of the basal marker *KRT14,* which is associated

with squamous differentiation in the bladder (Sjodahl *et al.*, 2013), was non-significantly increased in RT112 R1 + PD, R1 no PD, R2 + PD and R2 no PD and non-significantly decreased in R3 + PD and R3 no PD compared to RT112 parental no PD (Fig. 6.40). qRT-PCR showed that there was a significant increase in *KRT14* expression in RT112 R1 + PD and R1 no PD (Fig. 6.40).

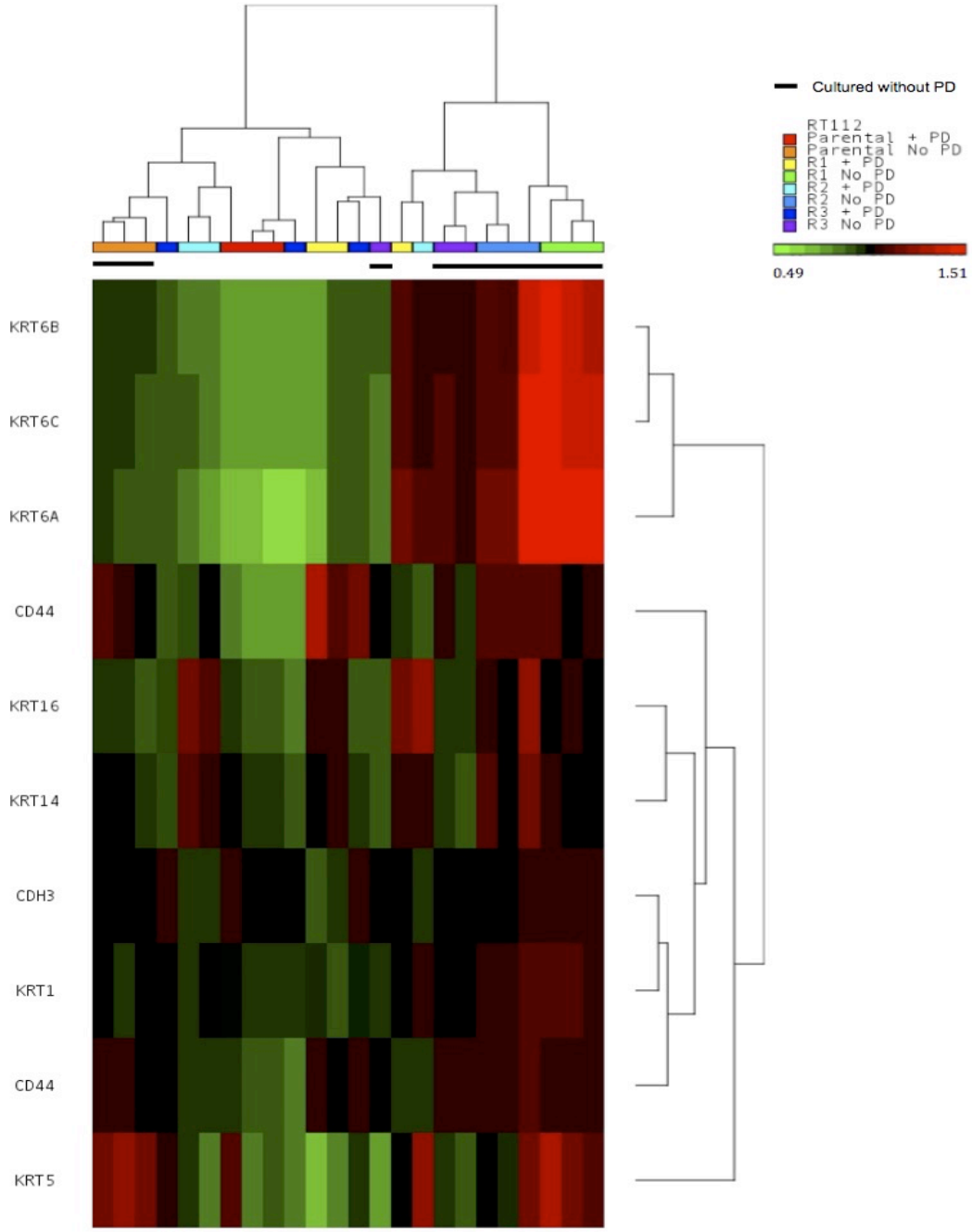

Figure 6.39 Unsupervised hierarchical cluster analysis of Choi *et al.* cohort of basal markers in RT112 microarray samples. The Log_2 gene expression was normalised by dividing each expression value by the probe's mean Log_2 gene expression. Following Log_2 gene expression normalisation, the expression profiles of samples and genes were clustered in Partek® Genomics Suite® 6.6 using Euclidean distance and complete linkage. Scale bar indicates the normalised Log_2 gene expression with colour depicting the level of gene expression as high (red), intermediate (black) and low (green).

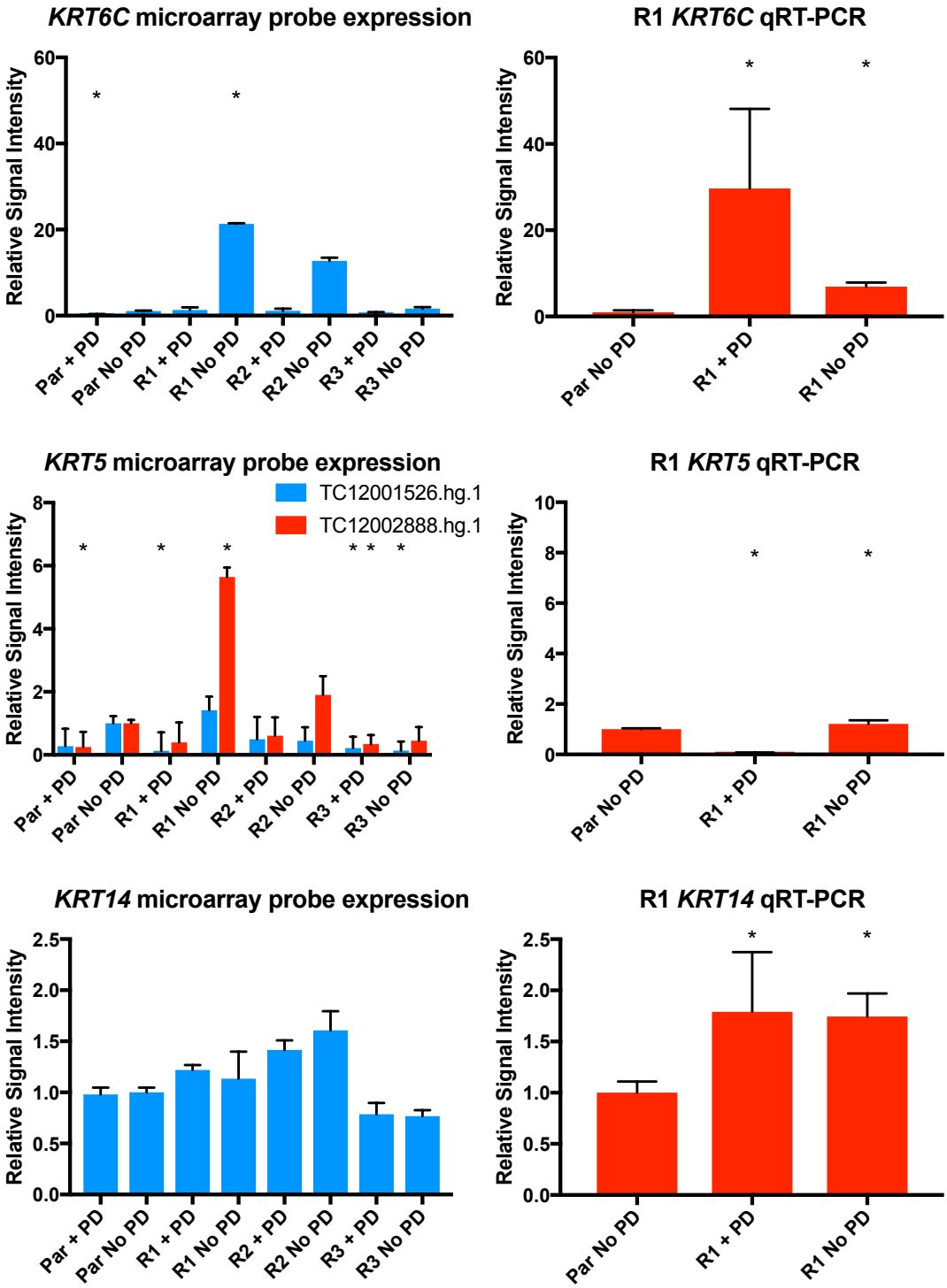

Figure 6.40 Expression of *KRT6C* and *KRT5* in RT112 determined by microarray and qRT-PCR analysis. Error bars indicate standard error of the mean. Signal intensity is given relative to parental no PD. Asterisks indicate the experimental conditions in which genes were significantly differentially expressed compared to parental no PD. Microarray analysis statistical test: ANOVA $p<0.05$, 2-fold expression change. qRT-PCR statistical test: Mann-Whitney U, 2-tailed test, $p<0.05$. For genes with specificity to more than one probe, the data generated from each probe is shown separately with a legend indicating the probe's Affymetrix IDs.

Immunoblot analysis showed that expression of cytokeratin 5/6 was much lower in RT112 samples than in the positive control SCaBER. The sample with the highest expression of cytokeratin 5/6 was RT112 parental no PD (Fig. 6.41). Therefore, treatment with PD, or subsequent removal of PD, did not induce an increase in cytokeratin 5/6 protein expression. The discrepancy between the *KRT5* and *KRT6C* mRNA and cytokeratin 5/6 protein levels could be due to post-transcriptional regulation of the mRNA.

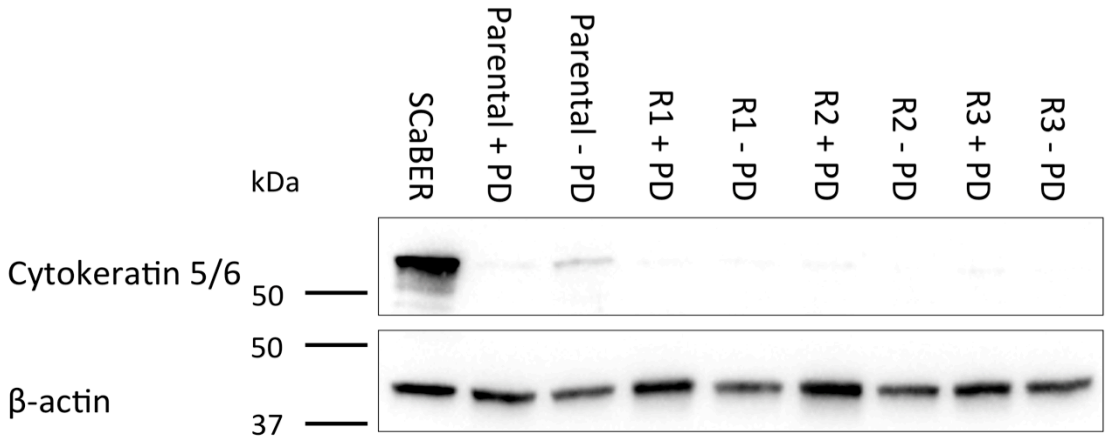

Figure 6.41 Immunoblot analysis of cytokeratin 5 and 6 protein expression in RT112. Expression was examined in parental, parental treated with PD173074 for 24 h, R1, R2 and R3 cultured with PD173074 and R1, R2 and R3 cultured without PD173074 for 4 passages. SCaBER was included as a positive control for cytokeratin 5 and 6 and β-actin was used as a loading control.

Microarray analysis showed that expression of the basal marker *CD44* was significantly decreased in RT112 parental + PD and R2 + PD compared to parental no PD (Fig. 6.42). However, no CD44 protein expression was detected in any RT112 samples with immunoblot (Fig. 6.43). This indicates that despite the observed differential expression of basal marker mRNA in the RT112 experimental conditions, this may be insufficient to induce detectable changes in protein expression. As the immunoblot analysis conducted to examine cytokeratin 5/6 and CD44 did not show that protein expression of these basal markers was increased in the RT112 resistant line, it is unlikely that the cells underwent a luminal to basal subtype switch.

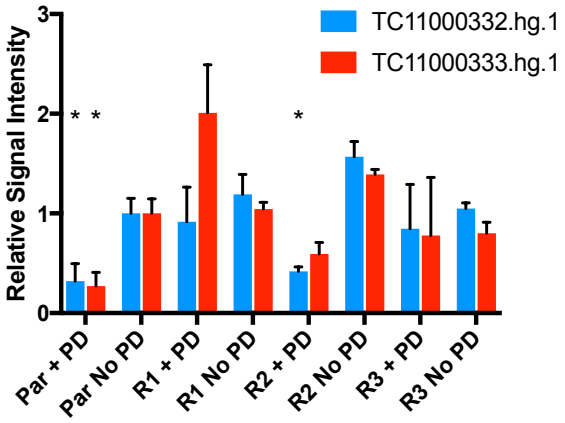

Figure 6.42 Expression of *CD44* in RT112 determined by microarray analysis. Error bars indicate standard error of the mean. Signal intensity is given relative to parental no PD. Asterisks indicate the experimental conditions in which *CD44* was significantly differentially expressed compared to parental no PD (ANOVA $p<0.05$, 2-fold expression change). The data generated from each probe with specificity to *CD44* is shown separately with a legend indicating the probe's Affymetrix IDs.

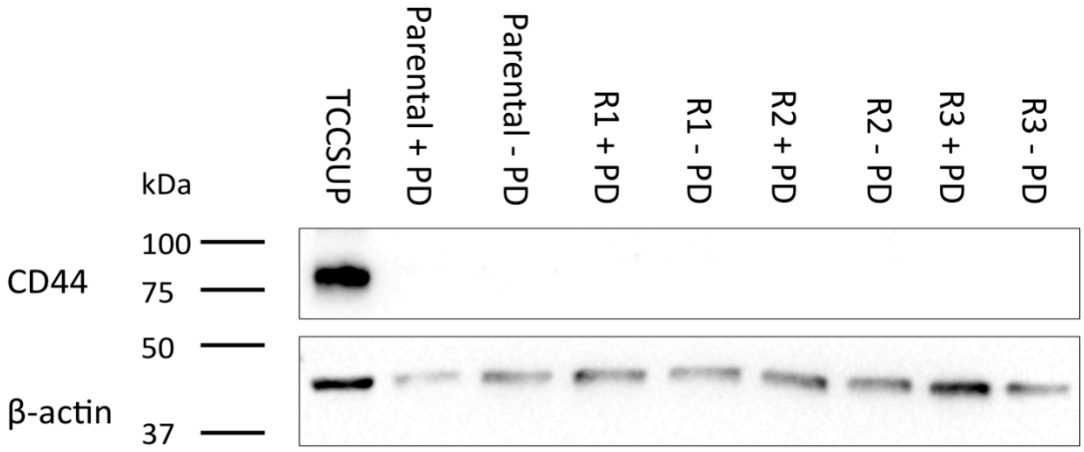

Figure 6.43 Immunoblot analysis of CD44 protein expression in RT112. Expression was examined in parental, parental treated with PD173074 for 24 h, R1, R2 and R3 cultured with PD173074 and R1, R2 and R3 cultured without PD173074 for 4 passages. TCCSUP was included as a positive control for CD44 and β-actin was used as a loading control.

6.2.10 Expression of luminal cell markers in RT4

It was noted that some basal and luminal markers were differentially expressed in RT4 microarray data (2-fold change lists). Additionally, an increase in activation of EGFR was observed in RT4 R1 (Chapter 4, Fig. 4.6) which is characteristic of the basal subtype in MIBC (Kiselyov *et al.*, 2016). Unsupervised hierarchical cluster analysis was performed with RT4 microarray expression data for the luminal subtype markers reported by Choi *et al.* (Fig. 6.44). Compared to RT4 parental no PD, expression of luminal markers was predominantly reduced in RT4 R1 no PD.

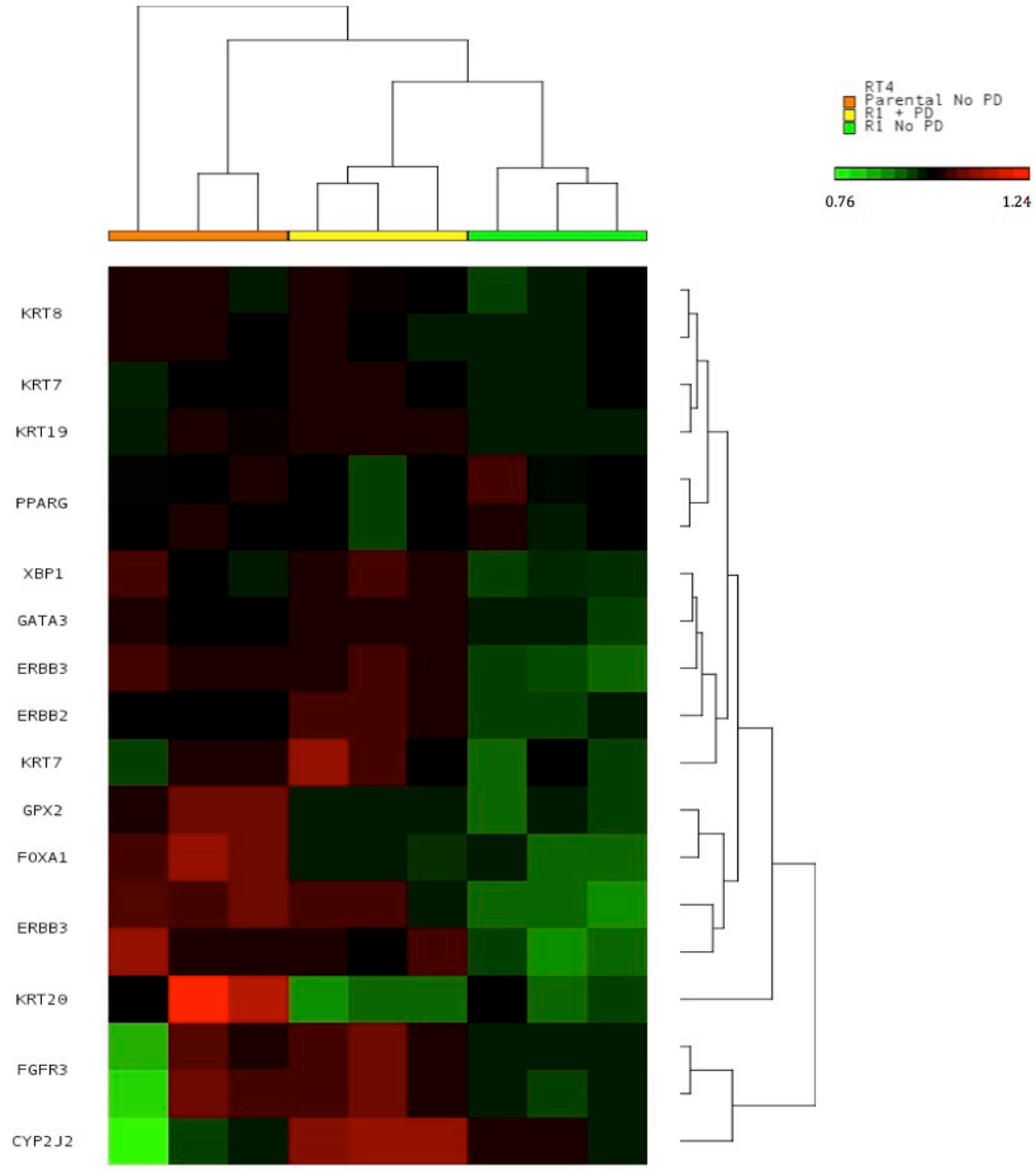

Figure 6.44 Unsupervised hierarchical cluster analysis of Choi *et al.* cohort of luminal markers in RT4 microarray samples. The Log_2 gene expression was normalised by dividing each expression value by the probe's mean Log_2 gene expression. Following Log_2 gene expression normalisation, the expression profiles of samples and genes were clustered in Partek® Genomics Suite® 6.6 using Euclidean distance and complete linkage. Scale bar indicates the normalised Log_2 gene expression with colour depicting the level of gene expression as high (red), intermediate (black) and low (green).

Expression of the luminal markers *FOXA1* and *GPX2* was significantly reduced in RT4 R1 + PD and RT4 R1 no PD to approximately half the level expressed in RT4 parental no PD (Fig. 6.45). Expression of *KRT20* was non-significantly reduced in RT4 R1 + PD and R1 no PD to approximately half the level expressed in parental no PD (Fig. 6.45). *GATA3* and *PPARG* were not significantly differentially expressed across RT4 experimental conditions (Fig. 6.45). Compared to RT4 parental no PD expression of the luminal marker *CYP2J2* was significantly

increased approximately 4-fold and non-significantly increased approximately 2-fold in R1 + PD and R1 no PD respectively (Fig. 6.45). qRT-PCR analysis found expression of *FGFR3* to be significantly increased in RT4 R1 + PD compared to RT4 parental no PD (Fig. 6.31). However, immunoblot analysis of FGFR3 in Chapter 3 found FGFR3 to be expressed at similar levels in RT4 parental and R1 + PD (Chapter 3, Fig. 3.13). Microarray analysis found a non-significant decrease in expression of *ERBB3* in RT4 R1 no PD compared to RT4 parental no PD (Fig. 6.46). qRT-PCR analysis showed that *ERBB3* expression was significantly reduced in RT4 R1 no PD to approximately half the expression level in RT4 parental no PD (Fig. 6.46). As expression of *FOXA1*, *GPX2* and *KRT20* was reduced in RT4 R1 + PD it is possible that RT4 R1 gained a less luminal phenotype during its derivation.

Microarray analysis showed that expression of *UPK1A* and *UPK2* was significantly increased and expression of *UPK3A*, *UPK3B* and *ELF3* was non-significantly increased in RT4 R1 + PD compared to PD (Fig. 6.47). Overall, microarray analysis showed that, as for RT112 R1 + PD and R2 + PD, expression of some luminal markers was increased in RT4 R1 + PD compared to the parental line, whilst other luminal markers exhibited a decrease or no change in expression.

p53-like subtype markers were not significantly differentially expressed across RT4 experimental conditions (Appendix D, D.14 and Fig. D.15) therefore it is unlikely that RT4 R1 has gained a more p53-like phenotype.

6.2.11 Expression of basal cell markers in RT4

Unsupervised hierarchical cluster analysis was performed on RT4 microarray samples with Choi *et al.* basal markers (Fig. 6.48). This suggested that expression of *CD44*, *KRT14* and *CDH3* could be differentially expressed between RT4 experimental conditions. Further examination of the microarray data showed that *KRT14* and *CDH3* were not significantly differentially expressed (Fig. 6.49). Expression of *CD44* was significantly lower in R1 + PD than in parental and R1 no PD (Fig. 6.49). As the microarray analysis showed that expression of basal markers was not significantly increased in RT4 R1 + PD compared to RT4 parental, it is unlikely that RT4 R1 underwent a luminal to basal subtype switch.

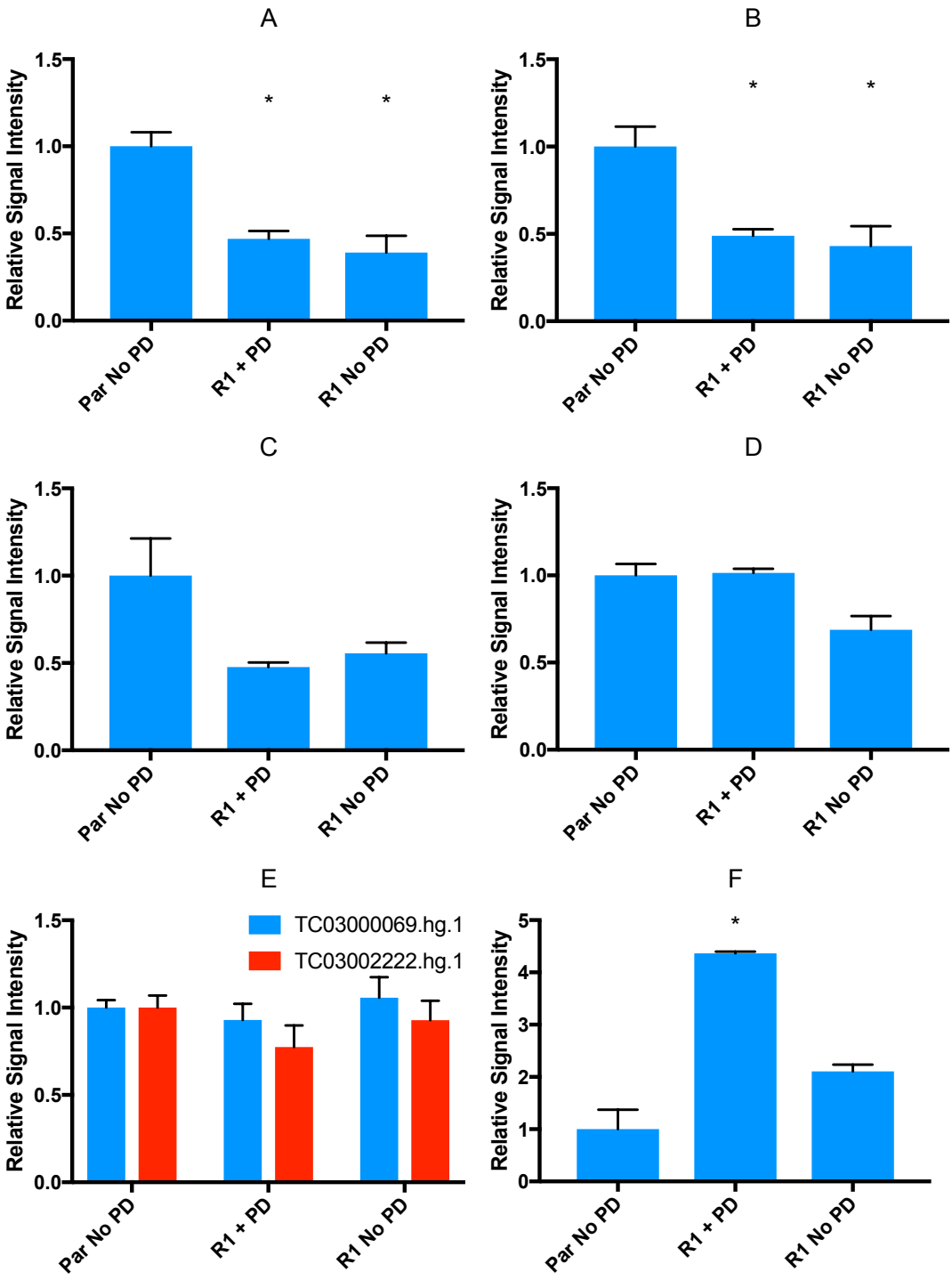

Figure 6.45 Expression of *FOXA1*, *GPX2, KRT20, GATA3, PPARG and CYP2J2* in RT4 determined by microarray analysis. A) *FOXA1* B) *GPX2* C) *KRT20* D) *GATA3* E) *PPARG* and F) *CYP2J2*. Error bars indicate standard error of the mean. Signal intensity is given relative to parental no PD. Asterisks indicate the experimental conditions in which *FOXA1*, *GPX2, KRT20, GATA3, PPARG and CYP2J2* were differentially expressed compared to parental no PD (ANOVA $p<0.05$, 2-fold expression change). For genes with specificity to more than one probe, the data generated from each probe is shown separately with a legend indicating the probe's Affymetrix IDs.

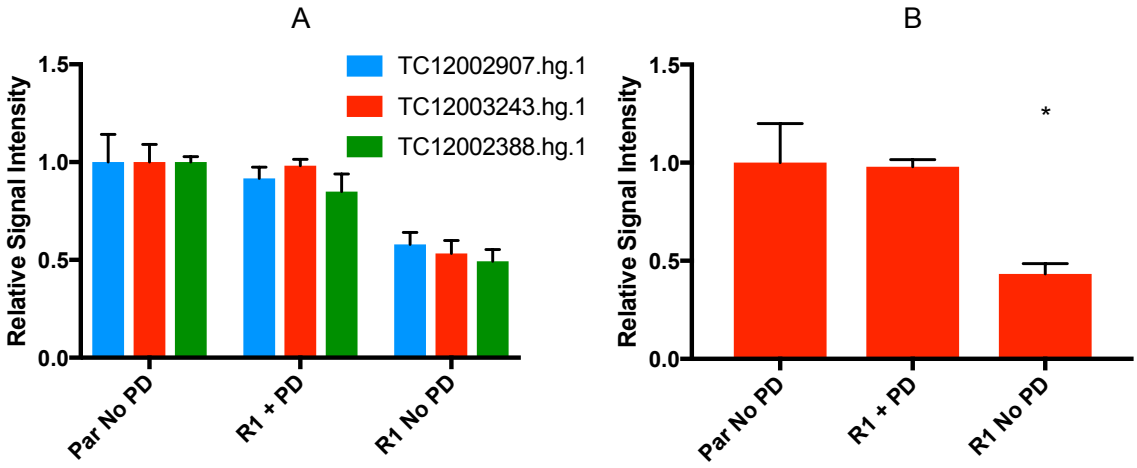

Figure 6.46 Expression of *ERBB3* in RT4 determined by microarray and qRT-PCR analysis. A) microarray analysis. B) qRT-PCR analysis. Error bars indicate standard error of the mean. Signal intensity is given relative to parental no PD. Asterisks indicate the experimental conditions in which *ERBB3* is differentially expressed compared to parental no PD. Microarray statistical test: ANOVA $p<0.05$, 2-fold expression change. qRT-PCR statistical test: Mann-Whitney U, 2-tailed test, $p<0.05$. For genes with specificity to more than one probe, the data generated from each probe is shown separately with a legend indicating the probe's Affymetrix IDs.

6.2.12 Expression of receptor tyrosine kinases

Examination of the expression and phosphorylation of RTKs previously implicated in resistance to FGFR inhibition in RT112 was conducted in Chapter 4. This showed that resistance to PD is not likely to have arisen in RT112 R1 and R2 via an increase in the activation of EGFR and ERBB2 (Chapter 4, Fig. 4.5 and Fig. 4.7). However, an increase in phosphorylation of ERBB3 was observed in RT112 R1 + PD and R2 + PD which may contribute to their resistance to PD. Immunoblot analysis found that total MET expression was reduced in RT112 R1 + PD and R2 + PD compared to parental no PD. However, MET phosphorylation was increased in RT112 R1 + PD, R2 + PD and R3 + PD supporting the notion that this RTK is mediating resistance to PD (Chapter 4, Fig. 4.11).

Unsupervised hierarchical cluster analysis was performed using expression array data for a selected panel of RTKs for RT112 microarray samples (Fig. 6.50). Expression of *KIT* was increased in parental + PD compared to parental no PD but not increased in the RT112 resistant derivatives therefore resistance is unlikely to be mediated in these lines by an increase in KIT expression. Expression of *ERBB2*, *ERBB3* and *INSR* was increased in RT112 parental + PD and R1 + PD and to a lesser extent R2 + PD compared to the other RT112 experimental conditions. qRT-PCR validation confirmed that *ERBB3* expression was increased in parental + PD, R1 + PD and R2 + PD (Fig. 6.37). Hierarchical clustering of microarray data also

identified an increase in *IGF1R, EGFR and MET* expression in R1 + PD and R2 + PD compared to the other RT112 samples (Fig. 6.50).

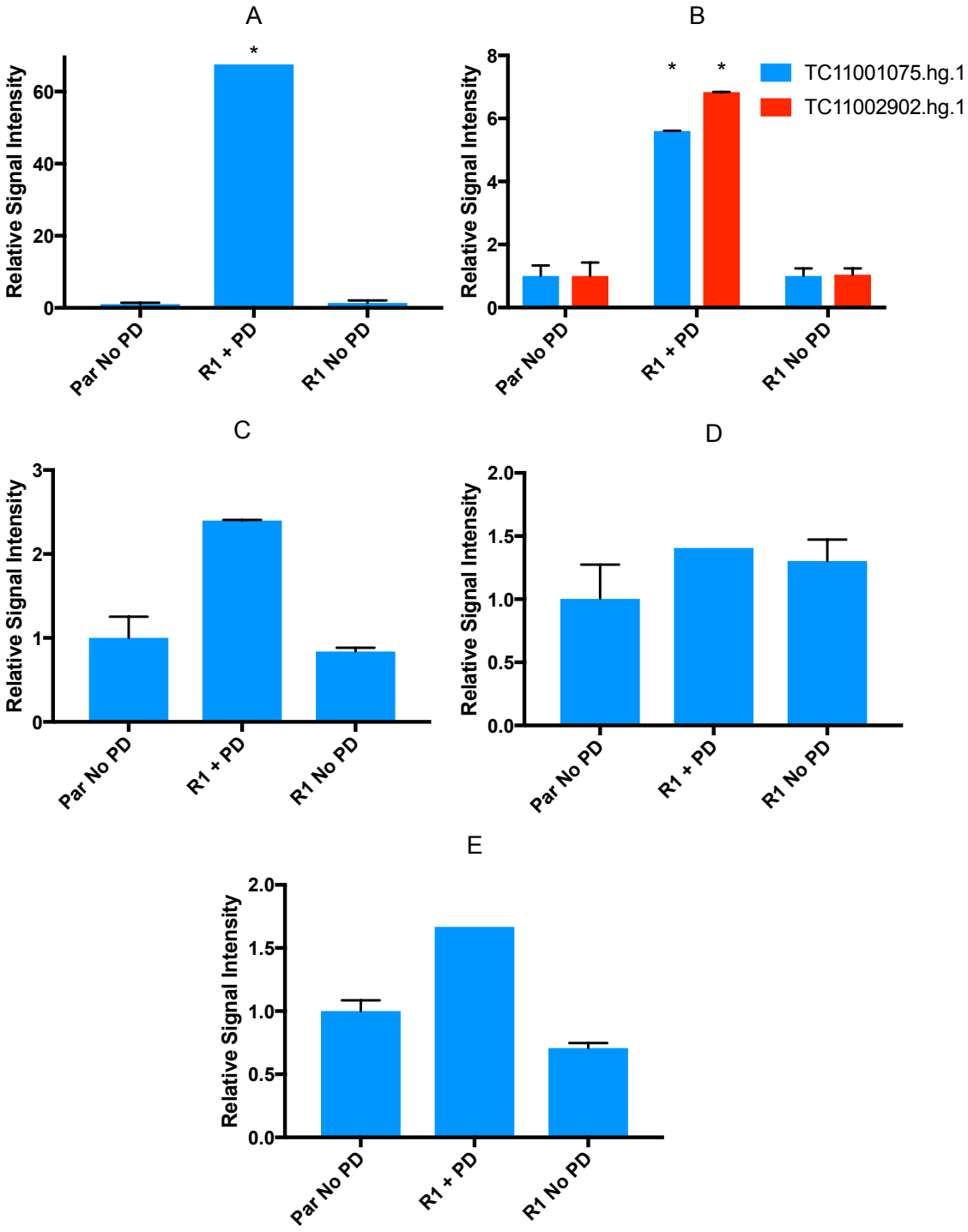

Figure 6.47 Expression of *UPK1A*, *UPK2, UPK3A, UPK3B* and *ELF3* in RT112 determined by microarray analysis. A) *UPK1A.* B) *UPK2.* C) *UPK3A.* D) *UPK3D.* E) *ELF3.* Error bars indicate standard error of the mean. Where error bars are not present this is due to the error being too small to plot. Signal intensity is given relative to RT112 no PD. Asterisks indicate the experimental conditions in which genes were significantly differentially expressed compared to parental no PD (ANOVA $p<0.05$, 2-fold expression change). For genes with specificity to more than one probe, the data generated from each probe is shown separately with a legend indicating the probe's Affymetrix IDs.

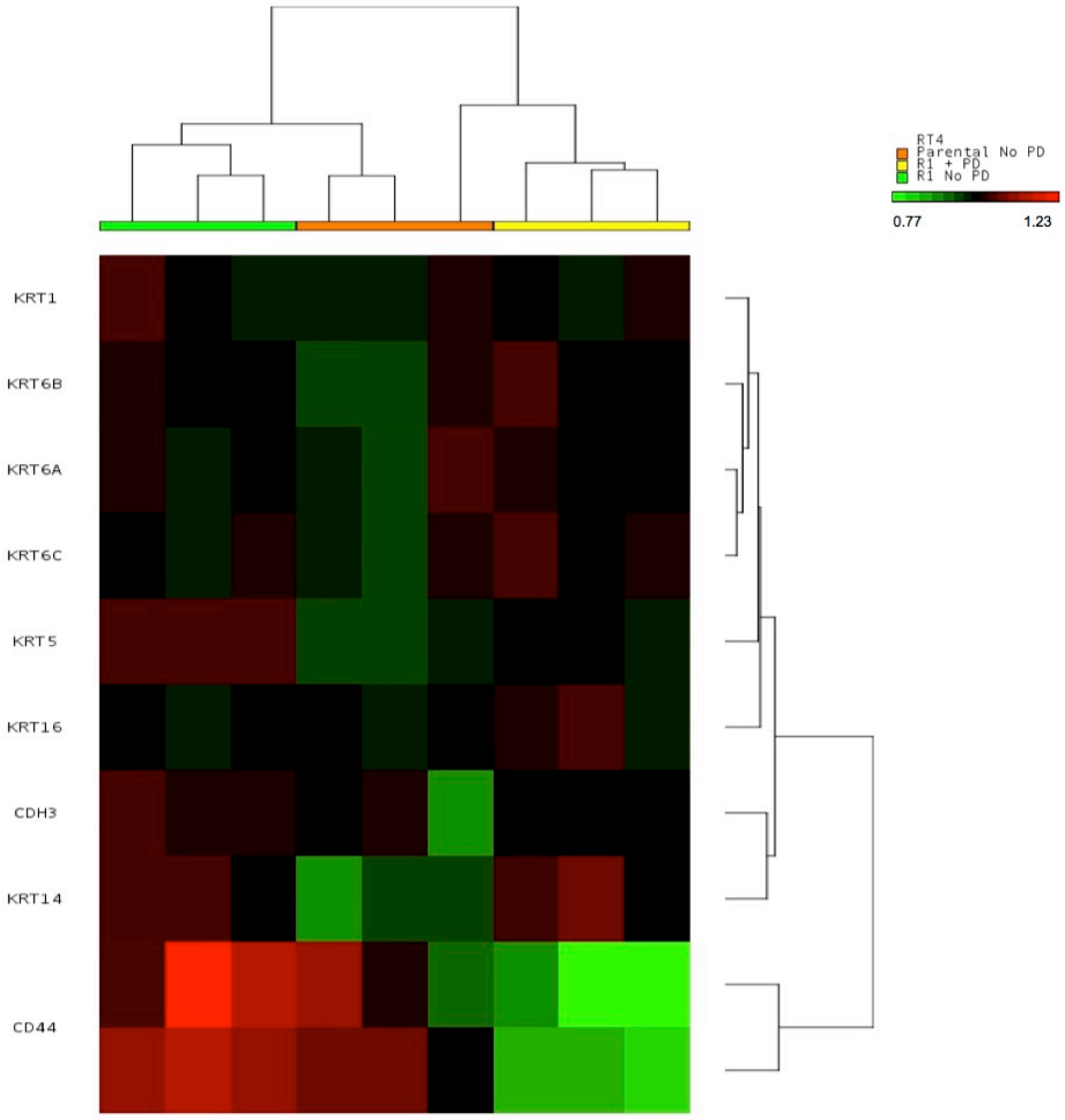

Figure 6.48 Unsupervised hierarchical cluster analysis of Choi *et al.* cohort of basal markers in RT4 microarray samples. The Log_2 gene expression was normalised by dividing each expression value by the probe's mean Log_2 gene expression. Following Log_2 gene expression normalisation, the expression profiles of samples and genes were clustered in Partek® Genomics Suite® 6.6 using Euclidean distance and complete linkage. Scale bar indicates the normalised Log_2 gene expression with colour depicting the level of gene expression as high (red), intermediate (black) and low (green).

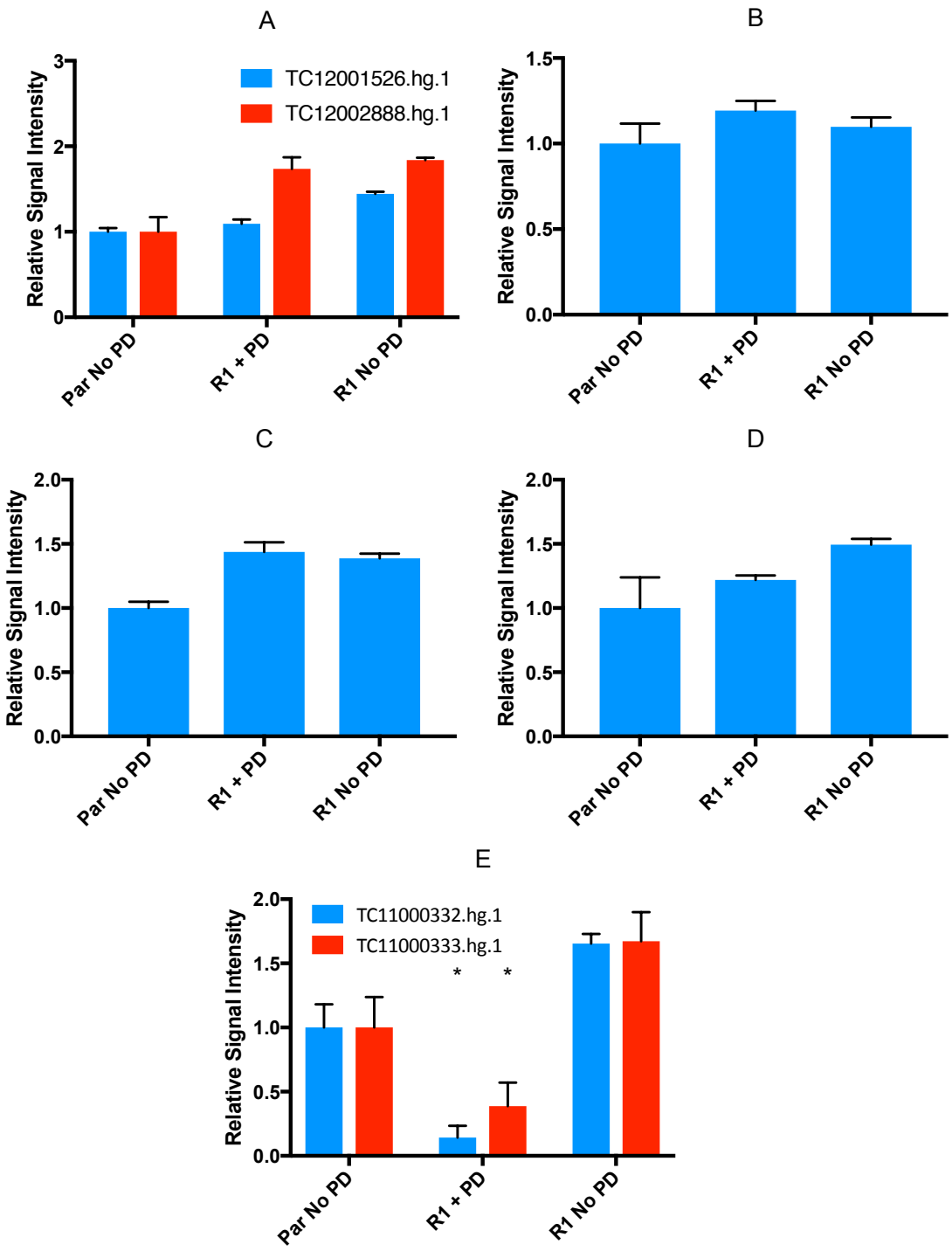

Figure 6.49 Expression of *KRT5, KRT6C, KRT14, CDH3* and *CD44* in RT4 determined by microarray analysis. A) *KRT5.* B) *KRT6C.* C) *KRT14.* D) *CDH3.* E) *CD44.* Error bars indicate standard error of the mean. Signal intensity is given relative to parental no PD. Asterisks indicate the experimental conditions in which *KRT5, KRT6C, KRT14, CDH3 and CD44* were significantly differentially expressed compared to parental no PD (ANOVA $p<0.05$, 2-fold expression change). For genes with specificity to more than one probe, the data generated from each probe is shown separately with a legend indicating the probe's Affymetrix IDs.

Further examination of the microarray data showed that for *IGF1R* expression was significantly increased in R1 + PD. One of the two IGF1R specific probes reported a significant increase in *IGF1R* expression in R2 + PD (Fig. 6.51). Immunoblot analysis was not conducted to examine *IGF1R* expression due to time limitations. The microarray analysis showed that *MET* expression was significantly increased in RT112 R1 + PD and iR3 + PD, and non-significantly increased in R2 + PD (Fig. 6.51). Resistance to PD in RT112 R1 and R2 could be mediated via increased signalling of IGF1R or MET and whether this is the case requires further investigation.

Increased expression of a RTK ligand could induce increased activation of an RTK and downstream signalling pathways, and therefore cause resistance to PD. As IGF1R, MET and ERBB3 had been identified as possible mediators of resistance to PD in RT112 R1 and R2, the expression of the ligands with specificity to these receptors was examined. Microarray analysis showed that expression of *IGF1*, which encodes the IGF1R ligand insulin-like growth factor 1, HGF, which encodes the MET ligand hepatocyte growth factor, *EREG* and *NRG2,* which encode the ERBB3 ligands epiregulin and neuregulin 2 respectively, were not significantly differentially expressed in the RT112 resistant derivatives compared to the parental line (Appendix D, Fig. D.16). Expression of *IGF2* which encodes the IGF1R ligand insulin-like growth factor 2 was significantly reduced in R1 + PD and R2 + PD (Fig. 6.52). One microarray probe set (TC08000250.hg.1) showed expression of *NRG1* was significantly increased in RT112 R1 + PD and R2 + PD. However, this increase in expression was of a small magnitude and the other probe sets with specificity to *NRG1* did not identify an increase in expression of this gene (Fig. 6.52). Therefore, it is most probable that R1 and R2 did not gain their PD-resistant phenotype due to an increase in expression of any of the ligands examined.

Microarray analysis showed that expression of *FGFR2 and FGFR3,* was increased in RT4 R1 + PD (Fig. 6.53), however these RTKs are unlikely to be inducing resistance as these receptors are inhibited by PD. Expression of *EPHA3,* which encodes ephrin receptor A3, was significantly increased approximately 2-fold in RT4 + PD compared to the parental line (Fig. 6.53 and Fig. 6.54).The Ephrin family of RTKS are implicated in angiogenesis (Pitulescu and Adams, 2014). Expression of EGFR family members was increased in R1 + PD (Fig. 6.53), including a significant increase in *EGFR* expression of approximately 3-fold in RT4 R1 + PD and R1 no PD (Fig. 6.54). The immunoblot analysis of phosphorylation of EGFR, ERBB2, ERBB3 in RT4 parental no PD and RT4 R1 + PD suggested that

EGFR could be inducing resistance to PD in RT4 R1 (Chapter 4, Fig. 4.6 and Fig. 4.9). Microarray analysis showed that expression of *ERBB4* was non-significantly increased in RT4 R1 + PD (Fig. 6.54), however, it is possible that increased expression of this receptor could contribute to resistance to PD in RT4 R1. EGFR activation remains the most likely mechanism of resistance in RT4 R1 + PD.

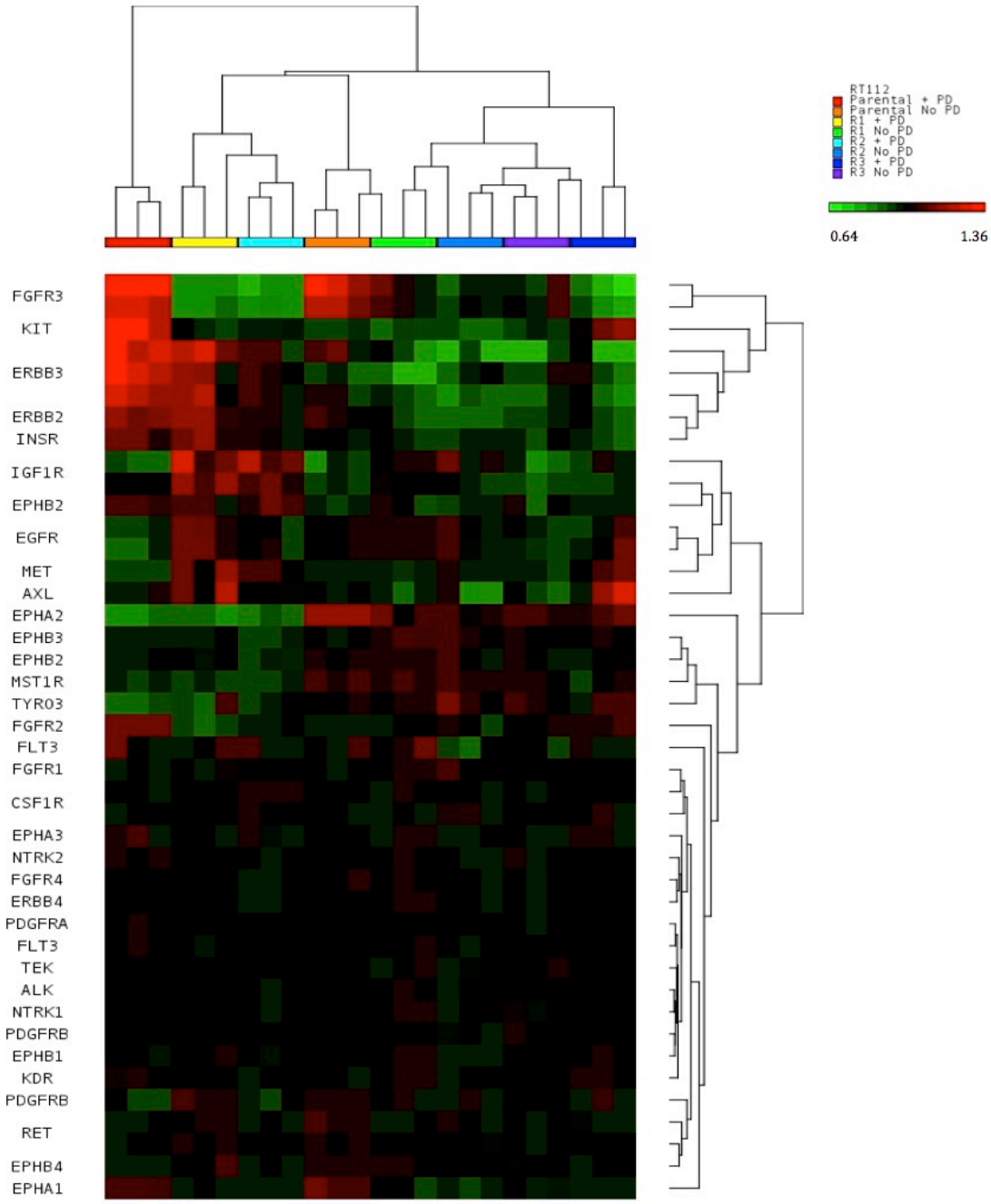

Figure 6.50 Unsupervised hierarchical cluster analysis of receptor tyrosine kinases in RT112 microarray samples. The Log_2 gene expression was normalised by dividing each expression value by the probe's mean Log_2 gene expression. Following Log_2 gene expression normalisation, the expression profiles of samples and genes were clustered in Partek® Genomics Suite® 6.6 using Euclidean distance and complete linkage. Scale bar indicates the normalised Log_2 gene expression with colour depicting the level of gene expression as high (red), intermediate (black) and low (green).

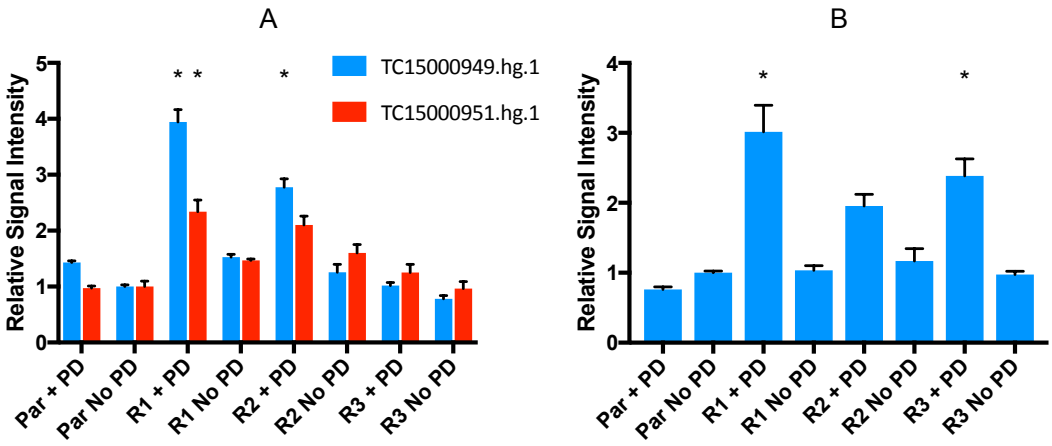

Figure 6.51 Expression of *IGF1R* and *MET* in RT112 determined by microarray analysis. A) *IGF1R.* B) *MET*. Error bars indicate standard error of the mean. Signal intensity is given relative to parental no PD. Asterisks indicate the experimental conditions in which *IGF1R* and *MET* were significantly differentially expressed compared to parental no PD (ANOVA p<0.05, 2-fold expression change). For genes with specificity to more than one probe, the data generated from each probe is shown separately with a legend indicating the probe's Affymetrix IDs.

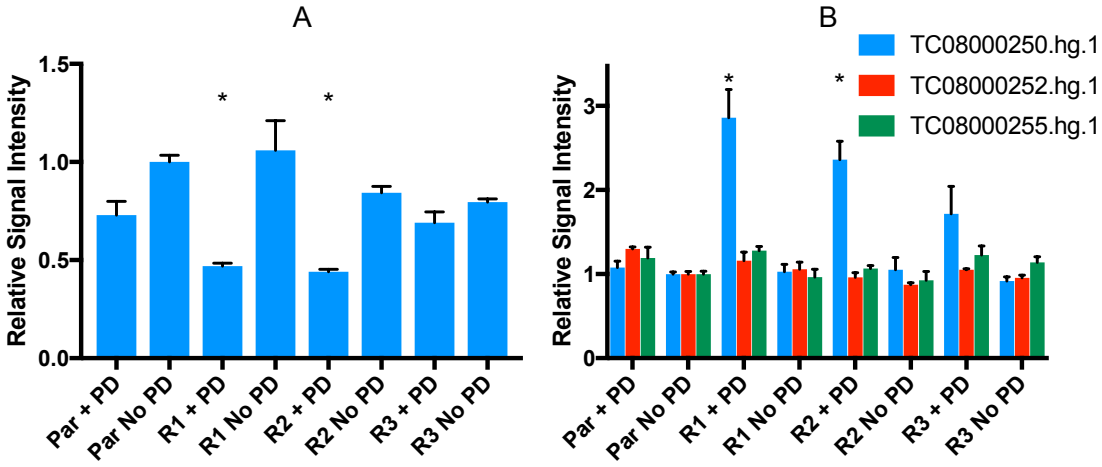

Figure 6.52 Expression of *IGF2* and *NRG1* in RT112 determined by microarray analysis. A) *IGF2.* B) *NRG1.* Error bars indicate standard error of the mean. Signal intensity is given relative to parental no PD. Asterisks indicate the experimental conditions in which *IGF2* and *NRG1* were significantly differentially expressed compared to parental no PD (ANOVA p<0.05, 2-fold expression change). For genes with specificity to more than one probe, the data generated from each probe is shown separately with a legend indicating the probe's Affymetrix IDs.

As EGFR activation was the most likely mechanism of resistance in RT4 R1 + PD, microarray analysis was used to examine expression of EGFR family ligands in RT4 experimental conditions. Expression of *EREG*, *HBEGF*, *EGF* and *EPGN,* which encode EGFR ligands, was not significantly increased in RT4 R1 + PD (Appendix D, Fig. D.17). Expression of *NRG1* and *NRG2* which encode the EGFR family ligands neuregulin 1 and neuregulin 2, was not significantly increased in RT4

R1 + PD compared to parental no PD (Appendix D, Fig. D.18). However, expression of *AREG* and *BTC*, which encode the EGFR ligands amphiregulin and betacellulin respectively, was significantly increased in RT4 R1 + PD compared to parental no PD (Fig. 6.55). Thus the increased activation of EGFR in RT4 R1 may be mediated by the increased expression of these ligands.

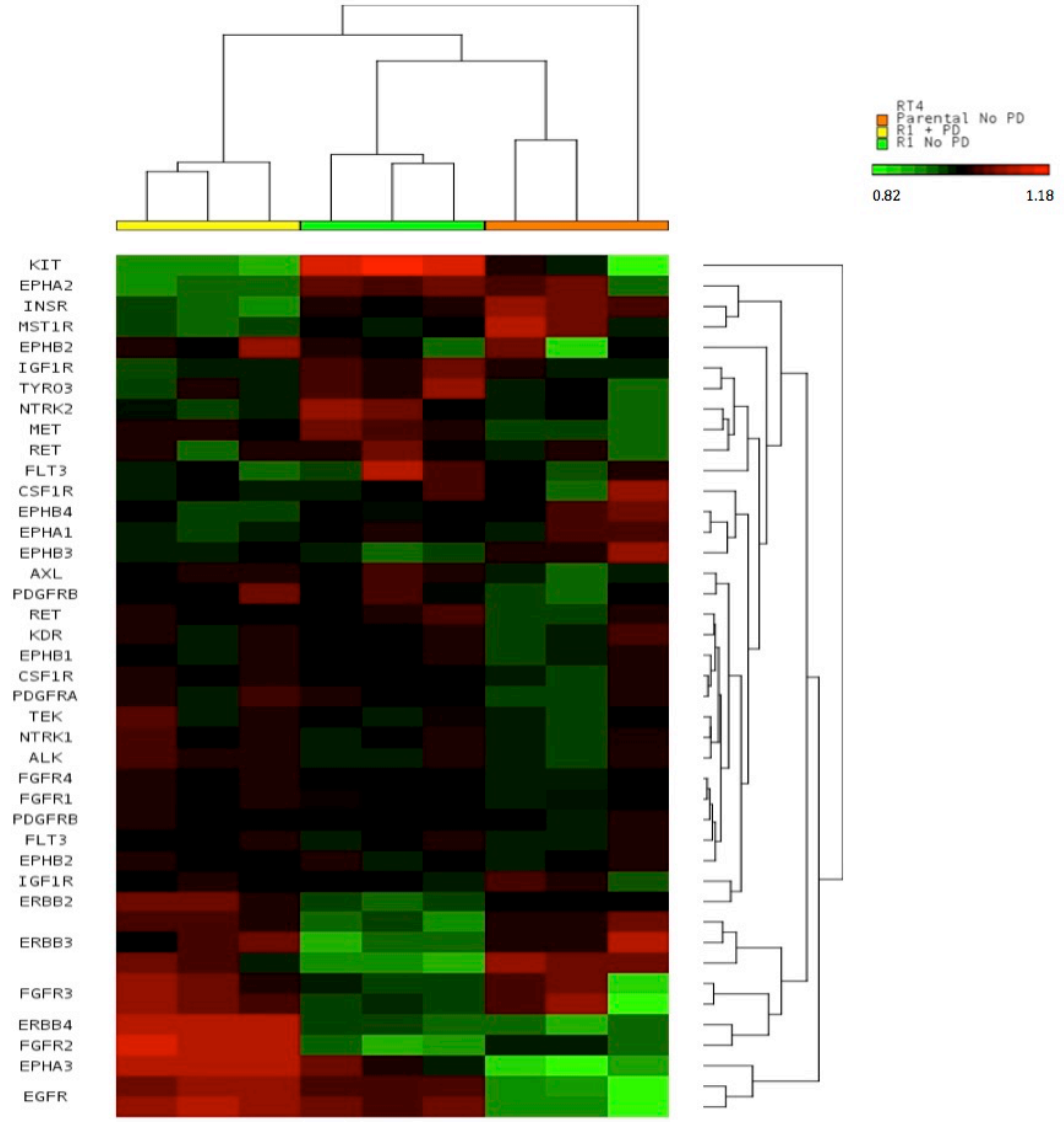

Figure 6.53 Unsupervised hierarchical cluster analysis of receptor tyrosine kinases in RT4 microarray samples. The Log_2 gene expression was normalised by dividing each expression value by the probe's mean Log_2 gene expression. Following Log_2 gene expression normalisation, the expression profiles of samples and genes were clustered in Partek® Genomics Suite® 6.6 using Euclidean distance and complete linkage. Scale bar indicates the normalised Log_2 gene expression with colour depicting the level of gene expression as high (red), intermediate (black) and low green.

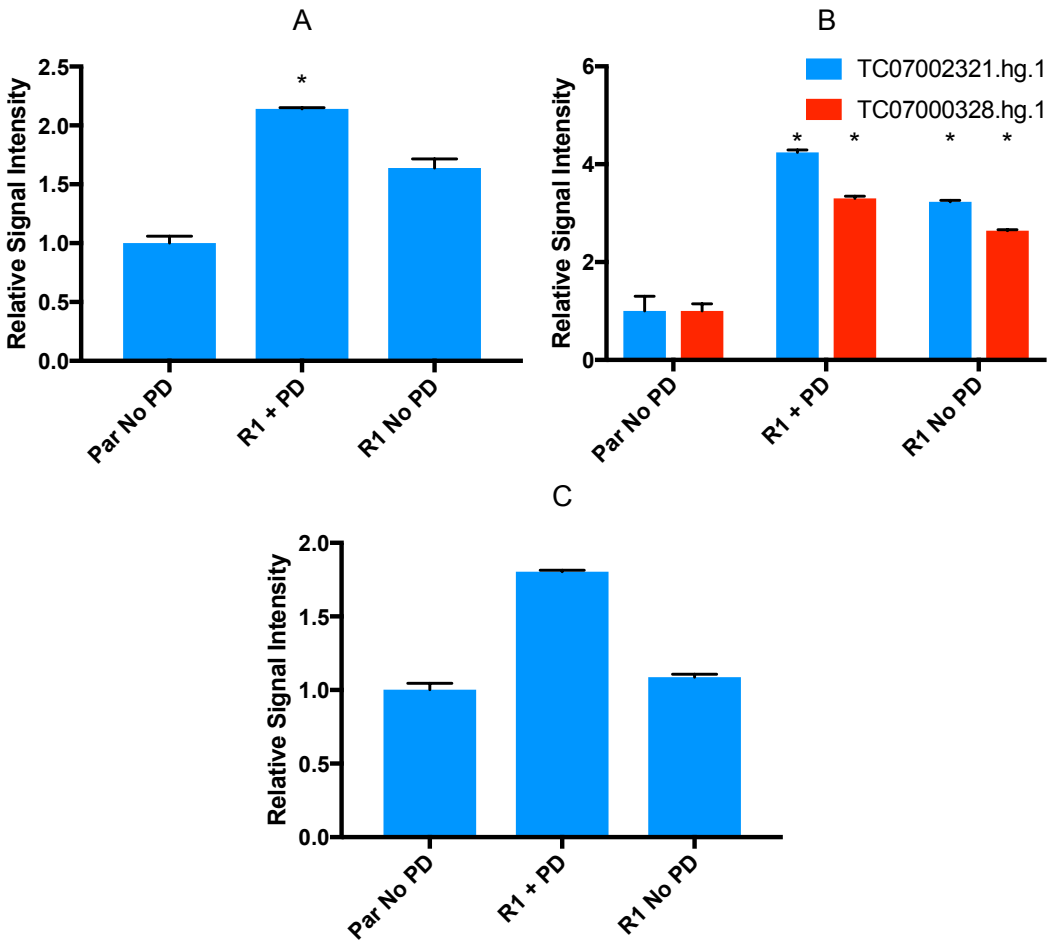

Figure 6.54 Expression of *EPHA3, EGFR* and *ERBB4* in RT4 determined by microarray analysis. A) *EPHA3.* B) *EGFR.* C) *ERBB4.* Error bars indicate standard error of the mean. Signal intensity is given relative to parental no PD. Asterisks indicate the experimental conditions and probes for which genes were significantly differentially expressed compared to parental no PD (ANOVA $p<0.05$, 2-fold expression change). For genes with specificity to more than one probe, the data generated from each probe is shown separately with a legend indicating the probe's Affymetrix IDs.

6.2.13 Expression of KDM5A and KDM6A

Sharma *et al.* generated derivatives of the NSCLC line PC9 tolerant to EGFR TKIs by culturing parental PC9 in gefitinib for 9 days. These cells mediated their resistance by activation of IGF1R. An increase in expression of histone demethylase KDM5A was observed in the resistant cells and the drug tolerant state of these cells was dependent upon KDM5A expression (Sharma *et al.*, 2010). It was observed that, upon culture without an EGFR TKI, resistant cells maintained their resistant phenotype for approximately 30 passages before regaining gefitinib sensitivity (Sharma *et al.*, 2010). It was considered that increased expression of KDM5A may be mediating resistance to PD in RT112, however, microarray analysis showed that *KDM5A* mRNA was not differentially expressed across RT112 conditions suggesting that this is unlikely (Fig. 6.56).

RT112 has a heterozygous P1139fs mutation in *KDM6A*. It was noted that expression of the histone demethylase *KDM6A* was significantly increased in the RT112 resistant derivatives cultured in PD compared to parental no PD (Fig. 6.56). *KDM6A* expression was also non-significantly increased in parental + PD, R1 no PD, R2 no PD and R3 no PD compared to parental no PD. It is possible that this increase in expression mediates the resistant phenotype.

Microarray analysis showed that expression of *KDM5A* was not significantly differentially expressed across RT4 experimental conditions (Fig. 6.56). Expression of the tumour suppressor *KDM6A* was significantly increased in RT4 R1 no PD and non-significantly increased in RT4 R1 no PD. Therefore, an increase in *KDM6A* expression may contribute to the resistant phenotype in RT4 R1.

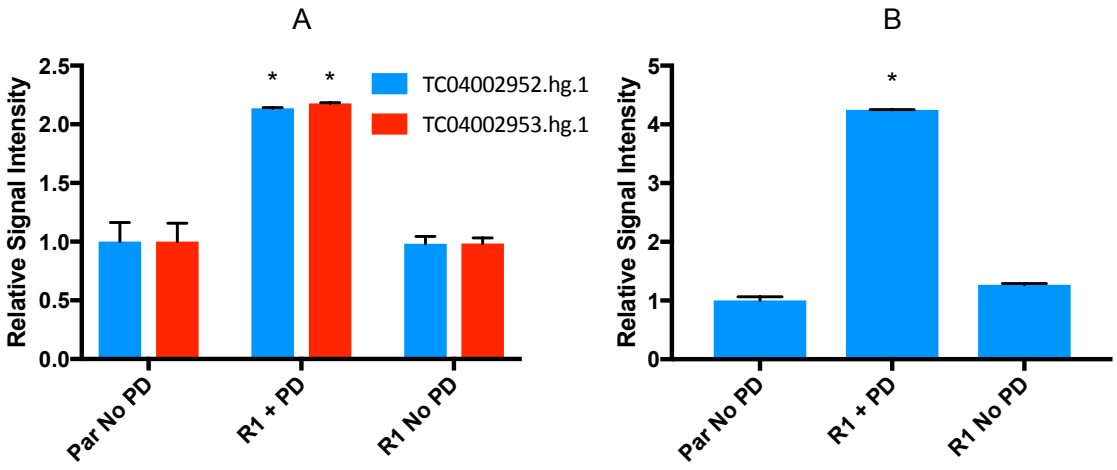

Figure 6.55 Expression of *AREG* and *BTC* in RT4 determined by microarray analysis. A) *AREG.* B) *BTC.* Error bars indicate standard error of the mean. Signal intensity is given relative to RT4 no PD. Asterisks indicate the experimental conditions in which genes were significantly differentially expressed compared to parental no PD (ANOVA $p<0.05$, 2-fold expression change). For genes with specificity to more than one probe, the data generated from each probe is shown separately with a legend indicating the probe's Affymetrix IDs.

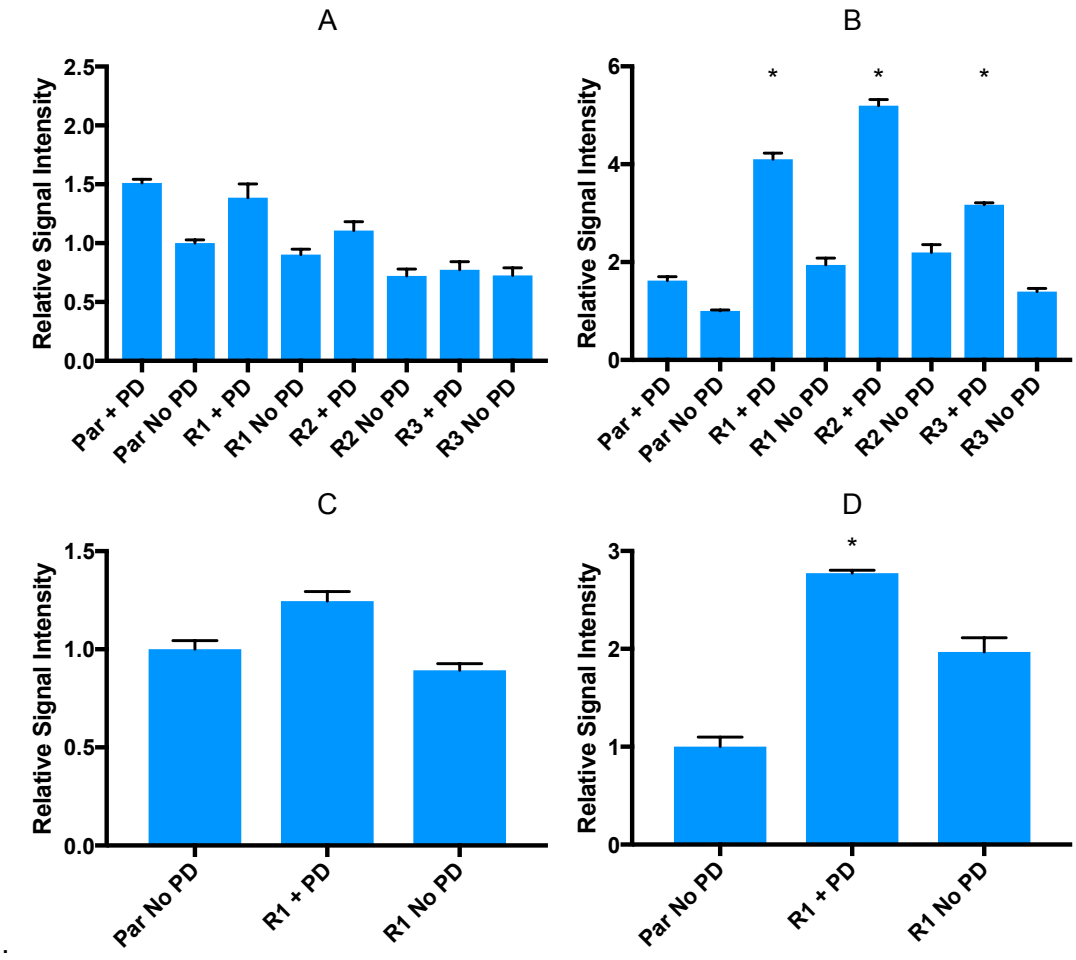

Figure 6.56 Expression of *KDM5A* and *KDM6A* in RT112 and RT4 determined by microarray analysis. A) *KDM5A* expression in RT112. B) *KDM6A* expression in RT112. C) *KDM5A* expression in RT4. D) *KDM6A* expression in RT4. Error bars indicate standard error of the mean. Signal intensity is given relative to parental no PD. Asterisks indicate the experimental conditions and Affymetrix probes for which genes were significantly differentially expressed compared to parental no PD (ANOVA $p<0.05$, 2-fold expression change).

6.3 Discussion

An online cancer microarray database such as Oncomine (Rhodes *et al*., 2007) could have been used to identify genes differentially expressed in urothelial carcinoma compared to normal urothelium. It would then have been possible to use the list of genes differentially expressed in urothelial carcinoma to filter our lists of significantly differentially expressed genes. This would have removed genes whose differential expression has not previously been implicated in urothelial carcinoma, therefore, removing potentially unimportant genes from our lists of significantly differentially expressed genes. However, it is possible that this would have removed gene expression changes implicated in resistance to FGFR inhibition that have yet to be reported in urothelial carcinoma.

Microarray analysis suggested that the OSM pathway could be mediating resistance to PD in RT112 resistant lines as a significant increase in the expression of *OSMR*, *LIFR* and *IL6ST* was observed in RT112 R1 + PD, R1 no PD and R2 + PD compared to parental no PD. A significant increase in expression of *LIFR* and *IL6ST* was also observed in RT112 R3 + PD. The increase in expression in RT112 R1 no PD may be due an increase in the copy number of these genes as copy number analysis showed that RT112 R1 has a gain of 5p15.33 - q11.1 which contains *LIFR* and *OSMR* and a gain of 5q11.1 - q11.2 which contains *IL6ST,* compared to RT112 parental (Chapter 5, Fig. 5.2, Table 5.2). However, the 5p gains cannot account for the increased expression of *IL6ST*, *OSMR* and *LIFR* in RT112 R1 + PD compared to R1 no PD. These copy number alterations were not observed in RT112 R3 (Chapter 5, Fig. 5.3, Table 5.3). Copy number analysis was not conducted in RT112 R2. qRT-PCR validated the increased expression of these receptors in RT112 resistant lines.

Microarray analysis showed that the ligands which activate the OSMR pathway, *OSM* and *IL31,* were not differentially expressed between RT112 experimental conditions. The protein expression levels of OSMRβ, LIFRβ and gp130 was not examined. STAT phosphorylation is commonly used as a readout of activation of the OSM pathway (Moidunny *et al.*, 2016; Zhang *et al.*, 2017). However, immunoblot analysis found that phosphorylation of STAT1 and STAT3 remained low in RT112 resistant derivatives. Therefore, the OSM signalling pathway is not activating STAT1 and STAT3 in the RT112 resistant derivatives. However, immunoblot analysis conducted in Chapter 4 showed that ERK was phosphorylated in RT112 resistant derivatives but not RT112 parental acutely treated with PD (Fig. 4.12). It is possible that the OSM signalling pathway is inducing resistance in RT112 resistant lines via activation of the MAP kinase pathway. No significant increase in OSM pathway ligands or receptors was observed in the microarray analysis of RT4 R1.

Microarray analysis showed that genes which regulate the synthesis of cholesterol and fatty acids were differentially expressed in RT112 and RT4 experimental conditions. It was thought that the resistance mechanism in the PD resistant lines might maintain the expression of fatty acid synthesis genes. Alternatively, the resistant lines could be proliferating despite reduced fatty acid synthesis. It was previously reported that expression of a cohort of genes regulating fatty acid and sterol biosynthesis was reduced in RT112 upon *FGFR3* knockdown for 48 h (Du *et al.*, 2012). Our microarray analysis found that expression of the majority of genes in this cohort was reduced in RT112 acutely treated in PD for 24

h compared to RT112 parental no PD. SCD1 is the rate-limiting enzyme in the production of mono-unsaturated fatty acids from saturated fatty acids and increases lipogenesis (Igal, 2016). As expression of this protein was reduced in RT112 resistant derivatives this suggests that the resistance mechanism employed in these lines does not restore fatty acid synthesis to the level observed in RT112 parental.

The *HRAS* mutation identified in RT112 R3 did not restore mSREBP1 or SCD1 expression to the level observed in the parental line. This indicates that the signalling via the mutant *HRAS* in RT112 R3 did not activate fatty acid synthesis to the same extent as the signalling via *FGFR3-TACC3* and wildtype *FGFR3* in RT112 parental no PD. However, expression of SCD1 was higher in RT112 R3 + PD than in R1 + PD and R2 + PD. Additionally, RT112 R3 + PD maintained expression of many of the Du *et al.* cohort of genes regulating fatty acid and sterol biosynthesis whilst expression was not maintained in R1 + PD and R2 + PD. This suggests that the *HRAS* mutation may have enabled RT112 R3 + PD to maintain fatty acid and sterol biosynthesis to a greater extent than it was maintained in RT112 R1 + PD and R2 + PD. The resistance mechanism in R3 may enable fatty acid and sterol biosynthesis and, therefore, could be the reason that R3 exhibits greater resistance to PD than RT112 R1 or R2 (Chapter 3, Fig. 3.8). Alternatively, the increased expression of genes regulating fatty acid and sterol biosynthesis in RT112 R3 may be due to the greater PD resistance exhibited by this line.

Expression of SCD1 and SREBP1 was not examined by immunoblot in RT4 experimental conditions but expression of the Du *et al.* gene cohort was predominantly reduced in RT4 + PD compared to RT4 parental. This suggests that there was reduced fatty acid and sterol biosynthesis in RT4 + PD. The effect of the reduced expression of genes regulating fatty acid and sterol biosynthesis on lipid metabolism in resistant lines could be investigated by measuring the incorporation of ^{14}C labelled acetate into fatty acids as conducted by Du *et al.* (Du *et al.*, 2012). Alternatively, cellular lipid composition of parental and resistant lines could be examined with mass spectrometry as conducted by Griffiths *et al.* (Griffiths *et al.*, 2013).

Wang *et al.* reported that RT112 cells cultured long-term in the FGFR TKIs BJG398 and ponatinib, to produce TKI-resistant derivatives, exhibited a mesenchymal morphology. It was found that removal of the FGFR TKIs resulted in the derivatives regaining an epithelial morphology within 2-4 weeks (Wang *et al.*, 2014). In Chapter 3 it was observed that RT112 R1 and R2 cultured in PD had a

mesenchymal morphology and had increased expression of the mesenchymal marker N-cadherin (Chapter 3, Fig. 3.4 and Fig. 3.11). These cells had low N-cadherin expression and regained an epithelial morphology following culture without PD for 4 passages (Chapter 3, Fig. 3.5 and Fig. 3.11). The mesenchymal phenotype is associated with greater cell migration and invasion. Therefore, if FGFR TKIs induce an EMT in patients this could lead to tumour metastasis (Singh *et al.*, 2017). EMT has been observed in NSCLC patients with acquired resistance to EGFR TKIs (Sequist *et al.*, 2011). The microarray analysis showed that expression of some epithelial and mesenchymal markers, such as the epithelial marker *CDH1*, remained similar in all RT112 experimental conditions whilst other markers were differentially expressed, such as the mesenchymal marker *FN1*. This supports the previously-held hypothesis that RT112 R1 and R2 underwent a partial EMT during their production. MetaCore™ pathway analysis also showed that R3 had undergone some EMT-like expression changes compared to parental. The evidence for an EMT in RT4 R1 is limited compared to the evidence in RT112 R1 and R2. However, MetaCore™ pathway analysis did find enrichment of the pathway 'regulation of epithelial to mesenchymal transition (EMT)' for the comparison RT4 R1 + PD and RT4 parental no PD (Fig. 6.12). EMT-like gene expression changes could pose a problem for patients treated with FGFR inhibitors if this facilitates tumour metastasis.

Basal bladder cancers tend to be more aggressive than luminal bladder cancers (Choi *et al.*, 2014a; Kiselyov *et al.*, 2016). Microarray and qRT-PCR analysis indicated that expression of some basal markers was increased and expression of some luminal markers was reduced in RT112 resistant derivatives. Expression of *GATA3* and *UPK1A* was increased in R1 + PD and R2 + PD whilst expression of FOXA1 was reduced in R1 + PD and R2 + PD. Immunoblot analysis would have confirmed whether the differences in mRNA expression resulted in differential protein expression. This was no conducted due to time limitations. Microarray and qRT-PCR analysis suggested that *KRT5*, *KRT6C* and *CD44* were differentially expressed between RT112 experimental conditions. However, as the expression of CD44 and cytokeratin 5/6 protein remained low it appears that mRNA expression changes did not result in corresponding changes in protein expression. Therefore, it is unlikely that RT112 resistant derivatives underwent a luminal to basal subtype switch.

As microarray analysis showed that expression of basal markers was not significantly increased in RT4 R1 + PD or R1 no PD, and expression of some luminal markers was increased in RT4 R1 + PD, it is unlikely that RT4 R1

underwent a luminal to basal switch during the derivation of this resistant line or upon culture without PD. Luminal/basal expression changes were not examined with qRT-PCR or immunoblot in RT4 due to time limitations. Expression of p53-like markers was not significantly different between RT4 or RT112 experimental conditions, therefore the RT4 and RT112 resistant derivatives did not undergo a luminal to p53-like subtype switch.

Sharma *et. al.* produced PC9 cells resistant to EGFR-TKIs, which mediated their resistance via activation of IGF1R, via culture in gefitinib for 9 days. It was observed that the resistant cells had increased expression of KDM5A and that *KDM5A* knockdown did not reduce the proliferation of parental PC9 cells but did reduce the production of resistant cells upon treatment with gefitinib (Sharma *et al.*, 2010). Gale *et al.* developed the KDM5A inhibitor YUKA1 and observed that treatment with this inhibitor reduced the formation of gefitinib-resistant colonies following the culture of PC9 in gefitinib for 35 days. Culture with YUKA1 as a single agent did not reduce the growth of PC9 (Gale *et al.*, 2016). Sharma *et al.* observed that, upon culture without an EGFR TKI, resistant cells maintained their resistant phenotype for approximately 30 passages before regaining gefitinib sensitivity (Sharma *et al.*, 2010). Microarray analysis showed that *KDM5A* was not differentially expressed between RT112 and RT4 parental cells and their resistant derivatives. Therefore, it is unlikely that PD resistance is mediated by an increase in *KDM5A* expression.

KDM6A mutations are present in approximately 25% of MIBCs and 40% of NMIBCs (Pietzak *et al.*, 2017; Robertson *et al.*, 2017). KDM6A demethylates lysine 27 of histone H3. One consequence of the histone demethylation activity of KDM6A in fibroblasts is an increase in expression of retinoblastoma binding proteins required for the function of RB1 as a tumour suppressor (Wang *et al.*, 2010). Its role in epithelial cells, including the urothelium, is unknown. Microarray analysis showed that expression of *KDM6A* was increased in the RT112 and RT4 resistant derivatives when cultured in PD. Whether the resistant derivatives are dependent upon *KDM6A* expression to maintain their PD resistance could be tested by examining whether knockdown of *KDM6A* re-sensitizes these cells to PD.

Resistance to RTK inhibition often arises via the activation of an alternative RTK as discussed in Chapter 1, section 1.2.2. Ma *et al.* reported that treatment with the IGF1R ligand IGF1 induced gefitinib resistance in glioblastoma cell lines. The combination of gefitinib and the small molecule inhibitor linsitinib, which has specificity for IGF1R and insulin receptor (InsR), reduced the cell viability of the

glioblastoma cell lines GBM39 and GBM76 more effectively than treatment with either inhibitor as a single agent (Ma *et al.*, 2016). Harris *et al.* found that breast cancer patients whose tumours expressed IGF1R were less likely to respond to the combination of trastuzumab and the chemotherapeutic agent vinorelbine (Harris *et al.*, 2007). Wang *et al.* reported that IGF1R knockdown induced greater sensitivity to gemcitabine in the bladder cancer cell line 5637. Additionally, a meta-analysis showed that bladder cancer patients with high expression of *IGF1R* mRNA have a lower overall survival time and lower time to disease recurrence (Wang *et al.*, 2017a). IGF1R activates the MAP kinase and PI3 kinase pathways (Hartog *et al.*, 2007). Immunoblot analysis in Chapter 4 showed that signalling via these pathways was reduced in RT112 parental acutely treated with PD whereas these pathways were activated in RT112 resistant lines cultured in PD (Fig. 4.12). Therefore, IGF1R could be mediating resistance via activation of the MAP kinase and PI3 kinase pathways in RT112 R1 and R2. Whether IGF1R protein expression is increased in the RT112 resistant lines and whether signalling via IGF1R is active in parental RT112 and the resistant lines could be confirmed with immunoblot analysis. A cell viability assay with the IGF1R inhibitor linsitinib will be described in Chapter 7 to examine the sensitivity of parental RT112 and the RT112 resistant lines to IGF1R inhibition.

Microarray analysis identified an increase in *MET* expression in the RT112 resistant derivatives. This is discrepant with the immunoblot analysis in Chapter 4, in which total MET protein expression was reduced in R1+ PD and R2 + PD (Fig. 4.11). As the immunoblot analysis identified an increase in the phosphorylation of MET, this RTK may be mediating resistance to PD. MET signalling has been reported as a mechanism of short term survival in response to FGFR inhibition (Harbinski *et al.*, 2012).

qRT-PCR analysis identified an increase in ERBB3 expression in RT112 parental acutely treated with PD, R1 + PD and R2 + PD. An increase in phospho-ERBB3 expression was observed in Chapter 4 (Fig. 4.8) but examination of total ERBB3 protein expression was unsuccessful. Signalling via ERBB3, together with its dimerization partner ERBB2, has been previously reported as a resistance mechanism to FGFR inhibition in RT112 (Wang *et al.*, 2014). ERBB3 remains a possible mediator of resistance in the RT112 resistant derivatives. MET has been reported to heterodimerize with ERBB3 (Pérez-Ramírez *et al.*, 2015; Tanizaki *et al.*, 2011), therefore it is possible that these two RTKs act together to induce PD resistance.

EPHA3 mRNA expression was significantly increased in RT4 + PD compared to RT4 R1 no PD. Conflicting evidence has found the EPH family of RTKs to be both oncogenic and tumour-suppressive. Agonistic and antagonistic targeted agents specific for EPH family members, such as ifabotuzumab which is a EphA3 agonist, have entered early stage clinical trials (Lodola *et al.*, 2017). Expression of *ERBB4* was non-significantly increased in RT4 R1 + PD. Canfield *et al.* showed that knockdown of *ERBB4* induced apoptosis in ERBB2-positive breast cancer cell lines with acquired resistance to the EGFR, ERBB2 and ERBB3 TKI lapatinib and the ERBB2-specific monoclonal antibody trastuzumab (Canfield *et al.*, 2015). Whether RT4 R1 exhibits sensitivity to inhibition or knockdown of EphA3 and ERBB4 is worthy of further examination

The increased expression of *EGFR* in RT4 R1 + PD observed in the microarray analysis is concordant with the previously observed increase in EGFR protein expression and phosphorylation. This increased activation of EGFR remains the most likely mediator of resistance in RT4 R1. Herrera-Abreu *et al.* showed that EGFR mediated short-term survival in RT112 treated with PD by re-activating the MAP kinase pathway (Herrera-Abreu *et al.*, 2013). Harbinski *et al.* screened a secreted protein cDNA library and identified that TGF-α, which activates EGFR signalling, was able to induce resistance to the FGFR TKI BGJ398 in RT112 (Harbinski *et al.*, 2012; Singh and Coffey, 2014). EGFR is reported to induce intrinsic resistance to BRAF inhibition via re-activation of the MAP kinase pathway in cell line models of colorectal cancer (Corcoran *et al.*, 2012; Prahallad *et al.*, 2012). Approximately 6% of MIBC tumours exhibit gain of copy number of 7p11.2 which contains *EGFR* (Robertson *et al.*, 2017). Approximately 60% of bladder cancer tumours express membranous EGFR (Ibrahim *et al.*, 2009). These tumours could be intrinsically resistant to FGFR inhibition.

In summary, the targets most worth examining with drug testing in RT112 are IGF1R, MET, ERBB3 and KDM6A, and in RT4 are EGFR, ERBB4, EPHA3 and KDM6A.

Chapter 7
Screening targeted agents to overcome PD173074 resistance

7.1 Introduction

The experimental work in this study so far was conducted with the aim of identifying the mechanisms of resistance in the PD resistant derivatives. Altered expression of several RTKs was identified by immunoblot and transcriptome analysis. Experiments described in this Chapter were performed in order to test whether these RTKs could be acting as mediators of resistance to PD.

Immunoblot analysis in Chapter 4 examined the phosphorylation of RTKs previously implicated in resistance to FGFR inhibition. An increase in phospho-ERBB3 was identified in RT112 R1 and R2. However, phosphorylation of ERBB2 and EGFR remained low in these lines. An increase in phospho-MET was also observed in the RT112 resistant lines. Total and phospho-EGFR expression was increased in RT4 R1 but expression of phospho-ERBB2 and phospho-ERBB3 remained low.

In Chapter 6, qRT-PCR showed *ERBB3* expression to be increased in RT112 parental acutely treated with PD, R1 and R2. Microarray analysis identified a significant increase in *IGF1R* mRNA in RT112 R1 and R2. Microarray analysis also showed *EGFR* mRNA expression to be increased in RT4 R1, concordant with the increase in total EGFR observed by immunoblot in Chapter 4.

The EGFR family, MET and IGF1R can be targeted with small-molecule inhibitors which have specificity to a small number of RTKs. In this Chapter, cell viability assays conducted with small-molecule inhibitors will be presented. These were carried out to test the dependency of resistant lines on RTKs for which an increase in expression or phosphorylation has been identified. This was carried out with the aim of determining which RTKs may be mediating resistance and to suggest which drug combinations could be used in the clinic to overcome resistance to FGFR inhibition. Cell viability assays were conducted with these small-molecule inhibitors, both as single agents and in combination with PD, in order to determine whether the continued inhibition of FGFR3 would elicit a greater reduction in cell proliferation and survival.

Exome sequencing, in Chapter 5, identified a *HRAS* G12S mutation in approximately 75% of RT112 R3 cells. Retroviral transduction of RT112 parental with mutant *HRAS* and subsequent cell viability assays showed that mutation of this gene alone induces resistance to PD. Inhibition of RTKs is thus unlikely to reduce cell viability in RT112 R3 cells with mutant *HRAS* as the constitutively active HRAS would be able to maintain cell proliferation and survival. The sub-population of RT112 R3 which does not possess the *HRAS* mutation may, however, be sensitive to RTK inhibition.

7.2 Results

7.2.1 Cell viability assays with RT112 and the MET TKI capmatinib

An increase in phosphorylation of MET was observed in RT112 R1, R2 and R3 by immunoblot analysis (Fig. 4.11). MET activation has been reported to overcome sensitivity to FGFR inhibition in RT112 (Harbinski *et al.*, 2012). Capmatinib is a selective, ATP-competitive inhibitor of MET. Liu *et al.* conducted a cell-free assay which showed that capmatinib inhibited MET with an IC50 of 0.13nM, whereas 2uM of capmatinib inhibited the other kinases in the panel tested by no more than 30%. Capmatinib inhibited cell viability in the *MET*-amplified gastric cancer cell line SNU-5 and the mouse fibroblast cell line S114, which expresses a high level of MET and HGF, with IC50s of 1.2 and 12.4 nM respectively. Capmatinib was inactive in the gastric cancer cell line SNU-1 and in the kidney cell line HEK293 which express no and a low level of MET respectively (Liu *et al.*, 2011). Capmatinib is currently being assessed in clinical trials for the treatment of EGFR TKI-resistant NSCLC (Wu *et al.*, 2017). As sensitivity to capmatinib had been previously reported at concentrations between 2 and 13nM in MET-dependent cell lines (Liu *et al.*, 2011), it was thought that 1μM capmatinib was a sufficiently high concentration to determine if the RT112 cells were sensitive to MET inhibition. Therefore, sensitivity to 1μM capmatinib was examined by cell viability assay (Fig. 7.1). 1μM capmatinib did not reduce cell viability in RT112 parental, R1, R2 or R3. The sensitivity of RT112 parental and resistant lines to a range of capmatinib concentrations in combination with 1μM PD was also tested (Fig. 7.2). Treatment with capmatinib + PD did not reduce cell viability any more than was observed with PD alone

(Chapter 3, Fig. 3.8). Therefore, RT112 parental and resistant lines are not dependent upon signalling via MET.

Expression of MET has previously been reported in the urothelial carcinoma cell line 5637 and activation of MET signalling by hepatocyte growth factor (HGF) has been reported to increase invasiveness in 5637 (Shintani *et al.,* 2017; Wang *et al.,* 2007). Immunoblot analysis showed that 5637 expressed phospho-MET and MET (Chapter 4, Fig 4.11). Therefore, 5637 was selected as a positive control to determine if capmatinib was successfully inhibiting MET. However, 5637 was insensitive to treatment with capmatinib (Fig. 7.3). This could indicate that capmatinib was not inhibiting MET at the concentrations used in this assay. One alternative explanation is that, whilst 5637 expresses phospho-MET and the activation of MET signalling increases the invasiveness of 5637, MET inhibition does not reduce 5637 cell proliferation or survival. It is also possible that MET could be promoting cell proliferation and survival in 5637 via crosstalk with another receptor, and when MET is inhibited activation of the other receptor compensates for the reduced MET activity. There was insufficient time to conduct immunoblot analysis to examine whether capmatinib inhibited MET phosphorylation in the RT112 resistant derivatives or 5637. This experiment would have clarified whether RT112 parental and the resistant derivatives were resistant to MET inhibition or capmatinib was not inhibiting MET activation. Possible explanations for insensitivity to capmatinib are discussed in greater detail later in this Chapter.

7.2.2 Cell viability assays with RT112 and the ERBB family TKI sapitinib

qRT-PCR analysis established that *ERBB3* was upregulated in RT112 parental acutely treated with PD, RT112 R1, R2 and R3 when compared to parental no PD (Fig. 6.46). Phosphorylation of ERBB3 was identified by immunoblot in R1 and R2 (Chapter 4, Fig. 4.8) whereas increased phosphorylation of EGFR and ERBB2 was not observed in R1 and R2 (Chapter 4, Fig. 4.5 and Fig. 4.7). Wang *et al.* reported activation of ERBB2 and ERBB3 as a mechanism of resistance in RT112 cultured in FGFR inhibitors (Wang *et al.*, 2014). Herrera-Abreu *et al.* reported EGFR activation as a mechanism of short term survival in response to treatment with PD in RT112 (Herrera-Abreu *et al.*, 2013).

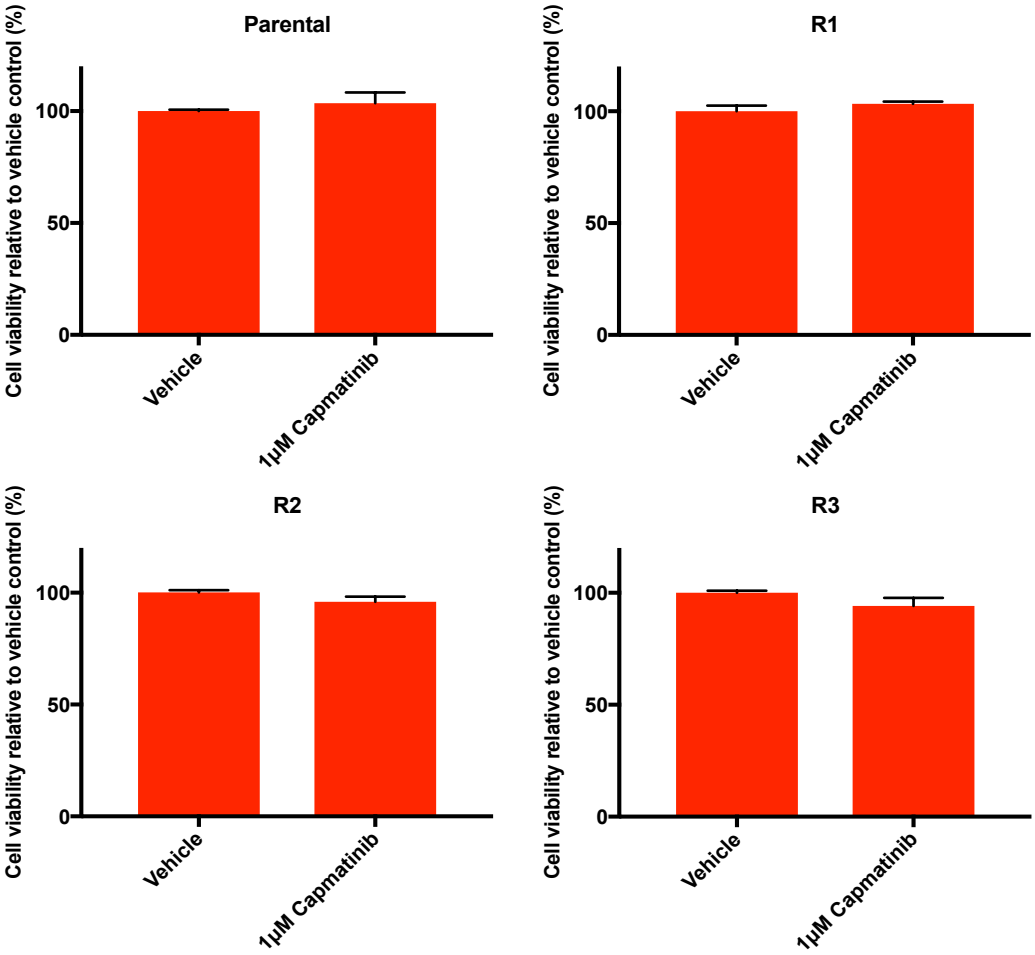

Figure 7.1 Cell viability of parental RT112 and resistant derivatives in capmatinib (MET TKI). Viability of cells was assayed using CellTiter-Blue following 120 h treatment with capmatinib and normalised to vehicle control. Error bars show the standard error of the mean. This assay was repeated twice and a representative example is shown.

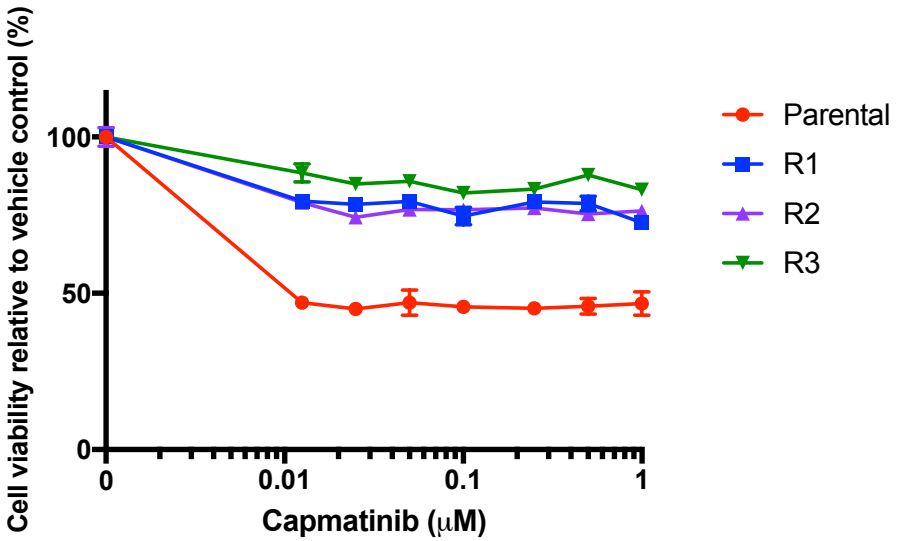

Figure 7.2 Cell viability of parental RT112 and resistant derivatives in capmatinib (MET TKI) + 1μM PD173074. Viability of cells was assayed using CellTiter-Blue following 120 h treatment with a range of capmatinib concentrations + 1μM PD173074 and normalised to vehicle control. Error bars show standard error of the mean; error bars are absent where the error was too small to plot. This assay was repeated twice and a representative example is shown.

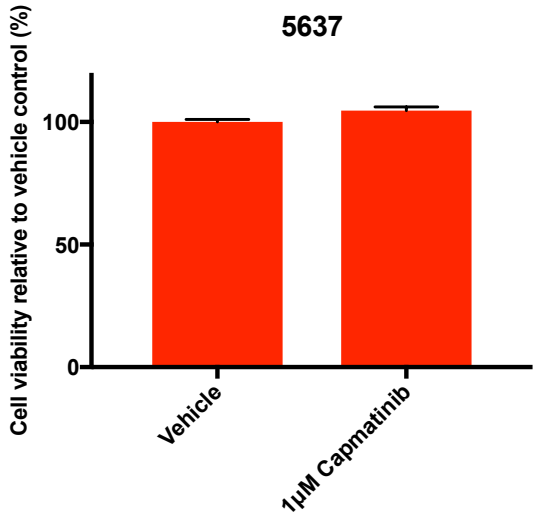

Figure 7.3 Cell viability of 5637 in capmatinib (MET TKI). Viability of cells was assayed using CellTiter-Blue following 120 h treatment with capmatinib and normalised to vehicle control. Error bars show standard error of the mean. This assay was conducted only once.

To determine if ERBB3 activation, or activation of an alternative EGFR family member, was contributing to the resistant phenotype of the RT112 resistant derivatives, cell viability was tested in RT112 parental and resistant derivatives when treated with sapitinib. Sapitinib is a reversible ATP-competitive TKI with specificity for EGFR, ERBB2 and ERBB3. A cell-free assay found sapitinib inhibited EGFR and ERBB2 with IC50s of 0.012 and 0.014μM respectively. No activity was observed at concentrations up to 10μM for other RTKs which were not members of the EGFR family. Sapitinib inhibited EGFR phosphorylation with an IC50 of 4nM in the buccal carcinoma cell line KB (Hickinson *et al.*, 2010). Sapitinib inhibited ERBB2 and ERBB3 phosphorylation in the breast adenocarcinoma cell line MCF7 with IC50s of 3 and 4nM respectively (Hickinson *et al.*, 2010). Sapitinib has been assessed in phase I and II clinical trials with breast cancer patients with limited success (Johnston *et al.*, 2016; Kurata *et al.*, 2014).

Single agent treatment with sapitinib did not appreciably reduce cell viability in RT112 parental or the resistant derivatives (Fig. 7.4). The combination of sapitinib and PD reduced the cell viability of the RT112 resistant derivatives to 50-60% of the vehicle control and viability in parental RT112 was reduced to approximately 20% (Fig. 7.5). It was observed in Chapter 3 that single agent treatment with PD reduced the viability of RT112 parental to 33%, R1 to 53%, R2 to 67% and R3 to 90% of the vehicle control (Fig. 3.8). Hence the combination of

sapitinib and PD was not effective in overcoming the resistance to PD in the RT112 resistant lines.

To confirm that the batch of sapitinib used to treat the RT112 parental and resistant lines was successfully inhibiting its target RTKs, it was decided to assay a cell line as a positive control for sensitivity to EGFR family inhibition. The urothelial carcinoma cell line DSH1, which expresses high levels of ERBB2 and is sensitive to ERBB2 inhibition, was selected as a positive control (de Martino *et al.*, 2014) (Fig. 7.6). The cell viability of DSH1 cultured in 1μM sapitinib was 34% of the vehicle control. As DSH1 was sensitive to sapitinib we can conclude that the sapitinib was inhibiting EGFR family members in the viability assays conducted with RT112 resistant derivatives. Therefore, these resistant derivatives displayed resistance to inhibition of the EGFR family.

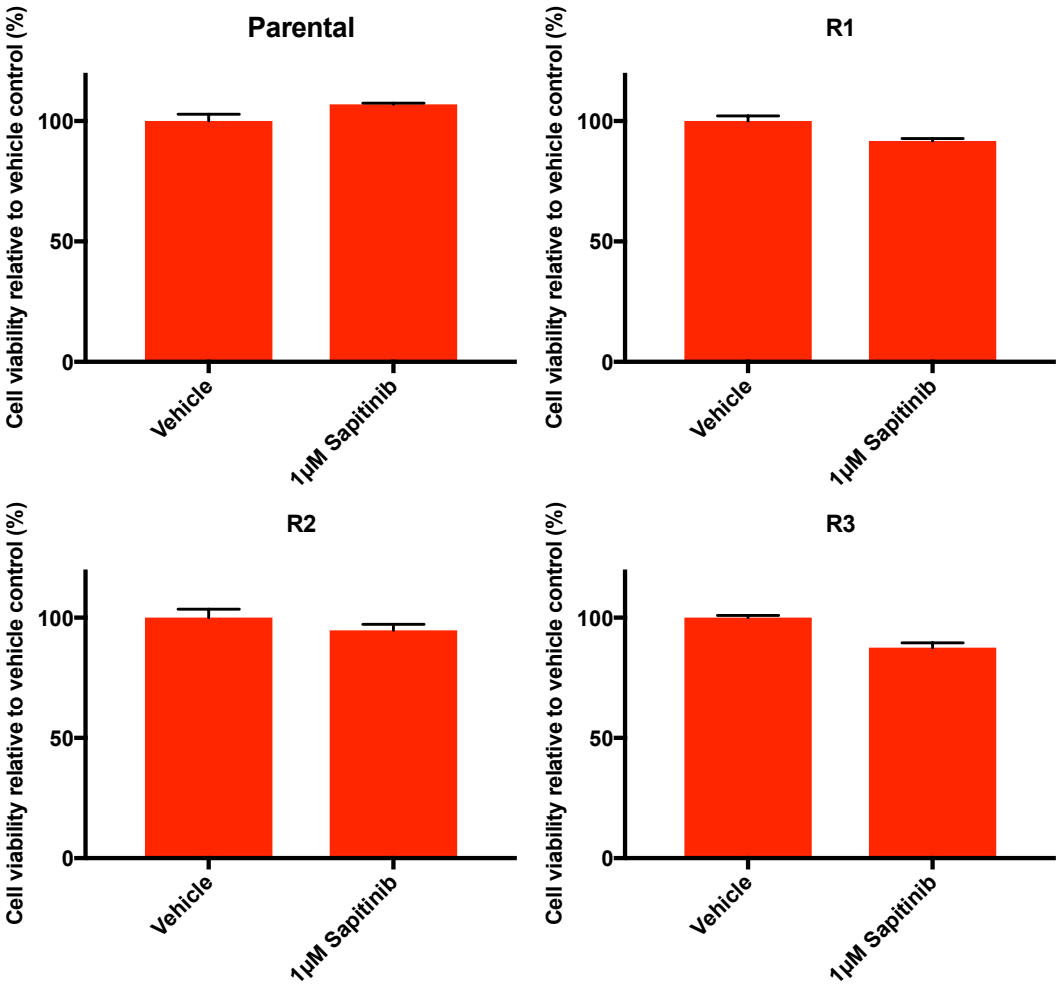

Figure 7.4 Cell viability of parental RT112 and resistant derivatives in sapitinib (EGFR, ERBB2 and ERBB3 TKI). Viability of cells was assayed using CellTiter-Blue following 120 h treatment with sapitinib and normalised to vehicle control. Error bars show the standard error of the mean. This assay was repeated twice and a representative example is shown.

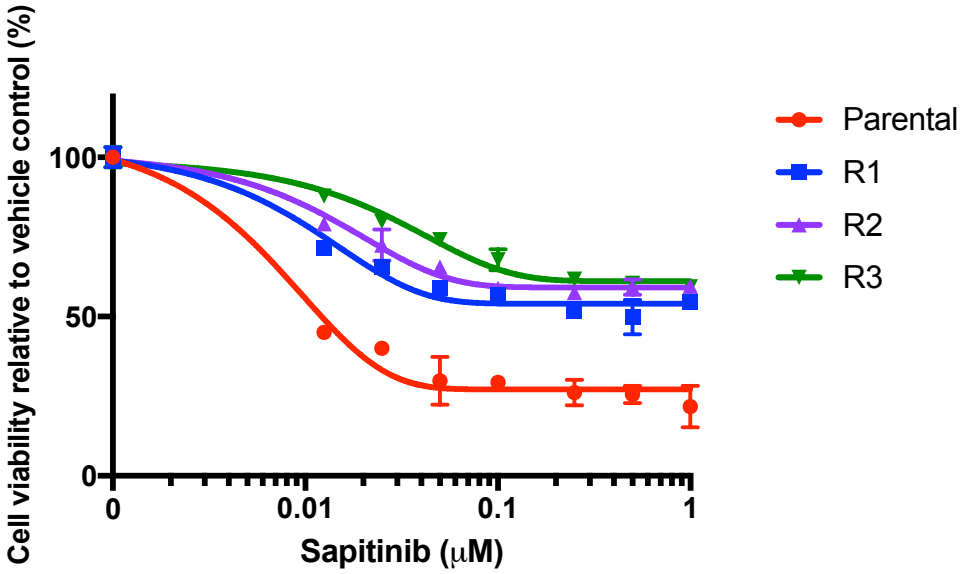

Figure 7.5 Cell viability of parental RT112 and resistant derivatives in sapitinib (EGFR, ERBB2 and ERBB3 TKI) + 1μM PD173074. Viability of cells was assayed using CellTiter-Blue following 120 h treatment with a range of sapitinib concentrations + 1μM PD. Cell viability was normalised to vehicle control. Error bars show the standard error of the mean; error bars are absent where the error was too small to plot. Sigmoidal dose response curves were plotted in GraphPad Prism®. This assay was repeated twice and a representative example is shown.

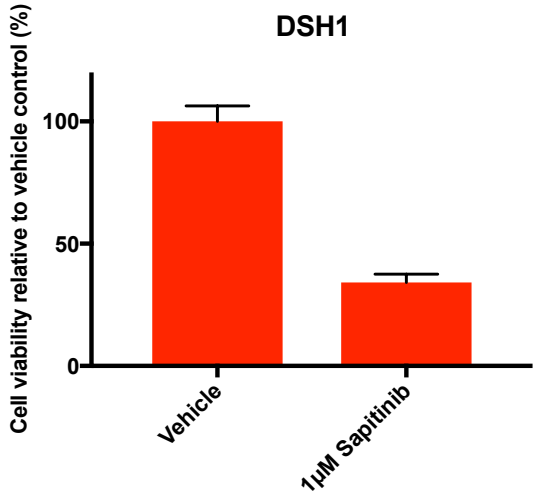

Figure 7.6 Cell viability of DSH1 in sapitinib (EGFR, ERBB2 and ERBB3 TKI). Viability of cells was assayed using CellTiter-Blue following 120 h treatment with 1μM sapitinib and normalised to vehicle control. Error bars show standard error of the mean. This assay was conducted only once.

7.2.3 Cell viability assays with RT112 and the IGF1R TKI linsitinib

Transcriptome analysis showed that *IGF1R* expression was upregulated in RT112 R1 and R2 (Chapter 6, Fig. 6.51). Linsitinib is a small-molecule ATP-competitive kinase inhibitor developed to inhibit IGF1R. A cell-free assay found that linsitinib inhibited IGF1R, the insulin receptor (IR) and insulin receptor-related protein (INSRR) with IC50s of 0.035, 0.075 and 0.075μM respectively but that concentrations greater than 10μM were required to inhibit other RTKs (Mulvihill *et al.*, 2009). Linsitinib has been assessed in clinical trials: for example, a phase III clinical trial was conducted with patients with locally advanced or metastatic adrenocortical carcinoma but was not found to increase patient survival (Fassnacht *et al.*, 2015).

To examine whether signalling via upregulated IGF1R might be inducing resistance to PD, sensitivity to linsitinib was assayed in RT112 parental and RT112 resistant derivatives (Fig. 7.7). The IC50s of linsitinib in RT112 parental, R1, R2 and R3 were 0.8, 0.4, 0.9 and 3.3μM respectively. This indicated that all lines were sensitive to linsitinib. The sensitivity of RT112 parental to linsitinib was unexpected as this cell line is able to signal via FGFR3 to promote cell growth and survival. It was also surprising that RT112 R3 was sensitive to linsitinib as it was hypothesised that the *HRAS* mutation in this line would enable constitutive activation of cell proliferation and cell survival. However, the IC50 values indicated that RT112 R3 was less sensitive to linsitinib than RT112 parental, R1 or R2.

RT112 parental and RT112 R1 were then assayed for their sensitivity to linsitinib in combination with 1μM PD (Fig. 7.8). RT112 parental and R1 treated with a range of linsitinib concentrations in combination with 1μM PD, had IC50s of 0.11μM and 0.34μM respectively. Therefore, in RT112 parental inhibition of IGF1R with linsitinib was more efficacious in combination with FGFR inhibition than treatment with either PD or linsitinib alone. In contrast, in RT112 R1, inhibition of IGF1R with linsitinib was not more efficacious in combination with FGFR inhibition than as a single agent.

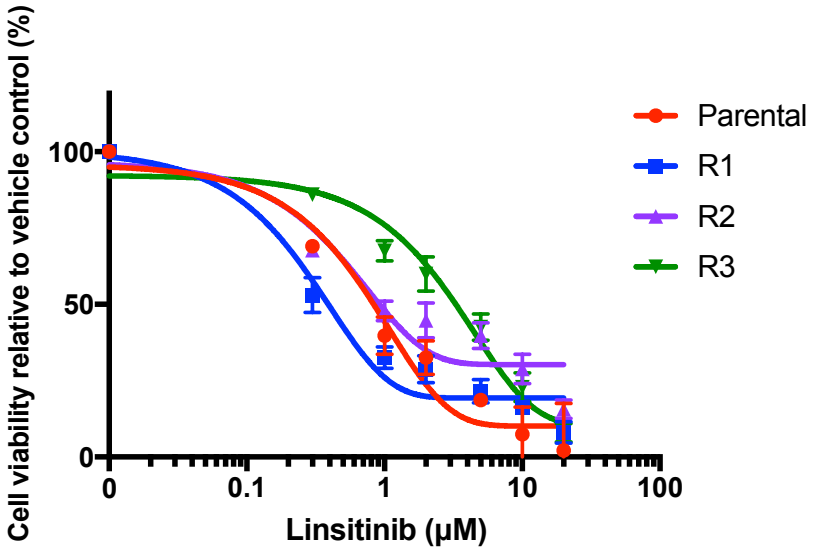

Figure 7.7 Cell viability of parental RT112 and RT112 resistant lines in linsitinib (IGF1R TKI). Viability of cells was assayed using CellTiter-Blue following 120 h treatment with a range of linsitinib concentrations and normalised to vehicle control. Error bars show standard error of the mean; error bars are absent where the error was too small to plot. Sigmoidal dose response curves were plotted in GraphPad Prism®. This assay was repeated twice and a representative example is shown.

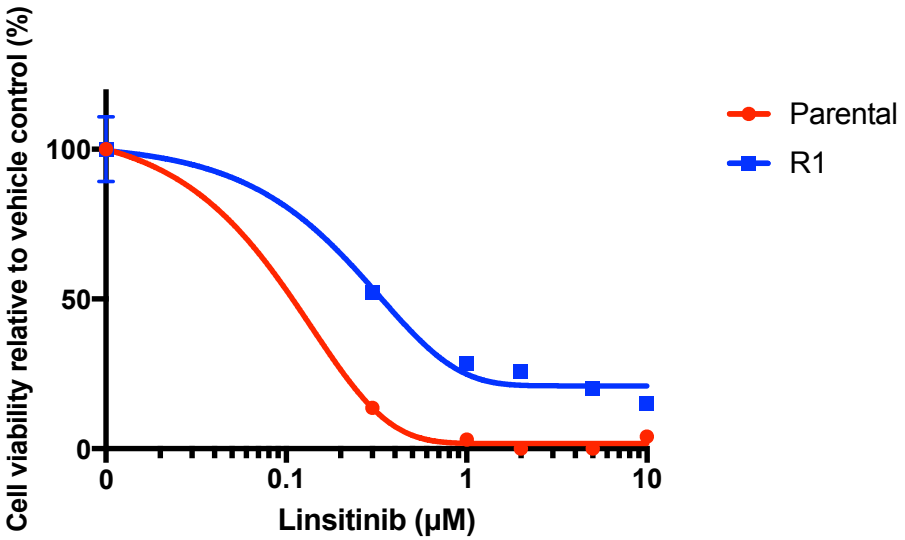

Figure 7.8 Cell viability of parental RT112 and RT112 R1 in linsitinib (IGF1R TKI) + 1μM PD173074. Viability of cells was assayed using CellTiter-Blue following 120 h treatment with a range of linsitinib concentrations + 1μM PD and normalised to vehicle control. Error bars show standard error of the mean; error bars are absent where the error was too small to plot. Sigmoidal dose response curves were plotted in GraphPad Prism®. This assay was repeated twice and a representative example is shown.

7.2.4 Cell viability assays with RT4 and the EGFR TKI erlotinib

Transcriptome analysis identified that expression of *EGFR* RNA was significantly increased in RT4 R1 cultured with and without PD compared to RT4 parental (Chapter 6, Fig. 6.52). Immunoblot analysis confirmed that both phospho-EGFR and total EGFR expression were increased in RT4 R1 compared to parental RT4 (Chapter 4, Fig. 4.5). Erlotinib is an ATP-competitive inhibitor with selectivity for EGFR (Moyer *et al.*, 1997). Moyer *et al.* examined the selectivity of erlotinib on purified RTKs and found that erlotinib inhibited EGFR with an IC50 of 2nM and exhibited over 1000-fold greater selectivity for EGFR than for the other kinases examined: SRC and ABL. Immunoblot analysis and densitometry showed that erlotinib inhibited the phosphorylation of EGFR following treatment with EGF in the head and neck squamous cell carcinoma cell line HN5 with an IC50 of 20nM (Moyer *et al.*, 1997). Erlotinib inhibited the proliferation of the colorectal carcinoma cell line DiFi with an IC50 of 100nM in an 8 day proliferation assay (Moyer *et al.*, 1997). Erlotinib is approved for treatment of NSCLC and pancreatic cancer (Mosquera *et al.*, 2016; Singh and Jadhav, 2017). To determine if activation of EGFR was mediating resistance to PD in RT4 R1, RT4 parental and RT4 R1 were assayed for their sensitivity to erlotinib (Fig. 7.9). RT4 parental had an IC50 of 6.1μM and RT4 R1 had an IC50 of 10μM. Erlotinib reduced viability in RT4 parental and RT4 R1 to approximately 15% and 20% of the vehicle control respectively. RT4 parental and RT4 R1 were then assayed for their sensitivity to erlotinib in combination with 1μM PD (Fig. 7.10). In combination with 1μM PD RT4 parental had an IC50 of 0.07μM and RT4 R1 had an IC50 of 0.37μM and viability was reduced in RT4 parental and RT4 R1 to approximately 15% and 6% of the vehicle control respectively. Therefore, simultaneous inhibition of the FGFRs and EGFR reduced cell viability in RT4 parental and RT4 R1 with greater efficacy than single agent treatment with erlotinib.

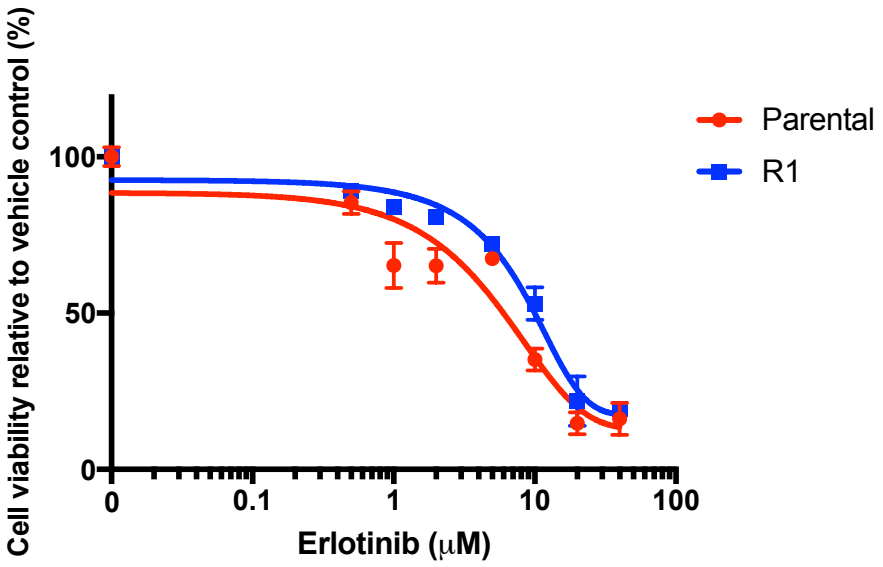

Figure 7.9 Cell viability of parental RT4 and R1 in erlotinib (EGFR TKI). Viability of cells was assayed using CellTiter-Blue following 120 h treatment with a range of erlotinib concentrations and normalised to vehicle control. Error bars show the standard error of the mean; error bars are absent where the error was too small to plot. Sigmoidal dose response curves were plotted in GraphPad Prism®. This assay was repeated twice and a representative example is shown.

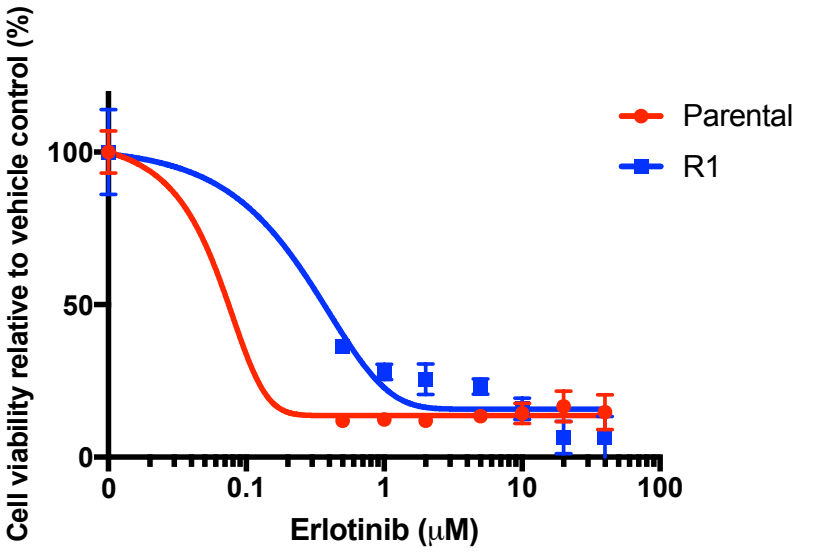

Figure 7.10 Cell viability of parental RT4 and R1 in erlotinib (EGFR TKI) + 1μM PD173074. Viability of cells was assayed using CellTiter-Blue following 120 h treatment with a range of erlotinib concentrations + 1μM PD173074 and normalised to vehicle control. Error bars show standard error of the mean; error bars are absent where the error was too small to plot. Sigmoidal dose response curves were plotted in GraphPad Prism®. This assay was repeated twice and a representative example is shown.

7.3 Discussion

It has been reported that the addition of HGF, which binds and upregulates MET, was able to rescue cell growth in RT112 treated with the FGFR TKI BGJ398 (Harbinski *et al.*, 2012). Additionally, immunoblot analysis in Chapter 4 showed that phospho-MET was expressed in RT112 R1, R2 and R3 cultured in PD (Fig. 4.11). It was therefore thought that MET could be mediating resistance to PD in the RT112 resistant derivatives. However, the resistant lines were not sensitive to treatment with the MET inhibitor capmatinib. It was hoped that treatment of 5637, which expresses phospho-MET, with capmatinib would demonstrate that the capmatinib used in the cell viability assays was successfully inhibiting MET and was not defective. Cell viability was not reduced in 5637 upon treatment with capmatinib. There was insufficient time to conduct immunoblot analysis to determine if capmatinib was inhibiting phosphorylation of MET in 5637 or the RT112 resistant derivatives. As we did not demonstrate that capmatinib was capable of reducing cell viability in a MET-dependent cell line or reducing MET phosphorylation it is possible that our batch of capmatinib was defective.

There are a number of other explanations which could explain the insensitivity of 5637 to capmatinib. It is possible that 5637 is not sensitive to MET inhibition under the conditions used in the viability assay. Previous research such as that conducted by Shintani *et al.* has examined the effect of stimulating MET signalling in 5637 via treatment with HGF, whereas the 5637 in this study 5637 was not cultured with exogenous HGF (Shintani *et al.*, 2017). It may be that exogenous HGF is required to induce cell proliferation mediated by MET in 5637. Therefore, as the 5637 cell viability assay was conducted in the absence of HGF this may be the reason that capmatinib did not reduce cell viability. It has been reported that HGF induced invasion in 5637 but cell proliferation was not examined (Wang *et al.*, 2007). Therefore, it is possible that signalling via MET in 5637 may induce invasion but not affect cell proliferation. An alternative explanation for the insensitivity of 5637 to capmatinib is that 5637 may express an ATP-binding cassette transporter such as P-glycoprotein which can induce drug resistance by transporting TKIs out of cancer cells (He and Wei, 2012). It was considered that 5637 may possess a gatekeeper mutation in MET which renders the line resistant to capmatinib. However, the exome of 5637 was previously sequenced by Nickerson *et al.* and a mutation in *MET* was not detected (Nickerson *et al.*, 2017). Finally, it is possible that MET could be promoting cell proliferation and survival in 5637 via crosstalk with another receptor, and when MET is inhibited activation of the other receptor

compensates for the reduced MET activity. Therefore, whether capmatinib was defective or RT112 parental and the resistant derivatives were resistant to MET inhibition not was not confirmed. Immunoblot analysis to examine whether capmatinib inhibited MET phosphorylation in the RT112 resistant derivatives or 5637 would have clarified this.

Cell viability was examined in RT112 parental and R1 for the combined treatment of the IGF1R inhibitor linsitinib and PD and for each drug as a single agent. RT112 parental was sensitive to linsitinib single agent treatment. This suggests that IGF1R signalling is active in RT112 parental cells rather than being activated as a mechanism of acquired resistance in the resistant derivatives. The RT112 resistant derivatives also displayed sensitivity to the IGF1R TKI linsitinib. In RT112 parental a greater sensitivity was displayed to the combination of linsitinib and PD than to either drug as a single agent. This suggests that if either FGFR3 or IGF1R is inhibited in parental RT112, signalling via the other receptor maintains some cell viability.

IGF1R has been implicated in resistance to inhibition of EGFR in NSCLC, ERBB2 in breast cancer and BRAF in melanoma (Harris *et al.*, 2007; Huang and Fu, 2015; Peled *et al.*, 2013; Villanueva *et al.*, 2010). Targeted agents specific for IGF1R are under clinical development. IGF1R expression has been associated with higher stage and grade in colorectal cancer and IGF1R targeted agents have been assessed in clinical trials for the treatment of this cancer (Hakam *et al.*, 1999; Shali *et al.*, 2016). A phase II/III clinical trial tested addition of the monoclonal antibody dalotuzumab specific for IGF1R to the standard treatment of irinotecan and cetuximab in metastatic colorectal cancer patients but found no increase in survival (Sclafani *et al.*, 2015). A phase III clinical trials in patients with non-adenocarcinoma NSCLC with the monoclonal antibody figitumumab, which inhibits IGF1R, indicated that the addition of this monoclonal antibody to treatment with chemotherapy or erlotinib did not increase patient survival (Langer *et al.*, 2014; Scagliotti *et al.*, 2015). The results in this Chapter suggest that single agent treatment with an inhibitor of IGF1R could overcome resistance to FGFR-targeted agents in some bladder cancers.

Single agent sapitinib had very little effect on the viability of RT112 resistant derivatives. The combination of sapitinib and PD did have some efficacy in RT112 parental and resistant derivatives but not enough to determine an IC50 in these lines. This suggests that ERBB family signalling is activated and does contribute to

cell proliferation or survival in RT112 parental and the RT112 resistant derivatives when these lines are cultured in PD.

The reduced cell viability in RT112 R3 was unexpected as exome sequencing and single cell cloning in Chapter 5 revealed that a *HRAS* G12S mutation was present in 73% of RT112 R3 cells. As *HRAS* is downstream of RTKs, it was thought that this mutation would constitutively promote cell proliferation and survival in RT112 R3 despite FGFR3 and EGFR family inhibition. It is unclear whether EGFR family signalling contributes to the cell proliferation or survival of all or only a subset of the RT112 parental and RT112 resistant derivative cells. It may be that the combinatorial treatment of sapitinib and PD primarily reduces the cell viability of RT112 R3 due to efficacy in the subpopulation of RT112 R3 cells which do not possess the *HRAS* G12S mutation.

It was considered that only a small reduction in cell viability observed in RT112 parental and resistant derivatives could be due to the batch of sapitinib being less active. For this reason the efficacy of the sapitinib was assessed in DSH1, which has been previously reported to be sensitive to the TKI lapatinib which exhibits specificity for EGFR and ERBB2 (de Martino *et al.*, 2014). DSH1 was found to be sensitive to single agent treatment with sapitinib. Therefore, it can be concluded that inhibition of the EGFR family of RTKs did not overcome PD resistance in the RT112 resistant lines.

Wang *et al.* generated RT112 derivatives resistant to FGFR inhibition via long term culture with the FGFR TKIs BGJ398 and ponatinib. These resistant derivatives had become resistant via activation of ERBB2 and ERBB3 (Wang *et al.*, 2014). Single agent treatment with sapitinib reduced the viability of the BGJ398 resistant derivatives to approximately 70% of the untreated control. They reported that treatment with sapitinib in combination with the FGFR TKI BGJ398 reduced cell viability to 20-30% of the untreated control in these resistant derivatives (Wang *et al.*, 2014). It can be concluded that the RT112 PD resistant derivatives in this study have become resistant to FGFR inhibition by a different mechanism than the mechanism observed by Wang *et al.* in their RT112 resistant derivatives.

IGF1R has been reported to heterodimerise with EGFR family members inducing resistance to EGFR family targeted agents. Morgillo *et al.* produced an EGFR TKI resistant derivative of the NSCLC cell line H460 via long term culture in erlotinib. Immunoblot analysis showed that this resistant line had increased expression of phospho-IGF1R compared to parental line. Coimmunoprecipitation showed that there was an increased binding of EGFR to IGF1R in the H460

erlotinib-resistant derivative, and in parental H460 acutely treated with erlotinib compared to the parental line cultured without erlotinib. Treatment with erlotinib and the IGF1R inhibitor AG1024 reduced colony formation in both parental H460 and the H460 erlotinib-resistant derivative to a greater extent than treatment with either drug as a single agent (Morgillo *et al.*, 2006). Nahta *et al.* produced trastuzumab resistant cells from the breast cancer cell line SKBR3 via long-term culture of the parental line in trastuzumab. These resistant cells had increased expression of phospho-IGF1R and coimmunoprecipitation of ERBB2 and IGF1R was observed in the resistant cells but not the parental line. Stimulation of the resistant cells with the IGF1R ligand IGF1 induced ERBB2 phosphorylation in the resistant cells but not parental SKBR3 (Nahta *et al.*, 2005). IGF1R has also been reported to interact with ERBB3 and ERBB4 in gefitinib-resistant cells derived from breast cancer cell line MCF-7 (Jones *et al.*, 2006). It is possible that IGF1R is heterodimerizing with EGFR family members in the RT112 parental and RT112 resistant derivatives and that this induces some sensitivity to the combination of sapitinib and PD.

Sensitivity to erlotinib was tested in RT4 parental and R1 as an increase in total and phosphorylated EGFR in RT4 R1 was observed via immunoblot analysis in Chapter 4. Additionally, microarray analysis showed an increase in *EGFR* mRNA in RT4 R1 compared to the parental line. Both these lines exhibited sensitivity to erlotinib which confirms that both RT4 parental and R1 are dependent on EGFR signalling. The inhibition of EGFR by erlotinib in parental RT4 and RT4 R1 could be confirmed by immunoblot analysis. The efficacy of erlotinib was potentiated by the addition of PD. This suggests that targeting the FGFR family and EGFR in combination could be an effective treatment for urothelial carcinoma. Signalling via EGFR has previously been implicated in resistance to FGFR-targeted agents in bladder cancer cell lines. An siRNA screen which identified EGFR as limiting the sensitivity to PD in three bladder cancer cell lines with mutant FGFR3, RT4, RT112 and MGH-U3 (Herrera-Abreu *et al.*, 2013). RT112 and 639V, a bladder cancer cell line with an *FGFR3* point mutation, showed increased phosphorylation of EGFR upon acute treatment with PD. A RT112 xenograft mouse model showed that treatment with PD and gefitinib reduced tumour volume to a greater extent than either of the drugs given separately (Herrera-Abreu *et al.*, 2013).

EGFR-targeted agents are already in use as treatments for treat lung and pancreatic and colorectal cancer (Lubner *et al.*, 2017; Mosquera *et al.*, 2016; Singh and Jadhav, 2017). EGFR-targeted agents may be efficacious in a subset of urothelial carcinoma patients who have relapsed on FGFR-targeted therapy. Approximately 60% of bladder cancer tumours express membranous EGFR and

expression does not correlate with the stage or grade of tumours (Ibrahim *et al.*, 2009). Approximately 6% of MIBC tumours exhibit gain of copy number of 7p11.2 which contains *EGFR* (Robertson *et al.*, 2017). TKIs targeting the EGFR family have entered clinical trials in urothelial carcinomas with EGFR or ERBB2 overexpression and have generally been found not to significantly benefit patients (Choudhury *et al.*, 2016; Miller *et al.*, 2016; Petrylak *et al.*, 2010; Powles *et al.*, 2017). It may be that combinatorial treatment with an EGFR and an FGFR family inhibitor would be beneficial in those patients who have *FGFR3* alterations.

The results of this Chapter have some limitations. There was large variability between individual cell viability assays, therefore, it would have been beneficial to have assayed the resistant lines for their sensitivity to PD as a single agent, as a control, at the same time as examining the sensitivity of the resistant lines to the combinatorial treatment of each small-molecule inhibitor + PD. This would have enabled a direct comparison of the efficacy of single agent PD and with the efficacy of each drug combination. Additionally, for each cell viability experiment it would have been more reliable to have presented the average of the cell viability assay repeats, rather than presenting one representative example. This would have enabled a statistical test to have been conducted to determine whether observed differences in viability were significant.

Chapter 8
Final Discussion

This project was conducted with the aim of examining the differences between the RT112 and RT4 resistant derivatives and their parental lines. It was hoped that examining these differences would identify the mechanisms by which the resistant derivatives have acquired reduced sensitivity to FGFR inhibition. The identification of these mechanisms would allow drugs to be tested for their ability to re-sensitize the resistant cells to FGFR inhibition.

Initial characterisation of the resistant lines identified that RT112 R1, RT112 R2 and RT4 R1 had a different morphology to their parental lines but that these changes in morphology were reversed upon culture without PD. RT112 resistant derivatives maintained resistance to PD following culture without PD and phenotypic reversion, whereas RT4 R1 did not. Reduced expression of FGFR3 was observed in the RT112 resistant derivatives indicating that FGFR3 overexpression or mutation or drug efflux is not the cause of resistance in these cells. Increased expression of N-cadherin was observed in RT112 R1 and R2 cultured in PD, suggesting these cells may have undergone an EMT. Following the initial characterisation of the parental and resistant cells, expression and phosphorylation of a number of RTKs was examined with immunoblot analysis. This identified increased expression of phospho-MET in the RT112 resistant derivatives, phospho-ERBB3 in RT112 R1 and R2 and phospho-EGFR in RT4 R1. Exome sequencing identified a *HRAS* G12S mutation in RT112 R3. Retroviral transfection of *HRAS* G12V into parental RT112 demonstrated that gain of constitutively active *HRAS* induces resistance to PD. Copy number analysis showed that *EGFR* was not amplified in RT4 R1 and a NGS assay which screens for common *EGFR* mutations did not identify an *EGFR* mutation in this line. Transcriptome analysis identified EMT-associated gene expression changes in the RT112 resistant derivatives compared to parental RT112 and identified a reduction in expression of genes which regulate fatty acid synthesis in RT112 and RT4 resistant derivatives. Immunoblot analysis confirmed reduced expression of mature SREBP1, a transcription factor which regulates the synthesis of unsaturated fatty acids, and SCD1, the rate limiting enzyme in the production of monounsaturated fatty acids, in RT112 resistant derivatives. Additionally, transcriptome analysis identified an

increase in expression of *IGF1R* in RT112 R1 and R2 and increase in expression of *KDM6A* in RT112 and RT4 resistant derivatives. Finally, a range of TKIs were tested for their efficacy at reducing the viability of resistant cells. The IGF1R TKI linsitinib and the EGFR TKI erlotinib proved effective at reducing viability in RT112 and RT4 resistant lines respectively.

A key finding of this project was the identification of the *HRAS* G12S mutation in RT112 R3 and the confirmation that the introduction of mutant *HRAS* into RT112 parental induces resistance to PD. This suggests that mutation of *HRAS* may occur in urothelial carcinoma patients as a mechanism of acquired resistance to FGFR-targeted agents. *RAS* and *FGFR3* mutations are mutually exclusive in urothelial carcinoma (Jebar *et al*., 2005). This suggests that these mutations have a similar function and therefore there is no selective pressure for a urothelial carcinoma to gain activating mutations in both these genes. It appears that the inhibition of FGFR3 induces a selective pressure to gain a mutation of similar functionality. RAS activates the MAP kinase and PI3 kinase pathways: two pathways also activated by FGFR3 (Klint *et al*., 1999; Rodriguez-Viciana *et al*., 1994; van Weering *et al*., 1998; Zhang *et al*., 1993). As activation of both these pathways was reduced in RT112 parental acutely treated with PD but not in RT112 resistant derivatives, the reactivation of these pathways may be key to inducing resistance to PD.

Despite decades of research, development of direct inhibitors of RAS has proved difficult due to RAS lacking deep hydrophobic binding pockets to which small molecule inhibitors could bind and the low affinity of RAS for GTP (Spencer-Smith and O'Bryan, 2017). Attempts to inhibit RAS with small molecule inhibitors have included inducing GTP hydrolysis with a GTP analogue which is more effectively hydrolysed by the mutant RAS than GTP (Ahmadian *et al*., 1999). Another possible way to directly inhibit RAS may be by inhibiting the interaction of RAS with guanine exchange factors. For example, Patgiri *et al*. developed a mimetic of the guanine exchange factor SOS which reduced the interaction of GDP-bound mutant RAS with SOS, thereby preventing the mutant RAS from binding GTP and reducing the activation of downstream signalling (Patgiri *et al*., 2011). Monoclonal antibodies have been developed which directly inhibit RAS, although full size antibodies cannot cross the plasma membrane to target intracellular molecules (Furth *et al*., 1982). A monoclonal antibody, RT11, has been developed which was able to enter the cytosol via clathrin-mediated endocytosis and bind to the protein-protein interface of the active GTP-bound form of *RAS.* This inhibited downstream signalling. Upon further engineering of RT11 so that it could bind

tumour-associated integrins, this antibody was able to inhibit the growth of RAS mutant xenografts in mice (Choi et al., 2014a; Shin et al., 2017). An alternative approach taken to reduce the activity of mutant RAS is by reducing the presence of RAS at the cell membrane. This can be achieved with farnesyltransferase and PDEδ inhibitors. Farnesyltransferase inhibitors disrupt the post-translational modifications of RAS which results in reduced RAS localisation at the cell membrane (Choy *et al*., 1999; Reiss *et al*., 1990). PDEδ inhibitors inhibit the binding of PDEδ to KRAS, reducing the trafficking of KRAS to the cell membrane (Zimmermann *et al*., 2013).

The development of inhibitors specific for molecules downstream of RAS has been more successful than direct RAS inhibition. MEK is a kinase in the MAP kinase pathway. The MEK inhibitor trametinib is approved by the EMA and FDA for the treatment of V600 mutant melanoma and NSCLC and cobimetinib is approved for the treatment of BRAF V600 mutant melanoma (Cheng and Tian, 2017). Inhibition of MEK has so far been unsuccessful as a mechanism of treating KRAS mutant colorectal cancer (Bahrami *et al*., 2018). A number of ongoing phase I and II trials are examining the efficacy of MEK inhibitors in combination with chemotherapy or other targeted agents, including PI3 kinase inhibitors, in KRAS mutant NSCLC (Tomasini *et al*., 2016). Bockorny *et al*. reported that the long-term culture of the *FGFR1*-amplified NSCLC cell line, NCI-H2077, produced a resistant derivative with an *NRAS* Q61R mutation. Treatment of the resistant cells with the pan-FGFR TKI BGJ398 and the MEK inhibitor trametinib reduced cell proliferation to a greater extent than treatment with BGJ398 as a single agent. It was observed that the combination of BGJ398 and trametinib was well tolerated, significantly slowed tumour progression and increased progression-free survival in a mouse NCI-H2077 xenograft model (Bockorny *et al*., 2018). Treatment with a MEK inhibitor such as trametinib may overcome the resistance to PD observed in RT112 R3 and could overcome resistance to FGFR inhibitors in urothelial carcinomas if they had gained mutations in the MAP kinase pathway. Examination of whether MEK inhibition would overcome PD resistance in RT112 R3 was not conducted due to time limitations.

Inhibition of EGFR with erlotinib overcame resistance to PD in RT4 R1. However, erlotinib was more effective in parental RT4 than RT4 R1 suggesting that EGFR inhibition may be more effective as a first line rather than second line treatment. Treatment of RT4 R1 with the combination of erlotinib and PD reduced cell viability to a greater extent than either TKI alone. Isobologram analysis would have determined if treatment with erlotinib and PD was additive in RT4 parental and

R1 but was not conducted due to time limitations. Herrera-Abreu *et al*. reported that activation of EGFR was a mechanism of short term survival in response to PD in RT112 that could be overcome by combined treatment with PD and the small molecule inhibitor of EGFR, gefitinib. Immunoblot analysis revealed that treatment with the MEK inhibitor CI-1040 induced an increase in EGFR phosphorylation and that PD treatment induced EGFR accumulation at the cell membrane and giant early endosomes. The mechanism by which expression of EGFR and phospho-EGFR was increased in RT4 R1 is unknown. Small molecule inhibitors and monoclonal antibodies which inhibit EGFR are approved for the treatment of lung, pancreatic and colorectal cancer (Lubner *et al*., 2017; Mosquera *et al*., 2016; Singh and Jadhav, 2017).

In addition to signalling as a homodimer, EGFR heterodimerises with other EGFR family members (Roskoski, 2014), therefore it is possible that other EGFR family members are implicated in the resistance to PD in RT4 R1. Wang *et al*. found RT112 activated ERBB2 and ERBB3 signalling as a mechanism of resistance to the FGFR TKIs BGJ398 and ponatinib upon long-term culture in these inhibitors (Wang *et al*., 2014). Canfield *et al*. showed that knockdown of *ERBB4* induced apoptosis in ERBB2-positive breast cancer cell lines with acquired resistance to the EGFR, ERBB2 and ERBB3 TKI lapatinib and the ERBB2-specific monoclonal antibody trastuzumab (Canfield *et al.*, 2015). Immunoblot analysis showed that expression of phospho-ERBB2 remained low in RT4 R1, whereas, phospho-ERBB3 expression was increased in RT4 R1. Immunoblot analysis of total ERBB4 and phospho-ERBB4 expression was not conducted with RT4 parental or R1 due to time limitations. Microarray analysis showed that expression of *ERBB4* was non-significantly increased in RT4 R1 + PD compared to parental no PD. It is possible that activation of ERBB3 or ERBB4 contributes to the RT4 R1 resistant phenotype via dimerisation with EGFR. Whether this is the case could be tested by examining whether knockdown of *ERBB3* or *ERBB4* expression or treatment with an ERBB3- or ERBB4-specific inhibitor re-sensitised RT4 R1 to PD.

Microarray analysis showed that expression of *AREG* and *BTC*, which encode the EGFR ligands amphiregulin and betacellulin respectively, was significantly increased in RT4 R1 + PD compared to parental no PD. Therefore, the increased activation of EGFR in RT4 R1 may be mediated by the increased expression of these ligands. Whether protein expression of amphiregulin and betacellulin was increased in RT4 R1 could have been examined with immunoblot analysis. Whether these ligands mediate PD resistance could be determined by examining whether knockdown of *AREG* or *BTC* expression re-sensitised RT4 R1

to PD. Additionally, whether treatment with amphiregulin or betacellulin induced resistance to PD in parental RT4 could be examined. These experiments were not conducted due to time limitations.

Urothelial carcinomas with expression or mutation of EGFR, ERBB2 or ERBB3 could be intrinsically resistant to FGFR-targeted agents as they may be able to signal via these EGFR family members. The sensitivity of urothelial carcinomas to EGFR-targeted agents has been assessed in clinical trials but unfortunately these have mainly been disappointing. A phase II clinical trial conducted by Pruthi *et al.* examined erlotinib as a neoadjuvant prior to radical cystectomy. Erlotinib was well tolerated and the results indicated that erlotinib may be efficacious as a single agent (Pruthi *et al*., 2010). A phase II clinical trial with gefitinib in metastatic urothelial carcinoma patients who had failed previous chemotherapy concluded that further study with this TKI in this setting was not justified (Petrylak *et al*., 2010). Another phase II clinical trial showed that the addition of gefitinib to treatment with chemotherapy did not significantly increase time to progression, the primary endpoint, in patients with advanced or metastatic urothelial carcinoma (Miller *et al*., 2016). Choudhury *et al.* conducted a phase II study in platinum-refractory metastatic urothelial carcinoma patients with the EGFR and ERBB2 TKI afatinib. They observed that treatment with afatinib showed significant activity in patients with *ERBB2* amplification and *ERBB3* mutations but *EGFR* amplification was not indicative of a response to afatinib (Choudhury *et al*., 2016). Powles *et al.* conducted a phase III clinical trial which found that treatment with the EGFR and ERBB2 TKI lapatinib following on from chemotherapy did not significantly improve outcomes in urothelial carcinoma patients with EGFR or ERBB2 overexpression (Powles *et al*., 2017). The findings in this project and the research conducted by Herrera-Abreu *et al*. indicate that EGFR-targeted agents may benefit urothelial carcinoma patients with resistance to FGFR-targeted agents. To my knowledge, clinical trials have not been conducted in urothelial carcinoma patients whose tumours are *FGFR3* mutant or overexpress FGFR3 with the combination of EGFR- and FGFR-targeted agents. Similarly, the efficacy of EGFR-targeted agents has not been assessed in urothelial carcinoma patients who have acquired resistance to FGFR-targeted agents. Whether the combination of FGFR and EGFR-targeted agents would be tolerated in patients with urothelial carcinoma is unknown.

Microarray analysis showed that *EPHA3* mRNA expression was significantly increased in RT4 R1 + PD compared to RT4 parental no PD. Conflicting evidence has found the EPH family of RTKs to be both oncogenic and tumour-suppressive.

Agonistic and antagonistic targeted agents specific for EPH family members, such as ifabotuzumab which is a EphA3 agonist, have entered early stage clinical trials (Lodola *et al*., 2017). Immunoblot analysis could have been used to confirm if expression of EphA3 and phospho-EphA3 was increased in RT4 R1. Whether the increase in expression of *EPHA3* contributes to the resistant phenotype in RT4 R1 could be tested by examining whether knockdown of *EPHA3* expression re-sensitised RT4 R1 to PD. This was not conducted due to time limitations.

Inhibition of IGF1R with linsitinib was efficacious in RT112 parental, R1, R2 and R3. As linsitinib reduced cell viability in parental RT112, signalling via IGF1R did not arise in the RT112 resistant lines as a mechanism of resistance to PD, rather the dependency on IGF1R signalling was pre-existing. It was surprising that RT112 R3 exhibited sensitivity to IGF1R, as this line had a *HRAS* mutation, resulting in a constitutively active protein, and it was thought that this mutation would diminish the dependency on RTK activation in RT112. Isobologram analysis could have been conducted to determine if treatment with linsitinib and PD was additive in RT112 parental and resistant derivatives, but was not due to time limitations. Immunoblot analysis to determine the expression of IGF1R and phospho-IGF1R in RT112 parental and the resistant lines was not conducted during this project due to time limitations. This would have determined whether the resistant lines cultured in PD or parental RT112 acutely treated with PD had increased activation of IGF1R, suggesting that IGF1R activation compensated for the loss of FGFR signalling. Alternatively, IGF1R may be activated at a similar level in RT112 parental and the RT112 resistant derivatives. Higher expression of *IGF1R* RNA correlates with a lower overall survival time in MIBC patients (Wang *et al*., 2017). Sun *et al.* reported that treatment of the urothelial carcinoma cell line, T24, with IGF1 significantly reduced mitomycin-induced apoptosis. Furthermore, depletion of IGF1R by treatment with an antisense oligodeoxynucleotide, in combination with mitomycin, induced apoptosis and cell proliferation to a greater extent than single agent treatment with either therapy (Sun *et al*., 2001).

Unfortunately, the results of clinical trials with targeted agents with specificity for IGF1R have been disappointing (Janssen and Varewijck, 2014). A phase III clinical trial was conducted with linsitinib in patients with advanced or metastatic adrenocortical carcinoma, but linsitinib did not increase overall survival (Fassnacht *et al*., 2015). EGFR is reported to transactivate IGF1R and signalling via IGF1R has been implicated in resistance to EGFR-targeted therapy in NSCLC (Burgaud and Baserga, 1996; Li *et al*., 2017; Morgillo *et al*., 2007). For this reason, phase II trials in NSCLC patients have compared treatment with erlotinib to

treatment with linsitinib in combination with erlotinib. Unfortunately, these trials have found that linsitinib did not improve patient outcomes (Ciuleanu *et al*., 2017; Leighl *et al*., 2017). Phase II/III clinical trials in colorectal cancer patients have examined the addition of the monoclonal antibody dalotuzumab, which has specificity for IGF1R, to treatment with the EGFR-specific monoclonal antibody cetuximab and chemotherapy. These trials have indicated that this targeted agent is ineffective at treating colorectal cancers. However, expression levels of IGF1R, IGF1 or IGF2 may indicate which patients would benefit from IGF1R-targeted therapy (Sclafani *et al*., 2015; Sclafani *et al*., 2017). As IGF1R has been implicated in resistance to EGFR-targeted agents it is logical that this RTK could also induce resistance to inhibition of other RTKs. Whilst IGF1R-targeted agents are still in the clinical trial stage, and the results of clinical trials have so far been disappointing, the use of biomarkers to stratify who receives IGF1R-targeted agents may yield more promising results.

The activation of RTKs in RT112 resistant lines was examined with a phospho-RTK array (PathScan® RTK signaling antibody array Kit #7982). However, as the results of this array were disappointing with a low signal detected from RTK specific spots, the results of this analysis were not presented in this thesis. An alternative phospho-RTK array from a different supplier was identified. However, analysis was not conducted with this array due time limitations. This analysis may have identified other RTKs which were activated in RT112 R1 and R2

The initial examination of RT112 R1 and R2 revealed that these cells had lost the parental RT112 epithelial morphology, gained a mesenchymal morphology and increased protein expression of N-cadherin. A complete EMT was not observed in these lines as E-cadherin expression remained constant between RT112 parental, R1 and R2. N-cadherin expression was not increased in parental RT112 acutely treated with PD and microarray analysis showed that EMT markers were not significantly differentially expressed between parental RT112 cultured without PD and parental RT112 acutely treated with PD. MetaCore™ analysis of microarray data found that pathways relating to EMT maps were upregulated in R1, R2 and R3 compared to RT112 parental and in RT4 R1 compared to RT4 parental. This is similar to what was reported by Wang *et al*. whose FGFR TKI-resistant RT112 derivatives, produced by long term culture in either ponatinib or BGJ398, reverted to a mesenchymal morphology and had increased expression of *CDH2* and *FN1* (Wang *et al*., 2014). EMT-like changes have been reported in *in vitro* models of adaptive resistance to other targeted therapies such as EGFR, ERBB2 and ALK TKIs (Brown *et al*., 2016; Gower *et al*., 2016; Lee *et al*., 2017). A

mesenchymal phenotype is associated with greater cell migration and invasion. It would be undesirable for treatment with a FGFR TKI to induce these characteristics in a patient as this could result in a greater risk of metastasis (Singh *et al*., 2017). This project has not determined whether the EMT-like changes observed in the resistant lines were fundamental to, or a by-product of, the resistant phenotype. Li *et al.* reported that activation of signalling via IGF1R in gefitinib resistant derivatives of the EGFR-mutant NSCLC cell lines PC9 and HCC827 induced an EMT. Treatment of the PC9 gefitinib resistant derivatives with the IGF1R inhibitor picropodophyllin increased sensitivity to gefitinib and reduced expression of mesenchymal markers (Li *et al*., 2017). Signalling via FGFR3 is associated with an epithelial morphology in urothelial carcinoma cell lines (Cheng *et al*., 2013). It is possible that, upon culture with PD, the resistant cells lose the signals from FGFR3 that induce an epithelial phenotype and gain a more mesenchymal phenotype. Signalling via EGFR has also been associated with EMT (Chang *et al*., 2012; Serrano *et al*., 2014). However, EGFR did not induce an EMT in RT4 R1 as this resistant derivative did not exhibit a mesenchymal morphology, exhibited low expression of N-cadherin and vimentin and maintained expression of E-cadherin. Cell migration and invasion was not examined in the parental lines and their resistant derivatives so the extent to which long term culture in PD induces these characteristics has not been established.

Bladder cancers can be classified as ‘luminal’ if their gene expression is more similar to the superficial or intermediate layers of the urothelium or ‘basal’ if their gene expression is more similar to the basal layer of the urothelium. Basal tumours exhibit upregulation of p63 target genes and are more likely to have mutations in *TP53* (Choi *et al*., 2014b; Robertson *et al*., 2017). Luminal tumours exhibit upregulation of PPARγ target genes and are more likely to have mutations in *FGFR3*, *ELF3*, *CDKN1A*, and *TSC1*. Basal MIBC are more aggressive and patients with basal tumours have shorter survival times than patients with luminal tumours (Dadhania *et al*., 2016). Therefore, if urothelial tumours switch towards a more basal phenotype upon being treated with FGFR-targeted agents this could result in a worse prognosis for patients. Both RT112 and RT4 have been previously classified as luminal (Warrick *et al.*, 2016). Microarray and qRT-PCR analysis suggested that the expression of some basal markers was increased and expression of some luminal markers was decreased in RT112 resistant derivatives compared to the parental line. However, immunoblot analysis showed that expression of the basal markers cytokeratin 5/6 and CD44 was low in RT112

parental and the RT112 resistant derivatives. Therefore, it is unlikely that the RT112 resistant derivatives have gained a basal phenotype.

Previous research has shown that fatty acid synthesis is reduced in RT112 upon *FGFR3* knockdown due to FGFR3 regulation of the transcription factor SREBP1 (Du *et al*., 2012). The weak base chloroquine induces lysosomal cell death by diffusing into lysosomes and raising the lysosomal pH. This induces lysosomal swelling, cathepsin leakage and cathepsin-mediated activation of caspases. King *et al.* reported that inhibition of FGFRs, PI3Kα, AKT or mTOR potentiated the lysosomal cell death induced by chloroquine in RT112. This was due to a reduction in the biosynthesis of cholesterol which can promote the integrity of lysosomal membranes (King *et al*., 2016). Here, microarray analysis indicated that there was differential expression of genes regulating lipid metabolism between RT112 experimental conditions and between RT4 experimental conditions. Immunoblot analysis indicated that expression of mature SREBP1, the transcription factor which regulates expression of fatty acid synthesis genes, was reduced in RT112 parental acutely treated with and RT112 R1 cultured in PD. Mature SREBP1 expression was reduced to a lesser extent in R2 and R3 cultured in PD. SCD1 is the rate-limiting enzyme in the production of mono-unsaturated fatty acids from saturated fatty acids (Igal, 2016). Immunoblot of SCD1 showed that expression of this protein was reduced in RT112 parental acutely treated with PD and R1 and R2 cultured in PD. Expression was also reduced but to a lesser extent in R3 + PD. These results confirmed that fatty acid synthesis was reduced in RT112 resistant derivatives. Protein expression of SCD1 and SREBP1 was not examined in RT4 parental and R1. However, microarray analysis indicated that genes involved in fatty acid synthesis were downregulated in RT4 R1 compared to RT4 parental. This indicates that the reduced sensitivity to PD exhibited by RT112 and RT4 resistant derivatives is not mediated by the restoration of fatty acid synthesis during FGFR3 inhibition. Even the *HRAS* mutation in RT112 R3 did not induce the return of fatty acid synthesis markers to the expression level observed in RT112 parental. This highlights that, although the two mutations are mutually exclusive, they do not have an identical function in the context of driving urothelial carcinoma. Further examination of fatty acid synthesis could have been conducted by examining the incorporation of ^{14}C-labelled acetate into fatty acids as conducted by Du *et al.* Alternatively, cellular lipid composition of parental and resistant lines could be examined with mass spectrometry as conducted by Griffiths *et al.* (Griffiths *et al*., 2013). This could have confirmed whether the observed changes in gene expression resulted in an overall reduction in fatty acid synthesis.

As RT4 R1, RT112 R1 and RT112 R2 exhibited morphological and gene expression changes which were reversible upon culture without PD, it was thought that these lines were in a resistant state mediated via epigenetic or gene expression changes rather than via a genetic mechanism. RT112 R1 and R2 maintained their resistance following culture without PD for 4 passages, despite reverting to a morphology similar to parental RT112. This was in contrast to the RT112 ponatinib and BGJ398 resistant derivatives produced by Wang *et al*. which regained sensitivity to FGFR inhibition following culture without drug for two to four weeks (Wang *et al*., 2014). It is not known whether culture of RT112 R1 and R2 for a longer period of time out of PD would have re-sensitized the lines to PD. Although the epigenetic state of RT112 R1 and R2 was not examined, these lines may have gained epigenetic alterations which enable the cells to maintain their resistance to FGFR inhibition.

As it was thought that the resistant state in RT4 R1, RT112 R1 and RT112 R2 was mediated via epigenetic or gene expression changes rather than via a genetic mechanism, the inhibition of epigenetic modifiers could be a useful strategy to overcome resistance FGFR TKIs. Examination of whether knockdown of epigenetic modifiers or treatment with inhibitors of epigenetic modifies re-sensitizes the resistant lines to PD could identify epigenetic alterations which facilitate PD resistance and therefore highlight an alternative therapeutic approach to overcoming PD resistance.

Epigenetic modifiers have been targeted to overcome resistance to targeted therapy. Gastrointestinal stromal tumours (GISTs) often have activating mutations in RTKs KIT and PDGFRA (Heinrich *et al*., 2003; Hirota *et al*., 1998). Mühlenberg *et al*. reported that treatment with the non-selective histone deacetylase inhibitor vorinostat and imatinib were additive in KIT-positive GIST cell lines. Vorinostat reduced *KIT* mRNA expression and increased acetylation of HSP90, a KIT chaperone, inducing KIT degradation (Muhlenberg *et al*., 2009). Bauer *et al*. conducted a phase I clinical trial which assessed the efficacy of imatinib in combination with the non-selective histone deacetylase inhibitor panobinostat in overcoming resistance in patients with gastrointestinal stromal tumours refractory to the combination of imatinib and the multitargeted TKI sunitinib. One out of the 11 patients showed a partial response, 7 had stable disease and 3 patients had progressive disease (Bauer *et al*., 2014).

Sharma *et. al.* produced PC9 cells resistant to EGFR-TKIs, which mediated their resistance via activation of IGF1R, via culture in gefitinib for 9 days. It was

observed that the resistant cells had increased expression of KDM5A and that *KDM5A* knockdown did not reduce the proliferation of parental PC9 cells but did reduce the production of resistant cells upon treatment with gefitinib. Upon culture without an EGFR TKI, resistant cells maintained their resistant phenotype for approximately 30 passages before regaining gefitinib sensitivity (Sharma *et al*., 2010). Treament with the KDM5A inhibitor YUKA1 reduced the formation of gefitinib-resistant colonies following the culture of PC9 in gefitinib for 35 days. Culture with YUKA1 as a single agent did not reduce the growth of PC9 (Gale *et al*., 2016). How long RT112 R1 and R2 would have to be cultured without PD to regain PD sensitivity is unknown. Hou *et al*. observed that expression of KDM5A was increased in the breast cancer lines SUM149 and SUM102 following 6 and 9 days culture in erlotinib. Stable knockdown of KDM5A in the breast cancer cell lines SUM149 and HCC1937 reduced the number of drug-tolerant SUM149 and HCC1937 cells following 30-day culture in erlotinib (Hou *et al*., 2012). Gale *et al*. cultured the breast cancer cell line BT474 with a low dose of trastuzumab for 35 days with and without YUKA1 and observed that YUKA1 reduced the formation of trastuzumab-resistant colonies. Culture with YUKA1 as a single agent did not reduce the growth of BT474 (Gale *et al*., 2016). Whether knockdown of *KDM5A* or treatment with a KDM5A inhibitor could re-sensitise RT112 R1 and R2 was not examined in this project due to time limitations. However, microarray analysis showed that *KDM5A* mRNA expression was not significantly differentially expressed between RT112 parental and the RT112 resistant lines. Expression of the histone demethylase *KDM6A* was significantly increased in the RT112 and RT4 resistant cells cultured in PD compared to their parental lines. Whether KDM6A contributes to the resistant phenotype could be tested by examining whether knockdown of *KDM6A* re-sensitizes these cells to PD.

Inhibition of the bromodomain and extraterminal (BET) family of chromatin readers has been previously examined in RT112 as a mechanism of increasing the efficacy of FGFR-targeted therapy. Binding of the BET bromodomain-containing protein BRD4 to MYC enhancers induces transcription of the oncogene MYC (Lovén *et al*., 2013). Mahe *et al.* observed that siRNA knockdown of the transcription factor *MYC* decreased FGFR3 expression in the bladder cancer cell lines MGH-U3, which has a Y375 FGFR3 activating mutation, and RT112. Treatment with PD reduced MYC expression in MGH-U3 and RT112 suggesting a MYC/FGFR3 positive feedback loop. In MGH-U3 and RT112, treatment with the PI3 kinase inhibitor LY294002 decreased phosphorylation of glycogen synthase kinase 3 β which induces the proteosomal degradation of MYC. Additionally, siRNA

knockdown of *MAPK14*, which encodes the MAP kinase protein p38α, reduced *MYC* mRNA expression. This demonstrated that both the MAP kinase and PI3 kinase pathway act downstream of FGFR3 to increase MYC expression. Treatment with the BET bromodomain inhibitor JQ1, in combination with PD, reduced cell viability in MGHU3 and RT112 in an additive fashion (Mahe *et al*., 2018). It is possible that treatment with a BET bromodomain inhibitor such as JQ1, in combination with an FGFR TKI might prevent the development of acquired resistance to FGFR3 inhibition.

A single cell clone of parental RT4 was used to generate RT4 R1, whereas a heterogenous population of RT112 cells, rather than a single cell clone, was used to generate the RT112 resistant derivatives. This was because a single cell clone of RT4 was available at the start of this project, whilst a single cell clone of RT112 was not. The use of a heterogenous population of RT112 cells made analysis of genetic and gene expression changes more challenging to interpret. For example, it is unclear whether the HRAS G12S mutation observed in RT112 R3 was present in a subpopulation of parental RT112 or was acquired by an RT112 cell during long-term culture in PD. Additionally a number of copy number differences were observed between parental RT112 and the RT112 R1 and between parental RT112 and the RT112 R3. These copy number differences may have been present in a subpopulation of cells prior to, or acquired during, the long-term culture of RT112 cells in PD. In contrast, as a single cell clone of parental RT4 was used to generate RT4 R1, the copy number differences observed between parental RT4 and RT4 R1 were likely to have been acquired during the long-term culture of RT4 cells in PD. A limitation of the transcriptome analysis was that, as this involved examining expression of a large number of genes, a number of genes will have been falsely classified as differentially expressed between experimental conditions. Raising the threshold for classifying genes as differentially expressed may have reduced the number of false positives. However, this would have reduced the detection of true gene expression differences. The use of a greater number of repeats per experimental condition would have increased the reliability of the microarray data. In order to validate the microarray data, immunoblotting and qRT-PCR were used to confirm gene expression changes.

There are a number of experiments which would have been conducted had there been more time available to continue this project. A limitation of this study is that short tandem repeat profiling was last used to authenticate the cell line identity of the parental RT112 and RT4 in 2012 and that short tandem repeat profiling has not been used to authenticate the identity of the RT112 and RT4 resistant

derivatives. Had more time been available, short tandem repeat profiling would have been conducted to confirm the cell line identity of the RT112 and RT4 parental lines and resistant derivatives. Immunoblot analysis could have been conducted to determine the expression of IGF1R and phospho-IGF1R in RT112 parental and the resistant lines. Additionally, immunoblot analysis could have been used to show that treatment with capmatinib reduced MET phosphorylation in RT112 resistant lines, demonstrating the efficacy of this TKI. Microarray analysis identified an increase in expression of *KDM6A* mRNA expression in RT112 and RT4 resistant derivatives when cultured in PD. Additionally, microarray analysis identified an increase in *ERBB4* and *EPHA3* mRNA expression in RT4 R1 + PD. Immunoblot analysis could have determined whether these changes in mRNA expression induced a change in protein expression of KDM6A, ERBB4 and EphA3 and to examine whether ERBB4 and EphA3 were phosphorylated in RT4 R1. Whether *KDM6A*, *ERBB4* or *EPHA3* contributed to PD resistance could have been tested by examining whether knockdown of these genes, or treatment with a specific inhibitor, re-sensitised the resistant lines to PD. A cell viability assay could have been conducted with a MEK inhibitor to determine whether this treatment would overcome the resistance to PD observed in RT112 R3. Isobologram analysis could have been conducted to determine if treatment with erlotinib and PD was additive in RT4 parental and R1 and if treatment with linsitinib and PD was additive in RT112 parental and resistant derivatives.

In conclusion, this project has shown that mutations downstream of FGFR3, in this case a *HRAS* G12S mutation, can be acquired as a mechanism of resistance to FGFR inhibition. Currently RAS mutations cannot be directly targeted with therapeutic agents. As RAS mutations are frequent in cancer there is a requirement for effective treatments for RAS mutant tumours and research is ongoing to meet this need. As the RT112 resistant derivatives exhibited sensitivity to linsitinib, this suggests that it may be possible to target IGF1R to overcome resistance to FGFR inhibition. EGFR was identified as a mediator of acquired resistance to FGFR inhibition in RT4 R1. EGFR activation has been previously identified as a mechanism of short-term survival following treatment with PD in RT112 (Herrera-Abreu *et al.*, 2013). A number of different RTKs have been reported in this study, and elsewhere, to induce resistance to FGFR-targeted agents in urothelial carcinoma cell lines. Therefore, the examination of the RTK expression profile of an FGFR-TKI resistant urothelial carcinoma, by a method such as immunohistochemistry, and screening for mutations in pathways activated downstream of FGFR3, may be key to treating refractory tumours.

A

	RT112 R1	RT112 R2	RT112 R3	RT4 R1
N-cadherin	Increased	Increased	Increased	Constant
FGFR3	Reduced	Reduced	Reduced	Constant
Phospho-EGFR	Reduced	Reduced	Not assayed	Increased
EGFR	Constant	Constant	Not assayed	Increased
Phospho-ERBB2	Not detected	Not detected	Not assayed	Not detected
ERBB2	Constant	Constant	Not assayed	Not detected
Phospho-ERBB3	Increased	Increased	Not assayed	Increased
Phospho-MET	Increased	Increased	Increased	Not assayed
MET	Reduced	Reduced	Increased	Not assayed

B

RT112 R1	RT112 R3	RT4 R1
Gain of 5p15.33–q11.1	*HRAS* G12S	Gain of 5p15.33–q11.1
ATF2 E349K		No *EGFR* amplification
MIB2 Q898R		No *EGFR* mutation

C

	RT112 R1	RT112 R2	RT112 R3	RT4 R1
OSMR, *LIFR* and *IL6ST*	Increased	Increased	Increased	Constant
IGF1R	Increased	Increased	Non significant increase	Constant
EPHA3	Constant	Constant	Constant	Increased
ERBB4	Constant	Constant	Constant	Increased
KDM5A	Non-significant increase	Non-significant increase	Non-significant reduction	Non-significant increase
KDM6A	Increased	Increased	Increased	Increased

D

RT112 R1	RT112 R2	RT112 R3	RT4 R1
Linsitinib (IGF1R TKI)	Linsitinib	Linsitinib	Erlotinib (EGFR TKI)

Figure 8.1 Summary of key findings from immunoblot analysis, copy number analysis, whole exome-sequencing, transcriptome analysis and screen of targeted agents. A) Protein expression changes identified by immunoblot analysis. B) Genetic alterations identified by whole exome sequencing and copy number analysis thought to be most likely to be inducing resistance to PD. C) RNA expression changes identified by transcriptome analysis. D) Small-molecule inhibitors identified to efficaciously reduce cell viability as monotherapies.

Appendix A
Tissue culture media, buffers and solutions

RPMI-1640 Medium
500ml RPMI-1640 medium
50ml FCS
2mM GlutaMax

Trypsin/versene
dH_20
0.25% (w/v) Trypsin
0.02% (w/v) EDTA
HBSS minus Ca^{2+} and Mg^{2+}

Ham's F12 complete medium
500ml Ham's F12 nutrient mixture
1% FCS
1% insulin-transferrin-selenium
1% minimal essential medium non-essential amino acids
25mM Hyrocortisone
2mM GlutaMax

Freezing medium
120ml Ham's F12
15ml FCS
15ml DMSO

Blocking solution for Western blotting
10ml PBS
0.1% (v/v) Tween 20
4% non-fat milk

Antibody diluent for Western blotting
10ml PBS
0.1% (v/v) Tween 20
2% non-fat milk

SDS loading buffer (5x)
1.25ml 2M Tris-HCl pH 6.8
3ml 30% glycerol
2mg bromophenol blue
5.75ml molecular biology grade water (Sigma Aldrich)

DNA loading buffer
2.5g Ficoll
0.04g bromophenol blue
0.04g Xylene cyanole
10ml molecular biology grade water (Sigma Aldrich)

Stripping buffer for Western blotting
120.12g Urea
10ml 2M Tris-HCl pH 6.8
200ml dH_20

RIPA lysis buffer
PBS
1% Triton x100
1mM EDTA
0.5% (w/v) Sodium deoxycholate
0.1% SDS

Appendix B
List of suppliers

Abcam
330 Cambridge Science Park, Cambridge, CB4 0FL, UK
http://www.abcam.com/

Adooq Bioscience
4000 Barranca Parkway, Suite 250, Irvine, California, 92604, USA
http://www.adooq.com/

Affymetrix
Supplied by Thermo Fisher Scientific
https://www.thermofisher.com/

Agilent
5301 Stevens Creek Boulevard, Santa Clara, California, 95051, USA
https://www.agilent.com

Applied Biosystems
Supplied by Life technologies
http://www.lifetechnologies.com

Apex Technology
4745 Sutton Park Court, Suite 402, Jacksonville, Florida, 32224, USA
http://www.apextechnology.com/

Beckman Coulter
Oakley Court, Kingsmead Business Park, London Road, High Wycombe, HP11 1JU, UK
https://www.beckmancoulter.com

Berthold Technologies
Calmbacher Strasse 22, 75323 Bad Wildbad, Germany
https://www.berthold.com

Bio-Rad
Bio-Rad House, Maxted Road, Hemel Hempstead, Hertfordshire, HP2 7DX, UK
http://www.bio-rad.com

Biosera
Rue de la Caille, 49340. Nuaille, France
http://www.biosera.com

Biovision
155 South Milpitas Boulevard, Milpitas, California, 95035, USA
https://www.biovision.com/

BMG labtech
8 Bell Business Park, Smeaton Close, Aylesbury, Buckinghamshire, HP19 8JR, UK
https://www.bmglabtech.com

Cambridge Bioscience
Munro House, Trafalgar Way, Bar Hill, Cambridge, CB23 8SQ, UK
https://www.bioscience.co.uk/

Cayman Chemical
Munro House Trafalgar Way Bar Hill, Cambridge, CB23 8SQ, UK
https://www.caymanchem.com

Cell Signalling Technology
3 Trask Lane, Danvers, Massachusetts, 01923, USA
https://www.cellsignal.com/

Corning Life Sciences B.V.
Fogostraat 12, 1060 LJ Amsterdam, The Netherlands, Amsterdam, 1060, The Netherlands
https://www.corning.com

Dako
Supplied by Agilent
https://www.agilent.com

Gibco
Supplied by Life technologies
http://www.lifetechnologies.com

Illumina
Chesterford Research Park, Little Chesterford, Near Saffron Walden, Essex, CB10 1XL UK
https://www.illumina.com/

Invitrogen
Supplied by Life technologies
http://www.lifetechnologies.com

Labtech international
Mytogen House, 11 Browning Road, Heathfield, East Sussex, TN21 8DB, UK
https://www.labtech.com/

Life Technologies
3 Fountain Drive, Inchinnan Business Park, Paisley, PA4 9RF, UK
https://www.lifetechnologies.com

Medical Air Technologies (MAT)
Unit 2, Mercury Way, Trafford Park, Manchester, M41 7LY
http://www.medicalairtechnology.com

Merk Millipore
Suite 21, Building 6, Croxley Green, Business Park, Watford, Hertfordshire, WD18 8YH,UK
http://www.merckmillipore.com

New England Biolabs
New England Biolabs,75-77 Knowl Piece, Wilbury Way, Hitchin, Hertfordshire, SG4 0TY, UK
https://www.neb.com

Panreac AppliChem
Surechem products LTD. Lion Barn Industrial Estate, Needham Market, Suffolk, IP6 8NZ, UK
https://www.applichem.com

Promega
Delta House, Southampton Science Park, Southampton, SO16 7NS
http://www.promega.co.uk

Qiagen
Skelton House, Lloyd Street North, Manchester, M15 6SH, UK
https://www.qiagen.com

R&D Systems
614 McKinley Place NE, Minneapolis, Minnesota, 55413, USA
https://www.rndsystems.com

Santa Cruz Biotechnology
10410 Finnell Street, Dallas, Texas, 75220, USA
https://www.scbt.com/

Sanyo Limited
9 The Office Village, North Road, Loughborough, Leicestershire, LE11 1QJ, UK
http://sanyo-biomedical.co.uk/

Sarstedt
68 Boston Road, Beaumont Leys, Leicester, LE4 1AW, UK
https://www.sarstedt.com

Severn Biotech Limited
Unit 2, Park Lane, Kidderminster, Worcestershire, DY11 6TJ, UK
http://www.severnbiotech.com

Sigma Aldrich Limited
The Old Brickyard, New Road, Gillingham, Dorset, SP8 4XT, UK
https://www.sigmaaldrich.com

Southern Biotech
Supplied by Cambridge Bioscience
https://www.bioscience.co.uk

Thermo Fisher Scientific
Bishop Meadow Road, Loughborough, LE11 5RG
https://www.thermofisher.com/

Appendix C
Copy number analysis and exome sequencing data

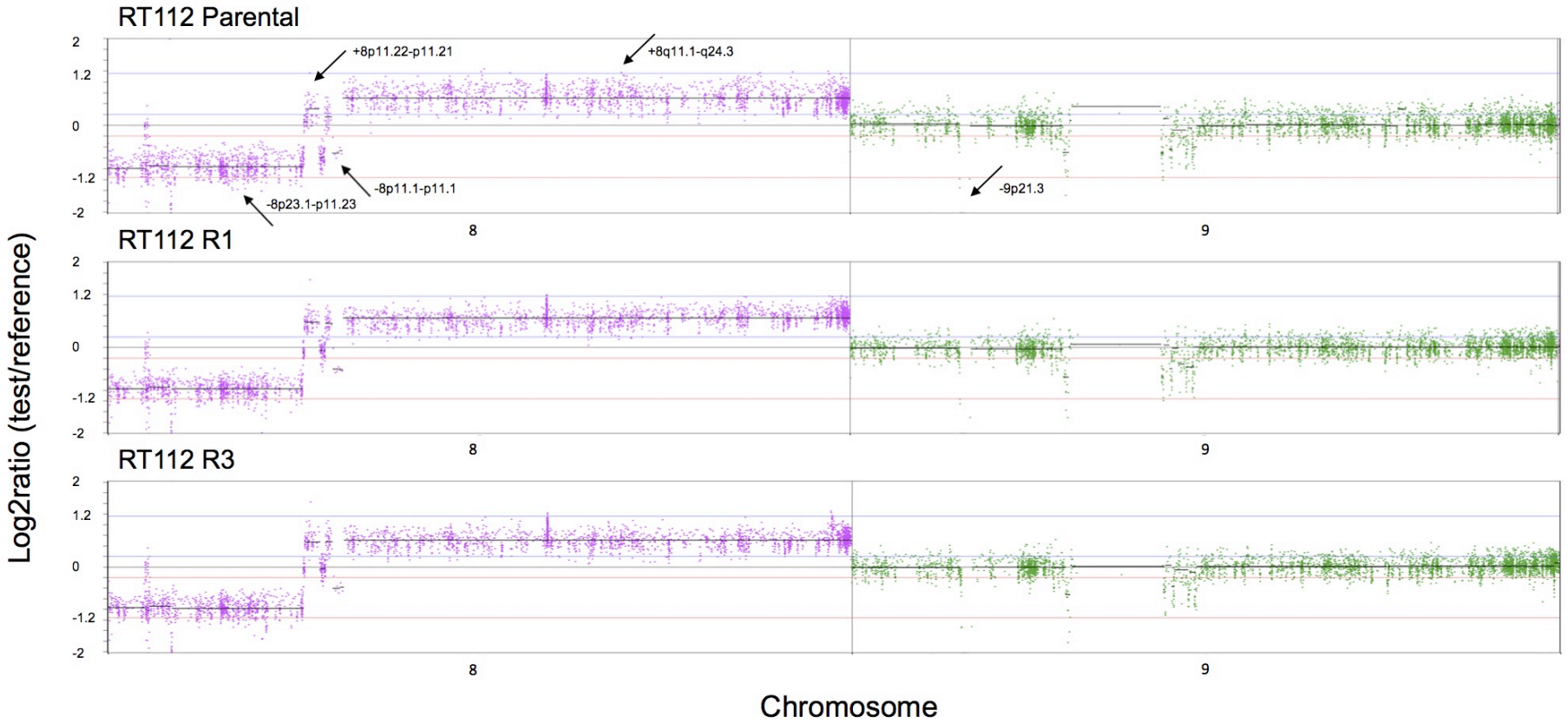

Figure C.1 Copy number profiles of chromosomes 8 and 9 for RT112 parental, R1 and R3 normalised to a patient blood sample. Copy number plots were generated in Nexus Copy Number 8.0. and show $\log_2$ ratio of the read counts of RT112 samples normalised to a patient blood sample for chromosomes 8 and 9 (GRch38 reference). Each point represents the $\log_2$ ratio for a section of DNA of window size 1000 bp. Copy number gains (above the zero line) and losses (below the zero line) shared by RT112 parental, R1 and R3 are highlighted with arrows and are also detailed in Table 5.1.

Table C.1 Mutations identified by whole exome sequencing in RT112 R1. The mutations met the following criteria: the mutation was absent from RT112 parental and had a variant allele frequency of greater than 20%

Gene	Ensembl transcript ID	Chromosome: Position (Mb; hg38)	Variant Effect Predictor (VEP) consequence	Coding DNA sequence change (position from start codon)	Amino acid change	COSMIC ID	Sorting Intolerant From Tolerant (SIFT) Prediction	Polymorphism Phenotyping v2 (PolyPhen) Prediction
MIB2	ENST00000355826	1:1629393	missense variant	c.A2693G	p.Q898R		tolerated	benign
KIAA2013	ENST00000376572	1:11925736	missense variant	c.G502A	p.G168S		tolerated low confidence	benign
ATF2	ENST00000264110	2:175093201	missense variant	c.G1045A	p.E349K		deleterious	possibly damaging
HACL1	ENST00000321169	3:15601421	missense variant	c.T43C	p.S15P		deleterious	benign
BTD	ENST00000417015	3:15601421	missense variant	c.A17G	p.D6G		-	unknown
SLC35G2	ENST00000393079	3:136854890	stop gained	c.C430T	p.Q144*		-	-
NDUFS4	ENST00000296684	5:53646367	synonymous variant	c.A312G	p.R104=		-	-
MIER3	ENST00000336942	5:56946947	synonymous variant	c.A78G	p.S26=		-	-
MDN1	ENST00000369393	6:89698985	missense variant	c.G9048A	p.M3016I		tolerated	benign
ZP3	ENST00000336517	7:76440270	synonymous variant	c.G699A	p.L233=		-	-
GIMAP8	ENST00000307271	7:150466710	synonymous variant	c.G12A	p.Q4=		-	-
SHB	ENST00000377707	9:38068185	missense variant	c.C461T	p.S154L		tolerated	benign
EPB41L4B	ENST00000374566	9:109320304	missense variant	c.C143T	p.S48L		tolerated low confidence	benign
PRRG4	ENST00000257836	11:32853436	missense variant	c.G590A	p.R197K		tolerated	benign
TRIM51	ENST00000449290	11:55886138	stop gained	c.A427T	p.K143*		-	-
SESN3	ENST00000278499	11:95185375	stop gained	c.G226T	p.E76*		-	-
WNK1	ENST00000315939	12:885517	synonymous variant	c.C4713T	p.1571=	COSM5376269 COSM5376270 COSM5376271	-	-

GRIP1	ENST00000359742	12:66517916	missense variant	c.G563A	p.G188E		deleterious	probably damaging
PAGR1	ENST00000320330	16:29819568	synonymous variant	c.G579A	p.R193=		-	-
CTD-2574D22.6	ENST00000562285	16:29819568	synonymous variant	c.G69A	p.R23=		-	-
IGHV3OR16-9	ENST00000354689	16:32066301	synonymous variant	c.G237A	p.L79=		-	-
USP43	ENST00000285199	17:9680360	missense variant	c.C1099T	p.L367F		tolerated	benign
WDR18	ENST00000251289	19:991968	synonymous variant	c.T936C	p.N312=		-	-
MUM1	ENST00000415183	19:1370676	synonymous variant	c.C1587G	p.V529=		-	-
NDUFS7	ENST00000233627	19:1388539	missense variant	c.C68T	p.P23L		tolerated low confidence	benign
DIRAS1	ENST00000323469	19:2717258	synonymous variant	c.G549C	p.G183=		-	-
ZNF554	ENST00000317243	19:2820107	synonymous variant	c.G36A	p.R12=		-	-
TBXA2R	ENST00000375190	19:3600458	synonymous variant	c.G177A	p.T59=	COSM5510987 COSM5510988	-	-
TMIGD2	ENST00000301272	19:4294626	missense variant	c.G503T	p.W168L		tolerated	benign
CTB-50L17.10	ENST00000589486	19:4493711	synonymous variant	c.A312G	p.P104=		-	-
ARHGEF18	ENST00000359920	19:7440096	synonymous variant	c.C156T	p.G52=		-	-
CYP4F8	ENST00000325723	19:15615676	synonymous variant	c.G60T	p.L20=		-	-
CYP4F3	ENST00000620621	19:15615676	synonymous variant	c.G60T	p.L20=		-	-
UNC13A	ENST00000519716	19:17656091	missense variant	c.G1075A	p.A359T		tolerated low confidence	benign
INSL3	ENST00000379695	19:17821329	missense variant	c.A178G	p.T60A		tolerated low confidence	benign
INSL3	ENST00000317306	19:17821381	synonymous variant	c.A126G	p.L42=		-	-
LRRC25	ENST00000339007	19:18392025	missense variant	c.C880T	p.P294S		tolerated	benign
GDF1	ENST00000247005	19:18869363	missense variant	c.C353T	p.A118V		tolerated	benign
CERS1	ENST00000623927	19:18869363	missense variant	c.C353T	p.A118V		tolerated	benign

CERS1	ENST00000429504	19:18895839	synonymous variant	c.T234C	p.T78=		-	-
SUGP1	ENST00000247001	19:19279376	synonymous variant	c.C1365T	p.Y455=		-	-
CILP2	ENST00000291495	19:19540331	synonymous variant	c.A291G	p.E97=		-	-
TMPRSS15	ENST00000284885	21:18329201	missense variant	c.G1748C	p.R583T		deleterious	probably damaging

Table C.2 Mutations identified by whole exome sequencing in RT112 R3. The mutations met the following criteria: the mutation was absent from RT112 parental and had a variant allele frequency of greater than 20%

Gene	Ensembl transcript ID	Chromosome: Position (Mb;hg38)	Variant Effect Predictor (VEP) consequence	Coding DNA sequence change (position from start codon)	Amino acid change	COSMIC ID	Sorting Intolerant From Tolerant (SIFT) Prediction	Polymorphism Phenotyping v2 (PolyPhen) Prediction
COL8A2	ENST00000481785	1:36098553	synonymous variant	c.G933A	p.G311=			
YY1AP1	ENST00000295566	1:155672698	missense variant	c.G643A	p.A215T		tolerated	benign
CD55	ENST00000314754	1:207331177	missense variant	c.A734T	p.Y245F		deleterious	probably damaging
XIRP2	ENST00000409195	2:167248119	stop gained	c.G6727T	p.E2243*			
SPATA3	ENST00000424440	2:230996329	synonymous variant	c.C96T	p.S32=			
PRR21	ENST00000408934	2:240042962	synonymous variant	c.A21G	p.T7=	COSM3695376 COSM3695377		
YIPF7	ENST00000332990	4:44624624	synonymous variant	c.T657C	p.G219=			
TENM3	ENST00000511685	4:182753541	synonymous variant	c.G3954T	p.L1318=			
UGT3A1	ENST00000333811	5:35962902	missense variant	c.T731A	p.V244E		deleterious low confidence	possibly damaging
DENND2A	ENST00000275884	7:140601525	synonymous variant	c.A873G	p.K291=			
IFNA21	ENST00000380225	9:21166592	synonymous variant	c.A21G	p.L7=			
PHF2	ENST00000359246	9:93676725	synonymous variant	c.G2964T	p.P988=	COSM3750192		

PHF2	ENST00000359246	9:93676737	synonymous variant	c.C2976A	p.T992=	-		
HRAS	ENST00000311189	11:534289	missense variant	c.G34A	p.G12S	COSM1644659 COSM1746299 COSM3931342 COSM480 COSM481 COSM482	deleterious	tolerated
MUC5AC	ENST00000621226	11:1190532	synonymous variant	c.A12387G	p.T4129=	-		
CRACR2A	ENST00000535292	12:3640718	missense variant	c.G301A	p.D101N			unknown
TUBGCP3	ENST00000464139	13:112547535	missense variant	c.A1253G	p.H418R		deleterious low confidence	benign
GOLGA6L6	ENST00000619213	15:20534627	synonymous variant	c.C1807A	p.R603=			
GOLGA6L6	ENST00000619213	15:20534645	missense variant	c.G1789A	p.E597K		tolerated	unknown
GOLGA6L6	ENST00000619213	15:20534648	missense variant	c.C1786T	p.R596W		tolerated	unknown
UNC13C	ENST00000260323	15:54293917	synonymous variant	c.C3841A	p.R1281	COSM3502389 COSM3502390 COSM3502391		
MESP2	ENST00000341735	15:89776918	synonymous variant	c.G561A	p.G187=			
KRTAP4-16	ENST00000440582	17:41101693	missense variant	c.G517C	p.V173L	COSM5177690		unknown
CCDC130	ENST00000588809	19:13759339	missense variant	c.C557A	p.P186H			unknown
ZNF114	ENST00000315849	19:48286708	missense variant	c.G1084A	p.E362K		tolerated	possibly damaging

Appendix D
Quality control, normalisation and analysis of transcriptomic data

This appendix contains the first stages of transcriptome analysis. Affymetrix GeneChip HTA 2.0 raw data files (.CEL files), were imported into Expression Console and the quality of the data was assessed using quality controls included on the microarray. Data was then normalised so that gene expression of different samples could be compared.

D.1 Quality control of expression data

Affymetrix Expression Console™ version 1.4 was used to assess the quality of the RNA microarray data. The area under the curve for the receiver operator curve for all microarray samples (Fig. D.1) was greater than or equal to 0.98 for microarray samples indicating a low false positive rate and a high true positive rate for the microarray positive and negative controls.

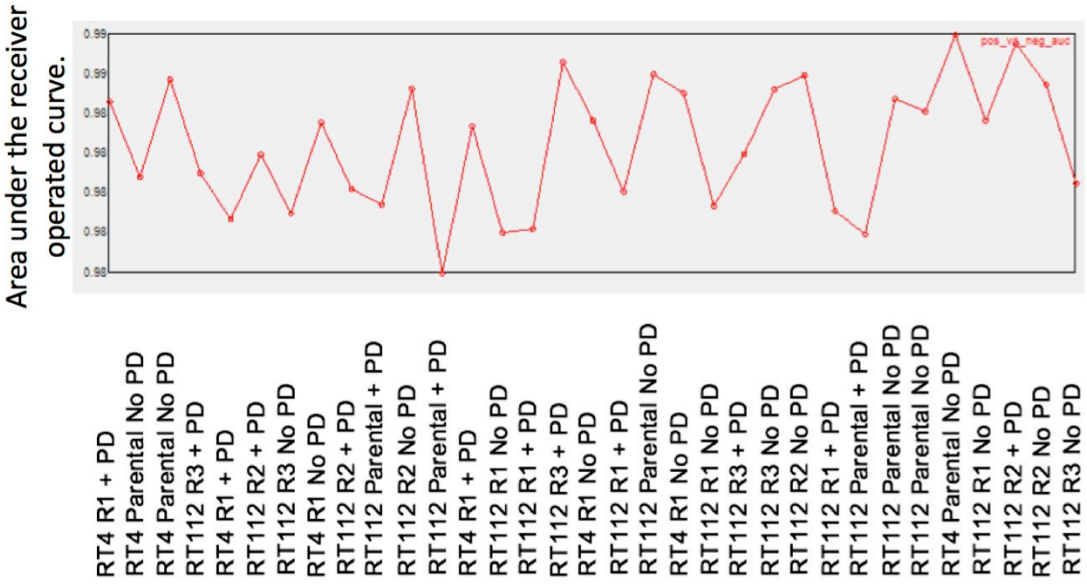

Figure D.1 The area under the curve for the receiver operator curve. The receiver operator curve plots the true positive rate against the false positive rate. The area under this curve gives an indication of how successfully positive and negative microarray controls were identified. The closer the AUC is to 1, the more accurate the identification of controls. This analysis was conducted in Affymetrix Expression Console™.

The Eukaryotic hybridisation controls were detected with signal values increasing in the order bioB, bioC, bioD and cre, matching the concentrations that these controls are spiked into the hybridisation cocktail (Fig. D.2). Affymetrix state that bioC, bioD and cre should be present in every array sample and bioB should present in a minimum of 70% of array samples. As the eukaryotic hybridisation controls are present as expected this indicates successful hybridisation.

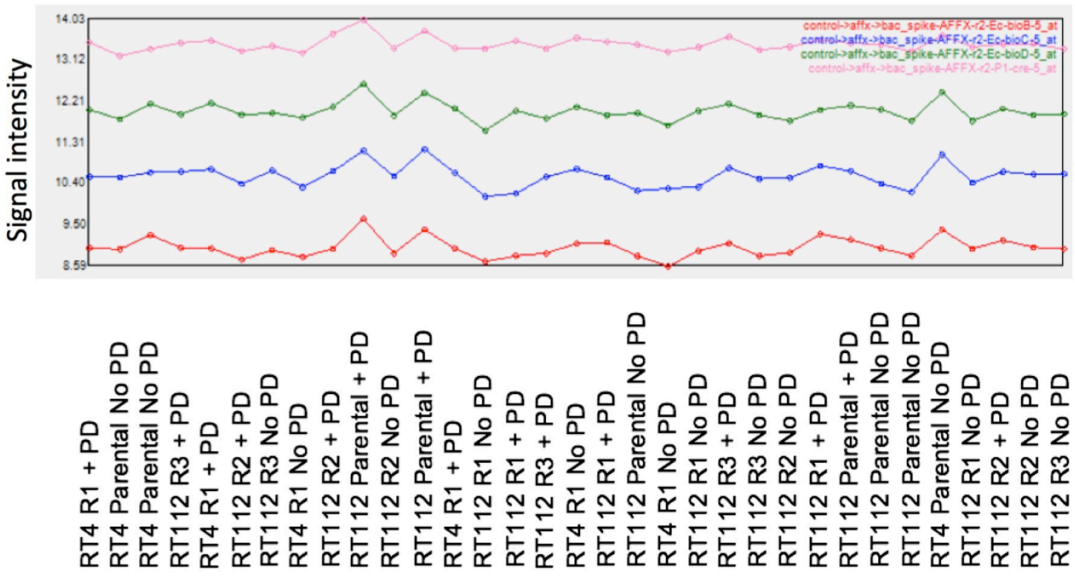

Figure D.2 Eukaryotic hybridisation controls (spike controls). The transcripts *bioB*, *bioC* and *bioD* take their sequence from genes of the *E.coli* biotin synthesis pathway and the probe *cre* takes its sequence from the bacteriophage P1 recombinase gene (all non-eukaryotic genes so not expressed in human cells). These controls are spiked into the hybridisation cocktail at different, known concentrations to enable signal alignment during image analysis. This analysis was conducted in Affymetrix Expression Console™.

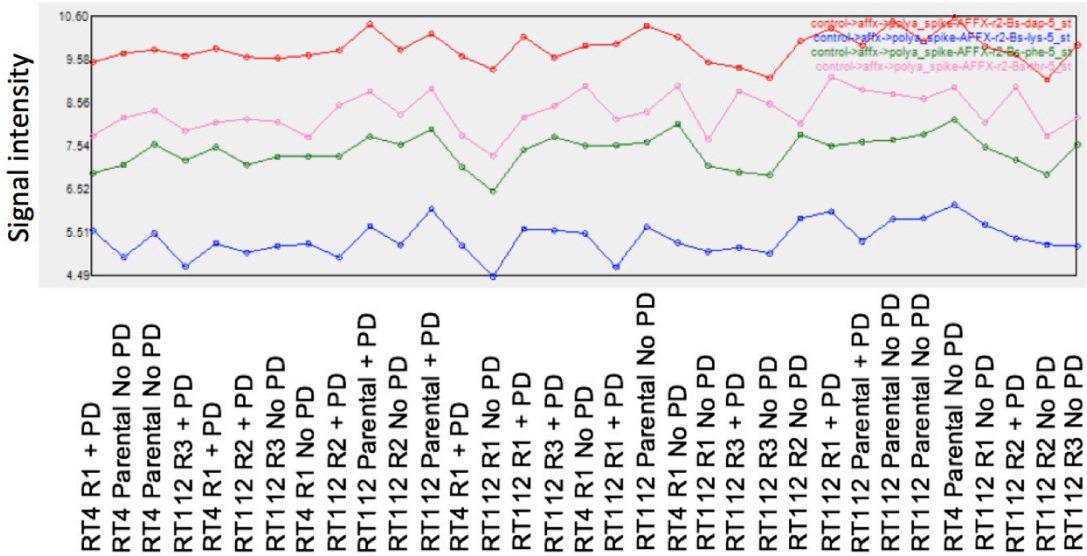

Figure D.3 Array labelling controls. The transcripts lys, phe, thr and dap take their sequence from *D.subtilis* genes, these genes are not expressed in eukaryotic cells. Different, known concentrations of these transcripts are amplified and labelled with the array samples to examine the labelling process. This analysis was conducted in Affymetrix Expression Console™.

D.2 Data normalisation

Normalisation of the microarray data was conducted in the Affymetrix Expression Console™ version 1.4. Due to experimental variation, such as that occurring during the fluorescent labelling of cDNA and hybridisation of cDNA to the microarray, there is some variability between the probe cell intensity data of the separate microarray samples, measured from CEL files, prior to normalisation (Fig. D.4).

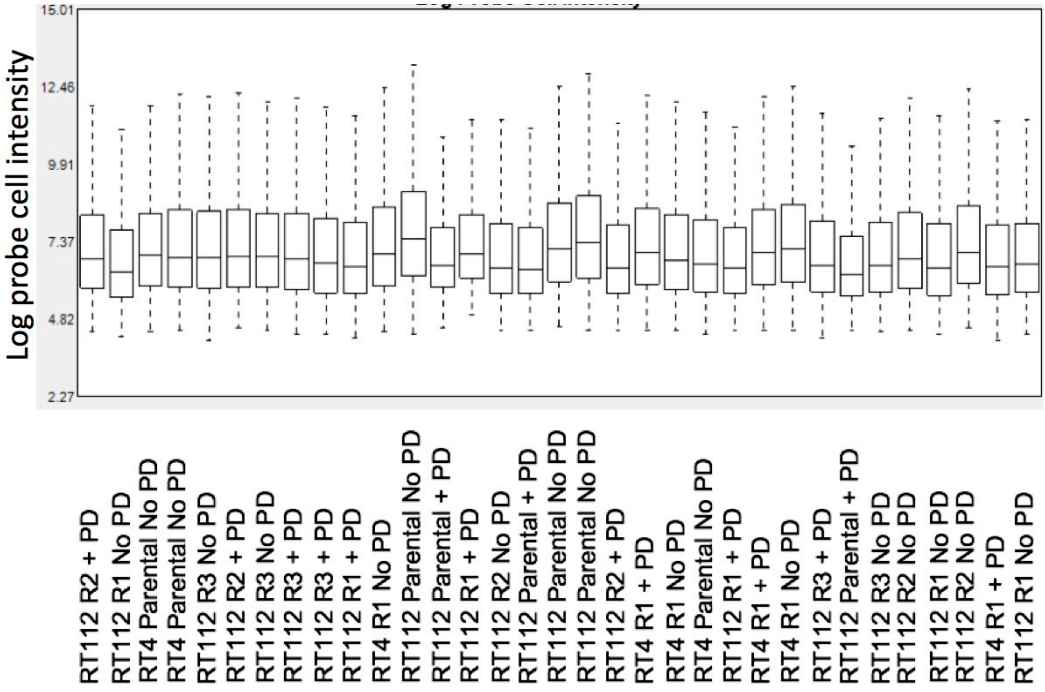

Figure D.4 Log probe cell intensity. The log probe cell intensity box plot shows the intensity of the signal from each array. As data normalisation is yet to be conducted, differences in signal intensity are expected. This analysis was conducted in Affymetrix Expression Console™.

To adjust for the variability in probe cell intensity data between microarray samples, Signal Space Transformation-Robust Multichip Average (SST-RMA) normalisation was conducted using the raw data from the CEL files generating CHP files. SST removes significant fold-change compression and RMA minimises probe variance (Irizarry *et al.*, 2003). After normalisation, CHP file summarized probe set signal values have a reduced variability compared to the probe cell intensity values of microarray samples measured from CEL files (Fig. D.5). This indicates that the data normalisation was successful and array samples can now be compared.

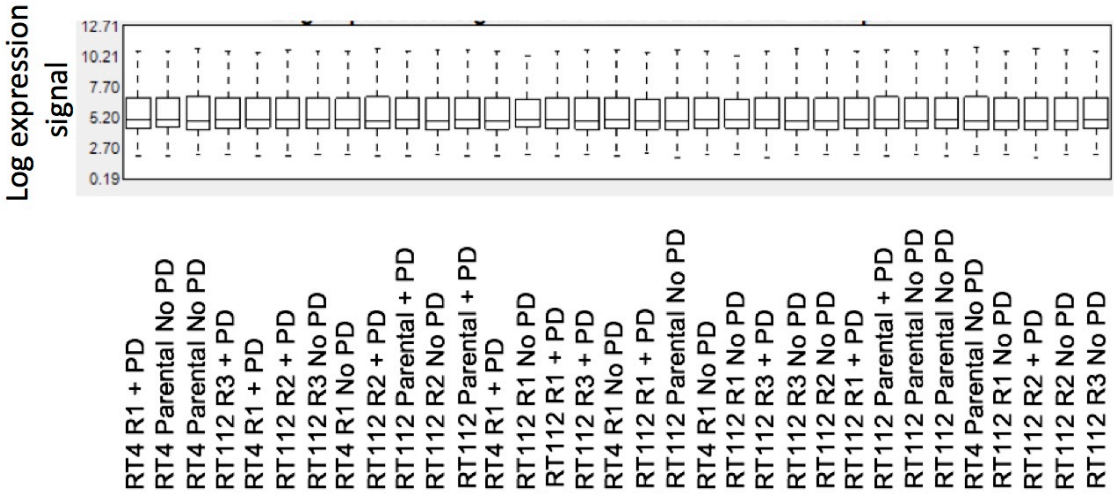

Figure D.5 Log expression signal of CHP files generated from the CEL files through SST-RMA normalisation. This box plot shows the signal intensity of each array following the SST-RMA normalisation and therefore differences in signal intensities between arrays should not be present. This analysis was conducted in Affymetrix Expression Console™.

D.3 Supplementary expression analysis

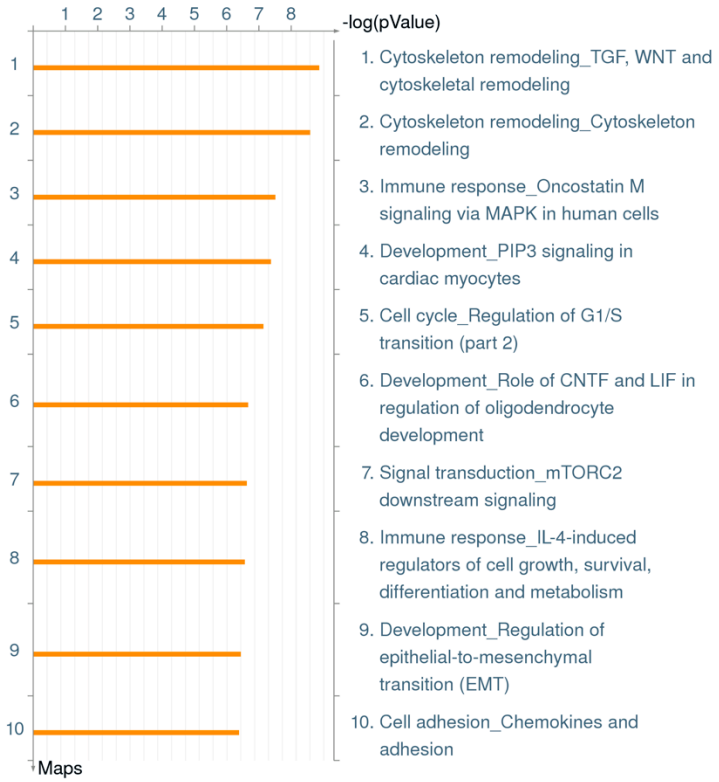

Figure D.6 The 10 most significantly differentially expressed pathway maps between RT112 R1 no PD and parental + PD according to MetaCore™.

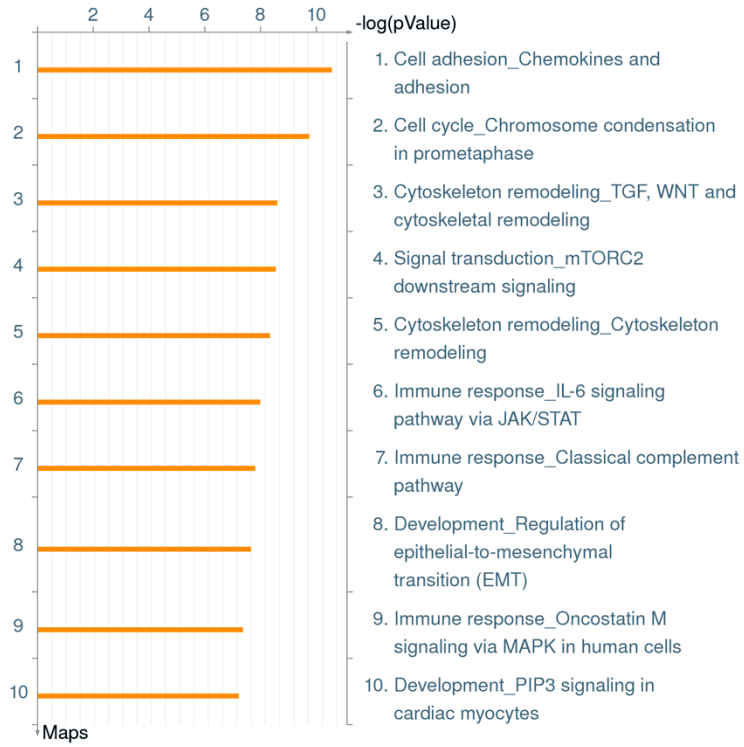

Figure D.7 The 10 most significantly differentially expressed pathway maps between RT112 R2 no PD and parental + PD according to MetaCore™.

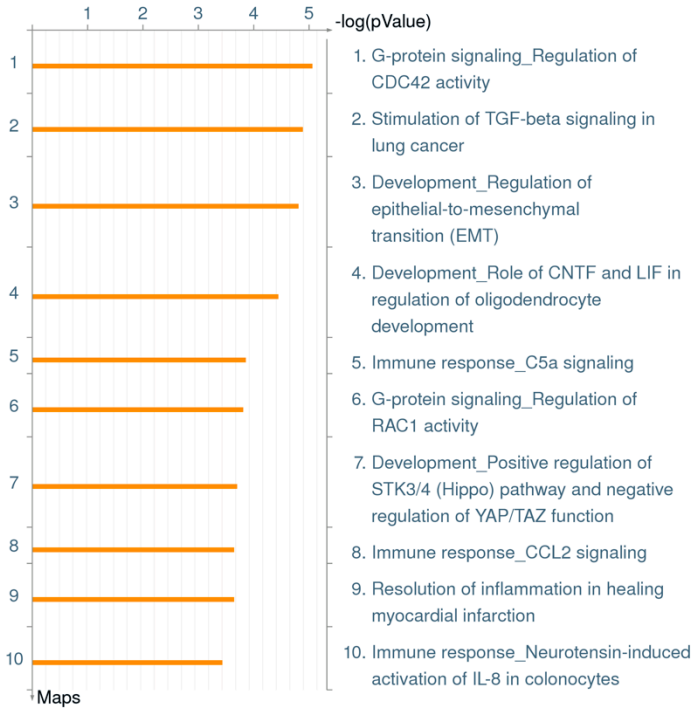

Figure D.8 The 10 most significantly differentially expressed pathway maps between RT112 R3 no PD and parental + PD according to MetaCore™.

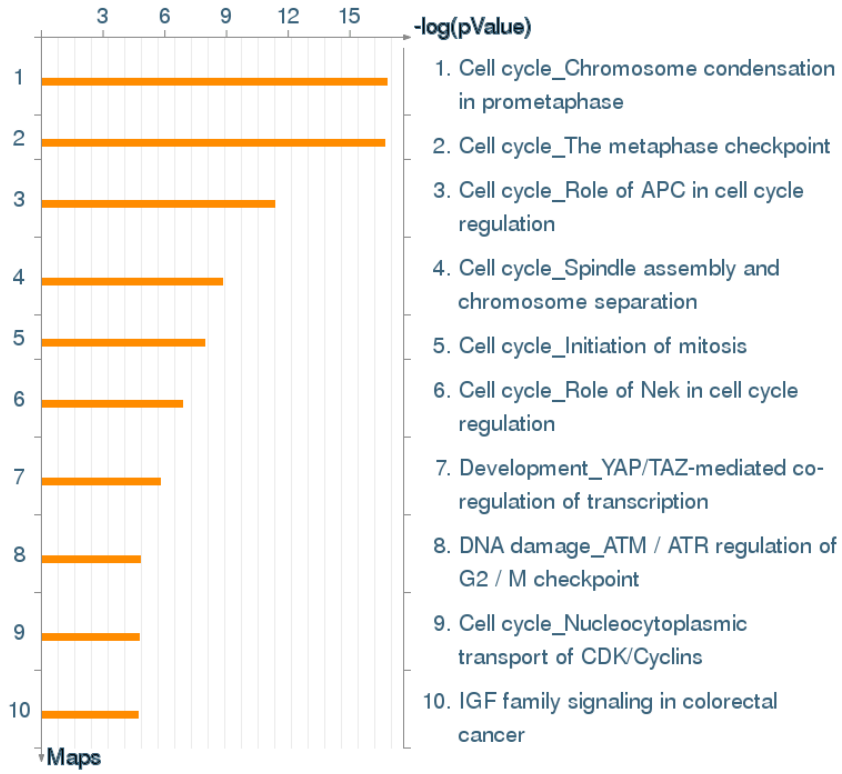

Figure D.9 The 10 most significantly differentially expressed pathway maps between RT4 R1 + PD vs R1 no PD according to MetaCore™.

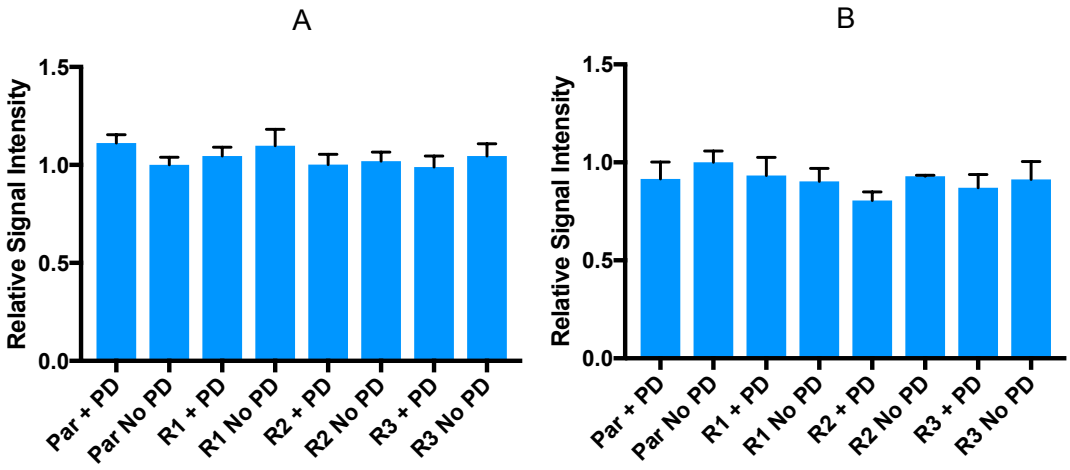

Figure D.10 Expression of *OSM* and *IL31* in RT112 determined by microarray analysis. A) *OSM* B) *IL31*. Error bars indicate standard error of the mean. Signal intensity is given relative to parental no PD. *OSM* and *IL31* were not differentially expressed in any experimental conditions compared to parental no PD (ANOVA $p<0.05$, 2-fold expression change).

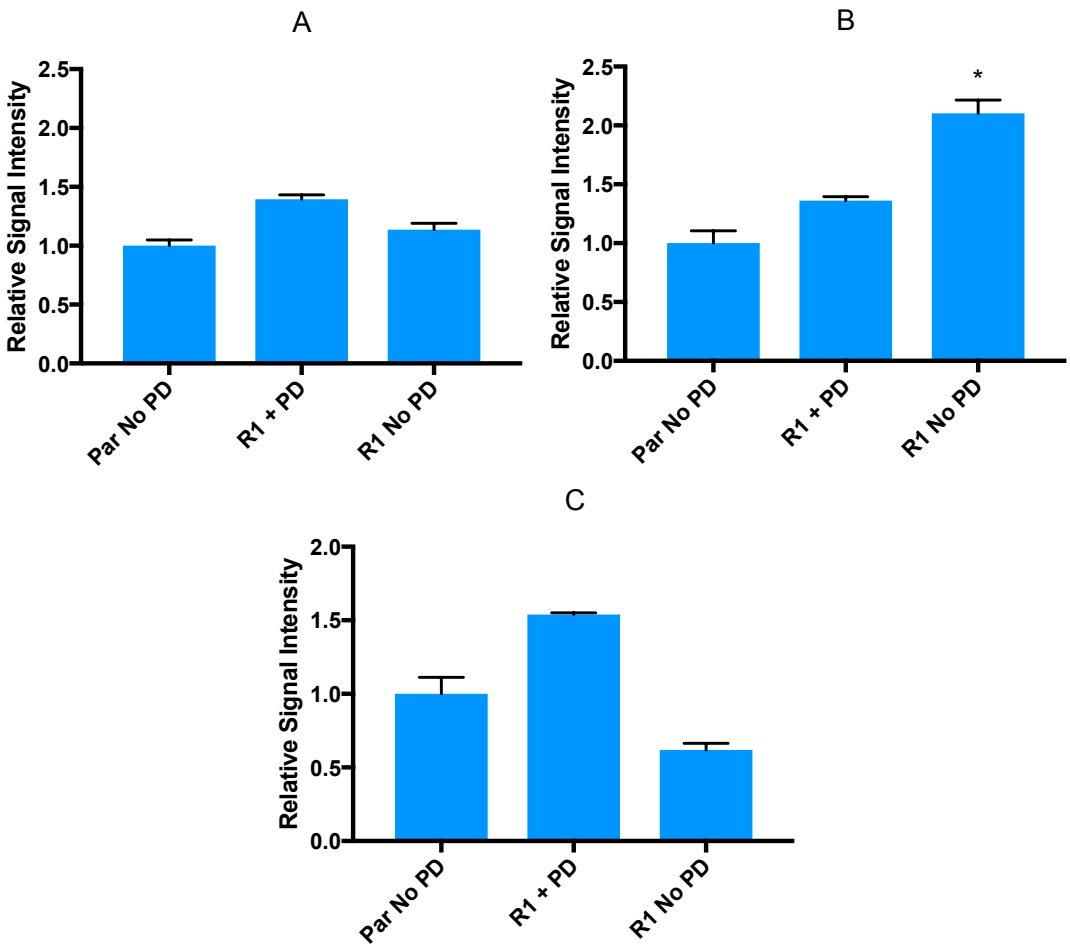

Figure D.11 Expression of *IL6ST*, *OSMR* and *LIFR* in RT4 determined by microarray analysis. A) *IL6ST.* B) *OSMR.* C) *LIFR*. Error bars indicate standard error of the mean. Signal intensity is given relative to RT112 no PD. Asterisks indicate the experimental conditions in which *IL6ST*, *OSMR* or *LIFR* were differentially expressed compared to parental no PD (ANOVA $p<0.05$, 2-fold expression change).

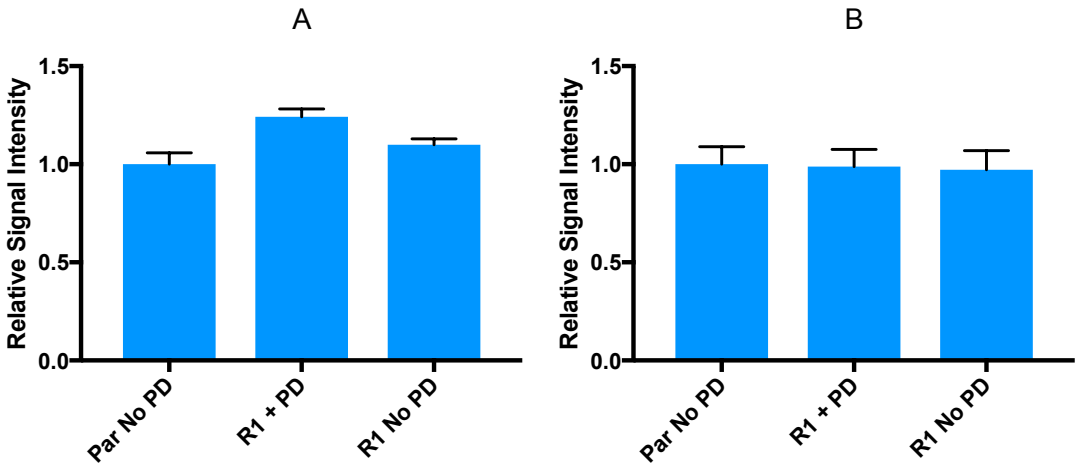

Figure D.12 Expression of *OSM* and *IL31* in RT4 determined by microarray analysis. Error bars indicate standard error of the mean. A) *OSM.* B) *IL31*. Signal intensity is given relative to parental no PD. *OSM* and *IL31* were not differentially expressed in any experimental conditions compared to parental no PD (ANOVA $p<0.05$, 2-fold expression change).

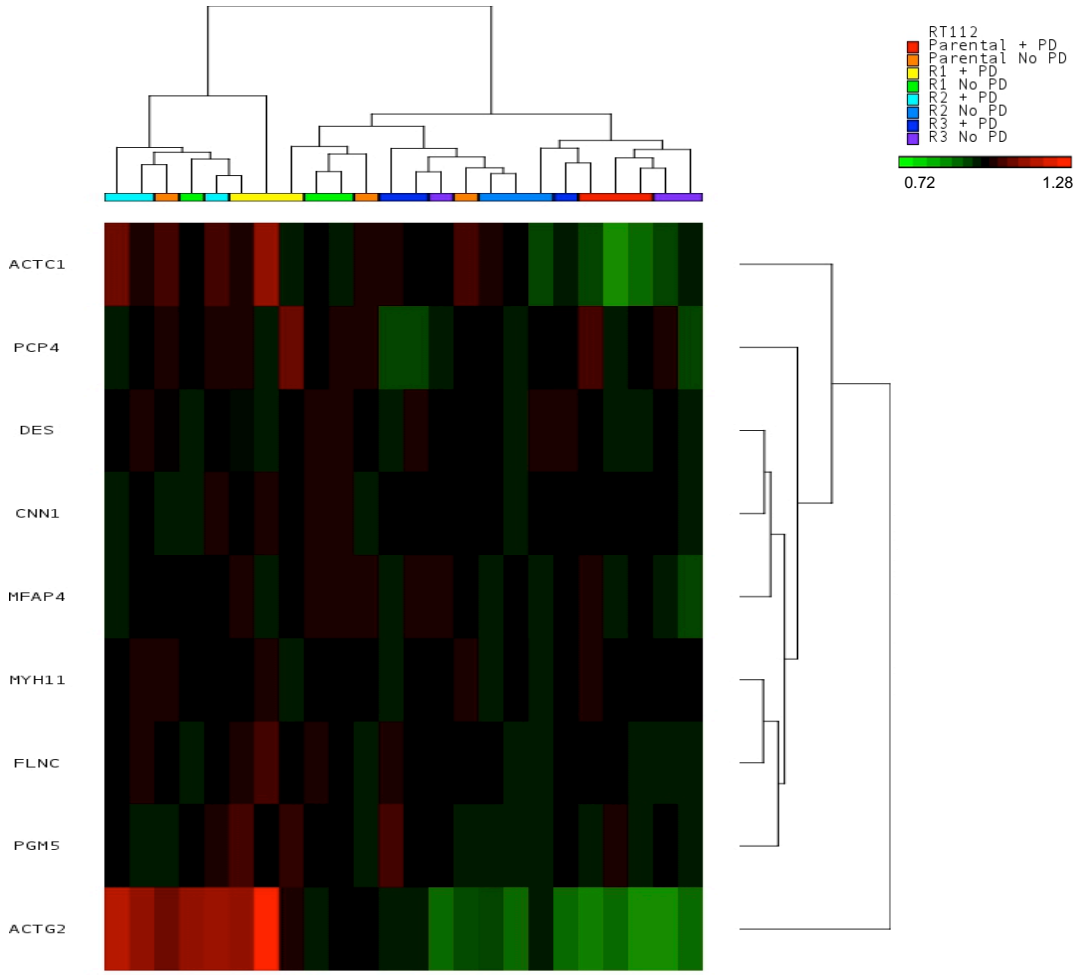

Figure D.13 Unsupervised hierarchical cluster analysis of Choi *et al.* cohort of p53-like markers in RT112 microarray samples. The Log_2 gene expression was normalised by dividing each expression value by the probe's mean Log_2 gene expression. Following Log2 gene expression normalisation, the expression profiles of samples and genes were clustered in Partek® Genomics Suite® 6.6 using Euclidean distance and complete linkage. Scale bar indicates the normalised Log_2 gene expression with colour depicting the level of gene expression as high (red), intermediate (black) and low (green).

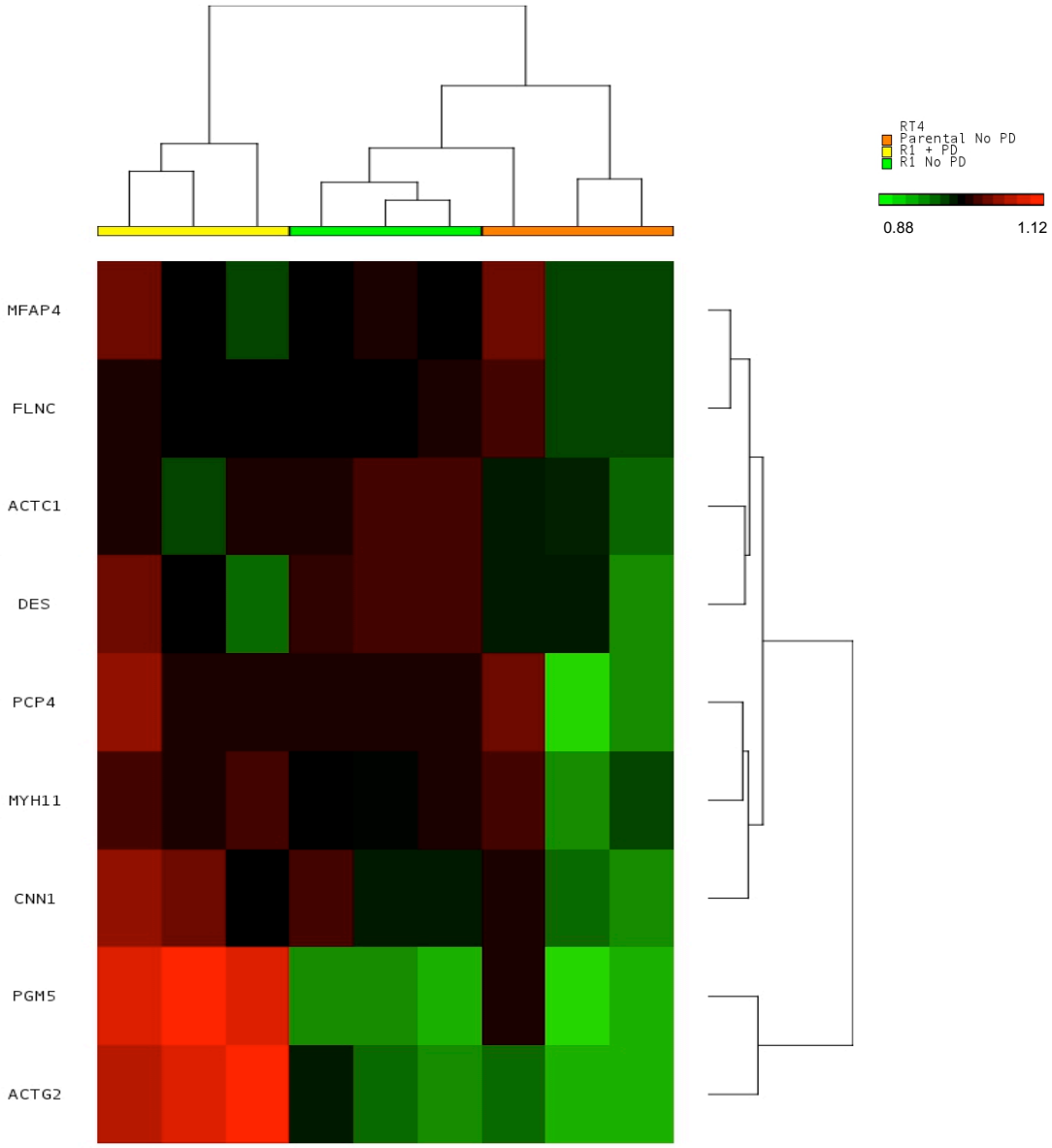

Figure D.14 Unsupervised hierarchical cluster analysis of Choi *et al.* cohort of p53-like markers in RT4 microarray samples. The Log_2 gene expression was normalised by dividing each expression value by the probe's mean Log_2 gene expression. Following Log_2 gene expression normalisation, the expression profiles of samples and genes were clustered in Partek® Genomics Suite® 6.6 using Euclidean distance and complete linkage. Scale bar indicates the normalised Log_2 gene expression with colour depicting the level of gene expression as high (red), intermediate (black) and low (green).

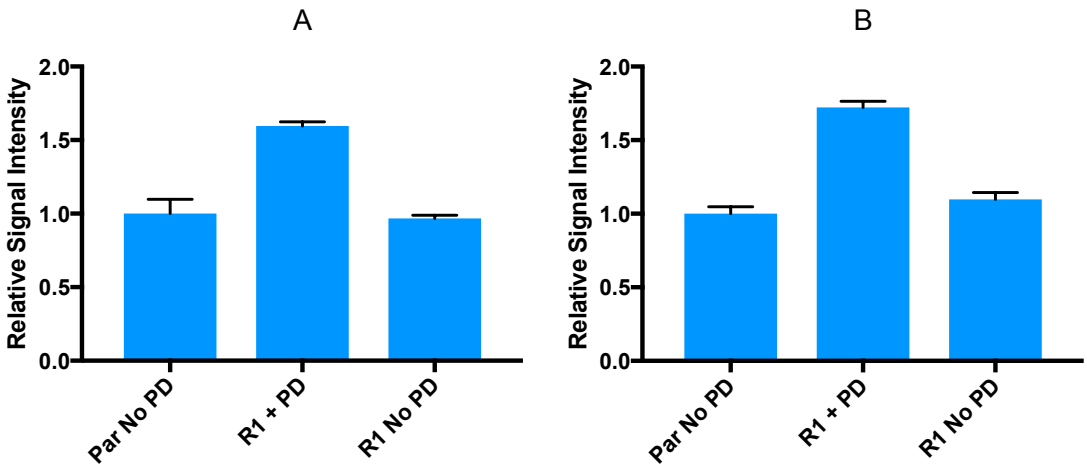

Figure D.15 Expression of *PGM5* and *ACTG2* in RT4 determined by microarray analysis. A) *PGM5.* B) *ACTG2.* Error bars indicate standard error of the mean. Signal intensity is given relative to parental no PD. Asterisks indicate the experimental conditions in which *PGM5* and *ACTG2* were differentially expressed compared to parental no PD (ANOVA p<0.05, 2-fold expression change).

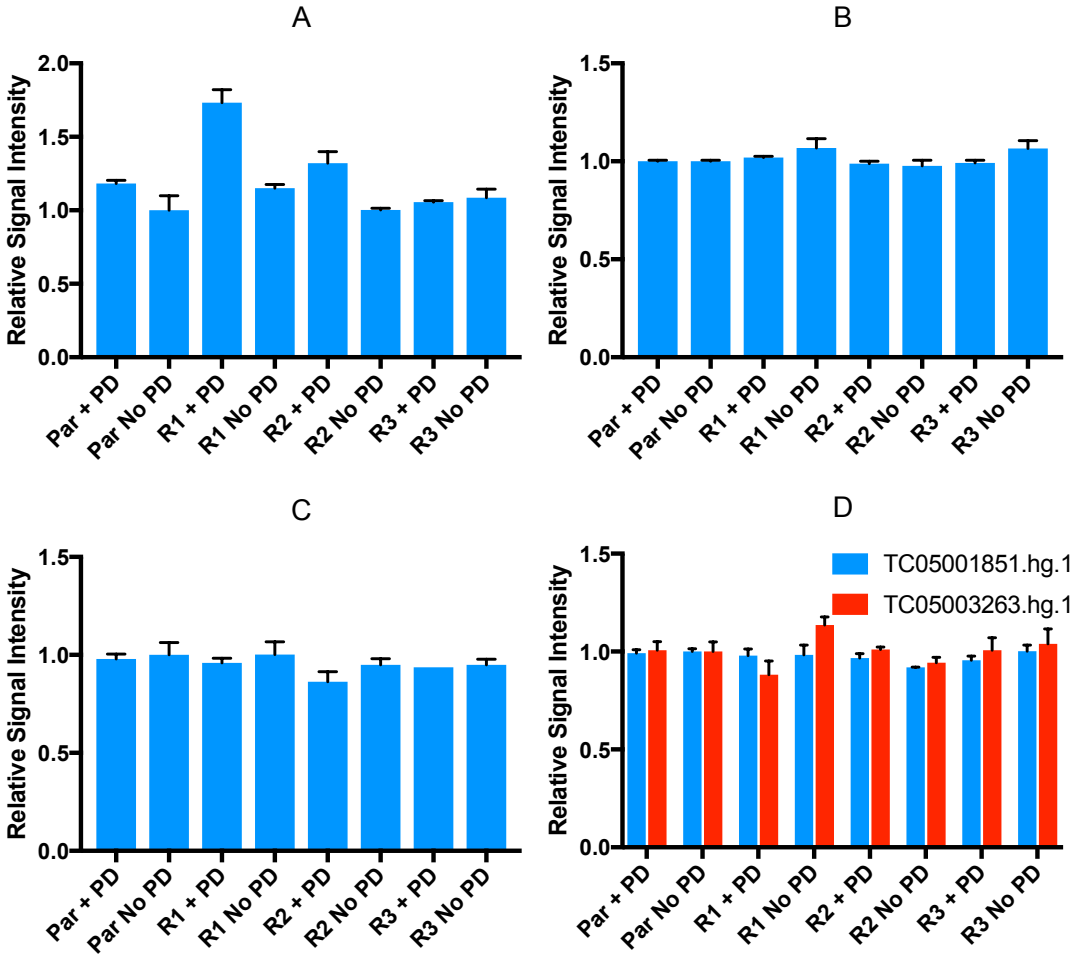

Figure D.16 Expression of *IGF1*, *HGF, EREG* and NRG2 in RT112 determined by microarray analysis. A) *IGF1.* B) *HGF.* C) *EREG*. D) *NRG2*. Error bars indicate standard error of the mean. Signal intensity is given relative to RT112 no PD. Asterisks indicate the experimental conditions in which genes were significantly differentially expressed compared to parental no PD (ANOVA p<0.05, 2-fold expression change). For genes with specificity to more than one probe, the data generated from each probe is shown separately with a legend indicating the probe's Affymetrix IDs.

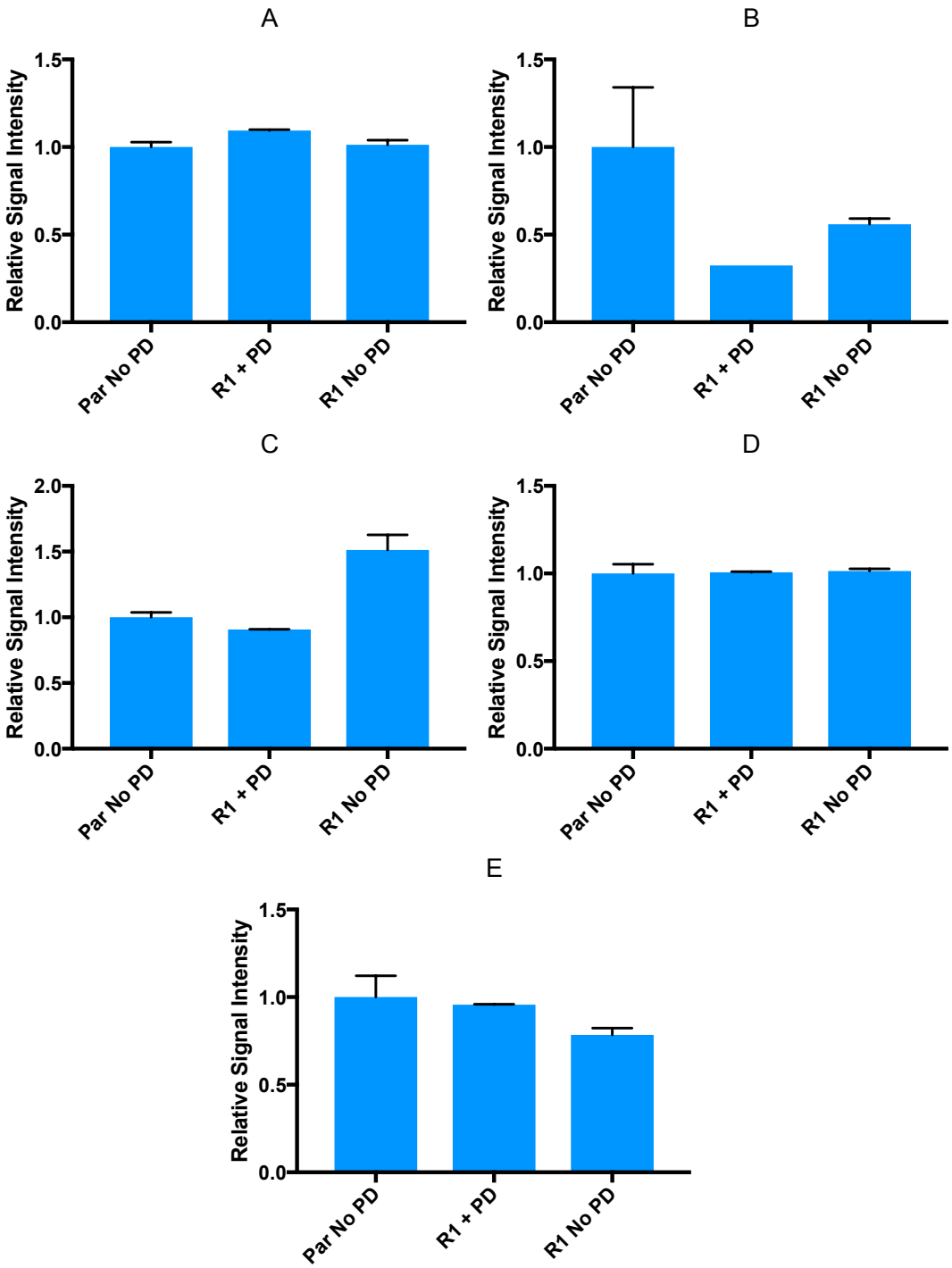

Figure D.17 Expression of *EREG*, *HBEGF, EGF, NRG2* and *EPGN* in RT4 determined by microarray analysis. A) *EREG.* B) *HBEGF.* C) *EGF*. D) *NRG2*. E) *EPGN*. Error bars indicate standard error of the mean. Error bars are absent where the standard error of the mean was too small to plot. Signal intensity is given relative to RT4 no PD. Asterisks indicate the experimental conditions in which genes were significantly differentially expressed compared to parental no PD (ANOVA $p<0.05$, 2-fold expression change).

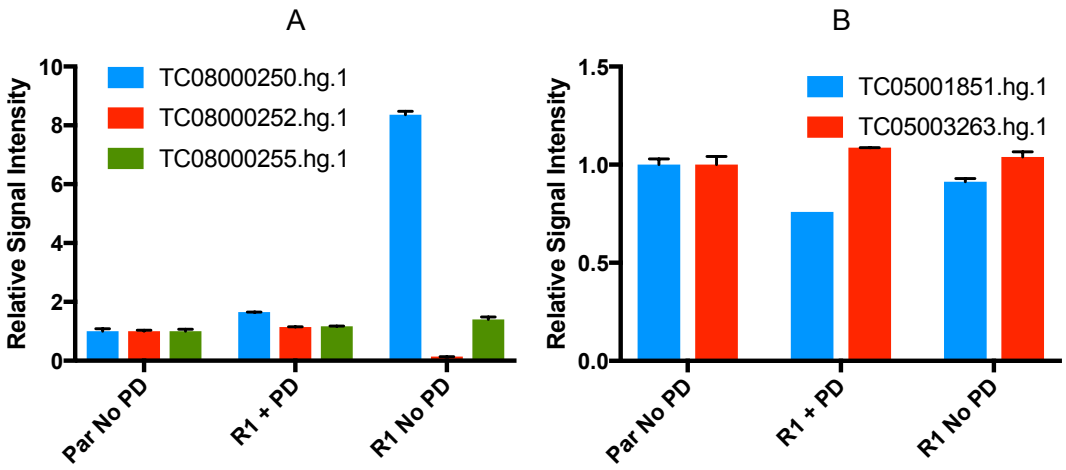

Figure D.18 Expression of *NRG1* and *NRG2* in RT4 determined by microarray analysis. A) *NRG1.* B) *NRG2.* Error bars indicate standard error of the mean. Error bars are absent where the standard error of the mean was too small to plot. Signal intensity is given relative to RT4 no PD. Asterisks indicate the experimental conditions in which genes were significantly differentially expressed compared to parental no PD (ANOVA $p<0.05$, 2-fold expression change). For genes with specificity to more than one probe, the data generated from each probe is shown separately with a legend indicating the probe's affymetrix IDs.

List of References

Ahmadian, M. R., Zor, T., Vogt, D., Kabsch, W., Selinger, Z., Wittinghofer, A., and Scheffzek, K. (1999). Guanosine triphosphatase stimulation of oncogenic Ras mutants. Proceedings of the National Academy of Sciences of the United States of America *96*, 7065-7070.

Akhavan, D., Pourzia, A. L., Nourian, A. A., Williams, K. J., Nathanson, D., Babic, I., Villa, G. R., Tanaka, K., Nael, A., Yang, H.*, et al.* (2013). De-repression of PDGFRbeta transcription promotes acquired resistance to EGFR tyrosine kinase inhibitors in glioblastoma patients. Cancer Discovery *3*, 534-547.

Allory, Y., Beukers, W., Sagrera, A., Flandez, M., Marques, M., Marquez, M., van der Keur, K. A., Dyrskjot, L., Lurkin, I., Vermeij, M.*, et al.* (2014). Telomerase reverse transcriptase promoter mutations in bladder cancer: high frequency across stages, detection in urine, and lack of association with outcome. European Urology *65*, 360-366.

Alves, C. C., Carneiro, F., Hoefler, H., and Becker, K. F. (2009). Role of the epithelial-mesenchymal transition regulator Slug in primary human cancers. Frontiers in Bioscience *14*, 3035-3050.

Amado, R. G., Wolf, M., Peeters, M., Van Cutsem, E., Siena, S., Freeman, D. J., Juan, T., Sikorski, R., Suggs, S., Radinsky, R.*, et al.* (2008). Wild-type KRAS is required for panitumumab efficacy in patients with metastatic colorectal cancer. Journal of Clinical Oncology *26*, 1626-1634.

André, F., O'Regan, R., Ozguroglu, M., Toi, M., Xu, B., Jerusalem, G., Masuda, N., Wilks, S., Arena, F., Isaacs, C.*, et al.* (2014). Everolimus for women with trastuzumab-resistant, HER2-positive, advanced breast cancer (BOLERO-3): a randomised, double-blind, placebo-controlled phase 3 trial. The Lancet Oncology *15*, 580-591.

Anido, J., Scaltriti, M., Bech Serra, J. J., Josefat, B. S., Rojo Todo, F., Baselga, J., and Arribas, J. (2006). Biosynthesis of tumorigenic HER2 C-terminal fragments by alternative initiation of translation. EMBO Journal *25*, 3234-3244.

Aquila, L., Ohm, J., and Woloszynska-Read, A. (2018). The role of STAG2 in bladder cancer. Pharmacological Research. *131*, 143-149

Arkenau, H.-T., Saggese, M., Hollebecque, A., Mathewson, A., Lemech, C. R., Landers, D., Frewer, P., Kilgour, E., and Brooks, N. (2014). A phase 1 expansion cohort of the fibroblast growth factor receptor (FGFR) inhibitor AZD4547 in patients (pts) with advanced gastric (GC) and gastroesophageal (GOJ) cancer. Journal of Clinical Oncology *32*, 2620-2620.

Arribas, J., Baselga, J., Pedersen, K., and Parra-Palau, J. L. (2011). p95HER2 and Breast Cancer. Cancer Research *71*, 1515-1519.

Askham, J. M., Platt, F., Chambers, P. A., Snowden, H., Taylor, C. F., and Knowles, M. A. (2010). AKT1 mutations in bladder cancer:

identification of a novel oncogenic mutation that can co-operate with E17K. Oncogene *29*, 150-155.

Atreya, C. E., Cutsem, E. V., Bendell, J. C., Andre, T., Schellens, J. H. M., Gordon, M. S., McRee, A. J., O'Dwyer, P. J., Muro, K., Tabernero, J.*, et al.* (2015). Updated efficacy of the MEK inhibitor trametinib (T), BRAF inhibitor dabrafenib (D), and anti-EGFR antibody panitumumab (P) in patients (pts) with BRAF V600E mutated (BRAFm) metastatic colorectal cancer (mCRC). Journal of Clinical Oncology *33*, 103-103.

Aveyard, J. S., and Knowles, M. A. (2004). Measurement of Relative Copy Number of CDKN2A/ARF and CDKN2B in Bladder Cancer by Real-Time Quantitative PCR and Multiplex Ligation-Dependent Probe Amplification. The Journal of Molecular Diagnostics *6*, 356-365.

Aveyard, J. S., Skilleter, A., Habuchi, T., and Knowles, M. A. (1999). Somatic mutation of PTEN in bladder carcinoma. British Journal of Cancer *80*, 904-908.

Azuma, K., Kawahara, A., Sonoda, K., Nakashima, K., Tashiro, K., Watari, K., Izumi, H., Kage, M., Kuwano, M., Ono, M., and Hoshino, T. (2014). FGFR1 activation is an escape mechanism in human lung cancer cells resistant to afatinib, a pan-EGFR family kinase inhibitor. Oncotarget *5*, 5908-5919.

Babjuk, M., Böhle, A., Burger, M., Capoun, O., Cohen, D., Compérat, E. M., Hernández, V., Kaasinen, E., Palou, J., Rouprêt, M.*, et al.* (2016). EAU Guidelines on Non–Muscle-invasive Urothelial Carcinoma of the Bladder: Update 2016. European Urology. *71*, 447-461

Bahrami, A., Hassanian, S. M., ShahidSales, S., Farjami, Z., Hasanzadeh, M., Anvari, K., Aledavood, A., Maftouh, M., Ferns, G. A., Khazaei, M., and Avan, A. (2018). Targeting RAS signaling pathway as a potential therapeutic target in the treatment of colorectal cancer. Journal of Cellular Physiology *233*, 2058-2066.

Balak, M. N., Gong, Y., Riely, G. J., Somwar, R., Li, A. R., Zakowski, M. F., Chiang, A., Yang, G., Ouerfelli, O., Kris, M. G.*, et al.* (2006). Novel D761Y and common secondary T790M mutations in epidermal growth factor receptor-mutant lung adenocarcinomas with acquired resistance to kinase inhibitors. Clinical Cancer Research *12*, 6494-6501.

Balbás-Martínez, C., Sagrera, A., Carrillo-de-Santa-Pau, E., Earl, J., Márquez, M., Vazquez, M., Lapi, E., Castro-Giner, F., Beltran, S., Bayés, M.*, et al.* (2013). Recurrent inactivation of STAG2 in bladder cancer is not associated with aneuploidy. Nature Genetics *45*, 1464-1469.

Bartley, A. N., Washington, M. K., Ventura, C. B., Ismaila, N., Colasacco, C., Benson, A. B., 3rd, Carrato, A., Gulley, M. L., Jain, D., Kakar, S.*, et al.* (2016). HER2 Testing and Clinical Decision Making in Gastroesophageal Adenocarcinoma: Guideline From the College of American Pathologists, American Society for Clinical Pathology, and American Society of Clinical Oncology. American Journal of Clinical Pathology *146*, 647-669.

Bauer, S., Hilger, R. A., Mühlenberg, T., Grabellus, F., Nagarajah, J., Hoiczyk, M., Reichardt, A., Ahrens, M., Reichardt, P., Grunewald, S.*, et al.* (2014). Phase I study of panobinostat and imatinib in patients

with treatment-refractory metastatic gastrointestinal stromal tumors. British Journal of Cancer *110*, 1155-1162.

Bean, J., Riely, G. J., Balak, M., Marks, J. L., Ladanyi, M., Miller, V. A., and Pao, W. (2008). Acquired resistance to epidermal growth factor receptor kinase inhibitors associated with a novel T854A mutation in a patient with EGFR-mutant lung adenocarcinoma. Clinical Cancer Research *14*, 7519-7525.

Bekaii-Saab, T., Williams, N., Plass, C., Calero, M. V., and Eng, C. (2006). A novel mutation in the tyrosine kinase domain of ERBB2 in hepatocellular carcinoma. BMC Cancer *6*, 278.

Bell, R. J. A., Rube, H. T., Kreig, A., Mancini, A., Fouse, S. D., Nagarajan, R. P., Choi, S., Hong, C., He, D., Pekmezci, M.*, et al.* (2015). The transcription factor GABP selectively binds and activates the mutant TERT promoter in cancer. Science *348*, 1036-1039.

Bellmunt, J., de Wit, R., Vaughn, D. J., Fradet, Y., Lee, J. L., Fong, L., Vogelzang, N. J., Climent, M. A., Petrylak, D. P., Choueiri, T. K.*, et al.* (2017). Pembrolizumab as Second-Line Therapy for Advanced Urothelial Carcinoma. The New England Journal of Medicine *376*, 1015-1026.

Bellmunt, J., Werner, L., Bamias, A., Fay, A. P., Park, R. S., Riester, M., Selvarajah, S., Barletta, J. A., Berman, D. M., de Muga, S.*, et al.* (2015). HER2 as a target in invasive urothelial carcinoma. Cancer Medicine *4*, 844-852.

Belov, A. A., and Mohammadi, M. (2013). Molecular Mechanisms of Fibroblast Growth Factor Signaling in Physiology and Pathology. Cold Spring Harbor Perspectives in Biology *5*. a015958

Benevolenskaya, E. V., Murray, H. L., Branton, P., Young, R. A., and Kaelin, W. G., Jr. (2005). Binding of pRB to the PHD protein RBP2 promotes cellular differentiation. Molecular Cell *18*, 623-635.

Bernard-Pierrot, I., Brams, A., Dunois-Lardé, C., Caillault, A., Diez de Medina, S. G., Cappellen, D., Graff, G., Thiery, J. P., Chopin, D., Ricol, D., and Radvanyi, F. (2006). Oncogenic properties of the mutated forms of fibroblast growth factor receptor 3b. Carcinogenesis *27*, 740-747.

Bianco, R., Rosa, R., Damiano, V., Daniele, G., Gelardi, T., Garofalo, S., Tarallo, V., De Falco, S., Melisi, D., Benelli, R.*, et al.* (2008). Vascular endothelial growth factor receptor-1 contributes to resistance to anti-epidermal growth factor receptor drugs in human cancer cells. Clinical Cancer Research *14*, 5069-5080.

Bock, M., Hinley, J., Schmitt, C., Wahlicht, T., Kramer, S., and Southgate, J. (2014). Identification of ELF3 as an early transcriptional regulator of human urothelium. Developmental Biology *386*, 321-330.

Bockorny, B., Rusan, M., Chen, W., Liao, R. G., Li, Y., Piccioni, F., Wang, J., Tan, L., Thorner, A. R., Li, T.*, et al.* (2018). RAS-MAPK reactivation facilitates acquired resistance in FGFR1-amplified lung cancer and underlies a rationale for upfront FGFR-MEK blockade. Molecular Cancer Therapeutics. *18*, 623-635

Boleij, A., Tack, V., Taylor, A., Kafatos, G., Jenkins-Anderson, S., Tembuyser, L., Dequeker, E., and van Krieken, J. H. (2016). RAS testing practices and RAS mutation prevalence among patients with

metastatic colorectal cancer: results from a Europe-wide survey of pathology centres. BMC Cancer *16*, 825.

Booth, D. G., Hood, F. E., Prior, I. A., and Royle, S. J. (2011). A TACC3/ch-TOG/clathrin complex stabilises kinetochore fibres by inter-microtubule bridging. The EMBO Journal *30*, 906-919.

Borah, S., Xi, L., Zaug, A. J., Powell, N. M., Dancik, G. M., Cohen, S., Costello, J. C., Theodorescu, D., and Cech, T. R. (2015). TERT promoter mutations and telomerase reactivation in urothelial cancer. Science *347*, 1006-1010.

Bose, R., Kavuri, S. M., Searleman, A. C., Shen, W., Shen, D., Koboldt, D. C., Monsey, J., Goel, N., Aronson, A. B., Li, S.*, et al.* (2013). Activating HER2 mutations in HER2 gene amplification negative breast cancer. Cancer Discovery *3*, 224-237.

Böttcher, R. T., and Niehrs, C. (2005). Fibroblast Growth Factor Signaling during Early Vertebrate Development. Endocrine Reviews *26*, 63-77.

Brown, W. S., Akhand, S. S., and Wendt, M. K. (2016). FGFR signaling maintains a drug persistent cell population following epithelial-mesenchymal transition. Oncotarget *7*, 83424-83436.

Bryan, R. T., Evans, T., Dunn, J. A., Iqbal, G., Bathers, S., Collins, S. I., James, N. D., Catto, J. W. F., and Wallace, D. M. A. (2015). A Comparative Analysis of the Influence of Gender, Pathway Delays, and Risk Factor Exposures on the Long-term Outcomes of Bladder Cancer. European Urology Focus *1*, 82-89.

Budhidarmo, R., Nakatani, Y., and Day, C. L. (2012). RINGs hold the key to ubiquitin transfer. Trends in Biochemical Sciences *37*, 58-65.

Burgaud, J.-L., and Baserga, R. (1996). Intracellular Transactivation of the Insulin-like Growth Factor I Receptor by an Epidermal Growth Factor Receptor. Experimental Cell Research *223*, 412-419.

Byron, S. A., Chen, H., Wortmann, A., Loch, D., Gartside, M. G., Dehkhoda, F., Blais, S. P., Neubert, T. A., Mohammadi, M., and Pollock, P. M. (2013). The N550K/H Mutations in FGFR2 Confer Differential Resistance to PD173074, Dovitinib, and Ponatinib ATP-Competitive Inhibitors. Neoplasia *15*, 975-988.

Cairns, P., Evron, E., Okami, K., Halachmi, N., Esteller, M., Herman, J. G., Bose, S., Wang, S. I., Parsons, R., and Sidransky, D. (1998). Point mutation and homozygous deletion of PTEN/MMAC1 in primary bladder cancers. Oncogene *16*, 3215-3218.

Canfield, K., Li, J., Wilkins, O. M., Morrison, M. M., Ung, M., Wells, W., Williams, C. R., Liby, K. T., Vullhorst, D., Buonanno, A.*, et al.* (2015). Receptor tyrosine kinase ERBB4 mediates acquired resistance to ERBB2 inhibitors in breast cancer cells. Cell Cycle *14*, 648-655.

Cappellen, D., De Oliveira, C., Ricol, D., de Medina, S., Bourdin, J., Sastre-Garau, X., Chopin, D., Thiery, J. P., and Radvanyi, F. (1999). Frequent activating mutations of FGFR3 in human bladder and cervix carcinomas. Nature Genetics *23*, 18-20.

Castellano, E., and Downward, J. (2011). RAS Interaction with PI3K: More Than Just Another Effector Pathway. Genes and Cancer *2*, 261-274.

Chakrabarti, R., Hwang, J., Blanco, M. A., Wei, Y., Lukačišin, M., Romano, R.-A., Smalley, K., Liu, S., Yang, Q., Ibrahim, T.*, et al.* (2012). Elf5 inhibits epithelial mesenchymal transition in mammary gland

development and breast cancer metastasis by transcriptionally repressing Snail2/Slug. Nature Cell Biology *14*, 1212-1222.

Chang, Z. G., Wei, J. M., Qin, C. F., Hao, K., Tian, X. D., Xie, K., Xie, X. H., and Yang, Y. M. (2012). Suppression of the epidermal growth factor receptor inhibits epithelial-mesenchymal transition in human pancreatic cancer PANC-1 cells. Digestive Diseases and Sciences *57*, 1181-1189.

Chantranupong, L., Wolfson, R. L., Orozco, J. M., Saxton, R. A., Scaria, S. M., Bar-Peled, L., Spooner, E., Isasa, M., Gygi, S. P., and Sabatini, D. M. (2014). The Sestrins interact with GATOR2 to negatively regulate the amino acid sensing pathway upstream of mTORC1. Cell Reports *9*, 1-8.

Chapman, P. B., Hauschild, A., Robert, C., Haanen, J. B., Ascierto, P., Larkin, J., Dummer, R., Garbe, C., Testori, A., Maio, M.*, et al.* (2011). Improved survival with vemurafenib in melanoma with BRAF V600E mutation. The New England Journal of Medicine *364*, 2507-2516.

Chell, V., Balmanno, K., Little, A. S., Wilson, M., Andrews, S., Blockley, L., Hampson, M., Gavine, P. R., and Cook, S. J. (2013). Tumour cell responses to new fibroblast growth factor receptor tyrosine kinase inhibitors and identification of a gatekeeper mutation in FGFR3 as a mechanism of acquired resistance. Oncogene *32*, 3059-3070.

Chellaiah, A. T., McEwen, D. G., Werner, S., Xu, J., and Ornitz, D. M. (1994). Fibroblast growth factor receptor (FGFR) 3. Alternative splicing in immunoglobulin-like domain III creates a receptor highly specific for acidic FGF/FGF-1. Journal of Biological Chemistry *269*, 11620-11627.

Chen, R., and Chen, B. (2015). The role of dasatinib in the management of chronic myeloid leukemia. Drug Design, Development and Therapy *9*, 773-779.

Cheng, H. L., Trink, B., Tzai, T. S., Liu, H. S., Chan, S. H., Ho, C. L., Sidransky, D., and Chow, N. H. (2002). Overexpression of c-met as a prognostic indicator for transitional cell carcinoma of the urinary bladder: a comparison with p53 nuclear accumulation. Journal of Clinical Oncology *20*, 1544-1550.

Cheng, L., Montironi, R., Davidson, D. D., and Lopez-Beltran, A. (2009). Staging and reporting of urothelial carcinoma of the urinary bladder. Modern Pathology *22*, S70-95.

Cheng, T., Roth, B., Choi, W., Black, P. C., Dinney, C., and McConkey, D. J. (2013). Fibroblast growth factor receptors-1 and -3 play distinct roles in the regulation of bladder cancer growth and metastasis: implications for therapeutic targeting. PLoS ONE *8*, e57284.

Cheng, Y., and Tian, H. (2017). Current Development Status of MEK Inhibitors. Molecules *22*, 1551.

Chesi, M., Nardini, E., Brents, L. A., Schröck, E., Ried, T., Kuehl, W. M., and Bergsagel, P. L. (1997). Frequent translocation t(4;14)(p16.3;q32.3) in multiple myeloma is associated with increased expression and activating mutations of fibroblast growth factor receptor 3. Nature Genetics *16*, 260-264.

Choi, D.-K., Bae, J., Shin, S.-M., Shin, J.-Y., Kim, S., and Kim, Y.-S. (2014a). A general strategy for generating intact, full-length IgG

antibodies that penetrate into the cytosol of living cells. mAbs *6*, 1402-1414.

Choi, W., Porten, S., Kim, S., Willis, D., Plimack, Elizabeth R., Hoffman-Censits, J., Roth, B., Cheng, T., Tran, M., Lee, I. L.*, et al.* (2014b). Identification of Distinct Basal and Luminal Subtypes of Muscle-Invasive Bladder Cancer with Different Sensitivities to Frontline Chemotherapy. Cancer Cell *25*, 152-165.

Choudhury, N. J., Campanile, A., Antic, T., Yap, K. L., Fitzpatrick, C. A., Wade, J. L., 3rd, Karrison, T., Stadler, W. M., Nakamura, Y., and O'Donnell, P. H. (2016). Afatinib Activity in Platinum-Refractory Metastatic Urothelial Carcinoma in Patients With ERBB Alterations. Journal of Clinical Oncology *34*, 2165-2171.

Choy, E., Chiu, V. K., Silletti, J., Feoktistov, M., Morimoto, T., Michaelson, D., Ivanov, I. E., and Philips, M. R. (1999). Endomembrane trafficking of ras: the CAAX motif targets proteins to the ER and Golgi. Cell *98*, 69-80.

Ciuleanu, T. E., Ahmed, S., Kim, J. H., Mezger, J., Park, K., Thomas, M., Chen, J., Poondru, S., VanTornout, J. M., Whitcomb, D., and Blackhall, F. (2017). Randomised Phase 2 study of maintenance linsitinib (OSI-906) in combination with erlotinib compared with placebo plus erlotinib after platinum-based chemotherapy in patients with advanced non-small cell lung cancer. British Journal of Cancer *117*, 757-766.

Codony-Servat, J., Albanell, J., Lopez-Talavera, J. C., Arribas, J., and Baselga, J. (1999). Cleavage of the HER2 ectodomain is a pervanadate-activable process that is inhibited by the tissue inhibitor of metalloproteases-1 in breast cancer cells. Cancer Research *59*, 1196-1201.

Cohen, E. E., Lingen, M. W., Martin, L. E., Harris, P. L., Brannigan, B. W., Haserlat, S. M., Okimoto, R. A., Sgroi, D. C., Dahiya, S., Muir, B.*, et al.* (2005). Response of some head and neck cancers to epidermal growth factor receptor tyrosine kinase inhibitors may be linked to mutation of ERBB2 rather than EGFR. Clinical Cancer Research *11*, 8105-8108.

Corcoran, R. B., Atreya, C. E., Falchook, G. S., Kwak, E. L., Ryan, D. P., Bendell, J. C., Hamid, O., Messersmith, W. A., Daud, A., Kurzrock, R.*, et al.* (2015). Combined BRAF and MEK Inhibition With Dabrafenib and Trametinib in BRAF V600-Mutant Colorectal Cancer. Journal of Clinical Oncology *33*, 4023-4031.

Corcoran, R. B., Ebi, H., Turke, A. B., Coffee, E. M., Nishino, M., Cogdill, A. P., Brown, R. D., Della Pelle, P., Dias-Santagata, D., Hung, K. E.*, et al.* (2012). EGFR-mediated re-activation of MAPK signaling contributes to insensitivity of BRAF mutant colorectal cancers to RAF inhibition with vemurafenib. Cancer Discovery *2*, 227-235.

Costa, D. B., Halmos, B., Kumar, A., Schumer, S. T., Huberman, M. S., Boggon, T. J., Tenen, D. G., and Kobayashi, S. (2007). BIM mediates EGFR tyrosine kinase inhibitor-induced apoptosis in lung cancers with oncogenic EGFR mutations. PLoS Medicine *4*, 1669-1679.

da Cunha Santos, G., Shepherd, F. A., and Tsao, M. S. (2011). EGFR mutations and lung cancer. Annual Review of Pathology *6*, 49-69.

Dadhania, V., Zhang, M., Zhang, L., Bondaruk, J., Majewski, T., Siefker-Radtke, A., Guo, C. C., Dinney, C., Cogdell, D. E., Zhang, S.*, et al.* (2016). Meta-Analysis of the Luminal and Basal Subtypes of Bladder Cancer and the Identification of Signature Immunohistochemical Markers for Clinical Use. EBioMedicine *12*, 105-117.

Damrauer, J. S., Hoadley, K. A., Chism, D. D., Fan, C., Tiganelli, C. J., Wobker, S. E., Yeh, J. J., Milowsky, M. I., Iyer, G., Parker, J. S., and Kim, W. Y. (2014). Intrinsic subtypes of high-grade bladder cancer reflect the hallmarks of breast cancer biology. Proceedings of the National Academy of Sciences of the United States of America *111*, 3110-3115.

Das, M., Padda, S. K., Frymoyer, A., Zhou, L., Riess, J. W., Neal, J. W., and Wakelee, H. A. (2015). Dovitinib and erlotinib in patients with metastatic non-small cell lung cancer: A drug-drug interaction. Lung Cancer *89*, 280-286.

de Martino, M., Zhuang, D., Klatte, T., Rieken, M., Rouprêt, M., Xylinas, E., Clozel, T., Krzywinski, M., Elemento, O., and Shariat, S. F. (2014). Impact of ERBB2 mutations on in vitro sensitivity of bladder cancer to lapatinib. Cancer Biology and Therapy *15*, 1239-1247.

De Roock, W., Claes, B., Bernasconi, D., De Schutter, J., Biesmans, B., Fountzilas, G., Kalogeras, K. T., Kotoula, V., Papamichael, D., Laurent-Puig, P.*, et al.* (2010). Effects of KRAS, BRAF, NRAS, and PIK3CA mutations on the efficacy of cetuximab plus chemotherapy in chemotherapy-refractory metastatic colorectal cancer: a retrospective consortium analysis. The Lancet Oncology *11*, 753-762.

Deeks, E. D. (2017). Neratinib: First Global Approval. Drugs *77*, 1695-1704.

Du, X., Wang, Q. R., Chan, E., Merchant, M., Liu, J., French, D., Ashkenazi, A., and Qing, J. (2012). FGFR3 stimulates stearoyl CoA desaturase 1 activity to promote bladder tumor growth. Cancer Research *72*, 5843-5855.

di Martino, E., Tomlinson, D. C., and Knowles, M. A. (2012). A Decade of FGF Receptor Research in Bladder Cancer: Past, Present, and Future Challenges. Advances in Urology *2012*, 429213.

di Martino, E., Tomlinson, D. C., Williams, S. V., and Knowles, M. A. (2016). A place for precision medicine in bladder cancer: targeting the FGFRs. Future Oncology *12*, 2243-2263.

Diez de Medina, S. G., Chopin, D., El Marjou, A., Delouvee, A., LaRochelle, W. J., Hoznek, A., Abbou, C., Aaronson, S. A., Thiery, J. P., and Radvanyi, F. (1997). Decreased expression of keratinocyte growth factor receptor in a subset of human transitional cell bladder carcinomas. Oncogene *14*, 323-330.

Ding, Z. M., Huang, C. J., Jiao, X. F., Wu, D., and Huo, L. J. (2017). The role of TACC3 in mitotic spindle organization. Cytoskeleton *74*, 369-378.

Dracopoli, N. C., Harnett, P., Bale, S. J., Stanger, B. Z., Tucker, M. A., Housman, D. E., and Kefford, R. F. (1989). Loss of alleles from the distal short arm of chromosome 1 occurs late in melanoma tumor progression. Proceedings of the National Academy of Sciences of the United States of America *86*, 4614-4618.

Du, X., Wang, Q. R., Chan, E., Merchant, M., Liu, J., French, D., Ashkenazi, A., and Qing, J. (2012). FGFR3 stimulates stearoyl CoA desaturase 1

activity to promote bladder tumor growth. Cancer Research *72*, 5843-5855.

Earl, J., Rico, D., Carrillo-de-Santa-Pau, E., Rodriguez-Santiago, B., Mendez-Pertuz, M., Auer, H., Gomez, G., Grossman, H. B., Pisano, D. G., Schulz, W. A.*, et al.* (2015). The UBC-40 Urothelial Bladder Cancer cell line index: a genomic resource for functional studies. BMC Genomics *16*, 403.

Eble, J. N., Sauter, G., I., E. J., and I.A., S. (2004). World Health Organization Classification of Tumours. Pathology and Genetics of Tumours of the Urinary System and Male Genital Organs. IARC Press Lyon.

Engelman, J. A., Zejnullahu, K., Mitsudomi, T., Song, Y., Hyland, C., Park, J. O., Lindeman, N., Gale, C. M., Zhao, X., Christensen, J.*, et al.* (2007). MET amplification leads to gefitinib resistance in lung cancer by activating ERBB3 signaling. Science *316*, 1039-1043.

Esrig, D., Spruck, C. H., 3rd, Nichols, P. W., Chaiwun, B., Steven, K., Groshen, S., Chen, S. C., Skinner, D. G., Jones, P. A., and Cote, R. J. (1993). p53 nuclear protein accumulation correlates with mutations in the p53 gene, tumor grade, and stage in bladder cancer. American Journal of Pathology *143*, 1389-1397.

Fabbro, D. (2015). 25 Years of Small Molecular Weight Kinase Inhibitors: Potentials and Limitations. Molecular Pharmacology *87*, 766-775.

Fassnacht, M., Berruti, A., Baudin, E., Demeure, M. J., Gilbert, J., Haak, H., Kroiss, M., Quinn, D. I., Hesseltine, E., Ronchi, C. L.*, et al.* (2015). Linsitinib (OSI-906) versus placebo for patients with locally advanced or metastatic adrenocortical carcinoma: a double-blind, randomised, phase 3 study. The Lancet Oncology *16*, 426-435.

Fattore, L., Marra, E., Pisanu, M. E., Noto, A., de Vitis, C., Belleudi, F., Aurisicchio, L., Mancini, R., Torrisi, M. R., Ascierto, P. A., and Ciliberto, G. (2013). Activation of an early feedback survival loop involving phospho-ErbB3 is a general response of melanoma cells to RAF/MEK inhibition and is abrogated by anti-ErbB3 antibodies. Journal of Translational Medicine *11*, 180-180.

Ferlay, J., Soerjomataram, I., Dikshit, R., Eser, S., Mathers, C., Rebelo, M., Parkin, D. M., Forman, D., and Bray, F. (2015). Cancer incidence and mortality worldwide: Sources, methods and major patterns in GLOBOCAN 2012. International Journal of Cancer *136*, E359-E386.

Fischbach, A., Rogler, A., Erber, R., Stoehr, R., Poulsom, R., Heidenreich, A., Schneevoigt, B. S., Hauke, S., Hartmann, A., Knuechel, R.*, et al.* (2015). Fibroblast growth factor receptor (FGFR) gene amplifications are rare events in bladder cancer. Histopathology *66*, 639-649.

Fischer, M. (2017). Census and evaluation of p53 target genes. Oncogene *36*, 3943-3956.

Forbes, S. A., Beare, D., Boutselakis, H., Bamford, S., Bindal, N., Tate, J., Cole, C. G., Ward, S., Dawson, E., Ponting, L.*, et al.* (2017). COSMIC: somatic cancer genetics at high-resolution. Nucleic Acids Research *45*, D777-D783.

Foulon, V., Sniekers, M., Huysmans, E., Asselberghs, S., Mahieu, V., Mannaerts, G. P., Van Veldhoven, P. P., and Casteels, M. (2005). Breakdown of 2-hydroxylated straight chain fatty acids via peroxisomal 2-hydroxyphytanoyl-CoA lyase: a revised pathway for the

alpha-oxidation of straight chain fatty acids. Journal of Biological Chemistry *280*, 9802-9812.

Fradet-Turcotte, A., Sitz, J., Grapton, D., and Orthwein, A. (2016). BRCA2 functions: from DNA repair to replication fork stabilization. Endocrine-Related Cancer *23*, T1-T17.

Fruman, D. A., Chiu, H., Hopkins, B. D., Bagrodia, S., Cantley, L. C., and Abraham, R. T. (2017). The PI3K Pathway in Human Disease. Cell *170*, 605-635.

Fukuhara, H., Ino, Y., and Todo, T. (2016). Oncolytic virus therapy: A new era of cancer treatment at dawn. Cancer Science *107*, 1373-1379.

Furth, M. E., Davis, L. J., Fleurdelys, B., and Scolnick, E. M. (1982). Monoclonal antibodies to the p21 products of the transforming gene of Harvey murine sarcoma virus and of the cellular ras gene family. Journal of Virology *43*, 294-304.

Gale, M., Sayegh, J., Cao, J., Norcia, M., Gareiss, P., Hoyer, D., Merkel, J. S., and Yan, Q. (2016). Screen-identified selective inhibitor of lysine demethylase 5A blocks cancer cell growth and drug resistance. Oncotarget *7*, 39931-39944.

Garrido-Laguna, I., McGregor, K. A., Wade, M., Weis, J., Gilcrease, W., Burr, L., Soldi, R., Jakubowski, L., Davidson, C., Morrell, G.*, et al.* (2013). A phase I/II study of decitabine in combination with panitumumab in patients with wild-type (wt) KRAS metastatic colorectal cancer. Investigational New Drugs *31*, 1257-1264.

Girotti, M. R., Pedersen, M., Sanchez-Laorden, B., Viros, A., Turajlic, S., Niculescu-Duvaz, D., Zambon, A., Sinclair, J., Hayes, A., Gore, M.*, et al.* (2013). Inhibiting EGF receptor or SRC family kinase signaling overcomes BRAF inhibitor resistance in melanoma. Cancer Discovery *3*, 158-167.

Godwin, J. L., Hoffman-Censits, J., and Plimack, E. (2018). Recent developments in the treatment of advanced bladder cancer. Urologic Oncology *36*, 109-114.

Gorre, M. E., Mohammed, M., Ellwood, K., Hsu, N., Paquette, R., Rao, P. N., and Sawyers, C. L. (2001). Clinical Resistance to STI-571 Cancer Therapy Caused by BCR-ABL Gene Mutation or Amplification. Science *293*, 876-880.

Gower, A., Hsu, W.-H., Hsu, S.-T., Wang, Y., and Giaccone, G. (2016). EMT is associated with, but does not drive resistance to ALK inhibitors among EML4-ALK non-small cell lung cancer. Molecular Oncology *10*, 601-609.

Greenwell, I. B., Ip, A., and Cohen, J. B. (2017). PI3K Inhibitors: Understanding Toxicity Mechanisms and Management. Oncology *31*, 821-828.

Gridelli, C., Maione, P., Bareschino, M. A., Schettino, C., Sacco, P. C., Ambrosio, R., Barbato, V., Falanga, M., and Rossi, A. (2010). Erlotinib in the Treatment of Non-small Cell Lung Cancer: Current Status and Future Developments. Anticancer Research *30*, 1301-1310.

Griffiths, B., Lewis, C. A., Bensaad, K., Ros, S., Zhang, Q., Ferber, E. C., Konisti, S., Peck, B., Miess, H., East, P.*, et al.* (2013). Sterol regulatory element binding protein-dependent regulation of lipid

synthesis supports cell survival and tumor growth. Cancer and Metabolism *1*, 3-3.

Grimaldi, A. M., Simeone, E., Festino, L., Vanella, V., Strudel, M., and Ascierto, P. A. (2017). MEK Inhibitors in the Treatment of Metastatic Melanoma and Solid Tumors. American Journal of Clinical Dermatology *18*, 745-754.

Grudinkin, P. S., Zenin, V. V., Kropotov, A. V., Dorosh, V. N., and Nikolsky, N. N. (2007). EGF-induced apoptosis in A431 cells is dependent on STAT1, but not on STAT3. European Journal of Cell Biology *86*, 591-603.

Gui, Y., Guo, G., Huang, Y., Hu, X., Tang, A., Gao, S., Wu, R., Chen, C., Li, X., Zhou, L.*, et al.* (2011). Frequent mutations of chromatin remodeling genes in transitional cell carcinoma of the bladder. Nature Genetics *43*, 875-878.

Guo, G., Sun, X., Chen, C., Wu, S., Huang, P., Li, Z., Dean, M., Huang, Y., Jia, W., Zhou, Q.*, et al.* (2013). Whole-genome and whole-exome sequencing of bladder cancer identifies frequent alterations in genes involved in sister chromatid cohesion and segregation. Nature Genetics *45*, 1459-1463.

Guo, Y., Scheuermann, T. H., Partch, C. L., Tomchick, D. R., and Gardner, K. H. (2015). Coiled-coil Coactivators Play a Structural Role Mediating Interactions in Hypoxia-inducible Factor Heterodimerization. Journal of Biological Chemistry *290*, 7707-7721.

Hafner, C., Toll, A., Fernández-Casado, A., Earl, J., Marqués, M., Acquadro, F., Méndez-Pertuz, M., Urioste, M., Malats, N., Burns, J. E.*, et al.* (2010). Multiple oncogenic mutations and clonal relationship in spatially distinct benign human epidermal tumors. Proceedings of the National Academy of Sciences of the United States of America *107*, 20780-20785.

Hafner, C., van Oers, J. M., Hartmann, A., Landthaler, M., Stoehr, R., Blaszyk, H., Hofstaedter, F., Zwarthoff, E. C., and Vogt, T. (2006). High frequency of FGFR3 mutations in adenoid seborrheic keratoses. The Journal of Investigative Dermatology *126*, 2404-2407.

Hagen, R. M., Rodriguez-Cuenca, S., and Vidal-Puig, A. (2010). An allostatic control of membrane lipid composition by SREBP1. FEBS Letters *584*, 2689-2698.

Hakam, A., Yeatman, T. J., Lu, L., Mora, L., Marcet, G., Nicosia, S. V., Karl, R. C., and Coppola, D. (1999). Expression of insulin-like growth factor-1 receptor in human colorectal cancer. Human Pathology *30*, 1128-1133.

Haling, Jacob R., Sudhamsu, J., Yen, I., Sideris, S., Sandoval, W., Phung, W., Bravo, Brandon J., Giannetti, Anthony M., Peck, A., Masselot, A.*, et al.* (2014). Structure of the BRAF-MEK Complex Reveals a Kinase Activity Independent Role for BRAF in MAPK Signaling. Cancer Cell *26*, 402-413.

Han, S.-W., Cha, Y., Paquet, A., Huang, W., Weidler, J., Lie, Y., Sherwood, T., Bates, M., Haddad, M., Park, I. H.*, et al.* (2012). Correlation of HER2, p95HER2 and HER3 Expression and Treatment Outcome of Lapatinib plus Capecitabine in her2-Positive Metastatic Breast Cancer. PLoS ONE *7*, e39943.

Hanahan, D., and Weinberg, R. A. (2011). Hallmarks of cancer: the next generation. Cell *144*, 646-674.

Hanze, J., Henrici, M., Hegele, A., Hofmann, R., and Olbert, P. J. (2013). Epithelial mesenchymal transition status is associated with anti-cancer responses towards receptor tyrosine-kinase inhibition by dovitinib in human bladder cancer cells. BMC Cancer *13*, 589.

Harbinski, F., Craig, V. J., Sanghavi, S., Jeffery, D., Liu, L., Sheppard, K. A., Wagner, S., Stamm, C., Buness, A., Chatenay-Rivauday, C.*, et al.* (2012). Rescue screens with secreted proteins reveal compensatory potential of receptor tyrosine kinases in driving cancer growth. Cancer Discovery *2*, 948-959.

Harris, L. N., You, F., Schnitt, S. J., Witkiewicz, A., Lu, X., Sgroi, D., Ryan, P. D., Come, S. E., Burstein, H. J., Lesnikoski, B. A.*, et al.* (2007). Predictors of resistance to preoperative trastuzumab and vinorelbine for HER2-positive early breast cancer. Clinical Cancer Research *13*, 1198-1207.

Hart, K. C., Robertson, S. C., and Donoghue, D. J. (2001). Identification of Tyrosine Residues in Constitutively Activated Fibroblast Growth Factor Receptor 3 Involved in Mitogenesis, Stat Activation, and Phosphatidylinositol 3-Kinase Activation. Molecular Biology of the Cell *12*, 931-942.

Hartog, H., Wesseling, J., Boezen, H. M., and van der Graaf, W. T. (2007). The insulin-like growth factor 1 receptor in cancer: old focus, new future. European Journal of Cancer *43*, 1895-1904.

Hata, A. N., Niederst, M. J., Archibald, H. L., Gomez-Caraballo, M., Siddiqui, F. M., Mulvey, H. E., Maruvka, Y. E., Ji, F., Bhang, H. E., Krishnamurthy Radhakrishna, V.*, et al.* (2016). Tumor cells can follow distinct evolutionary paths to become resistant to epidermal growth factor receptor inhibition. Nature Medicine *22*, 262-269.

Hatakeyama, S. (2011). TRIM proteins and cancer. Nature Reviews Cancer *11*, 792-804.

Hauschild, A., Grob, J.-J., Demidov, L. V., Jouary, T., Gutzmer, R., Millward, M., Rutkowski, P., Blank, C. U., Miller Jr, W. H., Kaempgen, E.*, et al.* (2012). Dabrafenib in BRAF-mutated metastatic melanoma: a multicentre, open-label, phase 3 randomised controlled trial. The Lancet *380*, 358-365.

Hayden, K. E. (2012). Human centromere genomics: now it's personal. Chromosome Research *20*, 621-633.

He, M., and Wei, M.-J. (2012). Reversing multidrug resistance by tyrosine kinase inhibitors. Chinese Journal of Cancer *31*, 126-133.

Hedegaard, J., Lamy, P., Nordentoft, I., Algaba, F., Hoyer, S., Ulhoi, B. P., Vang, S., Reinert, T., Hermann, G. G., Mogensen, K.*, et al.* (2016). Comprehensive Transcriptional Analysis of Early-Stage Urothelial Carcinoma. Cancer Cell *30*, 27-42.

Hegi, M. E., Diserens, A. C., Gorlia, T., Hamou, M. F., de Tribolet, N., Weller, M., Kros, J. M., Hainfellner, J. A., Mason, W., Mariani, L.*, et al.* (2005). MGMT gene silencing and benefit from temozolomide in glioblastoma. New England Journal of Medicine *352*, 997-1003.

Heidenreich, B., and Kumar, R. (2017). TERT promoter mutations in telomere biology. Mutation Research *771*, 15-31.

Heinrich, M. C., Corless, C. L., Duensing, A., McGreevey, L., Chen, C. J., Joseph, N., Singer, S., Griffith, D. J., Haley, A., Town, A.*, et al.* (2003). PDGFRA activating mutations in gastrointestinal stromal tumors. Science *299*, 708-710.

Heist, R. S., Mino-Kenudson, M., Sequist, L. V., Tammireddy, S., Morrissey, L., Christiani, D. C., Engelman, J. A., and Iafrate, A. J. (2012). FGFR1 Amplification in Squamous Cell Carcinoma of The Lung. Journal of Thoracic Oncology *7*, 1775-1780.

Helsten, T., Elkin, S., Arthur, E., Tomson, B. N., Carter, J., and Kurzrock, R. (2016). The FGFR Landscape in Cancer: Analysis of 4,853 Tumors by Next-Generation Sequencing. Clinical Cancer Research *22*, 259-267.

Hermanns, H. M. (2015). Oncostatin M and interleukin-31: Cytokines, receptors, signal transduction and physiology. Cytokine and Growth Factor Reviews *26*, 545-558.

Hermans, T. J. N., Voskuilen, C. S., van der Heijden, M. S., Schmitz-Drager, B. J., Kassouf, W., Seiler, R., Kamat, A. M., Grivas, P., Kiltie, A. E., Black, P. C., and van Rhijn, B. W. G. (2017). Neoadjuvant treatment for muscle-invasive bladder cancer: The past, the present, and the future. Urologic Oncology. 8, S1078-1493

Herrera-Abreu, M. T., Pearson, A., Campbell, J., Shnyder, S. D., Knowles, M. A., Ashworth, A., and Turner, N. C. (2013). Parallel RNA interference screens identify EGFR activation as an escape mechanism in FGFR3-mutant cancer. Cancer Discovery *3*, 1058-1071.

Hickinson, D. M., Klinowska, T., Speake, G., Vincent, J., Trigwell, C., Anderton, J., Beck, S., Marshall, G., Davenport, S., Callis, R.*, et al.* (2010). AZD8931, an equipotent, reversible inhibitor of signaling by epidermal growth factor receptor, ERBB2 (HER2), and ERBB3: a unique agent for simultaneous ERBB receptor blockade in cancer. Clinical Cancer Research *16*, 1159-1169.

Hirota, S., Isozaki, K., Moriyama, Y., Hashimoto, K., Nishida, T., Ishiguro, S., Kawano, K., Hanada, M., Kurata, A., Takeda, M.*, et al.* (1998). Gain-of-function mutations of c-kit in human gastrointestinal stromal tumors. Science *279*, 577-580.

Hobbs, G. A., Der, C. J., and Rossman, K. L. (2016). RAS isoforms and mutations in cancer at a glance. Journal of Cell Science *129*, 1287-1292.

Hochhaus, A., Kantarjian, H. M., Baccarani, M., Lipton, J. H., Apperley, J. F., Druker, B. J., Facon, T., Goldberg, S. L., Cervantes, F., Niederwieser, D.*, et al.* (2007). Dasatinib induces notable hematologic and cytogenetic responses in chronic-phase chronic myeloid leukemia after failure of imatinib therapy. Blood *109*, 2303-2309.

Hochhaus, A., Kreil, S., Corbin, A. S., La Rosee, P., Muller, M. C., Lahaye, T., Hanfstein, B., Schoch, C., Cross, N. C., Berger, U.*, et al.* (2002). Molecular and chromosomal mechanisms of resistance to imatinib (STI571) therapy. Leukemia *16*, 2190-2196.

Hochhaus, A., Larson, R. A., Guilhot, F., Radich, J. P., Branford, S., Hughes, T. P., Baccarani, M., Deininger, M. W., Cervantes, F., Fujihara, S.*, et al.* (2017). Long-Term Outcomes of Imatinib Treatment for Chronic

Myeloid Leukemia. The New England Journal of Medicine *376*, 917-927.

Hodges, C., Kirkland, J. G., and Crabtree, G. R. (2016). The many roles of BAF (mSWI/SNF) and PBAF complexes in cancer. Cold Spring Harbor Perspectives in Medicine *6*, a026930.

Holzinger, A., Maier, E. M., Bück, C., Mayerhofer, P. U., Kappler, M., Haworth, J. C., Moroz, S. P., Hadorn, H.-B., Sadler, J. E., and Roscher, A. A. (2002). Mutations in the Proenteropeptidase Gene Are the Molecular Cause of Congenital Enteropeptidase Deficiency. American Journal of Human Genetics *70*, 20-25.

Hong-Ji, X., Paul, C., Shi-Xue, H., A., K. M., and F., B. W. (1993). Loss of RB protein expression in primary bladder cancer correlates with loss of heterozygosity at the RB locus and tumor progression. International Journal of Cancer *53*, 781-784.

Horn, S., Figl, A., Rachakonda, P. S., Fischer, C., Sucker, A., Gast, A., Kadel, S., Moll, I., Nagore, E., Hemminki, K.*, et al.* (2013). TERT promoter mutations in familial and sporadic melanoma. Science *339*, 959-961.

Horowitz, J. M., Park, S. H., Bogenmann, E., Cheng, J. C., Yandell, D. W., Kaye, F. J., Minna, J. D., Dryja, T. P., and Weinberg, R. A. (1990). Frequent inactivation of the retinoblastoma anti-oncogene is restricted to a subset of human tumor cells. Proceedings of the National Academy of Sciences *87*, 2775-2779.

Hossam, M., Lasheen, D. S., and Abouzid, K. A. (2016). Covalent EGFR Inhibitors: Binding Mechanisms, Synthetic Approaches, and Clinical Profiles. Archiv der Pharmazie *349*, 573-593.

Hou, J., Wu, J., Dombkowski, A., Zhang, K., Holowatyj, A., Boerner, J. L., and Yang, Z.-Q. (2012). Genomic amplification and a role in drug-resistance for the KDM5A histone demethylase in breast cancer. American Journal of Translational Research *4*, 247-256.

Hu, P., Deng, F.-M., Liang, F.-X., Hu, C.-M., Auerbach, A. B., Shapiro, E., Wu, X.-R., Kachar, B., and Sun, T.-T. (2000). Ablation of Uroplakin III Gene Results in Small Urothelial Plaques, Urothelial Leakage, and Vesicoureteral Reflux. The Journal of Cell Biology *151*, 961-972.

Huang, J., and Manning, B. D. (2008). The TSC1–TSC2 complex: a molecular switchboard controlling cell growth. The Biochemical Journal *412*, 179-190.

Huang, L., and Fu, L. (2015). Mechanisms of resistance to EGFR tyrosine kinase inhibitors. Acta Pharmaceutica Sinica B *5*, 390-401.

Huang, Z., Chen, H., Blais, S., Neubert, T. A., Li, X., and Mohammadi, M. (2013). Structural Mimicry of A-Loop Tyrosine Phosphorylation by a Pathogenic FGF Receptor 3 Mutation. Structure *21*, 1889-1896.

Hurst, C. D., Alder, O., Platt, F. M., Droop, A., Stead, L. F., Burns, J. E., Burghel, G. J., Jain, S., Klimczak, L. J., Lindsay, H.*, et al.* (2017). Genomic Subtypes of Non-invasive Bladder Cancer with Distinct Metabolic Profile and Female Gender Bias in KDM6A Mutation Frequency. Cancer Cell *32*, 701-715.e707.

Hurst, C. D., Fiegler, H., Carr, P., Williams, S., Carter, N. P., and Knowles, M. A. (2004). High-resolution analysis of genomic copy number alterations in bladder cancer by microarray-based comparative genomic hybridization. Oncogene *23*, 2250-2263.

Hurst, C. D., Platt, F. M., and Knowles, M. A. (2014). Comprehensive mutation analysis of the TERT promoter in bladder cancer and detection of mutations in voided urine. European Urology *65*, 367-369.

Hurst, C. D., Platt, F. M., Taylor, C. F., and Knowles, M. A. (2012). Novel tumor subgroups of urothelial carcinoma of the bladder defined by integrated genomic analysis. Clinical Cancer Research *18*, 5865-5877.

Hussain, M. H., MacVicar, G. R., Petrylak, D. P., Dunn, R. L., Vaishampayan, U., Lara, P. N., Jr., Chatta, G. S., Nanus, D. M., Glode, L. M., Trump, D. L.*, et al.* (2007). Trastuzumab, paclitaxel, carboplatin, and gemcitabine in advanced human epidermal growth factor receptor-2/neu-positive urothelial carcinoma: results of a multicenter phase II National Cancer Institute trial. Journal of Clinical Oncology *25*, 2218-2224.

Ibrahim, N., Elzagheid, A., El-Hashmi, H., Syrjänen, K., and Alhakim, S. (2009). The Potential Value of EGFR and P53 Immunostaining in Tumors of the Urinary Bladder. Libyan Journal of Medicine *4*, 143-145.

Igal, R. A. (2016). Stearoyl CoA desaturase-1: New insights into a central regulator of cancer metabolism. Biochimica et Biophysica Acta *1861*, 1865-1880.

Iqbal, N., and Iqbal, N. (2014). Human Epidermal Growth Factor Receptor 2 (HER2) in Cancers: Overexpression and Therapeutic Implications. Molecular Biology International *2014*, 852748.

Irizarry, R. A., Bolstad, B. M., Collin, F., Cope, L. M., Hobbs, B., and Speed, T. P. (2003). Summaries of Affymetrix GeneChip probe level data. Nucleic Acids Research *31*, e15-e15.

Ishikawa, J., Xu, H.-J., Hu, S.-X., Yandell, D. W., Maeda, S., Kamidono, S., Benedict, W. F., and Takahashi, R. (1991). Inactivation of the Retinoblastoma Gene in Human Bladder and Renal Cell Carcinomas. Cancer Research *51*, 5736-5743.

Iyer, G., Hanrahan, A. J., Milowsky, M. I., Al-Ahmadie, H., Scott, S. N., Janakiraman, M., Pirun, M., Sander, C., Socci, N. D., Ostrovnaya, I.*, et al.* (2012). Genome Sequencing Identifies a Basis for Everolimus Sensitivity. Science *338*, 221-221.

Jabbour, E., Kantarjian, H., and Cortes, J. (2015). Use of Second- and Third-Generation Tyrosine Kinase Inhibitors in the Treatment of Chronic Myeloid Leukemia: An Evolving Treatment Paradigm. Clinical Lymphoma, Myeloma and Leukemia *15*, 323-334.

Jang, J. H., Shin, K. H., and Park, J. G. (2001). Mutations in fibroblast growth factor receptor 2 and fibroblast growth factor receptor 3 genes associated with human gastric and colorectal cancers. Cancer Research *61*, 3541-3543.

Jebar, A. H., Hurst, C. D., Tomlinson, D. C., Johnston, C., Taylor, C. F., and Knowles, M. A. (2005). FGFR3 and Ras gene mutations are mutually exclusive genetic events in urothelial cell carcinoma. Oncogene *24*, 5218-5225.

Jelinek, J., Gharibyan, V., Estecio, M. R. H., Kondo, K., He, R., Chung, W., Lu, Y., Zhang, N., Liang, S., Kantarjian, H. M.*, et al.* (2011). Aberrant DNA Methylation Is Associated with Disease Progression, Resistance

to Imatinib and Shortened Survival in Chronic Myelogenous Leukemia. PLoS ONE *6*, e22110.

Johnson, D. E., Lu, J., Chen, H., Werner, S., and Williams, L. T. (1991). The human fibroblast growth factor receptor genes: a common structural arrangement underlies the mechanisms for generating receptor forms that differ in their third immunoglobulin domain. Molecular and Cellular Biology *11*, 4627-4634.

Johnston, S., Basik, M., Hegg, R., Lausoontornsiri, W., Grzeda, L., Clemons, M., Dreosti, L., Mann, H., Stuart, M., and Cristofanilli, M. (2016). Inhibition of EGFR, HER2, and HER3 signaling with AZD8931 in combination with anastrozole as an anticancer approach: Phase II randomized study in women with endocrine-therapy-naive advanced breast cancer. Breast Cancer Research and Treatment *160*, 91-99.

Jones, H. E., Gee, J. M., Hutcheson, I. R., Knowlden, J. M., Barrow, D., and Nicholson, R. I. (2006). Growth factor receptor interplay and resistance in cancer. Endocrine-Related Cancer *13*, S45-51.

Kalff, A., and Spencer, A. (2012). The t(4;14) translocation and FGFR3 overexpression in multiple myeloma: prognostic implications and current clinical strategies. Blood Cancer Journal *2*, e89.

Kamat, A. M., Li, R., O'Donnell, M. A., Black, P. C., Roupret, M., Catto, J. W., Comperat, E., Ingersoll, M. A., Witjes, W. P., McConkey, D. J., and Witjes, J. A. (2017). Predicting Response to Intravesical Bacillus Calmette-Guerin Immunotherapy: Are We There Yet? A Systematic Review. European Urology. *73*, 738-748

Kantarjian, H. M., Giles, F., Gattermann, N., Bhalla, K., Alimena, G., Palandri, F., Ossenkoppele, G. J., Nicolini, F. E., O'Brien, S. G., Litzow, M.*, et al.* (2007). Nilotinib (formerly AMN107), a highly selective BCR-ABL tyrosine kinase inhibitor, is effective in patients with Philadelphia chromosome-positive chronic myelogenous leukemia in chronic phase following imatinib resistance and intolerance. Blood *110*, 3540-3546.

Karapetis, C. S., Khambata-Ford, S., Jonker, D. J., O'Callaghan, C. J., Tu, D., Tebbutt, N. C., Simes, R. J., Chalchal, H., Shapiro, J. D., Robitaille, S.*, et al.* (2008). K-ras mutations and benefit from cetuximab in advanced colorectal cancer. The New England Journal of Medicine *359*, 1757-1765.

Kataoka, Y., Mukohara, T., Shimada, H., Saijo, N., Hirai, M., and Minami, H. (2010). Association between gain-of-function mutations in PIK3CA and resistance to HER2-targeted agents in HER2-amplified breast cancer cell lines. Annals of Oncology *21*, 255-262.

Katoh, M. (2012). Function and cancer genomics of FAT family genes. International Journal of Oncology *41*, 1913-1918.

Keam, B., Kim, S. B., Shin, S. H., Cho, B. C., Lee, K. W., Kim, M. K., Yun, H. J., Lee, S. H., Yoon, D. H., and Bang, Y. J. (2015). Phase 2 study of dovitinib in patients with metastatic or unresectable adenoid cystic carcinoma. Cancer *121*, 2612-2617.

Killela, P. J., Reitman, Z. J., Jiao, Y., Bettegowda, C., Agrawal, N., Diaz, L. A., Friedman, A. H., Friedman, H., Gallia, G. L., Giovanella, B. C.*, et al.* (2013). TERT promoter mutations occur frequently in gliomas and a subset of tumors derived from cells with low rates of self-renewal.

Proceedings of the National Academy of Sciences of the United States of America *110*, 6021-6026.

Kim, Y.-M., and Kim, D.-H. (2013). dRAGging Amino Acid-mTORC1 Signaling by SH3BP4. Molecules and Cells *35*, 1-6.

Kimura, T., Suzuki, H., Ohashi, T., Asano, K., Kiyota, H., and Eto, Y. (2001). The incidence of thanatophoric dysplasia mutations in FGFR3 gene is higher in low-grade or superficial bladder carcinomas. Cancer *92*, 2555-2561.

Kinde, I., Munari, E., Faraj, S. F., Hruban, R. H., Schoenberg, M., Bivalacqua, T., Allaf, M., Springer, S., Wang, Y., Diaz, L. A., Jr.*, et al.* (2013). TERT promoter mutations occur early in urothelial neoplasia and are biomarkers of early disease and disease recurrence in urine. Cancer Research *73*, 7162-7167.

King, M. A., Ganley, I. G., and Flemington, V. (2016). Inhibition of cholesterol metabolism underlies synergy between mTOR pathway inhibition and chloroquine in bladder cancer cells. Oncogene *35*, 4518-4528.

Kiselyov, A., Bunimovich-Mendrazitsky, S., and Startsev, V. (2016). Key signaling pathways in the muscle-invasive bladder carcinoma: Clinical markers for disease modeling and optimized treatment. International Journal of Cancer *138*, 2562-2569.

Klein, S., McCormick, F., and Levitzki, A. (2005). Killing time for cancer cells. Nature Reviews Cancer *5*, 573-580.

Klein-Szanto, A. J., and Bassi, D. E. (2017). Proprotein convertase inhibition: Paralyzing the cell's master switches. Biochemical Pharmacology *140*, 8-15.

Klint, P., and Claesson-Welsh, L. (1999). Signal transduction by fibroblast growth factor receptors. Frontiers in Bioscience *4*, D165-177.

Knowles, M. A., Habuchi, T., Kennedy, W., and Cuthbert-Heavens, D. (2003). Mutation spectrum of the 9q34 tuberous sclerosis gene TSC1 in transitional cell carcinoma of the bladder. Cancer Research *63*, 7652-7656.

Knowles, M. A., and Hurst, C. D. (2015). Molecular biology of bladder cancer: new insights into pathogenesis and clinical diversity. Nature reviews Cancer *15*, 25-41.

Kobayashi, S., Boggon, T. J., Dayaram, T., Janne, P. A., Kocher, O., Meyerson, M., Johnson, B. E., Eck, M. J., Tenen, D. G., and Halmos, B. (2005). EGFR mutation and resistance of non-small-cell lung cancer to gefitinib. The New England Journal of Medicine *352*, 786-792.

Konecny, G. E., Finkler, N., Garcia, A. A., Lorusso, D., Lee, P. S., Rocconi, R. P., Fong, P. C., Squires, M., Mishra, K., Upalawanna, A.*, et al.* (2015). Second-line dovitinib (TKI258) in patients with FGFR2-mutated or FGFR2-non-mutated advanced or metastatic endometrial cancer: a non-randomised, open-label, two-group, two-stage, phase 2 study. The Lancet Oncology *16*, 686-694.

Koo, B. K., Yoon, K. J., Yoo, K. W., Lim, H. S., Song, R., So, J. H., Kim, C. H., and Kong, Y. Y. (2005). Mind bomb-2 is an E3 ligase for Notch ligand. Journal of Biological Chemistry *280*, 22335-22342.

Kosugi, S., Hasebe, M., Entani, T., Takayama, S., Tomita, M., and Yanagawa, H. (2008). Design of peptide inhibitors for the importin

alpha/beta nuclear import pathway by activity-based profiling. Chemistry and Biology *15*, 940-949.

Kubo, T., Kuroda, Y., Shimizu, H., Kokubu, A., Okada, N., Hosoda, F., Arai, Y., Nakamura, Y., Taniguchi, H., Yanagihara, K.*, et al.* (2009). Resequencing and copy number analysis of the human tyrosine kinase gene family in poorly differentiated gastric cancer. Carcinogenesis *30*, 1857-1864.

Kurata, T., Tsurutani, J., Fujisaka, Y., Okamoto, W., Hayashi, H., Kawakami, H., Shin, E., Hayashi, N., and Nakagawa, K. (2014). Inhibition of EGFR, HER2 and HER3 signaling with AZD8931 alone and in combination with paclitaxel: phase I study in Japanese patients with advanced solid malignancies and advanced breast cancer. Investigational New Drugs *32*, 946-954.

Laé, M., Couturier, J., Oudard, S., Radvanyi, F., Beuzeboc, P., and Vieillefond, A. (2010). Assessing HER2 gene amplification as a potential target for therapy in invasive urothelial bladder cancer with a standardized methodology: results in 1005 patients. Annals of Oncology *21*, 815-819.

Lamont, F. R., Tomlinson, D. C., Cooper, P. A., Shnyder, S. D., Chester, J. D., and Knowles, M. A. (2011). Small molecule FGF receptor inhibitors block FGFR-dependent urothelial carcinoma growth in vitro and in vivo. British Journal of Cancer *104*, 75-82.

Langer, C. J., Novello, S., Park, K., Krzakowski, M., Karp, D. D., Mok, T., Benner, R. J., Scranton, J. R., Olszanski, A. J., and Jassem, J. (2014). Randomized, phase III trial of first-line figitumumab in combination with paclitaxel and carboplatin versus paclitaxel and carboplatin alone in patients with advanced non-small-cell lung cancer. Journal of Clinical Oncology *32*, 2059-2066.

le Coutre, P., Tassi, E., Varella-Garcia, M., Barni, R., Mologni, L., Cabrita, G., Marchesi, E., Supino, R., and Gambacorti-Passerini, C. (2000). Induction of resistance to the Abelson inhibitor STI571 in human leukemic cells through gene amplification. Blood *95*, 1758-1766.

Lee, J. W., Soung, Y. H., Seo, S. H., Kim, S. Y., Park, C. H., Wang, Y. P., Park, K., Nam, S. W., Park, W. S., Kim, S. H.*, et al.* (2006). Somatic mutations of ERBB2 kinase domain in gastric, colorectal, and breast carcinomas. Clinical Cancer Research *12*, 57-61.

Lee, A.-F., Chen, M.-C., Chen, C.-J., Yang, C.-J., Huang, M.-S., and Liu, Y.-P. (2017). Reverse epithelial-mesenchymal transition contributes to the regain of drug sensitivity in tyrosine kinase inhibitor-resistant non-small cell lung cancer cells. PLoS ONE *12*, e0180383.

Leighl, N. B., Rizvi, N. A., de Lima, L. G., Jr., Arpornwirat, W., Rudin, C. M., Chiappori, A. A., Ahn, M. J., Chow, L. Q., Bazhenova, L., Dechaphunkul, A.*, et al.* (2017). Phase 2 Study of Erlotinib in Combination With Linsitinib (OSI-906) or Placebo in Chemotherapy-Naive Patients With Non-Small-Cell Lung Cancer and Activating Epidermal Growth Factor Receptor Mutations. Clinical Lung Cancer *18*, 34-42.e32.

Leow, J. J., Martin-Doyle, W., Rajagopal, P. S., Patel, C. G., Anderson, E. M., Rothman, A. T., Cote, R. J., Urun, Y., Chang, S. L., Choueiri, T. K., and Bellmunt, J. (2014). Adjuvant chemotherapy for invasive

bladder cancer: a 2013 updated systematic review and meta-analysis of randomized trials. European Urology *66*, 42-54.

Lianes, P., Orlow, I., Zhang, Z. F., Oliva, M. R., Sarkis, A. S., Reuter, V. E., and Cordon-Cardo, C. (1994). Altered patterns of MDM2 and TP53 expression in human bladder cancer. Journal of the National Cancer Institute *86*, 1325-1330.

Li, L., Gu, X., Yue, J., Zhao, Q., Lv, D., Chen, H., and Xu, L. (2017). Acquisition of EGFR TKI resistance and EMT phenotype is linked with activation of IGF1R/NF-κB pathway in EGFR-mutant NSCLC. Oncotarget *8*, 92240-92253.

Lin, W., Cao, J., Liu, J., Beshiri, M. L., Fujiwara, Y., Francis, J., Cherniack, A. D., Geisen, C., Blair, L. P., Zou, M. R.*, et al.* (2011). Loss of the retinoblastoma binding protein 2 (RBP2) histone demethylase suppresses tumorigenesis in mice lacking Rb1 or Men1. Proceedings of the National Academy of Sciences of the United States of America *108*, 13379-13386.

Lindgren, D., Sjödahl, G., Lauss, M., Staaf, J., Chebil, G., Lövgren, K., Gudjonsson, S., Liedberg, F., Patschan, O., Månsson, W.*, et al.* (2012). Integrated Genomic and Gene Expression Profiling Identifies Two Major Genomic Circuits in Urothelial Carcinoma. PLOS ONE *7*, e38863.

Liu, H., Deng, X., Shyu, Y. J., Li, J. J., Taparowsky, E. J., and Hu, C.-D. (2006). Mutual regulation of c-Jun and ATF2 by transcriptional activation and subcellular localization. EMBO Journal *25*, 1058-1069.

Liu, X., Wang, Q., Yang, G., Marando, C., Koblish, H. K., Hall, L. M., Fridman, J. S., Behshad, E., Wynn, R., Li, Y.*, et al.* (2011). A novel kinase inhibitor, INCB28060, blocks c-MET-dependent signaling, neoplastic activities, and cross-talk with EGFR and HER-3. Clinical Cancer Research *17*, 7127-7138.

Liu, X., Wu, G., Shan, Y., Hartmann, C., von Deimling, A., and Xing, M. (2013). Highly prevalent TERT promoter mutations in bladder cancer and glioblastoma. Cell Cycle *12*, 1637-1638.

Lodola, A., Giorgio, C., Incerti, M., Zanotti, I., and Tognolini, M. (2017). Targeting Eph/ephrin system in cancer therapy. European Journal of Medicinal Chemistry *142*, 152-162.

López-Knowles, E., Hernández, S., Kogevinas, M., Lloreta, J., Amorós, A., Tardón, A., Carrato, A., Kishore, S., Serra, C., Malats, N., and Real, F. X. (2006). The p53 Pathway and Outcome among Patients with T1G3 Bladder Tumors. Clinical Cancer Research *12*, 6029-6036.

Lopez-Knowles, E., Hernandez, S., Malats, N., Kogevinas, M., Lloreta, J., Carrato, A., Tardon, A., Serra, C., and Real, F. X. (2006). PIK3CA mutations are an early genetic alteration associated with FGFR3 mutations in superficial papillary bladder tumors. Cancer Research *66*, 7401-7404.

Lovén, J., Hoke, H. A., Lin, C. Y., Lau, A., Orlando, D. A., Vakoc, C. R., Bradner, J. E., Lee, T. I., and Young, R. A. (2013). Selective Inhibition of Tumor Oncogenes by Disruption of Super-Enhancers. Cell *153*, 320-334.

Lu, C.-H., Wyszomierski, S. L., Tseng, L.-M., Sun, M.-H., Lan, K.-H., Neal, C. L., Mills, G. B., Hortobagyi, G. N., Esteva, F. J., and Yu, D. (2007). Preclinical Testing of Clinically Applicable Strategies for Overcoming

Trastuzumab Resistance Caused by PTEN Deficiency. Clinical Cancer Research *13*, 5883-5888.

Lubner, S. J., Uboha, N. V., and Deming, D. A. (2017). Primary and acquired resistance to biologic therapies in gastrointestinal cancers. Journal of Gastrointestinal Oncology *8*, 499-512.

Ma, Y., Tang, N., Thompson, R., Mobley, B. C., Clark, S. W., Sarkaria, J. N., and Wang, J. (2016). InsR/IGF1R pathway mediates resistance to EGFR inhibitors in glioblastoma. Clinical Cancer Research *22*, 1767-1776.

Mackenzie, P. I., Rogers, A., Treloar, J., Jorgensen, B. R., Miners, J. O., and Meech, R. (2008). Identification of UDP Glycosyltransferase 3A1 as a UDP N-Acetylglucosaminyltransferase. The Journal of Biological Chemistry *283*, 36205-36210.

Mahe, M., Dufour, F., Neyret-Kahn, H., Moreno-Vega, A., Beraud, C., Shi, M., Hamaidi, I., Sanchez-Quiles, V., Krucker, C., Dorland-Galliot, M.*, et al.* (2018). An FGFR3/MYC positive feedback loop provides new opportunities for targeted therapies in bladder cancers. EMBO molecular medicine *10*. e8163

Malats, N., and Real, F. X. (2015). Epidemiology of bladder cancer. Hematology/oncology clinics of North America *29*, 177-189, vii.

Malats, N., Bustos, A., Nascimento, C. M., Fernandez, F., Rivas, M., Puente, D., Kogevinas, M., and Real, F. X. (2005). P53 as a prognostic marker for bladder cancer: a meta-analysis and review. Lancet Oncology *6*, 678-686.

Maluf, F. C., Cordon-Cardo, C., Verbel, D. A., Satagopan, J. M., Boyle, M. G., Herr, H., and Bajorin, D. F. (2006). Assessing interactions between mdm-2, p53, and bcl-2 as prognostic variables in muscle-invasive bladder cancer treated with neo-adjuvant chemotherapy followed by locoregional surgical treatment. Annals of Oncology *17*, 1677-1686.

Mao, C., Wu, X.-Y., Yang, Z.-Y., Threapleton, D. E., Yuan, J.-Q., Yu, Y.-Y., and Tang, J.-L. (2015). Concordant analysis of KRAS, BRAF, PIK3CA mutations, and PTEN expression between primary colorectal cancer and matched metastases. Scientific Reports *5*, 8065.

Mao, Z., Hine, C., Tian, X., Van Meter, M., Au, M., Vaidya, A., Seluanov, A., and Gorbunova, V. (2011). SIRT6 promotes DNA repair under stress by activating PARP1. Science *332*, 1443-1446.

Maréchal, A., and Zou, L. (2013). DNA Damage Sensing by the ATM and ATR Kinases. Cold Spring Harbor Perspectives in Biology *5*, a012716.

Marshall, C. J., Franks, L. M., and Carbonell, A. W. (1977). Markers of neoplastic transformation in epithelial cell lines derived from human carcinomas. Journal of the National Cancer Institute *58*, 1743-1751.

Martin, D., Abba, M. C., Molinolo, A. A., Vitale-Cross, L., Wang, Z., Zaida, M., Delic, N. C., Samuels, Y., Lyons, J. G., and Gutkind, J. S. (2014). The head and neck cancer cell oncogenome: a platform for the development of precision molecular therapies. Oncotarget *5*, 8906-8923.

Martin, V., Landi, L., Molinari, F., Fountzilas, G., Geva, R., Riva, A., Saletti, P., De Dosso, S., Spitale, A., Tejpar, S.*, et al.* (2013). HER2 gene copy number status may influence clinical efficacy to anti-EGFR

monoclonal antibodies in metastatic colorectal cancer patients. British Journal of Cancer *108*, 668-675.

Masters, J. R., Hepburn, P. J., Walker, L., Highman, W. J., Trejdosiewicz, L. K., Povey, S., Parkar, M., Hill, B. T., Riddle, P. R., and Franks, L. M. (1986). Tissue culture model of transitional cell carcinoma: characterization of twenty-two human urothelial cell lines. Cancer Research *46*, 3630-3636.

Merkel, O., Taylor, N., Prutsch, N., Staber, P. B., Moriggl, R., Turner, S. D., and Kenner, L. (2017). When the guardian sleeps: Reactivation of the p53 pathway in cancer. Mutation Research *773*, 1-13.

Midha, A., Dearden, S., and McCormack, R. (2015). EGFR mutation incidence in non-small-cell lung cancer of adenocarcinoma histology: a systematic review and global map by ethnicity (mutMapII). American Journal of Cancer Research *5*, 2892-2911.

Mieulet, V., and Lamb, R. F. (2010). Tuberous sclerosis complex: linking cancer to metabolism. Trends in Molecular Medicine *16*, 329-335.

Millard, T. H., Dawson, J., and Machesky, L. M. (2007). Characterisation of IRTKS, a novel IRSp53/MIM family actin regulator with distinct filament bundling properties. Journal of Cell Science *120*, 1663-1672.

Miller, K., Morant, R., Stenzl, A., Zuna, I., and Wirth, M. (2016). A Phase II Study of the Central European Society of Anticancer-Drug Research (CESAR) Group: Results of an Open-Label Study of Gemcitabine plus Cisplatin with or without Concomitant or Sequential Gefitinib in Patients with Advanced or Metastatic Transitional Cell Carcinoma of the Urothelium. Urologia Internationalis *96*, 5-13.

Milowsky, M. I., Dittrich, C., Duran, I., Jagdev, S., Millard, F. E., Sweeney, C. J., Bajorin, D., Cerbone, L., Quinn, D. I., Stadler, W. M.*, et al.* (2014). Phase 2 trial of dovitinib in patients with progressive FGFR3-mutated or FGFR3 wild-type advanced urothelial carcinoma. European Journal of Cancer *50*, 3145-3152.

Milowsky, M. I., Iyer, G., Regazzi, A. M., Al-Ahmadie, H., Gerst, S. R., Ostrovnaya, I., Gellert, L. L., Kaplan, R., Garcia-Grossman, I. R., Pendse, D.*, et al.* (2013). Phase II study of everolimus in metastatic urothelial cancer. BJU International *112*, 462-470.

Miyake, M., Ishii, M., Koyama, N., Kawashima, K., Kodama, T., Anai, S., Fujimoto, K., Hirao, Y., and Sugano, K. (2010). 1-tert-butyl-3-[6-(3,5-dimethoxy-phenyl)-2-(4-diethylamino-butylamino)-pyrido[2,3 -d]pyrimidin-7-yl]-urea (PD173074), a selective tyrosine kinase inhibitor of fibroblast growth factor receptor-3 (FGFR3), inhibits cell proliferation of bladder cancer carrying the FGFR3 gene mutation along with up-regulation of p27/Kip1 and G1/G0 arrest. The Journal of Pharmacology and Experimental Therapeutics *332*, 795-802.

Miyazaki, J., and Nishiyama, H. (2017). Epidemiology of urothelial carcinoma. International Journal of Urology *24*, 730-734.

Moelans, C. B., de Weger, R. A., Monsuur, H. N., Vijzelaar, R., and van Diest, P. J. (2010). Molecular profiling of invasive breast cancer by multiplex ligation-dependent probe amplification-based copy number analysis of tumor suppressor and oncogenes. Modern Pathology *23*, 1029-1039.

Mohammadi, M., Froum, S., Hamby, J. M., Schroeder, M. C., Panek, R. L., Lu, G. H., Eliseenkova, A. V., Green, D., Schlessinger, J., and

Hubbard, S. R. (1998). Crystal structure of an angiogenesis inhibitor bound to the FGF receptor tyrosine kinase domain. EMBO Journal *17*, 5896-5904.

Moidunny, S., Matos, M., Wesseling, E., Banerjee, S., Volsky, D. J., Cunha, R. A., Agostinho, P., Boddeke, H. W., and Roy, S. (2016). Oncostatin M promotes excitotoxicity by inhibiting glutamate uptake in astrocytes: implications in HIV-associated neurotoxicity. Journal of Neuroinflammation *13*, 144.

Mojarad, E. N., Kuppen, P. J. K., Aghdaei, H. A., and Zali, M. R. (2013). The CpG island methylator phenotype (CIMP) in colorectal cancer. Gastroenterology and Hepatology From Bed to Bench *6*, 120-128.

Morgillo, F., Woo, J. K., Kim, E. S., Hong, W. K., and Lee, H.-Y. (2006). Heterodimerization of Insulin-like Growth Factor Receptor/Epidermal Growth Factor Receptor and Induction of Survivin Expression Counteract the Antitumor Action of Erlotinib. Cancer Research *66*, 10100-10111.

Mosquera, C., Maglic, D., and Zervos, E. E. (2016). Molecular targeted therapy for pancreatic adenocarcinoma: A review of completed and ongoing late phase clinical trials. Cancer Genetics *209*, 567-581.

Moyer, J. D., Barbacci, E. G., Iwata, K. K., Arnold, L., Boman, B., Cunningham, A., DiOrio, C., Doty, J., Morin, M. J., Moyer, M. P.*, et al.* (1997). Induction of Apoptosis and Cell Cycle Arrest by CP-358,774, an Inhibitor of Epidermal Growth Factor Receptor Tyrosine Kinase. Cancer Research *57*, 4838-4848.

Muhlenberg, T., Zhang, Y., Wagner, A. J., Grabellus, F., Bradner, J., Taeger, G., Lang, H., Taguchi, T., Schuler, M., Fletcher, J. A., and Bauer, S. (2009). Inhibitors of deacetylases suppress oncogenic KIT signaling, acetylate HSP90, and induce apoptosis in gastrointestinal stromal tumors. Cancer Research *69*, 6941-6950.

Mulvihill, M. J., Cooke, A., Rosenfeld-Franklin, M., Buck, E., Foreman, K., Landfair, D., O'Connor, M., Pirritt, C., Sun, Y., Yao, Y.*, et al.* (2009). Discovery of OSI-906: a selective and orally efficacious dual inhibitor of the IGF-1 receptor and insulin receptor. Future Medicinal Chemistry *1*, 1153-1171.

Nahta, R., Yuan, L. X., Zhang, B., Kobayashi, R., and Esteva, F. J. (2005). Insulin-like growth factor-I receptor/human epidermal growth factor receptor 2 heterodimerization contributes to trastuzumab resistance of breast cancer cells. Cancer Research *65*, 11118-11128.

Nakata, S., Tanaka, H., Ito, Y., Hara, M., Fujita, M., Kondo, E., Kanemitsu, Y., Yatabe, Y., and Nakanishi, H. (2014). Deficient HER3 expression in poorly-differentiated colorectal cancer cells enhances gefitinib sensitivity. International Journal of Oncology *45*, 1583-1593.

Naldini, L. (2015). Gene therapy returns to centre stage. Nature *526*, 351-360.

Nazarian, R., Shi, H., Wang, Q., Kong, X., Koya, R. C., Lee, H., Chen, Z., Lee, M.-K., Attar, N., Sazegar, H.*, et al.* (2010). Melanomas acquire resistance to B-RAF(V600E) inhibition by RTK or N-RAS upregulation. Nature *468*, 973-977.

Nedjadi, T., Al-Maghrabi, J., Assidi, M., Dallol, A., Al-Kattabi, H., Chaudhary, A., Al-Sayyad, A., Al-Ammari, A., Abuzenadah, A., Buhmeida, A., and Al-Qahtani, M. (2016). Prognostic value of HER2 status in bladder

transitional cell carcinoma revealed by both IHC and BDISH techniques. BMC Cancer *16*, 653.

Nelson, K. N., Meyer, A. N., Siari, A., Campos, A. R., Motamedchaboki, K., and Donoghue, D. J. (2016). Oncogenic Gene Fusion FGFR3-TACC3 Is Regulated by Tyrosine Phosphorylation. Molecular Cancer Research *14*, 458-469.

Niault, T. S., and Baccarini, M. (2010). Targets of Raf in tumorigenesis. Carcinogenesis *31*, 1165-1174.

Nickerson, M. L., Witte, N., Im, K. M., Turan, S., Owens, C., Misner, K., Tsang, S. X., Cai, Z., Wu, S., Dean, M.*, et al.* (2017). Molecular analysis of urothelial cancer cell lines for modeling tumor biology and drug response. Oncogene *36*, 35-46.

Nishiyama, N., Arai, E., Nagashio, R., Fujimoto, H., Hosoda, F., Shibata, T., Tsukamoto, T., Yokoi, S., Imoto, I., Inazawa, J., and Kanai, Y. (2011). Copy number alterations in urothelial carcinomas: their clinicopathological significance and correlation with DNA methylation alterations. Carcinogenesis *32*, 462-469.

Nogova, L., Sequist, L. V., Garcia, J. M. P., Andre, F., Delord, J.-P., Hidalgo, M., Schellens, J. H. M., Cassier, P. A., Camidge, D. R., Schuler, M.*, et al.* (2017). Evaluation of BGJ398, a Fibroblast Growth Factor Receptor 1-3 Kinase Inhibitor, in Patients With Advanced Solid Tumors Harboring Genetic Alterations in Fibroblast Growth Factor Receptors: Results of a Global Phase I, Dose-Escalation and Dose-Expansion Study. Journal of Clinical Oncology *35*, 157-165.

O'Brien, N. A., Browne, B. C., Chow, L., Wang, Y., Ginther, C., Arboleda, J., Duffy, M. J., Crown, J., O'Donovan, N., and Slamon, D. J. (2010). Activated Phosphoinositide 3-Kinase/AKT Signaling Confers Resistance to Trastuzumab but not Lapatinib. Molecular Cancer Therapeutics *9*, 1489-1502.

O'Brien, S. G., Guilhot, F., Larson, R. A., Gathmann, I., Baccarani, M., Cervantes, F., Cornelissen, J. J., Fischer, T., Hochhaus, A., Hughes, T.*, et al.* (2003). Imatinib Compared with Interferon and Low-Dose Cytarabine for Newly Diagnosed Chronic-Phase Chronic Myeloid Leukemia. New England Journal of Medicine *348*, 994-1004.

Obaid, N. M., Bedard, K., and Huang, W.-Y. (2017). Strategies for Overcoming Resistance in Tumours Harboring BRAF Mutations. International Journal of Molecular Sciences *18*, 585.

Ohashi, K., Sequist, L. V., Arcila, M. E., Moran, T., Chmielecki, J., Lin, Y.-L., Pan, Y., Wang, L., de Stanchina, E., Shien, K.*, et al.* (2012). Lung cancers with acquired resistance to EGFR inhibitors occasionally harbor BRAF gene mutations but lack mutations in KRAS, NRAS, or MEK1. Proceedings of the National Academy of Sciences of the United States of America *109*, E2127-E2133.

Ohl, F., Jung, M., Radonic, A., Sachs, M., Loening, S. A., and Jung, K. (2006). Identification and validation of suitable endogenous reference genes for gene expression studies of human bladder cancer. Journal of Urology *175*, 1915-1920.

Oleksiewicz, U., Gładych, M., Raman, A. T., Heyn, H., Mereu, E., Chlebanowska, P., Andrzejewska, A., Sozańska, B., Samant, N., Fąk, K.*, et al.* (2017). TRIM28 and Interacting KRAB-ZNFs Control Self-Renewal of Human Pluripotent Stem Cells through Epigenetic

Repression of Pro-differentiation Genes. Stem Cell Reports *9*, 2065-2080.

Olsen, S. K., Ibrahimi, O. A., Raucci, A., Zhang, F., Eliseenkova, A. V., Yayon, A., Basilico, C., Linhardt, R. J., Schlessinger, J., and Mohammadi, M. (2004). Insights into the molecular basis for fibroblast growth factor receptor autoinhibition and ligand-binding promiscuity. Proceedings of the National Academy of Sciences of the United States of America *101*, 935-940.

Ornitz, D. M., Xu, J., Colvin, J. S., McEwen, D. G., MacArthur, C. A., Coulier, F., Gao, G., and Goldfarb, M. (1996). Receptor Specificity of the Fibroblast Growth Factor Family. Journal of Biological Chemistry *271*, 15292-15297.

Pacholsky, D., Vakeel, P., Himmel, M., Lowe, T., Stradal, T., Rottner, K., Furst, D. O., and van der Ven, P. F. (2004). Xin repeats define a novel actin-binding motif. Journal of Cell Science *117*, 5257-5268.

Paik, P. K., Shen, R., Berger, M. F., Ferry, D., Soria, J. C., Mathewson, A., Rooney, C., Smith, N. R., Cullberg, M., Kilgour, E.*, et al.* (2017). A Phase Ib Open-Label Multicenter Study of AZD4547 in Patients with Advanced Squamous Cell Lung Cancers. Clinical Cancer Research *23*, 5366-5373.

Pan, W., Yang, Y., Zhu, H., Zhang, Y., Zhou, R., and Sun, X. (2016). KRAS mutation is a weak, but valid predictor for poor prognosis and treatment outcomes in NSCLC: A meta-analysis of 41 studies. Oncotarget *7*, 8373-8388.

Pao, W., Wang, T. Y., Riely, G. J., Miller, V. A., Pan, Q., Ladanyi, M., Zakowski, M. F., Heelan, R. T., Kris, M. G., and Varmus, H. E. (2005). KRAS Mutations and Primary Resistance of Lung Adenocarcinomas to Gefitinib or Erlotinib. PLoS medicine *2*, e17.

Pardo, O. E., Latigo, J., Jeffery, R. E., Nye, E., Poulsom, R., Spencer-Dene, B., Lemoine, N. R., Stamp, G. W., Aboagye, E. O., and Seckl, M. J. (2009). The fibroblast growth factor receptor inhibitor PD173074 blocks small cell lung cancer growth in vitro and in vivo. Cancer Research *69*, 8645-8651.

Park, J.-Y., Zhang, F., and Andreassen, P. R. (2014). PALB2: The Hub of a Network of Tumor Suppressors involved in DNA damage responses. Biochimica et Biophysica Acta *1846*, 263-275.

Park, S., Jiang, Z., Mortenson, E. D., Deng, L., Radkevich-Brown, O., Yang, X., Sattar, H., Wang, Y., Brown, N. K., Greene, M.*, et al.* (2010). The therapeutic effect of anti-HER2/neu antibody depends on both innate and adaptive immunity. Cancer Cell *18*, 160-170.

Patgiri, A., Yadav, K. K., Arora, P. S., and Bar-Sagi, D. (2011). An orthosteric inhibitor of the Ras-Sos interaction. Nature Chemical Biology *7*, 585-587.

Paulsson, J., Rydén, L., Strell, C., Frings, O., Tobin, N. P., Fornander, T., Bergh, J., Landberg, G., Stål, O., and Östman, A. (2017). High expression of stromal PDGFRβ is associated with reduced benefit of tamoxifen in breast cancer. Journal of Pathology *3*, 38-43.

Peled, N., Wynes, M. W., Ikeda, N., Ohira, T., Yoshida, K., Qian, J., Ilouze, M., Brenner, R., Kato, Y., Mascaux, C., and Hirsch, F. R. (2013). Insulin-like growth factor-1 receptor (IGF-1R) as a biomarker for

resistance to the tyrosine kinase inhibitor gefitinib in non-small cell lung cancer. Cellular Oncology *36*, 277-288.

Perez, E. A., Romond, E. H., Suman, V. J., Jeong, J. H., Sledge, G., Geyer, C. E., Jr., Martino, S., Rastogi, P., Gralow, J., Swain, S. M.*, et al.* (2014). Trastuzumab plus adjuvant chemotherapy for human epidermal growth factor receptor 2-positive breast cancer: planned joint analysis of overall survival from NSABP B-31 and NCCTG N9831. Journal of Clinical Oncology *32*, 3744-3752.

Pérez-Ramírez, C., Cañadas-Garre, M., Molina, M. Á., Faus-Dáder, M. J., and Calleja-Hernández, M. Á. (2015). MET/HGF targeted drugs as potential therapeutic strategies in non-small cell lung cancer. Pharmacological Research *102*, 90-106.

Peset, I., and Vernos, I. (2008). The TACC proteins: TACC-ling microtubule dynamics and centrosome function. Trends in Cell Biology *18*, 379-388.

Peters, J. M., Tedeschi, A., and Schmitz, J. (2008). The cohesin complex and its roles in chromosome biology. Genes and Development *22*, 3089-3114.

Petrylak, D. P., Tangen, C. M., Van Veldhuizen, P. J., Jr., Goodwin, J. W., Twardowski, P. W., Atkins, J. N., Kakhil, S. R., Lange, M. K., Mansukhani, M., and Crawford, E. D. (2010). Results of the Southwest Oncology Group phase II evaluation (study S0031) of ZD1839 for advanced transitional cell carcinoma of the urothelium. BJU International *105*, 317-321.

Pietzak, E. J., Bagrodia, A., Cha, E. K., Drill, E. N., Iyer, G., Isharwal, S., Ostrovnaya, I., Baez, P., Li, Q., Berger, M. F.*, et al.* (2017). Next-generation Sequencing of Nonmuscle Invasive Bladder Cancer Reveals Potential Biomarkers and Rational Therapeutic Targets. European Urology *72*, 952-959.

Pitulescu, M. E., and Adams, R. H. (2014). Regulation of signaling interactions and receptor endocytosis in growing blood vessels. Cell Adhesion and Migration *8*, 366-377.

Platt, F. M., Hurst, C. D., Taylor, C. F., Gregory, W. M., Harnden, P., and Knowles, M. A. (2009). Spectrum of phosphatidylinositol 3-kinase pathway gene alterations in bladder cancer. Clinical Cancer Research *15*, 6008-6017.

Pollock, P. M., Gartside, M. G., Dejeza, L. C., Powell, M. A., Mallon, M. A., Davies, H., Mohammadi, M., Futreal, P. A., Stratton, M. R., Trent, J. M., and Goodfellow, P. J. (2007). Frequent activating FGFR2 mutations in endometrial carcinomas parallel germline mutations associated with craniosynostosis and skeletal dysplasia syndromes. Oncogene *26*, 7158-7162.

Pomerantz, J., Schreiber-Agus, N., Liegeois, N. J., Silverman, A., Alland, L., Chin, L., Potes, J., Chen, K., Orlow, I., Lee, H. W.*, et al.* (1998). The Ink4a tumor suppressor gene product, p19Arf, interacts with MDM2 and neutralizes MDM2's inhibition of p53. Cell *92*, 713-723.

Powles, T., Duran, I., van der Heijden, M. S., Loriot, Y., Vogelzang, N. J., De Giorgi, U., Oudard, S., Retz, M. M., Castellano, D., Bamias, A.*, et al.* (2018). Atezolizumab versus chemotherapy in patients with platinum-treated locally advanced or metastatic urothelial carcinoma

(IMvigor211): a multicentre, open-label, phase 3 randomised controlled trial. Lancet *391*, 748-757.

Powles, T., Huddart, R. A., Elliott, T., Sarker, S. J., Ackerman, C., Jones, R., Hussain, S., Crabb, S., Jagdev, S., Chester, J.*, et al.* (2017). Phase III, Double-Blind, Randomized Trial That Compared Maintenance Lapatinib Versus Placebo After First-Line Chemotherapy in Patients With Human Epidermal Growth Factor Receptor 1/2-Positive Metastatic Bladder Cancer. Journal of Clinical Oncology *35*, 48-55.

Powles, T., Kilgour, E., Mather, R., Galer, A., Arkenau, H.-T., Farnsworth, A., Wilde, J., Ratnayake, J., and Landers, D. (2016). BISCAY, a phase Ib, biomarker-directed multidrug umbrella study in patients with metastatic bladder cancer. Journal of Clinical Oncology *34*, TPS4577-TPS4577.

Pradere, B., Thibault, C., Vetterlein, M. W., Leow, J. J., Peyronnet, B., Roupret, M., and Seisen, T. (2017). Peri-operative chemotherapy for muscle-invasive bladder cancer: status-quo in 2017. Translational Andrology and Urology *6*, 1049-1059.

Prahallad, A., Sun, C., Huang, S., Di Nicolantonio, F., Salazar, R., Zecchin, D., Beijersbergen, R. L., Bardelli, A., and Bernards, R. (2012). Unresponsiveness of colon cancer to BRAF(V600E) inhibition through feedback activation of EGFR. Nature *483*, 100-103.

Prout, G. R., Jr., Barton, B. A., Griffin, P. P., and Friedell, G. H. (1992). Treated history of noninvasive grade 1 transitional cell carcinoma. The National Bladder Cancer Group. The Journal of Urology *148*, 1413-1419.

Pruthi, R. S., Nielsen, M., Heathcote, S., Wallen, E. M., Rathmell, W. K., Godley, P., Whang, Y., Fielding, J., Schultz, H., Grigson, G.*, et al.* (2010). A phase II trial of neoadjuvant erlotinib in patients with muscle-invasive bladder cancer undergoing radical cystectomy: clinical and pathological results. BJU International *106*, 349-354.

Ramirez, M., Rajaram, S., Steininger, R. J., Osipchuk, D., Roth, M. A., Morinishi, L. S., Evans, L., Ji, W., Hsu, C. H., Thurley, K.*, et al.* (2016). Diverse drug-resistance mechanisms can emerge from drug-tolerant cancer persister cells. Nature Communications *7*, 10690.

Ranieri, D., Rosato, B., Nanni, M., Magenta, A., Belleudi, F., and Torrisi, M. R. (2016). Expression of the FGFR2 mesenchymal splicing variant in epithelial cells drives epithelial-mesenchymal transition. Oncotarget *7*, 5440-5460.

Razis, E., Bobos, M., Kotoula, V., Eleftheraki, A. G., Kalofonos, H. P., Pavlakis, K., Papakostas, P., Aravantinos, G., Rigakos, G., Efstratiou, I.*, et al.* (2011). Evaluation of the association of PIK3CA mutations and PTEN loss with efficacy of trastuzumab therapy in metastatic breast cancer. Breast Cancer Research and Treatment *128*, 447-456.

Rebouissou, S., Herault, A., Letouze, E., Neuzillet, Y., Laplanche, A., Ofualuka, K., Maille, P., Leroy, K., Riou, A., Lepage, M. L.*, et al.* (2012). CDKN2A homozygous deletion is associated with muscle invasion in FGFR3-mutated urothelial bladder carcinoma. Journal of Pathology *227*, 315-324.

Reis, E. S., Mastellos, D. C., Ricklin, D., Mantovani, A., and Lambris, J. D. (2018). Complement in cancer: untangling an intricate relationship. Nature Reviews Immunology *18*, 5-18.

Reiss, Y., Goldstein, J. L., Seabra, M. C., Casey, P. J., and Brown, M. S. (1990). Inhibition of purified p21ras farnesyl:protein transferase by Cys-AAX tetrapeptides. Cell *62*, 81-88.

Rexer, B. N., Chanthaphaychith, S., Dahlman, K. B., and Arteaga, C. L. (2014). Direct inhibition of PI3K in combination with dual HER2 inhibitors is required for optimal antitumor activity in HER2+ breast cancer cells. Breast Cancer Research *16*, R9-R9.

Rexer, B. N., Ghosh, R., Narasanna, A., Estrada, M. V., Chakrabarty, A., Song, Y., Engelman, J. A., and Arteaga, C. L. (2013). Human breast cancer cells harboring a gatekeeper T798M mutation in HER2 overexpress EGFR ligands and are sensitive to dual inhibition of EGFR and HER2. Clinical Cancer Research *19*, 5390-5401.

Rhodes, D. R., Kalyana-Sundaram, S., Mahavisno, V., Varambally, R., Yu, J., Briggs, B. B., Barrette, T. R., Anstet, M. J., Kincead-Beal, C., Kulkarni, P.*, et al.* (2007). Oncomine 3.0: Genes, Pathways, and Networks in a Collection of 18,000 Cancer Gene Expression Profiles. Neoplasia *9*, 166-180.

Rigby, C. C., and Franks, L. M. (1970). A human tissue culture cell line from a transitional cell tumour of the urinary bladder: growth, chromosone pattern and ultrastructure. British Journal of Cancer *24*, 746-754.

Robak, P., and Robak, T. (2017). Novel synthetic drugs currently in clinical development for chronic lymphocytic leukemia. Expert Opinion on Investigational Drugs *26*, 1249-1265.

Robbins, J., Dilworth, S. M., Laskey, R. A., and Dingwall, C. (1991). Two interdependent basic domains in nucleoplasmin nuclear targeting sequence: identification of a class of bipartite nuclear targeting sequence. Cell *64*, 615-623.

Robertson, A. G., Kim, J., Al-Ahmadie, H., Bellmunt, J., Guo, G., Cherniack, A. D., Hinoue, T., Laird, P. W., Hoadley, K. A., Akbani, R.*, et al.* (2017). Comprehensive Molecular Characterization of Muscle-Invasive Bladder Cancer. Cell *171*, 540-556.e525.

Rodriguez-Viciana, P., Warne, P. H., Dhand, R., Vanhaesebroeck, B., Gout, I., Fry, M. J., Waterfield, M. D., and Downward, J. (1994). Phosphatidylinositol-3-OH kinase as a direct target of Ras. Nature *370*, 527-532.

Roh, Y. G., Mun, M. H., Jeong, M. S., Kim, W. T., Lee, S. R., Chung, J. W., Kim, S. I., Kim, T. N., Nam, J. K., and Leem, S. H. (2018). Drug resistance of bladder cancer cells through activation of ABCG2 by FOXM1. BMB Reports. *51*, 98-103

Rojas, M., Yao, S., and Lin, Y. Z. (1996). Controlling epidermal growth factor (EGF)-stimulated Ras activation in intact cells by a cell-permeable peptide mimicking phosphorylated EGF receptor. Journal of Biological Chemistry *271*, 27456-27461.

Rosenberg, J. E., Hoffman-Censits, J., Powles, T., van der Heijden, M. S., Balar, A. V., Necchi, A., Dawson, N., O'Donnell, P. H., Balmanoukian, A., Loriot, Y.*, et al.* (2016). Atezolizumab in patients with locally advanced and metastatic urothelial carcinoma who have progressed following treatment with platinum-based chemotherapy: a single-arm, multicentre, phase 2 trial. Lancet *387*, 1909-1920.

Roskoski, R. (2014). The ErbB/HER family of protein-tyrosine kinases and cancer. Pharmacological Research *79*, 34-74.

Ross, J. S., Wang, K., Al-Rohil, R. N., Nazeer, T., Sheehan, C. E., Otto, G. A., He, J., Palmer, G., Yelensky, R., Lipson, D.*, et al.* (2014). Advanced urothelial carcinoma: next-generation sequencing reveals diverse genomic alterations and targets of therapy. Modern Pathology *27*, 271-280.

Ross, R. L., Burns, J. E., Taylor, C. F., Mellor, P., Anderson, D. H., and Knowles, M. A. (2013). Identification of mutations in distinct regions of p85 alpha in urothelial cancer. PLoS One *8*, e84411.

Russo, A., Franchina, T., Rita Ricciardi, G. R., Picone, A., Ferraro, G., Zanghì, M., Toscano, G., Giordano, A., and Adamo, V. (2015). A decade of EGFR inhibition in EGFR-mutated non small cell lung cancer (NSCLC): Old successes and future perspectives. Oncotarget *6*, 26814-26825.

Salesse, S., and Verfaillie, C. M. (2002). BCR/ABL: from molecular mechanisms of leukemia induction to treatment of chronic myelogenous leukemia. Oncogene *21*, 8547-8559.

Santarpia, M., Liguori, A., Karachaliou, N., Gonzalez-Cao, M., Daffinà, M. G., D'Aveni, A., Marabello, G., Altavilla, G., and Rosell, R. (2017). Osimertinib in the treatment of non-small-cell lung cancer: design, development and place in therapy. Lung Cancer: Targets and Therapy *8*, 109-125.

Santos-Rosa, H., Schneider, R., Bannister, A. J., Sherriff, J., Bernstein, B. E., Emre, N. C., Schreiber, S. L., Mellor, J., and Kouzarides, T. (2002). Active genes are tri-methylated at K4 of histone H3. Nature *419*, 407-411.

Sartore-Bianchi, A., Trusolino, L., Martino, C., Bencardino, K., Lonardi, S., Bergamo, F., Zagonel, V., Leone, F., Depetris, I., Martinelli, E.*, et al.* (2016). Dual-targeted therapy with trastuzumab and lapatinib in treatment-refractory, KRAS codon 12/13 wild-type, HER2-positive metastatic colorectal cancer (HERACLES): a proof-of-concept, multicentre, open-label, phase 2 trial. The Lancet Oncology *17*, 738-746.

Scagliotti, G. V., Bondarenko, I., Blackhall, F., Barlesi, F., Hsia, T. C., Jassem, J., Milanowski, J., Popat, S., Sanchez-Torres, J. M., Novello, S.*, et al.* (2015). Randomized, phase III trial of figitumumab in combination with erlotinib versus erlotinib alone in patients with nonadenocarcinoma nonsmall-cell lung cancer. Annals of Oncology *26*, 497-504.

Scaltriti, M., Chandarlapaty, S., Prudkin, L., Aura, C., Jimenez, J., Angelini, P. D., Sánchez, G., Guzman, M., Parra, J. L., Ellis, C.*, et al.* (2010). Clinical benefit of lapatinib-based therapy in patients with HER2-positive breast tumors co-expressing the truncated p95HER2 receptor. Clinical Cancer Research *16*, 2688-2695.

Scaltriti, M., Rojo, F., Ocana, A., Anido, J., Guzman, M., Cortes, J., Di Cosimo, S., Matias-Guiu, X., Ramon y Cajal, S., Arribas, J., and Baselga, J. (2007). Expression of p95HER2, a truncated form of the HER2 receptor, and response to anti-HER2 therapies in breast cancer. Journal of the National Cancer Institute *99*, 628-638.

Scheid, C., Reece, D., Beksac, M., Spencer, A., Callander, N., Sonneveld, P., Kalimi, G., Cai, C., Shi, M., Scott, J. W., and Stewart, A. K. (2015). Phase 2 study of dovitinib in patients with relapsed or refractory

multiple myeloma with or without t(4;14) translocation. European Journal of Haematology *95*, 316-324.

Schellens, J. H. M., van Geel, R., Bendell, J. C., Spreafico, A., Schuler, M., Yoshino, T., Delord, J.-P., Yamada, Y., Lolkema, M. P., Faris, J. E.*, et al.* (2015). Abstract CT136: Final biomarker analysis of the phase I study of the selective BRAF V600 inhibitor encorafenib (LGX818) combined with cetuximab with or without the α-specific PI3K inhibitor alpelisib (BYL719) in patients with advanced BRAF-mutant colorectal cancer. Cancer Research *75*, CT136-CT136.

Schindler, T., Bornmann, W., Pellicena, P., Miller, W. T., Clarkson, B., and Kuriyan, J. (2000). Structural Mechanism for STI-571 Inhibition of Abelson Tyrosine Kinase. Science *289*, 1938-1942.

Schroeder, A., Mueller, O., Stocker, S., Salowsky, R., Leiber, M., Gassmann, M., Lightfoot, S., Menzel, W., Granzow, M., and Ragg, T. (2006). The RIN: an RNA integrity number for assigning integrity values to RNA measurements. BMC Molecular Biology *7*, 3-3.

Sclafani, F., Kim, T. Y., Cunningham, D., Kim, T. W., Tabernero, J., Schmoll, H. J., Roh, J. K., Kim, S. Y., Park, Y. S., Guren, T. K.*, et al.* (2015). A Randomized Phase II/III Study of Dalotuzumab in Combination With Cetuximab and Irinotecan in Chemorefractory, KRAS Wild-Type, Metastatic Colorectal Cancer. Journal of the National Cancer Institute *107*, djv258.

Sclafani, F., Kim, T. Y., Cunningham, D., Kim, T. W., Tabernero, J., Schmoll, H. J., Roh, J. K., Kim, S. Y., Park, Y. S., Guren, T. K.*, et al.* (2017). Dalotuzumab in chemorefractory KRAS exon 2 mutant colorectal cancer: Results from a randomised phase II/III trial. International Journal of Cancer *140*, 431-439.

Scott, A. J., Lieu, C. H., and Messersmith, W. A. (2016). Therapeutic Approaches to RAS Mutation. Cancer Journal *22*, 165-174.

Scott, A. M., Allison, J. P., and Wolchok, J. D. (2012). Monoclonal antibodies in cancer therapy. Cancer Immunity *12*, 14.

Scully, R., Chen, J., Plug, A., Xiao, Y., Weaver, D., Feunteun, J., Ashley, T., and Livingston, D. M. (1997). Association of BRCA1 with Rad51 in mitotic and meiotic cells. Cell *88*, 265-275.

Seiler, R., Ashab, H. A. D., Erho, N., van Rhijn, B. W. G., Winters, B., Douglas, J., Van Kessel, K. E., Fransen van de Putte, E. E., Sommerlad, M., Wang, N. Q.*, et al.* (2017). Impact of Molecular Subtypes in Muscle-invasive Bladder Cancer on Predicting Response and Survival after Neoadjuvant Chemotherapy. European Urology *72*, 544-554.

Sequist, L. V., Waltman, B. A., Dias-Santagata, D., Digumarthy, S., Turke, A. B., Fidias, P., Bergethon, K., Shaw, A. T., Gettinger, S., Cosper, A. K.*, et al.* (2011). Genotypic and Histological Evolution of Lung Cancers Acquiring Resistance to EGFR Inhibitors. Science Translational Medicine *3*, 75ra26-75ra26.

Seront, E., Rottey, S., Sautois, B., Kerger, J., D'Hondt, L. A., Verschaeve, V., Canon, J. L., Dopchie, C., Vandenbulcke, J. M., Whenham, N.*, et al.* (2012). Phase II study of everolimus in patients with locally advanced or metastatic transitional cell carcinoma of the urothelial tract: clinical activity, molecular response, and biomarkers. Annals of Oncology *23*, 2663-2670.

Serrano, M. J., Ortega, F. G., Alvarez-Cubero, M. J., Nadal, R., Sanchez-Rovira, P., Salido, M., Rodríguez, M., García-Puche, J. L., Delgado-Rodriguez, M., Solé, F.*, et al.* (2014). EMT and EGFR in CTCs cytokeratin negative non-metastatic breast cancer. Oncotarget *5*, 7486-7497.

Sforza, V., Martinelli, E., Ciardiello, F., Gambardella, V., Napolitano, S., Martini, G., della Corte, C., Cardone, C., Ferrara, M. L., Reginelli, A.*, et al.* (2016). Mechanisms of resistance to anti-epidermal growth factor receptor inhibitors in metastatic colorectal cancer. World Journal of Gastroenterology *22*, 6345-6361.

Shali, H., Ahmadi, M., Kafil, H. S., Dorosti, A., and Yousefi, M. (2016). IGF1R and c-met as therapeutic targets for colorectal cancer. Biomedicine and Pharmacotherapy *82*, 528-536.

Sharma, P., Retz, M., Siefker-Radtke, A., Baron, A., Necchi, A., Bedke, J., Plimack, E. R., Vaena, D., Grimm, M. O., Bracarda, S.*, et al.* (2017). Nivolumab in metastatic urothelial carcinoma after platinum therapy (CheckMate 275): a multicentre, single-arm, phase 2 trial. The Lancet Oncology *18*, 312-322.

Sharma, S. V., Lee, D. Y., Li, B., Quinlan, M. P., Takahashi, F., Maheswaran, S., McDermott, U., Azizian, N., Zou, L., Fischbach, M. A.*, et al.* (2010). A chromatin-mediated reversible drug tolerant state in cancer cell subpopulations. Cell *141*, 69-80.

Shaulian, E. (2010). AP-1 — The Jun proteins: Oncogenes or tumor suppressors in disguise? Cellular Signalling *22*, 894-899.

Shi, E., Kan, M., Xu, J., Wang, F., Hou, J., and McKeehan, W. L. (1993). Control of fibroblast growth factor receptor kinase signal transduction by heterodimerization of combinatorial splice variants. Molecular and Cellular Biology *13*, 3907-3918.

Shi, F., Telesco, S. E., Liu, Y., Radhakrishnan, R., and Lemmon, M. A. (2010). ErbB3/HER3 intracellular domain is competent to bind ATP and catalyze autophosphorylation. Proceedings of the National Academy of Sciences of the United States of America *107*, 7692-7697.

Shi, H., Hugo, W., Kong, X., Hong, A., Koya, R. C., Moriceau, G., Chodon, T., Guo, R., Johnson, D. B., Dahlman, K. B.*, et al.* (2014). Acquired resistance and clonal evolution in melanoma during BRAF inhibitor therapy. Cancer Discovery *4*, 80-93.

Shimoyama, Y., Takeda, H., Yoshihara, S., Kitajima, M., and Hirohashi, S. (1999). Biochemical characterization and functional analysis of two type II classic cadherins, cadherin-6 and -14, and comparison with E-cadherin. The Journal of Biological Chemistry *274*, 11987-11994.

Shin, S. M., Choi, D. K., Jung, K., Bae, J., Kim, J. S., Park, S. W., Song, K. H., and Kim, Y. S. (2017). Antibody targeting intracellular oncogenic Ras mutants exerts anti-tumour effects after systemic administration. Nature Communications *8*, 15090.

Singh, M., and Jadhav, H. R. (2017). Targeting non-small cell lung cancer with small-molecule EGFR tyrosine kinase inhibitors. Drug Discovery Today *17*, 30371-30379.

Singh, M., Yelle, N., Venugopal, C., and Singh, S. K. (2017). EMT: Mechanisms and therapeutic implications. Pharmacology and Therapeutics. *182*, 80-94.

Shintani, T., Kusuhara, Y., Daizumoto, K., Dondoo, T.-O., Yamamoto, H., Mori, H., Fukawa, T., Nakatsuji, H., Fukumori, T., Takahashi, M., and Kanayama, H. (2017). The Involvement of Hepatocyte Growth Factor-MET-Matrix Metalloproteinase 1 Signaling in Bladder Cancer Invasiveness and Proliferation. Effect of the MET Inhibitor, Cabozantinib (XL184), on Bladder Cancer Cells. Urology *101*, 169.e167-169.e113.

Sholl, L. M. (2016). The Molecular Pathology of Lung Cancer. Surgical Pathology Clinics *9*, 353-378.

Silva, P. N., Altamentova, S. M., Kilkenny, D. M., and Rocheleau, J. V. (2013). Fibroblast growth factor receptor like-1 (FGFRL1) interacts with SHP-1 phosphatase at insulin secretory granules and induces beta-cell ERK1/2 protein activation. The Journal of Biological Chemistry *288*, 17859-17870.

Simpson, R. J., Yi Lee, S. H., Bartle, N., Sum, E. Y., Visvader, J. E., Matthews, J. M., Mackay, J. P., and Crossley, M. (2004). A classic zinc finger from friend of GATA mediates an interaction with the coiled-coil of transforming acidic coiled-coil 3. The Journal of Biological Chemistry *279*, 39789-39797.

Singh, B., and Coffey, R. J. (2014). From wavy hair to naked proteins: The role of transforming growth factor alpha in health and disease. Seminars in Cell and Developmental Biology *28*, 12-21.

Singh, D., Chan, J. M., Zoppoli, P., Niola, F., Sullivan, R., Castano, A., Liu, E. M., Reichel, J., Porrati, P., Pellegatta, S.*, et al.* (2012). Transforming Fusions of FGFR and TACC Genes in Human Glioblastoma. Science *337*, 1231-1235.

Singh, M., and Jadhav, H. R. (2017). Targeting non-small cell lung cancer with small-molecule EGFR tyrosine kinase inhibitors. Drug Discovery Today *17*, 30371-30379.

Singh, M., Yelle, N., Venugopal, C., and Singh, S. K. (2017). EMT: Mechanisms and therapeutic implications. Pharmacology and Therapeutics. *182*, 80-94

Sjödahl, G., Eriksson, P., Liedberg, F., and Höglund, M. (2017). Molecular classification of urothelial carcinoma: global mRNA classification versus tumour-cell phenotype classification. The Journal of Pathology *242*, 113-125.

Sjodahl, G., Lauss, M., Lovgren, K., Chebil, G., Gudjonsson, S., Veerla, S., Patschan, O., Aine, M., Ferno, M., Ringner, M.*, et al.* (2012). A molecular taxonomy for urothelial carcinoma. Clinical Cancer Research *18*, 3377-3386.

Sjodahl, G., Lovgren, K., Lauss, M., Patschan, O., Gudjonsson, S., Chebil, G., Aine, M., Eriksson, P., Mansson, W., Lindgren, D.*, et al.* (2013). Toward a molecular pathologic classification of urothelial carcinoma. American Journal of Pathology *183*, 681-691.

Sleeman, M., Fraser, J., McDonald, M., Yuan, S., White, D., Grandison, P., Kumble, K., Watson, J. D., and Murison, J. G. (2001). Identification of a new fibroblast growth factor receptor, FGFR5. Gene *271*, 171-182.

Smyth, E. C., Turner, N. C., Peckitt, C., Pearson, A., Brown, G., Chua, S., Gillbanks, A., Johnston, S. R. D., TARAZONA, N., Cutts, R.*, et al.* (2015). Phase II multicenter proof of concept study of AZD4547 in FGFR amplified tumours. Journal of Clinical Oncology *33*, 2508-2508.

Snell, L. M., McGaha, T. L., and Brooks, D. G. (2017). Type I Interferon in Chronic Virus Infection and Cancer. Trends in Immunology *38*, 542-557.

Sohl, C. D., Ryan, M. R., Luo, B., Frey, K. M., and Anderson, K. S. (2015). Illuminating the Molecular Mechanisms of Tyrosine Kinase Inhibitor Resistance for the FGFR1 Gatekeeper Mutation: The Achilles' Heel of Targeted Therapy. ACS Chemical Biology *10*, 1319-1329.

Solomon, D. A., Kim, J.-S., Bondaruk, J., Shariat, S. F., Wang, Z.-F., Elkahloun, A. G., Ozawa, T., Gerard, J., Zhuang, D., Zhang, S.*, et al.* (2013). Frequent truncating mutations of STAG2 in bladder cancer. Nature Genetics *45*, 1428-1430.

Solomon, D. A., Kim, J.-S., and Waldman, T. (2014). Cohesin gene mutations in tumorigenesis: from discovery to clinical significance. BMB Reports *47*, 299-310.

Song, Z. (2013). Roles of the nucleotide sugar transporters (SLC35 family) in health and disease. Molecular Aspects of Medicine *34*, 590-600.

Soria, J. C., DeBraud, F., Bahleda, R., Adamo, B., Andre, F., Dienstmann, R., Delmonte, A., Cereda, R., Isaacson, J., Litten, J.*, et al.* (2014). Phase I/IIa study evaluating the safety, efficacy, pharmacokinetics, and pharmacodynamics of lucitanib in advanced solid tumors. Annals of Oncology *25*, 2244-2251.

Soverini, S., Branford, S., Nicolini, F. E., Talpaz, M., Deininger, M. W. N., Martinelli, G., Müller, M. C., Radich, J. P., and Shah, N. P. (2014). Implications of BCR-ABL1 kinase domain-mediated resistance in chronic myeloid leukemia. Leukemia Research *38*, 10-20.

Spencer-Smith, R., and O'Bryan, J. P. (2017). Direct inhibition of RAS: Quest for the Holy Grail? Seminars in Cancer Biology. doi: 10.1016/j.semcancer.2017.12.005.

Steinberg, F., Zhuang, L., Beyeler, M., Kälin, R. E., Mullis, P. E., Brändli, A. W., and Trueb, B. (2010). The FGFRL1 Receptor Is Shed from Cell Membranes, Binds Fibroblast Growth Factors (FGFs), and Antagonizes FGF Signaling in Xenopus Embryos. The Journal of Biological Chemistry *285*, 2193-2202.

Stephens, P., Hunter, C., Bignell, G., Edkins, S., Davies, H., Teague, J., Stevens, C., O'Meara, S., Smith, R., Parker, A.*, et al.* (2004). Lung cancer: intragenic ERBB2 kinase mutations in tumours. Nature *431*, 525-526.

Striz, I. (2017). Cytokines of the IL-1 family: recognized targets in chronic inflammation underrated in organ transplantations. Clinical Science *131*, 2241-2256.

Sun, H. Z., Wu, S. F., and Tu, Z. H. (2001). Blockage of IGF-1R signaling sensitizes urinary bladder cancer cells to mitomycin-mediated cytotoxicity. Cell Research *11*, 107-115.

Svatek, R. S., Hollenbeck, B. K., Holmang, S., Lee, R., Kim, S. P., Stenzl, A., and Lotan, Y. (2014). The economics of bladder cancer: costs and considerations of caring for this disease. European Urology *66*, 253-262.

Sylvester, R. J., van der Meijden, A. P. M., Oosterlinck, W., Witjes, J. A., Bouffioux, C., Denis, L., Newling, D. W. W., and Kurth, K. (2006). Predicting Recurrence and Progression in Individual Patients with Stage Ta T1 Bladder Cancer Using EORTC Risk Tables: A Combined

Analysis of 2596 Patients from Seven EORTC Trials. European Urology *49*, 466-477.

Tabernero, J., Bahleda, R., Dienstmann, R., Infante, J. R., Mita, A., Italiano, A., Calvo, E., Moreno, V., Adamo, B., Gazzah, A.*, et al.* (2015a). Phase I Dose-Escalation Study of JNJ-42756493, an Oral Pan–Fibroblast Growth Factor Receptor Inhibitor, in Patients With Advanced Solid Tumors. Journal of Clinical Oncology *33*, 3401-3408.

Tabernero, J., Bahleda, R., Dienstmann, R., Infante, J. R., Mita, A., Italiano, A., Calvo, E., Moreno, V., Adamo, B., Gazzah, A.*, et al.* (2015b). Phase I Dose-Escalation Study of JNJ-42756493, an Oral Pan-Fibroblast Growth Factor Receptor Inhibitor, in Patients With Advanced Solid Tumors. Journal of Clinical Oncology *33*, 3401-3408.

Takeuchi, T., Adachi, Y., Sonobe, H., Furihata, M., and Ohtsuki, Y. (2006). A ubiquitin ligase, skeletrophin, is a negative regulator of melanoma invasion. Oncogene *25*, 7059-7069.

Tan, H. L., Queenan, B. N., and Huganir, R. L. (2015). GRIP1 is required for homeostatic regulation of AMPAR trafficking. Proceedings of the National Academy of Sciences of the United States of America *112*, 10026-10031.

Tanizaki, J., Okamoto, I., Sakai, K., and Nakagawa, K. (2011). Differential roles of trans-phosphorylated EGFR, HER2, HER3, and RET as heterodimerisation partners of MET in lung cancer with MET amplification. British Journal of Cancer *105*, 807-813.

Taylor, C. F., Platt, F. M., Hurst, C. D., Thygesen, H. H., and Knowles, M. A. (2014). Frequent inactivating mutations of STAG2 in bladder cancer are associated with low tumour grade and stage and inversely related to chromosomal copy number changes. Human Molecular Genetics *23*, 1964-1974.

Taylor, J. G., Cheuk, A. T., Tsang, P. S., Chung, J.-Y., Song, Y. K., Desai, K., Yu, Y., Chen, Q.-R., Shah, K., Youngblood, V.*, et al.* (2009). Identification of FGFR4-activating mutations in human rhabdomyosarcomas that promote metastasis in xenotransplanted models. The Journal of Clinical Investigation *119*, 3395-3407.

Teh, M.-T., Gemenetzidis, E., Patel, D., Tariq, R., Nadir, A., Bahta, A. W., Waseem, A., and Hutchison, I. L. (2012). FOXM1 Induces a Global Methylation Signature That Mimics the Cancer Epigenome in Head and Neck Squamous Cell Carcinoma. PLoS ONE *7*, e34329.

Theelen, W. S. M. E., Mittempergher, L., Willems, S. M., Bosma, A. J., Peters, D. D. G. C., van der Noort, V., Japenga, E. J., Peeters, T., Koole, K., Šuštić, T.*, et al.* (2016). FGFR1, 2 and 3 protein overexpression and molecular aberrations of FGFR3 in early stage non-small cell lung cancer. The Journal of Pathology *2*, 223-233.

Thorvaldsdottir, H., Robinson, J. T., and Mesirov, J. P. (2013). Integrative Genomics Viewer (IGV): high-performance genomics data visualization and exploration. Briefings in Bioinformatics *14*, 178-192.

Tomasini, P., Walia, P., Labbe, C., Jao, K., and Leighl, N. B. (2016). Targeting the KRAS Pathway in Non-Small Cell Lung Cancer. Oncologist *21*, 1450-1460.

Tomlinson, D. C., Baldo, O., Harnden, P., and Knowles, M. A. (2007). FGFR3 protein expression and its relationship to mutation status and

prognostic variables in bladder cancer. The Journal of Pathology *213*, 91-98.

Tomlinson, D. C., Baxter, E. W., Loadman, P. M., Hull, M. A., and Knowles, M. A. (2012). FGFR1-Induced Epithelial to Mesenchymal Transition through MAPK/PLCγ/COX-2-Mediated Mechanisms. PLoS ONE *7*, e38972.

Tomlinson, D. C., and Knowles, M. A. (2010). Altered Splicing of FGFR1 Is Associated with High Tumor Grade and Stage and Leads to Increased Sensitivity to FGF1 in Bladder Cancer. The American Journal of Pathology *177*, 2379-2386.

Tomlinson, D. C., Lamont, F. R., Shnyder, S. D., and Knowles, M. A. (2009). FGFR1 promotes proliferation and survival via activation of the MAPK pathway in bladder cancer. Cancer Research *69*, 4613-4620.

Topalian, S. L., Drake, C. G., and Pardoll, D. M. (2015). Immune checkpoint blockade: a common denominator approach to cancer therapy. Cancer Cell *27*, 450-461.

Trouche, D., Le Chalony, C., Muchardt, C., Yaniv, M., and Kouzarides, T. (1997). RB and hbrm cooperate to repress the activation functions of E2F1. Proceedings of the National Academy of Sciences of the United States of America *94*, 11268-11273.

Trudel, S., Ely, S., Farooqi, Y., Affer, M., Robbiani, D. F., Chesi, M., and Bergsagel, P. L. (2004). Inhibition of fibroblast growth factor receptor 3 induces differentiation and apoptosis in t(4;14) myeloma. Blood *103*, 3521-3528.

Trudel, S., Li, Z. H., Wei, E., Wiesmann, M., Chang, H., Chen, C., Reece, D., Heise, C., and Stewart, A. K. (2005). CHIR-258, a novel, multitargeted tyrosine kinase inhibitor for the potential treatment of t(4;14) multiple myeloma. Blood *105*, 2941-2948.

Trueb, B., Zhuang, L., Taeschler, S., and Wiedemann, M. (2003). Characterization of FGFRL1, a novel fibroblast growth factor (FGF) receptor preferentially expressed in skeletal tissues. The Journal of Biological Chemistry *278*, 33857-33865.

Tseng, L.-C., Zhang, C., Cheng, C.-M., Xu, H., Hsu, C.-H., and Jiang, Y.-J. (2014). New Classes of Mind Bomb-Interacting Proteins Identified from Yeast Two-Hybrid Screens. PLoS ONE *9*, e93394.

Tsiambas, E., Lefas, A. Y., Georgiannos, S. N., Ragos, V., Fotiades, P. P., Grapsa, D., Stamatelopoulos, A., Kavantzas, N., Patsouris, E., and Syrigos, K. (2016). EGFR gene deregulation mechanisms in lung adenocarcinoma: A molecular review. Pathology - Research and Practice *212*, 672-677.

Tuna, B., Yorukoglu, K., Tuzel, E., Guray, M., Mungan, U., and Kirkali, Z. (2003). Expression of p53 and mdm2 and their significance in recurrence of superficial bladder cancer. Pathology, research and practice *199*, 323-328.

Turner, N., Pearson, A., Sharpe, R., Lambros, M., Geyer, F., Lopez-Garcia, M. A., Natrajan, R., Marchio, C., Iorns, E., Mackay, A*., et al.* (2010). FGFR1 amplification drives endocrine therapy resistance and is a therapeutic target in breast cancer. Cancer Research *70*, 2085-2094.

Ullrich, A., and Schlessinger, J. (1990). Signal transduction by receptors with tyrosine kinase activity. Cell *61*, 203-212.

Ungefroren, H., Witte, D., and Lehnert, H. (2017). The role of small GTPases of the Rho/Rac family in TGF-beta-induced EMT and cell motility in cancer. Developmental Dynamics. *247*, 451-461

van de Wetering, M., Francies, H. E., Francis, J. M., Bounova, G., Iorio, F., Pronk, A., van Houdt, W., van Gorp, J., Taylor-Weiner, A., Kester, L.*, et al.* (2015). Prospective derivation of a living organoid biobank of colorectal cancer patients. Cell *161*, 933-945.

Van Emburgh, B. O., Arena, S., Siravegna, G., Lazzari, L., Crisafulli, G., Corti, G., Mussolin, B., Baldi, F., Buscarino, M., Bartolini, A.*, et al.* (2016). Acquired RAS or EGFR mutations and duration of response to EGFR blockade in colorectal cancer. Nature Communications *7*, 13665.

van Haaften, G., Dalgliesh, G. L., Davies, H., Chen, L., Bignell, G., Greenman, C., Edkins, S., Hardy, C., O'Meara, S., Teague, J.*, et al.* (2009). Somatic mutations of the histone H3K27 demethylase, UTX, in human cancer. Nature Genetics *41*, 521-523.

van Weering, D. H., de Rooij, J., Marte, B., Downward, J., Bos, J. L., and Burgering, B. M. (1998). Protein kinase B activation and lamellipodium formation are independent phosphoinositide 3-kinase-mediated events differentially regulated by endogenous Ras. Molecular and Cellular Biology *18*, 1802-1811.

Villanueva, J., Vultur, A., Lee, J. T., Somasundaram, R., Fukunaga-Kalabis, M., Cipolla, A. K., Wubbenhorst, B., Xu, X., Gimotty, P. A., Kee, D.*, et al.* (2010). Acquired resistance to BRAF inhibitors mediated by a RAF kinase switch in melanoma can be overcome by cotargeting MEK and IGF-1R/PI3K. Cancer Cell *18*, 683-695.

von der Maase, H., Sengelov, L., Roberts, J. T., Ricci, S., Dogliotti, L., Oliver, T., Moore, M. J., Zimmermann, A., and Arning, M. (2005). Long-term survival results of a randomized trial comparing gemcitabine plus cisplatin, with methotrexate, vinblastine, doxorubicin, plus cisplatin in patients with bladder cancer. Journal of Clinical Oncology *23*, 4602-4608.

Vu, T., and Claret, F. X. (2012). Trastuzumab: Updated Mechanisms of Action and Resistance in Breast Cancer. Frontiers in Oncology *2*, 62.

Wang, D. S., Rieger-Christ, K., Latini, J. M., Moinzadeh, A., Stoffel, J., Pezza, J. A., Saini, K., Libertino, J. A., and Summerhayes, I. C. (2000). Molecular analysis of PTEN and MXI1 in primary bladder carcinoma. International Journal of Cancer *88*, 620-625.

Wang, F., Kan, M., Yan, G., Xu, J., and McKeehan, W. L. (1995). Alternately spliced NH2-terminal immunoglobulin-like Loop I in the ectodomain of the fibroblast growth factor (FGF) receptor 1 lowers affinity for both heparin and FGF-1. The Journal of Biological Chemistry *270*, 10231-10235.

Wang, F., Marshall, C. B., and Ikura, M. (2013a). Transcriptional/epigenetic regulator CBP/p300 in tumorigenesis: structural and functional versatility in target recognition. Cellular and Molecular Life Sciences *70*, 3989-4008.

Wang, H., Li, Q., Niu, X., Wang, G., Zheng, S., Fu, G., and Wang, Z. (2017a). miR-143 inhibits bladder cancer cell proliferation and enhances their sensitivity to gemcitabine by repressing IGF-1R signaling. Oncology Letters *13*, 435-440.

Wang, J., Mikse, O., Liao, R. G., Li, Y., Tan, L., Janne, P. A., Gray, N. S., Wong, K. K., and Hammerman, P. S. (2014). Ligand-associated ERBB2/3 activation confers acquired resistance to FGFR inhibition in FGFR3-dependent cancer cells. Oncogene *34*, 2167-2177.

Wang, J. K., Tsai, M.-C., Poulin, G., Adler, A. S., Chen, S., Liu, H., Shi, Y., and Chang, H. Y. (2010). The histone demethylase UTX enables RB-dependent cell fate control. Genes and Development *24*, 327-332.

Wang, L., Sustic, T., Leite de Oliveira, R., Lieftink, C., Halonen, P., van de Ven, M., Beijersbergen, R. L., van den Heuvel, M. M., Bernards, R., and van der Heijden, M. S. (2017b). A Functional Genetic Screen Identifies the Phosphoinositide 3-kinase Pathway as a Determinant of Resistance to Fibroblast Growth Factor Receptor Inhibitors in FGFR Mutant Urothelial Cell Carcinoma. European Urology *71*, 858-862.

Wang, P., Nishitani, M.-A., Tanimoto, S., Kishimoto, T., Fukumori, T., Takahashi, M., and Kanayama, H.-O. (2007). Bladder Cancer Cell Invasion Is Enhanced by Cross-Talk with Fibroblasts Through Hepatocyte Growth Factor. Urology *69*, 780-784.

Wang, S., Cang, S., and Liu, D. (2016). Third-generation inhibitors targeting EGFR T790M mutation in advanced non-small cell lung cancer. Journal of Hematology and Oncology *9*, 34.

Wang, Y., Liu, Y., Du, Y., Yin, W., and Lu, J. (2013b). The predictive role of phosphatase and tensin homolog (PTEN) loss, phosphoinositol-3 (PI3) kinase (PIK3CA) mutation, and PI3K pathway activation in sensitivity to trastuzumab in HER2-positive breast cancer: a meta-analysis. Current Medical Research and Opinion *29*, 633-642.

Warrick, J. I., Walter, V., Yamashita, H., Chung, E., Shuman, L., Amponsa, V. O., Zheng, Z., Chan, W., Whitcomb, T. L., Yue, F.*, et al.* (2016). FOXA1, GATA3 and PPARɣ Cooperate to Drive Luminal Subtype in Bladder Cancer: A Molecular Analysis of Established Human Cell Lines. Scientific Reports *6*, 38531.

Watson, G., Ronai, Z. A., and Lau, E. (2017). ATF2, a paradigm of the multifaceted regulation of transcription factors in biology and disease. Pharmacological Research *119*, 347-357.

Weisberg, E., Manley, P., Mestan, J., Cowan-Jacob, S., Ray, A., and Griffin, J. D. (2006). AMN107 (nilotinib): a novel and selective inhibitor of BCR-ABL. British Journal of Cancer *94*, 1765-1769.

Williams, S. V., Adams, J., Coulter, J., Summersgill, B. M., Shipley, J., and Knowles, M. A. (2005). Assessment by M-FISH of karyotypic complexity and cytogenetic evolution in bladder cancer in vitro. Genes, Chromosomes and Cancer *43*, 315-328.

Williams, S. V., Hurst, C. D., and Knowles, M. A. (2013). Oncogenic FGFR3 gene fusions in bladder cancer. Human Molecular Genetics *22*, 795-803.

Witjes, J. A., Compérat, E., Cowan, N. C., De Santis, M., Gakis, G., Lebret, T., Ribal, M. J., Van der Heijden, A. G., and Sherif, A. (2014). EAU Guidelines on Muscle-invasive and Metastatic Bladder Cancer: Summary of the 2013 Guidelines. European Urology *65*, 778-792.

Witjes, J. A., Lebret, T., Comperat, E. M., Cowan, N. C., De Santis, M., Bruins, H. M., Hernandez, V., Espinos, E. L., Dunn, J., Rouanne, M.*, et al.* (2016). Updated 2016 EAU Guidelines on Muscle-invasive and Metastatic Bladder Cancer. European Urology *71*, 462-475.

Wolff, A. C., Hammond, M. E. H., Hicks, D. G., Dowsett, M., McShane, L. M., Allison, K. H., Allred, D. C., Bartlett, J. M. S., Bilous, M., Fitzgibbons, P.*, et al.* (2013). Recommendations for Human Epidermal Growth Factor Receptor 2 Testing in Breast Cancer: American Society of Clinical Oncology/College of American Pathologists Clinical Practice Guideline Update. Journal of Clinical Oncology *31*, 3997-4013.

Wong, S., and Witte, O. N. (2004). The BCR-ABL story: bench to bedside and back. Annual Review of Immunology *22*, 247-306.

World Health Organization (1973). Histological Typing of Urinary Bladder Tumours.

Wu, Y.-M., Su, F., Kalyana-Sundaram, S., Khazanov, N., Ateeq, B., Cao, X., Lonigro, R. J., Vats, P., Wang, R., Lin, S.-F.*, et al.* (2013). Identification of Targetable FGFR Gene Fusions in Diverse Cancers. Cancer Discovery *3*, 636.

Wu, Y. L., Soo, R. A., Locatelli, G., Stammberger, U., Scagliotti, G., and Park, K. (2017). Does c-Met remain a rational target for therapy in patients with EGFR TKI-resistant non-small cell lung cancer? Cancer Treatment Reviews *61*, 70-81.

Yaeger, R., Cercek, A., O'Reilly, E. M., Reidy, D. L., Kemeny, N., Wolinsky, T., Capanu, M., Gollub, M. J., Rosen, N., Berger, M. F.*, et al.* (2015). Pilot Trial of Combined BRAF and EGFR Inhibition in BRAF Mutant Metastatic Colorectal Cancer Patients. Clinical Cancer Research *21*, 1313-1320.

Yonesaka, K., Zejnullahu, K., Okamoto, I., Satoh, T., Cappuzzo, F., Souglakos, J., Ercan, D., Rogers, A., Roncalli, M., Takeda, M.*, et al.* (2011). Activation of ERBB2 signaling causes resistance to the EGFR-directed therapeutic antibody cetuximab. Science Translational Medicine *3*, 99ra86-99ra86.

Yoza, K., Himeno, R., Amano, S., Kobashigawa, Y., Amemiya, S., Fukuda, N., Kumeta, H., Morioka, H., and Inagaki, F. (2016). Biophysical characterization of drug-resistant mutants of fibroblast growth factor receptor 1. Genes to Cells *21*, 1049-1058.

Zabriskie, M. S., Eide, C. A., Tantravahi, S. K., Vellore, N. A., Estrada, J., Nicolini, F. E., Khoury, H. J., Larson, R. A., Konopleva, M., Cortes, J. E.*, et al.* (2014). BCR-ABL1 compound mutations combining key kinase domain positions confer clinical resistance to ponatinib in Ph chromosome-positive leukemia. Cancer Cell *26*, 428-442.

Zerbino, D. R., Achuthan, P., Akanni, W., Amode, M. R., Barrell, D., Bhai, J., Billis, K., Cummins, C., Gall, A., Giron, C. G.*, et al.* (2018). Ensembl 2018. Nucleic Acids Research *46*, D754-D761.

Zhang, H. (2016). Three generations of epidermal growth factor receptor tyrosine kinase inhibitors developed to revolutionize the therapy of lung cancer. Drug Design, Development and Therapy *10*, 3867-3872.

Zhang, X. F., Settleman, J., Kyriakis, J. M., Takeuchi-Suzuki, E., Elledge, S. J., Marshall, M. S., Bruder, J. T., Rapp, U. R., and Avruch, J. (1993). Normal and oncogenic p21ras proteins bind to the amino-terminal regulatory domain of c-Raf-1. Nature *364*, 308-313.

Zhang, X., Ibrahimi, O. A., Olsen, S. K., Umemori, H., Mohammadi, M., and Ornitz, D. M. (2006). Receptor Specificity of the Fibroblast Growth Factor Family: The Complete Mammalian FGF Family. The Journal of Biological Chemistry *281*, 15694-15700.

Zhang, X., Li, J., Qin, J.-J., Cheng, W.-L., Zhu, X., Gong, F.-H., She, Z., Huang, Z., Xia, H., and Li, H. (2017). Oncostatin M receptor β deficiency attenuates atherogenesis by inhibiting JAK2/STAT3 signaling in macrophages. Journal of Lipid Research *58*, 895-906.

Zhao, R., Choi, B. Y., Lee, M.-H., Bode, A. M., and Dong, Z. (2016). Implications of Genetic and Epigenetic Alterations of CDKN2A (p16(INK4a)) in Cancer. EBioMedicine *8*, 30-39.

Zimmermann, G., Papke, B., Ismail, S., Vartak, N., Chandra, A., Hoffmann, M., Hahn, S. A., Triola, G., Wittinghofer, A., Bastiaens, P. I., and Waldmann, H. (2013). Small molecule inhibition of the KRAS-PDEdelta interaction impairs oncogenic KRAS signalling. Nature *497*, 638-642.

Zito, C. I., Riches, D., Kolmakova, J., Simons, J., Egholm, M., and Stern, D. F. (2008). Direct resequencing of the complete ERBB2 coding sequence reveals an absence of activating mutations in ERBB2 amplified breast cancer. Genes, Chromosomes and Cancer *47*, 633-638.